Titre: Title:	Numerical, Analytical and Experimental Studies of the Hydrogeotechnical Behaviors of Slurried Materials
Auteur: Author:	Jian Zheng
Date:	2018
Type:	Mémoire ou thèse / Dissertation or Thesis
Référence: Citation:	Zheng, J. (2018). Numerical, Analytical and Experimental Studies of the Hydrogeotechnical Behaviors of Slurried Materials [Thèse de doctorat, École Polytechnique de Montréal]. PolyPublie. https://publications.polymtl.ca/3760/

UNIVERSITÉ DE MONTRÉAL

NUMERICAL, ANALYTICAL AND EXPERIMENTAL STUDIES OF THE HYDRO-GEOTECHNICAL BEHAVIORS OF SLURRIED MATERIALS

JIAN ZHENG

DÉPARTEMENT DE GÉNIES CIVIL, GÉOLOGIQUE ET DES MINES

ÉCOLE POLYTECHNIQUE DE MONTRÉAL

THÈSE PRÉSENTÉE EN VUE DE L'OBTENTION

DU DIPLÔME DE PHILOSOPHIAE DOCTOR

(GÉNIE MINÉRAL)

NOVEMBRE 2018

UNIVERSITÉ DE MONTRÉAL

ÉCOLE POLYTECHNIQUE DE MONTRÉAL

Cette thèse intitulée :

NUMERICAL, ANALYTICAL AND EXPERIMENTAL STUDIES OF THE HYDRO-GEOTECHNICAL BEHAVIORS OF SLURRIED MATERIALS

présentée par : ZHENG Jian

en vue de l'obtention du diplôme de : Philosophiae Doctor

a été dûment acceptée par le jury d'examen constitué de :

M. SIMON Richard, Ph. D., président

M. LI Li, Ph. D., membre et directeur de recherche

M. MARTIN Vincent, Ph. D., membre

M. SIMMS Paul, Ph. D., membre externe

DEDICATION

To my family

To my country

ACKNOWLEDGEMENTS

First of all, I would like to express my deepest appreciation and respect to my supervisor, Prof Li Li, for your constant support, guidance and encouragement for my pre-doctoral research proposal, journal articles and this Ph.D. thesis, for your patience, motivation and immense knowledge. Thank you for always taking time out of your busy schedule to discuss with me and help me overcome many difficulties in my research project. Also, many thanks for giving me the chance to present my research in many occasions.

I'm very grateful to Prof. Richard Simon, Prof. Paul Simms, Dr. Vincent Martin and Prof. Anoui Lakis for your acceptance to be members of jury for my Ph.D. thesis. I'm aware that you are very busy with many commitments. Thank you!

I would also like to thank Prof. Mamert Mbonimpa and Prof. Thomas Pabst for their time, discussion and comments on my pre-doctoral proposal and articles. I especially want to thank Prof. Yuchao Li for his support, advices and encouragements during my studies in both China and Canada. Many thanks to Prof. Robert P Chapuis, Michael James, and Tikou Belem for their courses. Noura EI-Harrak, Samuel Chénier, Vincent Martin, Karim Essayad, Natasha Carrière, Maxime Daviault, Ghislain Charly Mube Soh and Yousra EI Bahraoui are also acknowledged for their kind help in my laboratory work.

My time in Montréal was so enjoyable and enriched due to many friends and groups. I would like to thank all my colleagues, friends and members of RIME-IRME research group for their kind help and advices. Also, many thanks to my teammates, friends and leaders I met in the volunteer organization "les amis de la montagne Montréal", we had a great time in the past three years.

I acknowledge the financial support from Natural Sciences and Engineering Research Council of Canada (NSERC), Institut de recherche Robert-Sauvé en santé et en sécurité du travail (IRSST), Fonds de recherche du Québec - Nature et Technologies (FRQNT), and also our industrial partners of the Research Institute on Mines and the Environment (RIME UQAT-Polytechnique).

Lastly, I would like to express my profound appreciation to my family, for their unconditional support, love and patient during my life and studies. I love them so much, it is impossible for me to make it so far without their support. There are no words to express how grateful I am to the sacrifices they have made on my behalf.

RÉSUMÉ

Les mines produisent des minéraux précieux, mais aussi une grande quantité de rejets miniers solides, y compris des résidus miniers et des stériles. Dans la plupart des cas, les résidus sont transportés par des canalisations et confinés dans des parcs à résidus, tandis que les stériles sont entreposés sous forme de haldes à stérile. Ces méthodes traditionnelles de gestion des rejets miniers peuvent poser des problèmes environnementaux et géotechniques. Une autre méthode consiste à utiliser les rejets miniers pour remblayer les chantiers miniers sous terre, ce qui peut améliorer la stabilité du terrain, augmenter la récupération du minerai et réduire le stockage en surface des rejets miniers.

Cependant, les digues des parcs à résidus et les barricades dans les chantiers miniers peuvent se rompre. Dans la plupart des cas, les conséquences d'une rupture d'une digue de retenue ou d'une barricade sont très graves et même catastrophiques. Il est donc très important d'évaluer correctement la pression interstitielle lors du remplissage afin de garantir la stabilité des digues de retenue des résidus et des barricades de chantiers remblayés. C'est l'objectif principal de la thèse.

Pour le dépôt de matières en suspension (résidus miniers ou boues de dragage), Gibson a proposé un modèle en 1958 pour évaluer la pression interstitielle en excès. Sa solution contient une intégrale qui ne peut être évaluée que numériquement. Des solutions analytiques sont donc proposées dans le cadre de cette thèse basées sur le modèle de Gibson (1958). Les solutions analytiques proposées peuvent être résolues à l'aide d'outils de calcul couramment disponibles (e.g. Excel de Microsoft). Les solutions proposées ont été validées par les résultats numériques obtenus par SIGMA/W. Le bon accord entre les résultats analytiques et numériques indique que les solutions proposées peuvent être un outil utile pour évaluer la pression interstitielle pendant le dépôt de matière en suspension, en particulier au stade préliminaire du projet. Dans le cas d'une opération après la fin du dépôt, Gibson n'a proposé qu'une équation différentielle en 1958. Cette équation différentielle ne peut pas être appliquée directement pour évaluer la pression interstitielle ou l'excès de celle-ci. De nouveaux développements ont été réalisés, menant à une nouvelle solution qui peut être utilisée pour évaluer la pression interstitielle avec des outils de calcul tels que MATLAB. Les solutions proposées ont également été validées par les résultats numériques obtenus par SIGMA/W. Elles peuvent être utilisées pour évaluer la pression interstitielle après le dépôt de matières en suspension (résidus miniers ou boues de dragage) au stade préliminaire d'un projet.

Pour la conception de barricade dans les chantiers remblayés, le facteur le plus important à considérer est la contrainte totale exercée sur celle-ci pendant et peu de temps après le dépôt du remblai. Au cours de ce processus, une consolidation du dépôt sous son poids propre peut avoir lieu, accompagnée de la génération d'une contrainte effective et d'un effet d'arche le long des interfaces de contact. Jusqu'à présent, la consolidation sous le poids propre et l'effet d'arche n'avaient jamais été pris en compte simultanément dans l'évaluation des contraintes dans les chantiers remblayés. Dans cette thèse, de nouvelles solutions sont proposées pour évaluer les contraintes totales et effectives des chantiers remblayés en prenant en compte la consolidation sous le poids propre et l'effet d'arche. Pour les remblais à très haute perméabilité, la solution proposée pour le cas de base imperméable peut être réduite à la solution proposée par Li et Aubertin en 2009 pour les chantiers remblayés à pression hydrostatique. Les solutions proposées sont également validées par une modélisation numérique réalisée avec Plaxis2D. Un exemple d'application des solutions proposées montre qu'un coefficient de consolidation élevé et un faible taux de remblayage sont favorables au drainage, ce qui se traduit par une contrainte effective élevée et une contrainte totale faible dans le chantier remblayé.

Malgré les nombreuses études sur la pression et les contraintes exercées sur les chantiers remblayés, un dilemme existe. Dans les quelques manuels disponibles sur les remblais miniers, les pressions dans les chantiers remblayés avec du remblai en pâte ont été jugées très faibles. Une légère construction de barricade a été recommandée pour conserver le remblai en pâte dans les chantiers miniers. Cela ne correspond pas aux mesures in situ, qui ont montré que les pressions interstitielles et les contraintes totales au cours de l'opération de remblayage peuvent être aussi élevées que la pression iso-géostatique due au poids des terres. Une révision de la définition du remblai en pâte donnée dans les manuels révèle qu'un remblai en pâte répondant au critère en termes de saignement d'eau peut être très visqueux et probablement non saturé. Lorsque ce remblai est placé dans un chantier, il se produit un effet d'arche associé à la cohésion apparente, ce qui entraîne de faibles contraintes dans les chantiers remblayés. En pratique, l'application d'un tel remblai en pâte peut être très difficile. Il faut ajouter plus d'eau dans le remblai pour réduire la consommation d'énergie nécessaire au pompage et au transport, pour obtenir une surface de remblayage horizontale ou pour assurer des contacts étroits entre le remblai et le plafond du chantier. Lorsque le remblai en pâte est placé dans le chantier sous forme de boue, le remblai n'a aucune résistance effective au cisaillement. Les pressions interstitielles et les contraintes totales

peuvent être aussi élevées que la pression iso-géostatique due au poids des terres. Ces deux cas extrêmes indiquent que les pressions et les contraintes dans les chantiers remblayés dépendent de la teneur en eau ou en solides du remblai. Pour étayer cette hypothèse, une série d'essais sur colonne a été réalisée avec un remblai en pâte de différents pourcentages de solides. Les contraintes totales verticales ont été mesurées au centre et près du mur. Les résultats montrent que les contraintes totales verticales dans un chantier diminuent à mesure que le pourcentage de solides augmente. Lorsque le pourcentage de solide du remblai est très élevé, une contrainte totale verticale faible au centre et près du mur a été obtenue. Une légère construction de barricade suffit. Lorsque le pourcentage de solides est faible, les contraintes totales verticales aussi élevées que la pression iso-géostatique ont été obtenues. Une légère construction de barricade peut ne pas suffire.

Les principaux résultats de ce projet sont présentés dans sept articles de revue, dont deux publiés et cinq soumis. Les résultats des travaux connexes ont été présentés dans les annexes, incluant notamment les résultats des essais de laboratoire effectués pour mesurer le coefficient de pression des terres dans les chantiers remblayés et ceux sur l'efficacité de la réduction du frottement en utilisant différents matériaux lubrifiants.

ABSTRACT

Mines produce not only valuable minerals, but also a large amount of solid wastes including tailings and waste rocks. For most cases, the tailings are transported by pipes and confined in tailings impoundments while the waste rocks are disposed as waste rock piles. These traditional mine waste management methods can pose some environmental and geotechnical problems. Thus, more and more mines use the mine wastes to fill underground mine stopes. This practice allows improved ground stability, increased ore recovery and reduced surface disposal of mine wastes.

However, tailings dams and barricades can fail. In most cases, the consequences associated with a tailing dam or barricade failure are very serious and catastrophic. It is thus very important to correctly evaluate the pore water pressure (PWP) in the tailings impoundments and in mine backfilled stopes during and after the deposition operation to ensure stable tailings dams and barricades of backfilled stopes. This is the main objective of the thesis.

For the case of ongoing deposition of a slurry, Gibson proposed a model in 1958 to evaluate the excess PWP. His solution contains an integral part, which can only be evaluated numerically. Analytical solutions are thus proposed in the context of this thesis based on the Gibson (1958) model. The proposed analytical solutions can be solved by commonly available tools of calculation (e.g. Excel of Microsoft). The proposed solutions have been validated by numerical results obtained by SIGMA/W. The good agreement between the analytical and numerical results indicates that the proposed solutions can be a useful tool to evaluate the PWP during the slurry deposition, especially in the preliminary stage of a project. For the case of after the end of deposition operation, Gibson only proposed a governing equation in 1958. The differential equations cannot directly be applied to evaluate the PWP or excess PWP. New development has been done, resulting in a new solution that can be used to evaluate the PWP with some commercial calculation tools like MATLAB. The proposed solutions have also been validated by numerical results obtained by SIGMA/W. They can be used to evaluate the PWP after the slurry deposition, in the preliminary stage of a project.

For the case of barricade design in backfilled stopes, the most critical factor is the total stresses during and shortly after the slurry deposition. During theses processes, self-weight consolidation can take place, accompanied with the generation of effective stress and arching effect along the fill-wall contact interfaces. Until now, the self-weight consolidation and the arching effect have never been considered simultaneously in the evaluation of stresses in backfilled stopes. In this

thesis, new solutions are proposed to evaluate the total and effective stresses in backfilled stopes by considering the self-weight consolidation and arching effect. For backfill with very high permeability, the proposed solution for the case of impervious base can reduce to the solution proposed by Li and Aubertin in 2009 for backfilled stopes with hydrostatic pressure. The proposed solutions are also validated by numerical modeling conducted with Plaxis2D. Sample application of the proposed solutions shows that high consolidation coefficient and low filling rate are favorable to the drainage, resulting in high effective stress and low total stress in the backfilled stope.

Despite the numerous studies on the pressure and stresses in backfilled stopes, a dilemma exists. In the few available handbooks on mine backfills, light barricades are recommended to retain paste backfill in mine stopes because the pressures in stopes backfilled with paste backfill were evaluated as very small. This does not correspond to the in situ measurements, which showed that the PWP and total stresses during the backfilling operation can be as high as the iso-geostatic pressure based on the overburden of the backfill. A revision on the definition of paste backfill given in the handbooks reveals that a paste backfill meeting the criterion in terms of water bleeding can be very viscous and probably unsaturated. When such backfill is placed in a stope, arching associated with the apparent cohesion takes place, resulting in small stresses in the backfilled stopes. In practice, the application of such paste backfill can be very difficult. More water has to be added in the backfill to minimize the energy consumption for the pumping and transportation, to obtain horizontal backfill surface or to ensure tight contacts between the backfill and stope roofs. When the paste backfill is placed in the stope in form of slurry, the backfill has no effective shear strength. The PWP and total stresses can be as high as the iso-geostatic pressure based on the overburden of the backfill. These two extreme cases indicate that the pressures and stresses in the backfilled stope depend on the water or solid content of the backfill. To verify this hypothesis, a series of column tests were conducted with a paste backfill of different solid contents. The vertical total stresses were measured at the center and near the wall. The results show that the vertical total stresses in a backfilled stope decrease as the solid content increases. When the solid content of backfill is very high, low vertical total stress at the center and near the wall were obtained. A light barricade may be enough. When the solid content is low, the vertical total stresses as high as the iso-geostatic pressure were obtained. A light barricade may not be enough.

The main results of this project are presented in seven journal articles with two published and five submitted. The laboratory test results conducted to measure the earth pressure coefficient in backfilled stopes and those performed to investigate the efficiency of friction reduction by using different lubricant materials have been presented in Appendices.

TABLE OF CONTENTS

LIST OF TABLES

LIST OF FIGURES

LIST OF SYMBOLS AND ABBREVIATIONS

Symbols

A	sectional area of the silo (m^2)
C	compressive force (kN)
C_u	uniformity coefficient
C_c	curvature coefficient
C_w	solid content (%)
D_{10}	particle size at which 10% of particles can pass the sieve (mm)
D_{60}	particle size at which 60% of particles can pass the sieve (mm)
E'	drained Young's modulus (MPa)
G	shear modulus
G_s	specific gravity
H	final height at the end of deposition (m)
H_d	height of the access drift (m)
H_e	excess PWP in water height (m)
K	earth pressure coefficient
K_a	active earth pressure coefficient
K_0	at-rest earth pressure coefficient
M'	drained constrained modulus (MPa)
L	length of underground structure (m)
P_w	pore water pressure (kPa)
P_{w0}	pore water pressure at the end of deposition (kPa)
P_{w1}	pore water pressure after the end of deposition (kPa)
R_ξ	horizontal resistance (kPa)

S slump height (m)

S' normalized slump height (m)

T dimensionless time factor

U circumference of the silo (m)

V vertical force (kN)

W weight of the backfill layer element (kN)

W_d width of the access drift (m)

a and b two parameters in Li and Aubertin (2008) to control the normal stress distribution curvature

c cohesion (kPa)

c_i cohesion of the ith fill-wall interface (kPa)

c_v consolidation coefficient (m^2/s)

c' effective cohesion of the fill (kPa)

d inner diameter

e void ratio

h depth from the surface of the backfill (m)

h_0 height of unyielded region (m)

h'_0 normalized height of unyielded region

h_1 height of yielded region (m)

h'_1 normalized height of yielded region (m)

k hydraulic conductivity (m/s)

k_{sat} saturated hydraulic conductivity (m/s)

l length of stope (m)

m filling rate (m/h)

n	series number
q	surcharge on top of the backfill (kPa)
q_u	compressive strength (kPa)
t	filling time (h)
t_0	time during the accreting deposition (h)
t_1	time start from the moment when the deposition ceases (h)
u	excess pore water pressure (kPa)
u_0	the hydrostatic pore pressure (kPa)
u_1	excess PWP after the end of deposition (kPa)
w	width of the stope (m)
w_L	liquid limit
w_P	plastic limit
x	distance from the center line of the stope (m)
z	elevation of the calculation point from the base (m)
α_i	backfill state angle on the ith wall (°)
β	inclination angle to the horizontal surface (°)
γ	unit weight of the backfill (kN/m^3)
γ'	submerged unit weight of the slurry (kN/m^3)
γ_{sub}	submerged unit weight of backfill (kN/m^3)
γ_{sat}	saturated unit weight of backfill (kN/m^3)
ξ	arbitrary integration parameter
σ'	effective stress (kPa)
σ_v	vertical total stress (kPa)
σ_h	horizontal total stress (kPa)

σ'_v	vertical effective stress (kPa)
σ'_h	horizontal total stress (kPa)
σ_{vH}	vertical stress at the bottom of the stope (kPa)
σ_{vx}	vertical stress across the stope width (kPa)
σ_{v0}	vertical stress at the centerline of the stope (kPa)
δ	friction angle along the interfaces between the fill and surrounding walls (°)
δ_i	friction angle of the *i*th fill-wall interface (°)
ϕ'	effective friction angle between the backfill and surrounding walls (°)
ϕ	internal friction angle of the backfill (°)
ϕ_0	friction angle correction parameter
λ_1, λ_2	model parameters
ν	Poisson's ratio
μ	friction coefficient along the wall
τ_y	yield stress (kPa)
τ'_y	normalized yield stress (kPa)

Abbreviations

ASTM	American Society for Testing and Materials
C-S-H	Calcium silicate hydrate
CPB	Cemented paste backfill
DF	Distribution factor
FLAC	Fast Lagrangian Analysis of Continua
FLD	Full lateral drainage
HF	Hydraulic fill

HW	Hanging wall
KB	Kanowna Bell
MATLAB	Matrix laboratory
PLD	Partial lateral drainage
PWP	Pore water pressure
UCS	Unconfined compressive strength
VCL	Vertical center line
VCR	Vertical crater retreat

LIST OF APPENDICES

CHAPTER 1 INTRODUCTION

1.1 Statement of the problem

Mining industry is an important part of Canada's national economy. Despite the production of valuable minerals, the excavation of ore body also generates large mined-out voids (stopes), which need to be properly managed to improve the ground stability (Darling 2011). The extraction of the commercially valuable minerals from the ore body is also accompanied with the generation of large amount of mine wastes in terms of waste rock and tailings.

The mine wastes can be disposed of on the surface or returned to underground to fill the void spaces. In the former, the tailings are usually transported by pipes and confined by tailings dams while the waste rocks are disposed as piles. They can also be co-disposed with the installation of waste rock inclusions in the tailings impoundments to accelerate the drainage and consolidation (Bolduc and Aubertin 2014; Ferdosi et al. 2015). This mine waste management can pose great environmental and geotechnical challenges associated with the geotechnical and geochemical instabilities (Bussière 2007). When the waste rocks are reactive, the waste rock piles can be the generator of the acid mine drainage due to the high air and water permeability of the piles (Sracek et al. 2004; Molson et al. 2005).

Compared to the surface disposal method, underground mine backfilling can bring several advantages, including increased ore recovery, reduced mineral dilution, improved ground stability and reduced surface disposal of mine wastes (Hassani and Archibald 1998; Jung and Biswas 2002; Potvin et al. 2005). Not surprisingly, it has become a common practice in many underground mines around the world.

In general, backfill can be classified as rock fill, hydraulic fill, and paste backfill. Among them, the hydraulic and paste backfills are advantageous as they can be transported by pipes. However, they must contain sufficient water to facilitate their transportation by pipes. A confining structure, called barricade, needs to be built at the base of the stope to retain the slurried backfill in the stope. The stability of barricade is an important concern as the failure of barricade can lead to the trap of equipment, huge economic lose and even lose of lives (Grice 1998; Sivakugan et al. 2006a, 2006b, 2013; Yang et al. 2017). The barricade stability is generally determined by the backfill pressure

during and shortly after the end of the backfilling operation. It is thus critical to have a good understanding of the hydro-geotechnical behavior of the backfill during and after the deposition.

When tailings or slurried backfills are placed in a confining structure (dam or mine stope), the solid particles tend to settle down under the gravity. The tailings or the backfills tend to become denser and expel the pore water out of them. As the tailings or the backfills usually have low permeability, the drainage will be limited, resulting in the generation of excess pore water pressure (PWP). When the dissipation of excess PWP reaches a certain degree and the solid particles contact each other, effective stresses start to generate. This process is called self-weight consolidation.

If the slurried material is deposited at a very high filling rate to a high final height, excessive high PWP and pressure can generate in the slurried material, which may lead to the failure of dams or barricades. If the filling rate is low, drainage and excess PWP dissipation can take place during the filling operation, resulting in the generation of effective stresses. For the case of mine backfilled stopes, the shear stresses can generate along the fill-wall contact interfaces. For a narrow mine stopes, a part of the load can be transferred from the backfill to the stiff surrounding walls, resulting in smaller backfill stresses than the overburden pressure. This phenomenon is called arching effect, which can lead to the vertical stresses in the backfilled stopes smaller than the overburden pressure.

The stability of the tailings dams and backfill barricades requires a good understanding of all the above-mentioned aspects during and shortly after the deposition of the slurried materials.

1.2 Objectives of the research

The main objective of this research is to investigate the hydro-geotechnical behavior of slurried materials during and after the deposition in a confining structure (tailings impoundment or mine stope). This has been achieved through the realization of the following specific objectives:

1) To evaluate the excess PWP in slurried materials during and after the deposition;
2) To evaluate the PWP and stresses in backfilled stope during or shortly after the placement of the slurried backfill by considering self-weight consolidation and arching;
3) To evaluate the “short-term” pressure in paste backfilled stopes by considering different solid contents of the backfill.

1.3 Contributions

The realization of the project leads to the publication or submission of the following peer-reviewed journal and conference papers:

J.1 Zheng J, Li L, Mbonimpa M, Pabst T. (2018) An analytical solution of Gibson's model for estimating the pore water pressures in accreting deposition of slurried material under one-dimensional self-weight consolidation. Part I: Pervious base. *Indian Geotechnical Journal*. 48(1): 72-83. This article is presented in Chapter 3.

J.2 Zheng J, Li L, Mbonimpa M, Pabst T. (2018) An analytical solution of Gibson's model for estimating pore water pressures in accreting deposition of slurried material under one-dimensional self-weight consolidation. Part II: Impervious base. *Indian Geotechnical Journal*. 48(1): 188-195. This article is presented in Chapter 4.

J.3 Zheng J, Li L, Li YC, Mbonimpa M. (2018) A new solution to evaluate the PWP during and after slurry deposition on a pervious base. *Environmental Geotechnics*. Revision submitted in August 2018. This article is presented in Chapter 5.

J.4 Zheng J, Li L, Li YC, Mbonimpa M. (2018) A solution to estimate the excess PWP during and after slurry deposition on an impervious base. *Geomechanics and Engineering*. Submitted in July 2018. This article is presented in Chapter 6.

J.5 Zheng J, Li L, Li YC. (2018) A solution to estimate the total and effective stresses in backfilled stopes with an impervious base during the filling operation. *International Journal for Numerical and Analytical Methods in Geomechanics*. Submitted in July 2018. This article is presented in Chapter 7.

J.6 Zheng J, Li L, Li YC. (2018) Total and effective stresses in backfilled stopes during the fill placement on a pervious base for barricade design. *Minerals*. Submitted in November 2018. This article is presented in Chapter 8.

J.7 Zheng J, Li L. (2018) Variation of the "short-term" pressures of paste backfill as a function of the solid content. *Canadian Geotechnical Journal*. Submitted in November 2018. This article is presented in Chapter 9.

J.8 Zheng J, Li L. (2018) An experimental study of the vertical and horizontal stresses and earth pressure coefficient in a vertical backfilled opening. To be submitted in a peer review journal. Main results are presented in Appendix A.

J.9 Zheng J, Li L, Daviault M. (2018) An experimental study to investigate the effectiveness of typical lubricants in reducing the sidewall friction. To be submitted in a peer review journal. Main results are presented in Appendix B.

C.1 Zheng J, Li L, Mbonimpa M, Pabst T. (2017) Analytical solutions of Gibson's model for estimating the pore water pressures in accreting deposition of slurried material under one-dimensional self-weight consolidation. Published in the Proceedings of 70th Canadian Geotechnical Conference, Ottawa, Canada.

C.2 Li L, Zheng J. (2017) A conceptual analytical solution for estimating the short-term pressure of paste fill varying from viscous to liquid state, placed in mine stopes. Published in the Proceedings of 70th Canadian Geotechnical Conference, Ottawa, Canada.

C.3 Zheng J, Li L, Daviault M. (2017) An experimental study of the effectiveness of lubricants in reducing sidewall friction. Published in the Proceedings of 19th International Conference on Civil, Environmental and Infrastructure Engineering, Kyoto, Japan.

C.4 Zheng J, Li L. (2018) Analytical and experimental studies of the evolution of the excess pore water pressure during the deposition of a slurried material. Published in the Proceedings of GeoEdmonton 2018, Canadian Geotechnical Society.

C.5 Zheng J, Li L (2018) A solution to estimate stresses in backfilled stopes by considering self-weight consolidation and arching. Published in the Proceedings of 8th international congress on environmental geotechnics, Hangzhou, China.

The realization of the project contributes to a better understanding of the hydro-geotechnical behavior of slurried materials during and after the deposition in a tailings impoundment or underground mine stope. Analytical, numerical and experimental solutions presented in this document constitute useful tools to evaluate the PWP, effective and total stresses in the tailings impoundments or underground mine backfilled stopes during and after the deposition. The proposed analytical solutions can be useful for geotechnical and mining engineers to conduct

parametric sensitivity analysis for evaluating the stability of tailings dams or underground mine stope barricades in the preliminary stage of projects.

1.4 Organization

The thesis is organized in a paper-based format as follows:

Chapter 1 gives a general introduction and presents the problematics of the thesis. The main objective, contributions and organization of the thesis are also elucidated.

Chapter 2 presents a comprehensive literature review of the background information, including the deposition of slurried materials in tailings impoundments or underground mine stopes, properties of tailings and backfills, pressures and stresses estimation in backfilled stopes shortly and long-time after the slurry deposition.

Chapters 3 and 4 (Articles 1 and 2) present the analytical solutions based on the Gibson (1958) model for estimating the PWP during the deposition of slurried material on pervious and impervious bases, respectively.

Chapters 5 and 6 (Articles 3 and 4) present the solutions to estimate the excess PWP in slurried material after the end of the deposition of slurried material on pervious and impervious bases, respectively.

Chapters 7 and 8 (Articles 5 and 6) present new solutions to evaluate the effective and total stresses in backfilled stopes during the filling operation on pervious and impervious bases, respectively.

Chapter 9 (Article 7) illustrates the variation of the short-term pressure as a function of the solid contents shortly after the placement of the paste backfill in a column.

Chapter 10 presents a summary and discussion of the presented results in the thesis.

The conclusions and recommendations are presented in Chapter 11.

CHAPTER 2 LITERATURE REVIEW

This chapter first presents the different mining methods and the application of mine backfill for different engineering purposes. The hydraulic and mechanics properties of tailings and three types of backfills (i.e. hydraulic fill, paste fill and rock fill) are then presented. Focus is given on the self-weight consolidation of slurried materials and evaluation of excess PWP and stresses in tailings impoundments and underground mine backfilled stopes.

2.1 Underground mining with backfill

When ore bodies are in a deep position or when surface mining method is restricted by the environmental or other issues, underground mining method has to be adopted. This mining method can be divided into three categories: naturally supported methods (e.g. room and pillar, sublevel stoping and shrinkage stoping), artificially supported methods (e.g. cut and fill, drift and fill), and caving methods (e.g. block caving, sublevel caving and longwall) (Brady and Brown 1993).

Several variants mining methods based on the three basic types of mining methods have also been developed and applied in practice. In the following subsection, the mining methods with the application of backfill will be presented. Emphasis is given on the functions and challenges associated with the use of backfill.

2.1.1 Underground mining methods and the possible application of backfill

Naturally supported methods

Naturally supported methods refer to the methods with the ore pillars being left in the mined-out voids to support the mine roof and rock walls. This method is usually applied for low-grade orebodies as the ore recovery is low in the ore pillars. Backfill is not very common from an economic point of view as the ore recovery cannot justify the backfill cost (Potvin et al. 2005). However, backfill can also be used to help recovery the ore pillars or/and provide support for the adjacent excavation. The naturally supported method is thus jointly used with the artificially supported method. The combined methods with the application of backfill is also presented in this subsection.

Room and pillar mining

Room and pillar mining refers to the method by extracting the horizontal openings to form the rooms and leaving pillars to support the roof and rock walls (Darling 2011), as shown in Fig. 2-1. The extraction of ore body can probably cause mine roof caving and wall to wall convergence. Backfill can thus be used to fill the underground openings, which can help to recover the ore bodies in the pillars and improve the rock wall and ground stability (Hunt 1988; Roberts et al. 1999; Tesarik et al. 2009). The backfill is first placed around the perimeter pillars and then towards to the center of the openings. The confining structure, such as barricade or fence needs to be built to retain the backfill in place. The barricade stability and the strength of the backfill to support the roof and rock wall are the critical concerns.

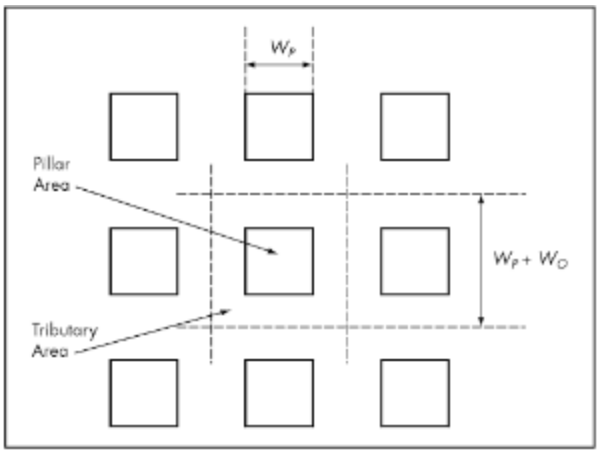

Figure 2-1: Plan view of a room-and-pillar mine (taken from Darling 2011)

Sublevel open stoping

Sublevel open stoping is a very common mining method in North America and accounts for 60% of all the underground mines (Pakalnis and Hughes 2011). It is normally used for competent and steep ore bodies with the dipping angle from 50° to 90°, which are surrounded by competent rock walls. The sublevel open stoping has mainly four types, including blasthole stoping, long-hole stoping, shrinkage stoping and VCR (vertical crater retreat).

Fig. 2-2(a) shows the schematic diagram of the blasthole stoping. In this mining method, ore bodies are broken using ring drilling or long parallels blast holes, which are drilled by top-hammer drills. The blasted ore bodies fall to the stope base under the effect of gravity, which are then extracted and collected from the drawpoints (Darling 2011). The long-hole stoping can be considered as one

variation of the blasthole stoping, as shown in Fig. 2-2(b). The hole can be as long as 100 m drilled by in-the-hole (ITH) technique (Hamrin 2001). Backfill can be used in blasthole and long-hole stoping to recover ore pillars and improve the ground stability. The uncemented backfill can be used when the pillars are not recovered.

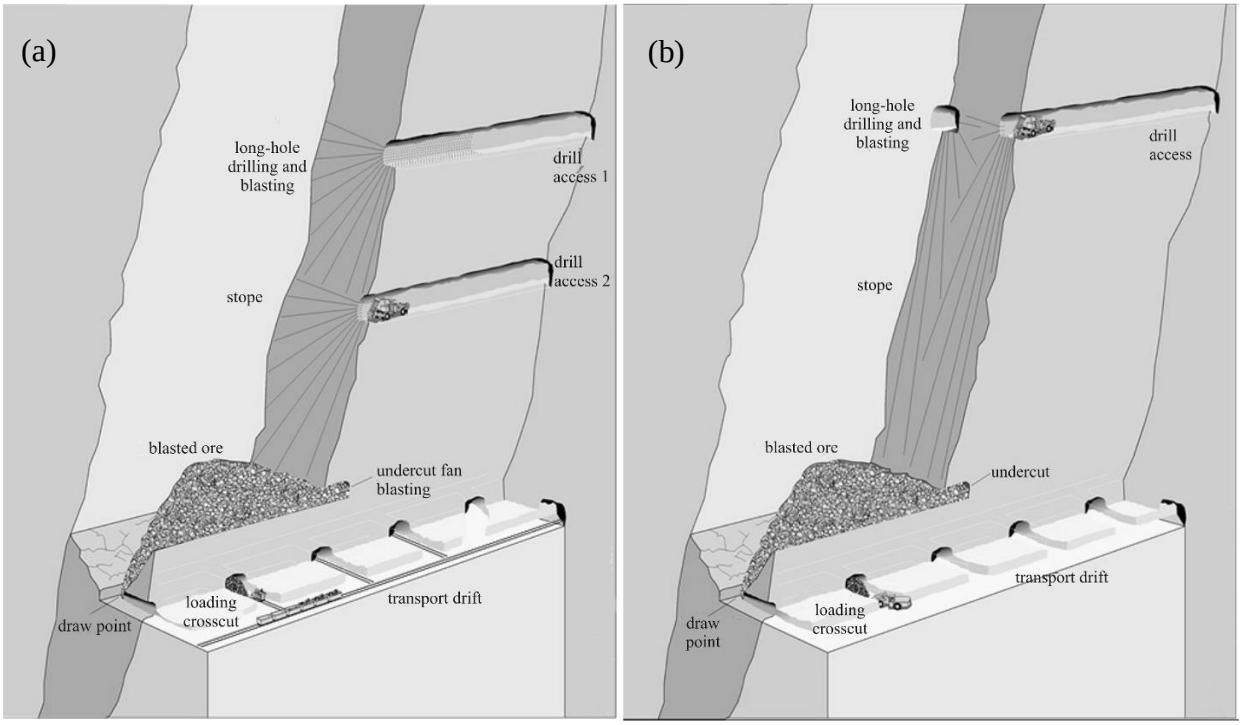

Figure 2-2: Schematic diagram of the (a) blasthole stoping and (b) long hole stoping (taken from Hamrin et al. 2001)

Shrinkage stoping is a vertical overhand stoping method, as shown in Fig. 2-3. It is usually applied for ore bodies, which are very narrow or not suitable for other mining methods. In this mining method, about 60% of the ore bodies are left in the stope to support the rock walls and provide work platform for the operators. When the mining operation is completed, the remaining broken ore bodies can be extracted from the stopes. Backfill is usually not necessary in the shrinkage stoping as the broken ore bodies remained in the stope can have the same effect. If all of the broken ore bodies are extracted from the stope after the completion of mining, uncemented rock fill can also be used to improve the stope stability.

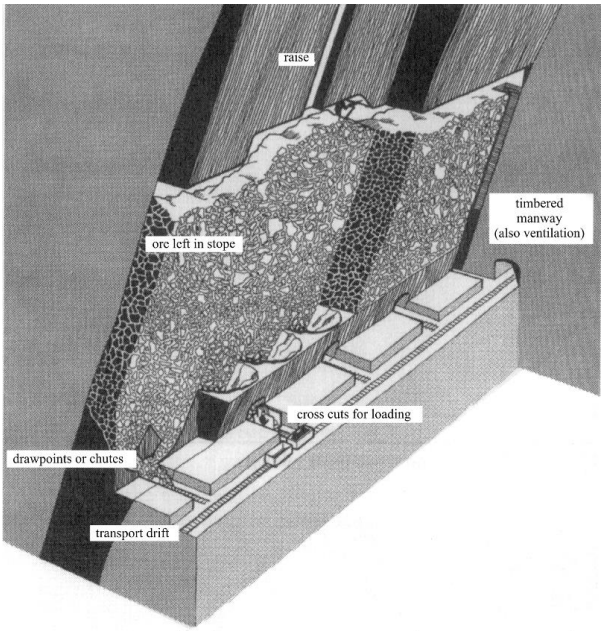

Figure 2-3: The layout of shrinkage stoping (taken from Hamrin et al. 2001)

Vertical crater retreat (VCR) is a variation mining method of sublevel open stoping. Fig. 2-4 shows the schematic diagram of VCR with primary stope being mined [Fig. 2-4(a)] and secondary stope being mined [Fig. 2-4(b)]. In this mining method, the ore bodies are blasted into slabs by the ITH holes drilled from the upper level. The broken ore is extracted at the base of the block. Backfill can be used when the whole stope is mined out (so called "delayed backfill"; Stephan 2011) to improve the ground stability and reduce the surface disposal of mine wastes. The primary stopes are filled with cemented backfill to obtain enough strength to self-stand after being exposed. When the placed backfill in the primary stopes gained required strength, the secondary stope can be filled with uncemented backfill as it is surrounded by the primary stopes and will not be exposed.

When the backfill is applied in the above-mentioned methods, barricade is normally built at the base of the stope near the drawpoint to retain the backfill in place. An important concern is to evaluate the stability of the barricade (see Section 2.4). Another important concern but not treated in this thesis is the determination of the minimum required strength of the cemented backfill used in the primary stopes.

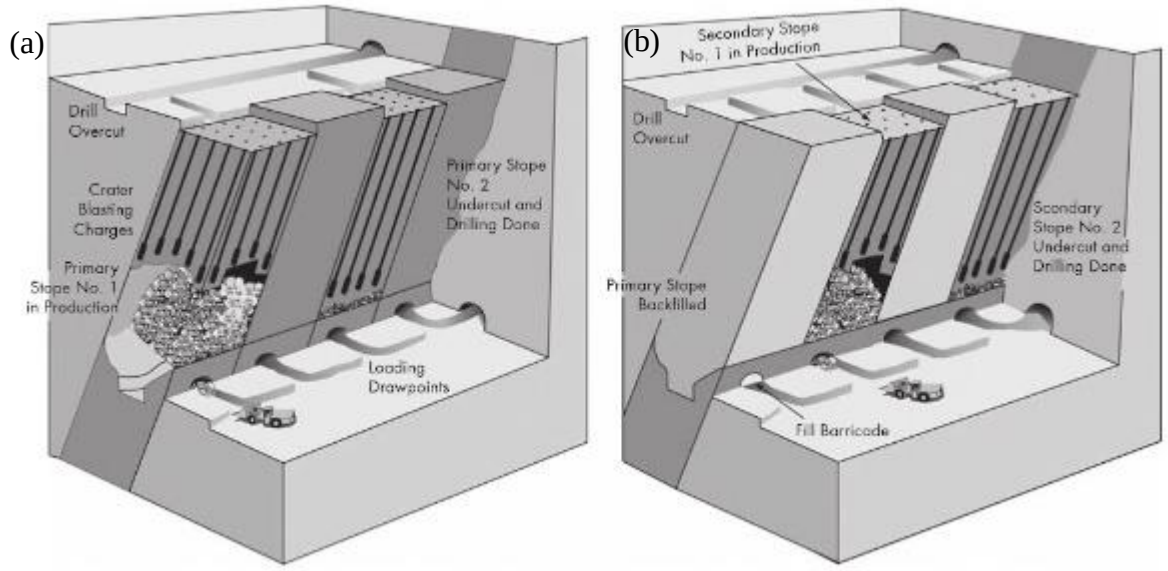

Figure 2-4: Schematic diagram of vertical crater retreat (a) primary stopes mined and (b) secondary stopes mined (taken from Darling 2011)

Artificially supported methods

Artificially supported methods consist to apply backfill progressively with the mining advancement to improve rock wall and ground stability, minimize void expose and reduce the surface disposal of mine wastes.

Cut-and-fill mining

Cut-and-fill mining is a typical artificially supported method in which the mined-out voids are filled with cemented or uncemented backfill during the extraction for continuous production.

There are two types of cut-and-fill mining, overhand and underhand, as shown in Fig. 2-5. The former method is suitable for competent ore bodies, which are narrow and steeply dipping. The uncemented hydraulic fill or rock fill is generally used to provide a stable work platform to ensure the subsequent ore extraction. In order to facilitate the machine operation, the top layer of the backfill is usually added with cement. Underhand cut-and-fill mining method can be used for incompetent ore bodies. In this mining method, the excavation and filling are conducted in a top-down sequence. The excavated stopes are usually filled with cemented backfill, which can develop required strength to provide a safe work space for the miners beneath it. The reinforcement

structures, such as fill mats or rock bolts are required to be built at the bottom of the stope prior to the backfilling.

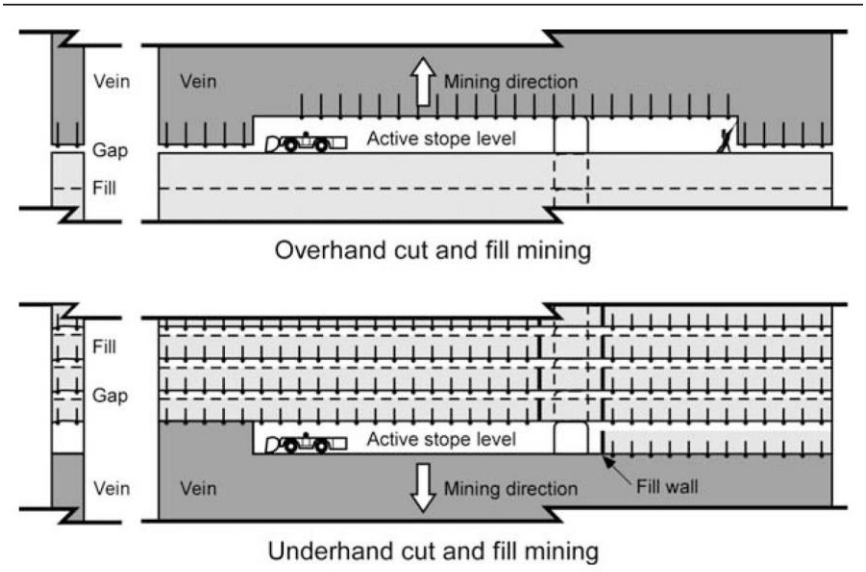

Figure 2-5: Schematic diagram of the overhand and underhand cut and fill mining methods (taken from Williams et al. 2007)

Variations of cut-and-fill mining

The cut-and-fill mining method has several variations, including the post pillar mining [Fig. 2-6(a)], drift and fill [Fig. 2-6(b)], and Avoca mining [Fig. 2-6(c)]. Post pillar mining is an overhand method and usually used for competent ore bodies large in width and thickness. In drift-and-fill method, the ore bodies are extracted from the ore zone through the excavation of parallel drifts. Avoca method is generally applied for ore bodies and rock wall with good strength. In these mining methods, the overhand mining usually uses uncemented backfill while the underhand mining uses cemented backfill.

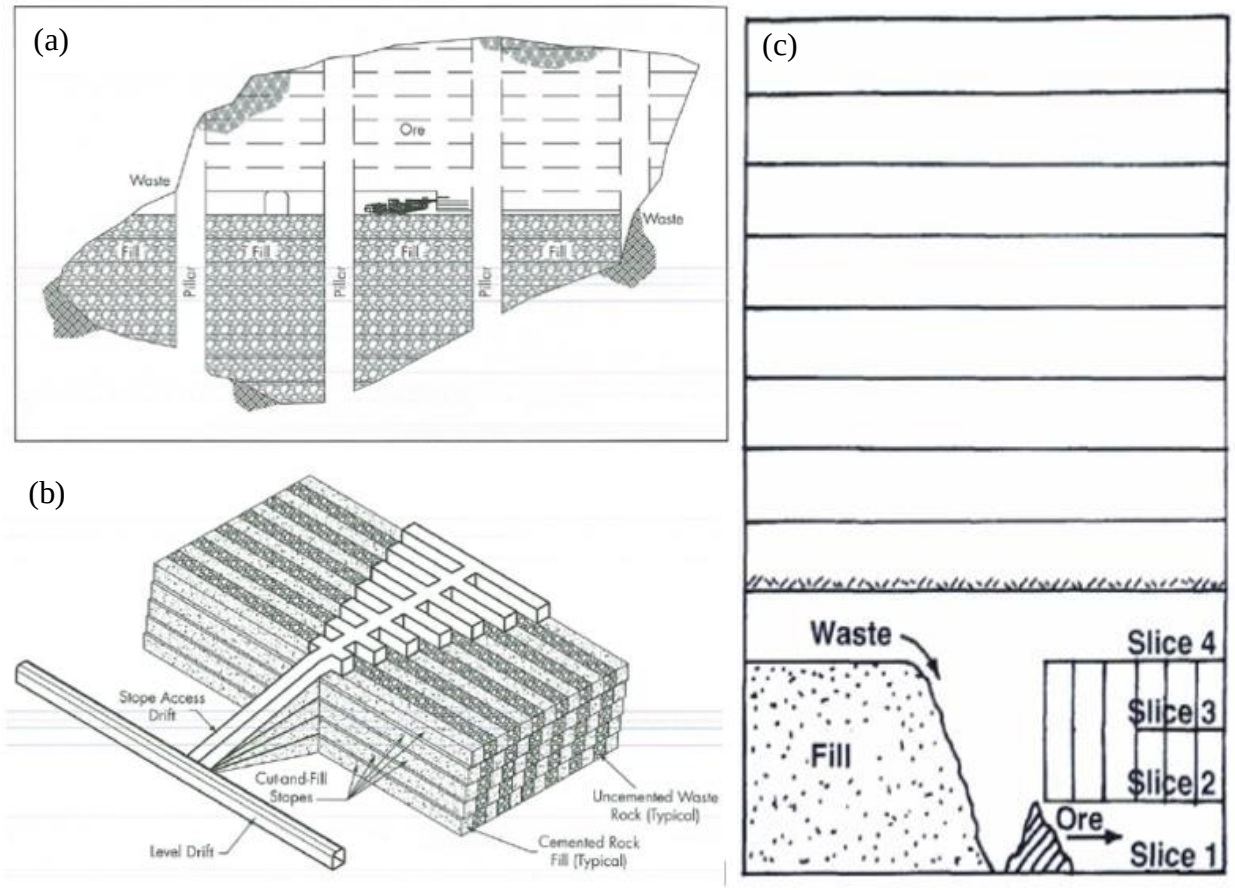

Figure 2-6: Variations of cut-and-fill mining methods (a) post pillar mining (taken from Darling 2011); (b) drift and fill (taken from Darling 2011), and (c) Avoca mining (taken from Hamrin et al. 2001)

Caving mining

In the caving mining method, the ore bodies are caved naturally following undercutting and recovered at the drawpoints. This mining method includes block caving, sublevel caving and longwall caving (Hartman and Britton 1992; Darling 2011).

Fig. 2-7(a) shows the schematic diagram of block caving. In this miming method, a thin horizontal layer at the bottom of the ore columns will be removed by commonly used mining methods. The unsupported overlying ore body can then be caved and falls to the base of stope under gravity and is then extracted at the drawpoints.

Fig. 2-7(b) shows the schematic diagram of sublevel caving. It is suitable for competent ore bodies, which are large and steeply dipping. The sublevel drifts can be excavated from the footwall drift to the hanging wall in the ore bodies. The excavated ore can then be extracted from the drifts.

Fig. 2-7(c) shows the schematic diagram of longwall mining. It is usually used for thin-bedded ore bodies, which have substantial horizontal extent and uniform thickness.

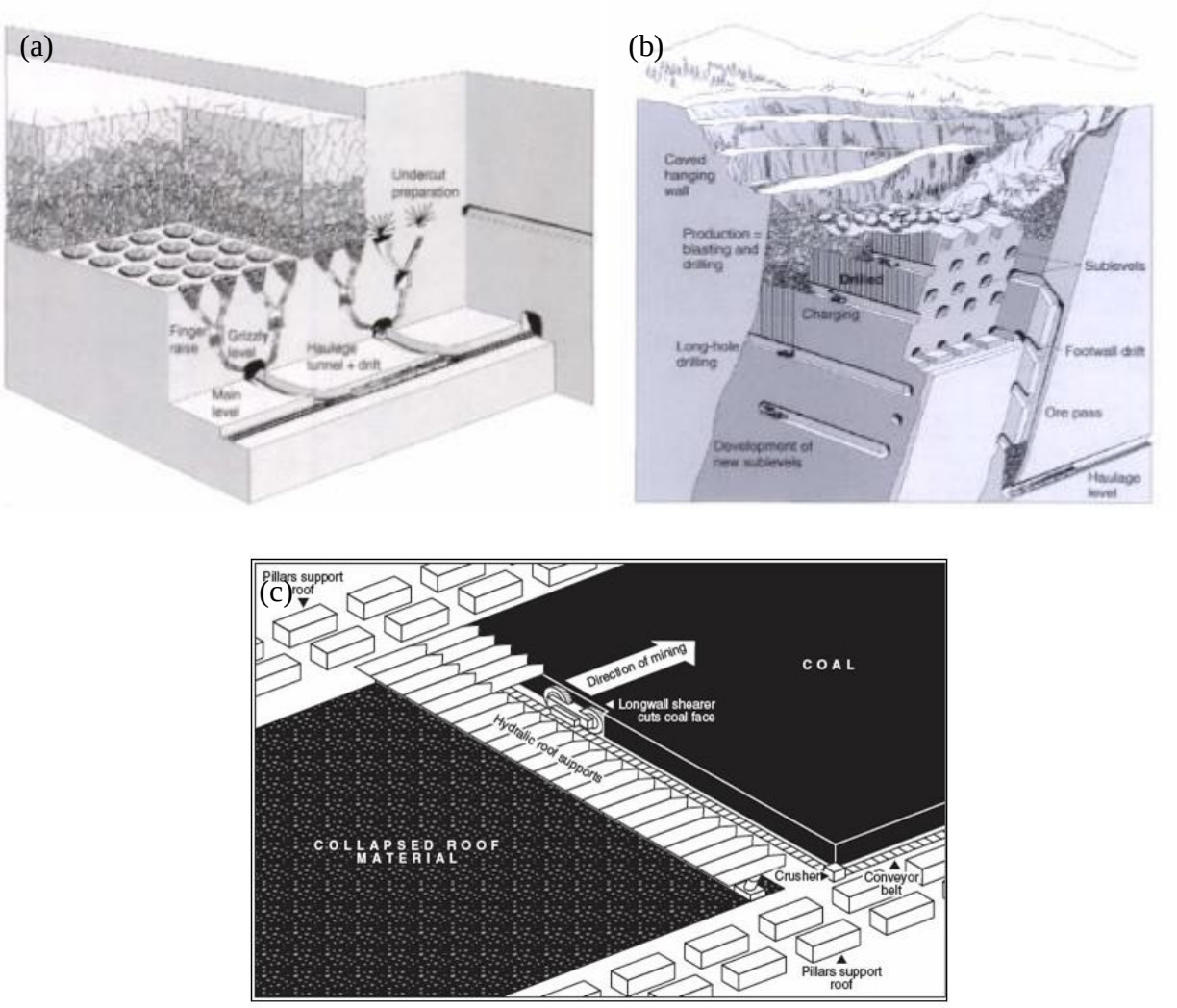

Figure 2-7: Schematic diagram of (a) block caving, (b) sublevel caving and (c) longwall mining (taken from Hamrin et al. 2001)

Backfill cannot be used for block caving and sublevel caving, while it can be used for longwall caving. Examples include the application of backfill in Polish and Chinese coal mines (Palarski 1994, 2014; Zhang et al. 2012, 2016). The backfill is mainly used to improve the rock wall stability and control ground subsidence. It can also act as an artificial hanging wall to support the mine roof

and increase the ore recovery. The commonly used backfill materials include the loosely dumped rock, hydraulic sand fills and densified paste fill with or without cement. When a slurried backfill is used, it is usually transported by pipeline system and deposited in underground stopes under the effect of gravity. Barricades are thus required to retain the slurried backfill in place.

2.1.2 Critical concerns in backfilled stope design

The brief review given above indicates that backfill can be used in several mining methods for different purposes, such as increasing ore recovery in pillars, providing work platforms or spaces for the subsequent mining, improving rock wall and ground stability and/or reducing the ground subsidence. To ensure a successful mining operation, the confining structure (i.e. barricades) and the backfill body upon exposure must be stable. For the first one, a good understanding of the hydro-geotechnical behavior of the backfill, in particularly the evaluation of the PWP and stresses during and shortly after the placement of the backfill in stopes is necessary.

2.2 Tailings and mining backfills

Tailings are the residual material, produced by concentrator mill, after physical and chemical processing and extraction of the valuable minerals from the crushed and ground ore bodies. They have no economic value and need to be disposed properly. For most cases, they are in form of slurry with high water content, typically between 40 to 60% by mass. Traditionally, they are transported by pipes and stocked in an area confined by tailings dams (Vick 1990; Aubertin et al. 2002; Bussière 2007). Tailings can also be used as a fill material, with or without cement, to fill the underground mined-out stopes, resulting in increased ground stability and ore recovery and reduced surface disposal of mine wastes. In the following subsections, a brief review will be given on the surface disposal of tailings as well as the three types of the most commonly used backfill.

2.2.1 Tailings

Tailings properties

Fig. 2-8 shows the grain size distribution curves of nine Canadian hard rock tailings (Bussière 2007). The particle size of 10% passing D_{10} varies from 0.001 to 0.004 mm while the particle size of 60% passing D_{60} is between 0.01 and 0.05 mm. The hard rock tailings can be classified as sandy

silts of low plasticity (ML) with the liquid limit (w_L) less than 40% and plastic limit (w_P) in the range of 0% to 15% (Barbour et al. 1993; Aubertin et al. 1996, 1999; Bussière 2007).

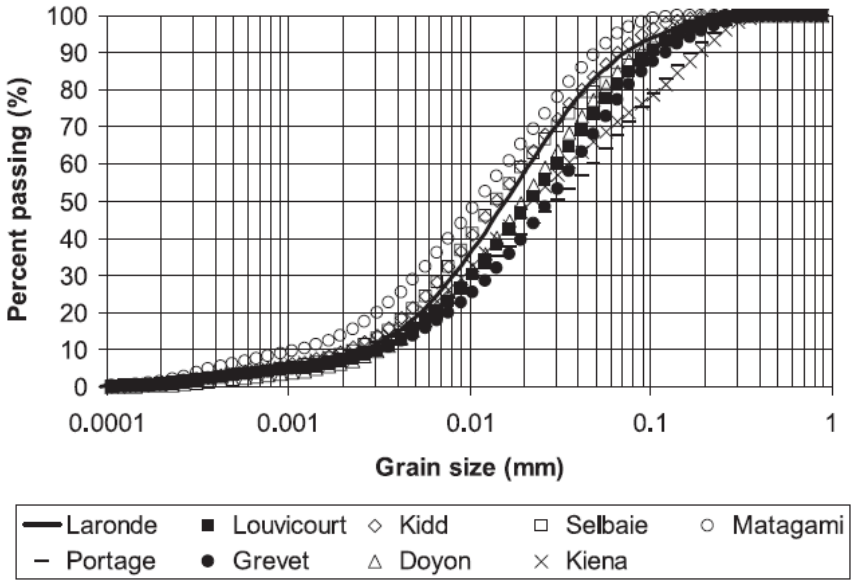

Figure 2-8: Grain size distribution curves of nine Canadian hard rock tailings (taken from Bussière 2007)

As the tailings contain a large portion of fine particles, the hydraulic conductivity k and consolidation coefficient c_v can be very low. Laboratory tests with remolded (homogenized) hard rock tailings samples have shown that the value of k_{sat} is between 10^{-6} and 10^{-4} cm/s for fine grained tailings and between 10^{-4} and 10^{-2} cm/s for coarse grained tailings. With undistributed tailings samples, the value of k_{sat} is measured to be between 10^{-7} and 10^{-4} cm/s. For remolded and undisturbed samples, the value of c_v is between 10^{-1} and 10^{2} cm^2/s for coarse tailings and 10^{-3} and 10^{-1} cm^2/s for fine tailings (Bussière 2007).

Tailings dams and deposition of tailings

A tailings dam is a retaining structure to retain the tailings and mine water. Tailings dams can be divided into two types. The first, called retention dam, is constructed to the full height before any deposition, method used in the construction of conventional water storage dam (EPA 1994). The second, called raised embankment dam, is progressively built with an increasing height due to the continuous addition of tailings (Priscu 1999). The raised embankment dams can be constructed in three ways: upstream, downstream and centerline (Vick 1990).

Fig. 2-9(a) shows the construction of an embankment with the upstream method. A free draining starter dyke is first constructed. The settled coarse particles near the discharge point can be used as foundation for the subsequent embankment construction (Vick 1990). This design method can thus reduce the construction cost as it requires less construction materials. However, the deposited tailings have the potential to liquefy and lose shear strength due to the dynamic loading induced by the earthquake or static loading induced by the excessive rising rate of the embankment (Jakubick et al. 2003; McLeod and Bjelkevik 2017). In order to prevent the accumulation of high excess pore water pressure and development of low shear strength in the deposited tailings, the rising rate of the upstream embankments should be also limited.

Fig. 2-9(b) shows the downstream tailings dam, which is first constructed with an impervious starter dyke with an impervious core and drainage zone on the upstream slope. The tailings are then deposited, and the new embankments are built on top of the downstream slope of the previously built dyke. Compared to upstream method, downstream method needs to use more construction materials, which can increase the construction costs. However, it is more stable than upstream method when subjected to earthquakes (ICOLD 2001). The downstream dams can be theoretically built with unlimited height, which requires large volume of fill materials and high cost. This will however be limited by the space around the tailings dams due to the outward movement of the dam toe (Vick 1990).

Figure 2-9(c) shows the centerline tailings dams, which is constructed progressively along the centerline of the starter dam. This design method is a combination of the upstream and downstream designs (Benckert and Eurenius 2001). It requires less building materials than the downstream method and is more stable than the upstream method in the event of an earthquake.

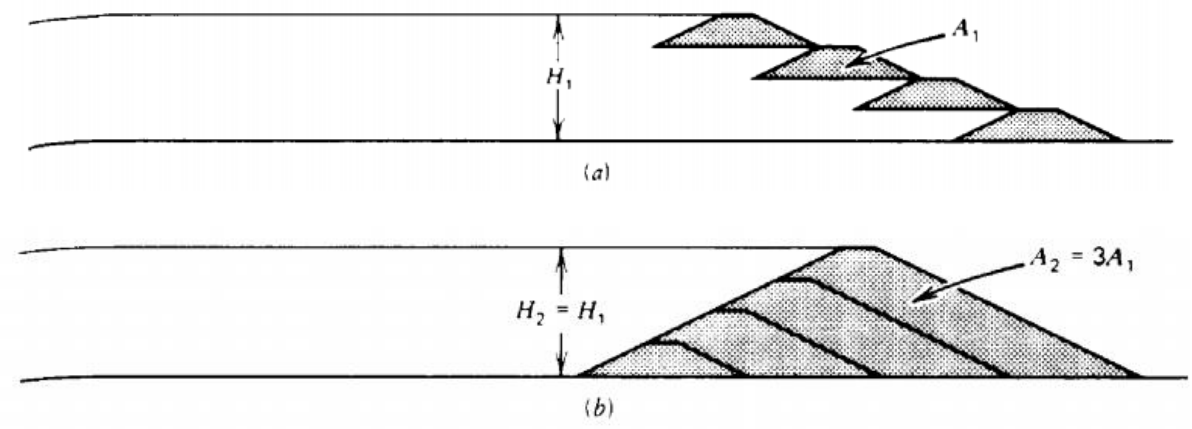

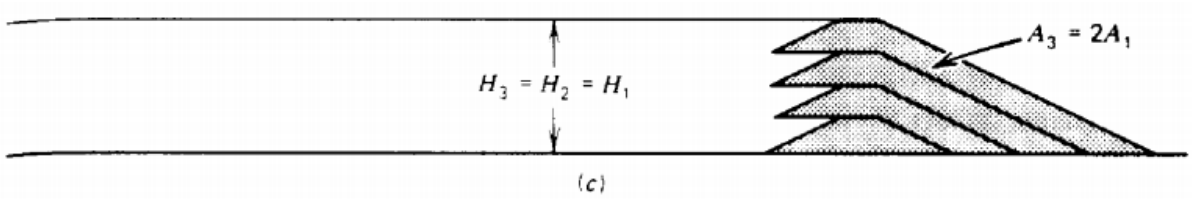

Figure 2-9: Three types of tailings dams constructed with: (a) upstream method, (b) downstream method and (c) centerline method (taken from Vick 1990)

Tailings are usually transported by centrifugal pumps and pipelines system and then confined by tailings dams, as shown in Fig. 2-10. Due to the low permeability, excess PWP will generate in the tailings during and after the deposition, which requires a long time to be dissipated. The high excess PWP of tailings is accompanied with the low shear strength, which pose a great challenge for the safety of tailings dams. This is particularly true for tailings dams constructed with upstream raised method. The failure of tailings dams can lead to severe consequences, such as release of large volume of tailings, environmental pollution, infrastructure damage and even loss of lives. In order to assess the stability of tailings dams or to establish a water balance sheet, a good understanding of the excess PWP associated with the self-weight consolidation during and after the accreting deposition is required.

Figure 2-10: Accreting deposition of slurried tailings through pipeline system and confined in tailings dams (photo taken by Li 2014 in a Québec mine)

2.2.2 Mining backfills

In practice, several types of backfill exist. But the most commonly used backfills are rock fill (RF), hydraulic fill (HF) and paste backfill (PF). A rock fill is mainly made of coarse waste rocks with or without cement. For the definition of hydraulic and paste backfills, there are some slight differences between different researchers.

According to Grice et al. (1993), the maximum particles size of HF should be less than 1 mm and the HF should contain less than 10% by weight of fine particles smaller than 10 μm. Hassani and Archibald (1998) do not have any specification on the maximum particle size of HF. They just defined that a HF should contain less than 20% by weight of fine particles smaller than 10 μm. According to Potvin et al. (2005), a HF should contain no more than 10% by weight of fine particles finer than 10 μm.

Regarding the definition of PF for underground mine backfilling, Potvin et al. (2005) specify that a PF should contain at least 15% of fine particles smaller than 20 μm while Aref et al. (1992) stated that a PF should contain 15% by weight of fine particles smaller than 45 μm. As shown in Fig. 2-8, the tailings of hard rock mines in Québec meet these criteria.

Fig. 2-11 shows typical grain size distribution curves of some paste fill, hydraulic fill and cemented hydraulic fill used in several Australian mines. It can be seen that the paste backfill contains nearly 70% of particles smaller than 75 μm and 20% of particles smaller than 10 μm. It is much finer than the hydraulic fill, which contains much less fine particles smaller than 10 μm.

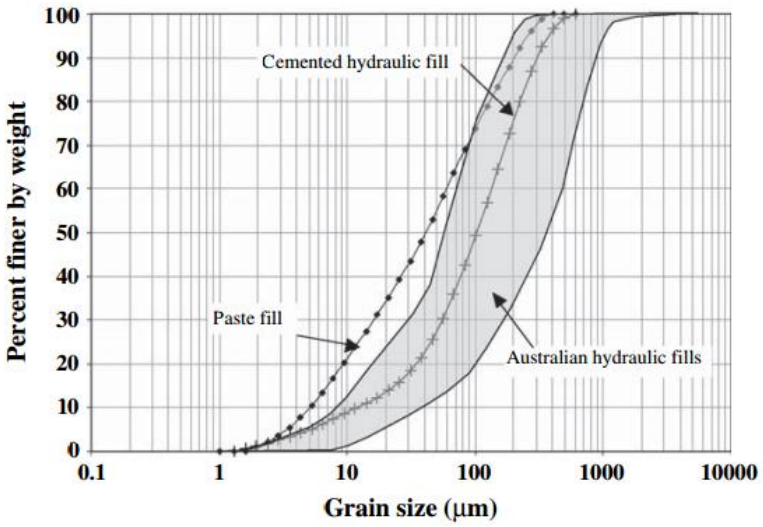

Figure 2-11: Grain size distribution curves of paste fill, hydraulic fill and cemented hydraulic fill used in Australian mines (taken from Sivakugan et al. 2006)

Hydraulic fill

Hydraulic fill (HF) has been first used in some coal mines in US in 1884 (Peele 1941). It still remains one of the most commonly used fill type around the world. HF is a type of high-density

slurry with 40% to 50% solid by volume and more than 70% solid by weight. It is usually produced by tailings dewatering and desliming processes, which can be conducted through the hydrocyclone technology to remove the fine particles. Another source to produce hydraulic fill is natural sand deposits.

Physical properties of hydraulic fill

Fig. 2-12 presents particle size distribution curves of 24 reconstituted hydraulic fills used in Australian mines (Rankine et al. 2006). It can be seen that the HF contains a large portion of sand, small portion of silt and very small portion of clay.

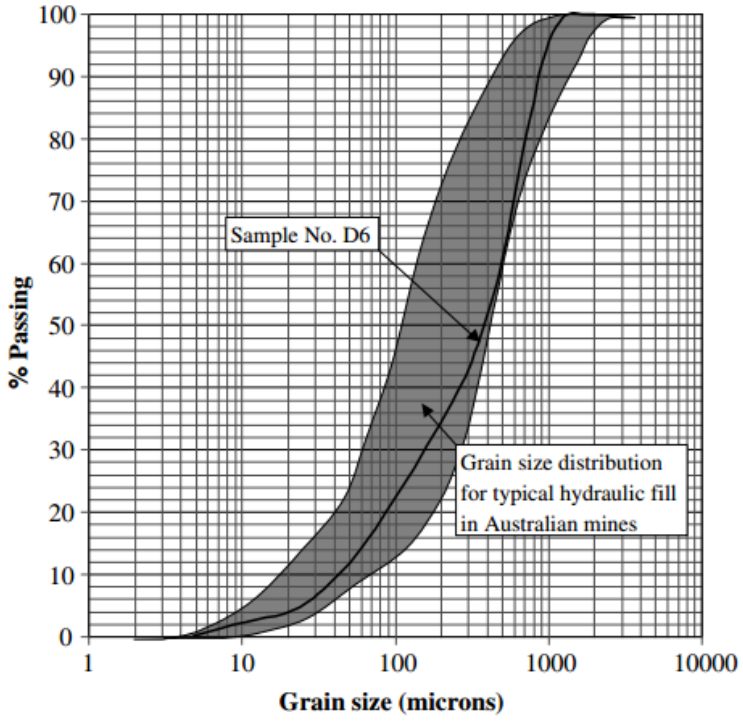

Figure 2-12: Typical grain size distribution curves of the hydraulic fills used in Australian mines (taken from Rankine et al. 2006)

Rankine et al. (2006) summarized the geotechnical properties of the HF used in Australian mines. Their results show that specific gravity G_s is typically in the range of 2.8 to 4.5 while the void ratio e is in the range of 0.58 and 0.96.

Hydraulic properties of hydraulic fill

The hydraulic conductivity can be measured by constant head infiltration tests for relatively high permeability backfill or by falling head infiltration tests for relatively low permeability backfill (Rankine 2005). The value of hydraulic conductivity *k* can also be estimated from the grain size distribution curve by using the Kozeny-Carman equation or modified Kozeny-Carman equation (Aubertin et al. 1996; Mbonimpa et al. 2002; Chapuis and Aubertin 2003).

Rankine et al. (2006) measured that the hydraulic conductivity *k* of Australian hydraulic fills is typically in the range of 1.7×10^{-7} to 1.1×10^{-5} m/s. These values are smaller than those typically in the range of 10^{-6} to 10^{-5} m/s obtained with in situ hydraulic fill (Grice 2001).

HF is usually transported by boreholes and pipelines to the underground mine stopes. In order to facilitate the transportation, HF is usually mixed with a large amount of water to increase the flowability. A barricade is required to be built at the access drift to retain the slurried backfill in place before the filling operation. Decanted water ponds are usually observed on top of the backfill (Potvin et al. 2005; Sivakugan et al. 2006; Yang et al. 2017). This water can lead to high hydrostatic pressure on the barricade. In case of barricade failure, the water becomes the source of inundation.

In order to accelerate the drainage and reduce the pressure on barricade, high permeability materials, such as porous brick or waste rocks (with the value of *k* in the range of 2×10^{-4} to 10^{-3} cm/s) are preferred to be used for the construction of the barricades.

Mechanical properties of hydraulic fill

Hydraulic fill can be used with or without binder. The addition of binder can significantly influence its mechanical properties, especially on the shear strength (cohesion) and stiffness.

Fig. 2-13 shows the variation of the uniaxial compressive strength as a function of the cement content by volume (Hambley 2011). It can be seen that the uniaxial compressive strength of cemented hydraulic fill increases as the cement content volume increases. The uniaxial compressive strength can also be influenced by other factors, such as segregation, arching effect, etc. (Potvin et al. 2005).

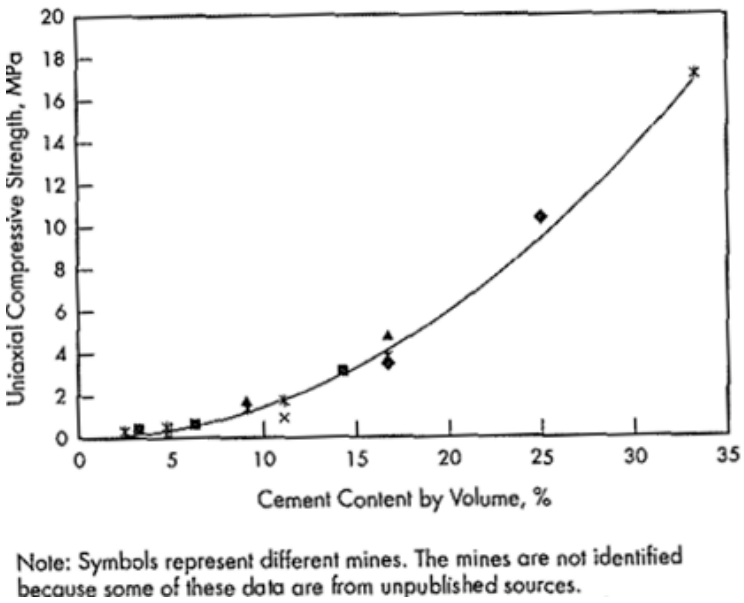

Figure 2-13: Variation of uniaxial compressive strength of CHF as a function of cement content by volume (taken from Hambley 2011)

Paste fill

Paste backfill has been initially used in Germany in the 1980s and then widely accepted as a common practice around the world. Paste backfill is usually transported by borehole or pipeline system through gravity flow. In order to avoid excessively high pressure on barricade, the mine stope is usually filled in two stages: plug pour and final pour. The former is usually 7 to 9 meters high, 2 to 3 meters higher than the access drift. In many cases, it has a cement content of 6 to 8% while the final pour usually has a lower cement content. The interval period between these two stages is varied between 24 hours or several days to allow the occurrence of consolidation and cement hydration. The interruption of backfill between the two stages may result in blockage of the pipeline and slowing down of the production.

Physical properties of CPB

According to the strict definition, a paste backfill should contain enough portion of fine particles, exempt of segregation and no bleeding of any water upon deposition. In order to satisfy this condition, paste backfill usually has high solid content, ranging from 75% to 85% (solids by weight). Li and Zheng (2007) have revised this definition and concluded that a paste backfill meeting these criteria would be unsaturated and difficult to transport. For large and wide stopes,

the application of such paste backfill could be problematic to ensure horizontal top surface or tight contact between the backfill and stope roof. In practice, saturated or at least slightly over saturated paste backfill has to be used unless superplasticizer is used to improve the flowability of the backfill.

Rheological properties of CPB

Paste backfill is a non-Newtonian fluid with varied viscosity under shear stress. A sufficient shear stress should be applied to initiate the flow (Boger 2002; Potvin et al. 2005; Cooke 2006). This minimum required shear stress to initiate the flow of the backfill is called yield stress. If the applied shear stress is smaller than the yield stress, the paste backfill will have an elastic behavior with a reversible deformation. When the applied shear stress is higher than the yield stress, the paste backfill can flow like a viscous material.

The yield stress of paste backfill is an important parameter for the design of transportation system and estimation of the pumping energy (Sofra and Boger 2001). It is primarily a function of the water content (or solid content) of the backfill. The yield stress can also be influenced by the hydration state, binder type and pore fluid chemistry (Sofra and Boger 2001; Simon and Grabinsky 2013). It can be measured by vane method or rheometer (Dzuy and Boger 1985; Gawu and Fourie 2004). To do vane tests, the vane spindle is immersed into the material and then slowly rotated at a constant speed. The torque value required to maintain the constant rotation speed is recorded. The maximum torque is then used to calculate the yield stress (Dzuy and Boger 1985). The rheometric tests can be conducted with a commercial rheometer through the measurement of the shear rate and required shear stress. The yield stress corresponds to the required shear stress at zero shear rate (Nehdi and Rahman 2004; Mahaut et al. 2008). An alternative method is to conduct slump tests to obtain an estimation of the yield stress. The test consists of filling a cylinder with the tested material. After removal of the cylinder, the difference between the initial and final heights of the tested sample is measured and called slump height (Pashias et al. 1996). The yield stress can then be estimated based on the empirical relationships between the slump height and yield stress (Pashias et al. 1996; Clayton et al. 2003; Boger et al. 2006).

In practice, the slump height of paste backfill should be less than 230 mm to ensure high flowability. The value of yield stress is generally in the range of 100 to 800 Pa (Potvin et al. 2005;

Boger et al. 2006; Niroshan et al. 2017). However, a value as high as 1100 Pa has been reported in the literature for paste backfill (Saebimoghaddam 2005; Simon and Grabinsky 2013).

Hydraulic properties of CPB

As paste backfill contains a large portion of fine particles, its hydraulic conductivity is usually small, typically much smaller than that of hydraulic fill. The hydraulic conductivity before any cementation is generally in the range of 10^{-8}~10^{-6} m/s (Aubertin et al. 1996; Bussière 2007; Fall et al. 2009).

Fig. 2-14 shows the evolution of the hydraulic conductivity with the curing time for paste backfill with different types and contents of cement (CPSG: prepared with ordinary Portland cement and slag at a ratio of 20/80; CPFA: prepared with ordinary cement and fly ash at a ratio of 70/30). One can see that the permeability decreases with the curing time for the two types of binder. For a given time and binder type, a higher binder content leads to a greater reduction of the permeability.

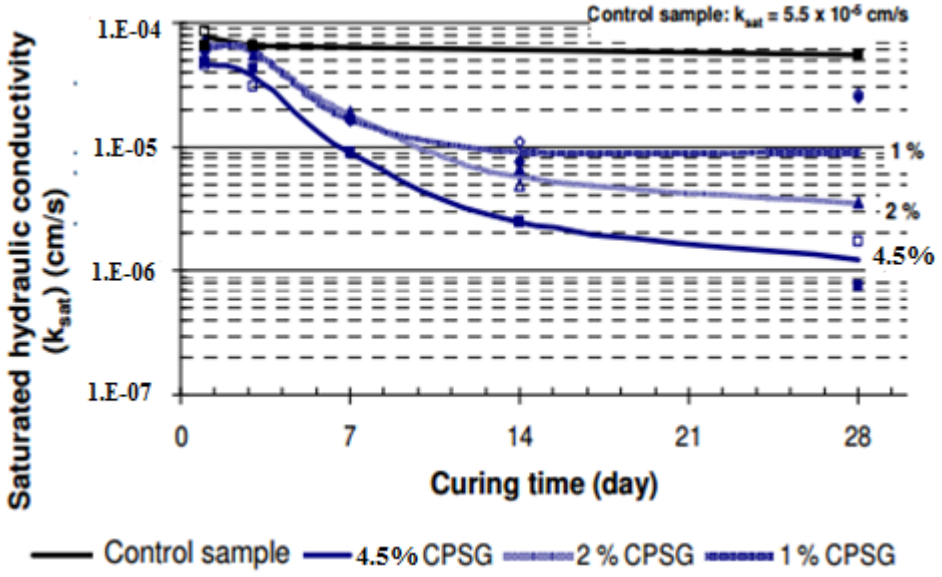

(a)

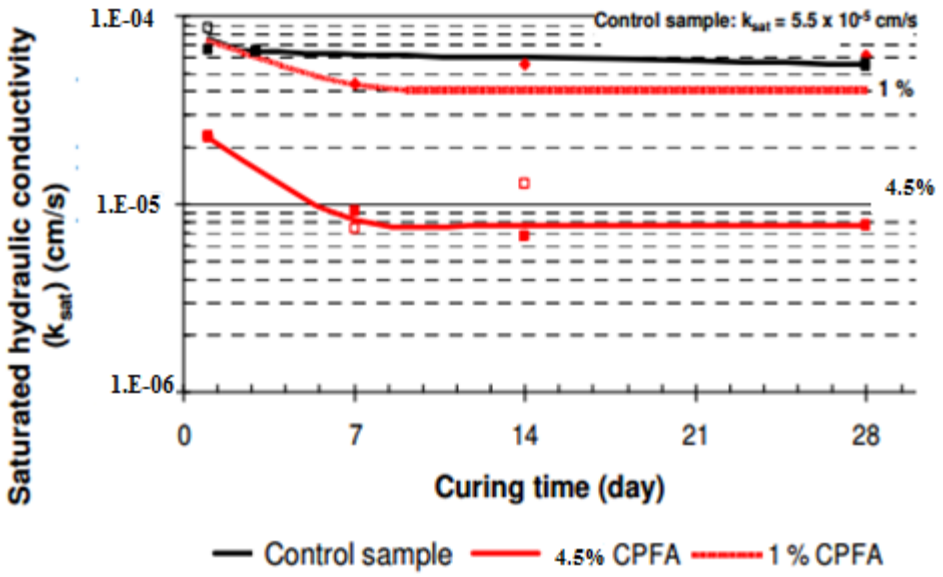

(b)

Figure 2-14: Evolution of saturated hydraulic conductivity with curing time for: (a) CPSG, and (b) CPFA, under different binder content (taken from Godbout et al. 2007)

Mechanics properties of CPB

Fig. 2-15 shows the evolution of shear modulus *G* of a paste backfill with the curing time (Abdelaal 2011). The stiffness of backfill increases with the curing time due to the generation of C-S-H bonds during the cement hydration.

Fig. 2-16 shows the evolution of the uniaxial compressive strength q_u of CPB with curing time by using different types and contents of binder, including PC (mixture of half Ordinary Portland cement and half type V Portland cement) and FP (mixture of half Ordinary Portland cement and half fly ash). The results show that the compressive strength for both PC and FP increases with the curing time from 14 to 28 days. After that, the compressive strength keeps almost constant for backfill using binder PC while shows a slightly increase for backfill using binder FP. For a given binder type, the compressive strength of the backfill increases with an increase in binder content.

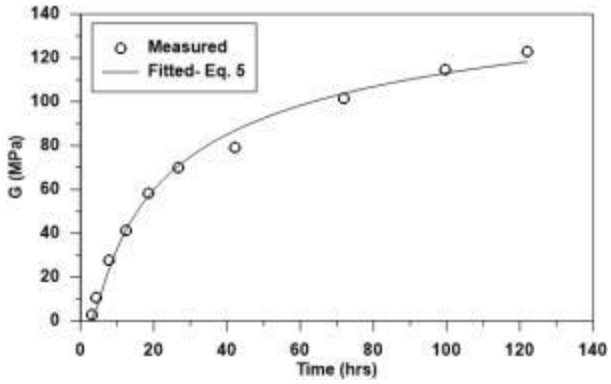

Figure 2-15: Evolution of the shear modulus of cemented paste backfill with curing time (taken from Abdelaal 2011)

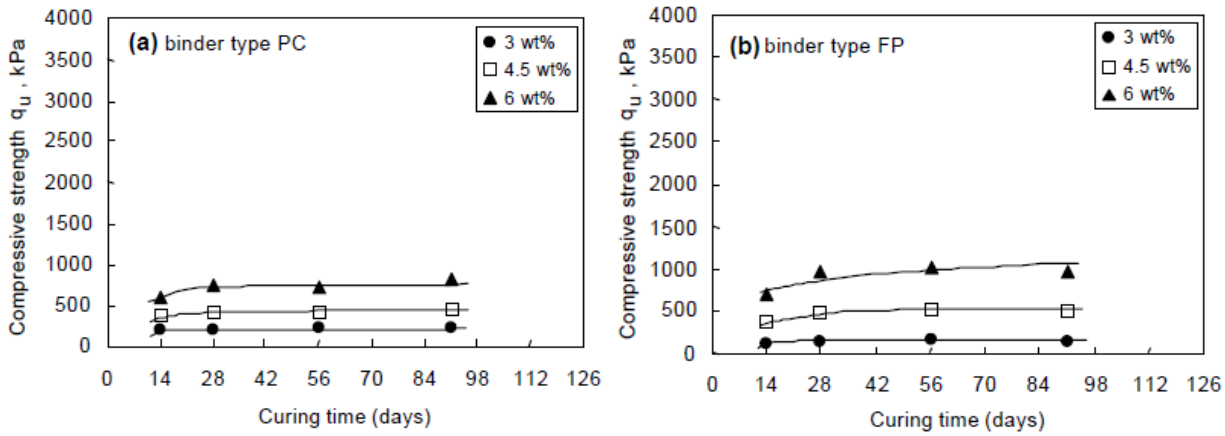

Figure 2-16: Evolution of the compressive strength q_u with curing time for paste backfill with different types of binder: (a) PC, (b) FP (taken from Belem et al. 2000)

Fig. 2-17 shows the effect of curing temperature on the unconfined compressive strength (UCS) development in CPB with different binder type (Portland cement and Portland cement/blast furnace slag (50/50)). The CPB specimens were tested under different curing periods (7, 28, 90, 150, 160 days) and temperatures (2ºC, 20ºC, 35ºC and 50ºC). One can see that the UCS increases as the curing temperature increases.

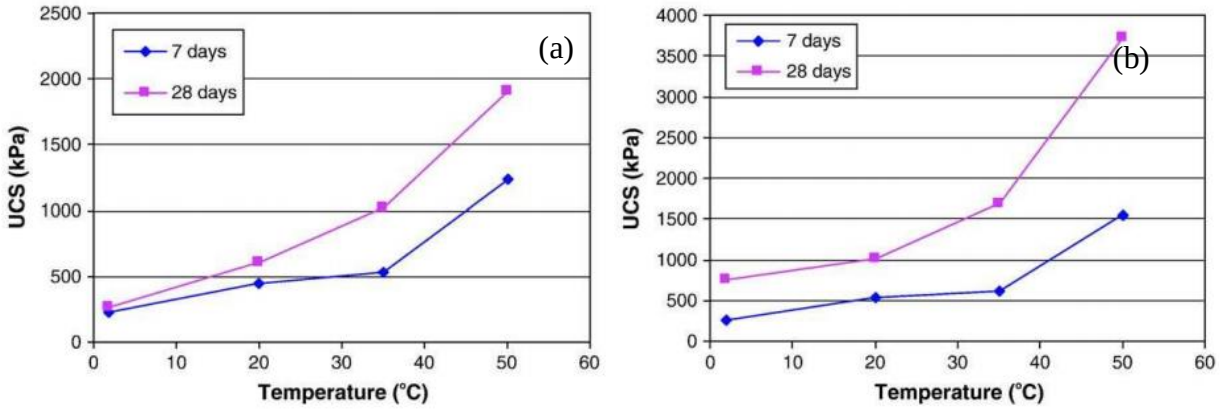

Figure 2-17: Effect of curing temperature on the UCS development of cemented paste backfill made of (a) Portland cement and (b) Portland cement/blast furnace Slag (50/50) (taken from Fall et al. 2010)

Rock fill

Rock fill (RF) is usually made of waste rocks generated in underground mines. The other sources of rock fill include quarry, smelter slag generated from furnace, rocky residue produced from leaching of metal heap, etc. (Potvin et al. 2005).

The uncemented RF and waste rock piles are made of similar materials with similar particle size distribution. Their hydraulic conductivity can be considered to be close to each other. Lessard (2011) reported that the hydraulic conductivity of the waste rock piles at Tio mine is in the range of 4×10^{-5} to 3×10^{-3} m/s measured by the infiltration tests. Peregoedova (2012) conducted column tests and reported that the hydraulic conductivity of waste rock is around 10^{-3} m/s. Aubertin (2013) reported that the hydraulic conductivity of waste rocks is usually higher than 10^{-5} m/s. The internal friction angle of (uncemented) rock fill is in the range of 35° to 55° (Potvin et al. 2005).

Rock fill can be filled in the underground mine stope alone or with the addition of cement. The uncemented rock fill can be applied if the filled stope will not be exposed for further excavation. In this case, the rock fill is mainly used to prevent wall slough and improve ground stability. If the filled mass is required to gain strength to maintain stability after adjacent excavation, it will be mixed with different types of binder materials, such as cement, slag and fly ash.

2.3 Pressure and stresses estimation in backfilled stopes and on barricades

2.3.1 Pressure and stresses during and shortly after the slurry deposition – Backfill in undrained or quasi undrained conditions

When a slurried material is deposited in a confining structure, which can be a tailings impoundment or an underground mine stope, it is important to have a good evaluation of the excess PWP. This requires a good understanding of the evolution of the excess PWP associated with the self-weight consolidation in the slurried materials during and after the deposition. Similar case is the deposition and confinement of dredged sludge excavated from the river or seabed.

When a slurried material is continuously deposited in a confining structure, the downward movement of the particles under the effect of gravity renders the backfill denser. The pore water tends to be expelled out of the slurried material. As the tailings or dredged sludge usually contain a high portion of fine particles and have low permeability, the outflow of pore water will be limited, resulting in the generation of excess PWP. The particles will approach each other during the drainage and dissipation of excess PWP. The dissipation of excess PWP before any contacts between the particles is called sedimentation. As drainage takes place furthermore, the solid particles start to contact each other. Effective stresses are generated. The process of the dissipation of excess PWP is called self-weight consolidation. The evaluation of excess PWP in slurried material is closely related to the stability of confining structures (dams or barricades) as well as water and fill volume management. When the slurried material has a very low permeability or/and the filling rate is very low, the consolidation can be very slow, resulting in high excess PWP and low effective stress. The stability of dams or barricades can become problematic. The failure of tailings dams or barricades can lead to severe consequences (Revell and Sainsbury 2007; Agurto-Detzel et al. 2016). It is thus very important to properly design these confining structures through a good understanding of the drainage and consolidation, especially during and shortly after the deposition of the slurried materials. A model proposed by Gibson (1958) can become useful to evaluate the excess PWP in slurried materials during and after the slurry deposition. The equations of Gibson (1958) model considering the evolution of the excess PWP during slurry deposition were used to evaluate the excess PWP in backfilled stopes and called analytical solution (Fahey et al. 2010; Doherty 2015; Shahsavari and Grabinsky 2014, 2015). However, these equations contain an integral that cannot be solved by hand calculations or commonly available calculation tools. Thus,

the equations of Gibson (1958) was not analytical solution. Gibson (1958) has also considered the evolution of the excess PWP after the slurry deposition. The proposed equation contains a mistake and cannot be directly used to evaluate the excess PWP. More development based on the Gibson (1958) model has been presented in Chapters 3 to 6.

Analytical model to evaluate the consolidation during and after the slurry deposition

During the slurry deposition, the consolidation of the slurry takes place under the effect of its own gravity and the load increments exerted by the subsequent layers of deposition. This is different from the traditional consolidation theory of Terzaghi (1943), in which the consolidation occurs due to the external load. Another aspect different from the traditional consolidation theory of Terzaghi (1943) is the moving top boundary. Thus, the consolidation theory of Terzaghi (1943) cannot be directly used to evaluate the consolidation of accreting slurry deposition.

Gibson (1958) is probably the first, who proposed a model to evaluate the consolidation of slurried material with an increasing thickness. Fig. 2-18 shows the Gibson's model with a slurried material deposited on a pervious/impervious base with a filling rate of m (m/h). On the figure, h (m) is the current height ($h = m \times t$, t (h) is the filling time); H (m) is the final height at the end of deposition; z (m) is the elevation of the calculation point.

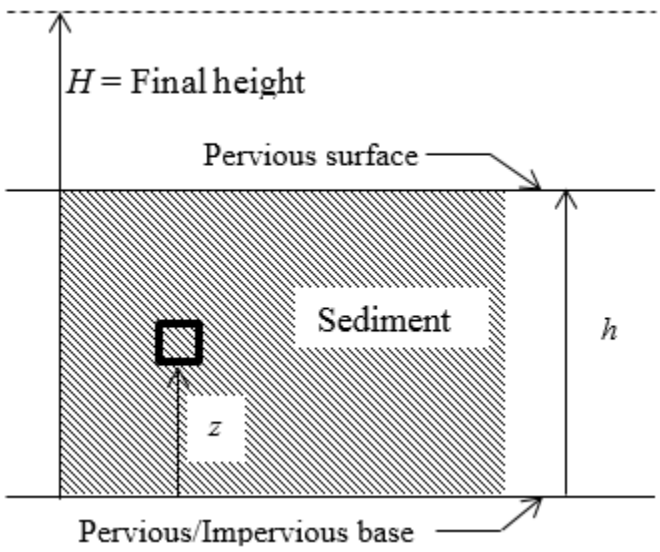

Figure 2-18: Accreting deposition of slurried material on a pervious/impervious base (taken from Gibson 1958)

By using the same assumptions as the Terzaghi (1943) theory, including the small strain consolidation with a constant consolidation coefficient, Gibson (1958) proposed the following governing equation for the case of impermeable base:

$$c_v \frac{\partial^2 u}{\partial z^2} = \frac{\partial u}{\partial t} - \gamma' \frac{dh}{dt} \tag{2-1}$$

where c_v (m^2/h) is the consolidation coefficient; u (kPa) is the excess PWP; γ' (kN/m^3) is the submerged unit weight of the slurry.

Considering the boundary conditions: $u = 0$ at $z = h$ and $du/dz = 0$ at $z = 0$, Eq. (2-1) can be solved as follows for the case of impervious base:

$$u = \gamma' mt - \gamma' (\pi c_v t)^{-\frac{1}{2}} \exp\left(\frac{-z^2}{4c_v t}\right) \int_0^\infty \xi \tanh\left(\frac{m\xi}{2c_v}\right) \cosh\left(\frac{z\xi}{2c_v t}\right) \exp\left(-\frac{\xi^2}{4c_v t}\right) d\xi \tag{2-2}$$

where ξ is an arbitrary integration parameter, ranging from 0 to ∞.

Gibson (1958) also gave the (excess) PWP during the accreting deposition for the case of pervious base as follows:

$$p_w = -\gamma z\left(1 + \frac{mz}{2c_v}\right) + \frac{\gamma m}{2c_v} (\pi c_v t)^{-\frac{1}{2}} \exp\left(-\frac{z^2}{4c_v t}\right) \int_0^\infty \xi^2 \coth\left(\frac{m\xi}{2c_v}\right) \sinh\left(\frac{z\xi}{2c_v t}\right) \exp\left(-\frac{\xi^2}{4c_v t}\right) d\xi \tag{2-3}$$

It should be noted that the excess PWP is defined as the excess of the current total PWP (in the transient state) over the final PWP (in the steady state). For the case of impervious base, the final PWP is equal to the hydrostatic pressure when the water reaches the final steady-state. The excess PWP is thus equal to the difference between the current total PWP and the hydrostatic pressure. This corresponds to the excess PWP definition in the Terzaghi's consolidation theory. For the case of pervious base, the water table will lower down to the base level in the final steady state. By neglecting the suction in the unsaturated region, the final PWP in the final steady state is equal to zero along the full height of the sediment. The excess PWP is thus always equal to the current total PWP. No distinction is needed between the current total PWP and the excess PWP.

Eqs. (2-2) and (2-3) were usually called analytical solutions. They have been used to evaluate the excess PWP in backfilled stopes (Fahey et al. 2010; Shahsavari and Grabinsky 2014; 2015; Walske and Doherty 2017). However, the two solutions contain an integral, which is impossible to be

solved by hand calculations. They are thus not analytical solution. Truly analytical solutions of Gibson (1958) model have been presented in Chapter 3 for the case of pervious base and Chapter 4 for the case of impervious bases.

When the deposition ceases at time t_0, the consolidation will continuously occur as the remained excess PWP in the slurry needs to be dissipated. By using the Terzaghi (1943) consolidation theory, Gibson (1958) proposed the following governing equation to evaluate the consolidation after the end of deposition:

$$c_v \frac{\partial^2 u_1}{\partial z^2} = \frac{\partial u_1}{\partial t_1} \tag{2-4}$$

where t_1 is the time start from the moment when the deposition ceases ($t_1 = t - t_0$).

Eq. (2-4) is in the form of differential equation. It cannot be used to evaluate the excess PWP in the slurried material after the end of deposition. Zheng et al. (2018c, 2018d) have solved the governing equation and proposed solutions for evaluating the (excess) PWP in slurried materials after the end of deposition. The corresponding solutions have been presented in Chapter 5 for the case of impervious base and Chapter 6 for the case of pervious base.

It should be noted that Eqs. (2-1) and (2-4) were developed based on the small strain consolidation theory with constant hydro-geotechnical properties (e.g. permeability, constrained modulus and consolidation coefficient). As slurried materials usually have high water content and high compressibility, the consolidation associated with the dissipation of excess PWP leads to the decrease of the hydraulic conductivity k and increase of the constrained modulus M'. The value of c_v ($= kM'/\gamma_w$) is thus rarely constant (usually increases with ongoing consolidation; Essayad 2015).

In order to investigate the applicability of the Gibson (1958) model, Fahey et al. (2010) compared the Gibson (1958) solution results with the numerical results obtained by MinTaCo code using constant and varied c_v. The constant c_v was obtained by using a combined varied manner of permeability and compression. They reported that the Gibson solution can be used with reasonable accuracy for backfill with a constant value of c_v. However, for a backfill with increased c_v during the consolidation, the Gibson model tends to underestimate the degree of consolidation. The degree of the underestimation increases as c_v increases during the filling operation.

It should also be noted that the Gibson (1958) model and ensuing solutions were developed based on the small strain consolidation theory. The variation of the backfill hydro-geotechnical properties and settlement during the consolidation were not considered. In addition, for slurried materials deposited on an impervious or pervious base, decanted water pond and unsaturated zone can develop at the top of the deposition. A new model is thus required to take into account these limitations.

Laboratory tests for the consolidation of slurried materials

Been and Sills (1981) carried out a series of column settling tests to investigate the self-weight consolidation of a soft clay. Their results showed that there is a suspension in the upper part of the column, in which the pore water pressure is equal to the total pressure and there is no effective stress. It was also observed that the density in the suspension is almost uniformly distributed. The clay behaved as a heavy liquid in this suspension. This process is known as sedimentation. Below the suspension, the pore water pressure in the sediment becomes smaller than the total pressure due to the dissipation of excess PWP. The effective stress started to generate, resulting in the formation of real soil. This process is known as consolidation.

Been and Sills (1981) also reported that the height of the sediment continuously decreased during the settling time. The sediment-water interface went down during the settlement of the soil particles. The excess PWP dissipated progressively after the deposition of the clay. They also measured the void ratio at the surface of the sediment during the settling. Their results showed that the void ratio near the sediment surface decreased with settling time while the effective stress remained negligible.

Lin (1983) conducted column tests to investigate the settling and consolidation behaviors of dredged slurry. The concentration was uniform along the height of the slurry when the slurry was initially filled in the column ($t = 0$). After the settling commenced, the slurry particles settled down under the effect of gravity, resulting in the decrease of slurry concentration in the upper part and increase in the lower part. Lin (1983) also observed that the supernatant water on the upper part of the slurry remained turbid in the initial stage of settling. They attributed it to the suspended fine particles and upward movement from the lower part. As the upward flow slowed down, the turbid supernatant water turned into clean; the water-soil interface formed at this moment and the below settled slurry behaved as real soil.

Pedroni and Aubertin (2008) carried out consolidation tests to study the consolidation of high water content of sludge under the effect of hydraulic gradient instead of external load. Their results showed that the water content in the sludge decreased during the consolidation. The sludge at the bottom of the column decreased more rapidly in the initial stage of consolidation. They also observed that the excess pore water pressures progressively dissipated during the consolidation. The void ratio and effective stress were calculated for each layer by using the measured water contents and pore water pressures. While the hydraulic conductivity was calculated for each layer by using the hydraulic gradient between the sensors. Fig. 2-19 shows the relationship of void ratio-effective stress and permeability-void ratio of the sludge. Two simple relationships, as shown in Fig. 2-19, were also proposed based on the experimental data shown in the figure.

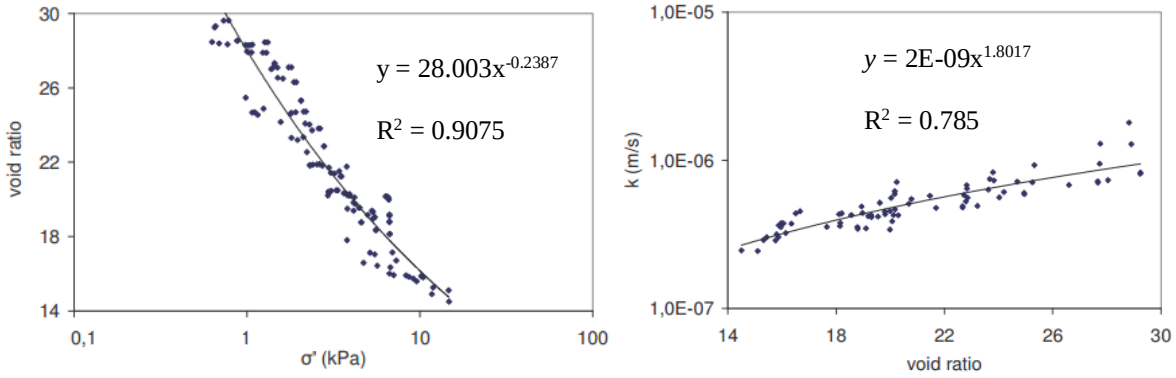

Figure 2-19: (a) void ratio-effective stress and (b) permeability-void ratio relationship based on the test results (taken from Pedroni and Aubertin 2008)

Li et al. (2013) carried out column tests to study the self-weight consolidation behavior of slurried clay. This test apparatus provided a simple way to visualize the generation and dissipation of the excess PWP during the consolidation, which was indicated as H_e in Fig. 2-20. With the measured variation of the sludge thickness and excess PWP during the consolidation, they proposed a series of equations to predict the hydraulic and mechanical properties of the sludge, including hydraulic gradient, upward flow velocity, hydraulic conductivity, settlement, total density, void ratio, excess PWP and vertical effective stress. Based on the variation of the physical and hydraulic properties of the slurried material with the consolidation time, they also proposed two equations to evaluate the relationship between the void ratio e and hydraulic conductivity k [Fig. 2-21(a)] or vertical effective stress σ_v' [Fig. 2-21(b)].

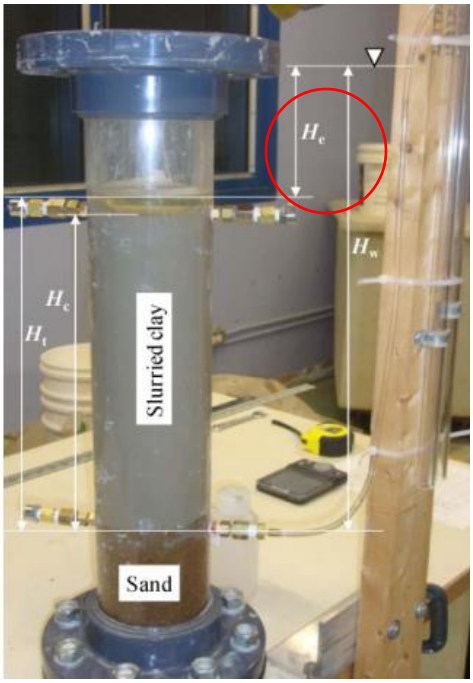

Figure 2-20: Photograph of the column test apparatus (taken from Li et al. 2013)

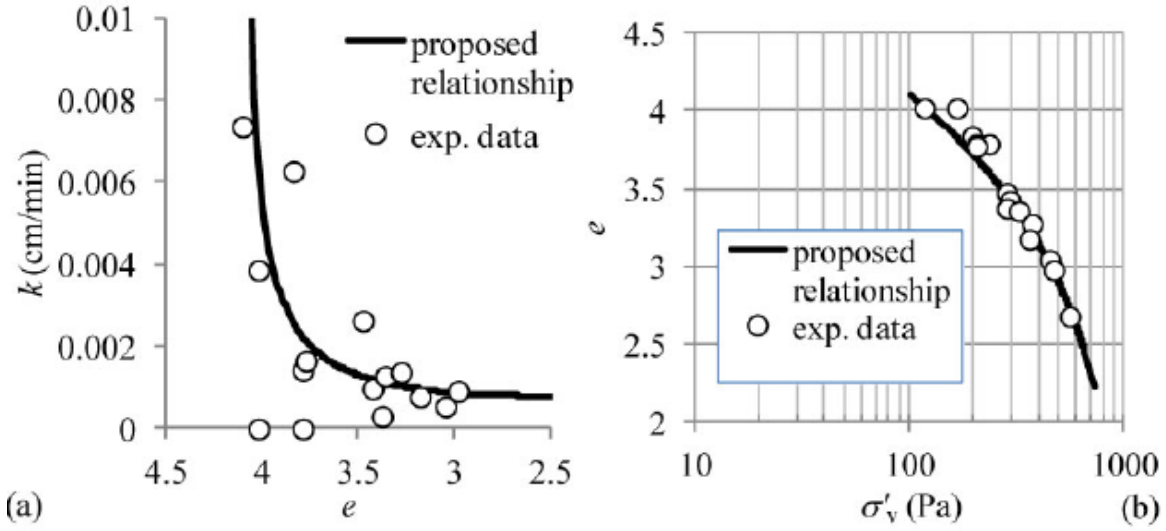

Figure 2-21: Relationship between (a) hydraulic conductivity and void ratio and (b) void ratio and vertical effective stress, obtained by the experimental data and predicted by the proposed relationships (taken from Li et al. 2013)

Belem et al. (2016) conducted column tests [Fig. 2-22] to investigate the effects of consolidation and cement hydration on the development of physical and mechanical properties in cemented paste backfills, prepared with tailings from two Canadian mines LRD (tailings CT1) and LVT (tailings

CT2). The tests were conducted in different drainage conditions of columns, including full (FLD) and partial (PLD) lateral draiange conditions. The lateral drainage is allowed along the full height of the column under the FLD condition and through the half lower part of the column under the PLD condition. Tests were also performed under based undrained (UD) condition.

They reported that most of the drainage and vertical settlement due to the self-weight consolidation took place in the first 48-72 h after the placement of the backfill in the column. The results revealed that the vertical strain (= measured final settlement/initial height of placed backfill) is 2.5% for undrained column, 2.8% for partial drained column, and 5.5% for full lateral drained column, respectively. The in situ measurement of the vertical strains for the LVT mine backfill varies from 3.3% to 5.0%, indicating that the placed backfill in mine stopes has similar behavior as the backfill in the column with FLD or PLD conditions.

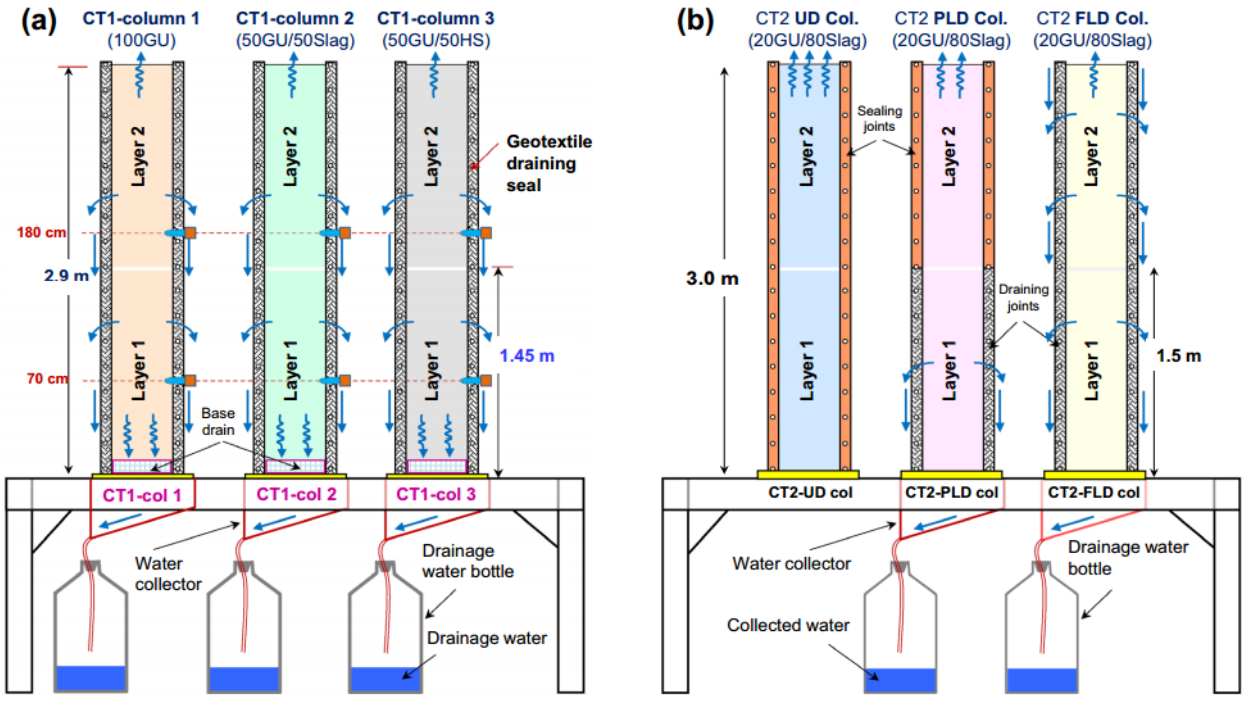

Figure 2-22: Schematic diagram of the self-weight consolidation tests with backfill from (a) LRD mine (CT1 tailings sample), and (b) LVT mine (CT2 tailings sample) (taken from Belem et al. 2016)

It should be noted that the above-mentioned laboratory tests were all conducted by filling the slurried materials in the column instantaneously or in a short period. This does not represent the

field conditions of tailings or backfill deposited in a dam or mine stope at a constant filling rate. Excess PWP can be generated and dissipated during the filling operation.

In situ measurement of the mine backfilled stope

Belem et al. (2004) conducted in situ measurements of stress variations and evolution in a mine stope at the Doyon Gold Mine, Canada. Fig. 2-23(a) shows that the stope was filled in three stages with the earth pressure cells installed at different places. Fig. 2-23(b) shows the evolution of the horizontal pressure measured by the sensor near the barricade during the filling operation. It can be seen that the horizontal pressure increased during the filling and reached a maximum value around 10 days. The maximum pressure at the end of the first stage of filling is 34 kPa, which is much smaller than the overburden pressure probably due to the occurrence of arching effect, drainage and consolidation during the filling operation.

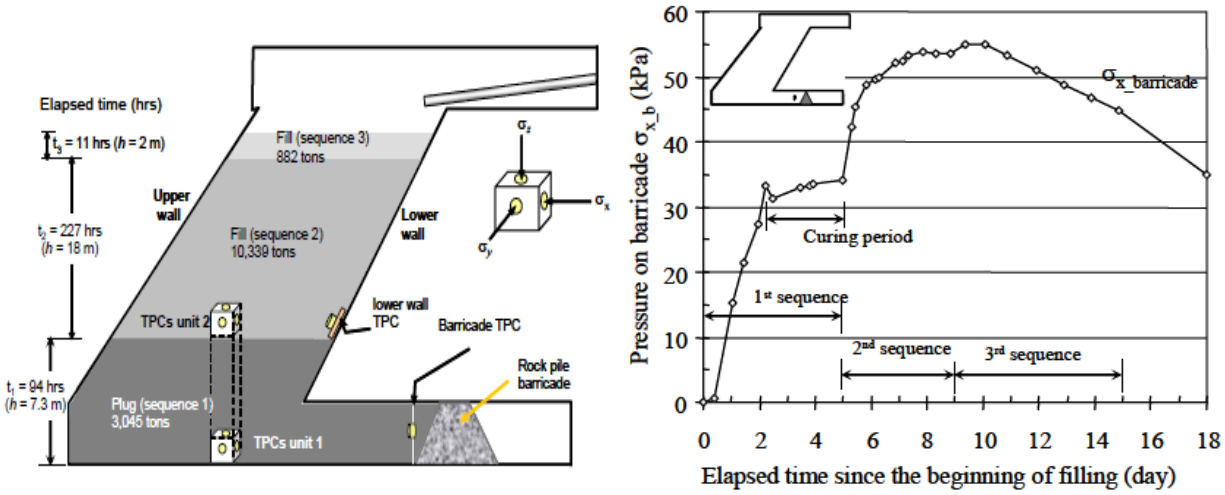

Figure 2-23: (a) a mine stope filled with backfill in two stages and the installation of earth pressure cells, (b) evolution of pressure on the barricade with the filling time (taken from Belem et al. 2004)

Helinski et al. (2011) conducted in situ measurements of the pore water pressure and total pressure at the Kanowna Bell (KB) mine, Australia. Fig. 2-24(a) shows the geometry of the stope and installation of the instruments in the stope. The stope was filled in two stages with a rest period of 24 h. Fig. 2-24(b) shows the variation of pore water pressure (u) and vertical total stress (σ_v) with the filling time. It can be seen that the pore water pressure and vertical total stress were equal to each other and increased at the same rate as the overburden pressure during the first 15 h of filling,

indicating no drainage and arching effect during this time. The pore water pressure and total pressure decreased with time during the resting period. The former decreased at a higher rate than the latter. Helinski et al. (2011) explained that it may be caused by the combined effect of drainage and consumption of pore water during the cement hydration. At the end of filling operation, the total vertical stress is 190 kPa, which is much smaller than the overburden pressure due to the occurrence of arching effect and cement hydration during the filling operation.

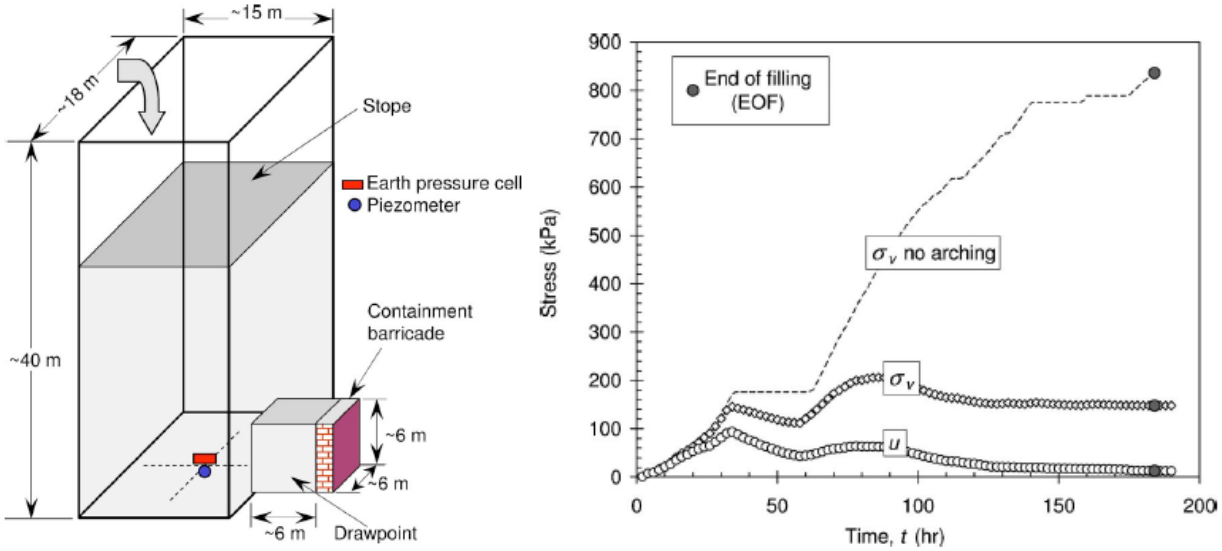

Figure 2-24: (a) The layout of the instruments in the KB mine stope, (b) the measured stresses during the filling operation (taken from Helinski et al. 2011)

Thompson et al. (2009) conducted in situ experiments to study the evolution of the total pressure at the Kidd Mine, Canada. Fig. 2-25 shows that four earth pressure cells were installed along the access drift at different distances from the stope brow. It can be seen that the total pressures are close to each other during the initial stage of filling (<1.5 days). After that, the measured total pressure decreased with the increase of the distance between the sensors and the stope brow, resulting from the aching effect in the access drift.

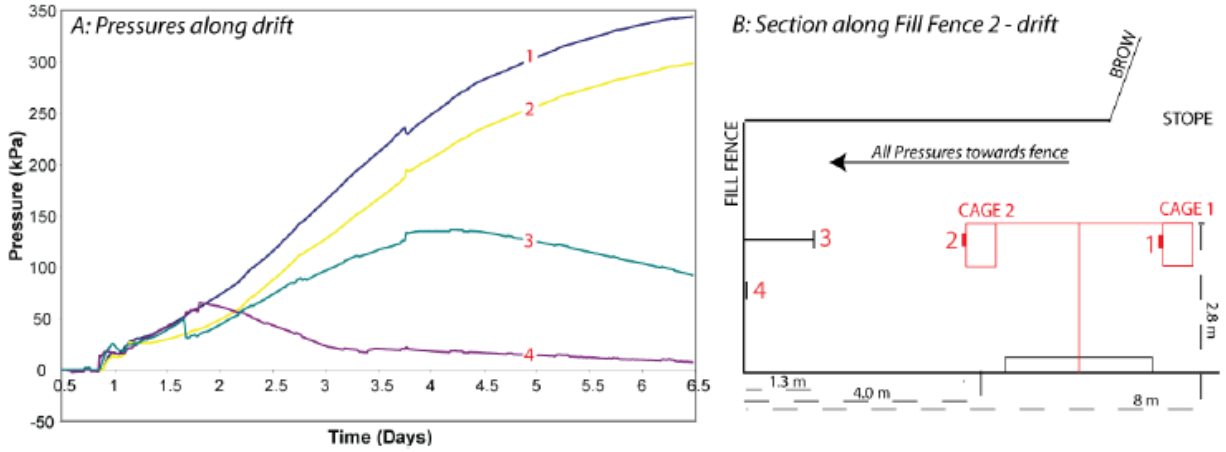

Figure 2-25: (a) Variation of the total pressure with the filling time, (b) layout of the pressure sensors in the drifts (taken from Thompson et al. 2009)

Thompson et al. (2012) performed in situ measurements in two mine stopes at Cayeli Mine, Turkey. The first stope (685) has 25 × 10 m in horizontal area and a height of 16.5 m, while the second stope (715) has 15 × 8.5 m in horizontal area and a height of 15 m. The 685 stope was filled continuously with a non-clastic tailings stream, the lower part of the stope from 0 to 8 m was filled with 8.5% binder content (by dry weight of solid) and the above part was filled with 6.5% binder content. The average filling rate is 22 cm/h. The 715 stope was filled in two stages with 6.5% binder content of tailings. The first filling stage is 20 hours, followed by a resting period of 3 days. The rest of the stope was filled within 21 hours. The average filling rate is 37 cm/h. Fig. 2-26 shows the layout of the instruments in the stope 685 and 715.

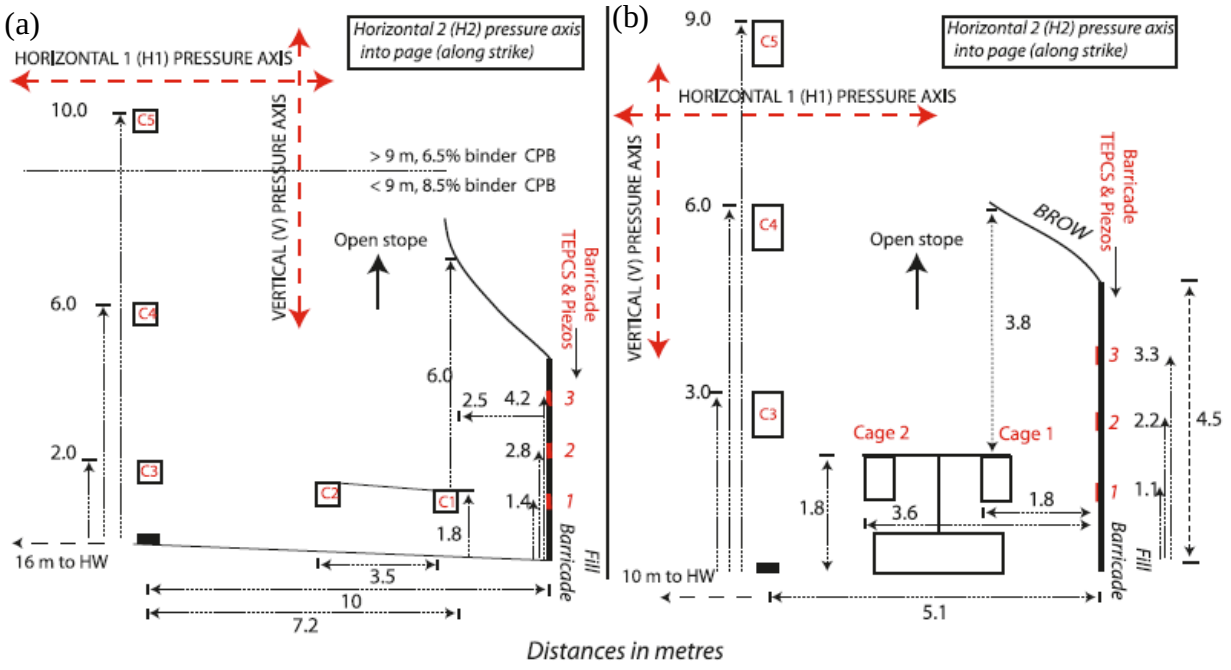

Figure 2-26: Schematic diagram of the layout of the instruments in the stope 685 and 715 (taken from Thompson et al. 2012)

Fig. 2-27(a) shows the measured vertical and horizontal total pressures, total pore water pressure and temperature on the barricade. It can be seen that the horizontal pressure, the pore water pressure, and the temperature on barricade increased in the initial stage of filling and then decreased during and after the filling operation. The pore water pressure decreased at a higher rate than the horizontal pressures due to the water drainage through the barricade and cracks on the rock wall. For the three sensors on the barricade, the measured pore water pressures increased at the same rate as the horizontal pressure in the initial stage of filling. These results indicate that the backfill had no effective stress and behaved as a heavy liquid during this time. Fig. 2-27(b) shows the horizontal pressure measured by the cages 1-3 and instruments on barricade. It can be seen that the horizontal pressures decreased when the installation point of the instruments was closer to the barricade, indicating the occurrence of arching effect in the access drift. As the backfill behaved as heavy liquid without effect stress, some other factors, such as viscosity of backfill may lead to the arching effect.

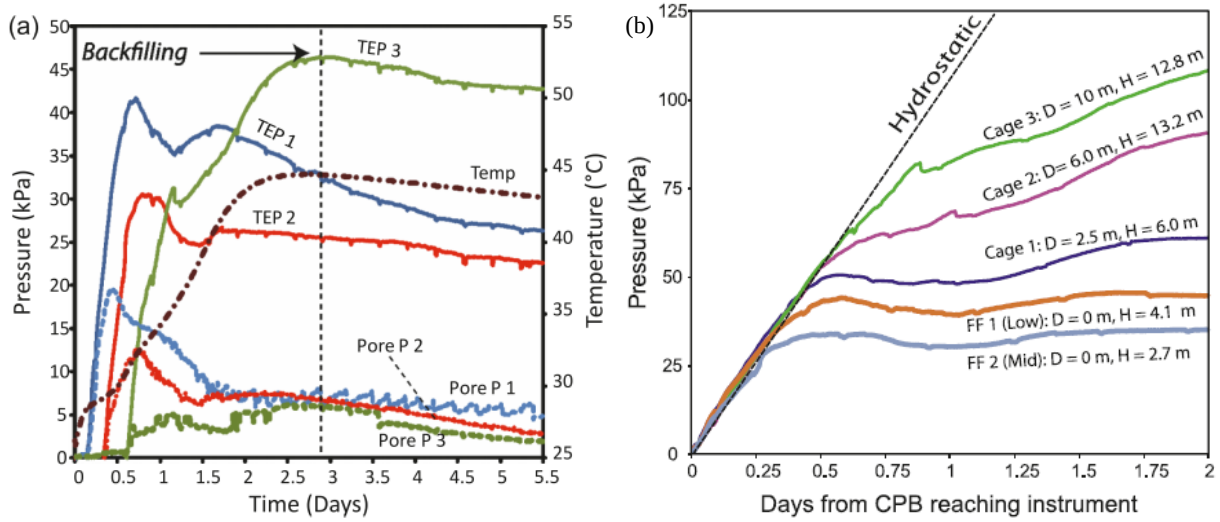

Figure 2-27: (a) Measured horizontal pressure, pore water pressure and temperature on the barricade; (b) Horizontal total pressure for Cages 1-3 and barricade TEPCs 1 (1.4m height) and 2 (2.8 m height) in the 685 stope, measured along the axis of the stope (toward the barricade) (taken from Thompson et al. 2012)

Fig. 2-28 shows the measured total pressure, pore water pressure and temperature by the instruments on the barricade and in cage 3 in the stope 715. Again, the pore water pressure increased at the same rate as the total pressure in the initial stage of filling for both the sensors on the barricade and in cage 3. During the curing period, the temperature in the backfill increased with time due to the exothermic reaction of the cement hydration. The pore water pressure decreased at a higher rate than the total earth pressure. This can be attributed to the consumption of pore water during the drainage and cement hydration processes. In the second stage of pouring, the pressures and temperature on the barricade kept almost constant. For cage 3, the vertical stress increased at a higher rate than the horizontal stress and pore water pressure.

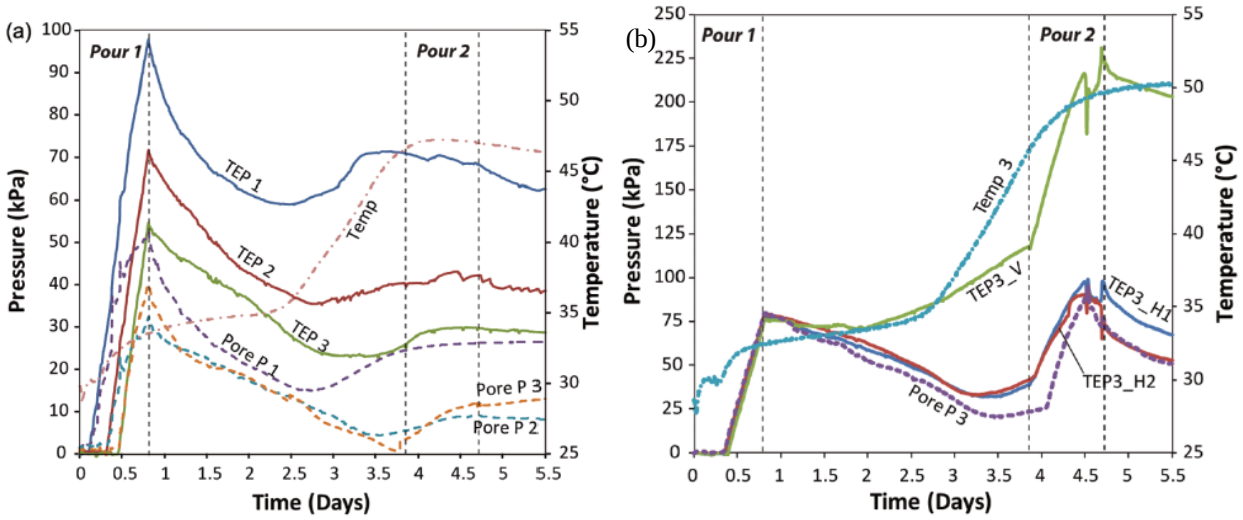

Figure 2-28: Evolution of the total pressure, pore water pressure and temperature with the filling time: (a) on the barricade; (b) cage 3 in the stope 685 (H1 = perpendicular to strike direction, H2 = along strike direction, V = vertical) (taken from Thompson et al. 2012)

Doherty et al. (2015) conducted in-stope measurements of total and pore water pressure in three stopes at the Raleigh mine, Australia. The three stopes have similar shape, with the heights of around 17 m, widths of 3.5 m and lengths of 18 m. The dip angles for the three stopes are in the range of 65° and 70° to the horizontal plane. The influence of the filling and resting period, the cement content and the drainage system of the barricade on the stress in the backfilled stopes were investigated. The results showed that the resting period between the stope filling plays a significant role in the stress development in the backfilled stopes. A very short resting period can lead to significant decrease of the pore water pressure and total pressure in the backfilled stopes. They also found that the volume of drainage water collected from the barricade is much smaller (less than 0.1%) than the water added to the backfill. The drainage may be not very obvious for the used cemented paste backfill. The water may also drain out of the backfill from the cracks on the rock walls, which has been studied by Belem et al. (2016).

Numerical simulation for the consolidation of slurried materials

Fahey et al. (2009) conducted numerical simulations with Plaxis to investigate the stresses in a stope filled with saturated backfill. Fig. 2-29 shows the distribution of vertical and horizontal total stresses along the full height of the backfilled stope. It can be seen that the backfill hydraulic conductivity has a significant influence on the vertical and horizontal total stresses development in

the backfilled stope. A high value of *k* leads to smaller horizontal and vertical total stresses in the backfilled stope, which can be attributed to the higher amount of drainage and consolidation during the filling operation.

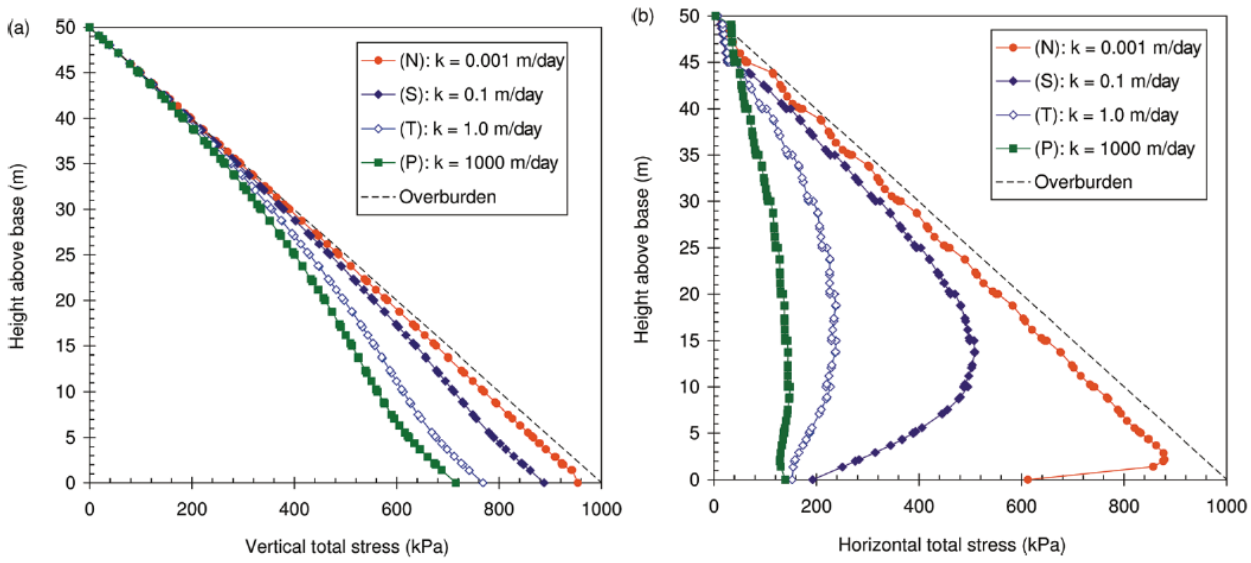

Figure 2-29: Distribution of the vertical and horizontal total stresses along the height of the backfilled stope obtained by Plaxis with different value of *k* (taken from Fahey et al. 2009)

El Mkadmi et al. (2014) conducted numerical simulations with SIGMA/W to investigate the influence of drainage and filling rate on the stress development in a backfilled stope. The interface was considered in the numerical simulation by adding two thin and softer layers on the two sides of rock wall. Fig. 2-30 shows the variation of vertical total stress, pore water pressure and vertical effective stress along the full height of the backfill after being instantaneously placed in a stope with progressive drainage. It can be seen that the vertical total stress is almost equal to the pore water pressure shortly after the placement (t = 34 min). There is almost no effective stress along the height of the placed backfill. As consolidation progressively takes place, the dissipation of excess PWP leads to the decrease of pore water pressure and increase of vertical effective stress. The decrease of vertical total stress can be attributed to the drainage and development of arching effect. An unsaturated zone was also observed after the drainage for a certain period of time. Their results showed that most of the variation of the total stress, pore water pressure and effective stress occurred within the first 3.7 days. After that, the stresses only changed slightly in the backfill.

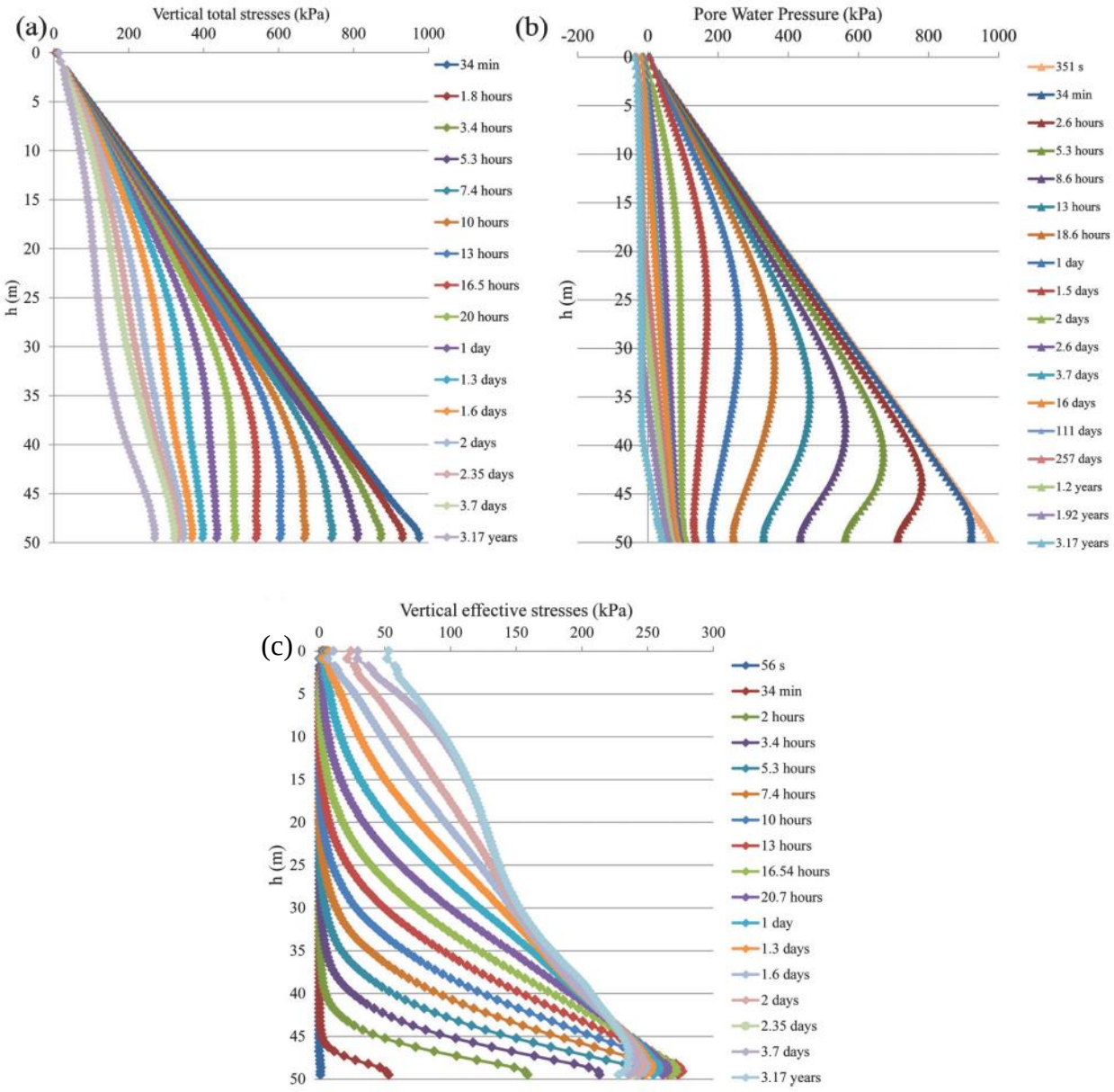

Figure 2-30: Variation of (a) vertical total stress, (b) pore water pressure and (c) vertical effective stresses in the backfilled stope obtained by SIGMA/W (taken from El Mkadmi et al. 2014)

Fig. 2-31 shows the influence of the filling rate on the evolution of the stresses near the base of the stope. One can see that the filling rate can significantly affect the stress near the base of the stope. When the filling rate is 5m/5days, the maximum vertical and horizontal total stresses at h = 47.5m are about 200 kPa and 50 kPa, respectively. When the filling rate increases to 5m/5hr, the maximum vertical and horizontal total stresses are around 600 kPa. The low filling rate can allow the high

degree of excess PWP dissipation, resulting in the generation of high effective stress and arching effect in the backfilled stope.

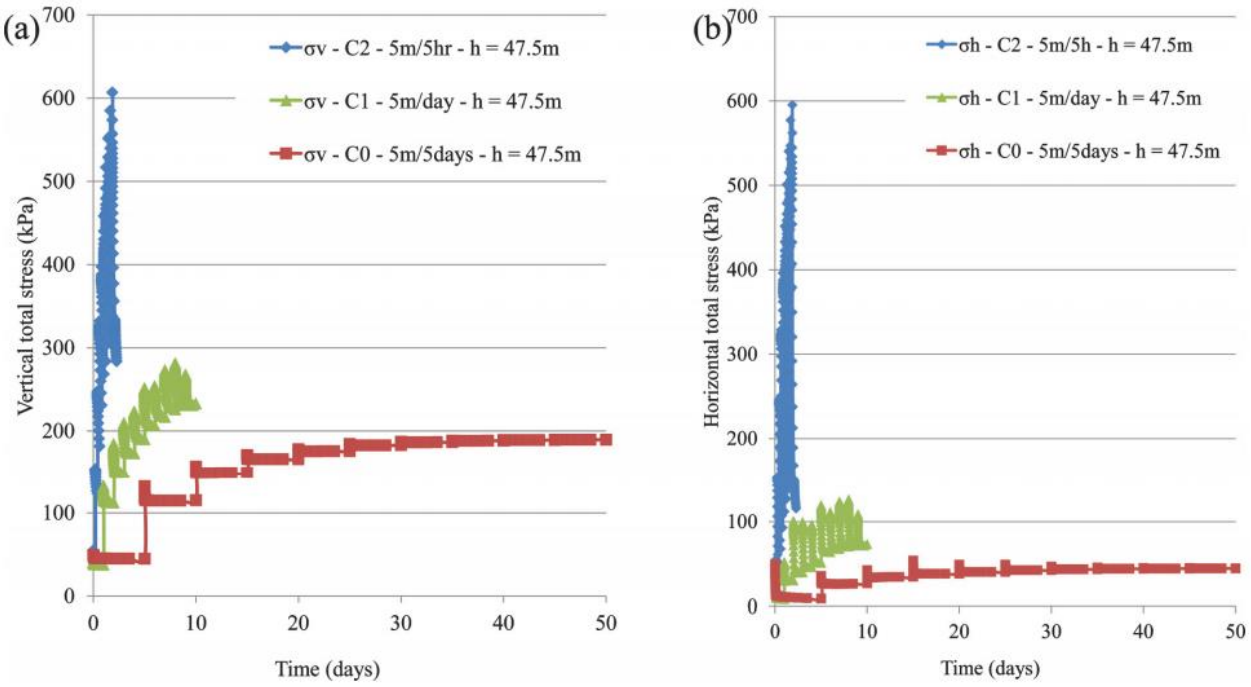

Figure 2-31: Evolution of the (a) vertical total stress and (b) horizontal total stress near the base of the stope with different filling rate (taken from El Mkadmi et al. 2014)

During the in situ measurements, Grabinsky et al. (2013, 2014) observed a layer of slurry on top of the placed backfill during the filling operation. In this slurry layer, the total stress and pore water pressure are almost equal to each other; there is almost no effective stress. It thus imposed a non-zero water pressure on top of the placed backfill. Shahsavari and Grabinsky (2014) used FLAC3D to investigate the influence of this slurry layer on the pore water pressure in the backfilled stope. Fig. 2-32 shows the pore water pressure distribution along the height of the backfill obtained by FLAC3D by considering slurry boundary and no slurry boundary (zero pore pressure). Their results showed that the consideration of slurry boundary increases the pore water pressure in the backfill. For a given height of backfill, Fig. 2-32(b) shows that higher thickness of the slurry leads to higher pore water pressure in the backfilled stopes.

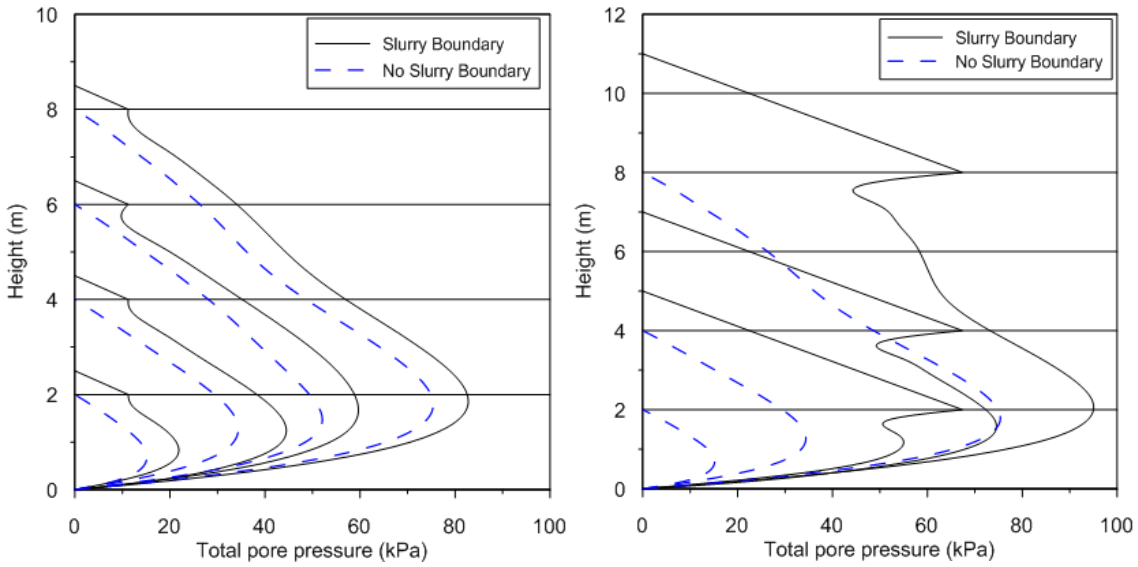

Figure 2-32: Distribution of the total pore water pressure along the height of the backfill with (a) 0.5 m and (b) 3.0 m slurry on top of the backfill (taken from Shahsavari and Grabinsky 2014)

The above-mentioned numerical simulations were conducted by considering impermeable stope rock walls. This may not be representative of the field conditions as the stope rock walls usually contain cracks and fractures (Belem et al. 2016). The excess pore water pressure can be dissipated through these cracks and fractures. In addition, the backfill properties (hydraulic conductivity, constrained modulus and consolidation coefficient, etc.) were considered to be constant or varied due to only the occurrence of cement hydration. The consolidation associated with the dissipation of excess PWP can also lead to the decrease of hydraulic conductivity and increase of the constrained modulus. These influences should be considered in the future work.

2.3.2 Pressures and stresses long-time after the slurry deposition − Backfill in or close to fully drained conditions

When the barricade is pervious, the backfill will become water-less when it reaches a fully drained and consolidated condition. Neglecting the suction, the backfill can be considered as dry. When the barricade is impervious, a hydrostatic pressure will be established when the backfill reaches the fully drained and consolidated condition. The backfill can be considered as in submerged condition. In both cases, effective stresses develop in the backfill. The tendency of the settlement of the backfill leads to the arching effect along the fill-wall interfaces and stress change in the backfill.

Arching theory

Janssen (1895) solution

Arching theory was first proposed by Janssen (1895) to evaluate the grain pressures confined by silos. Janssen (1895) presented the following equation to calculate the vertical effective stress in the fill:

$$\sigma_v' = \frac{\gamma}{K \tan\delta} \frac{A}{U} \left[1 - \exp\left(-K \tan\delta \frac{U}{A} z \right) \right] \tag{2-5}$$

where γ (kN/m^3) is the unit weight of the fill materials; K is the coefficient; U (m) is the circumference of the silo; A (m^2) is the sectional area of the silo; δ (°) is the friction angle along the interfaces between the fill and silo walls; z (m) is the depth of the fill materials.

The applicability of Janssen (1895) solution has been investigated by Take and Valsangkar (2001) who conducted centrifuge tests to study the lateral earth pressure on retaining walls. Their results show that the measured lateral pressure on the retaining wall is smaller than the overburden pressure due to the occurrence of arching effect. The measured results agree well with that predicted by the Janssen's arching theory.

Marston (1930) solution

Marston (1930) introduced Janssen (1895) arching theory to calculate the loads on conduits buried in trenches. The vertical stress on conduits is expressed as follows:

$$\sigma_v = \frac{\gamma B}{2K_a \mu} \left(1 - \exp\left(\frac{-2K_a h \mu}{B} \right) \right) \tag{2-6}$$

where γ (kN/m^3) is the unit weight of the backfill; B (m) is the width of the vertical openings; h (m) is the depth; μ is the friction coefficient along the wall, defined as $\mu = \tan\delta$ (δ (°) is the friction angle between the backfill and surrounding walls; K_a is the active earth pressure coefficient.

Li et al. (2003) conducted numerical simulations with FLAC2D to investigate the stresses in backfilled stopes. The filling sequence was considered by assuming that the wall convergence occurred before the placement of the backfill. The backfill obeyed Coulomb criterion while the rock walls were assumed to be homogeneous, isotropic and linearly elastic. The numerical results

were also compared to that calculated by the Marston (1930) theory. Fig. 2-33 shows that the Marston theory typically underestimates the horizontal and vertical stresses in the backfilled stope. Good agreements were obtained between the numerical and analytical results by using active earth pressure coefficient K_a for vertical stress and at rest earth pressure coefficient K_0 for horizontal stress.

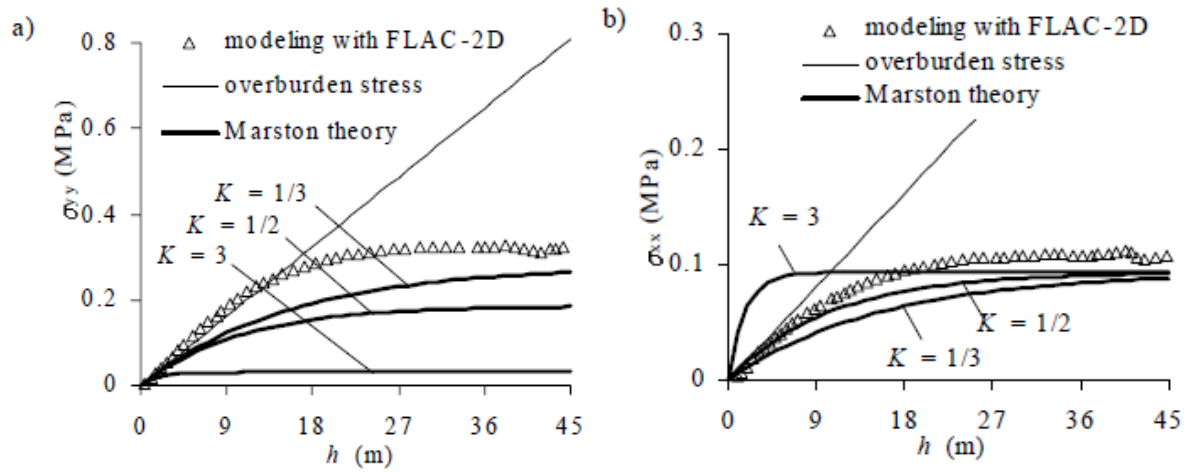

Figure 2-33: Variation of the (a) vertical and (b) horizontal stresses along the vertical center line of the backfilled stope obtained by the numerical simulations with FLAC and calculated by the Marston theory (taken from Li et al. 2003)

Terzaghi (1943) solution

Terzaghi (1943) proposed a solution based on the model of Marston (1930) to evaluate the stresses within two vertical surfaces of sliding. Fig. 2-34 shows the model of Terzaghi (1943) with the soil between two vertical sliding faces and an uniform surchage at the top surface. In the figure, q (kPa) is the surchage on top of backfill; b (m) is the half width between the two vertical sliding faces; γ (kN/m^3) is the unit weight of the soil. At position z (m) below the surface, a slice with a thickness dz and weight $2b\gamma dz$ is subjected to lateral stress σ_h (kPa), shear stress equaling to the shear strength $c + \sigma_h \tan\phi$ (where c (kPa) is the soil cohesion, ϕ (°) is the friction angle of the soil), and vertical stresses σ_v and $\sigma_v + d\sigma_v$ (kPa).

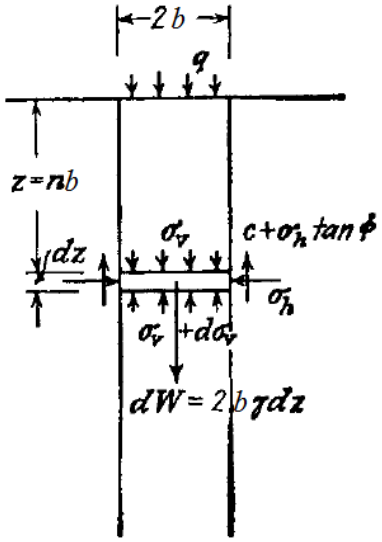

Figure 2-34: Model of Terzaghi (1943) to calculate the stresses in cohesion soil (taken from Terzaghi 1943)

The vertical stress (σ_v) at depth z were given as follows by Terzaghi (1943):

$$\sigma_v = \frac{b(\gamma - c/b)}{K\tan\phi}(1-\exp(-Kz\tan\phi/b)) + q\times\exp(-Kz\tan\phi/b) \quad (2\text{-}7)$$

Stress estimation in mine backfilled stopes

Traditionally, the stresses in mine backfilled stopes are calculated by the earth pressures based on the geo-static overburden solution. The vertical stress (σ_v) is equal to the unit weight of the backfill γ multiplied by the depth h ($\sigma_v = \gamma h$), while the horizontal stress (σ_h) is assumed to be proportional to the vertical stress ($\sigma_h = K\sigma_v$, where K is the earth pressure coefficient). This solution may be suitable for wide vertical stopes with very smooth walls in which the arching effect can be neglected. For narrow stopes with rough walls, the overburden solution leads to over-estimation of stresses in the backfilled stopes as shown in the following subsections.

2D analytical solution for vertical backfilled stopes

When the length of the mine stope is much larger than the other two dimensions (width and height), the stresses in the backfilled stope can be calculated by the following 2D analytical solution.

Aubertin et al. (2003) solution

Aubertin et al. (2003) considered arching effect in the estimation of stresses in backfilled stopes. Fig. 2-35 shows their model making use of that of Marston (1930).

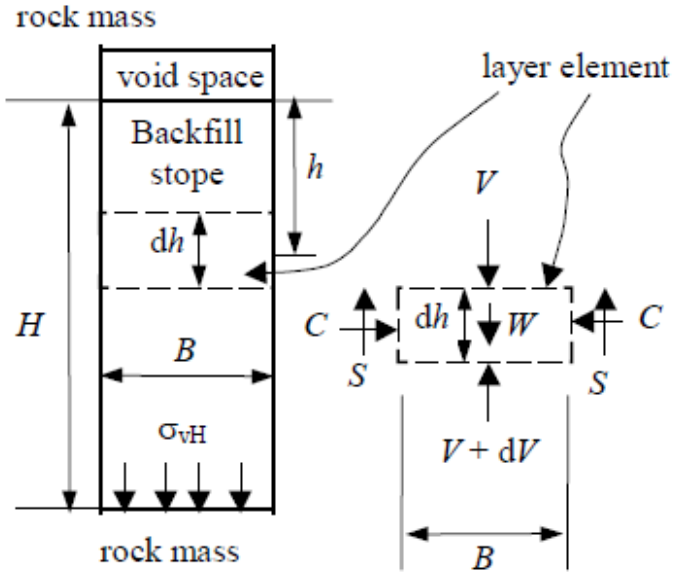

Figure 2-35: A vertical narrow backfilled stope with forces acted on an isolated layer and the floor (taken from Aubertin et al. 2003)

The vertical and horizontal stresses at the bottom of the backfilled stope can be expressed as (Aubertin et al. 2003):

$$\sigma_{vH} = \frac{\gamma B}{K}\left(\frac{1-\exp(-2KH\tan\delta'/B)}{2\tan\delta'}\right) \tag{2-8}$$

$$\sigma_{hH} = \gamma B\left(\frac{1-\exp(-2KH\tan\delta'/B)}{2\tan\delta'}\right) \tag{2-9}$$

where γ (kN/m^3) is the unit weight of the backfill; H (m) is the height of backfill; B (m) is the stope width; δ' (°) is the effective friction angle between the backfill and surrounding walls, which is assumed to be equal to the internal friction angle of the backfill ϕ (°) since most shear yielding can be expected to occur within the backfill part close to the wall (Aubertin et al. 2003); K is the earth pressure coefficient, which is dependent on the wall movement and material properties and can be defined as follow (Bowles 1988):

$$K = K_0 = 1-\sin\phi \qquad \text{At rest} \tag{2-10}$$

$$K = K_a = (1-\sin\phi)/(1+\sin\phi) \quad \text{Active condition} \tag{2-11}$$

$$K = K_p = (1+\sin\phi)/(1-\sin\phi) \quad \text{Passive condition} \tag{2-12}$$

Aubertin et al. (2003) also conducted numerical simulations with PHASES2 to investigate the stresses in vertical backfilled stopes and compared the numerical results with that predicted by Eqs. (2-8) and (2-9). Fig. 2-36 shows the distribution of the lateral stress on the wall [Fig. 2-36(a)] and vertical stress [Fig. 2-36(b)] along the height of the backfill. The arching effect does occur in the backfill as the lateral and vertical stresses calculated by Eqs. (2-8) and (2-9) as well as the numerical results at the bottom of the stope are lower than the overburden pressure. However, one can also see that the maximum lateral and vertical stresses occur around the mid-height of the backfill. This can be attributed to that the inward movement of the stope walls squeeze the backfill, resulting in high lateral and vertical stresses.

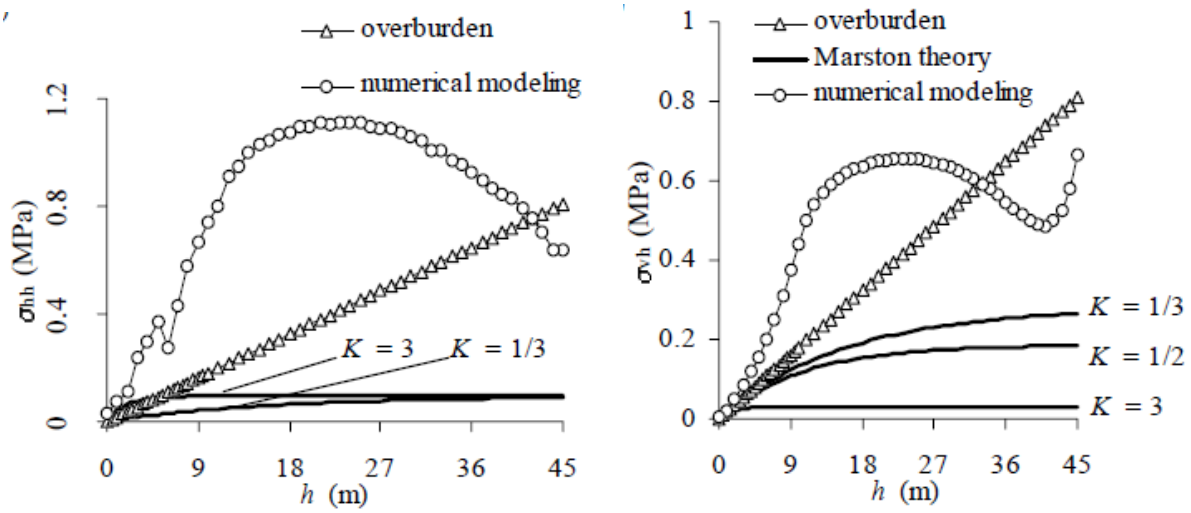

Figure 2-36: Distribution of the (a) lateral pressure on the wall and (b) vertical stress along the height of the backfill obtained by the numerical simulation and calculated by Eqs. (2-8) and (2-9) (taken from Aubertin et al. 2003)

Li and Aubertin (2008)

In the previous studies, the vertical and horizontal stresses were assumed to be uniformly distributed across the stopes width. The numerical simulations conducted by Li and Aubertin (2008) show that the horizontal stress is almost uniformly distributed across the width of the stope under plane strain conditions. However, the vertical stress at the center is obviously higher than

that close to the wall. Li and Aubertin (2008) proposed the following equations to calculate the vertical stress σ_{vx} across the stope width and horizontal stress σ_h:

$$\sigma_{vx} = \frac{\gamma B}{2K\tan\delta}\left\{1-\exp\left[-\frac{2K\tan\delta}{B(1-DF)}h\right]\right\}\times\left[1-a\left(\frac{|x|}{B}\right)^b\right] \tag{2-13}$$

$$\sigma_h = \frac{\gamma B}{2\tan\delta}\left[1-\exp\left(-\frac{2K\tan\delta}{B(1-DF)}\right)h\right] \tag{2-14}$$

where B (m) is the width of the stope, x (m) is the distance from the center line of the stope with a range of $-B/2$ to $B/2$, σ_{v0} (kPa) is the vertical stress at the centerline of the stope ($x = 0$), a and b are two parameters controlling the normal stress distribution curvature, γ (kN/m^3) is the unit weight of the backfill; δ (°) is the friction angle along the backfill-rock wall interface, which is usually taken as the friction angle of backfill, h (m) is the depth from the surface of the backfill. DF is the distribution factor, which was expressed as follows (Li and Aubertin 2008):

$$DF = \frac{a}{2^b(b+1)} = \frac{2^{\left(1-\lambda_1\frac{H}{B}\right)}\tan^{-\lambda_2}(\phi_0+\phi)}{2^b(b+1)} \tag{2-15}$$

where a and b are the parameters of the distribution factor, which can be determined from a series of numerical simulations using FLAC-2D; ϕ_0 (°) is a friction angle correction parameter, λ_1 and λ_2 are two addition model parameters. $\phi_0 = 50°$, $\lambda_1 = 0.02$ and $\lambda_2 = 0.1$ were obtained for calculations of the conditions at hand based on curve fitting technique on numerical results by Li and Aubertin (2008).

Jaouhar et al. (2018) solution

The above-mentioned arching solutions were developed by considering the uniform distribution of stress across a flat and horizontal layer element. This may not be representative as the principal stresses usually rotate near the walls. Jaouhar et al. (2018) proposed the following solutions to evaluate the vertical and horizontal principal stresses at any point (x, y) in a vertical backfilled opening by considering the equilibrium of a curved thin element.

$$\sigma_{v(x,y)} = \sigma_{1(x,y)}\left[1-(1-K_{ps})\left(\frac{x}{B\kappa}\right)^2\right] \tag{2-16}$$

$$\sigma_{h(x,y)} = \sigma_{1(x,y)}\left[K_{ps} + (1-K_{ps})\left(\frac{x}{B\kappa}\right)^2\right] \tag{2-17}$$

$$\sigma_{1(x,y)} = \frac{Q}{S}\left\{1-\exp\left(-\frac{S}{P}(y-\left[B\kappa-\sqrt{(B\kappa)^2-x^2}\right]\right)\right\} \tag{2-18}$$

$$K_{ps} = \tan^2(45^\circ - \phi/2) \qquad \kappa = \frac{1}{\sin(45^\circ - \phi/2)} \tag{2-19}$$

$$Q = \gamma B\kappa \sin\omega_w \qquad S = \frac{\tan\delta}{\cos\omega_w}\left(\sin^2\omega_w + K_{ps}\cos^2\omega_w\right) \tag{2-20}$$

$$P = B\kappa\sin\omega_w \qquad \omega_w = \sin^{-1}\left(\frac{1}{\kappa}\right) \tag{2-21}$$

where $\sigma_{1(x,y)}$ (kPa) is the major principal stress at a point (x, y) in the backfilled stope; x (m) is the distance between the vertical center line and the calculated point; B (m) is the half width of the vertical opening; ϕ (°) is the internal friction angle of the backfill; δ (°) is the friction angle along the backfill-rock wall interfaces, which is usually taken as two thirds of the backfill internal friction angle ($\delta \approx 2/3\phi$); γ (kN/m^3) is the unit weight of the backfill.

3D analytical solutions for vertical backfilled stopes

When the mine stopes have a limited length, the above-mentioned 2D solutions are not appropriate, 3D solutions should be applied.

Van Horn (1964) solution

Van Horn (1964) first proposed the following 3D analytical solutions to calculate the loads on the bottom of the soil prism at depth H from the natural ground surface:

$$\sigma_v = \frac{\gamma\left(\frac{BL}{L+B}\right)-2c}{2K\tan\delta}\left(1-\exp\left(\frac{-2KH\tan\delta(L+B)}{LB}\right)\right) \tag{2-22}$$

where γ (kN/m^3) is the unit weight of the fill material; B (m) and L (m) are the width and length of the underground structure; c (kPa) is the cohesion of the fill; δ (°) is the friction angle between the fill and rock; K is the earth pressure coefficient.

Li et al. (2005) solution

The previous 2D and 3D arching solutions generally consider a unique friction angle along the fill-wall interfaces. However, it is possible that the surrounding walls of vertical openings have different properties. Li et al. (2005) developed a three-dimensional analytical solution for evaluating the vertical and horizontal stresses in a narrow backfilled opening by taking into account the different properties along the four opening walls.

The vertical stress acted on the horizontal plane at a depth h from the top of the stope has been expressed as follows (Li et al. 2005):

$$\sigma_{vh} = \frac{\gamma - (\kappa_{13}B^{-1} + \kappa_{24}L^{-1})}{(\lambda_{13}B^{-1} + \lambda_{24}L^{-1})}\left\{1 - \exp\left[-h(\lambda_{13}B^{-1} + \lambda_{24}L^{-1}\right]\right\} \tag{2-23}$$

$$\lambda_{13} = K_1 \tan\delta_1 + K_3 \tan\delta_3 \tag{2-24}$$

$$\lambda_{24} = K_2 \tan\delta_2 + K_4 \tan\delta_4 \tag{2-25}$$

$$\kappa_{13} = c_1 + c_3 + 2c(\tan\alpha_1 \tan\delta_1 + \tan\alpha_3 \tan\delta_3) \tag{2-26}$$

$$\kappa_{24} = c_2 + c_4 + 2c(\tan\alpha_2 \tan\delta_2 + \tan\alpha_4 \tan\delta_4) \tag{2-27}$$

where γ (kN/m^3) is the unit weight of the backfill; α_i (°) is the backfill state angle on the i^{th} wall (i = 1-4); c_i (kPa) and δ_i (°) are the cohesion and friction angle of the ith fill-wall interface. K_i is the earth pressure coefficient and the value is between the at rest (K_0) and active (K_a) state.

Pirapakaran & Sivakugan (2007) solution

Pirapakaran and Sivakugan (2007a) extended the Marston (1930) analytical solution to evaluate the stress state in 3-dimensional mine stopes. The vertical stress for a rectangular stope can be expressed as (Pirapakaran and Sivakugan 2007a):

$$\sigma_v = \frac{\gamma B}{2K\tan\delta}\left(\frac{L}{L+B}\right)\left[1 - \exp\left\{-2\left(\frac{L+B}{LB}\right)Kh\tan\delta\right\}\right] \tag{2-28}$$

where γ (kN/m^3) is the unit weight of the mine backfill; B (m) is the width of the stope; L (m) is the length of the stope; K is the earth pressure coefficient, which is assumed to be K_0 due to the small movement of rock walls; δ (°) is the angle of the wall friction, which is assumed to be equal

to 2/3ϕ, where ϕ (°) is the internal friction angle of backfill; h (m) is the depth from the top surface of the backfill.

Solutions for inclined stopes

In practice, many stopes can be more or less inclined. Several solutions have been developed over the years by different researchers to evaluate the stresses in inclined backfilled stopes.

Blight (1984) solution

Blight (1984) investigated the stresses in an inclined mine stope. The two side walls were assumed to be parallel with same properties and applied with same shear stress and compressive stress. The existence of PWP was considered by using the linear relationship $u = u_0 + B'\sigma_z$ (where u_0 (kPa) is the hydrostatic pore pressure; σ_z (kPa) is the total stress, and coefficient B' (m) is related to the dissipation of excess PWP, $B' = 0$ means the excess PWP is dissipated completely while $B' = 1$ means the excess PWP is equal to total stress without any dissipation).

Blight (1984) proposed the following equation to evaluate the total stresses (along the center line and parallel to the stope walls) in an inclined stope by considering the equilibrium of the fill element:

$$\sigma_z = \frac{1}{A}\left\{\gamma \sin\beta - \frac{2}{w}(c' - u_0 K \tan\phi')\right\}\left\{1 - e^{-Az}\right\} \tag{2-29}$$

$$A = \frac{2K \tan\phi'(1 - B')}{w} \tag{2-30}$$

where γ (kN/m^3) is the unit weight of the fill; β (°) is the inclination angle to the horizontal surface; w (m) is the width of the stope; c' (kPa) is the effective cohesion of the fill; ϕ' (°) is the effective friction angle of the fill; K is the earth pressure coefficient, which is related to the state of the backfill.

Blight (1984) defined K as the Jaky expression K_0 (= 1 - sinϕ') for normally consolidated backfill and as the Reimbert expression $K_0 = (45° - \phi'/2) / (45° + \phi'/2)$ for loose granular backfill. The lateral total stress can be expressed as follows:

$$\sigma_y = K(\sigma_z - u) + u \tag{2-31}$$

Caceres (2005) solution

Based on Janssen's arching theory, Caceres (2005) proposed a solution to evaluate the stresses in an inclined backfilled stope. The two sides wall were assumed to have same properties for the fill-wall interface and applied with same shear and compressive stresses.

Caceres (2005) proposed the following equation to evaluate the stresses in the backfilled stope:

$$\sigma_y(z) = \frac{\gamma B \sin^2\beta}{2K\tan\phi'}\left[1-\exp\left(-\frac{2K\tan\phi'}{B\sin^2\beta}h\right)\right] \tag{2-32}$$

where B (= 2b; m) is the width of the stope; β (°) is the dip angle of the stope; K is the earth pressure coefficient. Caceres (2005) proposed the following equation to calculate the value of K by applying the curve fitting on the numerical results:

$$K = 1.4\sin^2\phi' - 2\sin\phi' + 1 \tag{2-33}$$

After revision of Eq. (2-32), Ting et al. (2011) and Yang (2016) have proposed the following expression to evaluate the vertical stress in backfilled stopes:

$$\sigma_y(z) = \frac{\gamma B \sin\beta}{2K\tan\phi'}\left[1-\exp\left(-\frac{2K\tan\phi'}{B\sin\beta}h\right)\right] \tag{2-34}$$

Ting et al. (2011)

Ting et al. (2011) proposed another analytical expression to evaluate the stresses in inclined backfilled stopes with two parallel walls. They assumed that the vertical normal stresses are uniformly distributed at any height; the adhesion along the hanging wall (HW) and footwall (FW) fill-walls interface is equal to the cohesion of the backfill; the shear and compressive forces applied on the HW and FW are the same.

Ting et al. (2011) proposed the following equation for an inclined stope with a uniform surcharge q on top of the backfill:

$$\sigma_z = \frac{\gamma B - 2c(1+\sin 2\beta\tan\delta)}{2K'\tan\delta}\left(1-\exp\left(-2K'\frac{z}{B}\tan\delta)\right)\right) + q\exp\left(-2K'\frac{z}{B}\tan\delta\right) \tag{2-35}$$

$$K' = \left(\frac{1+K}{2} + \frac{1-K}{2} \cos 2\beta + K \tan\delta \sin 2\beta \right) \tag{2-36}$$

where γ (kN/m^3) is the backfill unit weight; B (m) is the stope width; c (kPa) is the cohesion of the backfill; β (°) is the dip angle of the stope; δ (°) is the friction angle along the fill-wall interfaces (δ = 2/3ϕ, ϕ is the internal friction angle of backfill); q (kPa) is the surcharge on the top of the backfill; K is the earth pressure coefficient.

The results obtained by applying the solution showed that the combined effects of arching and stope inclination lead to 65-70% reduction of vertical stresses compared to the overburden pressure. The results also revealed that the vertical stresses calculated by Eq. (2-35) are much smaller than the solution for vertical stopes when the stope inclination is 30° to the vertical.

Ting et al. (2014) solution

Ting et al. (2014) extended the solution of Ting et al. (2011) to consider the backfilled stopes with non-parallel stope walls as shown in Fig. 2-37.

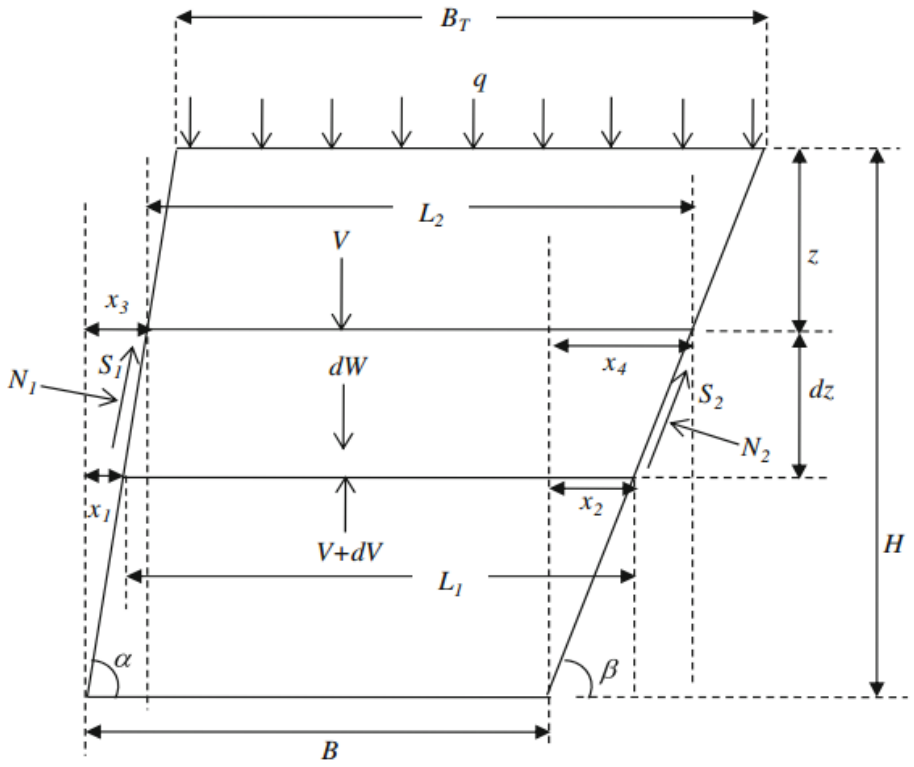

Figure 2-37: Schematic diagram of an inclined stope with two non-parallel walls (taken from Ting et al. 2014)

The vertical stress at a depth z can be expressed as follows:

$$\sigma_z = -\frac{(R-Sz)}{T} + \frac{S(P-Qz)}{T(T+Q)} + \left(q + \frac{R}{T} - \frac{SP}{T(T+Q)}\right)\left[\left(1-\frac{Qz}{P}\right)^{\frac{1}{Q}}\right]^{-T} \tag{2-37}$$

where α and β are the inclination angles of the HW and FW, respectively; other parameters are defined as follows:

$$P = B + \frac{H(\tan\alpha - \tan\beta)}{\tan\beta\tan\alpha}, \quad Q = \frac{\tan\alpha - \tan\beta}{\tan\beta\tan\alpha}, \; S = \frac{\gamma(\tan\alpha - \tan\beta)}{\tan\beta\tan\alpha} \tag{2-38}$$

$$R = \gamma B - \zeta_1 - \zeta_2 - c\sin 2\beta\cot\beta + c\sin 2\alpha\cot\alpha + \frac{\gamma H(\tan\alpha - \tan\beta)}{\tan\beta\tan\alpha} \tag{2-39}$$

$$T = \frac{(\tan\alpha - \tan\beta)}{\tan\beta\tan\alpha} - K_1\tan\phi - K_2\tan\phi - K_2\cot\beta + K_1\cot\alpha \tag{2-40}$$

$$\zeta_1 = c(1+\sin 2\alpha\tan\phi), \; \zeta_2 = c(1+\sin 2\beta\tan\phi) \tag{2-41}$$

$$K_1 = \frac{1+K}{2} + \frac{1-K}{2}\cos 2\alpha + K\tan\phi\sin 2\alpha, \; K_2 = \frac{1+K}{2} + \frac{1-K}{2}\cos 2\beta + K\tan\phi\sin 2\beta \tag{2-42}$$

Jahanbakhshzadeh et al. (2017) solution

Jahanbakhshzadeh et al. (2017) studied the effect of stope geometry and backfill properties on the value of K and stresses in inclined backfilled stopes. Based on the Marston theory, they proposed the following equation to calculate the stresses in inclined stopes:

$$\sigma_{vh} = \frac{\gamma B(\sin\beta)}{2K_\beta\tan\phi}\left(1-\exp\left(-\frac{2K_\beta\tan\phi}{B(\sin\beta)}\times h\right)\right) \tag{2-43}$$

$$\sigma_{hh} = K_\beta\sigma_{vh} \tag{2-44}$$

where γ (kN/m^3) is the backfill unit weight; B (m) is the stope width; h is the depth of calculation point; β is the inclination angle of the stope walls; ϕ (°) is the internal friction angle of backfill; K_β is the earth pressure coefficient in the inclined stope, expressed as follows.

$$K_\beta = K_a \times \left(\left(1+\cos\beta\right) - \left[\frac{h}{H} \tan\phi \cos^2\beta \right] \right) \times \left(1+3\times\left(1-\frac{l}{B}\right)^4 \times \tan\phi \cos(\beta - 10°) \right) \quad (2\text{-}45)$$

where l is the horizontal distance of the calculation point from the hanging wall.

Jahanbakhshzadeh et al. (2018b) solution

Based on the 3D arching solution for vertical backfilled stopes (Li et al. 2005), Jahanbakhshzadeh et al. (2018b) extended their 2D solution to 3D by considering the effect of the stope wall inclination as follows:

$$\sigma_{zz} = \frac{\gamma \sin\beta}{2(B^{-1}+L^{-1})K_\beta \tan\phi} \times \left\{ 1 - \exp\left[-\frac{2(B^{-1}+L^{-1})K_\beta \tan\phi}{\sin\beta} h \right] \right\} \quad (2\text{-}46)$$

$$K_\beta = K_a \left[1+3\tan\phi\cos(\beta-10°) \times \left(1-\frac{r}{B}\right)^4 \right] \times \left[(1+\cos\beta) - \left(\frac{h}{H} \tan\phi \cos^2\beta \right) \right] \quad (2\text{-}47)$$

where γ (kN/m^3) is the backfill unit weight; B (m) and L (m) are the width and length of the opening; β (°) is the inclination angle of the wall; ϕ (°) is the internal friction angle of backfill; h (m) is the depth of the calculation point from the top surface; r (m) is the horizontal distance from the HW.

Considering the effect of pore water pressure

In the previous studies (except Blight 1981 solution), the backfills were all assumed to be dry without any pore water pressure in the backfill. However, hydraulic and paste backfills usually contain large amount of water. When the backfill is retained by an impervious barricade, the final PWP will be hydrostatic pressure at the fully drained and consolidated state. This is the case considered by the three solutions presented below.

Li and Aubertin (2009a) solution

Li and Aubertin (2009a) considered a hydrostatic water pressure within the backfill and proposed analytical solutions to evaluate the vertical and horizontal stresses in submerged or partially submerged backfilled stopes. Fig. 2-38 shows a vertical backfilled stope with partially submerged backfill. On the figure, B (m) is the stope width, H_m (m) is the thickness of the wet backfill above the water surface; H_b (m) is the total backfill height; H_w (m) is the height of water within the

backfill; ϕ (°) and ϕ' (°) are the friction angle and effective friction angle of the wet backfill and saturated backfill, respectively; γ_m and γ_{sat} (kN/m^3) are the unit weight and saturated unit weight of the backfill, respectively.

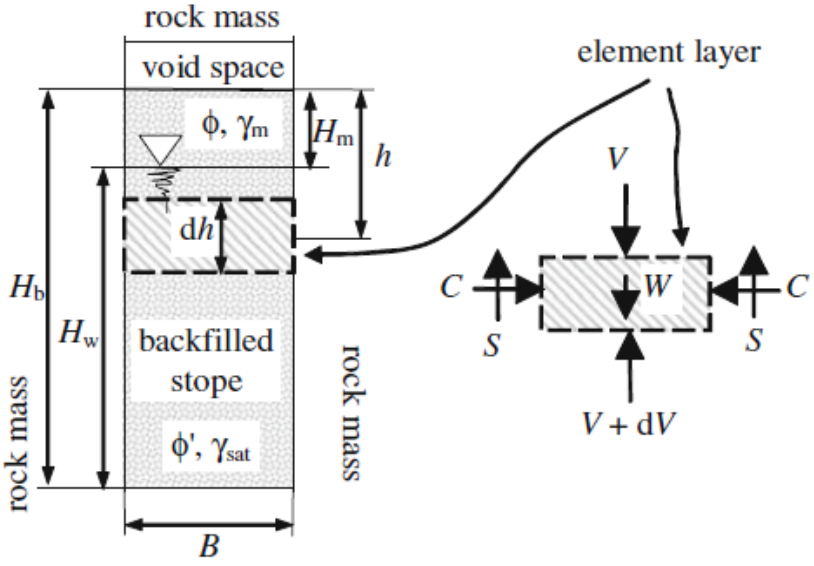

Figure 2-38: Partially submerged backfill in a vertical backfilled stope (take from Li and Aubertin 2009a)

The stresses above the phreatic table have been given by Aubertin et al. (2003). The total vertical and horizontal stresses in the saturated backfill can be expressed as follows (Li and Aubertin 2009a):

$$\sigma_v = \frac{B\gamma_{sub}}{2K_s \tan\phi'}\left[1-\exp\left(-\frac{2K_s(h-H_m)}{B}\tan\phi'\right)\right] + \frac{\gamma_m B}{2K\tan\phi}\left[1-\exp\left(-\frac{2KH_m}{B}\tan\phi\right)\right]\times\exp\left(-\frac{2K_s(h-H_m)}{B}\tan\phi'\right)+\gamma_w(h-H_m) \quad (2\text{-}48)$$

$$\sigma_h = K_s\sigma_v' + \gamma_w(h-H_m) \quad (2\text{-}49)$$

where h is the position below the backfill surface; K_s is the earth pressure coefficient.

Li and Aubertin (2009b) solution

Li and Aubertin (2009b) also took into account the pore water pressure within the backfill in three-dimensional analytical solutions. Fig. 2-39 shows a submerged vertical backfilled stope and an

isolated layer element, the uniform surface load p_0 (kN) is applied on the backfill surface. H_b and H_m (m) are the total backfill height and wet backfill height, respectively; B and L (m) are the width and length of the stope, respectively.

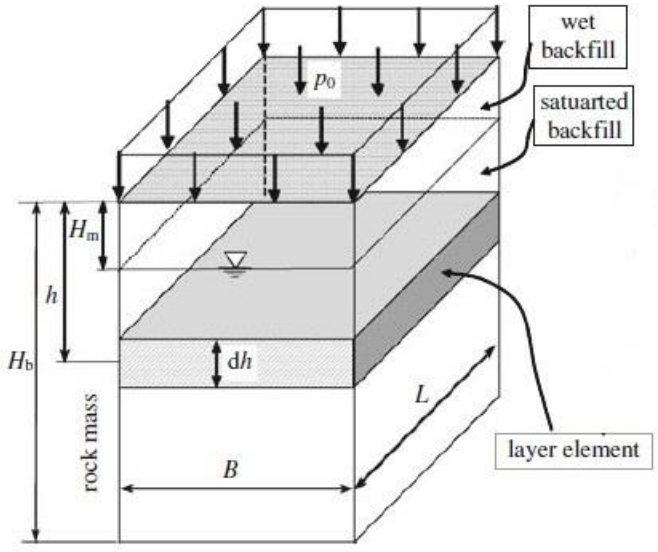

Figure 2-39: Schematic diagram of a vertical backfilled opening (taken from Li and Aubertin 2009b)

For the backfill below the water level ($h > H_m$), the vertical total stress can be obtained as (Li and Aubertin 2009b):

$$\sigma_{vh} = \frac{\gamma_m - 2c_m(\lambda_{1m}B^{-1} + \lambda_{2m}L^{-1})}{M_m} \times \{1 - \exp(-H_m M_m)\} \exp[(H_m - h)M_{sat}] + \frac{\gamma_{sub} - 2c_{sat}(\lambda_{1sat}B^{-1} + \lambda_{2sat}L^{-1})}{M_{sat}} \times \{1 - \exp[(H_m - h)M_{sat}]\} + p_0 \exp[(H_m - h)M_{sat} - H_m M_m] + \gamma_w(h - H_m) \quad (2\text{-}50)$$

$$M_{sat} = 2(K_{1sat}B^{-1} + K_{2sat}L^{-1}) \tan\delta_{sat} \quad (2\text{-}51)$$

$$M_m = 2(K_{1m}B^{-1} + K_{2m}L^{-1}) \tan\delta_m \quad (2\text{-}52)$$

$$\lambda_{1m} = 1 + 2\tan\alpha_{1m} \tan\delta_m \quad (2\text{-}53)$$

$$\lambda_{2m} = 1 + 2\tan\alpha_{2m} \tan\delta_m \quad (2\text{-}54)$$

$$\lambda_{1sat} = 1 + 2\tan\alpha_{1sat}\tan\delta_{sat} \tag{2-55}$$

$$\lambda_{2sat} = 1 + 2\tan\alpha_{2sat}\tan\delta_{sat} \tag{2-56}$$

where γ_m (kN/m^3) is the unit weight of the wet backfill; c_m (kPa) is the cohesion of the backfill; α_{im} and α_{isat} (°) are the fill state angle for the moist backfill and saturated backfill; δ_{im} and δ_{sat} (°) are the frictional angle between moist fill/saturated fill and rock walls, respectively; K_{im} and K_{isat} are the reaction coefficient for moist backfill and saturated fill, respectively.

Li and Aubertin (2010) solution

Li and Aubertin (2010) proposed the following more representative analytical solutions to evaluate the stresses in submerged or partially submerged backfilled stopes by considering the combined effects of non-uniform stress distribution and pore water pressure.

$$\sigma'_{v0} = \frac{\gamma_{sub}B}{K_{sat}\tan\delta_{sat}}\left\{1-\exp\left[\frac{K_{sat}(\langle H_m\rangle - h)}{B(1-DF_{sat}/4)}\tan\delta_{sat}\right]\right\} + \frac{\gamma_m B}{K_m\tan\delta_m}\left\{1-\exp\left[-\frac{K_m\langle H_m\rangle}{B(1-DF_m/4)}\tan\delta_m\right]\right\}\times\exp\left[\frac{K_{sat}(\langle H_m\rangle - h)}{B(1-DF_{sat}/4)}\tan\delta_{sat}\right] \tag{2-57}$$

$$\sigma'_{vx} = \sigma'_{v0}\left\{1-DF_{sat}\left(\frac{|x|}{B}\right)^3\right\} \tag{2-58}$$

$$DF_{sat} = \frac{2^{-\lambda}}{\tan^{0.1}(50°+\phi_{sat})} \qquad DF_m = \frac{2^{-\lambda}}{\tan^{0.1}(50°+\phi_m)} \qquad \lambda = 2+\frac{H_b}{100B} \tag{2-59}$$

$$\sigma_{vx} = \sigma'_{vx} + \gamma_w(h - H_m) \tag{2-60}$$

$$\sigma'_h = K_{sat}\sigma'_{v0} \tag{2-61}$$

$$\sigma_h = \sigma'_h + \gamma_w(h - H_m) \tag{2-62}$$

$$K_{sat} = \tan^2(45° - \phi_{sat}/2) \qquad K_m = (1-\sin\phi_m)/(1+\sin\phi_m) \tag{2-63}$$

where σ'_{v0} (kPa) is the effective vertical stress at the VCL of the stope; γ_m (kN/m^3) is the unit weight of the wet backfill; γ_{sub} (kN/m^3) is the submerged unit weight of the backfill; γ_w (kN/m^3) is the unit

weight of water; B (m) is the width of the stope; K_{sat} and K_m are the active reaction coefficient of the saturated and wet backfill, respectively; δ_{sat} (°) and δ_m (°) are the friction angle along the interface between the rock mass and saturated and wet backfill, respectively; H_b is the total height of the backfill; H_m is the height of the wet backfill; h (m) is the depth of the backfill from the top surface; ϕ_{sat} and ϕ_m are the internal friction angle of the saturated and wet backfill; x (m) is the distance from the VCL of the stope.

Horizontal stress on barricade

The stability of barricades is mainly dependent on the horizontal total stresses acted on it by the backfill in the drift. When the backfill is in fully drained and consolidated conditions (i.e. dry or in hydrostatic equilibrium state), arching can take place in the stope and in the drift. The existing solutions are summarized in the following subsection.

Mitchell et al. (1975) solution

Mitchell et al. (1975) considered the overburden solution and proposed the following equation to calculate the horizontal pressure σ_h on bulkhead in a hydraulic filled stope:

$$\sigma_h = K_0 H \gamma_t \tag{2-64}$$

where γ_t (kN/m^3) is the total unit weight of fill; H (m) is the backfill height above the bulkhead; K_0 is the horizontal at-rest pressure coefficient.

Mitchell et al. (1975) also conducted in situ measurement of the bulkhead pressure in a hydraulic filled stope and compared the measured results with pressure calculated from Eq. (2-64). The results indicate that the measured pressures at both footwall and hanging wall bulkhead are significantly lower than those calculated by Eq. (2-64). They attributed this to that Eq. (2-64) neglected the strength gain in the fill and arching in the drift opening.

Mitchell and coworkers (1982; 1984) solutions

Smith and Mitchell (1982) and Mitchell and Roettger (1984) proposed an empirical equation to evaluate the horizontal stress (σ_h) on barricade by considering the stress transfer between the backfill and rock walls:

$$\sigma_h = 0.4\gamma H\left(1 - 0.6\frac{l}{W_d}\right) \tag{2-65}$$

where γ (kN/m^3) is the unit weight of fill; H (m) is the height of backfill (Mitchell and Roettger 1984) or a range over which arching can occur (Smith and Mitchell 1982); l (m) is the distance between the bulkhead and the stope wall brow; W_d (m) is the drift width. However, this solution neglected the effect of barricade height.

With Eq. (2-65), Li and Aubertin (2009) proposed the following solution to evaluate the load on the barricade:

$$P = 0.2\gamma H^2(W_d - 0.6l) \quad H \le H_d \tag{2-66}$$

$$P = 0.2\gamma H_d^2(2H - H_d)(W_d - 0.6l) \quad H \ge H_d \tag{2-67}$$

where H_d (m) is the height of the access drift.

Li and Aubertin (2009c) solution

The previous solutions neglected the arching effect in the access drift, which may significantly influence the stress on barricade when the barricade is located far away from the stope brow. Li and Aubertin (2009c) thus proposed a new 3-D analytical solution by taking into account the arching effect in both the stope and access drift. Fig. 2-40 shows a vertical backfilled stope with an access drift. In the figure, H (m) is the backfill height, B (m) is the width of the stope, L (m) is the distance between the barricade and the wall at the other side of the stope, l (m) is the distance between the vertical layer element and the stope entrance.

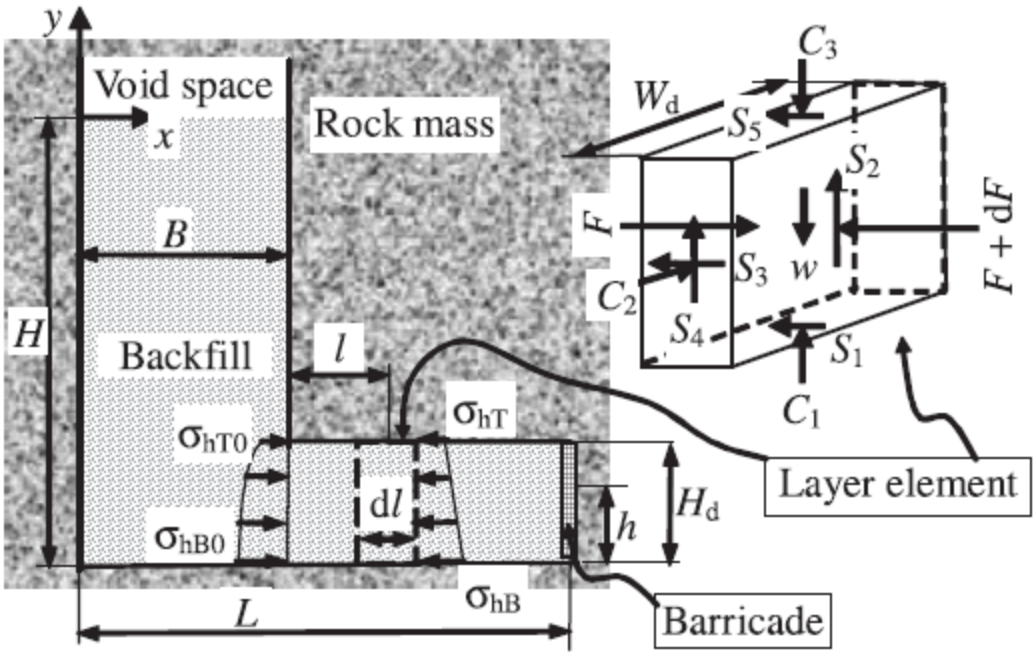

Figure 2-40: Schematic diagram of a vertical backfilled stope (without water) with its access drift and an isolated layer element (taken from Li and Aubertin 2009c).

The horizontal stress σ_h on the barricade at an elevation h from the base of the access drift can be expressed as:

$$\sigma_h = \left[\frac{h}{H_d}\sigma_{hT0} + \left(1-\frac{h}{H_d}\right)\sigma_{hB0}\right]\exp\left[-l\frac{2\tan\delta}{K_{dl}}\left(\frac{1}{H_d}+\frac{K_{dt}}{W_d}\right)\right] \tag{2-68}$$

where K_{dl} and K_{dt} are the earth pressure coefficient in the longitudinal direction of the drift axis l and transverse direction of the drift width W_d; δ (°) is the fill-wall interface frictional angle; σ_{hT0} and σ_{hB0} (kPa) are the horizontal stresses at the top and bottom of the access drift at the stope entrance, respectively, which can be expressed as:

$$\sigma_{hT0} = \frac{\gamma}{M}\{1-\exp[-K_s M(H-H_d)]\} \tag{2-69}$$

$$\sigma_{hB0} = \frac{\gamma}{M}[1-\exp(-K_s MH)] \tag{2-70}$$

Parametric sensitivity analysis with the proposed solution show that the effective and total stresses on barricade can be significantly influenced by the backfill properties, stope geometry and distance between the barricade and stope brow. The horizontal pressure on barricade tends to increase with

the decrease of distance between the barricade and stope brow. The increase of the internal friction angle of backfill and decrease of the drift width and height will decrease the effective and total stresses in the access drift and on barricade.

Li and Aubertin (2009d) solution

Li and Aubertin (2009d) also extended Li and Aubertin (2009c) solution to evaluate the pressure on barricade by taking into account the effect of pore water pressure for backfill in the submerged condition. Fig. 2-41 shows a vertical backfilled stope in a submerged condition. On the figure, p_0 (kPa) is the uniform pressure applied on the backfill, H_b (m) is the total backfill height, B (m) is the stope width, H_m and H_w (m) are the backfill thickness above the water table and below the water table, respectively, H_d (m) is the height of the access drift, ϕ_m (°) and γ_m (kPa) are the friction angle and unit weight for the wet backfill, while ϕ_{sat} (°) and γ_{sat} (kPa) are friction angle and unit weight for the saturated backfill, respectively.

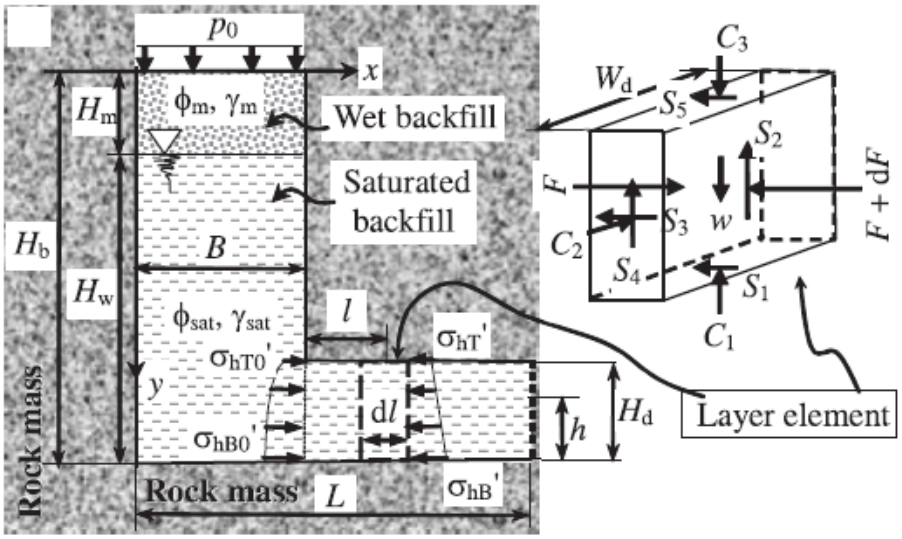

Figure 2-41: Schematic diagram of a vertical backfilled stope in submerged condition and access drift with an isolated vertical layer element (taken from Li and Aubertin 2009d).

The effective and total horizontal stresses along the axis direction of the access drift at an elevation h were given as follows (Li and Aubertin 2009d):

$$\sigma_h' = \left[\frac{h}{H_d}\sigma_{hT0}' + \left(1-\frac{h}{H_d}\right)\sigma_{hB0}'\right]\exp\left[-l\frac{2\tan\delta_{sat}}{K_{dl}}\left(\frac{1}{H_d}+\frac{K_{dt}}{W_d}\right)\right] \quad (2\text{-}71)$$

$$\sigma_h = \sigma_h^{'} + \gamma_w (H_w - h) \tag{2-72}$$

where σ'_{hT0} (kPa) and σ'_{hB0} (kPa) are the effective stresses at the top and bottom of the access drift at the stope entrance; K_{dl} and K_{dt} are the earth pressure coefficients in the longitudinal direction of the axis l and transverse direction of width axis W_d of the drift, respectively.

Li and Aubertin (2009d) also conducted parametric sensitivity analysis with the proposed solution. The results show that the stress in the access drift reduces with decreased friction angle of the backfill while increases with increased width and/or height of the drift.

2.3.3 Earth pressure coefficient

The application of the above-mentioned arching solutions to evaluate the stresses in backfilled stopes can be significantly influenced by the value of earth pressure coefficient K. The earth pressure coefficient was initially proposed in soil mechanics to evaluate the stresses on retaining walls. The value of K is related to the horizontal movement of the retaining wall. When the retaining wall remains static, the retained soil can be considered in an at-rest state and the earth pressure coefficient can be expressed as the Jaky at-rest earth pressure coefficient (Jaky 1948):

$$K_0 = 1 - \sin\phi \tag{2-73}$$

When the pressure on the retaining wall applied by the retained soil is not large enough, the retained soil tends to expand, resulting in the reduction of the horizontal stress. As the horizontal stress reduces to a certain degree, the retained soil can reach an active state and the earth pressure coefficient can be expressed as the Rankine active earth pressure coefficient as follows (CGS 2006; Das 2010):

$$K_a = \frac{1-\sin\phi}{1+\sin\phi} = \tan^2(45 - \frac{\phi}{2}) \tag{2-74}$$

As mine stope walls are very stiff, some researchers suggested to use the Jaky at-rest earth pressure coefficient for the placed backfill. For instance, Pirapakaran and Sivakugan (2007a) proposed 3D analytical solutions for square and circular stopes. Their results revealed that the vertical normal stresses along the center line of the circular and square stopes calculated by the proposed analytical solutions using K_0 correlated well with the numerical results obtained by FLAC. Fahey et al. (2009) conducted numerical simulations to study the stresses in backfilled stopes by using Plaxis 2D. For

the case of axisymmetric and plan-strain stopes filled with dry backfill, their results showed that the earth pressure coefficient along the height of the stope does not fully agreed with the at-rest earth pressure coefficient K_0 calculated by $K_0 = \nu/(1 - \nu)$ or $K_0 = 1 - \sin\phi'$ (where ν is the Poisson's ratio and ϕ' is the internal friction angle of the backfill). However, the value of K is closer to K_0 than to K_a.

However, some researchers suggested to use Rankine earth pressure coefficient for vertical backfilled stopes based on the numerical simulations and indirect experimental results. For instance, the numerical modellings performed by Li et al. (2003) with FLAC show that the vertical and horizontal stresses agreed well with that predicted by Marston's arching solution using K_0 near the wall while using K_a along the vertical central line. Li et al. (2005) also proposed a 3D analytical solution and compared the analytical results with the centrifuge test results of Take and Valsangkar (2001). The results show that the horizontal stresses on the walls correlated well with the proposed 3D analytical results using Rankine active earth pressure coefficient K_a. Ting et al. (2012) conducted laboratory tests in an inclined stope filled with dry backfill. The experimental results were compared with that obtained by numerical simulations performed with FLAC. Their results showed that the experimental results for the inclined stope correlated well with the numerical results when the Rankine active earth pressure coefficient K_a was used. Numerical simulations conducted by Sobhi et al. (2017) show that the value of K along the center line of a vertical backfilled stope is close to the Rankine active earth pressure coefficient K_a. They attributed the active state of the backfill to the occurrence of yielding during the placement. Yang et al. (2017) conducted numerical simulations to study the stress ratio in vertical backfilled stopes by considering the relationship between the Poisson's ratio (ν) and international friction angle (ϕ') of the backfill. Their results indicate that for backfill near the wall, the value of K is close to K_0 for related ν and ϕ' while depends on their respective values for unrelated ν and ϕ'. For backfill along the center line of the stope, the value of K_{ps} ($= \sigma'_3/\sigma'_1$) is near K_a when the value of ν and ϕ' satisfy the relationship ($\nu \leq (1-\sin\phi')$). Otherwise, the K_{ps} is close to K_0 calculated by Poisson's ratio ($K_0 = \nu/(1-\nu)$). Analytical and numerical studies performed by Yang et al. (2018) show that the earth pressure coefficient K along the VCL of a vertical backfilled opening is close to K_a when the Poisson's ratio or effective internal friction angle of the backfill are equal to or smaller than critical values; Otherwise, K is close to the at-rest earth pressure coefficient K_0.

The above-mentioned studies mainly focus on analytical and numerical studies. Experimental data is thus deemed necessary to validate the analytical and numerical results. The in situ measurements conducted by Thompson et al. (2012) show that the state of the backfill in the continuously poured stope is close to the active state in the lower portion while close to the at-rest state in the upper portion. For the backfill in the two-stage poured stope, the value of K is close to the at-rest state in the lower portion while is higher than the at-rest state (less than passive state) in the upper portion. They attributed the high value of K in the low portion of the two-stage poured stope to the cement hydration during the resting period. Zheng and Li (2018h) conducted column tests to measure the stresses and earth pressure coefficient in a vertical backfilled opening. To ensure the reliability of the experimental results, several methods have been examined in order to calibrate the stress sensors. It is found that lubricant materials are commonly used between the confining structure walls and backfill to reduce the friction (Zhu et al. 2009; Pedroni and Aubertin 2013; Gade and Dasaka 2018). To test the efficiency, a series of column backfilling tests and direct shear tests were conducted. The results showed that for the small scale laboratory tests, the commonly used lubricant materials are not efficient in reducing the friction along the interface between the backfill and walls. Some lubricant materials can even increase the friction due to the cohesion. More details are presented in Appendix B.

Regarding the earth pressure coefficient, the experimental results obtained by Zheng and Li (2018h) showed that the earth pressure coefficient calculated by the measured horizontal and vertical stresses is close to K_a along the center and close to K_0 near the wall. More details of the paper can be found in the article given in Appendix A.

2.4 Barricades to retain different types of backfills

For backfill in the form of slurry with high water content (e.g. hydraulic fill and paste fill), the barricade/bulkhead is required to be built at the base of the stope to retain the slurried backfill in place. There are mainly two types of retaining structure: barricade and bulkhead (Grice 1998; Potvin 2005). The former is made of high permeability materials such as porous brick or waste rock (Sivakugan et al. 2006a; Yumlu and Guresci 2007; Yang et al. 2016). The permeability of barricade is usually much higher than backfill to ensure a good drainage condition. Fig. 2-42(a) shows a typical barricade made of porous bricks with the hydraulic conductivity in the range of 0.1 to 0.3 cm/s (Rankine 2005). The latter usually refers to impermeable structure with high pressure

acting on the barricade (Grice 1998a; Potvin et al. 2005). Fig. 2-42(b) shows a bulkhead made of reinforced shotcrete. As the drainage condition for the bulkhead is poor, drainage pipes are usually installed to accelerate the drainage. The barricade and bulkhead are thus used interchangeably. They are all represented by barricade in this thesis.

Figure 2-42: The confining structure to retain the backfill: a) permeable barricade (Rankine 2005); b) impermeable bulkhead (taken from Revell 2007)

The barricade can fail if it is not properly designed or constructed. Fig. 2-43 shows a case of barricade failure (Revell and Sainsbury 2007). Other cases of barricade failure have been reported around the world in the past decades (Bloss and Chen 1998; Grice 1998a, 1998b, 2001; Sivakugan et al. 2006a, 2006b; Yumlu and Guresci 2007). The consequences are usually very serious. It is important to have a good evaluation of the pressure and stresses in backfilled stopes and on barricades to properly design the barricade.

Figure 2-43: A barricade failure (taken from Revell and Sainsbury 2007)

2.4.1 Barricades to retain dry or high hydraulic conductivity backfill

In Section 2.3, several analytical, numerical and experimental solutions have been presented by considering the backfill in fully drained and consolidated conditions. In other words, the backfill is dry or in hydraulic equilibrium state with a hydrostatic water pressure. The solutions are mostly valid for dry backfill or hydraulic backfill having a large hydraulic conductivity.

When the backfill is saturated and has a large hydraulic conductivity, the drainage and consolidation can take place quickly. An assumption can be made by considering the backfill in fully drained and consolidated condition during or shortly after the placement of the backfill. The solutions presented in Section 2.3 can be used to evaluate the pressure and stresses for the barricade design.

2.4.2 Barricades to retain low hydraulic conductivity backfill

When the backfill is saturated and has low permeability, the drainage and consolidation may take place slowly. The newly added backfill can continuously increase the stresses in the backfill until to the end of the deposition. The PWP, (excess) PWP and stresses increase to the maximum value during or shortly after the end of the filling operation. The most critical moments to be considered for the barricade design should thus be during or shortly after the filling operation.

When a slurried backfill is placed in a mine stope, two processes can take place simultaneously. The first one is the generation and dissipation of excess PWP, which is called self-weight consolidation (Fahey et al. 2010; Pedroni 2013; Shahsavari and Grabinsky 2014, 2015; Zheng et al. 2018a, 2018b). The dissipation of excess PWP leads to the generation of effective stress and shear strength along the fill-wall contact interfaces, which in turn can reduce the stresses in the backfilled stope and on the barricades. This is known as arching effect. The two processes can significantly influence the stresses in backfilled stopes and pressures on barricades. However, they have never been simultaneously considered in the previous studies. Zheng et al. (2018e, 2018f) have proposed some solutions to evaluate the stresses in backfilled stopes by considering the combined effects of self-weight consolidation and arching when the barricade is impervious (Chapter 7) or pervious (Chapter 8).

Finally, it should be mentioned that many works have been published on the self-desiccation of cemented backfill. For example, Wood et al. (2016) proposed a solution to evaluate the excess

PWP in the CPB during the deposition by considering the combined effects of self-weight consolidation and cement hydration (volume shrinkage). The effects of time dependent volume shrinkage were incorporated into the Gibson (1958) model. Fig. 2-44 shows the distribution and evolution of the excess PWP by considering respectively the effect of shrinkage, the effect of consolidation and the combined effects of consolidation and shrinkage during the deposition. The results showed that shrinkage has effect to generate negative pore water pressure in the backfill. The combined effects of shrinkage and self-weight consolidation thus leads to lower pore water pressure than considering only the effect of self-weight consolidation.

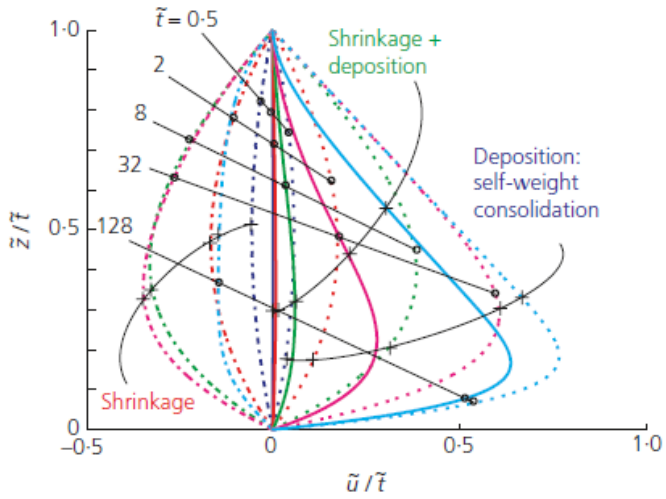

Figure 2-44: Evolution and variation of pore water pressure for three cases: considering only consolidation (represented by dotted lines), only shrinkage (represented by chain dotted lines), and combined effects of consolidation and shrinkage (represented by solid lines) (taken from Wood et al. 2016)

As previously indicated, the most critical moment for the barricade stability and design is during or shortly after the end of the deposition. When the cement content of the backfill is high, the cementation and shrinkage may take place quickly, especially when the filling rate is low. The negligence of the shrinkage may lead to overly conservative barricade design. In Canada and many countries elsewhere, depending on the mining method and purpose of the backfill, the cement content is usually low, typically between 2 to 8% (Belem et al. 2016). The effect of cementation or self-desiccation of the cemented backfill can be non-significant (Kazambua Beya 2016). It is conservative to neglect the effect of the cementation and self-desiccation of the cemented backfill in the barricade design.

CHAPTER 3 ARTICLE 1: AN ANALYTICAL SOLUTION OF GIBSON'S MODEL FOR ESTIMATING THE PORE WATER PRESSURES IN ACCRETING DEPOSITION OF SLURRIED MATERIAL UNDER ONE-DIMENSIONAL SELF-WEIGHT CONSOLIDATION. PART I: PERVIOUS BASE

Jian Zheng, Li Li, Mamert Mbonimpa and Thomas Pabst

Article published in Indian Geotechnical Journal, 2018, 48(1): 72-83.

Abstract: Every year, mines produce a large amount of tailings that must properly be managed. For most cases, the tailings are sent by pipes and disposed of in tailings dams. Another more and more common practice is to send a part of the tailings with or without cement binder to underground to fill mine voids (stopes). In civil engineering, a similar practice is the deposition of dredged sludge pumped and confined in a containment structure (dam for most cases). In these cases, an important challenge is to determine the pore water pressure (PWP) associated with the self-weight consolidation of the slurried backfill disposed layer by layer. A solution to the self-weight consolidation of accreting (increase in thickness) deposition of slurried material was first proposed by Gibson in 1958. Recently, it has been revisited and applied to mine stopes backfilled with slurried materials. The solution can only be evaluated numerically. In this paper, a truly analytical solution is proposed that is based on the Gibson approach and can be readily used to manually calculate the variation and evolution of the PWP within accreting deposition. The effect of the filling rate, fill height and backfill properties on the variation and evolution of the PWP is analyzed. The solution is proposed for accreting deposition of slurried backfill placed on pervious base. An analytical solution for estimating the PWP within slurried backfill disposed on impervious base is presented in a companion paper.

Keywords: Tailings dam; Backfilled stope; Dredged sludge; Self-weight consolidation; Gibson's solution; Analytical solution; Pore water pressure (PWP); Pervious base

3.1 Introduction

Every day and every year, mines produce a large amount of solid wastes in terms of waste rock and tailings that need to be adequately managed. For most cases, the tailings are sent by pipes,

poured in a storage area, and confined by dams, resulting in a tailings impoundment [Fig. 3-1(a)]. Another more and more common practice is to return a part of the tailings (with or without cement binder) underground to fill mine voids (stopes; in Fig. 3-1(b)). Similarly, in civil engineering, dredged sludge extracted from sea or river beds during maintenance need to be confined in a dam and properly managed. A common point between these cases is the continuous increase in the thickness (or height) of the deposition, commonly called accreting deposition of slurried materials (Gibson 1958; Fox 2000). A key issue for this problem is to determine the pore water pressure (PWP) associated with the self-weight consolidation of the slurried backfill having a low permeability.

Upon placement in a dam or a stope, the (grains) solids in the slurried material tend to settle down due to the gravity (i.e. self-weight). This moving tendency of the solids has effect to expel the water out of the backfill, while the out flow (drainage) is limited by the low permeability of the material, resulting in the generation of excess PWP in the backfill (Pedroni 2011; Li 2013; Li et al. 2013; El Mkadmi 2014). This phenomenon is called self-weight consolidation, which involves two processes associated with the dissipation of the excess PWP. When the slurried material remains in a state of slurry and the effective stress is zero (i.e. before grains come in contact), the dissipation of the excess pore water pressure is called sedimentation (Ahmed and Siddiqua 2014). Once the dissipation of the excess PWP is developed enough, the grain-grain contact begins. Effective stress begins to develop and the dissipation of the excess PWP is called self-weight consolidating (Been and Sills 1981; Pane and Schiffman 1985).

For tailings or dredged sludge dam, the knowledge of the PWP is closely related to the water and fill volume management (Aubertin and McKenna 2016). It is also a serious concern for the safety of the confining dams (Dobry and Alvarez 1967; Jeyapalan et al. 1983), especially for tailings dams constructed by upstream method (Vick 1990; Priscu 1999; Azam and Li 2010). For mine backfilled stopes, the knowledge of the PWP is closely related to the safety of barricades constructed at the base of stopes to retain the slurried backfill in place. In fact, several cases of barricade failure have been reported, resulting in serious undesirable consequences (Grice 1998; Sivakugan et al. 2006a, 2006b, 2013; Li and Aubertin 2009; Li and Aubertin 2011; Yang et al. 2016).

(a)  (b) 

Figure 3-1: Deposition of slurried material in a (a) tailings pond (photo taken by Li 2014 in one Québec mine) and (b) mine stope (photo taken by Li 2013 in another Québec mine)

The self-weight consolidation of the slurried material disposed layer by layer in tailings or dredged sludge dams and backfilled stopes is a complex process. The addition of new backfill layers lead to the generation and increase of excess PWP, while the dissipation of the excess PWP in previous layers can occur during the placement of new backfill layers. These indicate that a self-weight consolidating of accreting deposition involves simultaneously the dissipation (decrease) and generation (increase) of excess PWP with the continuous increase in the backfill thickness.

A solution to the self-weight consolidation of accreting deposition of slurried material was first proposed by Gibson (1958) for clayey soils. Recently, this solution has been revisited and applied to mine backfilled stopes to analyze the backfill consolidation during filling (Fahey et al. 2010; Doherty 2015; Shahsavari and Grabinsky 2014, 2015; Cui and Fall 2016). These works contributed to a better understanding of the pore water pressure evolution in the early stage of stopes backfilling. However, these existing solutions can only be evaluated numerically by qualified persons with the required numerical resources. This limits the practical application of these solutions.

In this paper, the Gibson (1958) approach is revisited for the case of a pervious base; the case of impervious base is presented in a companion paper (Part II). The equation of the Gibson (1958) solution is transformed into a form that can readily be calculated by commonly available computing tools, such as Excel®. The new solution can thus be considered as a truly analytical solution for estimating the variation and evolution of the PWP within an accreting deposition of slurried backfill in tailings or dredged sludge dams or backfilled stopes. The analytical solution is compared with

numerical results and applied to investigate the influence of filling rate, total fill height and material properties on the PWP variation and evolution.

3.2 Formulation of an analytical expression for the Gibson solution

Gibson (1958) investigated the one-dimensional self-weight consolidation problem of an accreting clayey layer. The governing equation is given as follows (Gibson 1958):

$$c_v \frac{\partial^2 p_w}{\partial z^2} = \frac{\partial p_w}{\partial t} - \gamma \frac{dh}{dt} \tag{3.1}$$

where p_w (kPa) is the PWP; γ (kN/m^3) is the unit weight of the backfill; c_v (m^2/h) is the consolidation coefficient; t (hour) is the filling time; z (m) is the elevation from the base of the sediment with the range of $0 \le z \le h$ (see Fig. 3-2); h (m) is the current thickness (height) of the backfill, which can be expressed as

$$h = mt \tag{3.2}$$

for fill deposition (in tailings or dredged sludge dam) or backfilling (in mine stopes) at a constant deposition or filling rate m (m/h).

Excess PWP is defined as the positive difference between the current PWP (when the water is in a transient state) and the final PWP (when the water reaches a steady-state). Two cases have been considered by Gibson et al. (1989):

1) When the water reaches an equilibrium state (no flux), the (final) PWP is equal to the hydrostatic pressure. The excess PWP is defined as the excess of the current PWP compared to the hydrostatic pressure. This corresponds to the traditional definition of excess PWP used in Terzaghi's consolidation theory (Holtz and Kovacs 1981).
2) When the water reaches a steady-state, the final PWP is different from the hydrostatic pressure. The excess PWP is defined as the excess of the current PWP compared to the final steady-state PWP (Lambe and Whitman 1969).

When the base of the accreting deposition is impervious, the hydrostatic pressure is considered as the reference. The first definition of the excess PWP should be applied and the hydrostatic pressure is not part of the excess PWP. This case is treated in a companion paper (Zheng et al. 2018).

In this study, the base is pervious, draining and imposed a zero PWP hydraulic boundary condition. The final level of the water table will lower to the base level and the final PWP will reduce to zero everywhere above the base when the water reaches a steady- state. The current total PWP is then always equal to the excess PWP. No more distinction is needed between the (current) total PWP and excess PWP through the remaining of the paper.

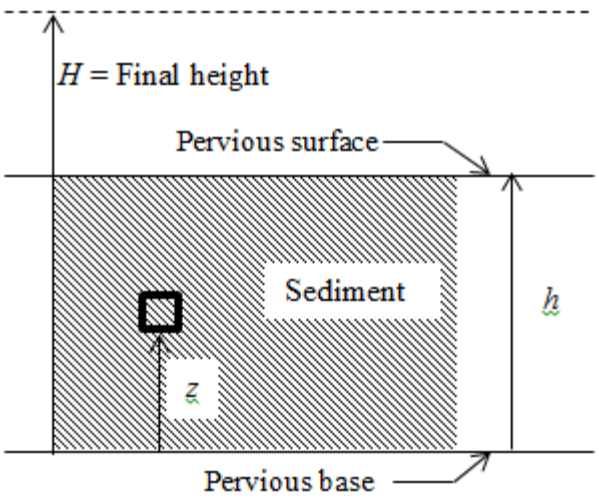

Figure 3-2: Model of Gibson (1958)

By considering both the top surface ($z = h$) and bottom ($z = 0$) of the sediment as pervious with zero PWP, the following equation has been given by Gibson (1958) to describe the variation (in space) and evolution (with time) of the PWP within the sediment:

$$p_w = -\gamma z\left(1+\frac{mz}{2c_v}\right)+\frac{\gamma m}{2c_v}(\pi c_v t)^{-\frac{1}{2}}\times\exp\left(-\frac{z^2}{4c_v t}\right) \times\int_0^{\infty}\xi^2\coth\left(\frac{m\xi}{2c_v}\right)\sinh\left(\frac{z\xi}{2c_v t}\right)\exp\left(-\frac{\xi^2}{4c_v t}\right)d\xi \quad (3.3)$$

where ξ (m) is an arbitrary integration variable, ranging from zero to infinity (∞).

As the Gibson (1958) solution [Eq. (3.3)] contains an integral that cannot be solved by hand calculations, it is not truly an analytical solution. The integral included in Eq. (3.3) has to be evaluated by numerical mean (Fahey et al. 2010; Shahsavari and Grabinsky 2014, 2015).

In order to obtain a truly analytical solution for evaluating the PWP within the sediment, the integral of Eq. (3.3) can be represented by a function as follows:

$$F(y)=\int_0^{\infty} f(y)\exp(-y^2)dy \tag{3.4}$$

where

$$f(y)=8(c_v t)^{3/2}\times y^2\times\coth\left(m\sqrt{\frac{t}{c_v}}y\right)\times\sinh\left(\frac{z}{\sqrt{c_v t}}y\right) \tag{3.5}$$

and,

$$y^2=\frac{\xi^2}{4c_v t} \tag{3.6}$$

As $f(y)$ is an even function, Eq. (3.4) can be re-written as

$$F(y)=\frac{1}{2}\int_{-\infty}^{\infty} f(y)\exp(-y^2)dy \tag{3.7}$$

This type of integral has been resolved with approximation by Goodwin (1949), who made the following transformation:

$$\int_{-\infty}^{\infty} f(y)\exp(-y^2)dy \approx h_0\sum_{n=-\infty}^{\infty}\left[f(nh_0)\exp(-n^2h_0^2)\right] \tag{3.8}$$

where h_0 (≤ 1) is the step interval of y, n is a series number varying from -∞ to +∞. Goodwin (1949) has shown that the sum of the series on the right side of Eq. (3.8) can be solved with high accuracy as long as the interval h_0 takes a value smaller than the unity.

Comparing Eqs. (3.7) and (3.8) leads to the following expression for $F(y)$

$$F(y)=4\left(h_0\sqrt{c_v t}\right)^3\sum_{n=-\infty}^{\infty}\left\{n^2\coth\left(mnh_0\sqrt{\frac{t}{c_v}}\right)\sinh\left(\frac{znh_0}{\sqrt{c_v t}}\right)\exp\left(-n^2h_0^2\right)\right\} \tag{3.9}$$

Substituting Eq. (3.9) into Eq. (3.3) leads to

$$\begin{aligned}p_w=&-\gamma z\left(1+\frac{mz}{2c_v}\right)+\frac{2\gamma mt}{\sqrt{\pi}}h_0^3\exp\left(-\frac{z^2}{4c_v t}\right)\\&\times\sum_{n=-\infty}^{\infty}\left\{n^2\coth\left(mnh_0\sqrt{\frac{t}{c_v}}\right)\sinh\left(\frac{znh_0}{\sqrt{c_v t}}\right)\exp\left(-n^2h_0^2\right)\right\}\end{aligned} \tag{3.10}$$

Similarly to the Terzaghi's consolidation theory, Gibson (1958) introduced the dimensionless time factor (T) as follows:

$$T = \frac{m^2 t}{c_v} = \frac{mh}{c_v} \tag{3.11}$$

Substituting time t of Eq. (3.10) by Eq. (3.11) leads to the following expression:

$$p_w = -\gamma z\left(1 + \frac{mz}{2c_v}\right) + \frac{2\gamma T c_v}{\sqrt{\pi} m} h_0^3 \exp\left(-\frac{z^2 m^2}{4Tc_v^2}\right) \times \sum_{n=-\infty}^{\infty} \left\{ n^2 \coth\left(nh_0\sqrt{T}\right) \sinh\left(\frac{zmnh_0}{c_v\sqrt{T}}\right) \exp\left(-n^2 h_0^2\right) \right\} \tag{3.12}$$

Eq. (3.12) can readily be solved by commonly available calculation means, such as Microsoft Excel®. It can thus be considered as a truly analytical solution for estimating the PWP within an accreting deposition of slurried backfill in tailings or dredged sludge dams or in mine stopes having a pervious base.

A sample calculation of PWP using Eq. (3.12) with Microsoft Excel® is presented in Appendix 1. The application of the proposed analytical solution [Eq. (3.12)] requires h_0 small enough and n large enough. Sensitivity analysis of h_0 and n should be made to ensure accurate and stable results. As shown in Appendix 2, the results tend to become stable and accurate enough when h_0 reduces to 0.5 and n ranges from -55 to 55.

3.3 Comparison with numerical results

As a first validation to the proposed analytical solution, the distribution and evolution of the PWP in a backfilled stope reported by Shahsavari and Grabinsky (2015) are compared with those calculated with the proposed analytical solution [Eq. (3.12)]. Shahsavari and Grabinsky (2015) considered a stope 1 m long and 1 m wide [Fig.3-3(a)] and a slurried backfill having a consolidation coefficient of c_v = 0.0864 m^2/h. The filling rate was m = 0.25 m/h. Figure 3-3(b) shows the distribution of the PWP from the base (z = 0) to the top (z = h) of the slurried deposition at different time of deposition (quantified by the dimensionless time factor $T = mh/c_v$), calculated with the proposed analytical solution [Eq. (3.12)] with h_0 = 0.5 and n = –55 to 55. Also plotted on the figure

are the PWP obtained by Shahsavari and Grabinsky (2015) through FLAC3D simulations. The agreements between the numerical and analytical solutions are excellent.

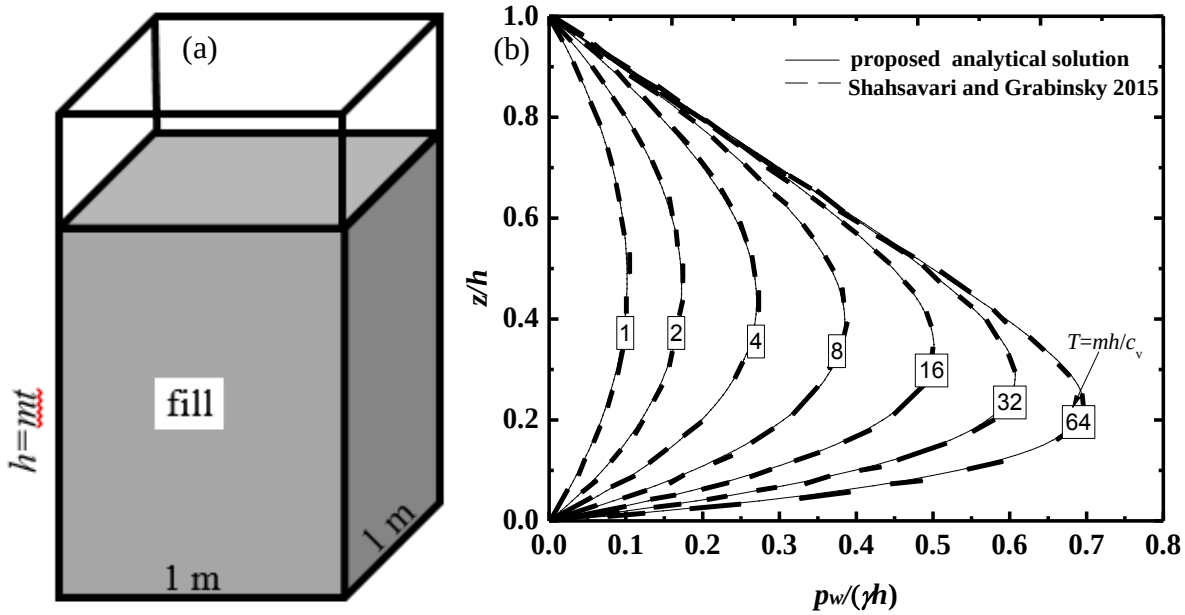

Figure 3-3: (a) a backfilled stope considered in the numerical model of Shahsavari and Grabinsky (2015); (b) comparisons between the PWP estimated by the proposed analytical solution [Eq. (3.12)] using h_0 = 0.5 and n = -55 to 55 and those obtained by Shahsavari and Grabinsky (2015) through FLAC3D simulations.

To further validate the proposed analytical solution, additional numerical simulations were performed using the 2D finite element code SIGMA/W (GEO-SLOPE 2008).

Fig. 3-4(a) shows the physical model of a stope to be filled with a slurried backfill. The stope has a width of 6 m and is filled to a height of H = 8 m for simulating a typical plug pour commonly used in backfilled stope (Li 2014). The slurried backfill is assumed to be linearly elastic with γ_{sat} = 20 kN/m^3 (unit weight), $M^{'}$ = 960 kPa (drained constrained modulus), μ = 0.2 (Poisson's ratio).

The drained Young's modulus, $E^{'}$ is defined as follows:

$$E^{'} = \frac{(1+\mu)(1-2\mu)M^{'}}{(1-\mu)} \tag{3.13}$$

The consolidation coefficient is given by

$$c_v = \frac{k \cdot M'}{\gamma_w} \tag{3.14}$$

where k (m/s) is the hydraulic conductivity (i.e. permeability coefficient), γ_w (kN/m^3) is the unit weight of water. In this study, two cases have been considered:

a) $k = 2.83\times10^{-7}$ m/s, $c_v = 0.1$ m^2/h (by applying [Eq. (3.14)], and $m = 0.2$ m/h.

b) $k = 2.83\times10^{-7}$ m/s, $c_v = 0.1$ m^2/h (by applying [Eq. (3.14)], and $m = 1.0$ m/h.

Fig. 3-4(b) shows a numerical model built with SIGMA/W for the physical model shown in Fig. 3-4(a). The two side walls are mechanically fixed in the horizontal direction and hydraulically impermeable. The bottom of the model is mechanically fixed in both the horizontal and vertical directions. After each layer deposition, the drainage is allowed through the top surface and the pervious base by imposing zero PWP across these two faces. The sensitivity analysis of meshing has been performed to find the optimal mesh for the numerical model. This resulted in quadrilateral and triangular mesh elements of 0.1 m.

In practice, the height of the backfill increases continuously with a rising rate, m. In numerical models, the continuous increase in backfill thickness can only be approximated by a series of instantaneous additions of backfill layers. If the thickness of each layer is dh, the time between the addition of two layers is dh/m. This difference in the numerical and physical models indicates that the layer thickness dh should be as small as possible to ensure that the numerical models represent well the continuous filling and increase in the backfill height.

Here, the backfilling of the stope was simulated by instantaneous additions of backfill of 0.1 m/layer. The numerical model required 80 additions of backfill layer to simulate a full filling of the total height of 8 m for the plug. With a filling rate of $m = 0.2$ m/h, the waiting time between the additions of two layers was 0.5 hours. When the filling rate was increased to $m = 1.0$ m/h, the time interval between two layers was reduced to 0.1 hours.

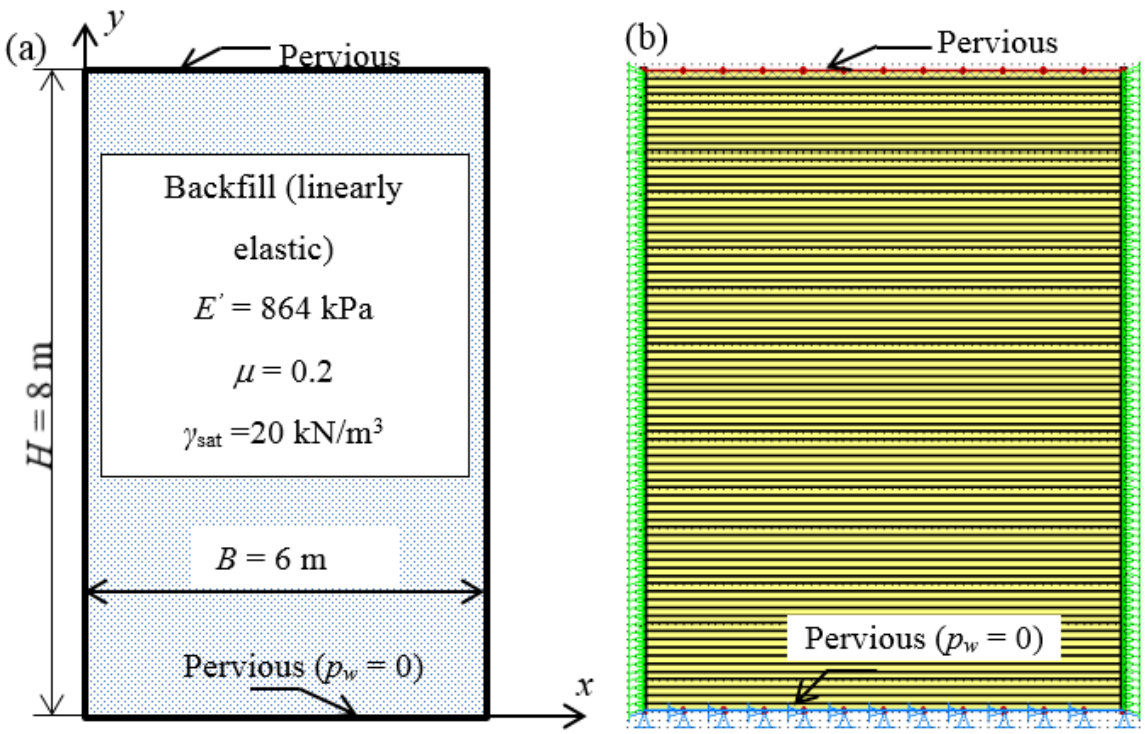

Figure 3-4: (a) A conceptual physical model of backfilled stope with the top and base as pervious and under zero PWP condition; (b) numerical model of (a) built by SIGMA/W.

Fig. 3-5 shows the distribution of the (excess) PWP at the end of the full filling of the plug 8 m high, obtained by the numerical modeling and calculated with the proposed analytical solution [Eq. (3.12)] for the two cases mentioned above. Despite the relatively large thickness of the numerical model (i.e. 0.1 m/layer), the (excess) PWP distributions predicted by the proposed analytical solution [Eq. (3.12)] agree well with those obtained by the numerical modeling. The proposed analytical solution is validated by the numerical modeling. It can be used to evaluate the (excess) PWP within an accreting deposition of slurried backfill on a pervious base.

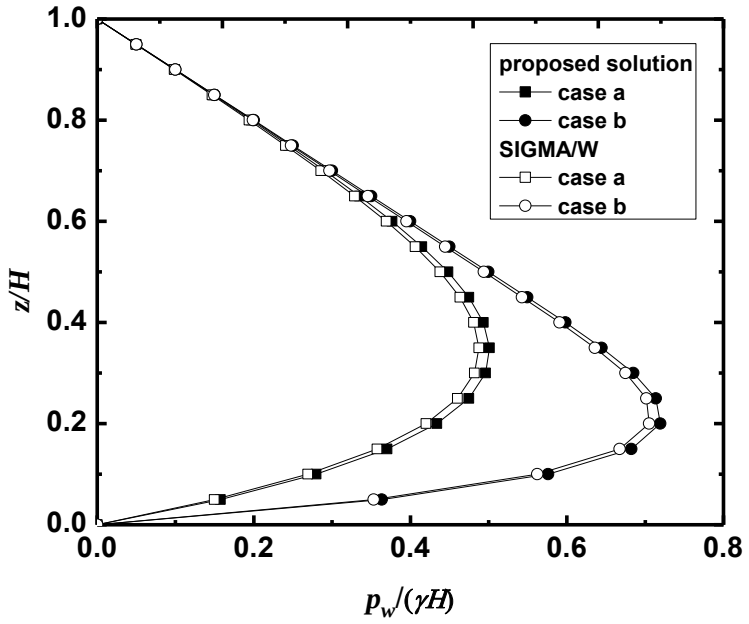

Figure 3-5: Distribution of the (excess) PWP obtained by numerical modeling and predicted by the analytical solution along the height of the backfill at the end of the full filling of the plug with different hydraulic properties and filling rate: (a) c_v = 0.1 m^2/h, m = 0.2 m/h; (b) c_v = 0.1 m^2/h and m = 1.0 m/h.

3.4 Sample applications

3.4.1 PWP estimation in tailings ponds

The proposed analytical solution [Eq. (3.12)] is used to evaluate the PWP in a tailings pond with different hydraulic properties (permeability or c_v) and rising rate. The final tailings height is H = 20 m and the filling rate varies between 4.8 and 9.6 m/yr (Seneviratne et al. 1996). The unit weight of the backfill γ_{sat} = 20 kN/m^3. The consolidation coefficient (c_v) of the backfill varies from 0.18 to 0.0018 m^2/h (Aubertin et al. 1996).

Fig. 3-6 shows the variation of the (excess) PWP distributions predicted by the analytical solution [Eq. (3.12)] at the end of the filling operation when the consolidation coefficient c_v varies from 0.18 to 0.0018 m^2/h. The filling rate and filling height were equal to 4.8 m/year and 20 m, respectively. The results show that an increase in the consolidation coefficient c_v lead to faster dissipation of the (excess) PWP. With a consolidation coefficient of 0.18 m^2/h, the (excess) PWP was almost completely dissipated at the end of the filling operation. When the c_v was reduced to

0.0018 m^2/h, the (excess) PWP at the end of the filling operation was largely dissipated near the base of the tailings pond, but remained close to the iso-geostatic pressure close to the top of the backfill. The maximum (excess) PWP increased to 135.4 kPa, compared to an almost zero (excess) PWP with c_v = 0.18 m^2/h.

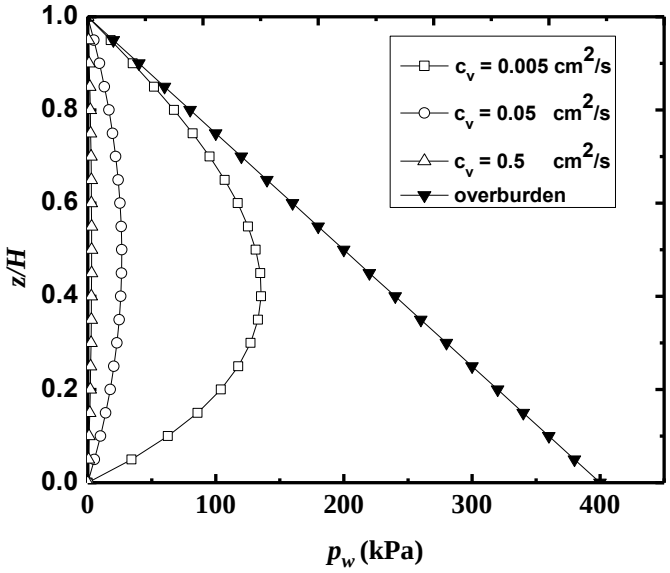

Figure 3-6: Variation of the (excess) PWP distribution with different c_v along the height of tailings pond at the end of the filling operation, calculated with the proposed analytical solution [Eq. (3.12)] by considering a tailings pond 20 m high realized at a filling rate m = 4.8 m/year.

Fig. 3-7 shows the variation of the (excess) PWP distributions predicted by the analytical solution [Eq. (3.12)] along the height of the tailings pond at the end of filling operation when the filling rate varies from 4.8 to 40 m/year. The filling height H and consolidation coefficient c_v were taken equal to 20 m and 0.018 m^2/h, respectively. A filling rate as high as 40 m/year is rare in practice; it is used here to better illustrate the effect on the dissipation and distribution of the (excess) PWP in the tailings ponds. The dissipation of the (excess) PWP slows down with faster filling, resulting in higher PWP in the tailings. These results indicate that a slow filling is preferred to avoid high PWP in the tailings. This can become particularly true with low permeability tailings.

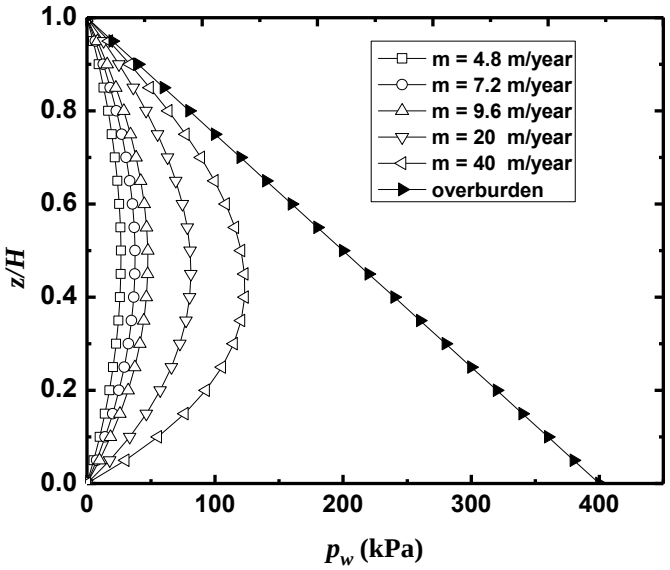

Figure 3-7: Variation of the (excess) PWP distribution predicted with the proposed analytical solution with different filling rates along the height of the tailing at the end of filling operation. Calculation made by considering a tailing height of 20 m and a consolidation coefficient c_v = 0.05 cm^2/s.

3.4.2 Sample application in mine backfilled stopes

As another sample application of the proposed analytical solution [Eq. (3.12)], the PWP within a backfilled stope is evaluated. A unit weight γ_{sat} = 20 kN/m^3 is used here for the backfill.

First, a backfill H = 8 m is considered, which corresponds to the thickness of plug pour that typically varies between 6 and 9 m and is typically 2 to 3 m higher than the drift (Thompson et al. 2009, 2012). The filling rate was taken as m = 0.2 m/h, a typical rate in mine operations (Thompson et al. 2012). Figure 8 shows the variation of the (excess) PWP distributions through the height of the plug pour at the end of the filling operation, calculated with the proposed analytical solution [Eq. (3.12)] as c_v increased from 0.01 to 1 m^2/h. The isostatic overburden pressure is also plotted on the figure. An increase in c_v significantly accelerates the dissipation of the (excess) PWP. When the mine backfill has a very low c_v (0.01 m^2/h), the PWP distribution is quite close to that based on the isostatic overburden solution along the whole height of the plug, except near the bottom of the stope where drainage and consolidation occur through the pervious base during the filling operation. This results in a maximum PWP of 125.3 kPa. When the backfill has a consolidation

coefficient c_v as high as 1 m^2/h, significant drainage and consolidation take place along the whole height of the plug during the filling operation, resulting in a maximum PWP of 23.4 kPa.

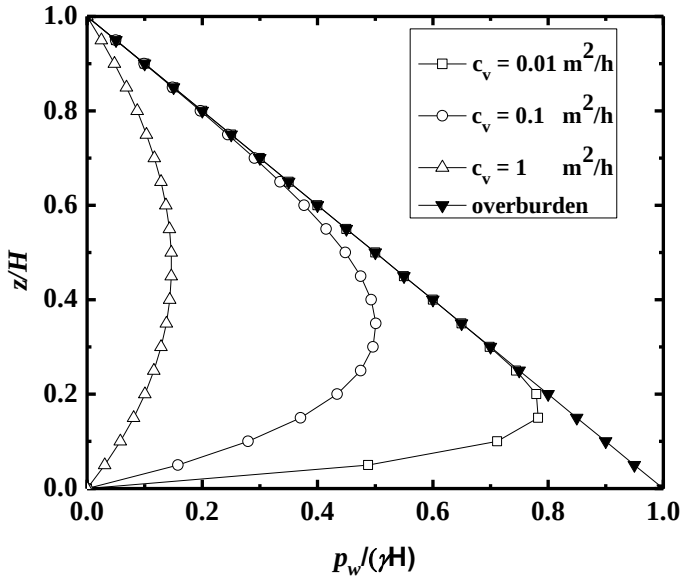

Figure 3-8: Variation of the (excess) PWP distribution with different c_v along the height of the plug at the end of the plug filling operation, calculated with the proposed analytical solution [Eq. (3.12)] by considering plug height of 8 m and a filling rate m = 0.2 m/h.

Fig. 3-9 shows the variation of the (excess) PWP distributions with different filling rates along the height of the plug at the end of the plug filling operation, calculated with the proposed analytical solution [Eq. (3.12)]. Again, a backfill 8 m high is considered in this sample calculation, while the consolidation coefficient was taken as c_v = 0.1 m^2/h. An increase in the filling rate slows down the dissipation of the (excess) PWP, resulting in peak PWP value of 61.6 kPa for m = 0.1 m/h, 101.7 kPa for m = 0.5 m/h, and 115.1 kPa for m = 1 m/h. These results indicate that high PWP can be limited by reducing the filling rate. These results also indicate that the application of the iso-geostatic overburden solution without any consideration of drainage and consolidation may largely overestimate the pressure and results in oversized (and uneconomic) barricade design. The overestimation is amplified with decreasing filling rates; this is the case with large mine stopes.

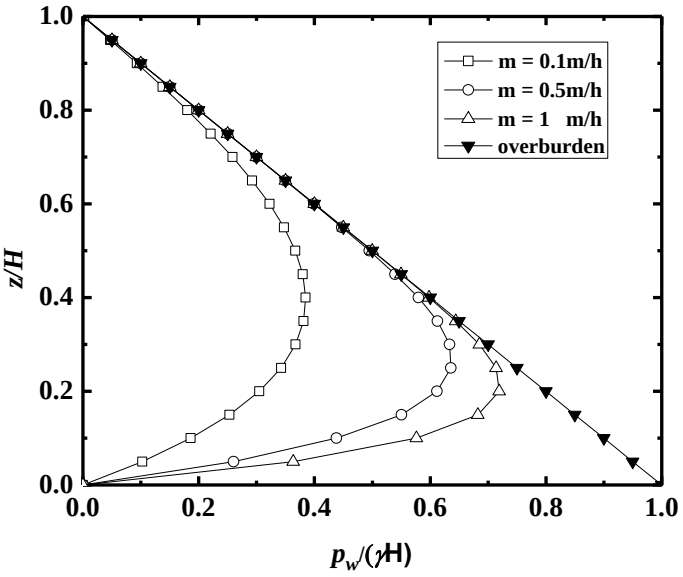

Figure 3-9: Variation of the (excess) PWP distribution with different filling rates along the height of the plug at the end of filling operation, calculated with the proposed analytical solution [Eq. (3.12)] by considering a plug height of 8 m and a consolidation coefficient c_v = 0.1 m^2/h.

Fig. 3-10 shows the variation of the (excess) PWP distributions with different backfill heights at the end of the backfilling operation, calculated with the proposed analytical solution [Eq. (3.12)] by considering a filling rate of m = 0.2 m/h and a consolidation coefficient of c_v = 0.1 m^2/h. The results show again that the drainage and consolidation occur during the stope backfilling operation, resulting in PWP smaller than the isostatic overburden pressure. For the given backfill and filling rate, higher backfill results in larger peak pressure with maximum PWP of 80.2 kPa for H = 8 m, 194.0 kPa for H = 16 m, and 444.3 kPa for H = 32 m, respectively. It is interesting to note that the position of the peak value of the (excess) PWP rises as the backfill height increases [Fig. 3-10(a)]. When the backfill height is 8 m, the peak PWP is located at an elevation of 2.8 m. The position of the peak PWP rises to an elevation of 4.8 m for a backfill height of 16 m and an elevation of 8.0 m for a backfill height of 32 m. With a typical access drift of 5 m in height, these results indicate that the peak PWP will apply near the mid-height of the barricade for a backfill height of 6 m and near the top level of the barricade for a backfill height of 24 m. If the barricade is not strong enough, the failure will be a horizontal movement in the former case and a top outside rotation for the latter case. It is also interesting to note that the normalized elevation of the peak PWP remains, however, relatively constant [Fig. 3-10(b)].

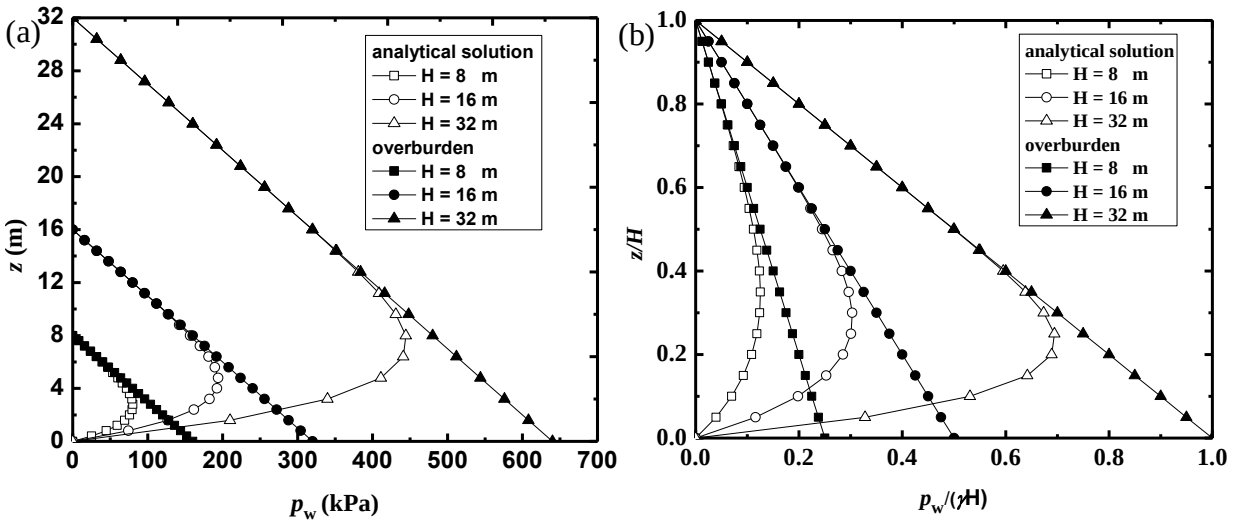

Figure 3-10: Variation of the (excess) PWP distribution as a function of the (a) elevation z and (b) normalized elevation z/H at the end of filling operation with different backfill height, calculated with the proposed analytical solution [Eq. (3.12)] by considering a filling rate of m = 0.2 m/h and a consolidation coefficient of c_v = 0.1 m^2/h.

3.5 Discussion

An analytical solution has been proposed to evaluate the PWP distribution and evolution within a slurried deposition confined in tailings or dredged sludge dams or mine stopes. The proposed analytical solution can readily be used for calculating the PWP within the slurried deposition. It constitutes a useful mean for parameter sensitivity analyses for tailings or dredged sludge dams and mine stope barricades design during the preliminary phase of the projects. It can particularly be useful for estimating the maximum height and filling rate allowed for continuous backfilling of a mine stope. It may also be used to estimate the sensitive zone on the barricade. However, as any other analytical solutions, the proposed analytical solution was developed based on several simplifying assumptions and contains some limitations.

For instance, using the same assumptions taken by Terzaghi (1943), the consolidation strain has been considered as small and the hydraulic properties (permeability, compressibility and consolidation coefficient) were considered as constant during the filling operation. A few experimental results seem to indicate that this is not the true behavior of mine backfills because the value of c_v can change with the self-weight consolidation (Fahey et al. 2010). More work is required

to take into account the large strain consolidation and variation of the hydraulic properties with time (Gibson et al. 1981; Cargill 1985; Feldkamp 1989; Morris 2002.

As indicated in the section “Introduction”, the self-weight consolidation of slurried material consists of two phases: sedimentation and consolidation. During the former process, excess pore water is being expelled but the particles remain in separate state and the effective stress is zero. Once the dissipation of excess water reaches a sufficient degree and the void ratio of the settled material reaches a critical value, the grain-grain contacts become effective. The consolidation process starts, and the effective stress become non-zero. In the Gibson (1958) model, the distinction of these two processes was not taken into account. This limitation is inherited by this study. More work on this aspect is ongoing and will be part of future publication.

Traditionally, excess PWP is usually defined as the part of the PWP higher than the hydrostatic water pressure, resulting from addition of overloading by construction or the moving tendency of the settling grains—i.e. “self-weight” consolidation. This is straightforward for the case of impervious base (Part II). In this study with a pervious and zero PWP base, a hydrostatic water pressure can also become excess PWP. Imagine the case where the backfill is initially on an impervious base and the water is in an equilibrium state. No excess PWP exists in the system. If the impervious base suddenly becomes pervious with zero PWP due to the adjacent lowering of water table by pumping or the creation of an underlying cavity, the water flow can readily be explained by the creation of hydraulic gradient. But the drainage and consolidation cannot be explained if the hydrostatic water pressure is not considered as excess PWP. In soil mechanics, the drainage and consolidation are inseparable with the dissipation of excess PWP (Holtz and Kovacs 1981). By applying the notion of Gibson et al. (1989), the hydrostatic water pressure is part of the excess PWP, the settlement of a saturated soft-soil after an underneath excavation or lowering of the water table by pumping can readily be explained by the drainage and consolidation associated with the dissipation of the excess PWP, even without any construction or self-weight consolidation. Subsequently, the excess PWP will be caused by the combined effects of moving tendency of the settling grains (i.e. self-weight consolidation) and hydrostatic water pressure in the case of accreting deposition of slurried material on a pervious zero PWP base.

Another limitation is related to the hydraulic boundary conditions in the conceptual model. The top surface of the backfill was assumed pervious under zero PWP. This condition is not totally

representative to the field condition, where decanted free water can be accumulated and forms water pond on the top surface of the backfill. To quantify the difference between the PWP distributions calculated with zero PWP and non-zero PWP boundary conditions along the top surface of the backfill, addition numerical simulations were performed with SIGMA/W. The filling rate was taken as 0.2 m/h and the permeability changed from 2.83×10^{-7} (case a) to 2.83×10^{-6} m/s (case b). The results shown in Fig. 11 indicate that the differences are not so significant in terms of peak maximum PWP. However, important differences are observed near the top part of the backfill. With non-zero PWP top boundary condition ($p_w \neq 0$), positive (water pond) or negative (suction) PWP can be developed on the top surface of the backfill, depending if the backfill has a low (case a, Fig. 3-11) or high (case b, Fig. 3-11) permeability. On the other hand, the pervious and zero PWP base can be considered reasonable for backfill placed in a mine stope with highly permeable barricade (usually called free draining (Li and Aubertin 2011; Yang et al. 2016)). It is however seldom the case with tailings or dredged sludge confined by dams due to their horizontal extension. More work is needed to take into account more representative boundary conditions with a pervious but non-zero PWP base.

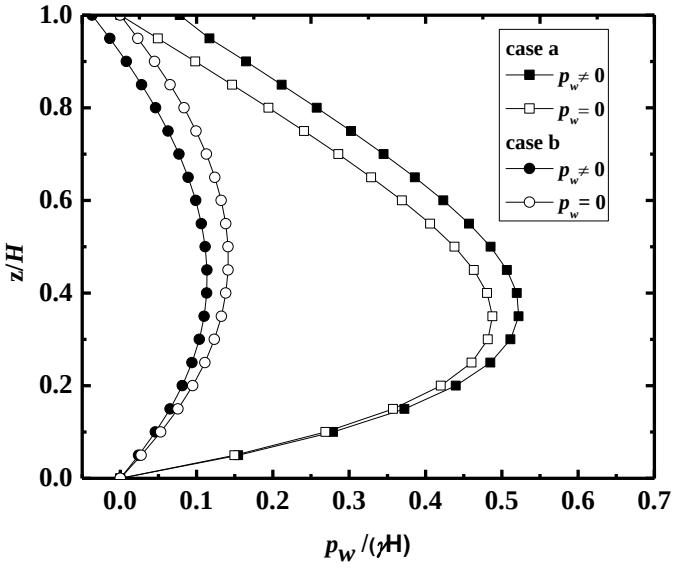

Figure 3-11: Variation and evolution of the PWP obtained by SIGMA/W with zero pressure (p_w=0) and non-zero PWP (p_w≠0) on the top of each new added layer backfill for case a: k = 2.83×10^{-7} m/s, m = 0.2 m/h and H = 8 m and case b: k = 2.83×10^{-6} m/s, m = 0.2 m/h and H = 8 m.

When the backfill has a high permeability, the drainage and consolidation during the filling operation may result in the development of effective stresses in the backfill. This may in turn lead to the development of arching effect in backfilled stopes (Li et al. 2005; Li and Aubertin 2009a, 2009b). The shear stresses developed along the fill-wall interfaces may have effect to prevent and slowdown the settlement of the backfill particles. Subsequently, neglecting the arching effect may overestimate the consolidation process.

Another limitation of the model is related to the unidimensional drainage and consolidation. This condition can be representative when the horizontal dimension of the slurried deposition is very large for the case of tailings dam or when the rock walls are impervious for the case of mine stopes. In practice, lateral drainage can take place in mine stopes through the horizontal drives and barricades placed at different height or when the rock walls of the stopes are fractured. For the case of tailings or dredged sludge dam, lateral drainage occurs when draining structures such as wick drains (Li 2014; Li and Yang 2015) or waste rock inclusions (James 2009; Bolduc and Aubertin 2014) are introduced to accelerate the drainage and consolidation of the slurried materials.

For mine stope filled with a cemented paste backfill, the effect of the cementation was not taken into consideration. Several researchers have shown that the cementation can be accompanied with volume shrinkage (Helinski et al. 2007; Wood et al. 2016), which may in turn affect the PWP in the backfill. In general, neglecting this aspect would lead to an overestimate of the (excess) PWP and conservative barricade design. On the other hand, the cementation of the cemented backfill can lead to reduction of hydraulic conductivity. This has effect to slow down the dissipation of the excess PWP and reduce the degree of the overestimation. More work is needed to take these two processes into account in the estimation of PWP within the backfill.

Finally, it should be noted that the PWP constitutes an important parameter in the stability and safety consideration of retaining structures such as tailings dams. For backfill barricades in mine stopes, the stability is controlled by the total stresses. Analytical solutions for estimating the total stresses within backfilled stopes and on barricades in access drifts have been given by Li and Aubertin (Li and Aubertin 2009c, 2009a, 2009b, 2009d) by considering hydrostatic water pressure. More work is needed and ongoing to develop analytical solutions that can be used to estimate the total stresses in backfilled stopes and on barricades by considering the drainage and consolidation of the accreting slurried backfill.

3.6 Conclusion

The understanding and estimation of the distribution and evolution of the (excess) PWP within a slurried material at the end of the deposition is essential for the stability and safety consideration of tailings or dredged sludge dams and mine backfill barricades. In this paper, a truly analytical solution has been proposed based on the Gibson (1958) model by considering a one dimensional self-weight consolidation with a pervious base. The proposed analytical solution can readily be solved by using commonly available computing means such as Excel®. It constitutes a useful tool for the design of tailings or dredged sludge dams and mine backfill barricades during the preliminary phase of projects. The proposed analytical solution has been validated against numerical modeling. It can thus be used to evaluate the distribution and evolution of the (excess) PWP in tailings or dredged sludge dams or in mine backfilled stopes. The results show that the consolidation coefficient, filling rate and backfill height can significantly influence the drainage and consolidation and the dissipation of the excess PWP. With high consolidation coefficient c_v, the self-weight consolidation can take place very fast, resulting in significantly reduced PWP in the backfill. The (excess) PWP in the slurried deposition can further be reduced by slow downing the filling rate or/and reducing the backfilling height. These results are particularly interesting for designing the maximum height allowed in continuous backfilling. Nevertheless, one should keep in mind that the proposed analytical solution has been developed based on several simplifying assumptions and contains some limitations.

Acknowledgements

The authors would like to acknowledge the financial support from the Natural Sciences and Engineering Research Council of Canada (NSERC 402318), Institut de recherche Robert-Sauvé en santé et en sécurité du travail (IRSST 2013-0029), Fonds de recherche du Québec—Nature et Technologies (FRQNT 2015-MI-191676, 2017-MI-202116), and industrial partners of the Research Institute on Mines and the Environment (RIME UQAT-Polytechnique; http://rime-irme.ca/).

3.7 Appendix I: Sample calculations of PWP distribution with Microsoft Excel®

Excel® of Microsoft is used to illustrate the application of the proposed analytical solution to estimate the PWP distribution and evolution in the backfill. The following geometry and material parameters are considered:

H = 8 m (pour height)

γ = 20 kN/m^3

c_v = 0.1 m^2/h

m = 0.2 m/h

Fig. 3-12 shows the detailed calculation considering h_0 = 0.5 and n ranging from -55 to 55. Beyond this range, the value of $f(y)$ becomes zero. In this illustrative calculation, the (excess) PWP at several points is calculated with z varying from 0.001 m to 8 m. It can be seen that the calculation is simple and easy to do with Excel®.

	A	B	C	D	E	F	G	H	T	U	V	W	X
1		h_0 =	0.5										
2		γ =	20	kN/m^3									
3		c_v =	0.1	m^2/h									
4		m =	0.2	m/h									
5		t =	40	h									
6		H =	8	m									
7		T=mH/c_v=	16										
8													
9													
10			$\frac{mnh_0}{c_v\sqrt{T}}$	z (m) =	0.001	0.005	0.01	0.1 ➡	6	6.5	7	7.5	8
11	n	$nh_0\sqrt{T}$			$f(y)$	$f(y)$	$f(y)$	$f(y)$	$f(y)$	$f(y)$	$f(y)$	$f(y)$	$f(y)$
12	-55	-110	-13.75		0	0	0	0	0	0	0	0	0
13	-54	-108	-13.5		0	0	0	0	5.5E-279	4.7E-276	4E-273	3.4E-270	2.9E-267
14	-53	-106	-13.25		3.9E-304	1.9E-303	3.9E-303	5.1E-302	4.9E-268	3.7E-265	2.8E-262	2.1E-259	1.6E-256
15	-52	-104	-13		9.2E-293	4.6E-292	9.2E-292	1.2E-290	2.6E-257	1.8E-254	1.2E-251	7.8E-249	5.2E-246
16	-51	-102	-12.75		1.3E-281	6.6E-281	1.3E-280	1.7E-279	8.7E-247	5.1E-244	3E-241	1.8E-238	1E-235
17	-50	-100	-12.5		1.2E-270	5.8E-270	1.2E-269	1.5E-268	1.7E-236	8.9E-234	4.6E-231	2.4E-228	1.2E-225
63	-5	-10	-1.25		6E-05	0.0003	0.0006	0.00605	43.6293	81.5102	152.281	284.499	531.514
64	-4	-8	-1		0.00029	0.00147	0.00293	0.02935	59.1121	97.4598	160.684	264.924	436.785
65	-3	-6	-0.75		0.00071	0.00356	0.00711	0.07121	42.6901	62.1177	90.3835	131.509	191.346
66	-2	-4	-0.5		0.00074	0.00368	0.00736	0.07366	14.7514	18.9597	24.3591	31.2889	40.1845
67	-1	-2	-0.25		0.0002	0.00101	0.00202	0.0202	1.72016	1.97179	2.25427	2.57201	2.93
68	0	0	0		0	0	0	0	0	0	0	0	0
69	1	2	0.25		0.0002	0.00101	0.00202	0.0202	1.72016	1.97179	2.25427	2.57201	2.93
70	2	4	0.5		0.00074	0.00368	0.00736	0.07366	14.7514	18.9597	24.3591	31.2889	40.1845
71	3	6	0.75		0.00071	0.00356	0.00711	0.07121	42.6901	62.1177	90.3835	131.509	191.346
72	4	8	1		0.00029	0.00147	0.00293	0.02935	59.1121	97.4598	160.684	264.924	436.785
73	5	10	1.25		6E-05	0.0003	0.0006	0.00605	43.6293	81.5102	152.281	284.499	531.514
117	50	100	12.5		1E-270	6E-270	1E-269	1E-268	2E-236	9E-234	5E-231	2E-228	1E-225
118	51	102	12.75		1E-281	7E-281	1E-280	2E-279	9E-247	5E-244	3E-241	2E-238	1E-235
119	52	104	13		9E-293	5E-292	9E-292	1E-290	3E-257	2E-254	1E-251	8E-249	5E-246
120	53	106	13.25		4E-304	2E-303	4E-303	5E-302	5E-268	4E-265	3E-262	2E-259	2E-256
121	54	108	13.5		0	0	0	0	6E-279	5E-276	4E-273	3E-270	3E-267
122	55	110	13.75		0	0	0	0	0	0	0	0	0
123				$F(y)$=	0.00402	0.0201	0.0402	0.40236	369.593	624.171	1079.88	1915.21	3483.82
124				p_w =	0.07073	0.35365	0.70551	6.87695	39.338	29.8244	20.1065	10.2689	0.36515

$$p_w = -\gamma z\left(1 + \frac{mz}{2c_v}\right) + \frac{2\gamma T c_v}{\sqrt{\pi}\, m} h_0^3 \exp\left(-\frac{z^2 m^2}{4 T c_v^2}\right) \times F(y)$$

$$F(y) = \sum_{n=-\infty}^{\infty} f(y) = \sum_{n=-\infty}^{\infty} n^2 \coth\left(nh_0\sqrt{T}\right) \times \sinh\left(\frac{zmnh_0}{\sqrt{T}\, c_v}\right) \times \exp\left(-n^2 h_0^2\right)$$

Figure 3-12: Sample calculations of the (excess) PWP using the proposed solution [Eq. (3.12)] with Excel®

3.8 Appendix II: Sensitivity analyses of h_0 and n in the application of the proposed analytical solution [Eq. (3.12)]

The proposed analytical solution [Eq. (3.12)] contains two parameters h_0 and n. To obtain accurate and reliable results, h_0 should be small enough while the range of n should be large enough. This requires a sensitivity analysis of these two parameters.

To illustrate this sensitivity analysis, the calculation example shown in Appendix 1 is taken again here. Fig. 3-13 shows the variation of the PWP at z = 6 m obtained by applying Eq. (3.12) with different h_0 and n. One sees that the results can be considered stable and accurate enough when h_0 reduces to 0.5 and n ranges from -55 to 55.

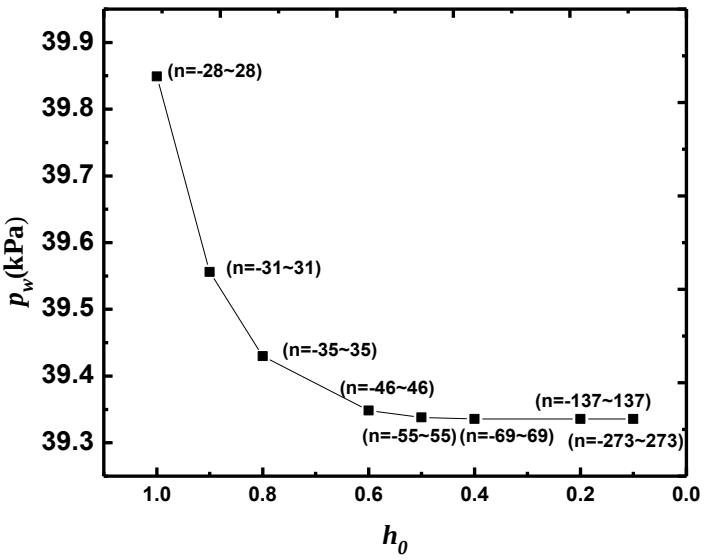

Figure 3-13: Sensitivity analysis of h_0 and n in application of the proposed analytical solution [Eq. (3.12)] to ensure stable results

3.9 References:

Ahmed, S.I., & Siddiqua, S. (2014). A review on consolidation behavior of tailings. *International Journal of Geotechnical Engineeering, 8*(1), 102-111.

Aubertin, M., Bussiere, B., & Chapuis, R.P. (1996). Hydraulic conductivity of homogenized tailings from hard rock mines. *Canadian Geotechnical Journal, 33*(3), 470-482.

Aubertin, M., & McKenna, G. (2016). *Tailings disposal challenges and prospects for oil sands mining operation*. Paper presented at the Geo-Chicago, Chicago, USA (pp. 359-371).

Azam, S., & Li, Q. (2010). Tailings dam failures: A review of the last one hundred years. *Geotechnical News, 28*(4), 50-54.

Been, K., & Sills, G.C. (1981). Self-weight consolidation of soft soils: an experimental and theoretical study. *Geotechnique, 31*(4), 519-535.

Bolduc, F.L., & Aubertin, M. (2014). Numerical investigation of the influence of waste rock inclusions on tailings consolidation. *Canadian Geotechnical Journal, 51*(9), 1021–1032.

Bussiere, B. (2007). Colloquium 2004: Hydrogeotechnical properties of hard rock tailings from metal mines and emerging geoenvironmental disposal approaches. *Canadian Geotechnical Journal, 44*(9), 1019-1052.

Cargill, K.W. (1984). Prediction of consolidation of very soft soil. *Journal of Geotechnical Engineering, 110*(6), 775–795.

Cui, L., & Fall, M. (2016). Multiphysics model for consolidation behavior of cemented paste backfill. *International Journal of Geomechanics, 17*(3), 04016077.

Darling, P. (2011). *SME mining engineering handbook* (3th ed.). Society for Mining, Metallurgy, and Exploration, Denver, US.

Dobry, R., & Alvarez, L. (1967). Seismic failures of Chilean tailings dams. *Journal of Soil Mechanics and Foundations Division, 93*(6), 237-260.

Doherty, J.P. (2015). A numerical study into factors affecting stress and PWP in free draining mine stopes. *Computers and Geotechnics, 63*, 331-341.

El Mkadmi, N., Aubertin, M., & Li, L. (2014). Effect of drainage and sequential filling on the behavior of backfill in mine stopes. *Canadian Geotechnical Journal, 51*(1), 1–15.

Fahey, M., Helinski, M., & Fourie, A. (2010). Consolidation in accreting sediments: Gibson's solution applied to backfilling of mine stopes. *Géotechnique, 60*(11), 877-882.

Feldkamp, J.R. (1989). Numerical analysis of one-dimensional nonlinear large-strain consolidation by the finite element method. *Transport in Porous Media, 4*(3), 239–257.

Ferdosi, B., James, M., & Aubertin, M. (2015). Effect of waste rock inclusions on the seismic stability of an upstream raised tailings impoundment: a numerical investigation. *Canadian Geotechnical Journal, 52*(12), 1930-1944.

Fox, P.J. (2000). *CS4: A large strain consolidation model for accreting soil layers*. Paper presented at the Geotechnics of high water content materials, ASTM International, West Conshohocken, PA.

GEO-SLOPE. (2008) Stress-deformation modeling with SIGMA/ W 2007 (3th ed.). GEO-SLOPE International Ltd, Calgary, Alberta, Canada.

Gibson, R.E. (1958). The progress of consolidation in a clay layer increasing in thickness with time. *Géotechnique, 8*(4), 171-182.

Gibson, R.E., Schiffman, R.L., & Cargill, K.W. (1981). The theory of one-dimensional consolidation of saturated clays. II. Finite nonlinear consolidation of thick homogeneous layers. *Canadian Geotechnical Journal, 18*(2), 280–293.

Goodwin, E.T. (1949). *The evaluation of integrals of the form* $\int_{-\infty}^{+\infty} f(x)e^{-x^2}\,dx$. Paper presented at the Mathematical Proceedings of the Cambridge Philosophical Society. Cambridge University, London, UK (pp. 241-245).

Grice, A.G. (1998a). *Stability of hydraulic backfill barricades*. Paper presented at the 6th International Symposium on Mining with Backfill, Brisbane, Australia (pp. 117-120).

Helinski, M., Fourie, A., Fahey, M., & Ismail, M. (2007). Assessment of the self-desiccation process in cemented mine backfills. *Canadian Geotechnical Journal, 44*(10), 1148-1156.

Helinski, M., Fourie, A., Fahey, M., & Ismail, M. (2007). Assessment of the self-desiccation process in cemented mine backfills. *Canadian Geotechnical Journal, 44*(10), 1148-1156.

James, M. (2009). The use of waste rock inclusions to control the effects of liquefaction in tailings impoundments. (Doctoral dissertation, Ecole Polytechnique de Montréal, Montréal, Canada).

Jeyapalan, J.K., Duncan, J.M., & Seed, H.B. (1983). Investigation of flow failures of tailings dams. *Journal of Geotechnical Engineering, 109*(2), 172-189.

Lambe, T.W., & Whitman, R.V. (1969). Soil mechanics. New York: John Wiley.

Li, L. (2013). Beneficial Experience from teaching and education to research and development. *Creative Education, 3*(7), 148–153.

Li, L. (2014). A numerical analysis of the application of wick drains for continuous backfilling in mine backfilled stopes. *Geosynthetic Mining Solutions*, (pp. 369-382).

Li, L. (2014). Analytical solution for determining the required strength of a side-exposed mine backfill containing a plug. *Canadian Geotechnical Journal, 51*(5), 508-519.

Li, L., Alvarez, I.C., & Aubertin, J.D. (2013). Self-weight consolidation of a slurried deposition: tests and interpretation. *International Journal of Geotechnical Engineering, 7*(2), 205–213.

Li, L., & Aubertin, M. (2009a). Influence of water pressure on the stress state in stopes with cohesionless backfill. *Geotechnical and Geological Engineering, 27*(1), 1–11.

Li, L., & Aubertin, M. (2009b). A three-dimensional analysis of the total and effective stresses in submerged backfilled stopes. *Geotechnical and Geological Engineering, 27*(4), 559–569.

Li, L., & Aubertin, M. (2009c) Horizontal pressure on barricades for backfilled stopes: Part I: Fully drained conditions. *Canadian Geotechnical Journal, 46*(1), 37–46.

Li, L., & Aubertin, M. (2009d). Horizontal pressure on barricades for backfilled stopes: Part II: Submerged conditions. *Canadian Geotechnical Journal, 46*(1), 47–56.

Li, L., & Aubertin, M. (2011). Limit equilibrium analysis for the design of backfilled stope barricades made of waste rock. *Canadian Geotechnical Journal, 48*(11), 1713-1728.

Li, L., Aubertin, M., & Belem, T. (2005). Formulation of a three dimensional analytical solution to evaluate stress in backfilled vertical narrow openings. *Canadian Geotechnical Journal, 42*(6), 1705–1717 (with Erratum 2006, 43(3), 338–339).

Li, L., & Yang, P.Y. (2015). A numerical evaluation of continuous backfilling in cemented paste backfilled stope through an application of wick drains. *International Journal of Mining Science and* Technology, 25(6), 897-904.

Morris, P.H. (2002). Analytical solutions of linear finite-strain one-dimensional consolidation. *Journal of Geotechnical and Geoenvironment Engineering, 128*(4), 319-326.

Pane, V., & Schiffman, R.L. (1985). A note on sedimentation and consolidation. *Géotechnique, 35*(1), 69-72.

Pedroni, L. (2011). Étude expérimentale et numérique de la sédimentation et de la consolidation des boues de traitement des eaux acides. (Doctoral dissertation, École Polytechnique de Montréal, Montréal, Canada).

Priscu, C. (1999). Behavior of mine tailings dams under high tailings deposition rates. (Doctoral dissertation, McGill University, Montréal, Canada).

Seneviratne, N.H., Fahey, M., Newson, T.A., & Fujiyasu, Y. (1996). Numerical modelling of consolidation and evaporation of slurried mine tailings. *International Journal for Numerical and Analytical Methods in Geomechanics, 20*(9), 647-671.

Shahsavari, M., & Grabinsky, M. (2014). *Cemented paste backfill consolidation with deposition-dependent boundary conditions*. Paper presented at the 67th Canadian Geotechnical Conference, Canadian Geotechnical Society, Regina, Saskatchewan, Canada.

Shahsavari, M., & Grabinsky, M. (2015). *Mine backfill porewater pressure dissipation: numerical predictions and field measurements*. Paper presented at the 68th Canadian Geotechnical Conference, Canadian Geotechnical Society, Québec City, Canada (pp. 1-8).

Sivakugan, N., Rankine, K., Lovisa, J., & Hall, W. (2013). Flow rate computations in hydraulic fill mine stopes. *Indian Geotechnical Journal, 43*(3), 195-202.

Sivakugan, N., Rankine, K., & Rankine, R. (2006a). Permeability of hydraulic fills and barricade bricks. *Geotechnical and Geological Engineering, 24*(3), 661-673.

Sivakugan, N., Rankine, R.M., Rankine, K.J., & Rankine, K.S. (2006b). Geotechnical considerations in mine backfilling in Australia. *Journal of Cleaner Production, 14*(12), 1168-1175.

Terzaghi, K. (1943). Theoretical Soil Mechanics. New York, USA: John Wiley and Sons.

Thompson, B.D., Bawden, W.F., & Grabinsky, M.W. (2012). In situ measurements of cemented paste backfill at the Cayeli Mine. *Canadian Geotechnical Journal, 49*(7), 755-772.

Thompson, B.D., Grabinsky, M.W., Bawden, W.F., & Counter, D.B. (2009). *In-situ measurements of cemented paste backfill in long-hole stopes*. Paper presented at the 3rd CANUS Rock Mechanics Symposium, Toronto, Canada (pp. 199).

Vick, SG. (1990) Planning, design, and analysis of tailings dams. New York: John Wiley and Sons, Inc.

Wood, D.M., Doherty, J.P., & Walske, M.L. (2016). Deposition and self-weight consolidation of a shrinking fill. *Géotechnical Letter, 6*(1), 72-76.

Yang, P.Y., Li, L., Aubertin, M., Brochu-Baekelmans, M., & Ouellet, S. (2016). Stability analyses of waste rock barricades designed to retain paste backfill. *International Journal of Geomechanics, 17*(3), 04016079.

Zheng, J., Li, L., Mbonimpa, M., & Pabst, T. (2018). An analytical solution of Gibson's model for estimating pore water pressures in accreting deposition of slurried material under one-dimensional self-weight consolidation. Part II: Impervious base. *Indian Geotechnical Journal, 48*(1), 188-195.

CHAPTER 4 ARTICLE 2: AN ANALYTICAL SOLUTION OF GIBSON'S MODEL FOR ESTIMATING PORE WATER PRESSURES IN ACCRETING DEPOSITION OF SLURRIED MATERIAL UNDER ONE-DIMENSIONAL SELF-WEIGHT CONSOLIDATION. PART Ⅱ: IMPERVIOUS BASE

Jian Zheng, Li Li, Mamert Mbonimpa and Thomas Pabst

Article published in Indian Geotechnical Journal, 2018, 48(1): 188-195.

Abstract: In mining engineering, tailings produced by concentrator mill must be properly managed. For most cases, they are sent by pipes and confined in tailings dams. Another very common practice is to use tailings as fill material to fill underground mine stopes. In coastal engineering, dredged sludge extracted from river or sea beds needs adequately be deposited and confined in containment structures. In these cases, one needs assess the pore water pressure (PWP) associated with the self-weight consolidation of accreting deposition of slurried material. To this end, a solution proposed by Gibson in 1958 had been revisited and applied to estimate the variation and evolution of the excess PWP within slurry deposition confined within tailings dams or mine stopes having an impervious base. The solution proposed in this paper can readily be solved manually with commonly available computing mean such as Excel® or any other commercially available calculation sheets to obtain the variation and evolution of PWP with different parameters involved in the analytical solution. The proposed analytical solution has been validated against numerical modeling performed with SIGMA/W of GeoStudio®. It constitutes a simple and useful tool for the design of tailings dams, dredged sludge dams, or backfilled stopes. A truly analytical solution has been given in a companion paper (Part I) for the case of pervious base.

Keywords: Tailings dams; Backfilled stopes; Dredged sludge; Self-weight consolidation; Gibson; Analytical solution; Pore water pressure(PWP); Impervious base

4.1 Introduction

Every year, mines produce considerable volume of tailings which must be properly managed. For most cases, they are sent by pipes and confined in tailings dams. It has also become a common practice to return tailings (with or without cement) underground to fill mine stopes. In coastal engineering, dredged slurry excavated from sea or river beds for maintenance needs to be properly disposed (pumped and confined in a dam for most cases). In these cases, one needs assess the pore water pressure (PWP) associated with the self-weight consolidation (addressed below) of accreting deposition of slurried material. For tailings or dredged sludge dams [Fig. 4-1(a)], this parameter is closely related to the stability of the confining dam and management of the tailings, dredged sludge and water volumes (Dobry and Alvarez 1967; Jeyapalan et al. 1983). A high excess PWP is particularly dangerous for the tailings pond constructed with the upstream method (Vick 1990; Priscu 1999; Azam and Li 2010). For mine backfilled stopes, assessing the PWP is a key concern for the stability of barricades, a structure constructed at the base of the stopes (usually near the drawpoints) to retain the slurried backfill in place [Fig. 4-1(b)] (Grice 1998; Sivakugan et al. 2006; Li and Aubertin 2011; Yang et al. 2016). The numerous cases of tailings dam failure and barricade failure reported in the literature and social media indicate that the consequence associated with the failure of such confining structures is usually very serious, involving environment disaster, damage and loss of equipment and lives (Sivakugan et al. 2006; Li and Aubertin 2011; Yang et al. 2016).

(a)  (b) 

Figure 4-1: Confining structures of mine slurried deposition: (a) a tailings dam on the surface; (b) a barricade in an underground mine

When a slurried material is poured within a confining structure, a process called “self-weight consolidation” takes place if the disposed material has a low permeability (Pedroni 2011; Li 2013; Li et al. 2013; El Mkadmi et al. 2014; Zhang and Zhu 2014). This process is accompanied by the

generation of excess PWP. At the placement of the slurry deposition, the PWP equals to the vertical total stress calculated based on the isostatic overburden solution, resulting in an excess PWP that is the difference between the PWP and the hydrostatic water pressure (Li 2013; Li et al. 2013). With the time and dissipation of the excess PWP, the PWP diminishes, resulting in a denser deposition and a decanted water pond on the top surface of the deposition.

The self-weight consolidation is complicated by the deposition rate (also called "filling rate" or "rising rate" in mine stopes). When the final height (or thickness) of a slurry deposition is large or when the filling rate is low, a coupled process involving the dissipation (decrease) of the excess PWP within the disposed slurried material and the generation (increase) of the excess PWP due to the addition of new slurried material on the top surface of previous layers. This phenomenon is commonly called "accreting deposition" of slurried material (Gibson 1958; Fox 2000).

The evolution and distribution of the excess PWP within a slurry deposition can be evaluated by either numerical modeling or analytical solution; each has advantages and limitations. The numerical solution is flexible and robust. More complicated and more representative field conditions can be taken into account in numerical modeling. However, the application of numerical modeling is usually limited by the availability of software, hardware and qualified personnel. Subsequently, the analytical solutions constitute a calculation tool commonly sought by practitioners and engineers.

For the case of accreting deposition of slurried material, a solution proposed by Gibson (1958) had been revisited and applied to estimate the variation and evolution of the PWP within slurry deposition confined within tailings dams or mine stopes. The formulation of Gibson (1958) has been taken and commonly called "analytical solution" (Fahey et al. 2010; Shahsavari and Grabinsky 2014, 2015; Doherty 2015; Cui and Fall 2016). The original formulation of Gibson (1958) is however not an "analytical solution" as it contains an integral that cannot be solved with the commonly available computing means and the equations have to be evaluated by numerical calculations (Shahsavari and Grabinsky 2014, 2015).

In this paper, the Gibson (1958) solution will be revisited for evaluating the excess PWP within slurried backfill confined in tailings or dredged sludge dams or backfilled stopes, having an impervious base. A truly analytical solution for the case of accreting deposition of slurry deposition with a pervious base has been presented in Part I (Zheng et al. 2018). The proposed solution in an

analytical expression can readily be solved manually to obtain the distribution and evolution of the excess PWP within a slurry deposition.

4.2 Formulation of an analytical expression for the Gibson solution

Fig. 4-2 schematically shows the deposition of a slurry on an impervious base. Here, the initial thickness of the deposition is assumed to be zero. *z* is the elevation of a point to be considered from the bottom of the slurry deposition. *h* and *H* are the current and final thickness (height) of the sediment, respectively.

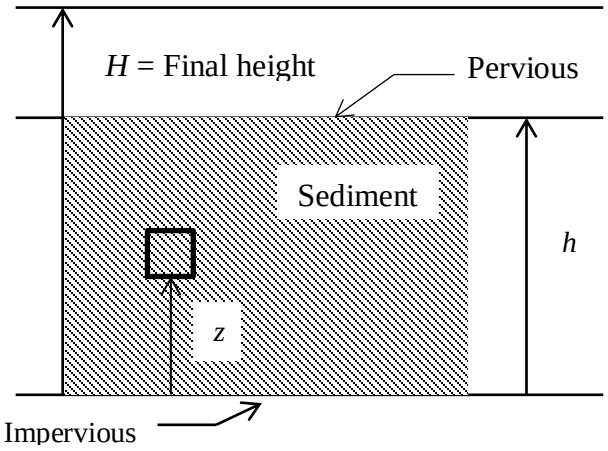

Figure 4-2: A slurry deposition on an impervious base (Gibson 1958)

To solve this type of problem, Gibson (1958) has made use of the same assumptions taken by Terzaghi's (1943) for the conventional consolidation theory. These include:

- The permeability coefficient and compressibility coefficient are constant;
- The pore-water and soil are incompressible;
- The soil is fully saturated and Darcy's law is strictly valid.

In Part I (Zheng et al. 2018), the governing equation was expressed with PWP in an accreting deposition. Here, the governing equation was given in terms of excess PWP as follows (Gibson 1958):

$$c_v \frac{\partial^2 u}{\partial z^2} = \frac{\partial u}{\partial t} - \gamma' \frac{dh}{dt} \tag{4.1}$$

where u (kPa) is the excess PWP equaling to the PWP minus the hydrostatic water pressure, t (hours) is the time starting from the beginning of the slurry deposition operation, c_v (m^2/h) is the consolidation coefficient which is taken as a constant because the permeability and constrained modulus are taken constant as in the Terzaghi's consolidation theory, γ' (kN/m^3) is the submerged unit weight of the slurry deposition (i.e. $\gamma' = \gamma - \gamma_w$; where γ is the unit weight of the saturated backfill and γ_w is the unit weight of water, $\gamma_w = 9.8$ kN/m^3).

By considering a constant rate of deposition, the current height of the slurry deposition can then be expressed as follows:

$$h = mt \tag{4.2}$$

where m (m/h) is the rising rate of the deposition.

Solving Eq. (4.1) and considering the drainage through the top surface of the slurry deposition lead to the excess PWP expressed as follows (Gibson 1958):

$$\begin{aligned} u = {} & \gamma' mt - \gamma' (\pi c_v t)^{-\frac{1}{2}} \exp\left(\frac{-z^2}{4c_v t}\right) \\ & \times \int_0^\infty \xi \tanh\left(\frac{m\xi}{2c_v}\right) \cosh\left(\frac{z\xi}{2c_v t}\right) \exp\left(-\frac{\xi^2}{4c_v t}\right) d\xi \end{aligned} \tag{4.3}$$

where ξ (m) is an arbitrary parameter varying from zero to infinity (∞). Again, the solution of Gibson (1958) cannot be considered as an analytical solution because it contains an integral that cannot be solved by commonly available computing mean.

To obtain a truly analytical solution that can directly be used to obtain the distribution and evolution of the excess PWP with a slurry deposition, the integral in Eq. (4.3) can be represented by the following function:

$$F(y) = \int_0^\infty f(y) \exp(-y^2) dy \tag{4.4}$$

where

$$f(y) = 4c_v t \times y \times \tanh\left(\frac{m\sqrt{t}y}{\sqrt{c_v}}\right) \times \cosh\left(\frac{z \times y}{\sqrt{c_v t}}\right) \tag{4.5}$$

and

$$y^2 = \frac{\xi^2}{4c_v t} \tag{4.6}$$

Since $f(y)$ is an even function, Eq. (4.4) can be expressed as follows:

$$F(y) = \frac{1}{2}\int_{-\infty}^{\infty} f(y)\exp(-y^2)dy \tag{4.7}$$

This type of integral has been approximated by Goodwin (1949) as follows:

$$\int_{-\infty}^{\infty} f(y)\exp(-y^2)dy \approx h_0 \sum_{n=-\infty}^{\infty} f(nh_0)\exp(-n^2h_0^2) \tag{4.8}$$

where n is a series number varying from -∞ to +∞, the variable y is divided into segments of h_0 ($h_0 \leq 1$). Goodwin (1949) had shown that a high accuracy can be obtained by applying Eq. (4.8) with a large value of h_0 smaller than the unity.

Introducing Eq. (4.8) into Eq. (4.7) leads to the following expression:

$$F(y) = 2c_v t h_0^2 \sum_{n=-\infty}^{\infty} n \times \tanh\left(\frac{mnh_0\sqrt{t}}{\sqrt{c_v}}\right) \times \cosh\left(\frac{znh_0}{\sqrt{c_v t}}\right) \times \exp(-n^2h_0^2) \tag{4.9}$$

Substitution of Eq. (4.9) into Eq. (4.3) results in

$$u = \gamma' mt - \frac{2\gamma'\sqrt{c_v t}h_0^2}{\sqrt{\pi}}\exp\left(\frac{-z^2}{4c_v t}\right) \times \sum_{n=-\infty}^{\infty} n \times \tanh\left(\frac{mnh_0\sqrt{t}}{\sqrt{c_v}}\right) \times \cosh\left(\frac{znh_0}{\sqrt{c_v t}}\right) \times \exp(-n^2h_0^2) \tag{4.10}$$

Introducing the dimensionless time factor (T) as follows:

$$T = \frac{m^2 t}{c_v} = \frac{mh}{c_v} \tag{4.11}$$

Replacing time (t) in the Eq. (4.10) with the dimensionless time factor (T) leads to

$$u = \frac{\gamma' T c_v}{m} - \frac{2\gamma' \sqrt{T} c_v h_0^2}{\sqrt{\pi} m} \exp\left(\frac{-z^2 m^2}{4 c_v^2 T}\right) \times \sum_{n=-\infty}^{\infty} n \times \tanh\left(n h_0 \sqrt{T}\right) \times \cosh\left(\frac{z n m h_0}{\sqrt{T} c_v}\right) \times \exp(-n^2 h_0^2) \quad (4.12)$$

Eq. (4.12) contains a sum of series with the number n varying from -∞ to ∞. It can readily be solved using commonly available computing mean such as Excel® (see the illustrative example given in Part I (Zheng et al. 2018) for the application of Eq. (4.12). Thus, it can be considered as a truly analytical solution for estimating the distribution and evolution of the excess PWP for tailings dams, dredged sludge dams, or backfilled stopes.

4.3 Comparison with numerical results

To assess the validity of the proposed analytical solution, the variation and evolution of the excess PWP in a backfilled stope are calculated using a finite element code, called SIGMA/W (GEO-SLOPE 2008). The numerical results are then compared with those predicted by the proposed analytical solution.

Fig. 4-3(a) shows the physical model of the backfilled stope with a width of 6 m. The backfill is poured to a final height of H = 8 m, which corresponds to a typical height of plug pour (Li 2014). The backfill is assumed to be homogeneous, isotropic and linearly elastic. Its geotechnical properties are: γ_{sat} = 20 kN/m^3 (unit weight), μ = 0.2 (Poisson's ratio), M' = 960 kPa (drained constrained modulus). Considering the relationship between the drained Young's modulus E' used in the SIGMA/W and the drained constrained modulus M'

$$E' = \frac{(1+\mu)(1-2\mu)M'}{(1-\mu)} \quad (4.13)$$

one obtains the drained Young's modulus E' = 864 kPa for the backfill.

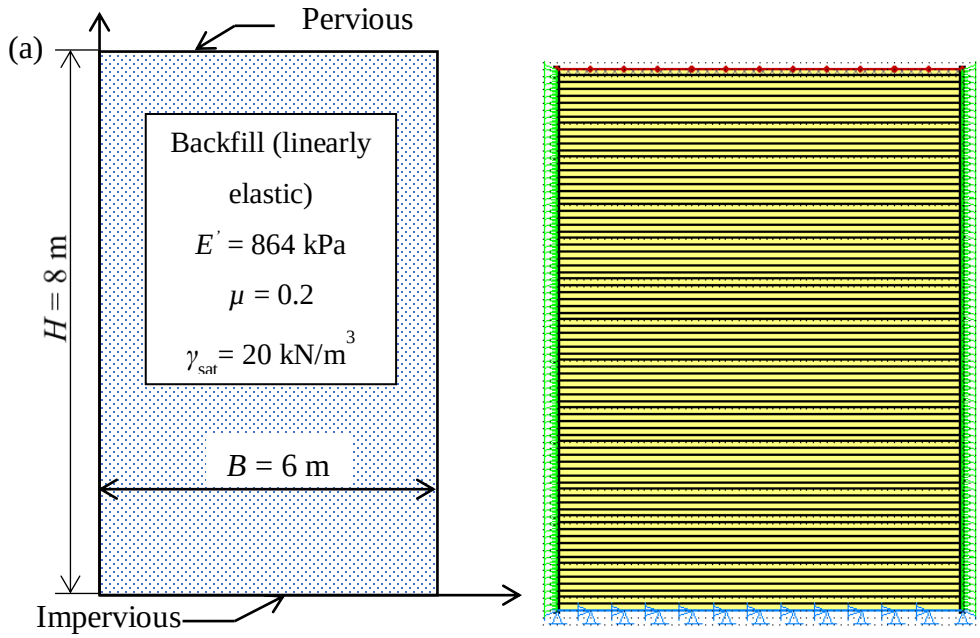

Figure 4-3: Simulation of a vertical sequentially backfilled stope with an impervious base (a) schematic representation of the physical model; (b) numerical model built with SIGMA/W

Knowing the hydraulic conductivity k (m/s) and the drained constrained modulus M' (kPa), the consolidation coefficient c_v (m^2/h) can be estimated by the following expression:

$$c_v = \frac{k \cdot M'}{\gamma_w} \tag{4.14}$$

In this study, we considered two cases as follows:

a) $k = 2.83\times10^{-7}$ m/s, $c_v = 0.1$ m^2/h (by applying Eq. (4.14)), and $m = 0.2$ m/h.

b) $k = 2.83\times10^{-7}$ m/s, $c_v = 0.1$ m^2/h (by applying Eq. (4.14)), and $m = 1.0$ m/h.

Fig. 4-3(b) shows the numerical model built by SIGMA/W. As shown in the figure, the two vertical walls are fixed in the horizontal direction and the bottom of the model is fixed in both the vertical and horizontal directions. The top surface of each newly added layer of backfill is allowed to drain with zero PWP. The two lateral vertical walls and the bottom of the model are considered to be impermeable.

Sensitivity analysis of meshing has been done. This resulted in an optimal mesh with quadrilateral and triangular elements of 0.1 m for the backfill to ensure a stable numerical result.

In practice, the backfill was continuously poured in the stope and the thickness of the backfill increases continuously with the filling time. In numerical modeling with SIGMA/W, this continuous backfilling has to be approximated by a series of instantaneous layer additions. For each layer of thickness Δh, the waiting time before the addition of a new layer is $\Delta h/m$. For a given rising rate m, the thinner the layer Δh is and the closer to the continuous backfilling the numerical modeling will be. When the thickness of each layer Δh is thin enough, the numerical models can be considered as a close reproduction of the continuous filling and increase in the backfill thickness. In this study, the thickness of each layer is taken as 0.1 m in the numerical model of SIGMA/W. This requires a filling operation of 80 layers to reach a backfill 8 m high. For the filling rates of 0.2 m/h and 1 m/h, the waiting time between two additions of layers is 0.5 h and 0.1 h, respectively.

Fig. 4-4 shows the distributions of the excess PWP along the height of the backfill at the end of the filling operation, obtained by the numerical modeling and calculated with the proposed analytical solution [Eq. (4.12)]. It can be seen that a close agreement is obtained between the excess PWP distributions predicted by the proposed analytical solution and those obtained by the numerical modeling. The proposed analytical solution [Eq. (4.12)] can thus be considered as validated. It can be used for estimating the excess PWP distribution and evolution in accreting deposition of slurried material with an impervious base.

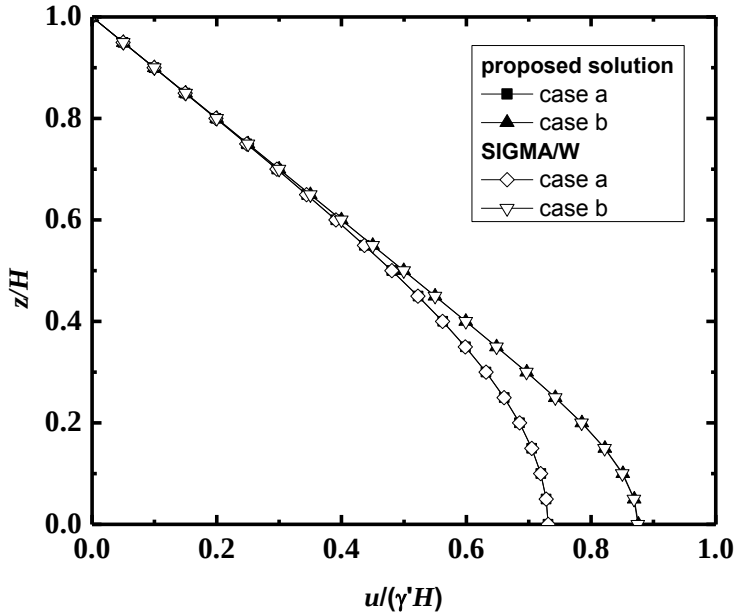

Figure 4-4: Distributions of the excess PWP obtained by the numerical simulations and calculated by the proposed analytical solution [Eq. (4.12)], using h_0 = 0.3 and n = -91 to 91) within the backfill at the end of deposition: (a) c_v = 0.1 m^2/h, m = 0.2 m/h; (b) c_v = 0.1 m^2/h and m = 1.0 m/h

4.4 Sample applications

4.4.1 Sample application in tailings pond

In this section, the proposed analytical solution [Eq. (4.12)] was applied to illustrate the PWP distribution in a tailings dam with a final height of H = 20 m. Here, the filling rate varied from 4.8 to 9.6 m/yr (Seneviratne et al.1996). The consolidation coefficient was varied from 0.18 to 0.0018 m^2/h (Aubertin et al. 1996). The unit weight of the backfill was considered as $\gamma_{sat} = 20$ kN/m^3.

Fig. 4-5 presents the distribution of the excess PWP along the height of the tailings pond at the end of the filling operation, corresponding to the c_v of 0.18, 0.018 and 0.0018 m^2/h. The filling rate and final filling height were considered as 4.8 m/year and 20 m, respectively. The distribution of the excess PWP for the case of undrained condition ($u = \gamma'(H - z)$; γ' (= γ_{sat} - γ_w) is the effective unit weight of the tailings) is also included in the figure. It can be seen that the value of c_v has a significant effect on the dissipation of the excess PWP. With an increased c_v, the excess PWP

dissipation rate increases significantly, resulting in reduced excess PWP. For the case of c_v = 0.18 m^2/h, the excess PWP was dissipated almost completely at the end of filling operation and resulted in a peak value of 5.9 kPa, while a peak value of 120.8 kPa was resulted in the case of c_v = 0.0018 m^2/h.

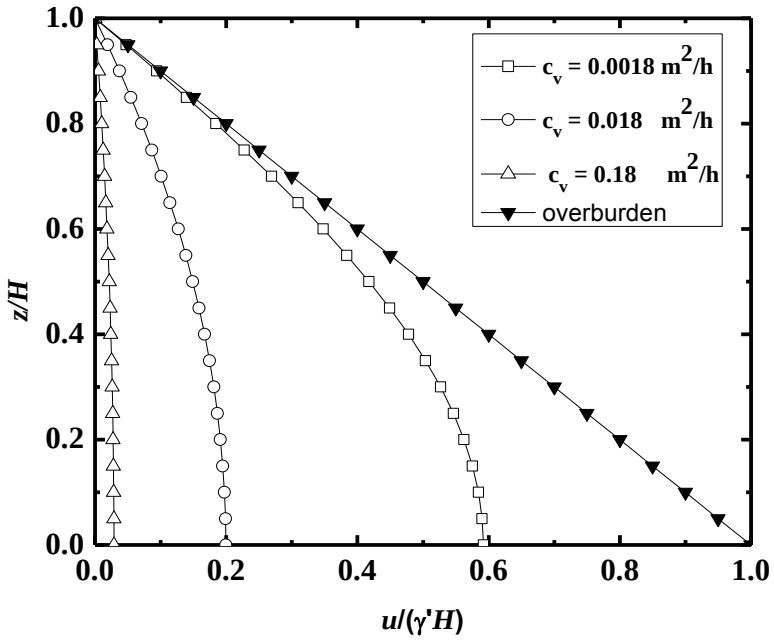

Figure 4-5: Distribution of excess PWP within the tailings pond at the end of the filling operation, calculated using the proposed analytical solution [Eq. (4.12)] by considering a tailings height of 20 m at a filling rate of m = 4.8 m/year

Fig. 4-6 shows the variation of the excess PWP distribution along the height of tailings pond at the end of the filling operation as the filling rate increases from 4.8 to 40 m/year, calculated with the proposed analytical solution. The final height of the backfill is 20 m and the consolidation coefficient is 0.018 m^2/h. The filling rates as high as 20 and 40 m/yr are quite scarce in practice; they were used to better illustrate the effect of the filling rate on the variation and evolution of the excess PWP. The results show that higher excess PWP can be generated with increased filling rate. This indicates that fast filling should be avoided in order to prevent the generation of excessively high excess PWP in tailings ponds, especially for the tailings of lower permeability.

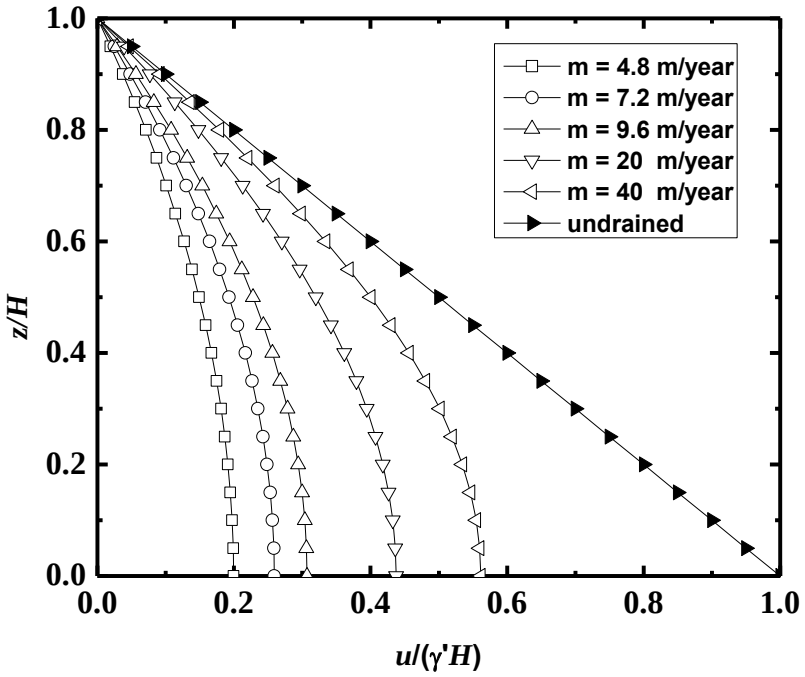

Figure 4-6: Variation of the excess PWP distribution with different filling rates at the end of filling operation, calculated by the proposed analytical solution [Eq. (4.12)] by considering a tailing height of 20 m and a consolidation coefficient c_v = 0.05 cm^2/s

4.4.2 Sample application in mine backfilled stopes

As another application, the proposed analytical solution [Eq. (4.12)] is applied to investigate the influence of backfill property, filling rate and total fill height on the PWP (i.e. excess PWP plus hydrostatic water pressure) distribution in the backfilled stopes. The unit weight of the backfill is taken as γ_{sat} = 20 kN/m^3.

Fig. 4-7 shows the variation of the PWP distribution along the height of the backfill at the end of the filling operation as the consolidation coefficient c_v increases from 0.01 to 1 m^2/h. The isostatic water pressure due to the overburden of the backfill is also plotted in the figure. The backfill height is 8 m, completed with a filling rate of m = 0.2 m/h. It can be seen that when the consolidation coefficient c_v is as high as 1 m^2/h, a large part of the excess PWP is dissipated during the stope filling operation, resulting in a peak PWP of 107.3 kPa. When the consolidation coefficient c_v reduces to 0.01 m^2/h, only a small part of the excess PWP is dissipated near the base of the slurried backfill, resulting in a peak PWP of 152.8 kPa. These results indicate that the barricade design

based on the isostatic pressure due to the overburden of the backfill is uneconomic for most cases. It can only be valid when the backfill has a very low permeability.

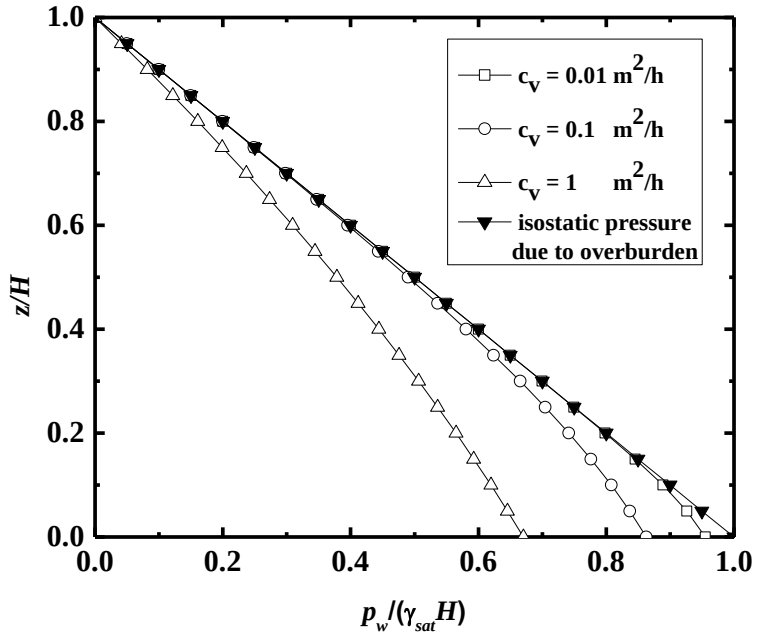

Figure 4-7: Variation of the PWP distribution within the stope at the end of filling operation with different consolidation coefficients, calculated with the proposed analytical solution [Eq. (4.12)] by considering a backfill height of 8 m and a filling rate of m = 0.2 m/h

Fig. 4-8 shows the variation of the PWP distribution at the end of filling operation when the filling rate changes from 0.1 to 1.0 m/h. The final backfill height is 8 m and the consolidation coefficient is c_v = 0.1 m^2/h. The PWP distribution based on the isostatic water due to the overburden of the backfill is also included in the figure. It can be seen that the PWP increases as the filling rate increases, resulting in peak values of 130.2, 145.8 and 149.9 kPa when the filling is performed at a rate of 0.1, 0.5 and 1.0 m/h, respectively. These results indicate again that the application of the iso-geostatic overburden solution without considering the self-weight consolidation would lead to overestimate of the PWP and uneconomical barricade design. The overestimation becomes more pronounced when the filling rate is lower.

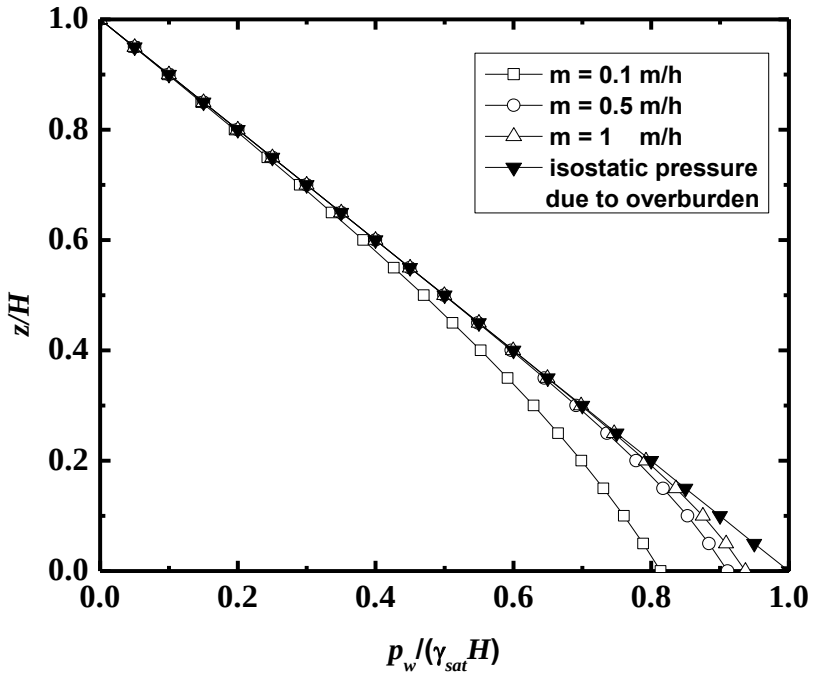

Figure 4-8: Variation of the PWP distribution at the end of filling operation with different filling rates, calculated with the proposed analytical solution [Eq. (4.12)] by considering H = 8 m and c_v = 0.1 m^2/h

Fig. 4-9 shows the variation of the PWP within the backfill at the end of the filling operation when the final backfill height increases from 8 to 32 m. The filling rate and consolidation coefficient were taken as 0.2 m/h and 0.1 m^2/h, respectively. It can be seen that the PWP distributions are all lower than those based on the isostatic water pressure due to the overburden of the backfill. The peak PWP increases as the final fill height increases. The proposed analytical solution can become useful in water management for tailings ponds or in barricade design for underground mine backfilled stopes.

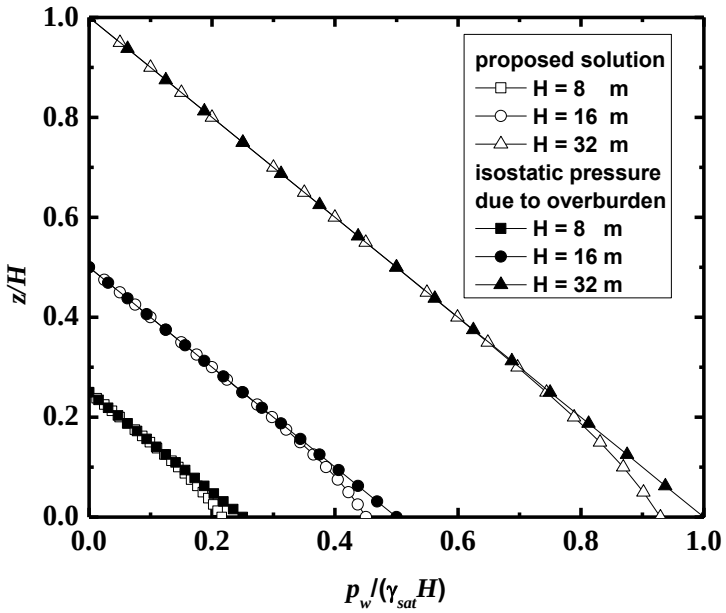

Figure 4-9: Variation of the PWP distribution at the end of the filling operation as the final backfill height increases from 8 to 32 m, calculated by the proposed analytical solution by considering a filling rate m = 0.2 m/h and a consolidation coefficient c_v = 0.1 m^2/h

4.5 Discussion

This paper proposed a truly analytical solution for estimating the variation and evolution of the PWP and excess PWP within the backfilled stopes, tailings ponds, or dredged sludge dams, having an impervious base. The analytical solution can readily be used with the common software such as Microsoft Excel®. It has been validated by the numerical modeling and constitutes an additional useful tool for the design of tailings ponds, dredged sludge dams, and mine backfilled stopes. Nevertheless, similar to Part I (Zheng et al. 2018) for the case of pervious base, the proposed solution contains some limitations associated with the simplifying assumptions, which include the one-dimensional consolidation model under small strain with constant hydro-mechanical properties and neglected arching that can develop during the dissipation of excess PWP. More work is needed to take into account these aspects in the future.

4.6 Conclusion

A good understanding of the PWP and excess PWP distribution and evolution for tailings dams, dredged sludge ponds and backfilled stopes is quite important for the safe design and management of these infrastructures. A truly analytical solution was proposed in this paper based on the Gibson (1958) model by considering one dimensional self-weight consolidation with an impervious base. The proposed analytical solution can readily be used with commonly available calculating means such as Excel® or any other calculation sheets. It has been validated against numerical modeling performed with SIGMA/W. The proposed analytical solution thus constitutes a useful and simple tool to evaluate the PWP and excess PWP distribution and evolution for tailings dams, dredged sludge ponds and backfilled stopes.

Acknowledgements

The authors would like to acknowledge the financial support from the Natural Sciences and Engineering Research Council of Canada (NSERC 402318), Institut de recherche Robert-Sauvé en santé et en sécurité du travail (IRSST 2013-0029), Fonds de recherche du Québec—Nature et Technologies (FRQNT 2015-MI-191676, 2017-MI-202116), and industrial partners of the ResearchInstitute on Mines and the Environment (RIME UQAT-Polytechnique; http://rime-irme.ca/).

4.7 References

Aubertin, M., Bussiere, B., & Chapuis, R.P. (1996). Hydraulic conductivity of homogenized tailings from hard rock mines. *Canadian Geotechnical Journal, 33*(3), 470-482.

Azam, S., & Li, Q. (2010). Tailings dam failures: A review of the last one hundred years. *Geotechnical News, 28*(4), 50-54.

Cui, L., & Fall, M. (2016). Multiphysics model for consolidation behavior of cemented paste backfill. *International Journal of Geomechanics, 17*(3), 04016077.

Dobry, R., & Alvarez, L. (1967). Seismic failures of Chilean tailings dams. *Journal of Soil Mechanics and Foundations Division, 93*(6), 237-260.

Doherty, J.P. (2015). A numerical study into factors affecting stress and PWP in free draining mine stopes. *Computers and Geotechnics, 63*, 331-341.

El Mkadmi, N., Aubertin, M., & Li, L. (2014). Effect of drainage and sequential filling on the behavior of backfill in mine stopes. *Canadian Geotechnical Journal, 51*(1), 1–15.

Fahey, M., Helinski, M., & Fourie, A. (2010). Consolidation in accreting sediments: Gibson's solution applied to backfilling of mine stopes. *Géotechnique, 60*(11), 877-882.

Fox, P.J. (2000). *CS4: A large strain consolidation model for accreting soil layers*. Paper presented at the Geotechnics of high water content materials, ASTM International, West Conshohocken, PA.

GEO-SLOPE. (2008) Stress-deformation modeling with SIGMA/ W 2007 (3th ed.). GEO-SLOPE International Ltd, Calgary, Alberta, Canada.

Gibson, R.E. (1958). The progress of consolidation in a clay layer increasing in thickness with time. *Géotechnique, 8*(4), 171-182.

Goodwin, E.T. (1949). *The evaluation of integrals of the form* $\int_{-\infty}^{+\infty} f(x)e^{-x^2}dx$. Paper presented at the Mathematical Proceedings of the Cambridge Philosophical Society. Cambridge University, London, UK (pp. 241-245).

Grice, T. (1998). *Stability of hydraulic backfill barricades*. Paper presented at the 6th International Symposium on Mining with Backfill, Victoria, Australia (pp. 117-120).

Jeyapalan, J.K., Duncan, J.M., & Seed, H.B. (1983). Investigation of flow failures of tailings dams. *Journal of Geotechnical Engineering, 109*(2), 172-189.

Li, L. (2013). Beneficial Experience from teaching and education to research and development. *Creative Education, 3*(7), 148–153.

Li, L. (2014). Analytical solution for determining the required strength of a side-exposed mine backfill containing a plug. *Canadian Geotechnical Journal, 51*(5), 508-519.

Li, L., Alvarez, I.C., & Aubertin, J.D. (2013). Self-weight consolidation of a slurried deposition: tests and interpretation. *International Journal of Geotechnical Engineering, 7*(2), 205–213.

Li, L., & Aubertin, M. (2011). Limit equilibrium analysis for the design of backfilled stope barricades made of waste rock. *Canadian Geotechnical Journal, 48*(11), 1713-1728.

Pedroni, L. (2011). Étude expérimentale et numérique de la sédimentation et de la consolidation des boues de traitement des eaux acides. (Doctoral dissertation, École Polytechnique de Montréal, Montréal, Canada).

Priscu, C. (1999). Behavior of mine tailings dams under high tailings deposition rates. (Doctoral dissertation, McGill University, Montréal, Canada).

Seneviratne, N.H., Fahey, M., Newson, T.A., & Fujiyasu, Y. (1996). Numerical modelling of consolidation and evaporation of slurried mine tailings. *International Journal for Numerical and Analytical Methods in Geomechanics, 20*(9), 647-671.

Shahsavari, M., & Grabinsky, M. (2014). *Cemented paste backfill consolidation with deposition-dependent boundary conditions*. Paper presented at the 67th Canadian Geotechnical Conference, Canadian Geotechnical Society, Regina, Saskatchewan, Canada.

Shahsavari, M., & Grabinsky, M. (2015). *Mine backfill porewater pressure dissipation: numerical predictions and field measurements*. Paper presented at the 68th Canadian Geotechnical Conference, Canadian Geotechnical Society, Québec City, Canada (pp. 1-8).

Sivakugan, N., Rankine, K., & Rankine, R. (2006). Permeability of hydraulic fills and barricade bricks. *Geotechnical and Geological Engineering, 24*(3), 661-673.

Terzaghi, K. (1943). Theoretical Soil Mechanics. New York, USA: John Wiley and Sons.

Vick, SG. (1990) Planning, design, and analysis of tailings dams. New York: John Wiley and Sons, Inc.

Yang, P.Y., Li, L., Aubertin, M., & Brochu-Baekelmans, M. (2017). Stability analyses of waste rock barricades designed to retain paste backfill. *International Journal of Geomechanics, 17*(3), 04016079.

Zhang, N., & Zhu, W. (2014). *Study of sedimentation and consolidation of soil particles in dredged slurry*. Paper presented at the Geo-Shanghai, Shanghai, China (pp.70-79).

Zheng, J., Li, L., Mbonimpa, M., & Pabst, T. (2018). An analytical solution of Gibson's model for estimating the pore water pressures in accreting deposition of slurried material under one-dimensional self-weight consolidation. Part I: Pervious base. *Indian Geotechnical Journal, 48*(1), 72-83.

CHAPTER 5 ARTICLE 3: A NEW SOLUTION TO EVALUATE THE PWP DURING AND AFTER SLURRY DEPPOSITION ON A PERVIOUS BASE

Jian Zheng, Li Li, Yu-Chao Li, Mamert Mbonimpa

Article submitted to *Environmental Geotechnics* in March 2018.

Abstract: In mining and geotechnical engineering, a good estimation of the pore water pressure (PWP) within a slurried material during and after the deposition is essential for analyzing the stability of the confining structures and for planning the slurry deposition. A model proposed by Gibson in 1958 can be used to evaluate the excess PWP during the slurry deposition on a pervious base. A truly analytical solution based on the Gibson model has also been proposed by the authors to evaluate the excess PWP during the slurry deposition. Starting from the end of slurry deposition, a differential equation involving the excess PWP was given by Gibson in 1958, but it cannot be directly used. In this paper, the differential equation in Gibson model is solved. The solution along with the authors' previous analytical solution can thus be used to evaluate the (excess) PWP during and after the slurry deposition on a pervious base. The proposed solutions are validated by numerical modeling performed with SIGMA/W of Geoslope. The influence of the consolidation coefficient and filling rate on the distribution and evolution of PWP is analyzed.

Keywords: tailings; backfill; dredged sludge; pore water pressure (PWP); consolidation; after slurry deposition; pervious base

5.1 Introduction

Nowadays, there are more and more projects involving the generation and management of slurried materials. In civil engineering, the maintenance of waterways usually need the excavation and deposition of dredged sludges (Dhanya et al. 2012; Jaditager and Sivakugan 2017). In mining engineering, hard rock or oil sand tailings need to be confined by dams (Ripley et al. 1978; Caughill et al. 1993; Qiu and Sego 2001; ERCB 2009; Alam et al. 2017). In underground mines, the backfill transported by pipes to fill the mined-out voids (stopes) usually contains a lot of water. All these slurried materials are characterized by high water content, low permeability, and low shear strength (Caughill et al. 1993; Qiu and Sego 2001; Beier et al. 2013; Malekzadeh and Sivakugan 2017).

Upon deposition in a dam confining pond or stope, the solid particles of the slurry tend to settle down due to the self-weight. The backfill thus tends to become denser and the water contained in the pores tends to be expelled out of the backfill. As the backfill and tailings, especially oil sand tailings, usually have a low permeability, the outflow of pore water is limited, resulting in the generation of excess PWP (pore-water pressure) (Pedroni 2011; Li 2013; Li et al. 2013; El Mkadmi et al. 2014). The excess PWP diminishes when the drainage and dissipation take place. The process is known as self-weight consolidation (Been and Sills 1981; Pane and Schiffman 1985). When the excess PWP is high, the effective stresses and strength of the backfill can be low while the total stresses can be high, threating the stability of the confining structures (dams for tailings or dredged sludge, barricades for underground mine backfilled stopes). One thus needs to have a good understanding of the excess PWP dissipation during and after the deposition of slurried material on an impervious or pervious base.

A model proposed by Gibson (1958) has been shown to be very useful to evaluate the excess PWP during the accreting deposition of slurried material (Fahey et al. 2010; Doherty 2015; Shahsavari and Grabinsky 2014, 2015; Zheng et al. 2018a, 2018b). However, the Gibson (1958) model and the ensuing solutions or applications were mostly limited to evaluate the excess PWP during the slurry deposition. After the slurry deposition, a differential equation was given by Gibson (1958) for the case of an impervious base. No solution was proposed to estimate the excess PWP after slurry deposition for the case of pervious base even though the disposition tailings or placement of mine backfill in mine stopes is equally frequently met in practice (e.g., Sivakugan et al. 2006a; Li and Aubertin 2011; Zheng et al. 2018a).

In this paper, a truly analytical solution based on the Gibson (1958) model for evaluating the (excess) PWP during the slurry deposition on a pervious base will first be recalled for the sake of completeness. A new solution is then proposed to estimate the (excess) PWP after the slurry deposition on a pervious. The proposed solution is validated by numerical results obtained with SIMGMA/W.

5.2 Proposed solutions

Fig. 5-1 schematically shows the deposition of a slurry on a pervious base. The thickness of the slurry is initially zero and increases at a constant filling rate of m (m/h). On the figure, h (m) and H (m) are the current and final thickness of the slurry, respectively; z (m) is the elevation of a calculation point from the base of the slurry deposition, ranging from 0 to h. At a given filling time t (h), the current thickness of the slurry can be expressed as:

$$h = mt \tag{5.1}$$

As can be seen from Fig. 5-1, the water table will fall down to the base level and the PWP will become zero everywhere in the slurry when the water reaches the final steady state. As the excess PWP is defined as the difference between the current and final steady state PWPs, the excess PWP is then always equal to the current PWP (Gibson 1989; Zheng et al. 2018a). No difference will be made between the PWP and excess PWP below through the paper.

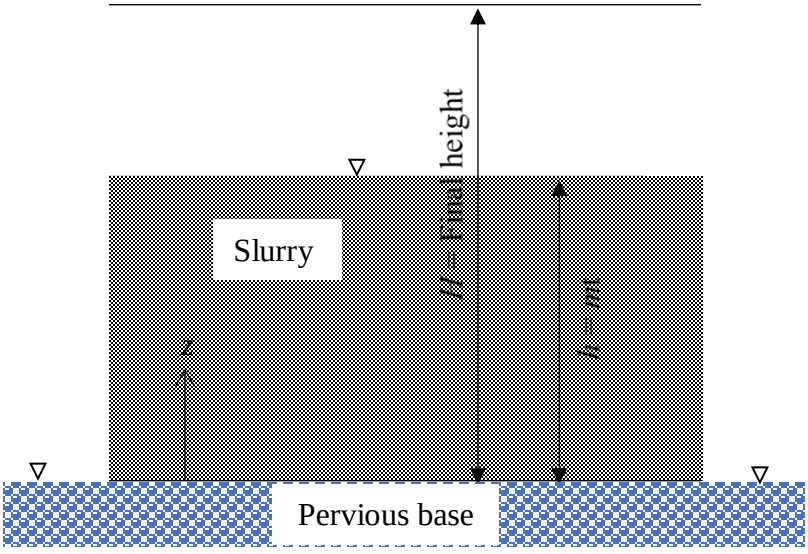

Figure 5-1: Deposition of a slurry on a pervious base (Gibson 1958)

5.2.1 Solution for PWP during the slurry deposition

The following differential equation was proposed by Gibson (1958) based on the classical Terzaghi (1943) consolidation theory to evaluate the (excess) PWP during the accreting deposition on a pervious base:

$$c_v \frac{\partial^2 p_w}{\partial z^2} = \frac{\partial p_w}{\partial t} - \gamma \frac{dh}{dt} \tag{5.2}$$

where p_w (kPa) is the PWP; c_v (m^2/h) is the consolidation coefficient; γ (kN/m^3) is the saturated unit weight of the backfill.

Considering the boundary conditions of $p_w = 0$ at $z = 0$ and $z = h$, Eq. (5.2) has been solved by Gibson (1958) and expressed as follows:

$$p_w = -\gamma z(1+\frac{mz}{2c_v}) + \frac{\gamma m}{2c_v}(\pi c_v t)^{-\frac{1}{2}} \times \exp\left(-\frac{z^2}{4c_v t}\right) \times \int_0^\infty \xi^2 \coth\left(\frac{m\xi}{2c_v}\right) \sinh\left(\frac{z\xi}{2c_v t}\right) \exp\left(-\frac{\xi^2}{4c_v t}\right) d\xi \tag{5.3}$$

where ξ (m) is an integration variable in the range of zero to infinite (∞).

Eq. (5.3) has been considered as an analytical solution and used to estimate the PWP in mine backfilled stopes during the deposition (Fahey et al. 2010; Doherty 2015; Shahsavari and Grabinsky 2014, 2015). It is however not a truly analytical solution because the integral contained in Eq. (5.3) cannot be solved by hand calculations or commonly available calculation tools.

By using a transformation proposed by Goodwin (1949), the integral of Eq. (5.3) has been approximated by a sum of series. This resulted in a truly analytical solution of the Gibson model, expressed as follows (Zheng et al. 2018a):

$$\begin{aligned} p_w(z,t) = &-\gamma z\left(1+\frac{mz}{2c_v}\right) + \frac{2\gamma m t}{\sqrt{\pi}} h_0^3 \exp\left(-\frac{z^2}{4c_v t}\right) \\ &\times \sum_{n=-\infty}^{\infty} \left\{ n^2 \coth\left(mnh_0\sqrt{\frac{t}{c_v}}\right) \sinh\left(\frac{znh_0}{\sqrt{c_v t}}\right) \exp\left(-n^2 h_0^2\right) \right\} \end{aligned} \tag{5.4}$$

where n is a series number in the range of -∞ to +∞, z is divided into step interval of h_0.

Eq. (5.4) is the truly analytical solution proposed by Zheng et al. (2018a) for estimating the PWP during the slurry deposition on a pervious base. As shown in Zheng et al. (2018a), stable results of p_w can be obtained when n is taken between -55 and 55 and h_0 is taken as 0.5.

5.2.2 Solution for PWP after the slurry deposition

When the slurry deposition stops at time t_0 with a final height H (=$m \times t_0$), the thickness ceases to increase while the excess PWP dissipation continues. Gibson (1958) proposed a differential equation for the dissipation of excess PWP after the slurry deposition on an impervious base. However, no equation exists for the case of pervious base.

Considering the traditional consolidation theory of Terzaghi (1943), the following equation can be obtained for the (excess) PWP p_{w1} after the slurry deposition:

$$c_v \frac{\partial^2 p_{w1}}{\partial z^2} = \frac{\partial p_{w1}}{\partial t_1} \tag{5.5}$$

where $t_1 = (t - t_0)$ is the time starting from the end of slurry deposition.

Considering Eq. (5.4), the (excess) PWP at the end of slurry deposition (i.e. at $t = t_0$ or $t_1 = 0$) can be expressed as follows:

$$\begin{aligned} p_{w0}(z,t_0) = &-\gamma z\left(1+\frac{mz}{2c_v}\right)+\frac{2\gamma m t_0}{\sqrt{\pi}} h_0^3 \exp\left(-\frac{z^2}{4c_v t_0}\right) \\ &\times \sum_{n=-\infty}^{\infty}\left\{n^2 \coth\left(mnh_0\sqrt{\frac{t_0}{c_v}}\right)\sinh\left(\frac{znh_0}{\sqrt{c_v t_0}}\right)\exp\left(-n^2 h_0^2\right)\right\} \end{aligned} \tag{5.6}$$

Solving Eq. (5.5) and considering the initial condition Eq. (5.6) and boundary conditions $p_{w1} = 0$ at $z = 0$, H, the PWP after the slurry deposition can be calculated by the following equation (see Appendix I for details of the formulation):

$$p_{w1}(z,t_1) = \frac{2}{H}\sum_{\alpha=1}^{\infty}\exp\left[-c_v\left(\frac{\alpha\pi}{H}\right)^2 t_1\right]\times\sin\left(\frac{\alpha\pi z}{H}\right)\times\int_0^H p_{w0}(z,t_0)\times\sin\left(\frac{\alpha\pi z}{H}\right)dz \tag{5.7}$$

Eq. (5.7) constitutes the proposed solution to evaluate the (excess) PWP after the slurry deposition. It can readily be solved by some mathematical tools, such as MATLAB (Mathworks 2011). A

MATLAB program developed for calculating (excess) PWP after slurry deposition is presented in Appendix II.

5.3 Comparison with numerical simulations

The finite-element software SIGMA/W (GEO-SLOPE 2008) is used here to validate the proposed solutions [Eqs. (5.4) and (5.7)]. Fig. 5-2(a) shows the physical model of an underground mine stope filled with a slurried backfill. The stope has a width of 6 m. It is filled to a final height of 8 m at a filing rate of m = 0.2 m/h (Thompson et al. 2012). The backfill is characterized as linearly elastic with the properties of: γ = 20 kN/m^3 (saturated unit weight), M' = 960 kPa (drained constrained modulus), μ = 0.2 (Poisson's ratio), k = 2.83×10^{-7} m/s (permeability) (Fahey et al. 2009, 2010). In the SIGMA/W, the drained Young's modulus E' can be calculated by the following equation:

$$E' = \frac{(1+\mu)(1-2\mu)M'}{(1-\mu)} \tag{5.8}$$

With μ = 0.2 and M' = 960 kPa, one obtains E' = 864 kPa.

With the hydraulic conductivity k (m/s) and the drained constrained modulus M' (kPa), the consolidation coefficient c_v (m^2/h) can be calculated as follows:

$$c_v = \frac{kM'}{\gamma_w} \tag{5.9}$$

where γ_w (= 9.8 kN/m^3) is the unit weight of water. With M' = 960 kPa, one obtains c_v = 0.1 m^2/h.

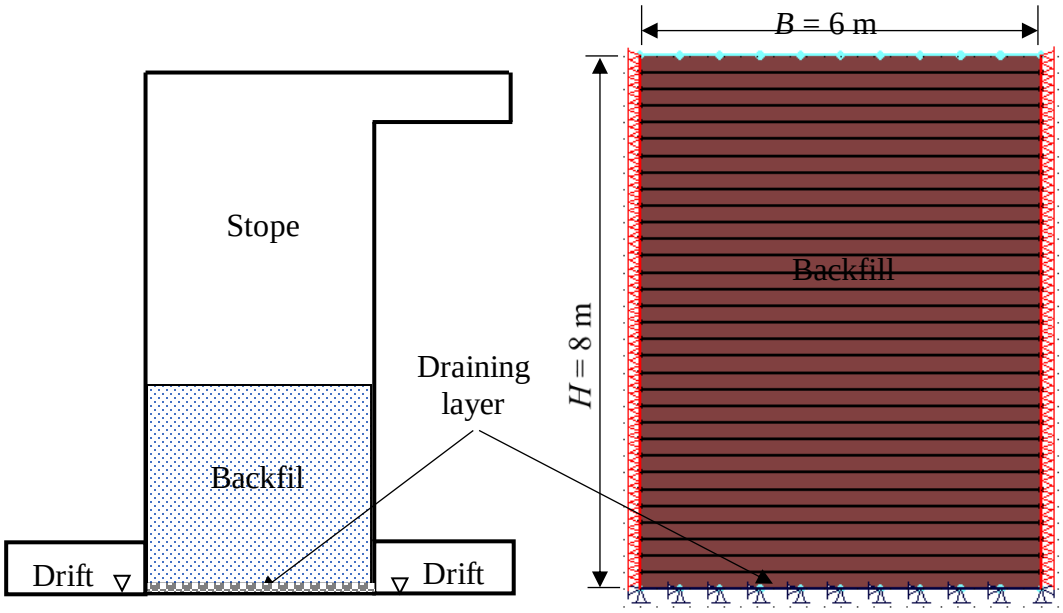

Figure 5-2 : An underground mine backfilled stope: (a) physical model; (b) numerical model built with SIGMA/W

Fig. 5-2(b) presents a numerical model built with SIGMA/W for the physical model [Fig. 5-2(a)]. The two vertical walls are impermeable. The displacements are prohibited in the horizontal direction, but allowed in the vertical direction. The base of the backfill is free draining and fixed in the horizontal and vertical directions. After addition of each new layer, a certain time is allocated to allow the drainage and consolidation through the bottom and top surfaces of backfill. The continuous backfilling is thus approximated in SIGMA/W by instantaneous additions of a series of thin layers. To approach a continuous backfilling, the thickness of each layer should be as small as possible (Zheng et al. 2018a, 2018b). Here, the thickness of each layer is taken as $\Delta h = 0.25$ m. At a filling rate of $m = 0.2$ m/h, the interval between two consecutive layers is 1.25 h.

Fig. 5-3 shows the distribution and evolution of the (excess) PWP along the height of backfill during and after the slurry deposition on a pervious (free draining) base, obtained by numerical modeling with SIGMA/W and calculated with the proposed solutions [Eqs. (5.4) and (5.7)]. It can be seen that an excellent agreement is obtained between the numerical and proposed solutions. The proposed solutions [Eqs. (5.4) and (5.7)] can thus be considered as valid and constitute a useful and simple tool to evaluate the (excess) PWP evolution in a slurried material during and after the deposition on a pervious base.

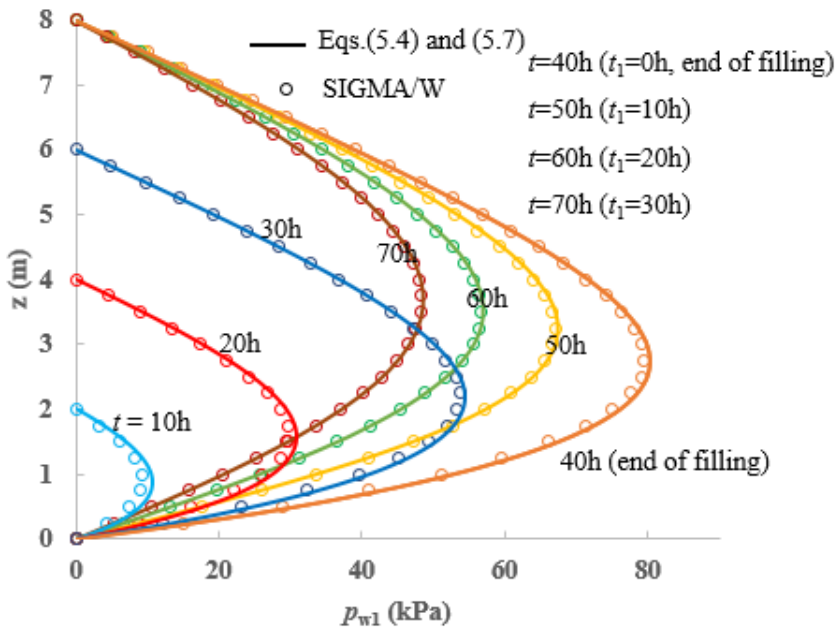

Figure 5-3: Distribution and evolution of the (excess) PWP along the height of the backfill during and after the deposition on a pervious base, obtained by numerical modeling with SIGMA/W and calculated with the proposed solutions [Eqs. (5.4) and (5.7)]. Calculation made with c_v = 0.1 m^2/h, m = 0.2 m/h, γ = 20 kN/m^3, and H = 8 m

5.4 Sample application of the proposed solutions

In this section, the proposed solutions [Eqs. (5.4) and (5.7)] are applied to investigate the PWP distribution and evolution in tailings dams or underground mine stopes during and after the deposition. The influence of the consolidation coefficient and filling rate on the (excess) PWP dissipation are investigated.

5.4.1 Tailings dams

As sample applications of the proposed solutions, one considers the deposition of a tailings at a filling rate of m = 4.8 m/year (= 0.548 mm/h; Seneviratne et al. 1996) up to a final height of H = 20 m.

Fig. 5-4 shows the distribution and evolution of the (excess) PWP along the height of a hard rock [Fig. 5-4(a)] and an oil sand [Fig. 5-4(b)] tailings during and after the deposition, calculated with the proposed solutions [Eqs. (5.4) and (5.7)]. The hard rock tailings are characterized by γ_{sat} = 20 kN/m^3 and c_v = 0.018 m^2/h (Seneviratne et al. 1996; Aubertin et al. 1996) while the oil sand tailings

by γ_{sat} = 13.3 kN/m^3 and c_v = 0.00057 m^2/h (Qiu and Sego 2001; Jeeravipoolvarn et al. 2009). It can be seen that the PWP increases continuously during the slurry deposition. At the end of slurry deposition (t = 4.167 years; t_1 = 0), the PWP reaches maximum along the height with a peak value of 26.6 kPa around an elevation of z = 11 m for hard rock tailings and 140.5 kPa for oil sand tailings. These peak values are much lower than the iso-static overburden pressure (= γH = 20 kN/m^3 × 20 m = 400 kPa) or hydrostatic pressure (= $\gamma_w H$ = 10 kN/m^3 × 20 m = 200 kPa). These results indicate the drainage and consolidation during the slurry deposition lead to considerable reduction of the (excess) PWP. Neglecting the drainage and consolidation of the slurry leads to significant overestimation of the (excess) PWP. After the end of slurry deposition, the drainage and consolidation process continue, accompanied with the dissipation and reduction of the (excess) PWP. The peak value of the (excess) PWP reduces from 26.6 kPa at the end of deposition (t_1 = 0) to 8.5 kPa, 0.3 year later after the end of the slurry deposition for hard rock tailings, while it takes 3 years for the peak value of (excess) PWP to reduce from 140.5 kPa at the end of deposition (t_1 = 0) to 92.8 kPa for oil sand tailings.

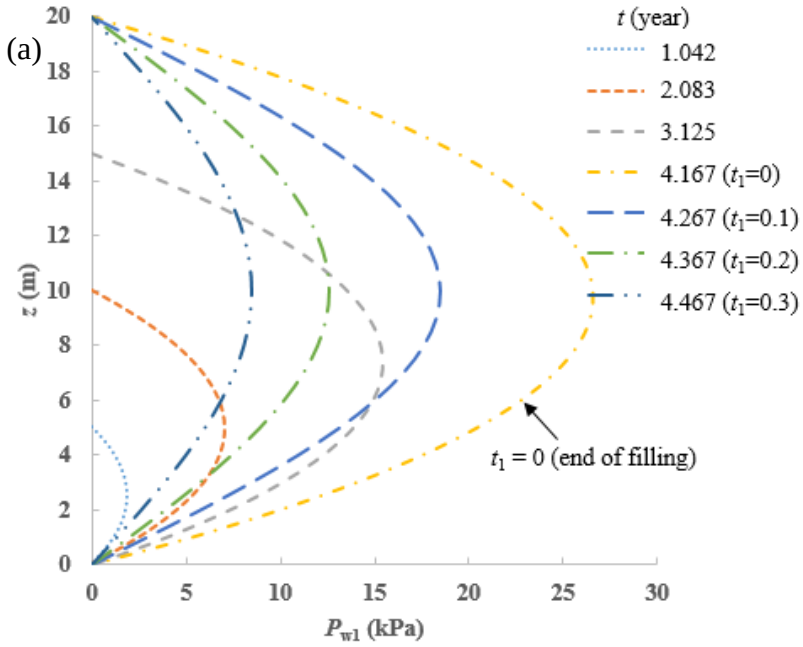

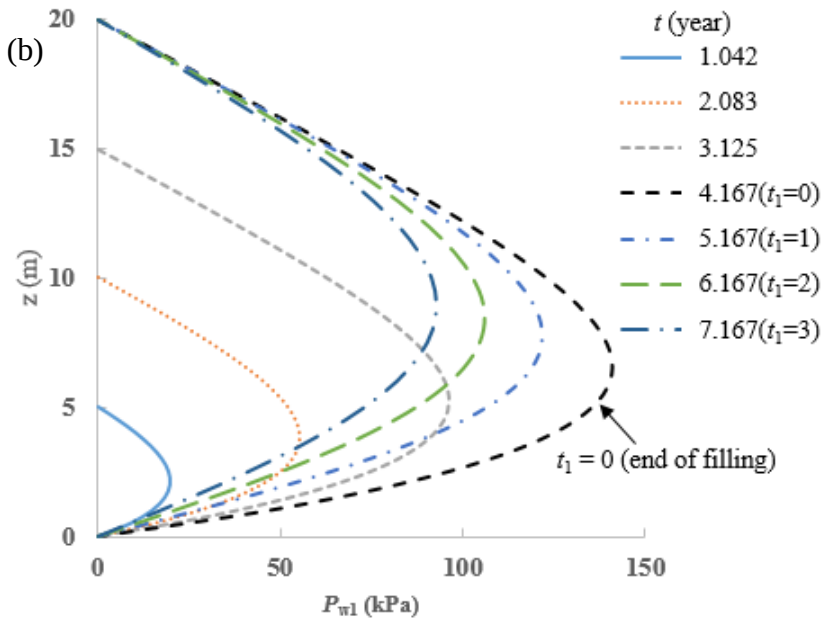

Figure 5-4: Distribution and evolution of the (excess) PWP in tailings during and after the deposition on a pervious base at a filling rate of m = 4.8 m/year (= 0.548 mm/h; Seneviratne et al. 1996) to a final height of H =20 m, calculated with the proposed solutions [Eqs. (5.4) and (5.7)]: (a) with c_v = 0.018 m^2/h for typical hard rock tailings; (b) with c_v = 0.00057 m^2/h for typical oil sand tailings

Fig. 5-5 shows the distribution and evolution of the (excess) PWP along the height of tailings after the end of tailings deposition, predicted by the proposed solutions [Eqs. (5.4) and (5.7)] as the consolidation coefficient c_v increases from 0.0018 to 0.045 m^2/h. The tailings have a saturated unit weight of γ_{sat} = 20 kN/m^3. It is deposited at a rate of m = 4.8 m/year (=0.548 mm/h) to a final height of H = 20 m. One sees that high consolidation coefficient leads to low (excess) PWP at the end of deposition (t_1 = 0 year) due to the high rate of (excess) PWP dissipation during the deposition. One year later after the tailings deposition, the (excess) PWP in the tailings having a high consolidation coefficient (c_v = 0.045 m^2/h) is almost completely dissipated with a peak value of 0.09 kPa while the peak value of the (excess) PWP in tailings having a low consolidation coefficient (c_v = 0.0018 m^2/h) remains as high as 112.2 kPa. These results are not surprising because the increase of the drainage and consolidation with higher consolidation coefficient is well known. It is however the first time that the influence is quantitatively evaluated through an analytical model.

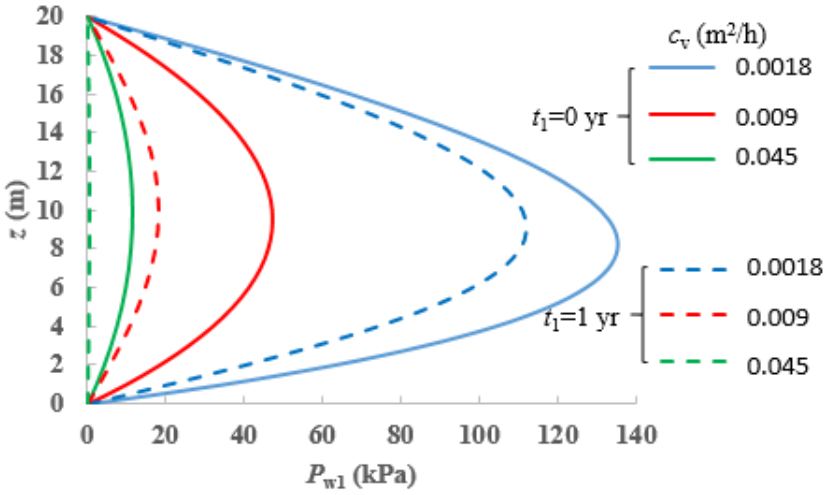

Figure 5-5: Distribution and evolution of the PWP along the height of a tailings after the end of slurry deposition, calculated with the proposed solutions [Eqs. (5.4) and (5.7)] by considering H = 20 m, m = 4.8 m/year, and γ_{sat}= 20 kN/m^3

Fig. 5-6 shows the distribution and evolution of the PWP along the height of the tailings after the end of tailings deposition as the filling rate increases from 4.8 to 9.6 m/year. The tailings have a saturated unit weight of γ_{sat} = 20 kN/m^3 and a consolidation coefficient c_v = 0.018 m^2/h. Its final height is H = 20 m. One can see that the (excess) PWP changes significantly with the filling rate. With a filling rate of 9.6 m/year, the peak value of the (excess) PWP can reach as high as 47.5 kPa at the end of deposition (t_1 = 0 year) or 22.4 kPa 0.2 years (t_1 = 0.2 years) later after the slurry deposition. With a filling rate of 4.8 m/year, the peak values of the (excess) PWP then reduce to 26.6 kPa at the end of deposition (t_1 = 0 year) or to 12.5 kPa, 0.2 years later after the slurry deposition. These results indicate that high filling rate leads to generation of high (excess) PWP at the end of deposition and longtime is needed to dissipate the (excess) PWP. Once again, this is well known. But it is the first time that the influence of the filling rate is quantitatively evaluated through an analytical model.

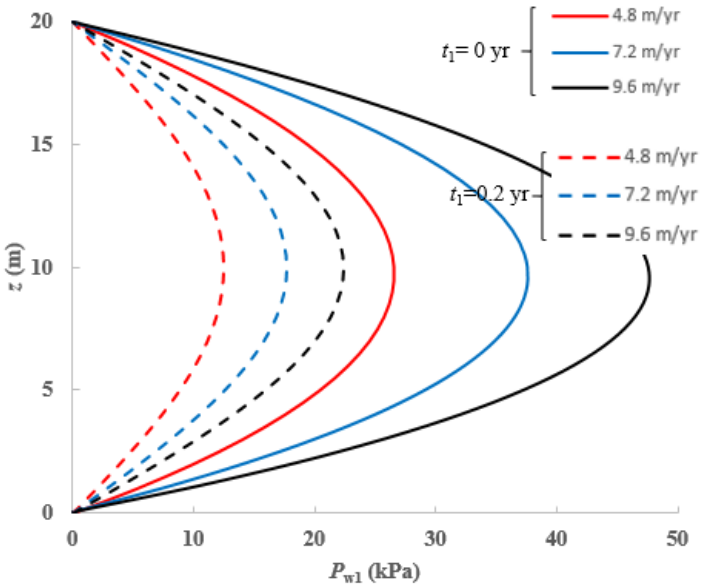

Figure 5-6: Distribution and evolution of the PWP within tailings after the tailings deposition, calculated with the proposed solution [Eqs. (5.4) and (5.7)] by considering H = 20 m, c_v = 0.018 m^2/h, and γ_{sat} = 20 kN/m^3

5.4.2 Underground mine backfilled stopes

The proposed solutions [Eqs. (5.4) and (5.7)] can also be used to evaluate the (excess) PWP distribution and evolution in slurried backfill during and after the placement in mine stopes. In the following, one considers an underground mine stope filled at a filling rate of m = 0.5 m/h to a final height of H = 8m. The backfill has a saturated unit weight of γ = 20 kN/m^3 and a consolidation coefficient of c_v = 1 m^2/h.

Fig. 5-7 shows the distribution and evolution of the (excess) PWP along the height of the backfill during and after the deposition. One sees that the (excess) PWP continuously increases with the deposition and reaches the maximum when the filling operation ceases (t_1 = 0 h), resulting in a peak value of 43.2 kPa. This value is much smaller than 160 kPa, a value based on iso-static overburden pressure. After the deposition, the (excess) PWP continues to decrease with the drainage and consolidation. The peak value reduces to 32.1, 23.7, and 17.4 kPa after 2, 4, and 6 h of waiting time, respectively. These results indicate that the PWP would be largely overestimated while the barricade design would be over conservative if the drainage and consolidation of the backfill during the filling operation are neglected.

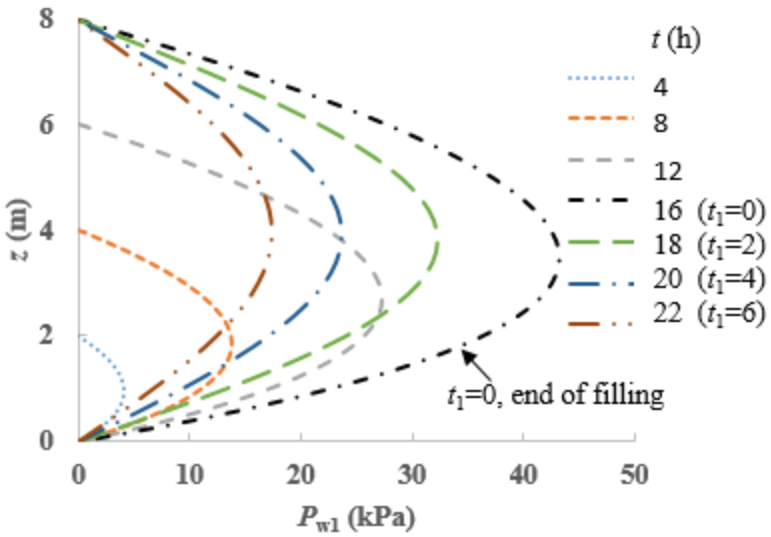

Figure 5-7: Distribution and evolution of the PWP within a backfilled stope during and after the deposition, calculated with the proposed solution [Eqs. (5.4) and (5.7)] by considering H = 8 m, c_v = 1 m^2/h, and m = 0.5 m/h

Fig. 5-8 shows the influence of the consolidation coefficient [Fig. 5-8(a)] and filling rate [Fig. 5-8(b)] on the distribution and evolution of the (excess) PWP along the height of the backfill after the deposition, calculated with the proposed solutions [Eqs. (5.4) and (5.7)]. Other parameters given (H = 8 m, γ = 20 kN/m^3 and m = 0.2 m/h), Fig. 5-8(a) shows that consolidation coefficient has a significant influence on the (excess) PWP dissipation during and after the placement of slurry backfill. At the end of backfilling, higher consolidation coefficient leads to the generation of higher PWP in the backfilled stope, with a peak value of 125.3 kPa for c_v = 0.01 m^2/h and 23.4 kPa for c_v = 1 m^2/h. 20 hours later after the end of backfilling, the peak value of the PWP slightly reduces to 115.9 kPa for c_v = 0.01 m^2/h, but almost to nil for c_v = 1 m^2/h. Other parameters given (H = 8 m, γ = 20 kN/m^3 and c_v = 0.01 m^2/h), Fig. 5-8(b) shows that the filling rate can considerably affect the distribution and evolution of the PWP in the backfilled stope during and after the backfilling operation. Filling at a higher filling rate leads to higher (excess) PWP at the end of the backfilling operation, with a peak value of 115.1 kPa at m = 1.0 m/h and 61.7 kPa at m = 0.1 m/h. 20 hours later after the end of filling operation, the peak value of the PWP reduces to 73.2 kPa at m = 1.0 m/h and 45.1 kPa at m = 0.1 m/h. These results show again that a slow filling is preferred to avoid the establishment of high (excess) PWP in backfilled stope (El Mkadmi et al. 2014).

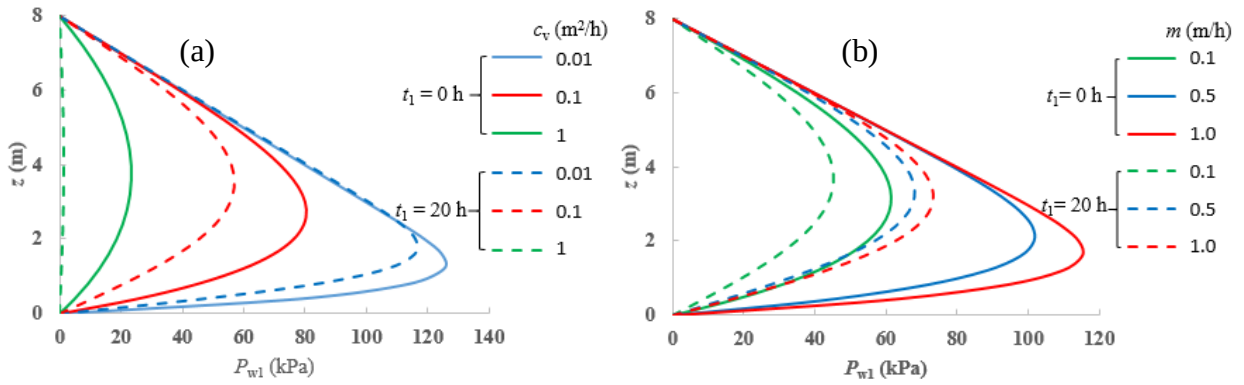

Figure 5-8: Distribution and evolution of the (excess) PWP along the height of the backfill after the end of backfilling operation, calculation made with the proposed solutions [Eqs. (5.4) and (5.7)] by considering H = 8 m and γ = 20 kN/m^3: (a) with m = 0.2 m/h and different coefficient consolidations, c_v; (b) with c_v = 0.1 m^2/h and different filling rates, m

5.5 Discussion

This paper proposed new solutions to evaluate the distribution and evolution of (excess) PWP in slurried material before and after the deposition on a pervious base, based on one-dimensional consolidation model of Gibson (1958). The proposed solutions constitute a simple and useful tool for design of slurry deposition (tailings or dredged sludge) or mine stope backfilling. However, one has to point out that the proposed solutions contain several limitations. For example, as the traditional consolidation theory of Terzaghi (1943), the Gibson (1958) model and the proposed solutions assume small strain consolidation with constant compressibility, permeability and consolidation coefficient. This assumption may be far from the reality and more work on this aspect is needed in the future.

Another limitation is related to the one-dimensional consolidation of the Gibson (1958) model. The model can be representative of field condition when the tailings or dredged sludge ponds are very large in horizontal directions or when the mine stope rock walls are impervious. Otherwise, horizontal drainage can occur and the application of the proposed solutions may lead to an underestimation of the (excess) PWP dissipation. This is particularly true when waste rock inclusions are applied to accelerate the drainage and consolidation of tailings (James 2009; Bolduc and Aubertin 2014) or when the stope rock walls are fractured or jointed (Belem et al. 2016).

Finally, one should note that the drainage and consolidation can lead to the development of effective stresses and shear strength, which, in turn, may lead to the generation of arching effect along the fill-wall contacts in underground mine stopes (Li et al. 2005; Li and Aubertin 2009a, 2009b). The (excess) PWP in mine backfilled stopes can thus be influenced by coupled process of consolidation and arching effect. More work is required and ongoing to take this aspect into account in the future.

5.6 Conclusion

A good understanding of the PWP distribution and evolution in slurried material during and after the deposition is essential to evaluate the stability and storage capacity of the confining structures, including tailings or dredged sludge dams and mine backfilled stopes. In this paper, a solution is proposed to evaluate the distribution and evolution of (excess) PWP evolution during and after the deposition of slurried material on a pervious base, based on the Gibson (1958) model. The proposed solutions have been validated by numerical modeling performed with SIGMA/W. Sample applications of the proposed solutions show that the dissipation of (excess) PWP accompanied with the drainage and consolidation of the slurry deposition can be slow as the consolidation coefficient (c_v) is small or/and the filling rate (m) is high, resulting in high (excess) PWP during and after the slurry deposition. High (excess) PWP can be avoided through the elimination of fine particles to increase the permeability or slow down the filling rate. Alternatively, longer time has to be allocated to allow the dissipation of the (excess) PWP. These results correspond to what have been observed in numerical simulations or field measurements. It is however the first time that the distribution and evolution of the (excess) PWP are quantitatively evaluated through a simple solution.

Acknowledgements

The authors would like to acknowledge the financial support from the Natural Sciences and Engineering Research Council of Canada (NSERC 402318), Fonds de recherche du Québec—Nature et Technologies (FRQNT 2015-MI- 191676), and industrial partners of the Research Institute on Mines and the Environment (RIME UQAT-Polytechnique; http://rime-irme.ca/).

5.7 Appendix I: Derivation process for the proposed solution [Eq. (5.7)]

Eq. (5.5) can be solved by applying the method of separation of variables (Asmar 2004). The function $p_{w1}(z, t_1)$ can be expressed as follows:

$$p_{w1}(z,t_1) = Z(z)T(t_1) \tag{5.10}$$

where $Z(z)$ and $T(t_1)$ are functions of z and t_1, respectively.

The boundary conditions $p_{w1} = 0$ at $z = 0, H$ can then be met by $Z(0) = 0$ and $Z(H) = 0$

Substituting Eq. (5.10) into Eq. (5.5) yields

$$\frac{1}{Z(z)}\frac{d^2Z}{dz^2} = -\lambda = \frac{1}{c_v T(t_1)}\frac{dT}{dt_1} \tag{5.11}$$

where λ is a non-zero constant ($\lambda \neq 0$).

The former equality of Eq. (5.11) can be rewritten as

$$Z''(z) + \lambda Z(z) = 0 \tag{5.12}$$

A general solution of Eq. (5.12) is given as follows

$$Z(z) = C_1 \sin(\sqrt{\lambda} z) + C_2 \cos(\sqrt{\lambda} z) \tag{5.13}$$

Taking the boundary conditions $Z(0) = 0$ and $Z(H) = 0$ into Eq. (5.13) leads to

$$C_2 = 0 \tag{5.14}$$

$$C_1 \sin\sqrt{\lambda} H = 0 \tag{5.15}$$

The characteristic value of λ can then be obtained from Eq. (5.15) as follows:

$$\lambda = \left(\frac{\alpha\pi}{H}\right)^2 \ (\alpha = 1, 2, \ldots, \infty) \tag{5.16}$$

The characteristic function of $Z(z)$ for Eq. (5.13) can be expressed as:

$$Z_\alpha(z) = A_\alpha \sin\left(\frac{\alpha\pi}{H} z\right) \tag{5.17}$$

where A_α is a series of constants.

The latter equability of Eq. (5.11) can be rewritten as follows:

$$T'(t_1) + \lambda c_v T(t_1) = 0 \tag{5.18}$$

The characteristic function of $T(t_1)$ for Eq. (5.18) can be solved as

$$T_\alpha(t_1) = B_\alpha \exp\left(-c_v\left(\frac{\alpha\pi}{H}\right)^2 t_1\right) \tag{5.19}$$

where B_α is a series of constants.

Introducing Eqs. (5.17) and (5.19) into Eq. (5.10) leads to:

$$p_{w1}(z,t_1) = \sum_{\alpha=1}^{\infty} Z_\alpha(t) T_\alpha(t_1) = \sum_{\alpha=1}^{\infty} C_\alpha \exp\left(-c_v\left(\frac{\alpha\pi}{H}\right)^2 t_1\right) \times \sin\left(\frac{\alpha\pi}{H} z\right) \tag{5.20}$$

where C_α is a series of constants.

Considering the initial condition (at $t_1 = 0$) of Eq. (5.6) for the post-deposition process, the following equation can be obtained:

$$p_{w0}(z,t_0) = p_{w1}(z,0) = \sum_{\alpha=1}^{\infty} C_\alpha \sin\left(\frac{\alpha\pi}{H} z\right) \tag{5.21}$$

or:

$$\int_0^H p_{w0}(z,t_0) \times \sin\left(\frac{\beta\pi z}{H}\right) dz = \int_0^H \sum_{\alpha=1}^{\infty} C_\alpha \times \sin\left(\frac{\alpha\pi z}{H}\right) \times \sin\left(\frac{\beta\pi z}{H}\right) dz \tag{5.22}$$

The orthogonality of trigonometric function stipulates $\alpha = \beta$ (otherwise, the right side of Eq. (5.22) is equal to zero for $\alpha \neq \beta$). One thus has,

$$\int_0^H p_{w0}(z,t_0) \times \sin\left(\frac{\alpha\pi z}{H}\right) dz = \int_0^H \sum_{\alpha=1}^{\infty} C_\alpha \left[\sin\left(\frac{\alpha\pi z}{H}\right)\right]^2 dz = C_\alpha \times \frac{H}{2} \tag{5.23}$$

or:

$$C_\alpha = \frac{2}{H} \int_0^H p_{w0}(z,t_0) \times \sin\left(\frac{\alpha\pi z}{H}\right) dz \tag{5.24}$$

Substituting Eq. (5.24) into Eq. (5.20) leads to

$$p_{w1}(z,t_1)=\frac{2}{H}\sum_{\alpha=1}^{\infty}\exp\left[-c_v\left(\frac{\alpha\pi}{H}\right)^2 t_1\right]\times\sin\left(\frac{\alpha\pi z}{H}\right)\times\int_0^H p_{w0}(z,t_0)\times\sin\left(\frac{\alpha\pi z}{H}\right)dz \tag{5.25}$$

5.8 Appendix II: MATLAB program for solving Eq. (5.7)

A MATLAB program to solve Eq. (5.7) and output the (excess) PWP at an elevation z at a given time t_1 is given here. An example of calculation is conducted by using typical geometry and property parameters. To note that the result by executing the program depends on the value of n_{max}. For a given problem at a given elevation z and at a given time t_1, sensitivity analysis must be conducted to see if n_{max} is large enough to ensure a stable and accurate result of the (excess) PWP. Fig. 5-9 shows the variation of the PWP at z = 2.4 m at t_1 = 5 h obtained by executing the program as the value of n_{max} increases from 11 to 161. It can be seen that the calculated (excess) PWP tends to become stable when n_{max} is larger than 101.

```
%=========================================================================%
%   A new solution to evaluate the PWP (= excess PWP) in slurried material
during and after its deposition on a pervious base %
%=========================================================================%
nmax = 101; % nmax = number of elements;
time_0 = 40; % filling time during the accreting deposition (h);
m = 0.2; % filling rate during the accreting deposition (m/h);
H = m*time_0; % Final thickness of the backfill (m);
c_v = 1; % consolidation coefficient of the backfill (m²/h);
h_0 = 0.5; %step interval of x (x is the elevation; x = 0 at the bottom);
gama = 20; % saturated unit weight of the slurried material (γsat = 20 kN/m³);
time_1 = 5; % time after the deposition ceases (corresponding to t1 in Eq. 7);

for i = 1:nmax
    z(i) = H/(nmax-1)*(i-1);
    pw_0(i) = 0.0;
    for n = -55:55;
        temp1 = m*n*h_0*sqrt(time_0)/sqrt(c_v);
        temp2 = z(i)*n*h_0/sqrt(c_v* time_0);
        a = exp(-(n*h_0)^2)*coth(temp1)*sinh(temp2);
         if (n == 0)
```

```
            a=0.0;
        else
        end
        pw_0(i) = pw_0(i)+h_0/2.0*8.*sqrt((c_v*time_0)^3)*(n*h_0)^2*a;
    end
    pre_multi = gama*m/2./c_v/sqrt(pi*c_v*time_0)*exp(-
z(i)*z(i)/4./c_v/time_0);
    pw_0(i)=((-gama*z(i)*(1+m*z(i)/2./c_v)+pre_multi*pw_0(i)));
    end


for i = 1:nmax
    z(i) = H/(nmax-1)*(i-1);
    sum(i) = 0.0;
    temp3 = i*pi/m/time_0;
    for j = 1:nmax;
        delta_y = m*time_0/nmax;
        sum(i) = sum(i)+pw_0(j)*sin(temp3*j*delta_y)*delta_y;
    end
end


for i=1:nmax
    z(i) = H/(nmax-1)*(i-1);
    pw_1(i)=0.0;
            for k=1:nmax;
            temp4=k*pi/m/time_0*z(i);
            pw_1(i)=pw_1(i)+exp(-
1*c_v*(k*pi/m/time_0)^2*(time_1))*sin(temp4)*sum(k);
    end
    pw_1(i)=2/m/time_0*pw_1(i);
end


%output
fid = fopen('output filename.txt','w')
for i=1:nmax
    fprintf(fid,'%g %g\n',z(i),pw_1(i))
end
fclose(fid)
plot(pw_1,z,'-.');
```

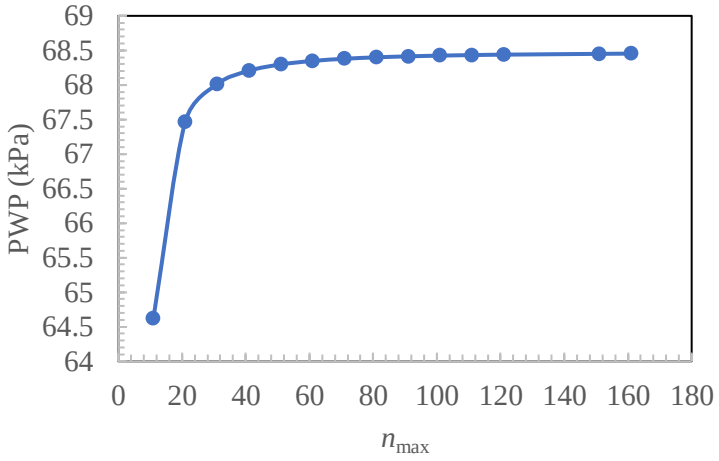

Figure 5-9 : A sensitivity analysis on the value of n_{max} to ensure stable and accurate (excess) PWP by using the MATLAB program

5.9 References

Alam, R., Shang, J.Q., & Islam, S. (2017). Electrophoresis and its applications in oil sand tailings management. *International Journal of Mineral Processing, 161*: 41-49.

Asmar NH. (2004) Partial differential equations and boundary value problems. Pearson Education, Upper Saddle River, NJ.

Aubertin, M., Bussiere, B., & Chapuis, R.P. (1996). Hydraulic conductivity of homogenized tailings from hard rock mines. *Canadian Geotechnical Journal, 33*(3), 470-482.

Been, K., & Sills, G.C. (1981). Self-weight consolidation of soft soils: an experimental and theoretical study. *Geotechnique, 31*(4), 519-535.

Beier, N., Wilson, W., Dunmola, A., & Sego, D. (2013). Impact of flocculation-based dewatering on the shear strength of oil sands fine tailings. *Canadian Geotechnical Journal, 50*(9), 1001-1007.

Belem, T., EI Aatar, O., Bussière, B., & Benzaazoua, M. (2016). Gravity-driven 1-D consolidation of cemented paste backfill in 3-m-high columns. *Innovative Infrastructure Solutions, 1*(1), 37.

Bolduc, F.L., & Aubertin, M. (2014). Numerical investigation of the influence of waste rock inclusions on tailings consolidation. *Canadian Geotechnical Journal, 51*(9), 1021–1032.

Caughill, D.L., Morgenstern, N.R., & Scott, J.D. (1993). Geotechnics of nonsegregating oil sand tailings. *Canadian Geotechnical Journal, 30*(5), 801-811.

Ganesalingam, D., Nagaratnam, S., & Ameratunga, J. (2012). Influence of settling behavior of soil particles on the consolidation properties of dredged clay sediment. *Journal of Waterway, Port, Coast, and Ocean Engineering, 139*(4), 295-303.

Doherty, J.P. (2015). A numerical study into factors affecting stress and PWP in free draining mine stopes. *Computers and Geotechnics, 63*, 331-341.

El Mkadmi, N., Aubertin, M., & Li, L. (2014). Effect of drainage and sequential filling on the behavior of backfill in mine stopes. *Canadian Geotechnical Journal, 51*(1), 1–15.

Energy Resources Conservation Board. (2009). *Directive 074: Tailings performance criteria and requirements for oil sands mining schemes.* Calgary, Alberta, Canada.

Fahey, M., Helinski, M., & Fourie, A. (2010). Consolidation in accreting sediments: Gibson's solution applied to backfilling of mine stopes. *Géotechnique, 60*(11), 877-882.

GEO-SLOPE. (2008) Stress-deformation modeling with SIGMA/ W 2007 (3th ed.). GEO-SLOPE International Ltd, Calgary, Alberta, Canada.

Gibson, R.E., Schiffman, R.L., & Whitman, R.V. (1989). On two definitions of excess pore water pressure. *Geotechnique, 39*(1), 169-171.

Gibson, R.E. (1958). The progress of consolidation in a clay layer increasing in thickness with time. *Géotechnique, 8*(4), 171-182.

Goodwin, E.T. (1949). *The evaluation of integrals of the form* $\int_{-\infty}^{+\infty} f(x)e^{-x^2}dx$. Paper presented at the Mathematical Proceedings of the Cambridge Philosophical Society. Cambridge University, London, UK (pp. 241-245).

Jaditager, M., & Sivakugan, N. (2017). Influence of fly ash–based geopolymer binder on the sedimentation behavior of dredged mud. *Journal of Waterwway, Port, Coastal, and Ocean Engineering, 143*(5), 04017012.

James, M. (2009). The use of waste rock inclusions to control the effects of liquefaction in tailings impoundments. (Doctoral dissertation, Ecole Polytechnique de Montréal, Montréal, Canada).

Jeeravipoolvarn, S., Scott, J.D., & Chalaturnyk, R.J. (2009). 10 m standpipe tests on oil sands tailings: long-term experimental results and prediction. *Canadian Geotechnical Journal, 46*(8), 875-888.

Li, L., Alvarez, I.C., & Aubertin, J.D. (2013). Self-weight consolidation of a slurried deposition: tests and interpretation. *International Journal of Geotechnical Engineering, 7*(2), 205–213.

Li, L., Aubertin, M., & Belem, T. (2005). Formulation of a three dimensional analytical solution to evaluate stress in backfilled vertical narrow openings. *Canadian Geotechnical Journal, 42*(6), 1705–1717 (with Erratum 2006, 43(3), 338–339).

Li, L., & Aubertin, M. (2009a). Influence of water pressure on the stress state in stopes with cohesionless backfill. *Geotechnical and Geological Engineering, 27*(1), 1–11.

Li, L., & Aubertin, M. (2009b). A three-dimensional analysis of the total and effective stresses in submerged backfilled stopes. *Geotechnical and Geological Engineering, 27*(4), 559–569.

Li, L. (2013). Beneficial Experience from teaching and education to research and development. *Creative Education, 3*(7), 148–153.

Malekzadeh, M., & Sivakugan, N. (2017). One-dimensional electrokinetic stabilization of dredged mud. *Marine Georesources & Geotechnology, 35*(5), 603-609.

Matlab, M (2011). MATLAB—The language of technical computing (Version 2014). [Computer software]. Retrieved from http://www.mathworks.com/products/matlab/

Pane, V., & Schiffman, R.L. (1985). A note on sedimentation and consolidation. *Géotechnique, 35*(1), 69-72.

Pedroni, L. (2011). Étude expérimentale et numérique de la sédimentation et de la consolidation des boues de traitement des eaux acides. (Doctoral dissertation, École Polytechnique de Montréal, Montréal, Canada).

Qiu, Y.X., & Sego, D.C. (2001). Laboratory properties of mine tailings. *Canadian Geotechnical Journal, 38*(1), 183-190.

Ripley, E.A., Redmann, R.E., & Maxwell, J. (1978). *Environmental impact of mining in Canada*. Centre for Resource Studies, Queen's University, Kingston, Ontario (pp. 101-203).

Seneviratne, N.H., Fahey, M., Newson, T.A., & Fujiyasu, Y. (1996). Numerical modelling of consolidation and evaporation of slurried mine tailings. *International Journal for Numerical and Analytical Methods in Geomechanics, 20*(9), 647-671.

Shahsavari, M., & Grabinsky, M. (2014). *Cemented paste backfill consolidation with deposition-dependent boundary conditions*. Paper presented at the 67th Canadian Geotechnical Conference, Canadian Geotechnical Society, Regina, Saskatchewan, Canada.

Shahsavari, M., & Grabinsky, M. (2015). *Mine backfill porewater pressure dissipation: numerical predictions and field measurements*. Paper presented at the 68th Canadian Geotechnical

Conference, Canadian Geotechnical Society, Québec City, Canada (pp. 1-8). Terzaghi K. (1943) Theory of consolidation. Wiley, New York, USA.

Zheng, J., Li, L., Mbonimpa, M., & Pabst, T. (2018a). An analytical solution of Gibson's model for estimating the pore water pressures in accreting deposition of slurried material under one-dimensional self-weight consolidation. Part I: Pervious base. *Indian Geotechnical Journal*, *48*(1), 72-83.

Zheng, Jian., Li, L., Mbonimpa, M., & Pabst, T. (2018b). An analytical solution of Gibson's model for estimating pore water pressures in accreting deposition of slurried material under one-dimensional self-weight consolidation. Part II: Impervious base. *Indian Geotechnical Journal*, *48*(1), 188-195.

CHAPTER 6 ARTICLE 4: A SOLUTION TO ESTIMATE THE EXCESS PWP DURING AND AFTER SLURRY DEPOSITION ON AN IMPERVIOUS BASE

Jian Zheng, Li Li, Yu-Chao Li, Mamert Mbonimpa

Article submitted to *Geomechanics and Engineering* in July 2018.

Abstract: In coastal engineering, the storage of dredged sludge needs the construction of containment structure. In mining engineering, the surface disposal of tailings slurry requires the construction of tailings dam while the placement of mining backfill in an underground opening (stope) has the necessity of a retaining structure, called barricade. A common task among them is to estimate the excess pore water pressure (PWP) in the slurry during and after its deposition. To this end, a model was proposed by Gibson in 1958. Equations were given to describe the evolution of the excess PWP during and after the slurry deposition. For the former case, the equation is not an analytical solution because it contains an integral that can only be solved by numerical method. For the latter case, the equation contains an error and cannot be directly used to evaluate the excess PWP. In this paper, the Gibson model is first revisited. For the sake of completeness, the authors' analytical solution for the case of during slurry deposition is also recalled. A new solution is then proposed, based on the Gibson's governing equation for the case of after slurry deposition on an impervious base. The proposed solutions are validated by numerical results obtained with SIGMA/W of Geoslope. Sample calculations are made to show the influence of the consolidation coefficient and filling rate on the distribution and evolution of the excess PWP in slurry deposited on an impervious base.

Keywords: Tailings dam; backfilled stope; dredged sludge; excess pore water pressure; drainage and consolidation; impervious base

6.1 Introduction

In geotechnical engineering, one often needs to design containment structures constructed to retain slurried materials (He et al. 2017; Zhang et al. 2017). In civil engineering, the storage of dredged sludge from river or seabed cleaning operations requires the construction of confining structures (Berilgen et al. 2006; Ganesalingam et al. 2012). In mining engineering, the surface disposal of tailings needs the building of tailings dams (Caughill et al. 1993; Qiu and Sego 2001; Aubertin et al. 2002; Bussière 2007; ERCB 2009; Aubertin and Mckenna 2016; Alam et al. 2017), while the placement of mining backfill in underground openings (mine stopes) has the necessity of a retaining structure, called barricade (Sivakugan et al. 2006a, 2006b; Belem and Benzaazoua 2008; El Mkadmi et al. 2014; Komurlu and Kesimal 2015; Komurlu et al. 2016; Jaouhar et al. 2018). Among them, a common task is to estimate the excess pore water pressure (PWP) during and after the deposition of the slurried material.

When a slurried material is deposited in a confining structure, the solid particles tend to settle down under the gravity. The backfill can then become denser while the pore water should be expelled out of the backfill. If the slurried backfill contains a large portion of fine particles, the hydraulic conductivity of the slurried backfill will be low and the pore water cannot flow out the backfill quickly. This leads to the generation of excess PWP (Pedroni 2011; Li 2013; Li et al. 2013; El Mkadmi et al. 2014). With the dissipation of the excess PWP, the particles approach each other and the slurried backfill becomes denser. The process of the dissipation of excess PWP before any contact between the solid particles (i.e. no effective stresses) is called sedimentation (Xu et al. 2012; Ahmed and Siddiqua 2014). As the drainage proceeds furthermore and the excess PWP dissipates enough, the solid particles start to get into contact each other and effective stresses are generated. The process of the dissipation of excess PWP accompanied with increasing effective stresses is called self-weight consolidation (Been and Sills 1981; Pane and Schiffman 1985).

The evaluation of the dissipation of excess PWP is critical to ensure the stability of the confining structures. The failure of such structures may result in serious consequence. For instance, the failure of tailings dam in Samarco mine, Brazil, in 2015 involved 20 killed, released more than 50 million cubic of mine waste into the Doce River and caused severe environmental hazard (Agurto-Detzel et al. 2016; Garcia et al. 2016; Queiroz et al. 2018). The barricade failure in Bronzewing mine,

Australia in 2000 led to the disappearance of three workers (Sivakugan et al. 2006b; Berndt et al. 2007).

The evaluation of the dissipation of excess PWP is also critical for tailings dam design as the drainage and consolidation are closely related to the water and tailings volume managements (Priscu 1999). With oil sand tailings, the Directive 074 of Energy Resource Conservation Board of Alberta, Canada (ERCB 2009) requires the development of undrained shear strength of at least 5 kPa within one year and minimum 10 kPa within 5 years in the deposited tailings. The 10 kPa is necessary to support the traffic of vehicles and secure the reclamation activities (Beier et al. 2013; Farkish and Fall 2014). The development of the undrained shear strength is closely related to the drainage and consolidation, which are inseparable from the dissipation of excess PWP.

Gibson (1958) has proposed a model to analyze the excess PWP in the accreting deposition of slurried materials. For the case of during slurry deposition, an equation was given. But it is not an analytical solution because it contains an integral that can only be solved by numerical method. A form of analytical solution has been developed (Zheng et al. 2018a, 2018b), who transformed the integral into a sum of series. For the case of after slurry deposition, Gibson (1958) proposed an equation, which contains an error.

In this paper, the Gibson (1958) model is first revisited for the case of an impervious base. For the sake of completeness, the authors' analytical solution for the case of during slurry deposition is also recalled. A new solution is then proposed, based on the Gibson's governing equation for the case of after slurry deposition on an impervious base. The proposed solution is validated against numerical results obtained with SIGMA/W. Sample calculations are made to show the influence of the consolidation coefficient and filling rate on the distribution and evolution of the excess PWP in slurry deposited on an impervious base.

6.2 Gibson model

Fig. 6-1 shows the model of Gibson (1958) considering accreting deposition of a slurried material on an impervious base. The thickness of the slurry deposition increases at a constant filling rate, m (m/h). H (m) and h (m) are the final and current thicknesses of the slurry deposition, respectively; x (m) is the elevation of a calculation point from the impervious base ($0 \leq x \leq h$). The solutions

proposed by Gibson (1958) for analyzing the excess PWP during and after the slurry deposition on an impervious base are presented below.

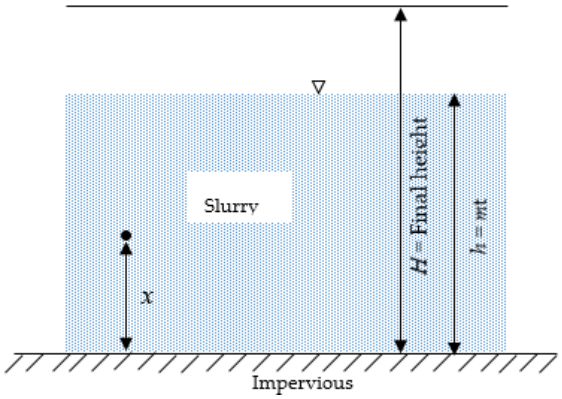

Figure 6-1: Accreting deposition of slurried material on an impervious base (Gibson 1958)

6.2.1 Gibson's solution for excess PWP during the slurry deposition

Based on the consolidation theory of Terzaghi (1943), Gibson (1958) proposed the following equation to evaluate the excess PWP distribution and evolution within the accreting slurry deposited on an impervious base:

$$c_v \frac{\partial^2 u}{\partial x^2} = \frac{\partial u}{\partial t} - \gamma' \frac{dh}{dt} \tag{6.1}$$

where c_v (m^2/h) is the consolidation coefficient; u (kPa) is the excess PWP, which is defined as the difference between the current total PWP and hydrostatic water pressure; t (h) is the filling time; γ' (kN/m^3) is the submerged unit weight of the slurry (i.e. $\gamma' = \gamma_{sat} - \gamma_w$; where γ_{sat} is the saturated unit weight of the slurry, γ_w is the unit weight of water with γ_w = 9.8 kN/m^3).

The current thickness h of the slurried material is expressed as follows:

$$h = mt \tag{6.2}$$

By considering boundary conditions $u = 0$ at $x = h$ and $du/dx = 0$ at $x = 0$, Gibson (1958) solved Eq. (6.1) and gave an expression of the excess PWP at elevation x as follows:

$$u = \gamma' mt - \frac{\gamma'}{\sqrt{\pi c_v t}} \exp\left(-\frac{x^2}{4c_v t}\right) \times \int_0^\infty \xi \tanh\left(\frac{m\xi}{2c_v}\right) \times \cosh\left(\frac{x\xi}{2c_v t}\right) \times \exp\left(-\frac{\xi^2}{4c_v t}\right) d\xi \tag{6.3}$$

where ξ (m) is an arbitrary integration parameter ($\infty > \xi > 0$).

To note that Eq. (6.3) has been called analytical solution by some researchers (Fahey et al. 2010; Doherty 2015; Shahsavari and Grabinsky 2014, 2015). However, it is not an analytical solution because it contains an integral, which can only be solved by numerical method.

6.2.2 Gibson's solution for excess PWP after the slurry deposition

When the deposition operation ceases at time $t = t_0$, the height of the deposition slurry h stops increasing and reaches its final height $h = H$. The dissipation of excess PWP within the deposition slurry continues. By applying again the classical theory of consolidation of Terzaghi (1943), Gibson (1958) gave an expression of the excess PWP u_1 at an elevation x after the deposition as follows:

$$c_v \frac{\partial^2 u_1}{\partial x^2} = \frac{\partial u_1}{\partial t_1} \tag{6.4}$$

where t_1 ($= t - t_0$) is the time starting from the end of the deposition operation.

By considering again the boundary conditions $u = 0$ at $x = h$ and du/d$x = 0$ at $x = 0$ to solve Eq. (6.4), the following equation was given by Gibson (1958):

$$u_1(x, t_1) = \frac{2}{H} \sum_{\alpha=1}^{\infty} \exp\left\{-\frac{\pi^2 c_v t_1}{4H^2}\right\} \times \cos\frac{(2\alpha - 1)\pi x}{2H} \int_0^H u_0(x, t_0) \times \cos\frac{(2\alpha - 1)\pi x}{2H} dx \tag{6.5}$$

Eq. (6.5) contains an error. A corrected equation will be given in the next subsection to evaluate the excess PWP after the slurry deposition.

6.3 Proposed solutions

The solution given by Gibson (1958) for the excess PWP during the slurry deposition has been considered as analytical solution (Fahey et al. 2010; Doherty 2015; Shahsavari and Grabinsky 2014, 2015). Zheng et al. (2018b) have shown that the solution of Gibson (1958) is not an analytical

solution because the integral contained in Eq. (6.3) cannot be solved by hand calculations or with commonly available and simple calculation tool such as Microsoft Excel. A truly analytical solution has been developed by Zheng et al. (2018b) and presented here for the sake of completeness. For the case of after the slurry deposition, the solution [Eq. (6.5)] of Gibson (1958) contains an error and cannot be used to calculate the excess PWP. More development is necessary and given in the following.

6.3.1 Solution for excess PWP during the slurry deposition

Zheng et al. (2018b) have shown that the integral contained in Eq. (6.3) can be approximated by a sum of series through the transformation of Goodwin (1949). A truly analytical solution for estimating the excess PWP during the slurry deposition was then given as follows (Zheng et al. 2018b):

$$u(x,t)=\gamma' mt-\frac{\gamma'}{\sqrt{\pi c_v t}}\times\exp\left(-\frac{x^2}{4c_v t}\right)\times\frac{h_0}{2}\sum_{n=-\infty}^{\infty}\left\{4c_v t n h_0\times\tanh\left(mnh_0\sqrt{\frac{t}{c_v}}\right)\times\cosh\left(\frac{xnh_0}{\sqrt{c_v t}}\right)\times\exp(-n^2h_0^2)\right\} \tag{6.6}$$

where h_0 is the step interval of x, n is the series number varying between -∞ and +∞.

Eq. (6.6) can be solved with hand or commonly available and simple calculation means (Excel of Microsoft, for example). For most cases, a stable result of u can be obtained when h_0 is taken as 0.3 and n ranges from -91 to 91.

6.3.2 Solution for excess PWP after the slurry deposition

When the deposition ceases at time $t = t_0$, the excess PWP at any point x within the sediment at time t_0 can be obtained with Eq. (6.6) and expressed as follows:

$$u_0(x,t_0)=\gamma' mt_0-\frac{\gamma'}{\sqrt{\pi c_v t_0}}\times\exp\left(-\frac{x^2}{4c_v t_0}\right)\times\frac{h_0}{2}\sum_{n=-\infty}^{\infty}4c_v t_0 n h_0\times\tanh\left(mnh_0\sqrt{\frac{t_0}{c_v}}\right)\times\cosh\left(\frac{xnh_0}{\sqrt{c_v t_0}}\right)\times\exp(-n^2h_0^2) \tag{6.7}$$

where $u_0(x, t_0)$ is the excess PWP at elevation x at the end of deposition $t = t_0$.

Considering the initial condition described by Eq. (6.7) at $t_1 = t - t_0 = 0$ and the hydraulic boundary conditions $u_1 = 0$ at $x = H$ ($= m \times t_0$) and $du_1/dx = 0$ at $x = 0$, the excess PWP after the deposition ($t_1 > 0$) can be expressed as follows (see formulation details given in Appendix I):

$$u_1(x,t_1) = \frac{2}{H}\sum_{\alpha=1}^{\infty}\exp\left\{-c_v t_1\left[\frac{(2\alpha-1)\pi}{2H}\right]^2\right\}\times\cos\frac{(2\alpha-1)\pi x}{2H}\int_0^H u_0(x,t_0)\times\cos\frac{(2\alpha-1)\pi x}{2H}dx \qquad (6.8)$$

Eq. (6.8) constitutes the solution for estimating the distribution and evolution of the excess PWP in the sediment for $t \geq t_0$ after the slurry deposition. It is different from Eq. (6.5) of Gibson (1958).

It is noted that the integral contained in Eq. (6.8) cannot be solved by hand or commonly available and simple calculation tools. However, it can readily be solved using some mathematic tools, such as MATLAB (Mathworks 2011). For these reasons, Eq. (6.8) is called pseudo analytical solution to evaluate the distribution and evolution of the excess PWP after the slurry deposition on an impervious base.

A MATLAB program to solve Eq. (6.8) for estimating the excess PWP is presented in Appendix II by considering $H = 8$ m, $\gamma_{sat} = 20$ kN/m^3, $\gamma_w = 9.8$ kN/m^3, $m = 0.5$ m/h, $c_v = 1$ m^2/h, $t_0 = 16$ h, and $t_1 = 10$ h. It should be noted that the value of n_{max} should be large enough to obtain accurate and reliable results of u_1. Sensitivity analysis of n_{max} is thus conducted here. Fig. 6-2 shows the variation of the excess PWP (u_1) at $x = 0$ at $t_1 = 10$ h calculated with the MATLAB program with different values of n_{max}. It can be seen that the stable results can be obtained when n_{max} is larger than 101. The sensitivity analysis should be conducted for each calculation to ensure stable and accurate results.

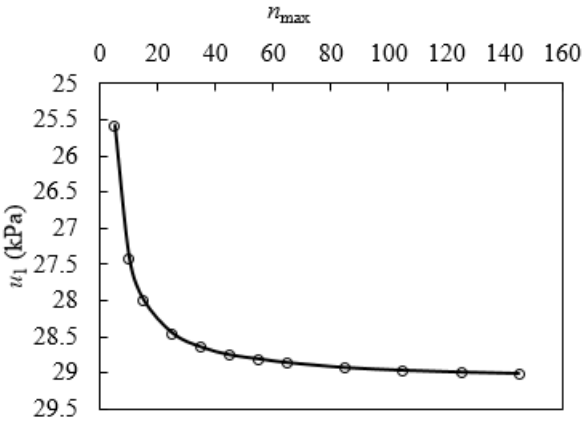

Figure 6-2: Sensitivity analysis of n_{max} to obtain stable and accurate excess PWP at x = 0 at t_1 = 10 h by using the MATLAB program; calculation made with H = 8 m, γ_{sat} = 20 kN/m^3, γ_w = 9.8 kN/m3, m = 0.5 m/h, c_v = 1 m2/h, t_0 = 16 h, and t_1 = 10 h

6.4 Validation of the proposed solutions by numerical modeling

In order to validate the proposed solutions [Eqs. (6.6) and (6.8)], numerical modeling with SIGMA/W (GEO-SLOPE 2008) was performed to evaluate the excess PWP distribution and evolution in a mine backfilled stope.

Fig. 6-3 shows the physical model [Fig. 6-3(a)] of an underground mine stope filled at a filling rate of m = 0.2 m/h with a slurried backfill. It is filled to a final height of H = 8 m, a typical value of plug pour in backfilled stopes (Li 2014). The stope has a width of 6 m. The backfill is considered as linearly elastic and characterized as γ_{sat} = 20 kN/m^3 (saturated unit weight), μ = 0.2 (Poisson's ratio), M' = 960 kPa (drained constrained modulus) and $k = 1.02\times10^{-2}$ m/h (hydraulic conductivity). The drained Young's modulus E' is deduced from the following relationship:

$$E' = \frac{(1+\mu)(1-2\mu)M'}{(1-\mu)} \tag{6.9}$$

Applying Eq. (6.9) with μ = 0.2 and M' = 960 kPa yields a drained constrained Young's modulus of E' = 864 kPa.

The consolidation coefficient of the backfill c_v (m^2/h) is calculated from the following relationship:

$$c_v = \frac{kM'}{\gamma_w} \tag{6.10}$$

Applying Eq. (6.10) with $k = 1.02\times10^{-2}$ m/h and $M' = 960$ kPa leads to a consolidation coefficient $c_v = 1.0$ m^2/h.

Fig. 6-3(b) shows the numerical model of SIGMA/W for the physical model shown in Fig. 6-3(a). The backfill is represented by a mesh of quadrilateral elements of 0.083 m (see more detail of the mesh with an enlarged view shown in the figure). This size was determined after a mesh sensitivity analysis. The two vertical walls are impermeable; they are mechanically fixed in the horizontal direction but free to move in the vertical direction. The bottom of the model is impermeable and mechanically fixed in both the horizontal and vertical directions. The top surface of each newly added backfill is permeable with zero PWP. The stope filling was simulated by instantaneously adding 32 backfill layers. The thickness of each layer is chosen as $\Delta h = 0.25$ m. This thickness was considered to be small enough to represent a continuous stope filling (see details in Zheng et al. 2018a, 2018b). The delay before the addition of new backfill layer is $\Delta h/m = 1.25$ h. The dissipation of the excess PWP in the backfill was monitored during and after the stope filling operation.

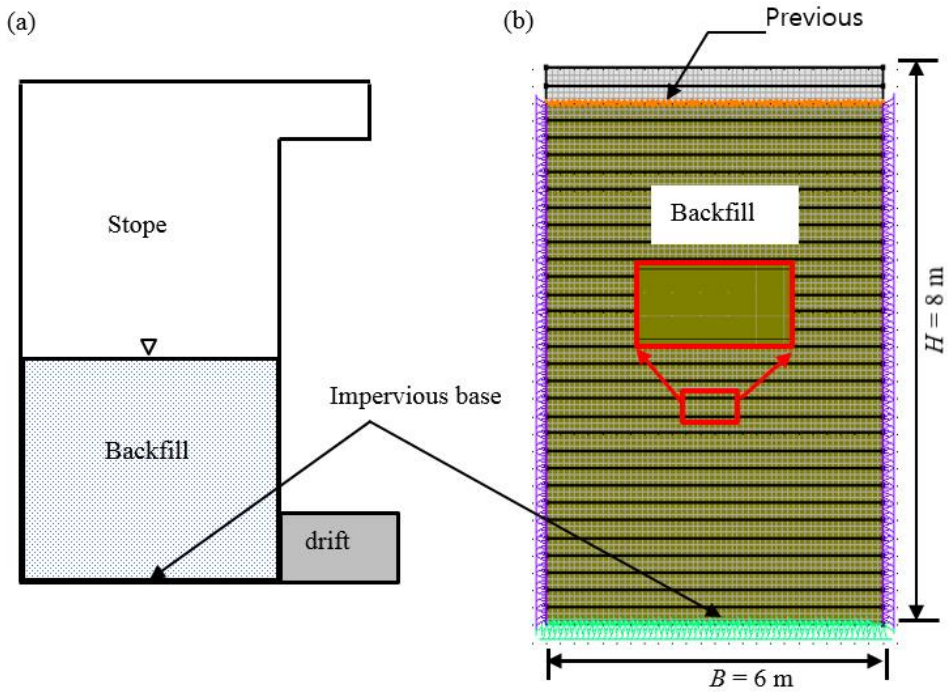

Figure 6-3: (a) Physical and (b) numerical model built in the SIGMA/W for the backfilled stope

Fig. 6-4 shows the distribution and evolution of the excess PWP before and after the end of deposition obtained by numerical modeling with SIGMA/W and calculated with the proposed solutions [Eqs. (6.6) and (6.8)]. Despite the relatively large thickness of each backfill layer (i.e.

0.25 m/layer) in SIGMA/W, the good agreement between the numerical and analytical results indicate that the proposed solutions [Eqs. (6.6) and (6.8)] are validated by the numerical modeling. The proposed solutions can thus be used to estimate the excess PWP distribution and evolution in slurried material deposited on an impervious base before and after the end of deposition.

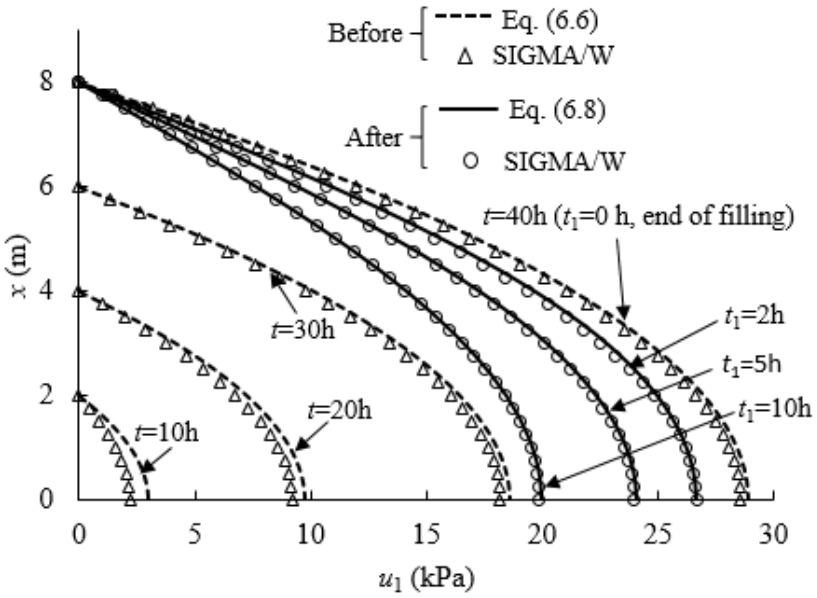

Figure 6-4: Distribution and evolution of the excess PWP obtained by the numerical modeling and calculated with the proposed solutions [Eqs. (6.6) and (6.8)] along the height of the backfill before and after the end of deposition. Calculations made with c_v = 1 m^2/h, m = 0.2 m/h, γ_{sat} = 20 kN/m^3, H = 8 m, μ = 0.2, E' = 864 kPa, k = 1.02×10^{-2} m/h

6.5 Sample application of the proposed solutions

The Gibson (1958) model was proposed to evaluate the one-dimensional consolidation of accreting material. The proposed solutions [Eqs. (6.6) and (6.8)] based on the Gibson (1958) model can thus be used to estimate the excess PWP in tailings or dredged sludge ponds or in mine backfilled stopes. In the following subsections, the proposed solutions will be applied to investigate the influence of some parameters on the excess PWP evolution in tailings ponds and in backfilled stopes.

6.5.1 Tailings ponds

One considers a tailings pond formed by the disposition of a hard rock or oil sand tailings at a filling rate of m = 0. 548 mm/h (4.8 m/year; Seneviratne et al. 1996) to a final height of H = 20 m.

The hard rock tailings have a saturated unit weight of γ_{sat} = 20 kN/m^3 and a consolidation coefficient of c_v = 0.018 m^2/h (Aubertin et al. 1996), while the oil sand tailings have a saturated unit weight of 13.3 kN/m^3 and a consolidation coefficient of c_v = 0.00057 m^2/h (Qiu and Sego 2001; Jeeravipoolvarn et al. 2009).

Fig. 6-5 shows the distribution and evolution of excess PWP during and after the tailings deposition along the height of the hard rock [Fig. 6-5(a)] and oil sand [Fig. 6-5(b)] tailings calculated with the proposed solutions [Eqs. (6.6) and (6.8)]. One sees that the excess PWP increases during the accreting deposition and reaches its peak value at the end of deposition (i.e. t = 4.2 years, t_1 = 0 year). The excess PWP distribution is not linearly distributed with the elevation during and after the slurry deposition. At the end of the tailings deposition, the excess PWP is about 40.7 kPa for hard rock tailings and 52.6 kPa for oil sand tailings, which are smaller than the expected values of 204 kPa (= $\gamma' H$ = 10.2 kN/m^3×20 m) and 70 kPa (= $\gamma' H$ = 3.5 kN/m^3×20 m) respectively for the hard rock and oil sand tailings if no drainage and consolidation occur. This indicates the occurrence of dissipation of the excess PWP during the tailings deposition due to the small filling rate (0.548 mm/h; Seneviratne et al. 1996) even though the tailings are relatively impermeable (c_v = 0.018 m^2/h for hard rock tailings and c_v = 0.00057 m^2/h for oil sand tailings).

After the end of tailings deposition, the excess PWP continues to be dissipated and diminish with time. Half year later after the end of hard rock tailings deposition (t_1 = 0.5 year), the peak value of the excess PWP reduces from 40.7 kPa to 25.6 kPa. The results show that one has to wait two years (t_1 = 2 years) in order for the peak value of the excess PWP to reduce to 6 kPa. For the oil sand tailings, the peak value of the excess PWP only slightly reduces from 52.6 kPa to 46.3 kPa three years (t_1 = 3 years) after the end of deposition, indicating a very slow process of the drainage and consolidation.

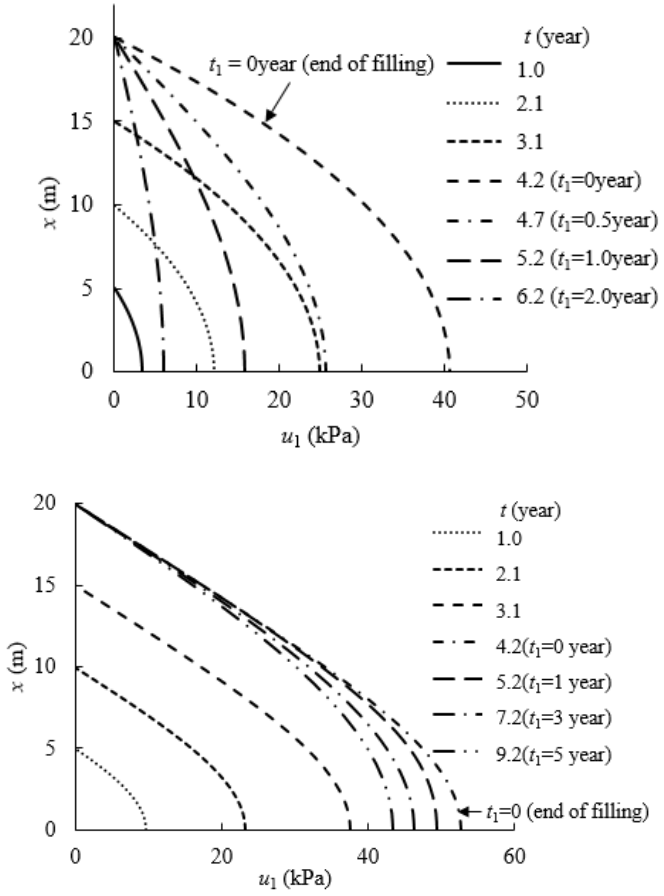

Figure 6-5: Distribution and evolution of the excess PWP within a tailings pond during and after the end of tailings deposition on an impervious base, calculated with the proposed solutions [Eqs. (6.6) and (6.8)]: (a) for hard rock tailings with H =20 m, γ_{sat} = 20 kN/m^3, c_v = 0.018 m^2/h, and m = 0.548 mm/h; (b) for oil sand tailings with H =20 m, γ_{sat} = 13.3 kN/m^3, c_v = 0.00057 m^2/h, and m = 0.548 mm/h

Fig. 6-6 shows the influence of the consolidation coefficient on the distribution and evolution of the excess PWP along the height of the tailings after the tailings deposition. Again, the tailings have a saturated unit weight of γ_{sat} = 20 kN/m^3. The deposition is realized at a filling rate of m = 4.8 m/year (= 0.548 mm/h) until a final height of H = 20 m. It can be seen that the excess PWP at the end of the tailings deposition (i.e. at t_1 = 0 h) decreases significantly as the consolidation coefficient c_v increases from 0.0018 to 0.045 m^2/h. One year later after the end of the tailings deposition (t_1 = 1 year or 8760 h), the dissipation of the excess PWP is almost complete with only a residual excess PWP of u_1 = 1.9 kPa for the tailings having a consolidation coefficient of c_v =

0.045 m^2/h while it remains as high as u_1 = 108.3 kPa for the tailings having a consolidation coefficient of c_v = 0.0018 m^2/h.

The influence of the consolidation coefficient on the dissipation of the excess PWP is a phenomenon well-know. But quantitatively, this is the first time that the distribution and evolution of the excess PWP during and after the tailings deposition are described by a mathematical model.

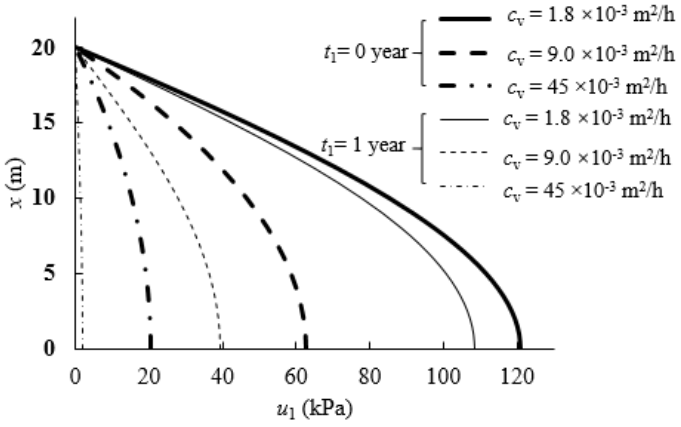

Figure 6-6: Distribution and evolution of the excess PWP within a tailings dam after the tailings deposition, calculated with the proposed solution [Eq. (6.8)] by considering H = 20 m, m = 4.8 m/year (= 0.548 mm/h), and γ_{sat}= 20 kN/m^3

Fig. 6-7 shows the distribution and evolution of the excess PWP along the height of the tailings pond after the tailings deposition as the filling rate m increases from 0.548 mm/h (4.8 m/year) to 1.096 mm/h (9.6 m/year) (Seneviratne et al. 1996). Again, the tailings slurry have a saturated unit weight of γ_{sat} = 20 kN/m^3, a consolidation coefficient of c_v = 0.018 m^2/h and a final height of H = 20 m. One sees that the filling rate significantly affect the drainage and consolidation of the tailings as well as the distribution and evolution of the excess PWP. When the 20 m high tailings pond is realized at a filling rate of m = 0. 548 mm/h, the peak excess PWP of u_1 = 40.7 kPa is reached at the end of tailings deposition (t_1 = 0 h). At a filling rate of m = 1.096 mm/h, the peak value of the excess PWP can reach 62.6 kPa at the end of the tailings deposition (t_1 = 0 h). Due to this initial difference in excess PWP at the end of tailings deposition, different excess PWP result one year later (t_1 = 1 year or 8760 h) after the end of tailings deposition, but the difference becomes smaller with u_1 = 15.8 kPa for m = 0.548 mm/h and u_1 = 24.2 kPa for m = 1.096 mm/h. These results are quite straightforward. With a higher filling rate, time allowed for dissipation of excess PWP is shorter, resulting in higher excess PWP (El Mkadmi et al. 2014; Zheng et al. 2018a, 2018b). From

the end of tailings deposition, higher excess PWP means higher hydraulic gradient, higher flowrate of drainage and faster dissipation of excess PWP. These results indicate that the proposed solutions can become useful in estimating the filling rate and time of rest if the allowed excess PWP is known to avoid any geotechnical stability problem of the tailings dams.

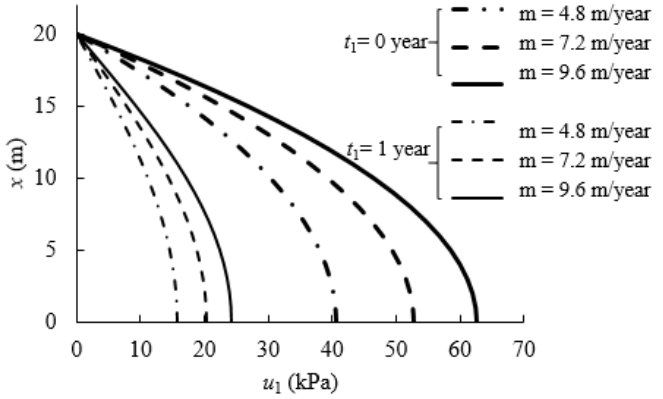

Figure 6-7: Distribution and evolution of the excess PWP in a tailings slurry after the tailings deposition for different filling rates m, calculated with the proposed solution [Eq. (6.8)] by considering H = 20 m, c_v = 0.018 m^2/h, and γ_{sat} = 20 kN/m^3

6.5.2 Underground mine backfilled stopes

Consider an underground mine stope filled at a filling rate of m = 0.5 m/h to a height of H = 8 m. The backfill has a saturated unit weight of γ_{sat} = 20 kN/m^3 and a consolidation coefficient of c_v = 1 m^2/h.

Fig. 6-8 shows the distribution and evolution of the excess PWP during and after the filling operation, obtained by applying the proposed solutions [Eqs. (6.6) and (6.8)]. It is seen that the excess PWP increases with the filling and reaches peak value at the end of filling operation (t = 16 h or t_1 = 0 h). Without any drainage and consolidation, a peak value of 81.6 kPa (= $\gamma' H$ = 10.2 kN/m^3 × 8 m) should be expected for the excess PWP at the bottom of the backfill. The peak value of u_1 = 42.5 kPa at the bottom of the backfill indicates significant dissipation of the excess PWP during the filling operation. After the end of filling operation, the excess PWP decrease with the rest time. These results indicate again that the pressure estimation by neglecting the drainage and consolidation during the filling operation can lead to an over conservative design of barricades (El Mkadmi et al. 2014; Zheng et al. 2018a, 2018b).

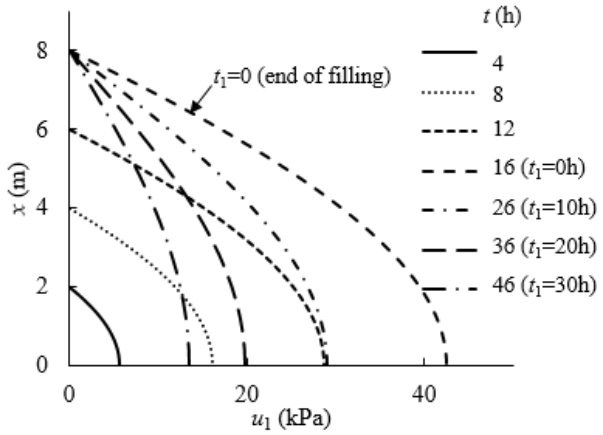

Figure 6-8: Distribution and evolution of the excess PWP in a backfilled stope before and after the backfill deposition, calculated with the proposed solutions [Eqs. (6.6) and (6.8)] by considering H = 8 m, γ_{sat} = 20 kN/m^3, c_v = 1 m^2/h, and m = 0.5 m/h

Fig. 6-9 shows the distribution and evolution of the excess PWP along the height of a mine backfilled stope after the filling operation as the filling rate increases from 0.1 to 1 m/h. The backfill has a final height of H = 8 m (plug pour) and a consolidation coefficient of c_v = 0.1 m^2/h. Again, one sees that the excess PWP reaches its peak values at the end of filling operation and a higher filling rate leads to higher excess PWP in the backfill. However, the peak values of the maximum excess PWP remain always smaller than that predicted by the iso-static pressure based on the overburden ($\gamma' H$ = 10.2 kN/m^3 × 8 m = 81.6 kPa). This indicates the occurrence of the dissipation of the excess PWP during the filling operation even though the backfill has a very small consolidation coefficient and the stope filling rate is as high as m = 1.0 m/h. When the filling rate is small, the peak values of the excess PWP at the end of filling operation become low. Due to the low consolidation coefficient of the backfill, the reduction of the excess PWP is not very significant 20 h (i.e. at t_1 = 20 h) after the end of the filling operation. These results indicate again that high excess PWP can be avoided through slow stope filling (El Mkadmi et al. 2014; Zheng et al. 2018a, 2018b).

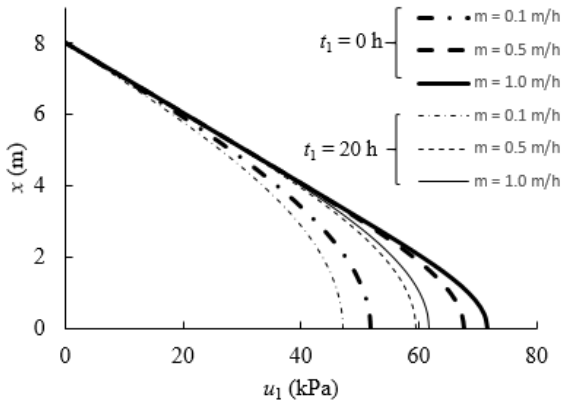

Figure 6-9: Distribution and evolution of the excess PWP in a backfilled stope during and after the backfill deposition for different filling rates m, calculated with the proposed solution [Eqs. (6.6) and (6.8)] by considering H = 8 m, c_v = 0.1 m^2/h, and γ_{sat} = 20 kN/m^3

Fig. 6-10 shows the distribution and evolution of excess PWP along the height of the mine stope after the filling operation, obtained by the proposed solutions [Eqs. (6.6) and (6.8)] as the consolidation coefficient c_v increases from 0.01 to 1 m^2/h. The backfill has a saturated unit weight of γ_{sat} = 20 kN/m^3 and a final height of H = 8 m. The filling rate m was taken as 0.2 m/h. Once again, one sees that higher excess PWP is generated at and after the end of stope filling with a backfill having lower consolidation coefficient c_v. Twenty hours later after the end of stope filling, the peak value of the excess PWP remains as high as 71.8 kPa for c_v = 0.01 m^2/h, but can fall to 13.6 kPa for c_v = 1 m^2/h. These results indicate that the consolidation coefficient of the backfill plays a key role in the dissipation of the excess PWP.

Again, the results shown above are qualitatively well-known and even shown by numerical modeling (El Mkadmi et al. 2014). However, it is for the first time that these results are illustrated quantitatively through the calculations of pseudo analytical solutions.

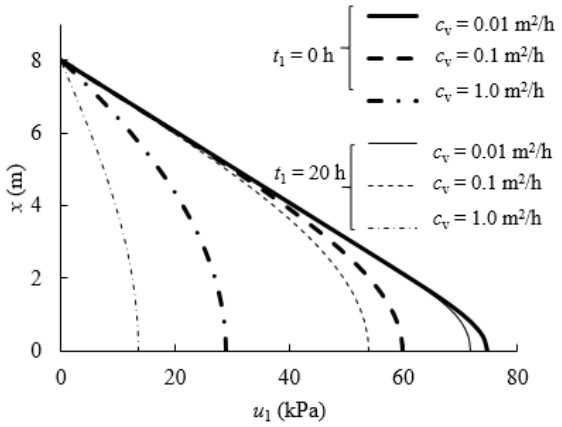

Figure 6-10: Distribution and evolution of the excess PWP in a backfilled stope during and after the backfill deposition for different consolidation coefficient c_v, calculated with the proposed solution [Eqs. (6.6) and (6.8)] by considering H = 8 m, m = 0.2 m/h, and γ_{sat} = 20 kN/m^3

6.6 Discussion

In this paper, a new solution is proposed to evaluate the excess PWP distribution and evolution using the one-dimensional consolidation model of Gibson (1958) before and after the slurry deposition. The proposed solution can be used to the cases of slurried material confined in tailings or dredge sludge dams or in mine stope. It is important to keep in mind that the proposed solutions contain several limitations. For instance, the Gibson (1958) model only considers unidimensional consolidation. The drainage only takes place in the vertical direction. This can be the case for dredged sludge or tailings dams with very large horizontal dimension or vertical mine stopes with impervious rock walls. The model and ensuing solutions can become invalid when lateral drainage takes place through jointed and pervious rock mass in mine stopes (Belem et al. 2016) or through conductive waste rock inclusions in tailings ponds (James 2009; Bolduc and Aubertin 2014).

Another limitation of the Gibson (1958) model and ensuing solutions is the consideration of small strain consolidation with constant consolidation coefficient c_v and without considering the settlement. In practice, the value of c_v changes with the drainage and consolidation (Fahey et al. 2010). In addition, the Gibson (1958) model and ensuing solutions do not make distinction between the sedimentation (dissipation of excess PWP without any development of effective stresses) and consolidation (dissipation of excess PWP with development of effective stresses). More work is needed to characterize the settlement and evolution of the hydraulic properties during the

sedimentation and consolidation. A more elaborate model can then be established to take into account the evolution of these hydraulic properties.

In underground mine stopes, the drainage and consolidation of the backfill will lead to the development of effective stress and arching effect along the fill-rock interfaces (Li et al. 2005; Li and Aubertin 2009a, 2009b). The arching effect or shear stresses along the interfaces tend to hold the particles in place and slow down the settlement or consolidation of the backfill. This aspect is part of ongoing work and will be part of future publications.

In the Gibson (1958) model and proposed solutions, the top surface of the slurry deposition was considered as permeable with zero PWP. In practice, water pond can form at the top of the tailings or backfill due to the sedimentation or consolidation. A new model is necessary to take into account the generation of the water pond.

The proposed solutions were developed by considering an impervious base. In practice, tailings or mine backfill can be deposited on a pervious base to accelerate their drainage and consolidation (Sivakugan et al. 2006a; Li and Aubertin 2011; Zheng et al. 2018a). More work is needed to account for pervious base on the estimation of the PWP.

Finally, it should be noted that the proposed solutions were not validated by experimental results. In the literature, a number of laboratory tests were reported, including the self-weight consolidation tests (Pedroni and Aubertin 2013; Li et al. 2013; Saleh-Mbemba and Aubertin 2018). These results cannot be used to validate or invalidate the proposed solution as the slurry deposition was done instantaneously in all these tests. Laboratory test work is needed to validate or calibrate the proposed solutions. This work is ongoing and will be part of future publications.

6.7 Conclusion

In this paper, the Gibson (1958) model considering one-dimensional drainage of accreting deposition on an impervious base has been revisited. For the case of during slurry deposition, an analytical solution proposed by the authors based on the Gibson model has first been recalled. For the case of after slurry deposition, a pseudo analytical solution based on the Gibson model was for the first time given. The two solutions constitute the proposed solutions to estimate the excess PWP in slurried material during and after the slurry deposition on an impervious base. The proposed solutions have been validated by numerical results obtained with SIGMA/W of Geoslope. They

can thus be used to evaluate the excess PWP in dredged sludge or tailings confined by dams or in underground mine stopes with an impervious base. Sample calculations using the proposed solutions showed that the consolidation coefficient is the most important controlling factor on the excess PWP during and after the slurry deposition. With high value of consolidation coefficient c_v, the drainage and consolidation can be very fast, resulting in low excess PWP within the slurried material during and after the slurry deposition. The filling rate can also affect the excess PWP in the slurred material, in particularly during the slurry deposition. With a given slurried material, a higher filling rate leads to higher excess PWP in the slurried material during the deposition, which may require longer time to be dissipated after the end of slurry deposition. The results also indicate that the peak value of the excess PWP at the bottom of accreting deposition are always smaller than that based on the overburden iso-static pressure before and after the slurry deposition even though the slurried material has a very low consolidation coefficient and filling operation is achieved very quickly. It is thus important to take into account the drainage and consolidation for estimating the excess PWP during and after the slurry deposition. Finally, it should be pointed out that these results confirm field observations or previously published numerical results. However, the distribution and evolution of the excess PWP during and after the slurry deposition on an impervious base are for the first time evaluated through an analytical model. They constitute a useful tool for design of dredges sludge or tailings dams or underground mine backfilled stopes.

Acknowledgements

The authors would like to acknowledge the financial support from the Natural Sciences and Engineering Research Council of Canada (NSERC 402318), Fonds de recherche du Québec—Nature et Technologies (FRQNT 2015-MI- 191676), and industrial partners of the Research Institute on Mines and the Environment (RIME UQAT-Polytechnique; http://rime-irme.ca/).

6.8 Appendix I: Derivation process for the proposed solution [Eq. (6.8)]

Eq. (6.4) has the same form as the heat conduction equation. It can be solved by separating the equation variables, a method commonly used to solve heat conduction problems (Asmar 2004). The excess PWP at moment t_1 ($= t - t_0$) at an elevation x can then be expressed by two new functions as follows:

$$u_1(x,t_1) = X(x)T(t_1) \tag{6.11}$$

where $X(x)$ is a function of the variable x, $T(t_1)$ is a function of the variable t_1.

Substituting Eq. (6.11) into Eq. (6.4) yields

$$\frac{1}{X(x)}\frac{d^2X}{dx^2} = -\lambda = \frac{1}{c_v T(t_1)}\frac{dT}{dt_1} \tag{6.12}$$

where λ is a constant ($\lambda \neq 0$).

Considering the former part of Eq. (6.12) leads to an expression as follows:

$$\frac{d^2X}{dx^2} + \lambda X = 0 \tag{6.13}$$

Solving Eq. (6.13) leads to a general solution expressed as follows:

$$X(x) = C_1 \sin\left(\sqrt{\lambda}x\right) + C_2 \cos\left(\sqrt{\lambda}x\right) \tag{6.14}$$

By considering Eq. (6.11) the boundary conditions $u_1 = 0$ at $x = H$ and $\mathrm{d}u_1/\mathrm{d}x$ at $x = 0$ can be met by imposing $X = 0$ at $x = H$ and $\mathrm{d}X/\mathrm{d}x = 0$ at $x = 0$. Considering these boundary conditions into Eq. (6.14) leads to the following expression for the eigenvalue λ

$$\lambda = \left[\frac{(2\alpha - 1)\pi}{2H}\right]^2 \quad (\alpha = 1, 2, \ldots, \infty) \tag{6.15}$$

The eigenfunction of $X(x)$ of Eq. (6.14) can be expressed as:

$$X_\alpha(x) = A_\alpha \cos\left[\frac{(2\alpha - 1)\pi}{2H}x\right] \tag{6.16}$$

where A_α is a series of constant.

Considering the latter part of Eq. (6.12) leads to an expression as follows:

$$\frac{dT(t_1)}{dt_1} + \lambda c_v T(t_1) = 0 \tag{6.17}$$

By performing the same processing of $X(x)$, one can obtain the characteristic function of $T(t_1)$ to Eq. (6.17) expressed as follows:

$$T_\alpha(t_1) = B_\alpha \exp\left\{-c_v\left[\frac{(2\alpha-1)\pi}{2H}\right]^2 t_1\right\} \tag{6.18}$$

where B_α is a series of constant.

The excess PWP can then be expressed as follows:

$$u_1(x,t_1) = \sum_{n=1}^{\infty} X_\alpha(x)T_\alpha(t_1) = \sum_{\alpha=1}^{\infty} C_\alpha \exp\left\{-c_v\left[\frac{(2\alpha-1)\pi}{2H}\right]^2 t_1\right\} \times \cos\left[\frac{(2\alpha-1)\pi}{2H}x\right] \tag{6.19}$$

where C_α is a series of constant.

Considering the initial condition (i.e. at $t_1 = 0$) of the post-deposition process leads to the following expression:

$$u_0(x,t_0) = u_1(x,0) = \sum_{\alpha=1}^{\infty}\left\{C_\alpha \cos\left[\frac{(2\alpha-1)\pi}{2H}x\right]\right\} \tag{6.20}$$

where $u_0\,(x,\, t_0)$ is given by Eq. (6.7).

Eq. (6.20) can be re-written as follows:

$$\int_0^H u_0(x,t_0)\times\cos\frac{(2\beta-1)\pi x}{2H}dx = \int_0^H \sum_{\alpha=1}^{\infty}\left\{C_\alpha\left[\cos\frac{(2\alpha-1)\pi x}{2H}\right]\right\}\times\cos\frac{(2\beta-1)\pi x}{2H}dx \tag{6.21}$$

where $\beta = 1, 2, \ldots, \infty$.

The orthogonality of trigonometric function stipulates that the right side of Eq. (6.21) becomes zero for $\alpha \neq \beta$ while can be rewritten as follows for $\alpha = \beta$ (Asmar 2004)

$$\int_0^H u_0(x,t_0)\times\cos\frac{(2\beta-1)\pi x}{2H}dx = \sum_{\alpha=1}^{\infty} C_\alpha \int_0^H\left(\cos\frac{(2\beta-1)\pi x}{2H}\right)^2 dx = C_\alpha \times \frac{H}{2} \tag{6.22}$$

The value of C_α can be calculated as

$$C_\alpha = \frac{2}{H}\int_0^H u_0(x,t_0)\times\cos\frac{(2\alpha-1)\pi x}{2H}dx \tag{6.23}$$

Substituting Eq. (6.23) into Eq. (6.19) yields

$$u_1(x,t_1)=\frac{2}{H}\sum_{\alpha=1}^{\infty}\exp\left\{-c_v t_1\left[\frac{(2\alpha-1)\pi}{2H}\right]^2\right\}\times\left[\cos\frac{(2\alpha-1)\pi x}{2H}\right]\int_0^H u_0(x,t_0)\times\left[\cos\frac{(2\alpha-1)\pi x}{2H}\right]dx \quad (6.24)$$

6.9 Appendix II: MATLAB program for solving Eq. (6.8)

A MATLAB program is given and applied to solve Eq. (6.8) and output the excess PWP at an elevation x at a given time t_1 in the backfill. The sample calculation is performed by considering H = 8 m, γ_{sat} = 20 kN/m^3, γ_w = 9.8 kN/m^3, m = 0.5 m/h, c_v = 1 m^2/h, t_0 = 16 h, and t_1 = 10 h.

```
%=========================================================================
%   A solution to estimate the excess PWP during and after slurry deposition
on an impervious base %
%=========================================================================%

nmax = 101; % number of division of H (here n_max = 101);
time_0 = 16; % filling time during the filling deposition (here t_0 = 16 h);
m = 0.5; % filling rate during the accreting deposition (here m = 0.5 m/h);
H = m*time_0; % Final thickness of the backfill (here H = 8 m);
h_0 = 0.3; %step interval of x (x is the elevation, see Fig. 1);
c_v = 1; % consolidation coefficient of the backfill (here c_v = 1 m^2/h);
time_1 = 10; % time after the deposition ceases (here t_1 = 10 h);
gama_sat = 20; % saturated unit weight of the slurried material (γ_sat = 20
kN/m^3);
gama_w = 9.8; % unit weight of water (γ_w = 9.8 kN/m^3);
gama_sub = gama_sat-gama_w; % submerged unit weight of the slurried material;


% calculate u_0(x,t_0) in the integral part of Eq.(6.8)
for i = 1:nmax
    x(i) = H/(nmax-1)*(i-1);
    u_0(i) = 0.0;
    for n = -91:91;
        temp1 = m*n*h_0*sqrt(time_0)/sqrt(c_v);
        temp2 = x(i)*n*h_0/sqrt(c_v*time_0);
        u_0(i) =
u_0(i)+h_0/2.*4.*c_v*time_0*n*h_0*tanh(temp1)*cosh(temp2)*exp(-(n*h_0)^2);
    end
    pre_multi = gama_sub/sqrt(pi*c_v*time_0)*exp(-(x(i))^2/4./c_v/time_0);
    u_0(i) = (gama_sub*m*time_0-pre_multi*u_0(i));
end

% calculate the integral part in Eq.(6.8)
for i = 1:nmax
    x(i) = H/(nmax-1)*(i-1);
    sum(i) = 0.0;
    temp3 = (2*i-1)*pi/2/m/time_0;
    for j = 1:nmax;
        delta_y = m*time_0/nmax;
        sum(i) = sum(i)+u_0(j)*cos(temp3*j*delta_y)*delta_y;
    end
end
% calculate the excess PWP distribution with Eq.(6.8)
```

```
for i=1:nmax
    x(i) = H/(nmax-1)*(i-1);
    u_1(i)=0.0;
            for k=1:nmax;
            temp4=(2*k-1)*pi/2/m/time_0*x(i);
            u_1(i)=u_1(i)+exp(-1*c_v*((2*k-
1)*pi/2/m/time_0)^2*(time_1))*cos(temp4)*sum(k);
    end
    u_1(i)=2/m/time_0*u_1(i);
end

% results output and saved in the file "output filename.txt"
fid = fopen('output filename.txt','w')
for i=1:nmax
    fprintf(fid,'%g %g\r\n',x(i),u_1(i))
end
fclose(fid)

plot(u_1,x,'-.');
```

6.10 References

Agurto-Detzel, H., Bianchi, M., Assumpção, M., Schimmel, M., Collaço, B., Ciardelli, C., … Calhau, J. (2016). The tailings dam failure of 5 November 2015 in SE Brazil and its preceding seismic sequence. *Geophysical Research Letters, 43*(10): 4929-4936.

Ahmed, S.I., & Siddiqua, S. (2014). A review on consolidation behavior of tailings. *International Journal of Geotechnical Engineeering, 8*(1): 102-111.

Alam, R., Shang, J.Q., & Islam, S. (2017). Electrophoresis and its applications in oil sand tailings management. *International Journal of Mineral Processing, 161*: 41-49.

Asmar NH. (2004) Partial differential equations and boundary value problems. Pearson Education, Upper Saddle River, NJ.

Aubertin, M., & McKenna, G. (2016). *Tailings disposal challenges and prospects for oil sands mining operation*. Paper presented at the Geo-Chicago, Chicago, USA (pp. 359-371).

Aubertin, M., Bussiere, B., & Bernier, L. (2002). *Environnement et gestion des rejets miniers. Presses* [Manual on CD-ROM]. Internationales Polytechnique, Montréal, Canada.

Aubertin, M., Bussiere, B., & Chapuis, R.P. (1996). Hydraulic conductivity of homogenized tailings from hard rock mines. *Canadian Geotechnical Journal, 33*(3), 470-482.

Been, K., & Sills, G.C. (1981). Self-weight consolidation of soft soils: an experimental and theoretical study. *Geotechnique, 31*(4), 519-535.

Beier, N., Wilson, W., Dunmola, A., & Sego, D. (2013). Impact of flocculation-based dewatering on the shear strength of oil sands fine tailings. *Canadian Geotechnical Journal, 50*(9), 1001-1007.

Belem, T., & Benzaazoua, B. (2008). Design and application of underground mine paste backfill technology. *Geotechnical and Geological Engineering, 26*(2), 147-174.

Belem, T., EI Aatar, O., Bussière, B., & Benzaazoua, M. (2016). Gravity-driven 1-D consolidation of cemented paste backfill in 3-m-high columns. *Innovative Infrastructure Solutions, 1*(1), 37.

Berilgen, S.A., Berilgen, M.M., & Ozaydin, K.I. (2006). Assessment of consolidation behavior of Golden Horn marine dredged material. *Marine Georesources Geotechnology, 24*(1): 1–16.

Berndt, C.C., Rankine, K.J., & Sivakugan, N. (2007). Materials properties of barricade bricks for mining applications. *Geotechnical and Geological Engineering, 25*(4): 449-471.

Bolduc, F.L., & Aubertin, M. (2014). Numerical investigation of the influence of waste rock inclusions on tailings consolidation. *Canadian Geotechnical Journal, 51*(9), 1021–1032.

Bussiere, B. (2007). Colloquium 2004: Hydrogeotechnical properties of hard rock tailings from metal mines and emerging geoenvironmental disposal approaches. *Canadian Geotechnical Journal, 44*(9), 1019-1052.

Caughill, D.L., Morgenstern, N.R., & Scott, J.D. (1993). Geotechnics of nonsegregating oil sand tailings. *Canadian Geotechnical Journal, 30*(5), 801-811.

Doherty, J.P. (2015). A numerical study into factors affecting stress and PWP in free draining mine stopes. *Computers and Geotechnics, 63*, 331-341.

Energy Resources Conservation Board. (2009). *Directive 074: Tailings performance criteria and requirements for oil sands mining schemes.* Calgary, Alberta, Canada.

El Mkadmi, N., Aubertin, M., & Li, L. (2014). Effect of drainage and sequential filling on the behavior of backfill in mine stopes. *Canadian Geotechnical Journal, 51*(1), 1–15.

Fahey, M., Helinski, M., & Fourie, A. (2010). Consolidation in accreting sediments: Gibson's solution applied to backfilling of mine stopes. *Géotechnique, 60*(11), 877-882.

Farkish, A., & Fall, M. (2014). Consolidation and hydraulic conductivity of oil sand mature fine tailings dewatered by using super absorbent polymer. *Journal of Geotechnical and Geoenvironmental Engineering, 140*(7), 06014006.

Ganesalingam, D., Nagaratnam, S., & Ameratunga, J. (2012). Influence of settling behavior of soil particles on the consolidation properties of dredged clay sediment. *Journal of Waterway, Port, Coast, and Ocean Engineering, 139*(4), 295-303.

Garcia, L.C., Ribeiro, D.B., Roque, F.O., Ochoa-Quintero, J.M., & Laurance, W.F. (2016). Brazil's worst mining disaster: corporations must be compelled to pay the actual environmental costs. *Ecological Applications, 27*(1), 5-9.

GEO-SLOPE. (2008) Stress-deformation modeling with SIGMA/ W 2007 (3th ed.). GEO-SLOPE International Ltd, Calgary, Alberta, Canada.

Gibson, R.E. (1958). The progress of consolidation in a clay layer increasing in thickness with time. *Géotechnique, 8*(4), 171-182.

Goodwin, E.T. (1949). *The evaluation of integrals of the form* $\int_{-\infty}^{+\infty} f(x)e^{-x^2}dx$. Paper presented at the Mathematical Proceedings of the Cambridge Philosophical Society. Cambridge University, London, UK (pp. 241-245).

He, J., Chu, J., Tan, S.K., Vu, T.T., & Lam, K.P. (2017). Sedimentation behavior of flocculant-treated soil slurry. *Marine Georesources & Geotechnology, 35*(5), 593-602.

James, M. (2009). The use of waste rock inclusions to control the effects of liquefaction in tailings impoundments. (Doctoral dissertation, Ecole Polytechnique de Montréal, Montréal, Canada).

Jaouhar, E.M., Li, L., & Aubertin, M. (2018). An analytical solution for estimating the stresses in vertical backfilled stopes based on a circular arc distribution. *Geomechanics and Engineering, 15*(3), 889-898.

Jeeravipoolvarn, S., Scott, J.D., & Chalaturnyk, R.J. (2009). 10 m standpipe tests on oil sands tailings: long-term experimental results and prediction. *Canadian Geotechnical Journal, 46*(8), 875-888.

Komurlu E and Kesimal A. (2015) Sulfide-rich mine tailings usage for short-term support purposes: An experimental study on paste backfill barricades. Geomech Eng Int J, 9(2): 195-205.

Komurlu, E., Kesimal, A., & Demir, S. (2016). Experimental and numerical analyses on determination of indirect (splitting) tensile strength of cemented paste backfill materials under different loading apparatus. *Geomechanics and Engineering, 10*(6), 775-791.

Li, L. (2013). Beneficial Experience from teaching and education to research and development. *Creative Education, 3*(7), 148–153.

Li, L. (2014). Analytical solution for determining the required strength of a side-exposed mine backfill containing a plug. *Canadian Geotechnical Journal, 51*(5), 508-519.

Li, L., & Aubertin, M. (2009a). Influence of water pressure on the stress state in stopes with cohesionless backfill. *Geotechnical and Geological Engineering, 27*(1), 1–11.

Li, L., & Aubertin, M. (2009b). A three-dimensional analysis of the total and effective stresses in submerged backfilled stopes. *Geotechnical and Geological Engineering, 27*(4), 559–569.

Li, L., & Aubertin, M. (2011). Limit equilibrium analysis for the design of backfilled stope barricades made of waste rock. *Canadian Geotechnical Journal, 48*(11), 1713-1728.

Li, L., Alvarez, I.C., & Aubertin, J.D. (2013). Self-weight consolidation of a slurried deposition: tests and interpretation. *International Journal of Geotechnical Engineering, 7*(2), 205–213.

Li, L., Aubertin, M., & Belem, T. (2005). Formulation of a three dimensional analytical solution to evaluate stress in backfilled vertical narrow openings. *Canadian Geotechnical Journal, 42*(6), 1705–1717 (with Erratum 2006, 43(3), 338–339).

Matlab, M (2011). MATLAB—The language of technical computing (Version 2014). [Computer software]. Retrieved from http://www.mathworks.com/products/matlab/

Pane, V., & Schiffman, R.L. (1985). A note on sedimentation and consolidation. *Géotechnique, 35*(1), 69-72.

Pedroni, L. (2011). Étude expérimentale et numérique de la sédimentation et de la consolidation des boues de traitement des eaux acides. (Doctoral dissertation, École Polytechnique de Montréal, Montréal, Canada).

Pedroni, L., & Aubertin, M. (2013). *Measurement and Simulation of the Large Strain Consolidation of AMD Treatment Sludge*. Paper presented at the 66th Canadian Geotechnical Conference, Geosciences for Sustainability, Montréal, Canada, GeoMontréal, Montréal, Canada.

Priscu, C. (1999). Behavior of mine tailings dams under high tailings deposition rates. (Doctoral dissertation, McGill University, Montréal, Canada).

Qiu, Y.X., & Sego, D.C. (2001). Laboratory properties of mine tailings. *Canadian Geotechnical Journal, 38*(1), 183-190.

Queiroz, H.M., Nóbrega, G.N., Ferreira, T.O., Almeida, L.S., Romero, T.B., Santaella, S.T., … Otero, X.L. (2018). The Samarco mine tailing disaster: A possible time-bomb for heavy metals contamination? *Science of the Total Environment, 637*, 498-506.

Saleh-Mbemba, F., & Aubertin, M. (2018). Characterization of self-weight consolidation of fine-grained mine tailings using moisture sensors. *Geotechnical Testing Journal, 41*(3), 543-554.

Seneviratne, N.H., Fahey, M., Newson, T.A., & Fujiyasu, Y. (1996). Numerical modelling of consolidation and evaporation of slurried mine tailings. *International Journal for Numerical and Analytical Methods in Geomechanics, 20*(9), 647-671.

Shahsavari, M., & Grabinsky, M. (2014). *Cemented paste backfill consolidation with deposition-dependent boundary conditions*. Paper presented at the 67th Canadian Geotechnical Conference, Canadian Geotechnical Society, Regina, Saskatchewan, Canada.

Shahsavari, M., & Grabinsky, M. (2015). *Mine backfill porewater pressure dissipation: numerical predictions and field measurements*. Paper presented at the 68th Canadian Geotechnical Conference, Canadian Geotechnical Society, Québec City, Canada (pp. 1-8).

Sivakugan, N., Rankine, K., & Rankine, R. (2006a). Permeability of hydraulic fills and barricade bricks. *Geotechnical and Geological Engineering, 24*(3), 661-673.

Sivakugan, N., Rankine, R.M., Rankine, K.J., & Rankine, K.S. (2006b). Geotechnical considerations in mine backfilling in Australia. *Journal of Cleaner Production, 14*(12), 1168-1175.

Terzaghi, K. (1943). Theoretical Soil Mechanics. New York, USA: John Wiley and Sons.

Xu, G.Z., Gao, Y.F., Hong, Z.S., & Ding, J.W. (2012). Sedimentation behavior of four dredged slurries in China. *Marine Georesources and Geotechnology, 30*(2), 143-156.

Yang, P.Y., Li, L., Aubertin, M., & Brochu-Baekelmans, M. (2017). Stability analyses of waste rock barricades designed to retain paste backfill. *International Journal of Geomechanics, 17*(3), 04016079.

Zhang, N., Zhu, W., He, H.T., Lv, Y.Y., & Wang, S.W. (2017). Experimental study on settling velocity of soil particles in dredged slurry. *Marine Georesources & Geotechnology, 35*(6), 747-757.

Zheng, J., Li, L., Mbonimpa, M., & Pabst, T. (2018a). An analytical solution of Gibson's model for estimating the pore water pressures in accreting deposition of slurried material under one-dimensional self-weight consolidation. Part I: Pervious base. *Indian Geotechnical Journal, 48*(1), 72-83.

Zheng, J., Li, L., Mbonimpa, M., & Pabst, T. (2018b). An analytical solution of Gibson's model for estimating pore water pressures in accreting deposition of slurried material under one-

dimensional self-weight consolidation. Part II: Impervious base. *Indian Geotechnical Journal, 48*(1), 188-195.

CHAPTER 7 ARTICLE 5: A SOLUTION TO ESTIMATE THE TOTAL AND EFFECTIVE STRESSES IN BACKFILLED STOPES WITH AN IMPERVIOUS BASE DURING THE FILLING OPERATION

Jian Zheng, Li Li, Yu-Chao Li

Article submitted to International Journal for Numerical and Analytical Methods in Geomechanics in July 2018.

Abstract: Mining backfill is commonly used in underground mines. A critical concern of this practice is to evaluate the pressures and total stresses in the backfilled stope to ensure a safe and economic design of barricades, constructed to retain the backfill. When a slurried backfill is placed in a mine stope, excess pore water pressure (PWP) can instantaneously generate and progressively dissipate. The dissipation of the excess PWP and consolidation lead to the development of effective stresses, which in turn lead to an arching effect in the backfilled stope. Until now, arching effect has been largely considered for stress estimation in dry or submerged backfill. The former corresponds to the final state at the end process of the drainage and consolidation of the backfill with a pervious while the latter with an impervious barricade. However, previous studies have shown that the most critical moment for the stability of barricades is during the stope filling. Therefore, the design of barricades requires a proper estimation of the pressure and total stresses during the filling operation. This in turn needs joint consideration of the arching effect and drainage and consolidation of the backfill. In this paper, a new solution is developed to evaluate the pressures and stresses in backfilled stope during the filling operation by considering the self-weight consolidation and arching effect. The proposed solution is validated by numerical modeling with Plaxis2D. It can thus be used to evaluate the pressures and stresses in backfilled stopes during the stope filling with an impervious barricade.

Keywords: backfill; self-weight consolidation; arching effect; effective and total stresses; excess pore water pressure (PWP); impervious base

7.1 Introduction

Mining backfill is widely used in underground mines to fill underground openings. Several advantages can be attributed to the application of mine backfill, including increased ore recovery, reduced mineral dilution, and improved ground stability (Hassani and Archibald 1998; Kump 2001; Jung and Biswas 2002; Cui and Fall 2018). Environment improvement through the reduction of the surface disposal of mine wastes is another important benefit of the mine backfilling (Aubertin et al. 2002; Bussiere 2007; Simms et al. 2007).

Despite the numerous advantages, successful application of backfill depends on the stability of a confining structure constructed at the stope base to retain the slurried backfill in place. This structure is called barricade. Several cases of barricade failure have been reported over the years and the consequences were usually very serious, such as huge economic loss, damage of equipment and even loss of lives (e.g., Grice 1998; Sivakugan et al. 2006a, 2006b, 2013; Yumlu and Guresci 2007; Revell et al. 2007). It is thus critical to ensure a safe and economic barricade design, which requires a good understanding of the pressures and stresses in the backfilled stopes.

When a slurried backfill is instantaneously placed in a mine stope, the solid particles tend to settle down under their own weight. The backfill then tends to become denser while the pore water tends to be expelled out of the backfill. As the backfill, especially paste backfill, usually contains a large portion of fine particles, the permeability is low and the drainage can be slow. This results in an instantaneous generation of excess pore water pressure (PWP), whose dissipation depends on the permeability and drainage time (Pedroni 2011; Li 2013; Li et al. 2013; El Mkadmi et al. 2014).

The problem becomes more complicated when the stope filling operation is considered. From one hand, the excess PWP can be continuously generated and increased with the addition of new backfill layers. On the other hand, the dissipation of excess PWP takes place with time during the filling operation. The resulted excess PWP depends on the rates of the generation (increase) and dissipation (decrease) of the excess PWP during the filling operation, which in turn depend on the hydraulic conductivity and filling rate of the backfill. This problem is known as self-weight consolidation of accreting deposition (constant increase in backfill thickness), which has been treated by Gibson (1958), who considered one-dimensional consolidation in the vertical direction and proposed a solution for estimating the distribution and evolution of the excess PWP. The application of the Gibson (1958) model in mine backfilled stopes has been shown by several

researchers (Fahey et al. 2010; Shahsavari and Grabinsky 2014, 2015; Doherty 2015; Wood et al. 2016; Zheng et al. 2018a, 2018b). It is noted that the Gibson (1958) model and the ensuing solutions did not consider any effective stresses during the filling operation.

However, field pressure and stress measurements showed that effective stresses develop during the filling operation (Thompson et al. 2012; Doherty 2015). Subsequently, shear strength and shear stresses can develop along the fill-wall contact interfaces, leading to the generation of arching effect.

Over the years, the consideration of arching effect in stress estimation in backfilled stopes has been largely reported (Askew et al. 1978; Knutsson 1981; Aubertin 1999; Aubertin et al. 2003; Li et al. 2003, 2005; Pirapakaran and Sivakugan 2007a, 2007b). Until now, arching effect has only been considered for dry and submerged (with a hydrostatic pressure; e.g., Li and Aubertin 2009a, 2009b) backfills, which correspond to the final states of uncemented backfill at the end of the drainage and self-weight consolidation process with a pervious and an impervious barricade, respectively.

However, the previous studies have shown that the most critical moment for the stability of barricades is during the filling operation of stopes, not at the end of the drainage and self-weight consolidation process (Revell and Sainsbury 2007; Yumlu and Guresci 2007). Therefore, the design of barricades requires a proper estimation of the pressure and total stresses during the filling operation, which in turn needs joint consideration of the arching effect and the drainage and consolidation of the backfill. This task can be realized by numerical modeling. However, a simple solution is preferred to allow parameter sensitivity analyses during the preliminary stage of projects.

In this paper, a solution is for the first time proposed to evaluate the pressures and stresses in backfilled stopes by considering the combined effects of arching and self-weight consolidation. The self-weight consolidation is first evaluated using an analytical solution proposed by the authors (Zheng et al. 2018b), based on the Gibson (1958) model. The dissipation of the excess PWP is then introduced into the arching model of Li and Aubertin (2009a). The proposed solution is validated by numerical results obtained with Plaxis2D. A few sample applications of the proposed solution are shown.

7.2 Proposed solution

7.2.1 Self-weight consolidation

Fig. 7-1 shows a typical mine stope filled with a saturated backfill at a constant filling rate m (m/h). On the figure, B (m) is the width of the stope; h (m) is the current height at the filing time t (h), i.e. $h = mt$; H (m) is the final height at the end of filling operation; y (m) is the elevation of the calculation point from the base of the stope, ranging from 0 to h; l (m) is the depth of the calculation point from the current top surface of the backfill, i.e. $l = h - y$.

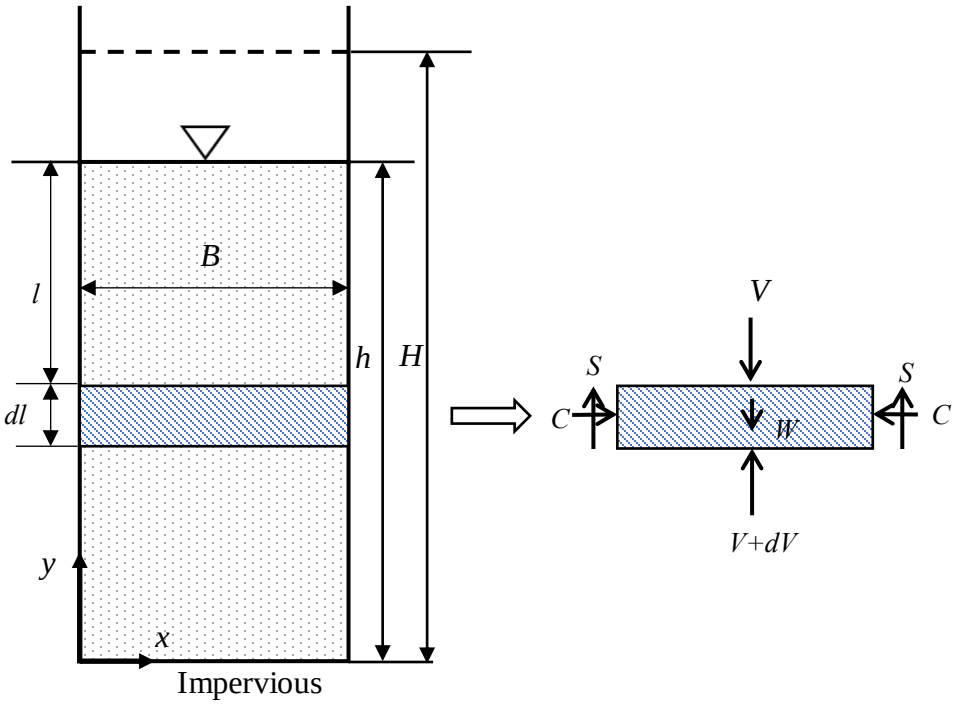

Figure 7-1: A vertical backfilled stope with saturated backfill and an isolated horizontal layer element.

The governing equation in terms of excess PWP is given by Gibson (1958) as follows:

$$c_v \frac{\partial^2 u}{\partial y^2} = \frac{\partial u}{\partial t} - \gamma' \frac{dh}{dt} \tag{7.1}$$

where u (kPa) is the excess PWP, c_v (m^2/h) is the consolidation coefficient, γ' (kN/m^3) is the submerged unit weight of the backfill ($\gamma' = \gamma_{sat} - \gamma_w$, where γ_{sat} (kN/m^3) is the saturated unit weight

of the backfill, γ_w (kN/m^3) is the unit weight of water). The excess PWP was further given by Gibson (1958) as follows:

$$u = \gamma' mt - \gamma' E(\pi c_v t)^{-\frac{1}{2}} \exp\left(\frac{-y^2}{4c_v t}\right) \tag{7.2}$$

with

$$E = \int_0^\infty \xi \tanh\left(\frac{m\xi}{2c_v}\right) \times \cosh\left(\frac{y\xi}{2c_v t}\right) \times \exp\left(-\frac{\xi^2}{4c_v t}\right) d\xi \tag{7.3}$$

where ξ (m) is an arbitrary integration variable in the range of zero to infinity (∞).

Eqs. (7.1) and (7.2) are the solution of Gibson (1958) for the variation and evolution of the excess PWP during the filling operation. However, the integral [Eq. (7.3)] of the Gibson (1958) solution cannot be solved by hand calculation or with simple and commonly available calculation tools. The following transformation has been done by the authors (Zheng et al. 2018b) to obtain an analytical solution of the Gibson (1958) solution.

Eq. (7.3) can be represented by a function as follows:

$$G(z) = \int_0^\infty g(z) \exp(-z^2) dz \tag{7.4}$$

where,

$$g(z) = 4c_v t \times z \times \tanh\left(\frac{mz\sqrt{t}}{\sqrt{c_v}}\right) \times \cosh\left(\frac{yz}{\sqrt{c_v t}}\right) \tag{7.5}$$

and

$$z^2 = \frac{\xi^2}{4c_v t} \tag{7.6}$$

Since g(z) is an even function of z, Eq. (7.4) can be re-written as

$$G(z) = \frac{1}{2} \int_{-\infty}^\infty g(z) \exp(-z^2) dz \tag{7.7}$$

Goodwin (1949) proposed the following transformation, which can give a good approximation of the integral with a high accuracy by using a value of h_0 in the range of 0 to 1 as long as the number n is taken large enough:

$$\int_{-\infty}^{\infty} g(z)\times\exp(-z^2)dz = h_0\sum_{n=-\infty}^{\infty} g(nh_0)e^{-n^2h_0^2} \tag{7.8}$$

Comparing Eqs. (7.7) and (7.8) yields the following equation for E:

$$E = \frac{h_0}{2}\sum_{n=-\infty}^{\infty} 4c_v t\times(nh_0)\times\tanh\left(\frac{mnh_0\sqrt{t}}{\sqrt{c_v}}\right)\times\cosh\left(\frac{ynh_0}{\sqrt{c_v t}}\right)\times\exp(-n^2h_0^2) \tag{7.9}$$

Introducing Eq. (7.9) into Eq. (7.2) yields

$$\begin{aligned} u = {} & \gamma' mt - \gamma'(\pi c_v t)^{-\frac{1}{2}}\exp\left(\frac{-y^2}{4c_v t}\right)\times \\ & \frac{h_0}{2}\sum_{n=-\infty}^{\infty} 4c_v t\times(nh_0)\times\tanh\left(\frac{mnh_0\sqrt{t}}{\sqrt{c_v}}\right)\times\cosh\left(\frac{ynh_0}{\sqrt{c_v t}}\right)\times\exp(-n^2h_0^2) \end{aligned} \tag{7.10}$$

Eq. (7.10) consists the analytical solution of Gibson (1958) model, proposed by Zheng et al. (2018b), for estimating the excess PWP during the filling operation with an impervious base. In order to obtain stable and accurate results, the value of h_0 should be small enough while the range of n should be large enough. For most cases, stable results can be obtained by taking a value of 0.3 for h_0 and n in the range of -91 to 91 (Zheng et al. 2018a, 2018b).

The derivation of the excess PWP can lead to

$$\frac{du}{dy} = -\gamma'(\pi c_v t)^{-\frac{1}{2}}\exp\left(\frac{-y^2}{4c_v t}\right)\times\left[\left(\frac{-y}{2c_v t}\right)\times E + F\right] \tag{7.11}$$

where F is expressed as

$$F = \int_0^{\infty}\xi\tanh\left(\frac{m\xi}{2c_v}\right)\times\sinh\left(\frac{y\xi}{2c_v t}\right)\times\left(\frac{\xi}{2c_v t}\right)\times\exp\left(-\frac{\xi^2}{4c_v t}\right)d\xi \tag{7.12}$$

Performing the same process to function E leads to the following expression for F:

$$F = \frac{h_0}{2}\sum_{n=-\infty}^{\infty} 4c_v t \times (nh_0) \times \tanh\left(\frac{mnh_0\sqrt{t}}{\sqrt{c_v}}\right) \times \sinh\left(\frac{ynh_0}{\sqrt{c_v t}}\right) \times \left(\frac{nh_0}{\sqrt{c_v t}}\right) \times \exp(-n^2 h_0^2) \tag{7.13}$$

Introducing Eqs. (7.9) and (7.13) into Eq. (7.11) leads to

$$\frac{du}{dy} = -\gamma'(\pi c_v t)^{-\frac{1}{2}} \exp\left(\frac{-y^2}{4c_v t}\right) \times \left[\begin{array}{l} \left(\frac{-y}{2c_v t}\right) \times \frac{h_0}{2}\sum_{n=-\infty}^{\infty} 4c_v t \times (nh_0) \times \tanh\left(\frac{mnh_0\sqrt{t}}{\sqrt{c_v}}\right) \times \cosh\left(\frac{ynh_0}{\sqrt{c_v t}}\right) \times \exp(-n^2 h_0^2) + \\ \frac{h_0}{2}\sum_{n=-\infty}^{\infty} 4c_v t \times (nh_0) \times \tanh\left(\frac{mnh_0\sqrt{t}}{\sqrt{c_v}}\right) \times \sinh\left(\frac{ynh_0}{\sqrt{c_v t}}\right) \times \left(\frac{nh_0}{\sqrt{c_v t}}\right) \times \exp(-n^2 h_0^2) \end{array}\right]$$

(7.14)

Eq. (7.14) will be used in the next section to consider the arching effect solution for the stresses during the placement of backfill in mine stopes.

7.2.2 Arching model

In order to take into account the arching effect in the process of self-weight consolidation, the forces acting on a layer element shown in Fig. 7-1 will be considered. *W* (kN) is the weight of the layer element; *C* (kN) and *S* (kN) are the compressive and shear forces on each side wall, respectively; *V* (kN) and *V* + d*V* (kN) are the vertical forces on top and at the base, respectively.

Considering the equilibrium of the layer element in the vertical direction yields:

$$dV + 2S = W \tag{7.15}$$

The weight of the layer element is calculated as:

$$W = \gamma_{sat} B\, \mathrm{d}l \tag{7.16}$$

where d*l* (m) is the thickness of the layer element.

The vertical force can be expressed as:

$$V = \sigma_v B \tag{7.17}$$

where σ_v (kPa) is the vertical total stress, which is assumed to be uniformly distributed across the width of the stope.

By assuming the effective friction angle δ' along the fill-wall interfaces to be equal to the effective internal friction angle of the backfill ϕ', the application of the Mohr-Coulomb criterion leads to the following expression for shearing force *S*:

$$S = \sigma_h' \tan\delta' dl = K\sigma_v' \tan\phi' dl \tag{7.18}$$

where σ'_h (kPa) and σ'_v (kPa) are the horizontal and vertical effective stresses, respectively; *K* (= σ'_h/σ'_v) is the earth pressure coefficient of the saturated backfill. In this study, the Rankine active earth pressure coefficient (K_a) and Jaky at-rest earth pressure coefficient (K_0) are considered for the earth pressure coefficient *K*. The former is expressed as follows (e.g., CGS 2006; Das 2010):

$$K_a = \tan^2(45° - \phi'/2) \tag{7.19}$$

while the latter is given as follows (e.g., Jaky 1948):

$$K_0 = 1 - \sin\phi' \tag{7.20}$$

The vertical and horizontal total stresses can be calculated as:

$$\sigma_v = \sigma_v' + u + \gamma_w l \tag{7.21}$$

$$\sigma_h = \sigma_h' + u + \gamma_w l = K\sigma_v' + u + \gamma_w l \tag{7.22}$$

From Eqs. (7.17) and (7.21), one can obtain the following expression:

$$dV = B[d\sigma_v' + du + \gamma_w dl] \tag{7.23}$$

Substituting Eqs. (7.16), (7.18), and (7.23) into Eq. (7.15) results in

$$Bd[\sigma_v' + u + \gamma_w l] + 2K\sigma_v' \tan\phi' dl = \gamma_{sat} B dl \tag{7.24}$$

Eq. (7.24) can be re-written as:

$$\frac{d\sigma_v'}{dl} + \frac{2K\tan\phi'}{B}\sigma_v' = \gamma' - \frac{du}{dl} \tag{7.25}$$

Solving Eq. (7.25) leads to:

$$\sigma_v^{'} = e^{\frac{-2K\tan\phi^{'}}{B}l}\left[\int(\gamma^{'} - \frac{du}{dl})e^{\frac{2K\tan\phi^{'}}{B}l}dl + A\right] \tag{7.26}$$

where A is an arbitrary constant.

Considering the boundary condition $\sigma'_v = 0$ at $l = 0$, one obtains the vertical effective stress as follows (see Appendix I for the details of derivation):

$$\sigma_v^{'} = e^{-\frac{2K\tan\phi^{'}}{B}l}\int_0^l\left(\gamma^{'} - \frac{du}{dl}\right)e^{\frac{2K\tan\phi^{'}}{B}l}dl \tag{7.27}$$

As $l = h - y$, one thus has:

$$\frac{du}{dl} = -\frac{du}{dy} \tag{7.28}$$

Eq. (7.27) can then be re-written as:

$$\sigma_v^{'} = e^{-\frac{2K\tan\phi^{'}}{B}l}\int_0^l\left(\gamma^{'} + \frac{du}{dy}\right)e^{\frac{2K\tan\phi^{'}}{B}l}dl \tag{7.29}$$

where du/dy can be obtained from Eq. (7.14).

The horizontal effective stress can then be obtained by the following expression:

$$\sigma_h^{'} = Ke^{-\frac{2K\tan\phi^{'}}{B}l}\int_0^l\left(\gamma^{'} + \frac{du}{dy}\right)e^{\frac{2K\tan\phi^{'}}{B}l}dl \tag{7.30}$$

Adding the total PWP leads to the following equations for the vertical (σ_v) and horizontal (σ_h) total stresses:

$$\sigma_v = e^{-\frac{2K\tan\phi^{'}}{B}l}\int_0^l\left(\gamma^{'} + \frac{du}{dy}\right)e^{\frac{2K\tan\phi^{'}}{B}l}dl + u + \gamma_w l \tag{7.31}$$

$$\sigma_h = Ke^{-\frac{2K\tan\phi^{'}}{B}l}\int_0^l\left(\gamma^{'} + \frac{du}{dy}\right)e^{\frac{2K\tan\phi^{'}}{B}l}dl + u + \gamma_w l \tag{7.32}$$

Eqs. (7.29) and (7.30) along with Eqs. (7.31) and (7.32) consist the proposed solution to evaluate the variation and evolution of the vertical and horizontal effective and total stresses in a backfilled stope during the filling operation.

A MATLAB program based on Eq. (7.32) to estimate the distribution of the horizontal total stress (very important for barricade design) within the backfilled stopes has been given in Appendix II. In the program, the backfill final thickness H is divided into n_{max} elements. Once again, the value of n_{max} should be large enough to obtain stable and reliable results of σ_h. The sensitivity analysis should be conducted case by case for each project to find the optimum value of n_{max}.

Fig. 7-2 shows the variation of the horizontal total stress (σ_h) at the bottom of the stope (l = 40 m) as the value of n_{max} varies from 11 to 151 calculated with the MATLAB program by considering one case with the parameters of H = 40 m, B = 6 m, m = 0.2 m/h, c_v = 5 m^2/h, γ_{sat} = 20 kN/m^3, γ_w = 10 kN/m^3, ϕ' = 20°, and $K = K_a$. One sees that stable results of σ_h can be obtained when n_{max} is larger than 101 by using the given parameters (σ_h = 600 kPa with n_{max} = 101 compared to σ_h = 599.3 kPa with n_{max} = 10001).

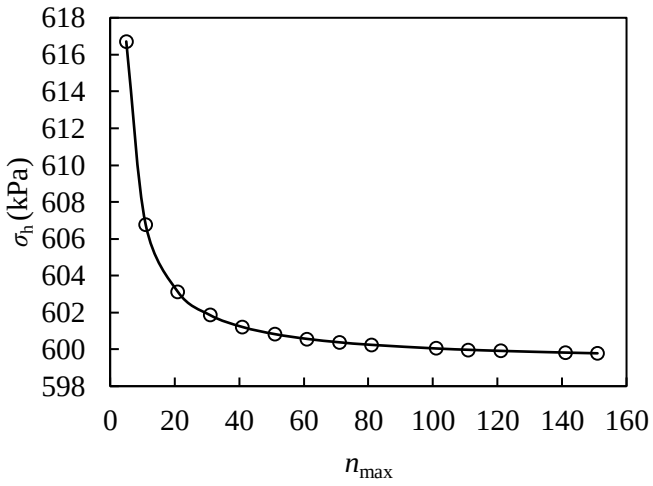

Figure 7-2: Sensitivity analysis of n_{max} to obtain stable and reliable results of σ_h by using the MATLAB program (plotted using Microsoft Excel); Calculation made with H = 40 m, B = 6 m, m = 0.2 m/h, c_v = 5 m^2/h, γ_{sat} = 20 kN/m^3, γ_w = 10 kN/m^3, ϕ' = 20°, and $K = K_a$

As a special case when the filling operation is very slow (i.e. $m \rightarrow 0$) or/and the consolidation coefficient is very large (i.e. $c_v \rightarrow \infty$), the excess PWP (u = 0) and hydraulic gradient approach zero (i.e. $u \rightarrow 0$, du/d$y \rightarrow 0$). The proposed solution [Eq. (7.29)] then reduces to the analytical solution of Li and Aubertin (2009a) as follows:

$$\sigma_v' = e^{-\frac{2K\tan\phi'}{B}l}\int_0^l \gamma' \times e^{\frac{2K\tan\phi'}{B}l}dl = \frac{B\gamma'}{2K\tan\phi'}\left[1-\exp\left(-\frac{2Kl\tan\phi'}{B}\right)\right] \tag{7.33}$$

Again, the solution of Li and Aubertin (2009a) only considers the final state of the backfill when the drainage and consolidation end and the water reaches a hydraulic equilibrium. This state can be reached when the filling rate is very small or/and the consolidation coefficient is very large.

Fig. 7-3 shows the variation of the vertical [Fig. 7-3(a)] and horizontal [Fig. 7-3(b)] total stresses along the height of a stope 40 m high and 6 m wide at the end of filling operation, calculated with the solution of Li and Aubertin (2009a) and the proposed solution [Eqs. (7.31) and (7.32)] by considering a filling rate of m = 0.2 m/h and friction angle of ϕ'=20° when the consolidation coefficient c_v changes from 399.96 to 0.39996 m^2/h. The results calculated with the iso-geostatic overburden pressure have also been plotted on the figure. One can see the total stresses calculated with the proposed solution are very close to those based on the iso-geostatic overburden pressure when the consolidation coefficient is very small, but approach the vertical and horizontal total stresses calculated with Li and Aubertin (2009a) solution as long as the consolidation coefficient reaches a value of 399.96 m^2/h.

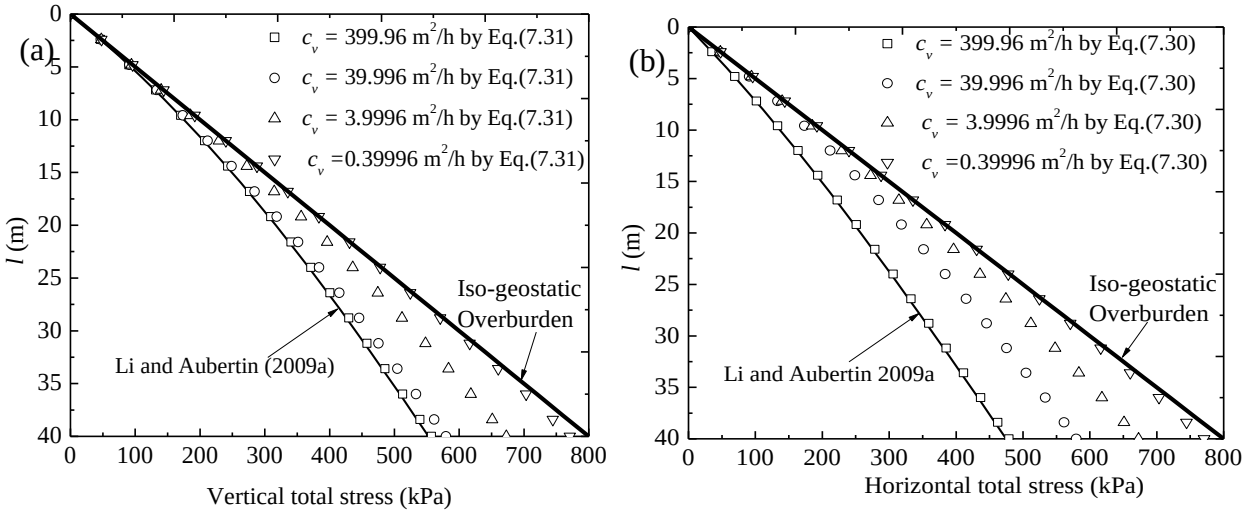

Figure 7-3: Variation of the (a) vertical and (b) horizontal total stresses along the VCL of the stope at the end of the stope filling for different consolidation coefficients, calculated with the Li and Aubertin (2009a) solution [Eq. (7.33)] and the proposed solution [Eqs. (7.31) and (7.32)]; calculation made with H = 40 m, B = 6 m, m =0.2 m/h, γ_{sat} = 20 kN/m^3, γ_w = 10 kN/m^3, ϕ' = 20°, and $K = K_a$

7.3 Validation of the proposed solution against numerical modeling

To verify the validity of the proposed solution, numerical modeling has been performed using Plaxis2D, a numerical code based on finite element method (Brinkgreve et al. 2014).

Fig. 7-4(a) shows a backfilled stope 4 m large and 12.4 m high. The backfill is filled at a filling rate of m = 0.5 m/h to a height of 12 m with a void space of 0.4 m left between the top surface of the backfill and the roof of the stope. The backfill and rock mass are elasto-plastic and obey the Mohr-Coulomb criterion.

The backfill is cohesionless and characterized as γ_{sat} = 20 kN/m^3 (saturated unit weight), k = 4.176 $\times 10^{-2}$ m/h (hydraulic conductivity), μ= 0.2 (Poisson's ratio), E' = 864 kPa (drained Young's Modulus), M' = 960 kPa (drained constrained modulus), ϕ' = 10° (effective friction angle) and ψ' = 0° (effective dilation angle). The consolidation coefficient (c_v) of the backfill can be calculated by the following equation:

$$c_v = \frac{k \times M'}{\gamma_w} \tag{7.34}$$

and one obtains c_v = 4 m^2/h.

The surrounding rock mass is impermeable and characterized as γ_r = 27 kN/m^3 (unit weight), μ_r = 0.25 (Poisson's ratio), E_r = 42 GPa (Young's modulus), c_r = 9400 kPa (cohesion), ϕ_r = 38° (friction angle), and ψ_r = 0° (dilation angle). The earth pressure coefficient of the rock mass is taken as K_r = 2, a typical value for the stress regime of Canadian Shield (Herget 1988). This value does not have any influence on the stresses in the backfill because the backfill is placed in the stope after the elastic deformation.

Fig. 7-4(b) shows the numerical model of the backfilled stope, built with Plaxis2D. By considering the vertical symmetry plane, only half of the full model is simulated. The upper boundary of the model is free while the lower boundary is fixed in all directions. The two side boundaries (rock mass and backfill) of the model are fixed in the horizontal direction but free for displacement in the vertical direction. In the stope, the vertical symmetry plane and the fill-rock contacts are impermeable, while the top of each newly added backfill layer is permeable with zero PWP.

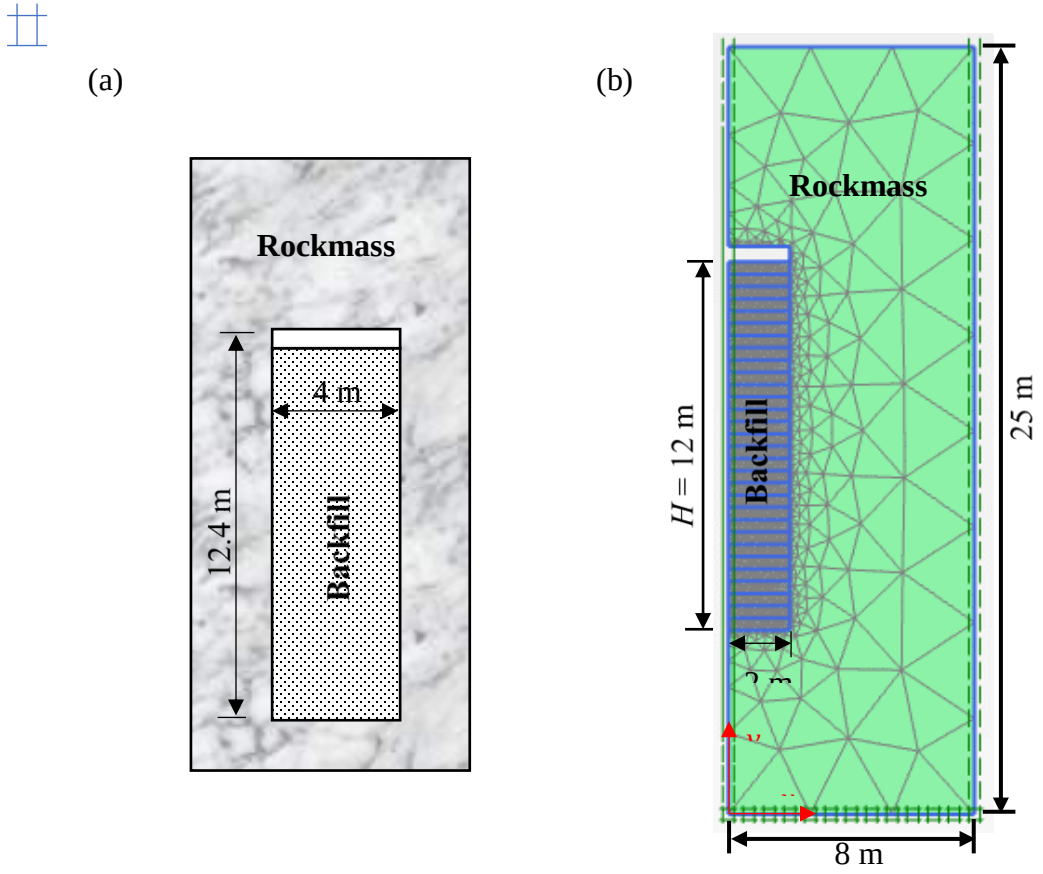

Figure 7-4: (a) A backfilled stope; (b) the numerical model of Plaxis2D by taking into account the plane of symmetry at $x = 0$

The numerical simulations have been carried out in three steps. The first step is to obtain an initial stress state in the rock mass prior to any excavation. The stope excavation is simulated in the second step. The third step consists of filling the stope layer by layer from the bottom to the top. The waiting delay for the addition of a new backfill layer is calculated by considering the filling rate *m*. If each of the backfill layer has a thickness of d*h*, the waiting delay should be d*h*/*m*. In order to simulate and approach as much as possible the continuous filling, the layer thickness d*h* should be enough small. In this study, the stope of 12 m high was filled in 30 layers with each layer having a thickness of 0.4 m. The waiting delay is 0.8 h for a filling rate of 0.5 m/h.

Fig. 7-5 shows the variation of the excess PWP [Fig. 7-5(a)], total and effective stresses [Fig. 7-5(b)] along the vertical center line (VCL) of the backfilled stope at the end of filling operation (at $t = 24$ h) obtained by numerical modeling with Plaxis2D and calculated with the proposed solution

[Eqs. (7.10), (7.29), (7.30), (7.31) and (7.32)] by considering H = 12 m, B = 4 m, m = 0.5 m/h, c_v = 4 m^2/h, γ_{sat} = 20 kN/m^3, γ_w = 10 kN/m^3, and ϕ' = 10°. The excess PWP (= $\gamma' h$) and the total stress (= $\gamma_{sat} h$) based on the iso-geostatic overburden pressure are also plotted on the figure. One sees that the calculated vertical and horizontal total stresses are lower than the overburden pressure, indicating the occurrence of arching effect within the backfill. The σ'_v and σ'_h calculated with the proposed solutions using K_a are more consistent with the results in the Plaxis2D. The excellent agreement between the numerical and proposed solution results indicates that the proposed solution using K_a can be used to evaluate the pressures and stresses in backfilled stope during and at the end of filling operation.

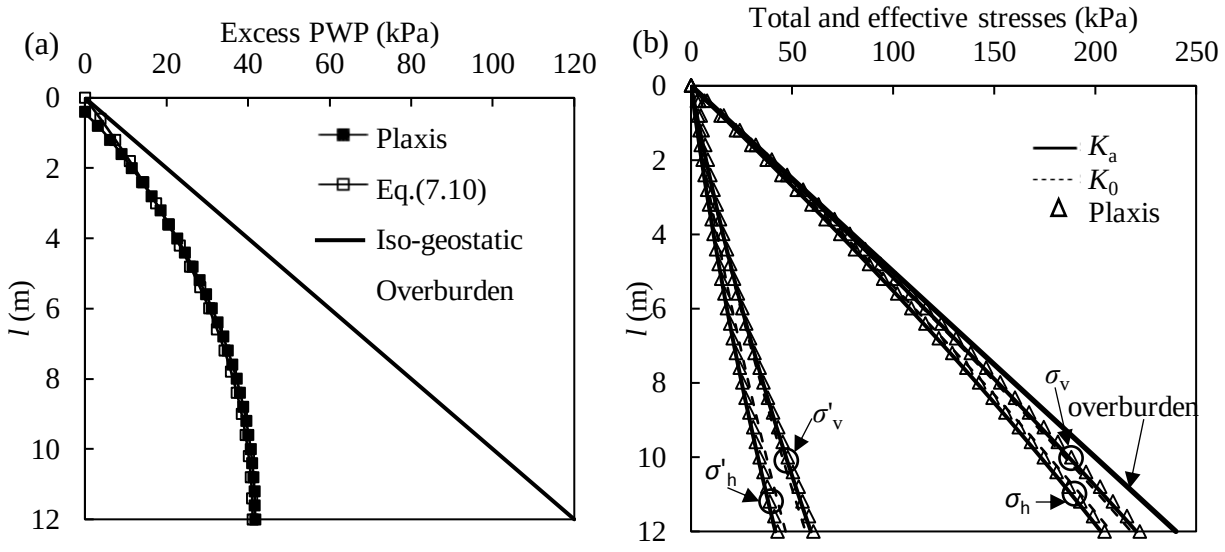

Figure 7-5: Variation of the (a) excess PWP, (b) total and effective stresses along the VCL of the stope at the end of filling operation (at t = 24 h and $h = H$ = 12 m), obtained by numerical modeling with Plaxis2D and calculated with the proposed solution [Eqs. (7.10), (7.29), (7.30), (7.31) and (7.32)] using Rankine active coefficient K_a and Jaky at-rest coefficient K_0; calculations made with H = 12 m, B = 4 m, m = 0.5 m/h, c_v = 4 m^2/h, γ_{sat} = 20 kN/m^3, γ_w = 10 kN/m^3, and ϕ' = 10°

7.4 Sample applications

Compared to numerical modeling that can be used simulate diverse problem, the proposed solution can be particularly useful to perform parametric sensitivity analysis in the preliminary stage of projects. In this study, the influence of the fill properties, stope width and filling rate on the stresses

in backfilled stopes will be evaluated by considering a backfill having a saturated unit weight of γ_{sat} = 20 kN/m^3 and a final height of H = 40 m.

Fig. 7-6 shows the variation of the effective [Fig. 7-6(a)] and total [Fig. 7-6(b)] stresses along the height of the stope, calculated by the proposed solution at the end of stope filling as the consolidation coefficient c_v varies from 0.1 to 10 m^2/h. The other parameters considered are B = 6 m, m = 0.2 m/h, and ϕ' = 20°. The Rankine active earth pressure coefficient K_a is used for the calculations. It is seen that the effective and total stresses at the end of stope filling change significantly with the change of c_v. When c_v takes a value of 0.1 m^2/h, the horizontal and vertical effective stresses at the end of filling along the upper part of the backfill are close to zero while the vertical and horizontal total stresses are close to the iso-geostatic overburden pressure. These results indicate the few drainage and consolidation during the filing operation in the upper part of the backfill. When c_v takes a value of 10 m^2/h, the horizontal and vertical effective stresses at the end of filling are not negligible while the vertical and horizontal total stresses are much smaller than the iso-geostatic overburden pressure.

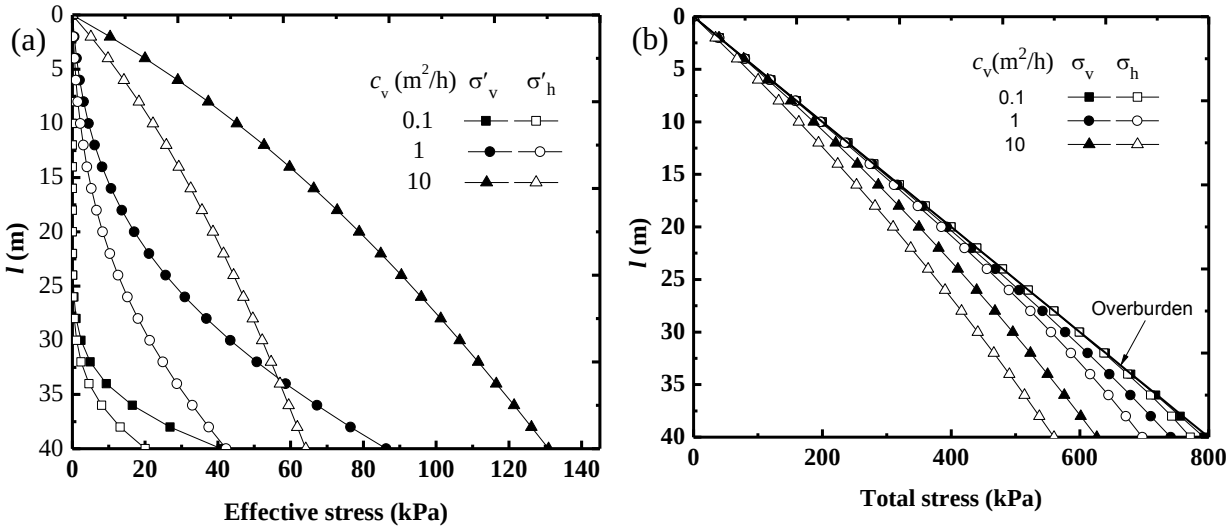

Figure 7-6: Variation of the horizontal and vertical effective (a) and total (b) stresses along the height of the stope at the end of filling for different consolidation coefficients c_v, calculated with the proposed solution [Eqs. (7.29), (7.30), (7.31) and (7.32)] by considering H = 40 m, B = 6 m, m = 0.2 m/h, γ_{sat} = 20 kN/m^3, γ_w = 10 kN/m^3, ϕ' = 20°, and $K = K_a$

Fig. 7-7 shows the variation of the effective [Fig. 7-7(a)] and total [Fig. 7-7(b)] stresses along the height of the stope at the end of the stope filling for different filling rates m, obtained by applying

the proposed solution [Eqs. (7.29), (7.30), (7.31) and (7.32)] and considering a consolidation coefficient c_v = 5 m^2/h, an effective friction angle ϕ' = 20° and the Rankine active earth pressure coefficient of $K = K_a$. One sees that an increase in the filling rate has effect to slow down the excess PWP dissipation, resulting in low effective stresses and high total stresses at the end of stope filling.

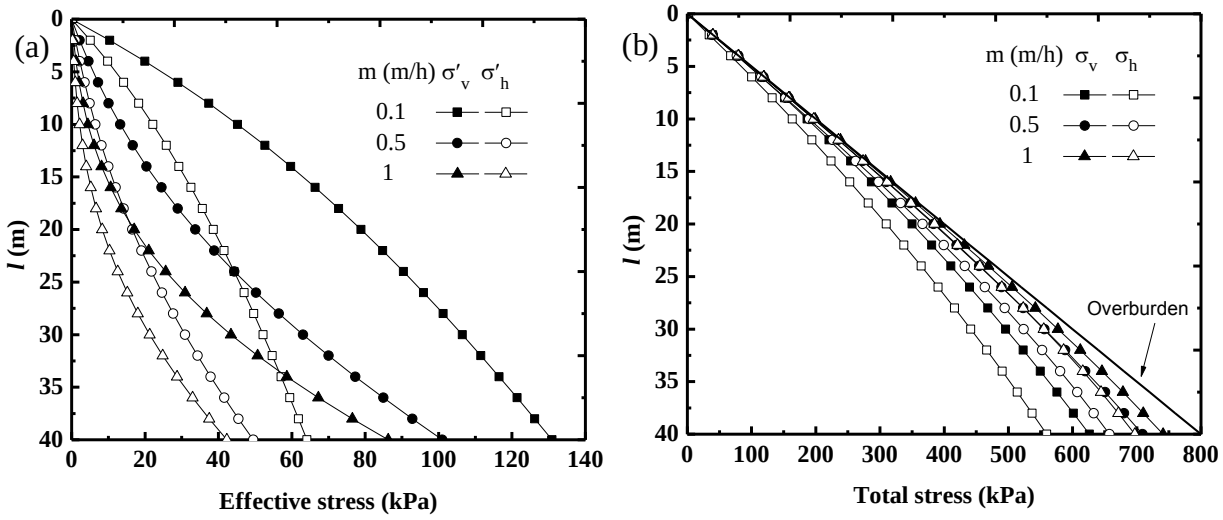

Figure 7-7: Variation of the horizontal and vertical effective (a) and total (b) stresses along the height of the stope at the end of filling for different filling rate *m*, calculated with the proposed solution [Eqs. (7.29), (7.30), (7.31) and (7.32)] by considering H = 40 m, B = 6 m, c_v = 5 m^2/h, γ_{sat} = 20 kN/m^3, γ_w = 10 kN/m^3, ϕ' = 20°, and $K = K_a$

Fig. 7-8 shows the variation of the effective [Fig. 7-8(a)] and total [Fig. 7-8(b)] stresses along the height of the stope at the end of filling for different effective friction angles of backfill ϕ', obtained by applying the proposed solution [Eqs. (7.29), (7.30), (7.31) and (7.32)] and considering a filling rate of m = 0.2 m/h, a consolidation coefficient of c_v = 5 m^2/h and the Rankine active earth pressure coefficient of K_a. One sees that the effective and total stresses decrease as the friction angle ϕ' increases from 10° to 30°. These results indicate that the increase in the friction angle mainly has effect to increase the arching effect and thus reduce the effective and total stresses.

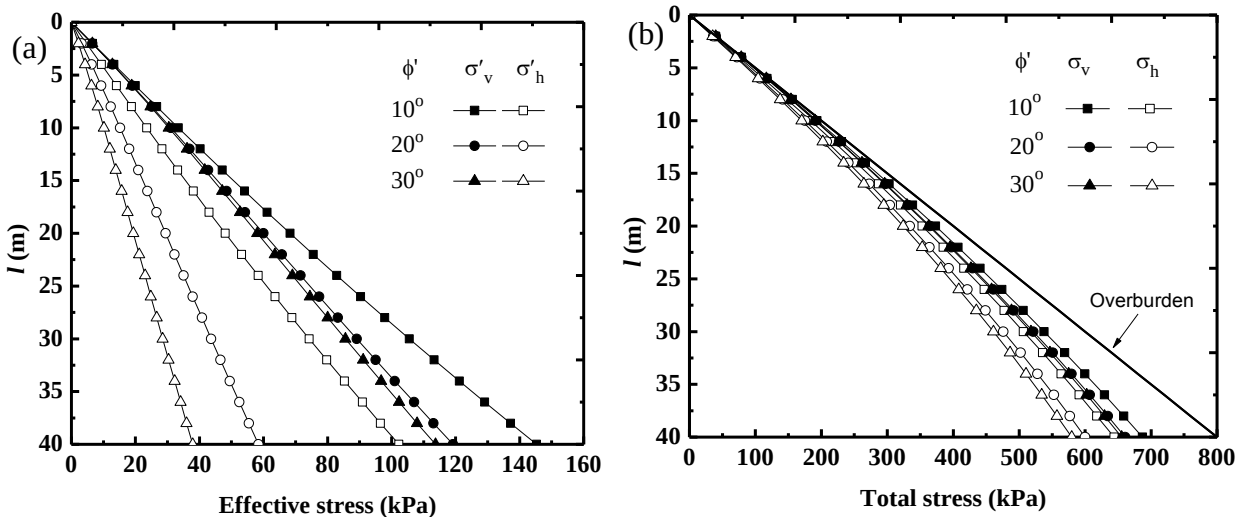

Figure 7-8: Variation of the horizontal and vertical effective (a) and total (b) stresses along the height of the stope at the end of filling, calculated with the proposed solution [Eqs. (7.29), (7.30), (7.31) and (7.32)] by considering H = 40 m, B = 6 m, m = 0.2 m/h, c_v = 5 m^2/h, γ_{sat} = 20 kN/m^3, γ_w = 10 kN/m^3, and $K = K_a$

Fig. 7-9 shows the variation of the effective [Fig. 7-9(a)] and total [Fig. 7-9(b)] stresses along the height of the stope at the end of filling for different stope widths B, obtained by applying the proposed solution [Eqs. (7.29), (7.30), (7.31) and (7.32)] as considering a filling rate of m = 0.2 m/h, a consolidation coefficient of c_v = 5 m^2/h, an effective friction angle ϕ' = 20° and an active earth pressure coefficient of $K = K_a$. One sees that the effective and total stresses decrease as the stope width decreases. These results are straightforward. With a small stope width, the degree of arching effect increases, resulting in low effective and total stresses.

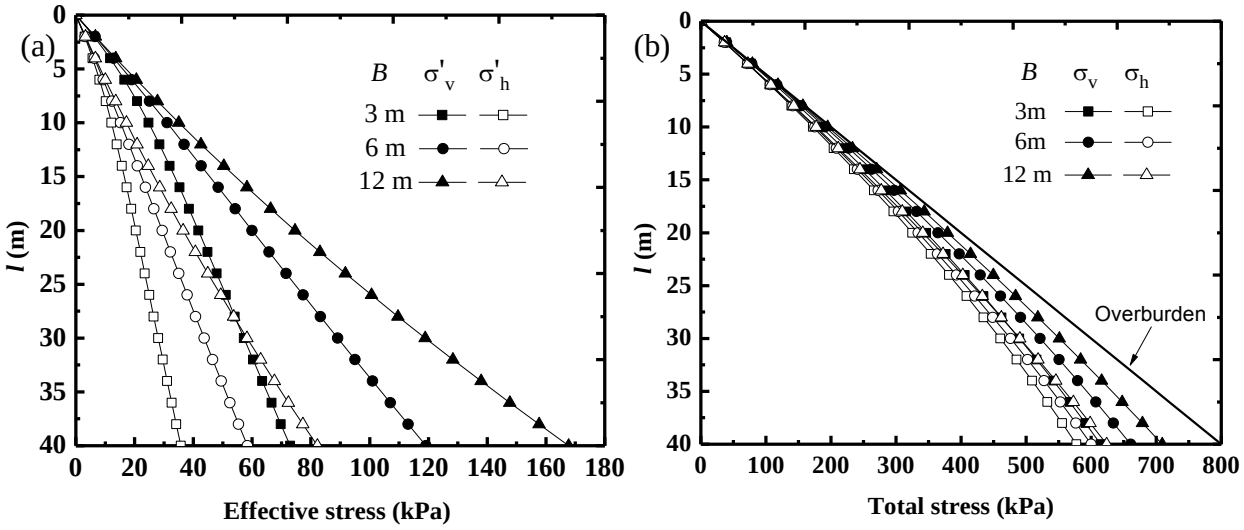

Figure 7-9: Variation of the horizontal and vertical effective (a) and total (b) stresses along the height of the stope at the end of filling, calculated with the proposed solution [Eqs. (7.29), (7.30), (7.31) and (7.32)] by considering H = 40 m, m = 0.2 m/h, c_v = 5 m^2/h, ϕ' = 20°, γ_{sat} = 20 kN/m^3, γ_w = 10 kN/m^3, and $K = K_a$

7.5 Discussion

A new solution has been proposed to evaluate the pressures and stresses in backfilled stopes during and at the end of stope filling operation with an impervious base. The consolidation and arching effect during the placement of backfill have been taken into account. The proposed solution has been validated by numerical modeling with Plaxis2D. It thus constitutes a simple and useful tool to evaluate the pressure and stresses in backfilled stopes and on barricades at the preliminary stage of projects. However, the proposed solution was developed with several simplifications and limitations. For instance, the excess PWP distribution was first calculated using Gibson (1958) model. The ensuing excess PWP solution was then taken into account in the arching solution to evaluate the effective and total stresses. The influence of the arching effect on the dissipation of the excess PWP was not taken into account. In reality, the process of drainage and consolidation and that of arching effect may influence each other during the placement of slurried backfill. The drainage and consolidation lead to the generation of arching effect, which tends to prevent the settlement of backfill particles and slow down the process of drainage and consolidation. Slower drainage and consolidation result in slower increase in the effective stress development, which in turn favors the drainage and consolidation. A coupled process takes place between the arching

effect and self-weight consolidation. More work is necessary to account for this coupled process in the estimation of the distribution and evolution of pressures and stresses in backfilled stopes.

Same as the traditional consolidation theory of Terzaghi (1943), the Gibson (1958) model also considered small strain consolidation with constant consolidation coefficient c_v. For mining backfills, the void ratio, the permeability and the constrained modulus can change with the drainage and consolidation. The consolidation coefficient c_v is thus rarely constant. More work is required to take into account the variation of the mechanical and hydraulic properties during the drainage and consolidation.

When a high water content backfill is placed in the stope, the dissipation of the excess PWP can begin with the sedimentation (i.e. no effective stress) and followed by the consolidation. This has been confirmed by laboratory (e.g., Li et al. 2013) and in situ measurements (e.g., Thompson et al. 2012). The sedimentation is not considered in the Gibson (1958) model. More work is needed to take this aspect into account in the future.

Another limitation is related to the one-dimensional drainage and consolidation. The stope base and side walls were considered to be impermeable. In reality, lateral drainage can occur through the fractures and discontinuities. Two- or three- dimensional consideration of the problem is necessary.

Finally, the proposed solution is developed for mine stopes with an impervious base. In practice, drainage can take place downward through porous barricades at the base of stopes. More work is necessary to develop a solution for estimating the stresses in backfilled stopes with a pervious base; this is ongoing and will be part of future publication.

7.6 Conclusion

In this paper, a new solution has been proposed to estimate the pressures and stresses in mine backfilled stopes with an impervious base by considering the combined effects of the process of drainage and consolidation and that of arching effect during the placement of slurried backfill. As a special case when the hydraulic conductivity is very high or/and when the filling rate is very small, the proposed solution reduces to the solution of Li and Aubertin (2009a) that was developed for estimating the stresses in backfilled stope with hydrostatic water pressure. The proposed solution was validated by numerical modeling with Plaxis2D. It can thus be used as a simple tool

to evaluate the pressures and stresses in backfilled stope during and at the end of stope filling at the preliminary stage of projects. Sample applications of the proposed solution have shown that the drainage and consolidation of backfill can be favored with high consolidation coefficient c_v and low filling rate m, resulting in high effective stress and low total stress in the backfilled stope. With increased backfill effective friction angle or decreased stope width, low effective and total stresses can be expected.

Acknowledgements

The authors would like to acknowledge the financial support from the Natural Sciences and Engineering Research Council of Canada (NSERC 402318), Fonds de recherche du Québec - Nature et Technologies (FRQNT 2015-MI-191676), and industrial partners of the Research Institute on Mines and the Environment (RIME UQAT-Polytechnique; http://rime-irme.ca/).

7.7 Appendix I: Process for the deduction of Eq. (7.27)

Eq. (7.26) can be re-written as follows:

$$\sigma_v^{'} = e^{\frac{-2K\tan\phi^{'}}{B}l}\left[\int f(l)dl + A\right] \tag{7.35}$$

where

$$f(l) = (\gamma^{'} - \frac{du}{dl})e^{\frac{2K\tan\phi^{'}}{B}l} \tag{7.36}$$

Assuming,

$$F^{'}(l) = f(l) \text{ or } \int f(l)dl = F(l) + C \tag{7.37}$$

Substituting Eq. (7.37) into Eq. (7.35) leads to

$$\sigma_v^{'} = e^{\frac{-2K\tan\phi^{'}}{B}l}\left[F(l) + C + A\right] \tag{7.38}$$

Considering the boundary condition, l = 0, σ'_v = 0, one can obtain

$$0 = F(0) + C + A \Rightarrow F(0) = -C - A \tag{7.39}$$

Substituting Eq. (7.39) into Eq. (7.38) leads to

$$\sigma_v^{'} = e^{\frac{-2K\tan\phi^{'}}{B}l}\left[F(l)-F(0)\right] \tag{7.40}$$

With Eq. (7.37), one can obtain

$$\int_0^l f(l)dl = F(l)-F(0) \tag{7.41}$$

Substituting Eq. (7.41) into Eq. (7.40) leads to

$$\sigma_v^{'} = e^{\frac{-2K\tan\phi^{'}}{B}l}\int_0^l f(l)dl = e^{-\frac{2K\tan\phi^{'}}{B}l}\int_0^l\left(\gamma^{'}-\frac{du}{dl}\right)e^{\frac{2K\tan\phi^{'}}{B}l}dl \tag{7.42}$$

7.8 Appendix II: MATLAB program for solving Eq. (7.32)

A MATLAB program is given below to solve Eq. (7.32). Sample calculation is conducted with the proposed program by considering a backfill having a saturated unit weight of γ_{sat} = 20 kN/m^3 and filled to a final height of H = 40 m. The other parameters are considered as B = 6 m, m = 0.2 m/h, c_v = 5 m^2/h, γ_w = 10 kN/m^3, ϕ' = 20° and $K = K_a$.

```
%=========================================================================%
% A solution to estimate the total and effective stresses in backfilled stopes
with an impervious base during the filling operation %
%=========================================================================%
nmax= 101; % number of division of H (here n_max= 101)
time = 200; % time of filling (here t = 200 h);
m = 0.2; % filling rate (here m = 0.2 m/h);
H = m*time; % final thickness of the backfill (here H = 40 m);
c_v = 5; % consolidation coefficient of the backfill (here c_v = 5 m^2/h);
h_0 = 0.3; % step interval of y (see Fig. 7-1);
gama_sat = 20; % saturated unit weight of the backfill (here γ_sat = 20 kN/m^3);
gama_w = 10; % unit weight of water (γ_w = 10 kN/m^3);
gama_sub = gama_sat-gama_w; % submerged unit weight of the backfill;
B = 6; % width of the mine stope (here B = 6 m)
Phi = 20; % effective internal friction angle of the backfill (here φ' = 20°);
K_a = (1-sind(Phi))/(1+sind(Phi)); % Rankine active earth pressure coefficient
of the backfill (used in this sample calculation);
K_0 = 1-sind(phi); %Jaky at-rest earth pressure coefficient (not used in this
sample calculation);
A = 2*K_a*tand(Phi)/B;
```

```
% calculate the excess PWP, u, in Eq.(7.10)
for i = 1:nmax
    l(i) = H/(nmax-1)*(i-1);
    y(i) = H-l(i);
    u(i) = 0.0;
    for j = -91:91;
        temp1 = m*j*h_0*sqrt(time)/sqrt(c_v);
        temp2 = y(i)*j*h_0/sqrt(c_v*time);
        u(i) = u(i)+h_0/2.*4.*c_v*time*j*h_0*tanh(temp1)*cosh(temp2)*exp(-
(j*h_0)^2);
    end
    pre_multi = gama_sub/sqrt(pi*c_v*time)*exp(-(y(i))^2/4./c_v/time);
    u(i) = (gama_sub*H-pre_multi*u(i));
end

% calculate the du/dy in Eq.(7.14)
for i = 1:nmax
    l(i) = H/(nmax-1)*(i-1);
    y(i) = H-l(i);
    derive_u(i) = 0.0;
    for j = -91:91;
        temp1 = m*j*h_0*sqrt(time)/sqrt(c_v);
        temp2 = (y(i))*j*h_0/sqrt(c_v*time);
        temp3 = j*h_0/sqrt(c_v*time);
        temp4 = -(y(i))/2./c_v/time;
        a = tanh(temp1)*cosh(temp2)*exp(-(j*h_0)^2);
        b = tanh(temp1)*sinh(temp2)*(j*h_0/sqrt(c_v*time))*exp(-(j*h_0)^2);
        derive_u(i) =
derive_u(i)+temp4*h_0/2.*4.*c_v*time*j*h_0*a+h_0/2.*4*c_v*time*j*h_0*b;
    end
    pre_multi = -gama_sub/sqrt(pi*c_v*time)*exp(-(y(i))^2/4./c_v/time);
    derive_u(i) = pre_multi*derive_u(i);
end

% calculate the horizontal total stress in Eq.(7.32)
for i = 1:nmax
    l(i) = H/(nmax-1)*(i-1);
```

```
    n_z = i;
    sigma_sub(i)=0.0;
    for k = 1:n_z
        delta_x = l(i)/(n_z);
        sigma_sub(i) =
sigma_sub(i)+(gama_sub+derive_u(k))*exp(A*(k*delta_x))*delta_x;
    end
    sigma_sub(i) = exp(-A*l(i))*sigma_sub(i);
    sigma_H(i)=K_a*sigma_sub(i)+gama_w*l(i)+u(i);
end
% results output and saved in the file "Output filename.txt"
fid = fopen('Output filename.txt','w')
for i=1:nmax
    fprintf(fid,'%g %g\r\n',l(i),sigma_H(i))
end
fclose(fid)

plot(sigma_H,l,'-.');
set(gca,'YDir','reverse');
```

7.9 References

Askew, J.E., McCarthy, P.L., & Fitzerald, D.J. (1978). *Backfill research for pillar extraction at ZC/NBHC*. Paper presented at the Proceedings of Mining with Backfill: 12th Canadian Rock Mechanics Symposium, CIM, Montréal, (pp. 100-110).

Aubertin, M. (1999). *Application de la mécanique des sols pour l'analyse du comportement des remblais miniers souterrains*. Short Course (unpublished notes). Paper presented at the 14th Colloque en Contrôle de Terrain, Val-d'Or, Québec.

Aubertin, M., Bussiere, B., & Bernier, L. (2002). *Environnement et gestion des rejets miniers. Presses* [Manual on CD-ROM]. Internationales Polytechnique, Montréal, Canada.

Aubertin, M., Li, L., Arnoldi, S., Belem, T., Bussière, B., Benzaazoua, M., & Simon, R. (2003). *Interaction between backfill and rock mass in narrow stopes*. Paper presented at the Soil and Rock America 2003, Essen, Germany (pp, 1157–1164).

Brinkgreve, R.B.J., Kumarswamy, S., & Swolfs, W.M. (2014). PLAXIS (2014) [Computer software]. Delft, Netherlands.

Bussiere, B. (2007). Colloquium 2004: Hydrogeotechnical properties of hard rock tailings from metal mines and emerging geoenvironmental disposal approaches. *Canadian Geotechnical Journal, 44*(9), 1019-1052.

Canadian geotechnical Society. (2006). *Canadian foundation engineering manual* (4th ed.), Vancouver, Canada.

Cui, L., & Fall, M. (2018). Modeling of self-desiccation in a cemented backfill structure. *International Journal for Numerical and Analytical Methods in Geomechanics, 42*(3), 558-583.

Darling, P. (2011). *SME mining engineering handbook* (3th ed.). Society for Mining, Metallurgy, and Exploration, Denver, US.

Doherty, J.P. (2015). A numerical study into factors affecting stress and PWP in free draining mine stopes. *Computers and Geotechnics, 63*, 331-341.

Doherty, J.P., Hasan, A., Suazo, G.H., & Fourie, A. (2015). Investigation of some controllable factors that impact the stress state in cemented paste backfill. *Canadian Geotechnical Journal, 52*(12), 1901-1912.

El Mkadmi, N., Aubertin, M., & Li, L. (2014). Effect of drainage and sequential filling on the behavior of backfill in mine stopes. *Canadian Geotechnical Journal, 51*(1), 1–15.

Fahey, M., Helinski, M., & Fourie, A. (2010). Consolidation in accreting sediments: Gibson's solution applied to backfilling of mine stopes. *Géotechnique, 60*(11), 877-882.

Gibson, R.E. (1958). The progress of consolidation in a clay layer increasing in thickness with time. *Géotechnique, 8*(4), 171-182.

Goodwin, E.T. (1949). *The evaluation of integrals of the form* $\int_{-\infty}^{+\infty} f(x)e^{-x^2}dx$. Paper presented at the Mathematical Proceedings of the Cambridge Philosophical Society. Cambridge University, London, UK (pp. 241-245).

Grice, A.G. (1998). *Stability of hydraulic backfill barricades*. Paper presented at the 6th International Symposium on Mining with Backfill, Brisbane, Australia (pp. 117-120).

Hassani, F., & Archibald, J. (1998). Mine backfill. (CD-ROM). Canadian Institute of Mining, Metallurgy and Petroleum, Montréal, Canada.

Herget, G. (1988). Stresses in rock. Rotterdam, Netherlands.

Jaky, J. (1948). *Pressure in silos*. Paper presented at the 2nd International Conference on Soil Mechanics and Foundation Engineering, Rotterdam, The Netherlands (pp. 103-107).

Jung, S.J., & Biswas, K. (2002). Review of current high density paste fill and its technology. *Minerral Resources Engineering, 11*(2), 165–182.

Knutsson, S. (1981). *Stresses in the hydraulic backfill from analytical calculations and in-situ measurements*. Paper presented at the Application of Rock Mechanics to Cut and Fill Mining, London. (pp. 261–268).

Kump, D. (2001). Backfill — whatever it takes. *Mining Engineering, 53*(1), 50–52.

Li, L. (2013). Beneficial Experience from teaching and education to research and development. *Creative Education, 3*(7), 148–153.

Li, L., Alvarez, I.C., & Aubertin, J.D. (2013). Self-weight consolidation of a slurried deposition: tests and interpretation. *International Journal of Geotechnical Engineering, 7*(2), 205–213.

Li, L., & Aubertin, M. (2009a). Influence of water pressure on the stress state in stopes with cohesionless backfill. *Geotechnical and Geological Engineering, 27*(1), 1–11.

Li, L., & Aubertin, M. (2009b). A three-dimensional analysis of the total and effective stresses in submerged backfilled stopes. *Geotechnical and Geological Engineering, 27*(4), 559–569.

Li., L, Aubertin, M., Simon, R., Bussière, B., & Belem, T. (2003). *Modeling arching effects in narrow backfilled stopes with FLAC*. Paper presented at the 3rd International FLAC Symposium, A. A. Balkema, Rotterdam, Netherlands. (pp. 211–219).

Li, L., Aubertin, M., & Belem, T. (2005). Formulation of a three dimensional analytical solution to evaluate stress in backfilled vertical narrow openings. *Canadian Geotechnical Journal, 42*(6), 1705–1717 (with Erratum 2006, 43(3), 338–339).

Pirapakaran, K., & Sivakugan, N. (2007a). A laboratory model to study arching within a hydraulic fill stope. *Geotechnical Testing Journal, 30*(6), 496–503.

Pirapakaran, K., & Sivakugan, N. (2007b). Arching within hydraulic fill stopes. *Geotechnical and Geological Engineering, 25*(1), 25-35.

Pedroni, L. (2011). Étude expérimentale et numérique de la sédimentation et de la consolidation des boues de traitement des eaux acides. (Doctoral dissertation, École Polytechnique de Montréal, Montréal, Canada).

Revell, M.B., & Sainsbury, D.P. (2007). *Paste bulkhead failures*. Paper presented at the 9th International Symposium on Mining with Backfill (Minefill'07), Montréal, Canada.

Shahsavari, M., & Grabinsky, M. (2014). *Cemented paste backfill consolidation with deposition-dependent boundary conditions*. Paper presented at the 67th Canadian Geotechnical Conference, Canadian Geotechnical Society, Regina, Saskatchewan, Canada.

Shahsavari, M., & Grabinsky, M. (2015). *Mine backfill porewater pressure dissipation: numerical predictions and field measurements*. Paper presented at the 68th Canadian Geotechnical Conference, Canadian Geotechnical Society, Québec City, Canada (pp. 1-8).

Simms, P., Grabinsky, M., & Zhan, G.S. (2007). Modelling evaporation of paste tailings from the Bulyanhulu mine. *Canadian Geotechnical Journal, 44*(12), 1417–1432.

Sivakugan, N., Rankine, K., & Rankine, R. (2006a). Permeability of hydraulic fills and barricade bricks. *Geotechnical and Geological Engineering, 24*(3), 661-673.

Sivakugan, N., Rankine, R.M., Rankine, K.J., & Rankine, K.S. (2006b). Geotechnical considerations in mine backfilling in Australia. *Journal of Cleaner Production, 14*(12), 1168-1175.

Sivakugan, N., Rankine, K., Lovisa, J., & Hall, W. (2013). Flow rate computations in hydraulic fill mine stopes. *Indian Geotechnical Journal, 43*(3), 195-202.

Terzaghi, K. (1943). Theoretical Soil Mechanics. New York, USA: John Wiley and Sons.

Thompson, B.D., Bawden, W.F., & Grabinsky, M.W. (2012). In situ measurements of cemented paste backfill at the Cayeli Mine. *Canadian Geotechnical Journal, 49*(7), 755-772.

Wood, D.M., Doherty, J.P., & Walske, M.L. (2016). Deposition and self-weight consolidation of a shrinking fill. *Géotechnical Letter, 6*(1), 72-76.

Yumlu, M., & Guresci, M. (2007). *Paste backfill bulkhead monitoring-A case study from Inmet's Cayeli mine*. Paper presented at the 9th International Symposium in Mining with Backfill (CD-ROM), Canadian Institute of Mining, Metallurgy and Petroleum, Montréal, Canada.

Zheng, J., Li, L., Mbonimpa, M., & Pabst, T. (2018a). An analytical solution of Gibson's model for estimating the pore water pressures in accreting deposition of slurried material under one-dimensional self-weight consolidation. Part I: Pervious base. *Indian Geotechnical Journal, 48*(1), 72-83.

Zheng, J., Li, L., Mbonimpa, M., & Pabst, T. (2018b). An analytical solution of Gibson's model for estimating pore water pressures in accreting deposition of slurried material under one-dimensional self-weight consolidation. Part II: Impervious base. *Indian Geotechnical Journal, 48*(1), 188-195.

CHAPTER 8 ARTICLE 6: TOTAL AND EFFECTIVE STRESSES IN BACKFILLED STOPES DURING THE FILL PLACEMENT ON A PERVIOUS BASE FOR BARRICADE DESIGN

Jian Zheng, Li Li, Yu-Chao Li

Article submitted to Minerals in November 2018.

Abstract: Backfill is increasingly used in underground mines worldwide. Its successful application depends on the stability of the barricades built at the base of the stopes to hold the backfill in place, which in turn depends on the knowledge of the pore water pressure (PWP) and stresses during or shortly after the placement of the slurried backfill. Until now, the self-weight consolidation is usually considered for the estimation of the PWP. There is no solution available to evaluate the total and effective stresses during and shortly after the filling operation. As excess PWP can simultaneously be generated (increased) and dissipated (decreased) during the backfilling operation, effective stresses can develop when the filling rate is low or/and hydraulic conductivity of the backfill is high. Arching effect has to be considered to evaluate the effective and total stresses in the backfilled stopes. In this paper, a pseudo-analytical solution is proposed to evaluate the effective and total stresses in backfilled stopes during the backfill deposition on a permeable base by considering the self-weight consolidation and arching effect. The proposed solution is validated by numerical results obtained by Plaxis2D. A few sample applications of the proposed solution are shown.

Keywords: Backfill; Self-weight Consolidation; Arching effect; Effective stress; Total stress; Excess pore water pressure (PWP); Pervious base

8.1 Introduction

Backfill is largely used in underground mines to fill stopes. The benefits of backfilling include improved ground stability, reduced mineral dilution, and increased ore recovery (Hassani and Archibald 1998; Jung and Biswas 2002). When mine wastes are used as the fill materials, the backfilling of underground mine stopes reduces the surface disposal of mine wastes and minimize the environment impact (Aubertin et al. 2002; Simms et al. 2007; Komurlu and Kesimal 2015; Cui and Fall 2018).

When the mining backfill is transported by boreholes and pipelines, it must contain sufficient water to ensure the workability and facilitate the transport. The construction of a confining structure called barricade (bulkhead) in the draw-point at the base of the stope is necessary to hold the slurried backfill in place. The stability of the barricade can thus become a critical concern because the barricade failures reported in the literature mostly resulted in serious consequences such as damage of equipment and personal injury and even life losses (e.g., Sivakugan et al. 2006a, 2006b, 2013; Yumlu and Guresci 2007; Revell et al. 2007; Li and Aubertin 2009c, 2011; Cui and Fall 2017; Yang et al. 2017; Ning et al. 2017).

The stability analyses of barricade require to properly estimate the pore water pressure (PWP) and the stresses in backfilled stopes and on barricades. It is important to know that the most critical moments for the stability of barricades are during and shortly after the placement of the slurried backfill. After these critical moments, the pressure and stresses can dramatically diminish due to the drainage and consolidation as well as the cementation of the cemented backfill (Thompson et al. 2012).

During the placement of the slurried backfill, excess PWP can be instantaneously generated (increased) with the addition of new backfill layers and progressively dissipated (decreased). This process is known as self-weight consolidation (Gibson 1958; Pedroni 2011; Li et al. 2013; El Mkadmi 2014; Park et al. 2014; Zhang et al. 2017). With the consolidation of slurried backfill, effective stresses and arching effect can develop in the backfilled stopes, especially when the filling rate is low and the hydraulic conductivity of the backfill is high.

Until now, the self-weight consolidation is largely considered for the estimation of the PWP during the placement of the slurried backfill without any consideration of effective stress development (Gibson 1958; Fahey et al. 2010; Shahsavari and Grabinsky 2014, 2015; Wood et al. 2016; Walske

and Doherty 2017; Zheng et al. 2018a, 2018b). The arching theory has been applied to evaluate the stresses either for dry backfill (Aubertin et al. 2003; Li et al. 2003, 2005; Pirapakaran and Sivakugan 2007a, 2007b; Li and Aubertin 2008, 2009c, 2009d; Jahanbakhshzadeh et al. 2017, 2018a, 2018b) or for submerged backfill with hydrostatic pressure (Li and Aubertin 2009a, 2009b, 2010). These conditions correspond to the final steady states of the slurried backfill when the drainage and self-weight consolidation are fully completed with a pervious (for dry backfill) or an impervious (for submerged backfill) barricade. The conditions do not correspond to the most critical moment for the stability of barricades during and after the filling operation. The question is how to evaluate the total and effective stresses during and shortly after the filling operation (the most critical moments for the stability of barricades). To reply to this question, the self-weight consolidation and arching effect have to be considered simultaneously.

In this paper, a pseudo-analytical solution is proposed to calculate the effective and total stresses in backfilled stopes during the deposition of slurried backfill on a permeable base. The self-weight consolidation and arching effect are taken into account. The PWP is first evaluated by using an analytical solution proposed by Zheng et al. (2018a). The effective and total stresses are then obtained by introducing the PWP expression in the arching model of Li and Aubertin (2009a). The proposed solution is validated by numerical modeling results obtained by Plaxis2D.

8.2 Proposed solution

Fig. 8-1 presents a typical vertical mine stope which is continuously filled with a slurried backfill at a filling rate of m (m/h). The stope has a width of B (m) and filled to a final height of H (m). At a given time t, the backfill reaches a height h (= mt). On the figure, x (m) is the elevation of a studied point ($0 \leq x \leq h$). Other parameters shown in the figure will be presented when their application appears.

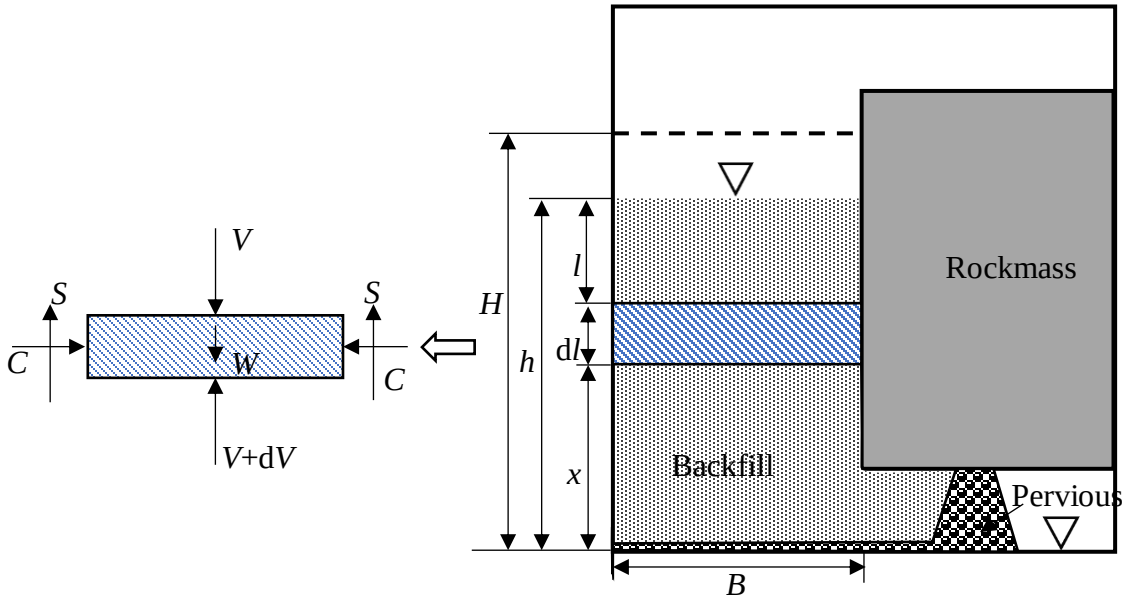

Figure 8-1: Schematic diagram of a vertical backfilled stope with a pervious base and continuously filled with slurried backfill.

As the stope has a permeable base, at the end of drainage and consolidation when the backfill water reaches the final steady state, the water table in the stope will fall down to the base level, resulting in zero PWP everywhere in the backfilled stope (negative PWP due to suction is neglected here). Since the excess PWP is defined as the current total PWP subtracted the final steady-state PWP (Gibson et al. 1989), the excess PWP is thus always equal to the current total PWP. Therefore, distinction between the excess PWP and current total PWP is not necessary. In the following sections, they are noted as (excess) PWP (Zheng et al. 2018a).

8.2.1 Solution to estimate the (excess) PWP

Gibson (1958) proposed a solution to evaluate the (excess) PWP in slurried materials placed on a pervious base with increasing thickness at a constant filling rate (m).

$$c_v \frac{\partial^2 p_w}{\partial x^2} = \frac{\partial p_w}{\partial t} - \gamma \frac{dh}{dt} \tag{8.1}$$

where p_w (kPa) is the (excess) PWP, t (h) is the filling time, γ (kN/m^3) is the saturated unit weight of the backfill, c_v (m^2/g) is consolidation coefficient of the backfill.

Using the boundary conditions $p_w = 0$ at $x = 0$ and $x = h$, Gibson (1958) gave the following solution:

$$p_w = -\gamma x(1+\frac{mx}{2c_v}) + \frac{\gamma m}{2c_v}(\pi c_v t)^{-\frac{1}{2}} \times \exp\left(-\frac{x^2}{4c_v t}\right) \times E \tag{8.2}$$

where

$$E = \int_0^\infty \xi^2 \coth\left(\frac{m\xi}{2c_v}\right) \times \sinh\left(\frac{x\xi}{2c_v t}\right) \times \exp\left(-\frac{\xi^2}{4c_v t}\right) d\xi \tag{8.3}$$

where ξ (m) is an arbitrary integration parameter ($0 < \xi < \infty$).

The gradient of the (excess) PWP can be calculated as:

$$\frac{dp_w}{dx} = -(\gamma + \frac{m\gamma x}{c_v}) + \frac{\gamma m}{2c_v}(\pi c_v t)^{-\frac{1}{2}} \times \exp\left(-\frac{x^2}{4c_v t}\right)\left[\left(-\frac{x}{2c_v t}\right) \times E + F\right] \tag{8.4}$$

where F is given as

$$F = \int_0^\infty \xi^2 \coth\left(\frac{m\xi}{2c_v}\right) \times \cosh\left(\frac{x\xi}{2c_v t}\right) \times \left(\frac{\xi}{2c_v t}\right) \times \exp\left(-\frac{\xi^2}{4c_v t}\right) d\xi \tag{8.5}$$

Equation (8.3) can be expressed as the following function:

$$G(y) = \int_0^\infty g(y) \exp(-y^2) dy \tag{8.6}$$

where

$$g(y) = 8(c_v t)^{\frac{3}{2}} \times y^2 \times \coth\left(\frac{m\sqrt{t} \times y}{\sqrt{c_v}}\right) \times \sinh\left(\frac{x \times y}{\sqrt{c_v t}}\right) \tag{8.7}$$

and

$$y^2 = \frac{\xi^2}{4c_v t} \tag{8.8}$$

As $g(y)$ is an even function, $G(y)$ is thus also an even equation and can be rewritten as follows:

$$G(y)=\frac{1}{2}\int_{-\infty}^{\infty} g(y)\exp(-y^2)dy \tag{8.9}$$

Goodwin (1949) proposed the following transformation to approximate the calculation of the integral:

$$\int_{-\infty}^{\infty} g(y)e^{-y^2}dy = h_0\sum_{n=-\infty}^{\infty} g(nh_0)e^{-n^2h_0^2} \tag{8.10}$$

where h_0 is step length of y; n is the series number in the range of -∞ to +∞. Goodwin (1949) has presented that the application of Eq. (8.10) can allow to obtain a good approximation of the integral with high accuracy when the value of h_0 is in the range of 0 to 1 and n is large enough through its sensitivity analysis.

Eq. (8.3) can thus be re-written as follows:

$$E=\frac{h_0}{2}\sum_{n=-\infty}^{\infty}8(c_vt)^{\frac{3}{2}}\times(nh_0)^2\times\coth\left(\frac{mnh_0\sqrt{t}}{\sqrt{c_v}}\right)\times\sinh\left(\frac{xnh_0}{\sqrt{c_vt}}\right)\times e^{-(nh_0)^2} \tag{8.11}$$

Substituting Eq. (8.11) into Eq. (8.2) leads to

$$\begin{aligned}p_w=&-\gamma x(1+\frac{mx}{2c_v})+\frac{\gamma m}{2c_v}(\pi c_vt)^{-\frac{1}{2}}\times\exp\left(-\frac{x^2}{4c_vt}\right)\times\\&\frac{h_0}{2}\sum_{n=-\infty}^{\infty}8(c_vt)^{\frac{3}{2}}\times(nh_0)^2\times\coth\left(\frac{mnh_0\sqrt{t}}{\sqrt{c_v}}\right)\times\sinh\left(\frac{xnh_0}{\sqrt{c_vt}}\right)\times e^{-(nh_0)^2}\end{aligned} \tag{8.12}$$

Eq. (8.12) is the analytical solution to evaluate the (excess) PWP in the slurried material during the accreting deposition on a pervious base, which was proposed by Zheng et al. (2018) based on the model of Gibson (1958). Stable results of (excess) PWP can be obtained with Eq. (8.12) when h_0 is taken as 0.5 and n is in the range of -55 and 55 for most cases (Zheng et al. 2018a).

Using the same derivation process as function E, function F can be expressed as follows:

$$F=\frac{h_0}{2}\sum_{n=-\infty}^{\infty}8(c_vt)^{\frac{3}{2}}\times(nh_0)^2\times\coth\left(\frac{mnh_0\sqrt{t}}{\sqrt{c_v}}\right)\times\frac{nh_0}{\sqrt{c_vt}}\times\cosh\left(\frac{xnh_0}{\sqrt{c_vt}}\right)\times e^{-(nh_0)^2} \tag{8.13}$$

Substituting Eqs. (8.11) and (8.13) into Eq. (8.4) yields

$$\frac{dp_w}{dx}=-(\gamma+\frac{m\gamma x}{c_v})+\frac{\gamma m}{2c_v}(\pi c_v t)^{-\frac{1}{2}}\times\exp\left(-\frac{x^2}{4c_v t}\right)\left[\begin{array}{l}\left(-\frac{x}{2c_v t}\right)\times\frac{h_0}{2}\sum_{n=-\infty}^{\infty}8(c_v t)^{\frac{3}{2}}\times(nh_0)^2\times\coth\left(\frac{mnh_0\sqrt{t}}{\sqrt{c_v}}\right)\times\sinh\left(\frac{xnh_0}{\sqrt{c_v t}}\right)\times e^{-(nh_0)^2}+\\ \frac{h_0}{2}\sum_{n=-\infty}^{\infty}8(c_v t)^{\frac{3}{2}}\times(nh_0)^2\times\coth\left(\frac{mnh_0\sqrt{t}}{\sqrt{c_v}}\right)\times\frac{nh_0}{\sqrt{c_v t}}\times\cosh\left(\frac{xnh_0}{\sqrt{c_v t}}\right)\times e^{-(nh_0)^2}\end{array}\right]$$

(8.14)

Eq. (8.14) will be introduced into the below section to evaluate the effective and total stresses in the backfilled stopes by taking into account the (excess) PWP and arching effect.

8.2.2 Solution to evaluate the effective and total stresses

In Fig. 8-1, the forces acted on the isolated layer element includes its own weight W (kN), two compressive forces C (kN) and two lateral shearing forces S (kN) on two side walls, a vertical total force V (kN) on the top and a vertical total force V + dV (kN) on the base. Considering the equilibrium state of the isolated layer element leads to:

$$dV+2S=W \tag{8.15}$$

The element layer weight W can be expressed as

$$W=\gamma Bdl \tag{8.16}$$

where l (= h – x) is the depth of the calculation point from the top of the slurried backfill, dl (m) is the thickness of the element layer.

Assuming the vertical total stress σ_v is uniformly distributed across the stope width, the vertical force V can be expressed as follows:

$$V=\sigma_v B \tag{8.17}$$

By applying the Mohr-Coulomb criterion and assuming the horizontal effective stress (σ'_h, kPa) be proportional to the vertical effective stress (σ'_v, kPa), the lateral shear force S can be calculated as follows:

$$S=\sigma_h^{'}\tan\delta^{'}dl=K\sigma_v^{'}\tan\phi^{'}dl \tag{8.18}$$

where δ' (°) is the effective friction angle along the backfill-wall contact interfaces, which is assumed here to be ϕ' (°); K is the earth pressure coefficient for the placed backfill. Based on

numerical and experimental results, some researchers suggested to use Rankine active earth pressure coefficient K_a (Li et al. 2003, 2005; Li and Aubertin 2009a, 2009b; Ting et al. 2012):

$$K_a = \sigma_h^{'} / \sigma_v^{'} = \tan^2(45° - \varphi^{'}/2) \tag{8.19}$$

while others proposed to take Jaky at-rest earth pressure coefficient K_0 as the rock walls do not move (Pirapakaran and Sivakugan 2007a, 2007b; Fahey et al. 2009; Ting et al. 2011):

$$K_0 = \sigma_h^{'} / \sigma_v^{'} = 1 - \sin\phi^{'} \tag{8.20}$$

Sobhi et al. (2017) and Yang et al. (2017) revealed that the wall immobilization is a necessary and sufficient condition for the backfill to be in an at-rest condition only when the natural soil (not backfill as shown in most textbook) before excavation (not backfilling) is initially in an at-rest state. For the case of placement of a backfill in a pre-existing confining structure (rather than construction of a retaining wall later to hold a pre-existing soil), an active state is possible for the newly deposited backfill. Yang et al. (2018) further show why the state of the backfill along the vertical center line of the backfilled stope can be in an at-rest or an active state, depending on the relationship between the value of friction angle and Poisson's ratio. In the case of at-rest state, the earth pressure coefficient will be expressed as K_0 by = $\mu/(1 - \mu)$, rather than the Jaky's expression. Further discussion on this aspect is beyond the scope of this paper. In the following sections, the Rankine active earth pressure coefficient of K_a will be used.

The vertical (σ_v, kPa) and horizontal (σ_h, kPa) total stresses can be expressed as follows:

$$\sigma_v = \sigma_v^{'} + p_w \tag{8.21}$$

$$\sigma_h = \sigma_h^{'} + p_w = K\sigma_v^{'} + p_w \tag{8.22}$$

Introducing Eq. (8.21) to Eq. (8.17) leads to:

$$dV = Bd[\sigma_v^{'} + p_w] \tag{8.23}$$

Substituting Eqs. (8.16), (8.18) and (8.23) into Eq. (8.15) yields

$$B[d\sigma_v^{'} + dp_w] + 2K\sigma_v^{'}\tan\phi^{'}dl = \gamma Bdl \tag{8.24}$$

or

$$\frac{d\sigma_v^{'}}{dl}+\frac{2K\tan\phi^{'}}{B}\sigma_v^{'}=\gamma-\frac{dp_w}{dl} \tag{8.25}$$

Solving Eq. (8.25) results in the following expression:

$$\sigma_v^{'}=e^{-\frac{2K\tan\phi^{'}}{B}l}[\int(\gamma-\frac{dp_w}{dl})\times e^{\frac{2K\tan\phi^{'}}{B}l}dl+A] \tag{8.26}$$

where A is an arbitrary constant.

By using the boundary condition $\sigma'_v = 0$ at $l = 0$, the σ'_v in the backfill can then be expressed as:

$$\sigma_v^{'}=e^{-\frac{2K\tan\phi^{'}}{B}l}\int_0^l(\gamma-\frac{dp_w}{dl})\times e^{\frac{2K\tan\phi^{'}}{B}l}dl \tag{8.27}$$

Considering that $l = h - x$, Eq. (8.27) can be re-written as:

$$\sigma_v^{'}=e^{-\frac{2K\tan\phi^{'}}{B}l}\int_0^l(\gamma+\frac{dp_w}{dx})\times e^{\frac{2K\tan\phi^{'}}{B}l}dl \tag{8.28a}$$

Knowing the vertical effective stress with Eq. (28a), the horizontal effective stress σ'_h can then be calculated as

$$\sigma'_h = K\sigma'_v. \tag{8.28b}$$

The horizontal (σ_h) and vertical (σ_v) total stresses can be calculated as:

$$\sigma_v=e^{-\frac{2K\tan\phi^{'}}{B}l}\int_0^l(\gamma+\frac{dp_w}{dx})\times e^{\frac{2K\tan\phi^{'}}{B}l}dl+p_w \tag{8.29}$$

$$\sigma_h=Ke^{-\frac{2K\tan\phi^{'}}{B}l}\int_0^l(\gamma+\frac{dp_w}{dx})\times e^{\frac{2K\tan\phi^{'}}{B}l}dl+p_w \tag{8.30}$$

Eqs. (8.28), (8.29) and (8.30) constitute the proposed pseudo-analytical solution to evaluate the vertical and horizontal effective and total stresses during the stope filling operation.

For the barricade design, the key parameter is the horizontal total stress. A MATLAB program to solve Eq. (8.30) for the horizontal total stress has been presented in Appendix A by considering a case with H = 20 m, B = 4 m, m = 0.1 m/h, c_v = 5 m^2/h, γ_w = 10 kN/m^3, γ = 20 kN/m^3, ϕ' = 10° and $K = K_a$. It is important to use a large enough value of n_{max} to ensure stable and accurate results of σ_h. Sensitivity analysis should be done to study the influence of n_{max} on the calculated σ_h.

Fig. 8-2 presents the variation of the calculated σ_h at the base of the stope (x = 0) as a function of n_{max}. It can be seen that a stable result of σ_h can be obtained when the value of n_{max} exceeds 101 for the given case (the results σ_h = 167.37 kPa for n_{max} = 1001 and σ_h = 167.27 kPa for n_{max} = 10001 are not presented in the figure). This sensitivity analysis should be conducted for each new calculation to ensure stable and reliable results.

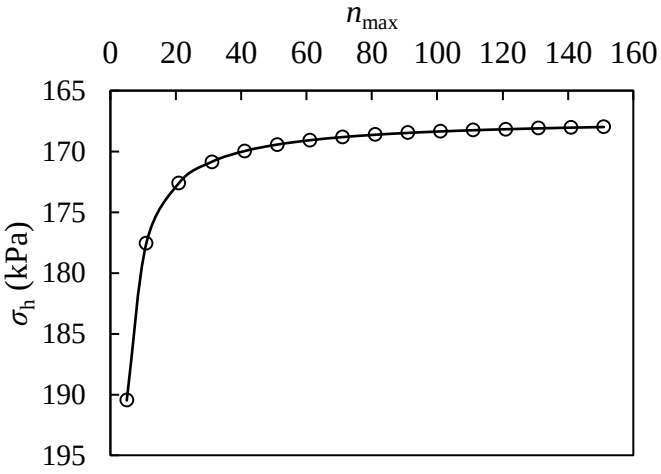

Figure 8-2: Variation of σ_h with the value of n_{max} obtained by calculations with the MATLAB program; calculated with H = 20 m, B = 4 m, m = 0.1 m/h, c_v = 5 m^2/h, γ_w = 10 kN/m^3, γ = 20 kN/m^3, ϕ' = 10° and $K = K_a$.

8.3 Validation of the analytical results by numerical results

In this section, the proposed pseudo-analytical solution will be validated by numerical results obtained by Plaxis2D (Brinkgreve et al. 2014).

Fig. 8-3(a) presents the physical model of an underground mine stope which is 4 m wide and 12.4 m high. The stope is continuously filled with a saturated backfill at a filling rate of m = 0.5 m/h to a final height of 12 m with a gap of 0.4 m being left between the stope roof and top surface of the backfill. In practice, a gap of 3 to 5 m high (the height of a drift) can be left to allow the passage of vehicles or workers. The backfill and rock walls are assumed to be elasto-plastic and obey the Mohr-Coulomb criterion.

The backfill is considered as cohesionless and has the properties of saturated unit weight γ = 20 kN/m^3, unit weight of water γ_w = 10 kN/m^3, drained Young's Modulus E' = 864 kPa, Poisson's

ratio μ= 0.2, drained constrained modulus M' = 960 kPa, effective friction angle ϕ' = 10° and effective dilation angle ψ' = 0°. The consolidation coefficient (c_v) can be calculated with the permeability (k) and drained constrained modulus (M') using the following equation:

$$c_v = \frac{k \cdot M'}{\gamma_w} \tag{8.31}$$

By considering $k = 4.2\times10^{-2}$ m/h (i.e. 1.2×10^{-5} m/s), one obtains $c_v = 4$ m^2/h.

The surrounding rock mass is assumed to be impermeable. Its geotechnical properties are unit weight γ_r = 27 kN/m^3, Poisson's ratio μ_r = 0.25, Young's modulus E_r = 42 GPa, cohesion c_r = 9.4 MPa, friction angle ϕ_r = 38°, and dilation angle ψ_r = 0°.

Fig. 8-3(b) presents the numerical model built by Plaxis2D, which shows only half of the full numerical model by considering the vertical symmetry plane (VSP). The VSP and the right outer boundary are restrained in the horizontal direction but can move freely in the vertical direction. The upper outer boundary of the model is free to move in the horizontal and vertical directions, while the lower outer boundary is restrained in all directions. The VSP and fill-wall interface are impermeable, while the top and bottom surfaces of the backfill after adding a new layer are permeable and imposed with zero PWP.

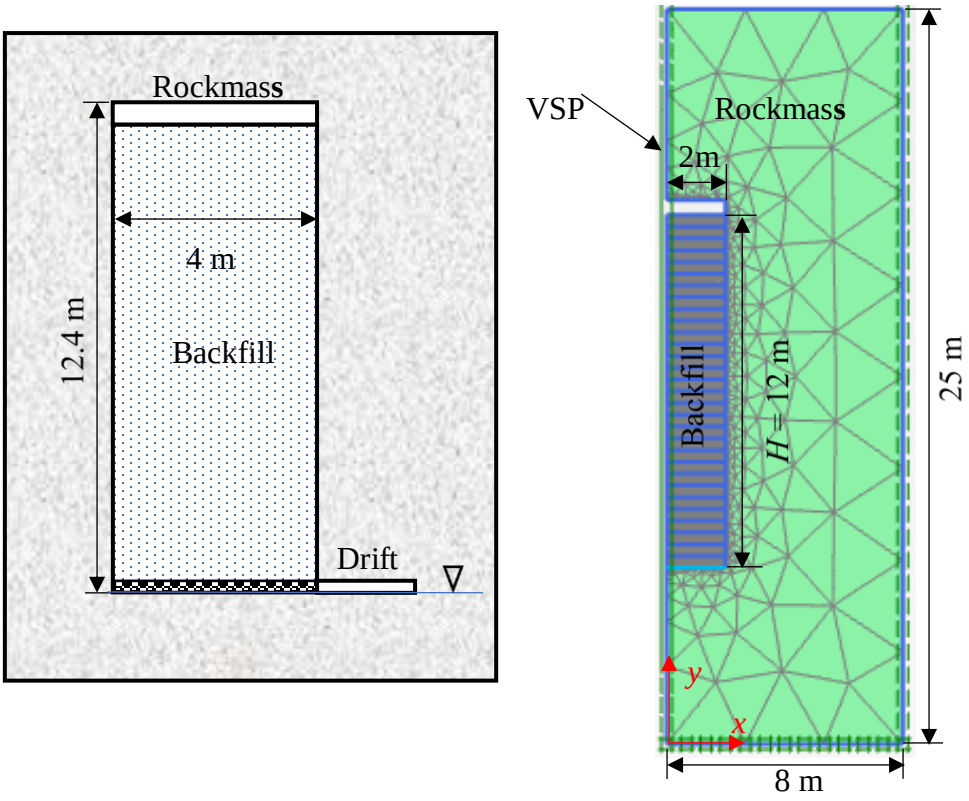

Figure 8-3: (a) The physical model and (b) numerical model of the backfilled stope built by Plaxis2D after considering the vertical symmetry plane (VSP).

The numerical modeling was conducted in three steps. The first step is to build the numerical model with rock mass and attain an initial stress state in it without any excavations. The stope is then excavated in the rock mass. The last step is to fill the stope in layers. In practice, the backfill is continuously filled in the underground mine stope with a gradual increase of thickness. In numerical model with Plaxis2D, this continuous and gradual increase of the backfill can only be approximately represented by instantaneously addition of a series of very thin backfill layers. If the backfill layer thickness is dh, the waiting delay before adding a new layer will be dh/dm. Drainage and consolidation take place during this waiting time. In order to well represent the continuous backfilling in a mine stope, the thickness of each layer dh should be as thin as possible. Therefore, the thickness of each layer should be as small as possible. Meanwhile, the calculation time increases exponentially as the layer thickness decrease and the number of layer increases. A compromise has been done between the accuracy and time calculation. In this paper, each layer has a thickness of 0.4 m. The waiting delay before adding a new layer is 0.8 h for a filling rate of 0.5

m/h. The sensitivity analysis (not shown) indicated that the thickness is indeed small enough to ensure numerically stable results, which has not been presented here.

Fig. 8-4 presents the distribution of the (excess) PWP [Fig. 8-4(a)], total [Fig. 8-4(b)], and effective [Fig. 8-4(c)] stresses along the vertical center line (VCL) of the stope at the end of backfill deposition, obtained by numerical simulation with Plaxis2D and calculated with the proposed solution [Eqs. (8.12), (8.28), (8.29) and (8.30)] using K_a. The (excess) PWP and total stresses based on the geostatic overburden solution ($p_w = \sigma_v = \sigma_h = \gamma h$) are also plotted on the figure. One sees that a good agreement is obtained between the analytical and numerical results.

Additional numerical simulations have been done. Good agreements were obtained again between the analytical and numerical results. These results are presented in the Ph.D. thesis of Zheng (2018). The proposed solution is thus considered to be validated by numerical modeling results. It can thus be applied to calculate the stresses and PWP in backfilled stopes during the accreting deposition.

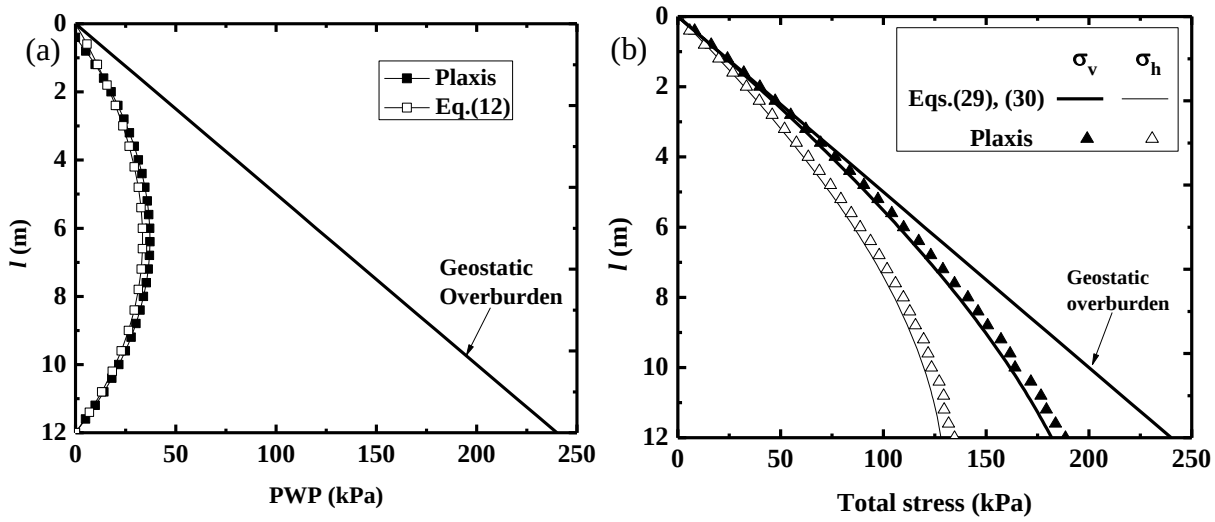

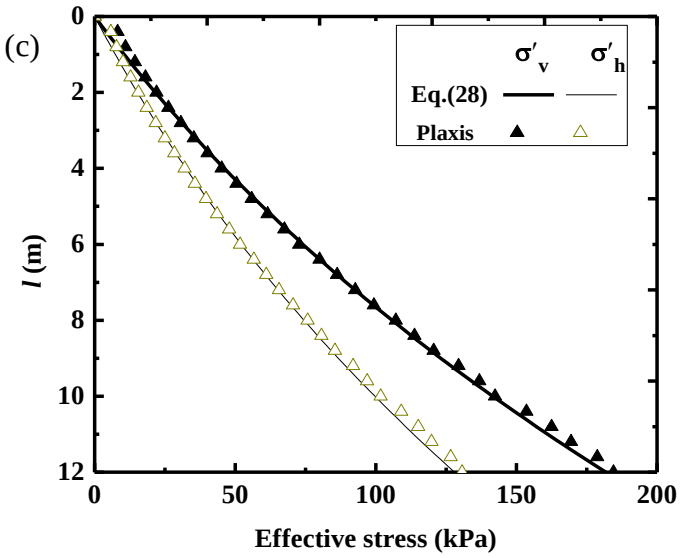

Figure 8-4 : Distribution of the (a) (excess) PWP, (b) total and (c) effective stresses along the VCL at the end of backfill deposition (at t = 24 h and h = H = 12 m), obtained by numerical modeling results performed with Plaxis2D and calculated using the proposed solution [Eqs. (8.12), (8.28), (8.29) and (8.30)] by considering K_a; calculations conducted with H = 12 m, B = 4 m, c_v = 4 m^2/h, m = 0.5 m/h, γ = 20 kN/m^3, γ_w = 10 kN/m^3, and ϕ' = 10°.

8.4 Sample applications

This section will use the proposed solution to investigate the influence of backfill properties, filling rate and stope geometry on the total and effective stresses in a backfilled stope at the end of backfill deposition. The slurried backfill having a saturated unit weight of γ = 20 kN/m^3 is filled to a final height of H = 40 m.

Fig. 8-5 presents the distribution of the total [Fig. 8-5(a)] and effective [Fig. 8-5(b)] stresses along the full height of the backfilled stope at the end of backfill deposition, predicted by the proposed solution when c_v increases from 0.1 to 10 m^2/h. The stope width B is taken as 6 m. The filling rate m is 0.2 m/h. The effective friction angle ϕ' is taken as 20°. The Rankine active earth pressure coefficient K_a is 0.49. Without any surprise, the results indicate that the value of c_v can significantly influence the effective and total stresses at the end of filling. With a very low value of c_v (= 0.1 m^2/h), the drainage and consolidation can be very slow, resulting in total stresses almost equal to the geostatic overburden pressure at the upper part of the backfill. When the consolidation coefficient is high (c_v = 10 m^2/h), significant drainage and consolidation take place during the

backfill accreting deposition, resulting in relative low total stresses and relative high effective stresses.

The similar results have been shown in previous publications, mostly through numerical modeling (e.g., Fahey et al. 2009; El Mkadmi et al. 2014). This is for the first time shown through pseudo-analytical solutions without numerical modeling.

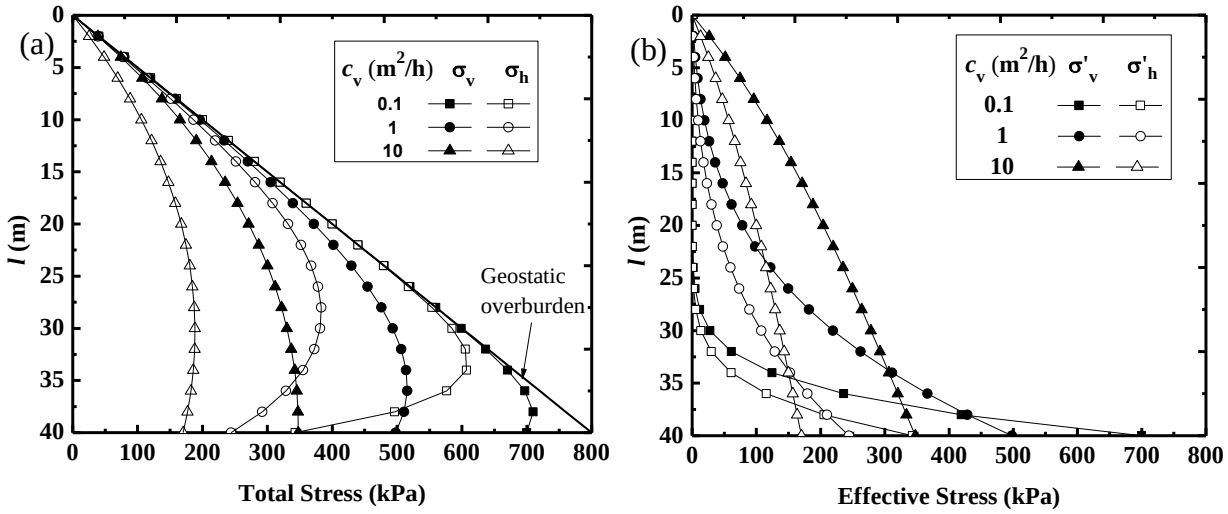

Figure 8-5: Distribution of the horizontal and vertical total (a) and effective (b) stresses with different consolidation coefficient c_v along the full height of the stope at the end of backfill accreting deposition, predicted by the proposed solution [Eqs. (8.28), (8.29) and (8.30)] by using: H = 40 m, B = 6 m, γ_w = 10 kN/m^3, γ = 20 kN/m^3, m = 0.2 m/h, ϕ' = 20°, and $K = K_a$.

Fig. 8-6 presents the distribution of the total [Fig. 8-6(a)] and effective [Fig. 8-6(b)] stresses along the full height of the backfilled stope when the deposition ceases as the filling rate m varies from 0.1 to 1 m/h, predicted by the proposed solution by considering a consolidation coefficient c_v = 5 m^2/h, an effective friction angle ϕ' = 20° and an earth pressure coefficient of $K = K_a$ = 0.49. One can see that high total stresses and low effective stresses result from high filling rate. Once again, these results are very similar to those shown in previous publications through numerical modeling (e.g., El Mkadmi et al. 2014). However, this is for the first time shown through pseudo-analytical solution.

Near the bottom of the backfill, abnormal high effective stress at high filling rate is observed. The same phenomenon has been observed in previous case with low consolidation coefficient [Fig. 8-5(b)]. When the filling rate is high or when the coefficient consolidation is low, the drainage and

consolidation become slow, resulting in high (excess) PWP, high total stresses and low effective stresses along the upper portion of the backfill. The high total stresses and low effective stresses in the upper portion mean that the high total stresses in the upper portion must be transferred to the backfill in the lower and bottom portion. This explains well the high total stresses along the full height of the stope with low consolidation coefficient [Fig. 8-5(a)] or high filling rate [Fig. 8-6(a)]. On the other hand, the (excess) PWP remains always zero at the bottom and very small near the bottom of the stope. The high total stresses near the bottom are thus assumed by high effective stresses.

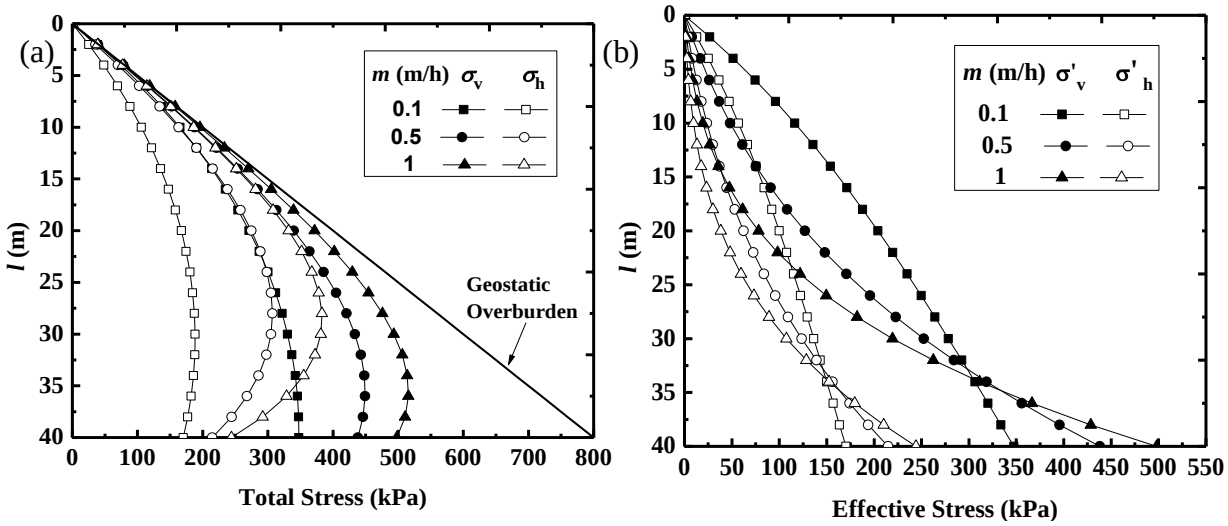

Figure 8-6: Distribution of the horizontal and vertical total (a) and effective (b) stresses with different filling rate m along the full height of the backfilled stope when the deposition ceases, predicted by the proposed solution [Eqs. (8.28), (8.29) and (8.30)] by considering H = 40 m, B = 6 m, c_v = 5 m^2/h, γ = 20 kN/m^3, γ_w = 10 kN/m^3, ϕ' = 20° and $K = K_a$.

Fig. 8-7 presents the distribution of the total [Fig. 8-7(a)] and effective [Fig. 8-7(b)] stresses along the full height of the backfilled stope at the end of filling with different effective friction angle of backfill ϕ', predicted by the proposed solution by using a consolidation coefficient of c_v = 5 m^2/h, a filling rate of m = 0.2 m/h, and an earth pressure coefficient of $K = K_a$. The geostatic overburden pressure is also included on the figure. The results show that the total and effective stresses decrease as the effective fiction angle increases. These results are straightforward because high effective friction angle of backfill leads to generation of high degree of arching effect and hence reduces effective and total stresses.

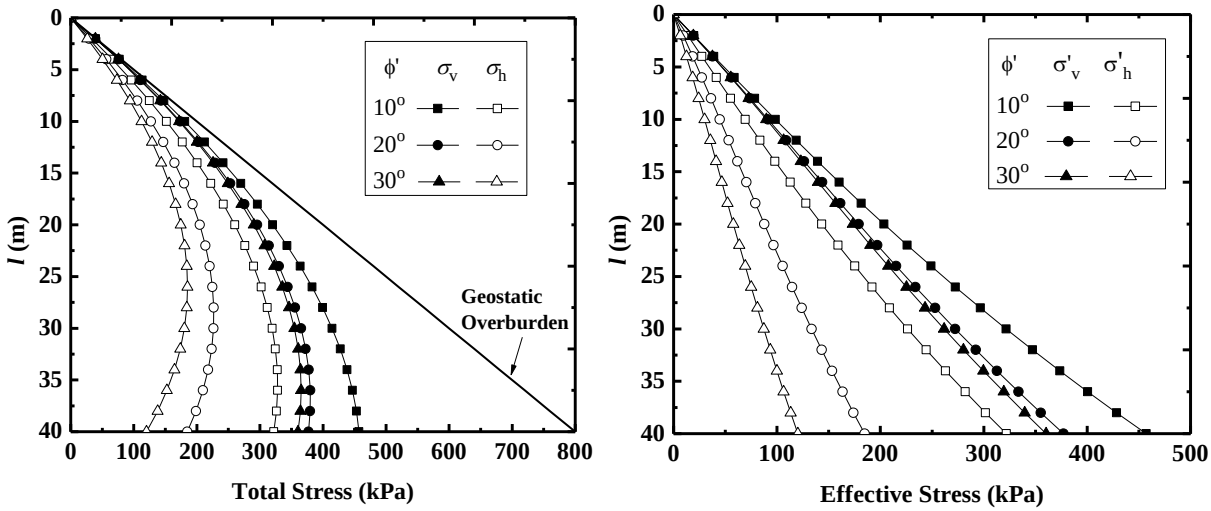

Figure 8-7: Distribution of the horizontal and vertical total (a) and effective (b) stresses with different effective friction angle ϕ' along the full height of the backfilled stope when the deposition ceases, predicted by the proposed solution [Eqs. (8.28), (8.29) and (8.30)] by using H = 40 m, B = 6 m, c_v = 5 m^2/h, m = 0.2 m/h, γ_w = 10 kN/m^3, γ = 20 kN/m^3 and $K = K_a$.

Fig. 8-8 presents the distribution of the total [Fig. 8-8(a)] and effective [Fig. 8-8(b)] stresses along the full height of the backfilled stope when the deposition ceases as stope width varies from 3 to 12 m, predicted by the proposed solution by considering a consolidation coefficient c_v = 5 m^2/h, a filling rate m = 0.2 m/h, an effective friction angle ϕ' = 20° and an earth pressure coefficient $K = K_a$ = 0.49. The results show that high total and effective stresses are generated with increased stope width. This is because the degree of arching effect decreases as the stope width increases, resulting in high effective and total stresses.

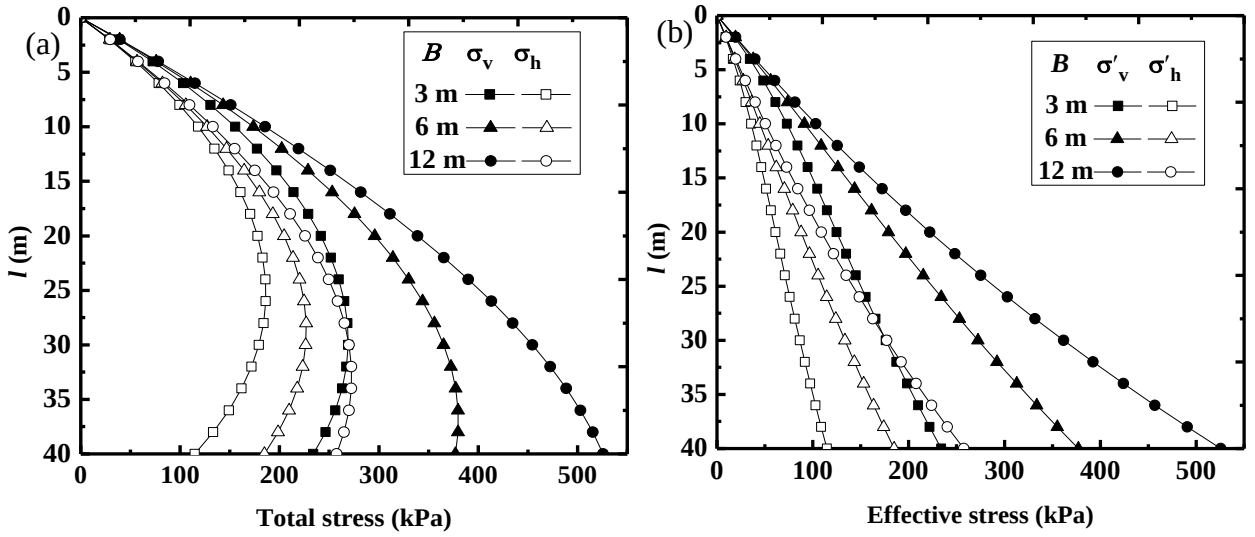

Figure 8-8: Distribution of the horizontal and vertical total (a) and effective (b) stresses along the full height of the backfilled stope with different stope widths when the filling operation ceases, predicted by the proposed solution [Eqs. (8.28), (8.29) and (8.30)] by considering H = 40 m, m = 0.2 m/h, c_v = 5 m^2/h, γ = 20 kN/m^3, γ_w = 10 kN/m^3, ϕ' = 20°, and $K = K_a$.

8.5 Discussion

This paper proposed a new pseudo-analytical solution to calculate the (excess) PWP as well as the total and effective stresses in a backfilled stope by considering the occurrence of self-weight consolidation and arching effect during the placement of the backfill. The proposed solution has been validated by numerical simulation results obtained by Plaxis2D. It thus provides a useful tool to evaluate the pressure and stresses in backfilled stopes. However, one should be reminded that the proposed solution presented in this paper contains some limitations due to the assumptions used in the development process. For instance, the (excess) PWP were evaluated first using the Gibson (1958) model without considering arching effect. In reality, the arching effect tends to hold the backfill in the original place and slowdown the consolidation. A slower consolidating may disfavor the arching development. A coupled phenomenon takes place between the consolidation and arching development. An equilibrium state can be reached after a number of iterations between the two processes. More work is required to consider the coupled processes in the future work.

Another limitation is related to the application of Gibson (1958) model, which considers one-dimensional consolidation model under small strain with constant physical, mechanical and

hydraulic properties. The one-dimensional model can be representative for tailing dams with large horizontal section. However, lateral drainage can take place in tailings dams when the waste rock inclusion is applied, or in mine stopes when the stope rock walls contain conductive fractures and joints.

Finally, experimental work is required to validate or calibrate the proposed solutions. This work is ongoing and will be part of future publications.

8.6 Conclusions

In this paper, a new pseudo-analytical solution is presented to evaluate the PWP as well as the effective and total stresses in backfilled stopes by considering the self-weight consolidation and arching effect during the placement of slurried backfill on a pervious base. The proposed solution has been validated against numerical results obtained by Plaxis2D. As the equations of the proposed solution can either be solved by MATLAB or Microsoft Excel, the proposed solution constitutes a simple and useful tool to calculate the pressures and stresses in backfilled stopes for the design of barricades. Sample applications with the proposed solution show that high total stresses along the full height of backfilled stopes can result from low consolidation coefficient, high filling rate, low effective friction angle or large stope width. Similar results have been reported in previous publications through numerical modeling. This is however for the first time shown through pseudo-analytical solutions without numerical modeling. The proposed solution can be particularly useful for parametric sensitivity analysis in the preliminary stage of barricade design.

Acknowledgements

The research received the financial support from NSERC (Natural Sciences and Engineering Research Council of Canada), FRQNT (Fonds de recherche du Québec—Nature et Technologies) and also the industrial partners of the Research Institute on Mines and the Environment (RIME UQAT-Polytechnique; http://rime-irme.ca/). The authors gratefully acknowledge for the support.

8.7 Appendix I: MATLAB program to solve Eq. (8.30)

A MTALAB program is developed to solve Eq. (8.30) for assessing the horizontal total stress along the full height of a stope at the end of backfill deposition. Sample calculation is conducted here by

considering: H = 20 m, B = 4 m, m = 0.1 m/h, γ_w = 10 kN/m^3, γ = 20 kN/m^3, c_v = 5 m^2/h, ϕ' = 10° and $K = K_a$.

```
%=========================================================================%
% Stresses estimation in backfilled stopes during the filling operation on a
pervious base %
%=========================================================================%


nmax= 101; % number of division of H (here n_max = 101);
time = 200; % time of filling (here t = 200 h);
m = 0.1; % filling rate during the filling operation (here m = 0.1 m/h);
H = m*time; % final thickness of the backfill (here H = 20 m);
c_v = 5; % consolidation coefficient of the backfill (here c_v = 5 m^2/h);
h_0 = 0.5; % step interval of x (x = 0 at the bottom, see Fig. 1);
gama = 20; % saturated unit weight of the backfill (here γ = 20 kN/m^3);
gama_w = 10; % unit weight of water (here γ_w = 10 kN/m^3);
gama_sub = gama-gama_w; submerged unit weight of the backfill;
B = 4; % stope width (here B = 4 m)
Phi = 10; % effective internal friction angle of the backfill (here φ' = 10°)
K_a = (1-sind(Phi))/(1+sind(Phi)); % Rankine active earth pressure coefficient
of the backfill (used in this sample calculation);
K_0 = 1-sind(Phi); %Jaky at-rest earth pressure coefficient (not used in this
sample calculation);
A = 2*K_a*tand(Phi)/B;


% calculate the PWP, pw, in Eq. (8.12)
for i = 1:nmax
    l(i)= H/(nmax-1)*(i-1);
    x(i)= H-l(i);
    pw(i) = 0.0;
    for jloop = -55:55
        temp1 = m*jloop*h_0*sqrt(time)/sqrt(c_v);
        temp2 = x(i)*jloop*h_0/sqrt(c_v*time);
        a = exp(-(jloop*h_0)^2)*coth(temp1)*sinh(temp2);
        if (jloop == 0)
            a=0.0;
        else
        end
```

```
        pw(i) = pw(i)+h_0/2.0*8.*sqrt((c_v*time)^3)*(jloop*h_0)^2*a;
    end
    pre_multi = gama*m/2./c_v/sqrt(pi*c_v*time)*exp(-x(i)*x(i)/4./c_v/time);
    pw(i)=((-gama*x(i)*(1+m*x(i)/2./c_v)+pre_multi*pw(i)));
end

%calculate the dpw/dx of Eq. (8.14)
for i = 1:nmax;
    l(i) = H/(nmax-1)*(i-1);
    x(i) = H-l(i);
    derive_pw(i) = 0.0;
    for j = -55:55;
        temp1 = m*j*h_0*sqrt(time)/sqrt(c_v);
        temp2 = x(i)*j*h_0/sqrt(c_v*time);
        temp3 = j*h_0/sqrt(c_v*time);
        temp4 = -x(i)/2./c_v/time;
        a = exp(-(j*h_0)^2)*coth(temp1)*sinh(temp2);
        b = exp(-(j*h_0)^2)*coth(temp1)*cosh(temp2)*(j*h_0/sqrt(c_v*time));
        if (j == 0)
            a=0.0;
            b=0.0;
        else
        end
        derive_pw(i)=
derive_pw(i)+temp4*h_0/2.*8.*sqrt((c_v*time)^3)*(j*h_0)^2*a+h_0/2.*8*sqrt((c_v
*time)^3)*(j*h_0)^2*b;
    end
    pre_multi = gama*m/2./c_v/sqrt(pi*c_v*time)*exp(-x(i)*x(i)/4./c_v/time);
    derive_pw(i)=(-gama-m*gama*x(i)/c_v)+pre_multi*derive_pw(i);
end

% calculate the horizontal total stress of Eq.(8.30)
for i = 1:nmax
    l(i) = H/(nmax-1)*(i-1);
    sigma_sub(i)=0.0;
    n_y = i;
    for k = 1:n_y
        delta_y = l(i)/(n_y);
```

```
        sigma_sub(i) =
sigma_sub(i)+(gama+derive_pw(k))*exp(A*(k*delta_y))*delta_y;
    end
    sigma_sub(i) = exp(-A*l(i))*sigma_sub(i);
    sigma_H(i)= K_a*sigma_sub(i)+ pw(i);
end

% results output and saved in the file "output filename.txt"
fid = fopen(Output filename. txt','w')
for i=1:nmax
    fprintf(fid,'%g %g\r\n',l(i),sigma_H(i))
end
fclose(fid)

plot(sigma_H,l,'-.');
set(gca,'Ydir','reverse');
```

8.8 References

Aubertin, M., Bussiere, B., & Bernier, L. (2002). *Environnement et gestion des rejets miniers. Presses* [Manual on CD-ROM]. Internationales Polytechnique, Montréal, Canada.

Aubertin, M., Li, L., Arnoldi, S., Belem, T., Bussière, B., Benzaazoua, M., & Simon, R. (2003). *Interaction between backfill and rock mass in narrow stopes*. Paper presented at the Soil and Rock America 2003, Essen, Germany (pp, 1157–1164).

Brinkgreve, R.B.J., Kumarswamy, S., & Swolfs, W.M. (2014). PLAXIS (2014) [Computer software]. Delft, Netherlands.

Cui, L., & Fall, M. (2008). Mathematical modelling of cemented tailings backfill: a review. *International Journal of Mining, Reclamation and Environment*, 1-20.

Cui, L., & Fall, M. (2017). Modeling of pressure on retaining structures for underground fill mass. *Tunnelling and Underground Space Technology*, *69*, 94-107.

El Mkadmi, N., Aubertin, M., & Li, L. (2014). Effect of drainage and sequential filling on the behavior of backfill in mine stopes. *Canadian Geotechnical Journal, 51*(1), 1–15.

Fahey, M., Helinski, M., & Fourie, A. (2010). Consolidation in accreting sediments: Gibson's solution applied to backfilling of mine stopes. *Géotechnique, 60*(11), 877-882.

Fahey, M., Helinski, M., & Fourie, A. (2009). Some aspects of the mechanics of arching in backfilled stopes. *Canadian Geotechnical Journal, 46*(11), 1322-1336.

Gibson, R.E. (1958). The progress of consolidation in a clay layer increasing in thickness with time. *Géotechnique, 8*(4), 171-182.

Gibson, R.E., Schiffman, R.L., & Whitman, R.V. (1989). On two definitions of excess pore water pressure. *Geotechnique, 39*(1), 169-171.

Goodwin, E.T. (1949). *The evaluation of integrals of the form* $\int_{-\infty}^{+\infty} f(x)e^{-x^2}\,dx$. Paper presented at the Mathematical Proceedings of the Cambridge Philosophical Society. Cambridge University, London, UK (pp. 241-245).

Hassani, F., & Archibald, J. (1998). Mine backfill. (CD-ROM). Canadian Institute of Mining, Metallurgy and Petroleum, Montréal, Canada.

Jahanbakhshzadeh, A., Aubertin, M., & Li, L. (2017). A new analytical solution for the stress state in inclined backfilled mine stopes. *Geotechnical and Geological Engineering, 35*(3), 1151-1167.

Jahanbakhshzadeh, A., Aubertin, M., & Li, L. (2018a). Analysis of the stress distribution in inclined backfilled stopes using closed-form solutions and numerical simulations. *Geotechnical and Geological Engineering, 36*(2), 1011-1036.

Jahanbakhshzadeh, A., Aubertin, M., & Li, L. (2018b). Three-dimensional stress state in inclined backfilled stopes obtained from numerical simulations and new closed-form solution. *Canadian Geotechnical Journal, 55*(6), 810-828.

Jung, S.J., & Biswas, K. (2002). Review of current high density paste fill and its technology. *Minerral Resources Engineering, 11*(2), 165–182.

Komurlu, E., & Kesimal, A. (2015). Sulfide-rich mine tailings usage for short-term support purposes: An experimental study on paste backfill barricades. *Geomechanics and Engineering, 9*(2), 195-205.

Li, L., Alvarez, I.C., & Aubertin, J.D. (2013). Self-weight consolidation of a slurried deposition: tests and interpretation. *International Journal of Geotechnical Engineering, 7*(2), 205–213.

Li L and Aubertin M. (2009a) Influence of water pressure on the stress state in stopes with cohesionless backfill. *Geotechnical and Geological Engineering, 27*(1), 1–11.

Li, L., & Aubertin, M. (2009b). A three-dimensional analysis of the total and effective stresses in submerged backfilled stopes. *Geotechnical and Geological Engineering, 27*(4), 559–569.

Li, L., & Aubertin, M. (2010). An analytical solution for the nonlinear distribution of effective and total stresses in vertical backfilled stopes. *Geomechanics and Geoengineering, 5*(4), 237-245.

Li, L., & Aubertin, M. (2008). An improved analytical solution to estimate the stress state in subvertical backfilled stopes. *Canadian Geotechnical Journal, 45*(10), 1487-1496.

Li, L., & Aubertin, M. (2009c) Horizontal pressure on barricades for backfilled stopes: Part I: Fully drained conditions. *Canadian Geotechnical Journal, 46*(1), 37–46.

Li, L., & Aubertin, M. (2009d). Horizontal pressure on barricades for backfilled stopes: Part II: Submerged conditions. *Canadian Geotechnical Journal, 46*(1), 47–56.

Li, L., & Aubertin, M. (2011). Limit equilibrium analysis for the design of backfilled stope barricades made of waste rock. *Canadian Geotechnical Journal, 48*(11), 1713-1728.

Li, L., Aubertin, M., & Belem, T. (2005). Formulation of a three dimensional analytical solution to evaluate stress in backfilled vertical narrow openings. *Canadian Geotechnical Journal, 42*(6), 1705–1717 (with Erratum 2006, 43(3), 338–339).

Li., L, Aubertin, M., Simon, R., Bussière, B., & Belem, T. (2003). *Modeling arching effects in narrow backfilled stopes with FLAC*. Paper presented at the 3rd International FLAC Symposium, A. A. Balkema, Rotterdam, Netherlands. (pp. 211–219).

Ning, J., Wang, J., Tan, Y., Zhang, L., & Bu, T. (2017). In situ investigations into mining-induced overburden failures in close multiple-seam longwall mining: a case study. *Geomechanics and Engineering, 12*(4), 657-673.

Park, J., Chun, Y.W., Trung, H.T., & Kim, Y.U. (2014). Effect of ultrasonic energy on self-weight consolidation of clay minerals. *KSCE Journal of Civil Engineering, 18*(4), 971-974.

Pedroni, L. (2011). Étude expérimentale et numérique de la sédimentation et de la consolidation des boues de traitement des eaux acides. (Doctoral dissertation, École Polytechnique de Montréal, Montréal, Canada).

Pirapakaran, K., & Sivakugan, N. (2007a). A laboratory model to study arching within a hydraulic fill stope. *Geotechnical Testing Journal, 30*(6), 496–503.

Pirapakaran, K., & Sivakugan, N. (2007b). Arching within hydraulic fill stopes. *Geotechnical and Geological Engineering, 25*(1), 25-35.

Revell, M.B., & Sainsbury, D.P. (2007). *Paste bulkhead failures*. Paper presented at the 9th International Symposium on Mining with Backfill (Minefill'07), Montréal, Canada.

Shahsavari, M., & Grabinsky, M. (2014). *Cemented paste backfill consolidation with deposition-dependent boundary conditions*. Paper presented at the 67th Canadian Geotechnical Conference, Canadian Geotechnical Society, Regina, Saskatchewan, Canada.

Shahsavari, M., & Grabinsky, M. (2015). *Mine backfill porewater pressure dissipation: numerical predictions and field measurements*. Paper presented at the 68th Canadian Geotechnical Conference, Canadian Geotechnical Society, Québec City, Canada (pp. 1-8).

Simms, P., Grabinsky, M., & Zhan, G.S. (2007). Modelling evaporation of paste tailings from the Bulyanhulu mine. *Canadian Geotechnical Journal, 44*(12), 1417–1432.

Sivakugan, N., Rankine, K., Lovisa, J., & Hall, W. (2013). Flow rate computations in hydraulic fill mine stopes. *Indian Geotechnical Journal, 43*(3), 195-202.

Sivakugan, N., Rankine, K., & Rankine, R. (2006a). Permeability of hydraulic fills and barricade bricks. *Geotechnical and Geological Engineering, 24*(3), 661-673.

Sivakugan, N., Rankine, R.M., Rankine, K.J., & Rankine, K.S. (2006b). Geotechnical considerations in mine backfilling in Australia. *Journal of Cleaner Production, 14*(12), 1168-1175.

Sobhi, M.A., Li, L., & Aubertin, M. (2017). Numerical investigation of earth pressure coefficient along central line of backfilled stopes. *Canadian Geotechnical Journal, 54*(1), 138-145.

Thompson, B.D., Bawden, W.F., & Grabinsky, M.W. (2012). In situ measurements of cemented paste backfill at the Cayeli Mine. *Canadian Geotechnical Journal, 49*(7), 755-772.

Ting, C.H., Shukla, S.K., & Sivakugan, N. (2011). Arching in soils applied to inclined mine stopes. *International Journal of Geomechanics, 11*(1), 29–35.

Ting, C.H., Sivakugan, N., & Shukla, S.K. (2012). Laboratory simulation of the stresses within inclined stopes. *Geotechnical Testing Journal, 35*(2), 280-294.

Walske, M.L., & Doherty, J. (2017). Incorporating chemical shrinkage volume into Gibson's solution. *Canadian Geotechnical Journal, 55*(6), 903-908.

Wood, D.M., Doherty, J.P., & Walske, M.L. (2016). Deposition and self-weight consolidation of a shrinking fill. *Géotechnical Letter, 6*(1), 72-76.

Yang, P.Y., Li, L., & Aubertin, M. (2017). Stress ratios in entire mine stopes with cohesionless backfill: A numerical study. *Minerals, 7*(10), 201.

Yang, P.Y., Li, L., & Aubertin, M. (2018). Theoretical and numerical analyses of earth pressure coefficient along the centerline of vertical openings with granular fills. *Applied Science, 8*(10), 1721.

Yang, P.Y., Li, L., Aubertin, M., & Brochu-Baekelmans, M. (2017). Stability analyses of waste rock barricades designed to retain paste backfill. *International Journal of Geomechanics, 17*(3), 04016079.

Yumlu, M., & Guresci, M. (2007). *Paste backfill bulkhead monitoring-A case study from Inmet's Cayeli mine*. Paper presented at the 9th International Symposium in Mining with Backfill (CD-ROM), Canadian Institute of Mining, Metallurgy and Petroleum, Montréal, Canada.

Zhang, N., Zhu, W., He, H.T., Lv, Y.Y., & Wang, S.W. (2017). Experimental study on settling velocity of soil particles in dredged slurry. *Marine Georesources & Geotechnology, 35*(6), 747-757.

Zheng, J., Li, L., Mbonimpa, M., & Pabst, T. (2018a). An analytical solution of Gibson's model for estimating the pore water pressures in accreting deposition of slurried material under one-dimensional self-weight consolidation. Part I: Pervious base. *Indian Geotechnical Journal, 48*(1), 72-83.

Zheng, J., Li, L., Mbonimpa, M., & Pabst, T. (2018b). An analytical solution of Gibson's model for estimating pore water pressures in accreting deposition of slurried material under one-dimensional self-weight consolidation. Part II: Impervious base. *Indian Geotechnical Journal, 48*(1), 188-195.

CHAPTER 9 ARTICLE 7: VARIATION OF THE "SHORT-TERM" PRESSURES OF PASTE BACKFILL AS A FUNCTION OF THE SOLID CONTENT

Jian Zheng; Li Li

Article submitted to Canadian Geotechnical Journal in November 2018.

Abstract: Paste backfill is increasingly used in underground mines to fill the stopes (mined-out voids). A critical concern is to estimate the pressures during or shortly after the placement of the paste fill exerted on the barricade constructed to retain the backfill in place. Several in situ measurements conducted in mine stopes showed that the backfill pressures shortly after the placement can be as high as the iso-geostatic pressure due to the absence of cementation and effective stresses. These results along with the numerous cases of barricade failure reported in the literature do not correspond to the recommendations given in the handbooks, which suggest slight construction of barricade for paste backfill. In this paper, a short review is first given on the definition of paste backfill. It will be seen that an important difference exists between the strictly defined paste backfill and the paste backfill commonly used in the practice. To meet the criteria of paste backfill defined in the handbooks, the paste backfill should have a very high solid content and probably be unsaturated while the paste backfill used in the practice contains much more water to ensure enough flowability so that the backfill behaves like a fluid. This explains the low pressure and slight construction of barricade in the handbooks and high pressure with the fluid-like paste backfill. These results indicate that the pressure should be dependent on the water or solid content of paste backfill. This is however never be analyzed in the past. In this paper, the results of a series of laboratory tests will be presented on the measurement of the "short-term" vertical total stress at a column center and near the wall with a paste backfill having different solid contents. The results show that the vertical total stresses near the wall and at the center decrease as the solid content of the backfill increases and the vertical total stress near the wall is always lower than that at the center. When the backfill has high solid content, the vertical total stress near the wall can be very low. As suggested in the handbook, a slight construction of barricade is indeed enough. Conversely,

with low solid content backfill, the vertical total stress at the stope wall can be high. A design and construction of adequately strong barricade is necessary.

Keywords: paste backfill; barricade; analytical solution; ratio of vertical total stress; yield stress; column tests

9.1 Introduction

Paste backfill made of full tailings (i.e. the tailings without any elimination of fine particles) is widely used in underground mines around the world. Compared to hydraulic fill, which needs to remove a part of the fine particles, paste backfill allows the mining industry to maximize the reuse of mine tailings and minimize the surface disposal of mine wastes, resulting in a better conservation of the environment (Aubertin et al. 2002; Benzaazoua et al. 2008). In addition, with the feature of non-segregation, paste backfill can be transported by pipes without any critical velocity (to avoid the problem of segregation like hydraulic fill). The slow velocity and the lubricant layer formed by the fine particles during the transportation can help to significantly reduce the pipe wear (Potvin et al. 2005). When binder is added, the utilization of paste backfill can allow increased ore recovery, reduced ore dilution and improved ground stability.

To use the paste backfill or other pulp backfills, one usually needs to construct a barricade (a confining structure) at the base of the stope near the draw-points (from where the blasted ore was withdrawn) to retain the backfill in place. A critical concern is to have a good estimation of the stresses in the backfilled stope and on the barricade.

Over the years, extensive studies have been conducted to investigate the stresses in backfilled stopes by considering arching effect (Askew et al. 1978; Knutsson 1981; Aubertin 1999; Aubertin et al. 2003; Li et al. 2003, 2005; Pirapakaran and Sivakugan 2007a, 2007b; Li and Aubertin 2008, 2009a, 2009b, 2010, 2009c, 2009d; Ting et al. 2010, 2012). These solutions constitute important tools to evaluate the stresses in dry and wet backfill or when the water in the saturated backfill is in a static equilibrium state. They can thus be used to estimate the stresses in stopes backfilled with dry, wet or very permeable backfill, like rock fill or hydraulic backfill.

For low permeability slurry like paste backfill (with the value of k in the range of 10^{-8} to 10^{-6} m/s), a dilemma exists. On one hand, the few handbooks on mine backfilling stipulates that the pressures on barricade exercised by paste backfill can be very small. Thus, the construction of light barricade

is enough (Hassani and Archibald 1998; Potvin et al. 2005). This point of view is mainly supported by the small amount of free water due to the drainage. The pressure can be further reduced if the hydration or desiccation of the cemented backfill is considered. On the other hand, a number of barricade failures have been reported in the literature, mostly involving serious consequences, such as the flooding of lower level working spaces, damage and trapping of equipment, personnel injury and even fatality (Bloss and Chen 1998; Grice 1998, 2001; Kuganathan 2001, 2002; Helinski et al. 2006; Sivakugan et al. 2006a, 2006b, 2013; Revell 2007; Yumlu and Guresci 2007; Hughes 2008). In addition, the in situ measurements performed by Thompson et al. (2012) showed that the effective stresses and arching effect are absent and the total stresses and PWP are as high as the iso-geostatic overburden pressure during the placement of slurried backfill in mine stopes. All these tend to indicate that the design of the barricade should be done properly. This requires a good understanding of the hydro-mechanical behavior of the paste backfill poured in mine stopes, especially during and shortly after the placement of the slurried backfill.

When a slurried backfill is poured in a mine stope, the fill particles tend to settle down upon the effect of the gravity and become closer to each other and denser. The pore water tends to be expelled out of the backfill. As the paste backfill has a low permeability (10^{-8} m/s < k < 10^{-6} m/s), the water drainage is limited, leading to the generation of excess pore water pressure (PWP), which can be dissipated with time. When the backfill is largely over-saturated, the dissipation of the excess PWP occurs without generation of effective stresses. This process is called sedimentation (Ahmed and Siddiqua 2014). The backfill pressure in this stage can be very high and equals to the iso-geostatic overburden pressure. When the dissipation of excess PWP reaches enough degree, tight grain-grain contact occurs with the generation and development of effective stresses. The dissipation of excess PWP is called self-weight consolidating (Gibson 1958; Been and Sills 1981; Fox 2000; Pedroni 2011; Li et al. 2013; Zheng et al. 2018a, 2018b). The theory of sedimentation and consolidation indicates that the pressure on barricades during and shortly after the placement of the slurried backfill can be as high as the iso-geostatic overburden pressure (Thompson et al. 2012; Shahsavari and Grabinsky 2014). This however does not correspond to the recommendations for the design of paste backfill barricades given in the handbooks (Hassani and Archibald 1998; Potvin et al. 2005).

In this paper, the contradiction between the field pressure measurement and barricade design recommendation will first be analyzed. A series of laboratory tests were conducted to investigate

the “short-term” vertical total stresses at the center and near the wall of a column backfilled with different solid content of tailings. The obtained vertical total stresses ratio at these two places are also compared with that predicted by the previous analytical solution. A good agreement is obtained.

9.2 Paste backfill and its pressure shortly after its placement in backfilled stopes

Although paste backfill has been used for more than thirty years, its definition is not yet unanimously accepted. Aref et al. (1992) defined that paste backfill should contain fine particles ($\leq$ 45 μm) less than 15% by weight. According to Hassani and Archibald (1998), a paste backfill should contain at least 15% of fine particles smaller than 45 μm. In Potvin et al. (2005), five criteria have been specified to define a paste backfill. Among the five criteria, the first one requires the backfill to contain at least 15% of fine particles smaller than 20 μm and the second one requires the backfill not to bleed of water not only upon its placement but also after a prolonged period of deposition. In our opinion, a backfill satisfying this last criterion is only possible when the fill is unsaturated or very slightly saturated; otherwise, bleeding certainly occurs more or less due to the drainage and self-weight consolidation.

Fig. 9-1 shows a backfill meeting the criteria of paste backfill. One sees that it is very viscous. Upon placement, a pile can form with a cone on the top. When such type of paste backfill is placed in a mine stope, the backfill pressure on lateral walls, including barricades, can indeed be small especially when the stope is very large or when the barricade is built far away from the stope (even nil if the barricade is far enough from the stope so that the paste backfill cannot touch the barricade). This explains well the recommendation of slight construction of barricades for paste backfill given in the handbooks (Hassani and Archibald 1998; Potvin et al. 2005). This kind of paste backfill can be interesting for surface disposal of tailings in the arid or semi-arid regions where water shortage and water recovery from mill tailings are critical concern (Simms et al. 2007). However, it is not suitable for filling underground mine stopes. The high viscosity (low flowability) of such paste backfill requires not only heavy pumps and energy-consuming to transport it from the surface backfill plant to underground stopes, but also renders difficult to fully fill wide stopes or to ensure tight contact between the backfill and stope roof. Subsequently, sufficient water has to be added in

the paste backfill to ensure a good flowability to facilitate the transportation and to ensure tight contact between the backfill and wide or long stope roof.

Figure 9-1: Solid-like high viscosity paste backfill (taken from Minewiki 2017)

Fig. 9-2(a) shows a typical paste backfill used in underground mines. It is seen that the backfill looks like a liquid. The almost horizontal surface of the backfill along the stope length indicates that the shear strength can be absent or very low. The arching effect and cementation shortly after the placement of the backfill can be absent, as confirmed by field measurements (Thompson et al. 2012), who showed that the vertical (σ_v) and horizontal (σ_h) total stresses and PWP (u_w) are equal to the iso-geostatic overburden pressure (i.e., $\sigma_h = \sigma_v = u_w = \gamma h$; where γ is the unit weight of saturated backfill, h is the backfill height) over the initial period of filling. Thus, the backfill pressure acted on the barricade can be very high. A slight construction of barricade recommended by the handbooks (Hassani and Archibald 1998; Potvin et al. 2005) may not be suitable. However, it should be noted that this type of backfill respects the criterion of paste backfill in terms of particle size distribution but not that in terms of water bleeding as shown in Fig. 9-2(b) with the draining water at the base. It should be noted also that the amount of draining water is not a reliable indicator of pressure due to the low permeability of the paste backfill (Li et al. 2013).

(a)  (b) 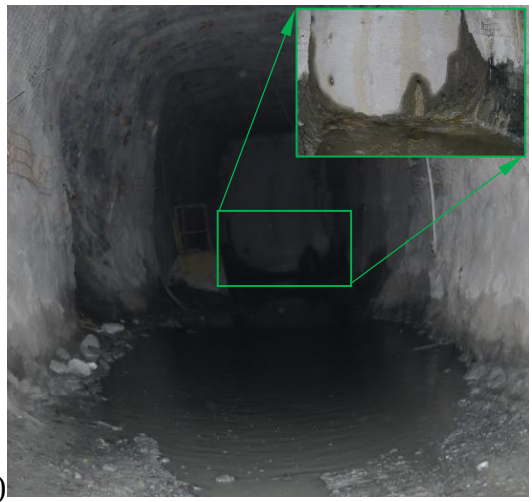

Figure 9-2: (a) A mine stope being filled with a fluid-like paste backfill; (b) A barricade with draining water at the base

This short review shows that there is a difference between the paste backfill defined in the handbooks and that used in practice, where the criterion of paste backfill in terms of fine particles is observed while that in terms of water bleeding is neglected. Fig. 9-3 shows typical grain size distribution curves of hard rock mine tailings in Québec, Canada. It is seen that the percentage of the particles smaller than 20 µm varies between 40 to 65%. The criterion of paste backfill in terms of fine particles is met for all of the mine tailings. Subsequently, a general tendency in practice is to call all backfill made of full tailings as paste backfill.

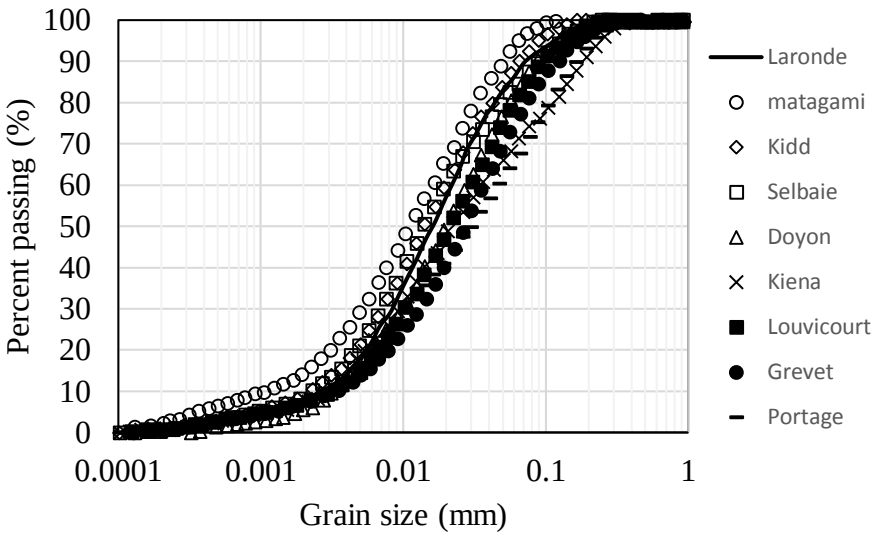

Figure 9-3: Typical grain size distribution curve of hard rock mine tailings (taken from Bussière 2007)

9.3 Laboratory tests

In the previous section, it has been shown that the paste backfill pressure shortly after the deposition in a stope can be very low when the paste backfill is very thick or very high when the paste backfill is very thin. This indicates that the backfill pressure depends on the water content (usually expressed by solid content) of the paste backfill. When the water content is very low, the paste backfill may have a solid-like behavior and the backfill pressure can be very low. When the water content is very high, the paste backfill will have a fluid-like behavior and the backfill pressure can be as high as the iso-geostatic overburden pressure. The question is what will be the behavior of the paste backfill when the water (or solid) content is intermediate between the two extreme cases.

To reply to this question, laboratory tests have been done to evaluate the "short-term" vertical total stresses in a paste backfilled stope (simulated by a column). The water (or solid) content has been taken into account through the yield stress of the backfill, which is defined as the minimum required shear stress to mobilize a Bingham fluid.

9.3.1 Testing material

The uncemented paste backfill tested in this study is made of tailings taken from a mine in Québec, Canada. The specific gravity (or relative density) is measured as D_r = 2.71. The grain size distribution curve of the tailings is shown in Fig. 9-4 with D_{60} = 0.048 mm, D_{10} = 0.003 mm and C_u = 16. The tailings contain 78% of particles smaller than 80 μm and 40% of particles smaller than 20 μm. The criterion of paste backfill in terms of fine particles is met (Potvin et al. 2005).

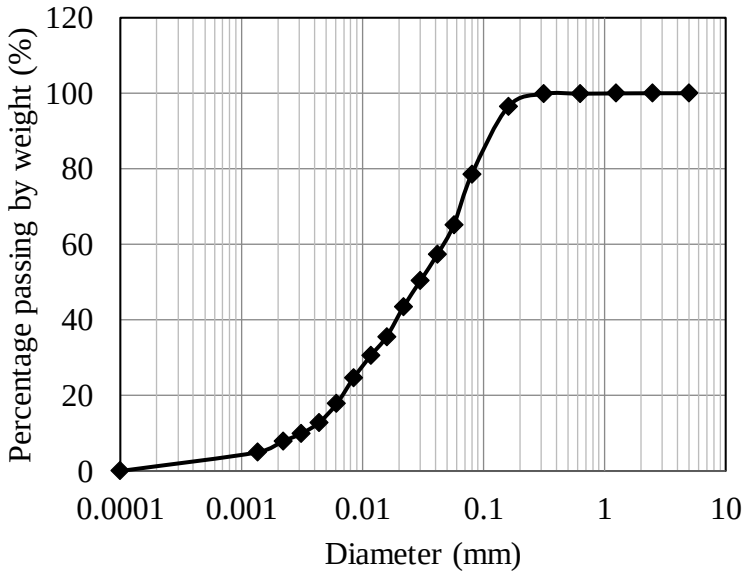

Figure 9-4: Grain size distribution curve of the tested mine tailings.

To prepare the paste backfill, a portion of dried tailings was put into a bucket. Water is added and mixing with the tailings until to a targeted solid content (water content). In this study, the solid content C_w of the tested paste backfill is in the range of 75.5 to 78.4% with the backfill density ranging between 1.877 and 1.945 g/cm^3. These values are in the range of the solid content normally used for paste backfill in practice (Potvin et al. 2005; Bussière 2007; Belem and Benzaazoua 2008). When the solid content is beyond this range, the backfill become too stiff or too runny and inappropriate for the slump tests. As an extreme case, a test was performed with a very runny backfill, which has a solid content of 62.5%.

9.3.2 Slump test

Slump tests were conducted with a cylindrical mold, which is made of Plexiglas and has an inner diameter d_1 = 100 mm, a thickness t_1 = 4.95mm, and a height H_1 = 214 mm. Fig. 9-5 shows a slump test before and after the removal of the cylindrical mold. The cylindrical mold was placed on a smooth, plane, nonabsorbent and moist plate. Paste backfill was poured to fill the cylindrical mold. A tamping rod with a hemispherical tip was used to avoid or reduce trapped airs (bubbles). The backfill exceeding the cylinder top was wiped. After the removal of the mold by vertical movement, the slump height S and the base diameter of the collapsed samples d were measured with a metal rule. The diameter was measured in two orthogonal directions to obtain an average value. The slope angle α was measured by carefully inserting a moist protractor into the backfill in four orthogonal directions to obtain an average value.

The test was evaluated as successful if the difference between the bottom diameters measured in the two directions and the maximum difference between the slope angles measured in four orthogonal directions is within 10%.

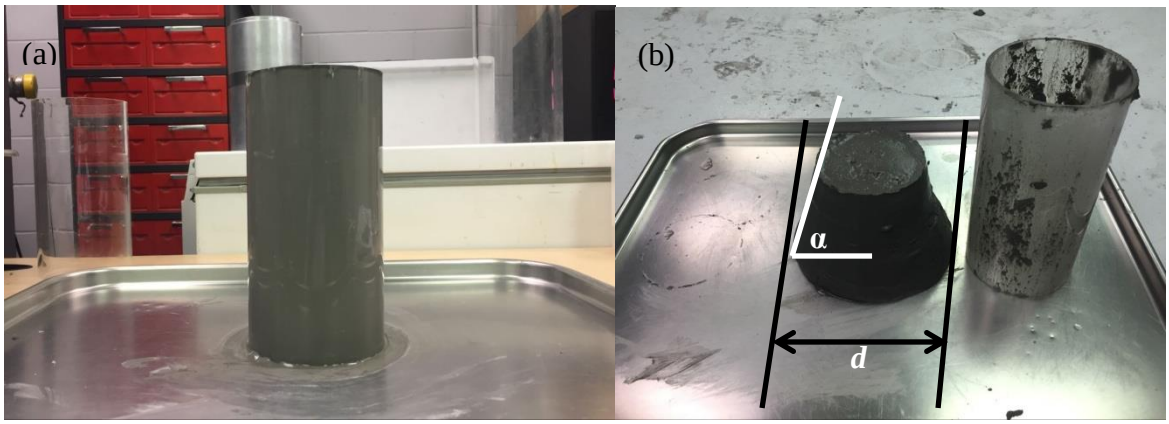

Figure 9-5: A slump test (a) before and (b) after the removal of the cylinder mold.

9.3.3 Pressure measurement with column tests

In this study, the pressure measurement was made with a column of Plexiglas, which has an inner diameter d_2 = 15.5 cm and a height H_2 = 50 cm. Two stress sensors of type TML-PDA-200 kPa were used (and available at the moment of tests) to measure the vertical total stresses at the bottom of the column. They have a diameter d_3 = 6.5 mm, a thickness t_3 = 1 mm and a capacity of 200 kPa.

Fig. 9-6 shows a schematic presentation [Fig. 9-6(a)] and a photograph [Fig. 9-6(b)] of the test instrumentation. A water-proof paper ruler with measuring range of 50 cm and resolution of 0.1 cm was stuck to the column inner wall. The two sensors were fixed at the bottom of the column, one was in the center and the other near the column wall (with a gap of about 2 mm). They were calibrated in the column with water. The input voltage for the sensors is 2 V. The output voltage is amplified by an amplifier and then measured with a multimeter. The initial voltage output before any water filling was first noted. Then, the column was filled with water in interval of 10 cm. At each interval, the voltage output was read from the multimeter.

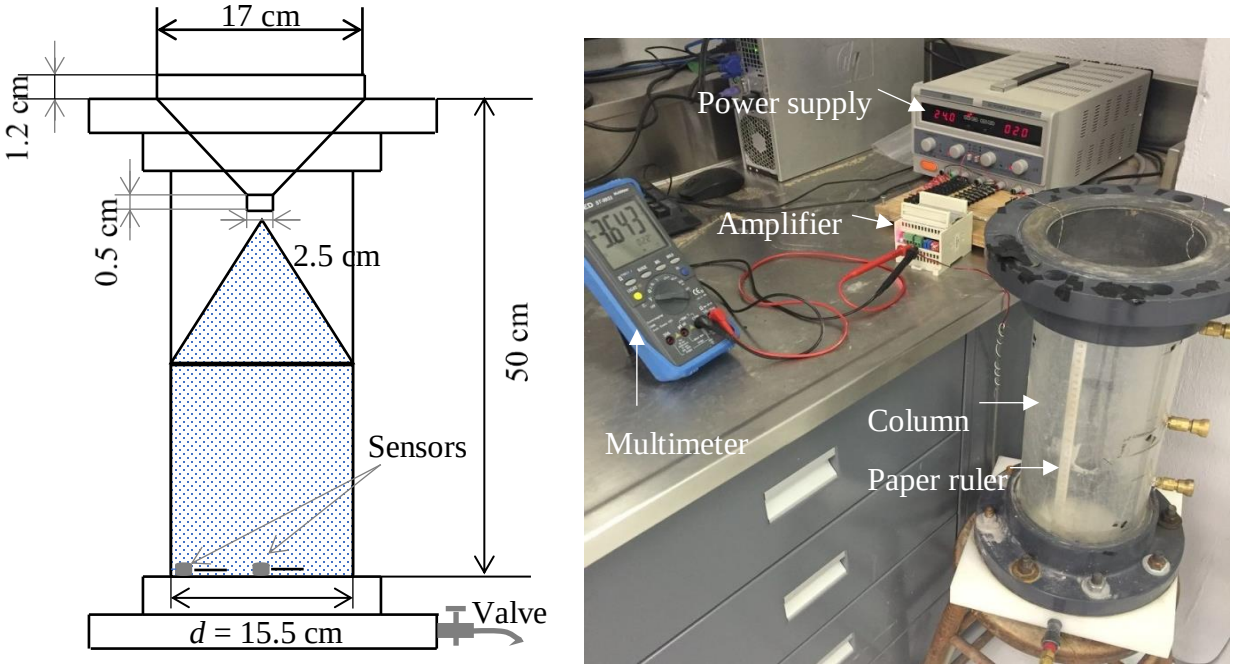

Figure 9-6: Instrumentation of the pressure measurement: (a) schematic presentation; (b) a photograph of the instrumentation.

Fig. 9-7 shows the calibration curves of the two stress sensors. The x–axis is the water pressure calculated from the water height in the column, while the y–axis represents the voltage difference ΔV between the voltage reading at a given water height and the initial voltage reading. It can be seen that the voltage difference increases linearly with the water height and pressure. The two sensors were calibrated at least two times before each column backfill pressure measurement test. The slopes of the calibration curves were then used to obtain the backfill pressure during the column filling tests.

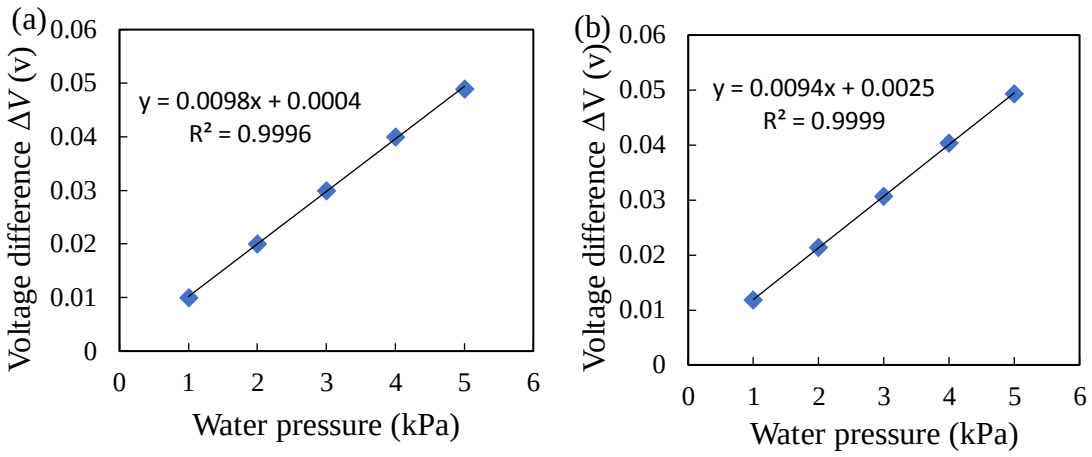

Figure 9-7: Calibration curves of the stress sensors: (a) at the column center and (b) close to the wall.

After the sensor calibration with water, the two stress sensors were left at their initial places and ready for the pressure measurement tests to measure the vertical total stresses at the center (σ_{v1}) and close to the wall (σ_{v2}) of the column. The backfill materials were the same used immediately after the slump tests. The water content of the backfill was measured before the slump tests and column tests. The column filling operation was made with a funnel placed at the top of the column. The funnel has an upper diameter of 17 cm and bottom diameter of 2.5 cm.

Fig. 9-8 shows the state of the placed backfill having different solid contents. When the solid content is as low as 62.5%, the backfill has enough flowability and behaves like a heavy liquid. The backfilling is easy and the backfill falls in the column under its own gravity, resulting in a fill mass having a horizontal surface at the top [Fig. 9-8(a)]. When the solid content is intermediate (75.5%) between very low and very high, a small cone forms at the top of the placed backfill [Fig. 9-8(b)]. When the solid content is as high as 78.4%, the backfill becomes too viscous and it cannot fall down into the column under its own gravity. A pressure has to be applied at the top surface of the backfill in the funnel to squeeze it out of the bottom of the funnel. The fill mass in the column is not continuous medium and contains many air bubbles [Fig. 9-8(c)]. For all of the tests (except for C_w = 62.5%), the filling operation was ended only when the placed backfill in the column reached the bottom of the funnel, resulting in the backfill height at the center of the column of H_3 (= 42 cm). Then, the output voltages of the two sensors were read and the vertical total stresses were calculated with the slopes of the calibration curves.

After each test, the backfill in the column was carefully vibrated and tamped to remove any trapped air bubbles in order for it to have a horizontal top surface. The backfill final height H_4 was measured to calculate the total volume of the backfill placed in the column.

Figure 9-8: The state of the placed backfill in the column with (a) very low solid content (C_w = 62.5%), (b) intermediate solid content (C_w = 75.5%) and (c) very high solid content (C_w = 78.4%).

9.4 Test results and interpretation

Table 9-1 shows the test results obtained with a paste backfill whose solid content varies between 62.5 and 78.4%. The measured parameters include the slump height S, slope angle α, bottom diameter d_2, the "short-term" vertical total stresses σ_{v1} and σ_{v2}, top height H_3, and average height H_4.

Table 9-1: Test results with paste backfill having different solid contents

C_w (%)	ρ (g/cm^3)	s (cm)	α (°)	d_2 (cm)	σ_{v1} (kPa)	σ_{v2} (kPa)	H_3 (cm)	H_4 (cm)	$\sigma_{v1}/(\gamma H_3)$	$\sigma_{v2}/(\gamma H_3)$
62.5	1.648	≈21.4	≈0	—	6.376	6.247	39	39.0	1.012	0.992
75.5	1.877	14.9	27.5	26.1	7.326	6.694	42	36.0	0.948	0.866
76.0	1.889	13.9	32.5	24.4	6.549	6.101	42	36.0	0.842	0.785
76.1	1.891	12.7	41.3	22.9	7.000	6.20	42	35.0	0.899	0.797
76.3	1.904	10.9	57.5	19.8	5.696	4.520	42	35.0	0.727	0.577
76.5	1.893	12.9	37.5	22.6	5.700	5.118	42	34.0	0.732	0.657
76.5	1.901	11.9	50.0	20.2	6.592	5.840	42	35.0	0.842	0.746
76.7	1.897	12.4	45.0	22.2	5.990	5.501	42	35.0	0.767	0.705
76.8	1.911	10.0	65.0	16.5	5.571	4.217	42	34.0	0.708	0.536
77.0	1.908	11.2	57.5	18.3	5.687	4.901	42	34.0	0.724	0.624
77.5	1.928	11.4	60.0	17.8	5.078	4.422	42	34.0	0.640	0.557
77.5	1.915	10.9	53.8	18.2	5.667	3.630	42	35.0	0.719	0.461
77.6	1.928	9.4	65.0	16.7	4.609	2.272	42	34.0	0.581	0.286
77.8	1.938	9.2	67.5	16.5	4.273	3.049	42	34.0	0.536	0.382
78.0	1.934	10.0	63.8	16.6	4.135	2.692	42	34.0	0.519	0.338
78.2	1.936	9.5	66.3	16.5	5.200	2.884	42	30.0	0.653	0.362
78.4	1.945	7.9	75.0	14.7	3.735	1.460	42	30.0	0.467	0.182

Fig. 9-9 shows the variation of the slump height S [Fig. 9-9(a)] and slope angle α [Fig. 9-9(b)] as a function of the backfill solid content C_w. The results for the backfill with a solid content of 62.5% is not shown because the backfill is too runny. After the removal of column, the backfill sample flowed around, resulting in a slump height almost equal to the column height and a slope angle of zero degree. One sees that an increased solid content leads to a decreased slump height S and an increased slope angle α. These results are straight forward. A high solid content means a low water content in the backfill. This in turn means a high viscosity and yield stress and a low flowability, and subsequently a low slump height and high slope angle.

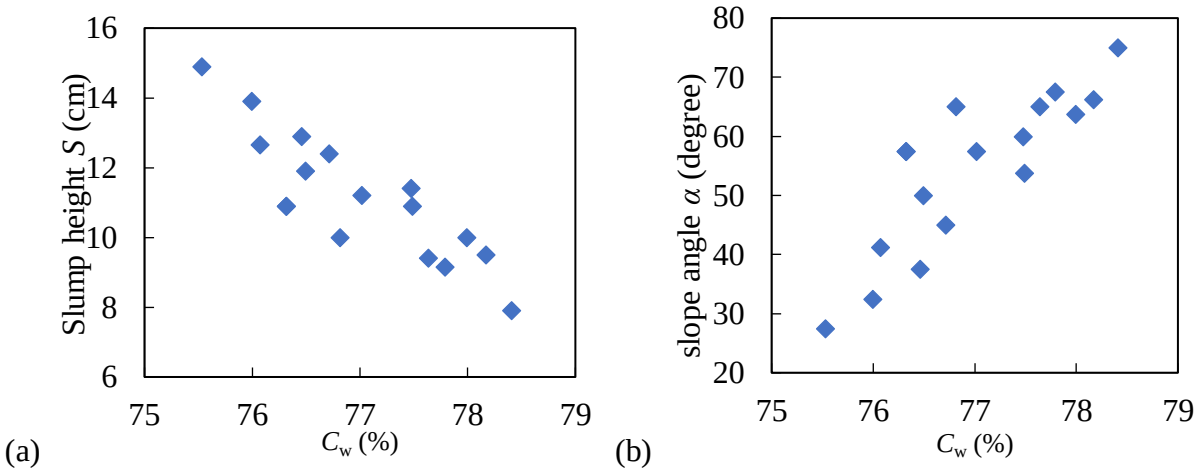

Figure 9-9: Measured (a) slump height and (b) slope angle as a function of the solid content.

Slump test is initially developed and used in civil engineering to evaluate the workability or consistency of fresh concrete. It is also used in mining engineering to evaluate the workability of mining backfill. Analytical models have been proposed to relate the yield stress with the slump height obtained with a standard cone (Murata 1984) or a cylindrical mold (Pashias et al. 1996).

Fig. 9-10 schematically shows a slump test conducted in a cylindrical mold along with the stress state before [Fig. 9-10(a)] and after [Fig. 9-10(b)] the removal of the cylinder. In the figure, d_1 and H_1 are the inner diameter and height of the mold, respectively. The slump height S is defined as the difference between the initial [Fig. 9-10(a)] and final [Fig. 9-10(b)] heights of the backfill. The upper un-deformed part is called intact or unyielded region with a height h_0 (or normalized height $h'_0 = h_0/H_1$) while the lower deformed part is considered as yielded region with a height h_1 (or normalized height $h'_1 = h_1/H_1$).

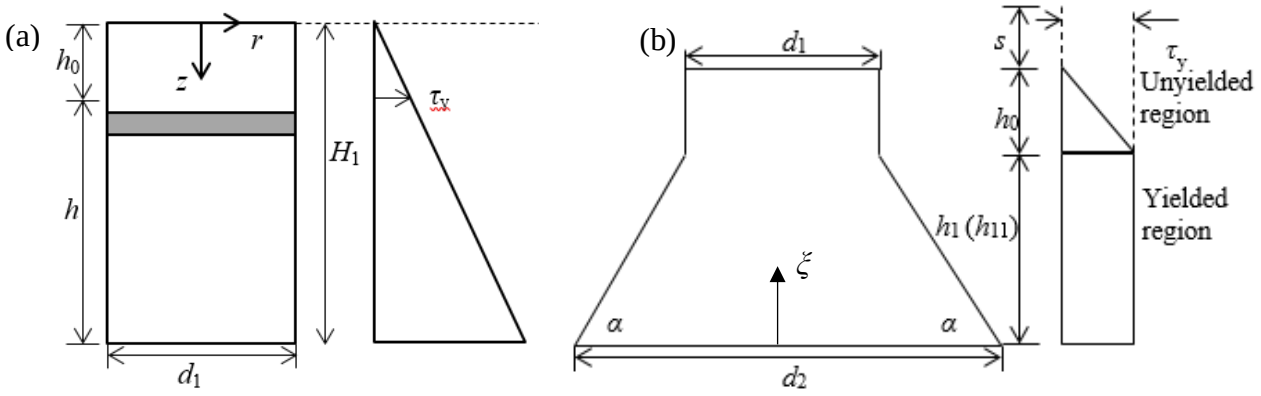

Figure 9-10: Schematic presentation of the (a) initial and (b) final geometry and state of the backfill during the slump test with a cylindrical mold (adapted from Pashias et al. 1996)

According to Pashias et al. (1996), the normalized heights h'_0 and h'_1 [Fig. 9-10(b)] after slumping can be calculated from the normalized yield stress τ'_y (= $\tau_y/(\gamma H_1)$; γ (kN/m^3) is unit weight of the backfill; τ_y (kPa) is the yield stress of the backfill) as follows:

$$h_0^{'} = 2\tau_y^{'} \tag{9.1}$$

$$h_1^{'} = -2\tau_y^{'}\mathrm{Ln}(h_0^{'}) \tag{9.2}$$

These relations have been proposed by neglecting the bottom resistance, which tends to limit the lateral expansion of the yielded fill. In this paper, the bottom resistance is considered to be equal to the yield stress at the cylinder bottom and the horizontal resistance R_ξ is assumed to be distributed linearly within the h_1 section as follow (Murata 1984):

$$R_\xi = (1-\frac{\xi}{h_1})\tau_y \tag{9.3}$$

where ξ is the axis with the origin point at the bottom of the cylinder and positive direction is upward.

When the horizontal resistance is considered, the height of the yielded region h_1 becomes h_{11} as follows

$$h_{11} = \int_0^{h_1} \frac{\tau_y + R_\xi}{\tau_y} d\xi = 1.5h_1 \tag{9.4}$$

The normalized height of h'_{11} can be expressed as:

$$h_{11}^{'} = 1.5h_1^{'} = -3\tau_y^{'}\mathrm{Ln}(h_0^{'}) \tag{9.5}$$

The normalized slump height S' (=S/H_1) is computed as

$$S' = 1 - h_0^{'} - h_{11}^{'} \tag{9.6}$$

Substituting Eqs. (9.1) and (9.5) into (9.6) results in

$$S' = 1 - 2\tau_y^{'} + 3\tau_y^{'} \times \mathrm{Ln}(2\tau_y^{'}) \tag{9.7}$$

Before the removal of the cylindrical mold, the volume of backfill V_1 (or normalized volume V'_1 = V_1/H_1^3) can be calculated as:

$$V_1^{'} = \frac{\pi}{4}(d_1^{'})^2 \times (h_0^{'} + h^{'}) \tag{9.8}$$

where

$$d_1^{'} = \frac{d_1}{H_1} \tag{9.9}$$

$$h^{'} = \frac{h}{H_1} \tag{9.10}$$

After the removal of the cylindrical mold, the volume of the backfill V_2 (or normalized volume V'_2 = V_2/H_1^3) can be expressed as:

$$\begin{aligned} V_2^{'} = {} & \frac{\pi}{4} \times \left(d_1^{'}\right)^2 h_0^{'} + \frac{1}{12}\pi\left(d_2^{'}\right)^2 \times \frac{d_2^{'}}{2}\tan\alpha \\ & - \frac{1}{12}\pi\left(d_1^{'}\right)^2 \times \frac{d_2^{'}}{2}\tan\alpha + \frac{1}{12}\pi\left(d_1^{'}\right)^2 h_{11}^{'} \end{aligned} \tag{9.11}$$

where d'_2 is the normalized bottom radius of the yielded portion which can be computed as follows:

$$d_2^{'} = d_1^{'} + 2h_{11}^{'}\cot\alpha \tag{9.12}$$

Considering the volume conservation before and after the removal of the cylindrical mold yields:

$$4\left(h_{11}^{'}\right)^3(\cot\alpha)^2 + 6\left(h_{11}^{'}\right)^2 d_1^{'}\cot\alpha + 3\left(d_1^{'}\right)^2 \times (h_{11}^{'} - h^{'}) = 0 \tag{9.13}$$

Solving Eq. (9.13) leads to

$$\tan\alpha = \frac{4\left(h_{11}^{'}\right)^2}{-3h_{11}^{'}d_1^{'} + d_1^{'} \times \sqrt{3h_{11}^{'}(4 - 4h_0^{'} - h_{11}^{'})}} \tag{9.14}$$

Substituting Eqs. (9.1) and (9.5) into (9.14) results in

$$\tan\alpha = \frac{36(\tau_y^{'})^2 \times \left[\ln(2\tau_y^{'})\right]^2}{9\tau_y^{'} \times \ln(2\tau_y^{'}) \times d_1^{'} + d_1^{'} \times \sqrt{-9\tau_y^{'} \times \ln(2\tau_y^{'}) \times (4 - 8\tau_y^{'} + 3\tau_y^{'} \times \ln(2\tau_y^{'}))}} \tag{9.15}$$

Fig. 9-11 shows the variation of the slope angle [Fig. 9-11(a)] and bottom diameter d_2 [Fig. 9-11(b)] with the normalized slump height of the backfill, obtained by the slump tests and calculated with the proposed solution [Eqs. (9.7) and (9.15)]. One can see that the slope angle decreases while the bottom diameter of the collapsed backfill increases as the normalized slump height S' increases. The agreements between the measured slope angles and bottom diameter of the collapsed backfill and those predicted by the proposed solution are good. The proposed analytical solution captures well the relationship between the slope angle, bottom diameter of the collapsed backfill and the normalized slump height.

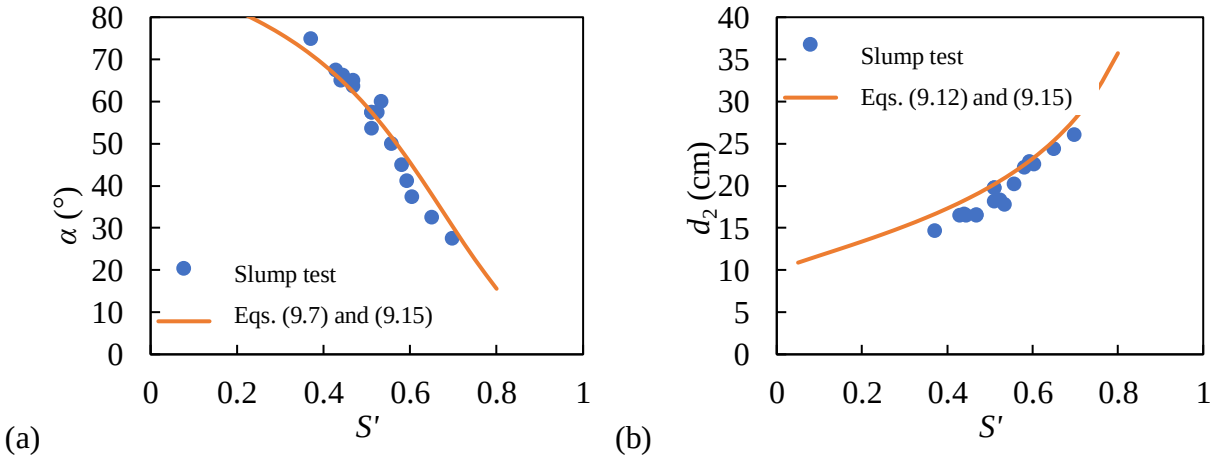

Figure 9-11: Variation of the (a) slope angle α and (b) bottom diameter d_2 with the normalized slump height S', obtained from the slump tests and estimated by applying the proposed solutions.

Fig. 9-12 shows the variation of the measured vertical total stresses [Fig. 9-12(a)] and the ratio between the stresses in the column center and close to the wall [Fig. 9-12(b)] as well as the vertical total stresses normalized by the iso-geostatic pressure based on the overburden [Fig. 9-12(c)], shortly after the deposition of the backfill as a function of the solid content. In all cases, the vertical total stress close to the wall is always smaller than that at the center. When the solid content

increases from 75.5 to 78.4%, the vertical total stresses at the center and near the wall decrease significantly while the difference between the stresses at the two positions increases, as shown in Fig. 9-12(a). To note that the vertical total stress corresponding to the solid content of C_w = 62.5% was not shown in Fig. 9-12(a) as the density and height of the backfill are much smaller than the backfill of higher solid content. Fig. 9-12(b) shows that the ratio between the stresses at the center and close to the wall increases as the solid content decreases. It becomes close to unity when the solid content is C_w = 62.5%.

From Fig. 9-12(c), one sees that the normalized vertical total stresses at the center and close to the wall decrease as the solid content increases. At a solid content of C_w = 62.5%, the normalized vertical total stresses at the two position are close to unity, indicating little arching effect. When the solid content increases from 75.5 to 78.4%, the normalized vertical total stresses decrease from around 0.9 to 0.4, clearly indicating the occurrence of arching effect.

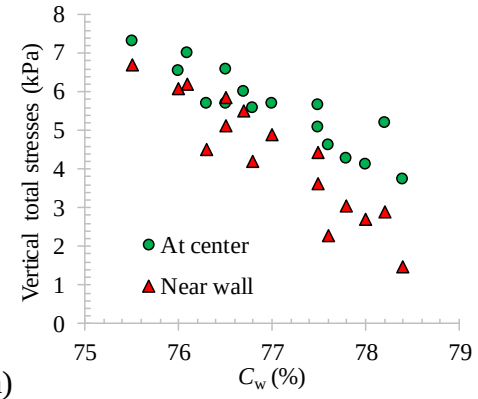

(a)

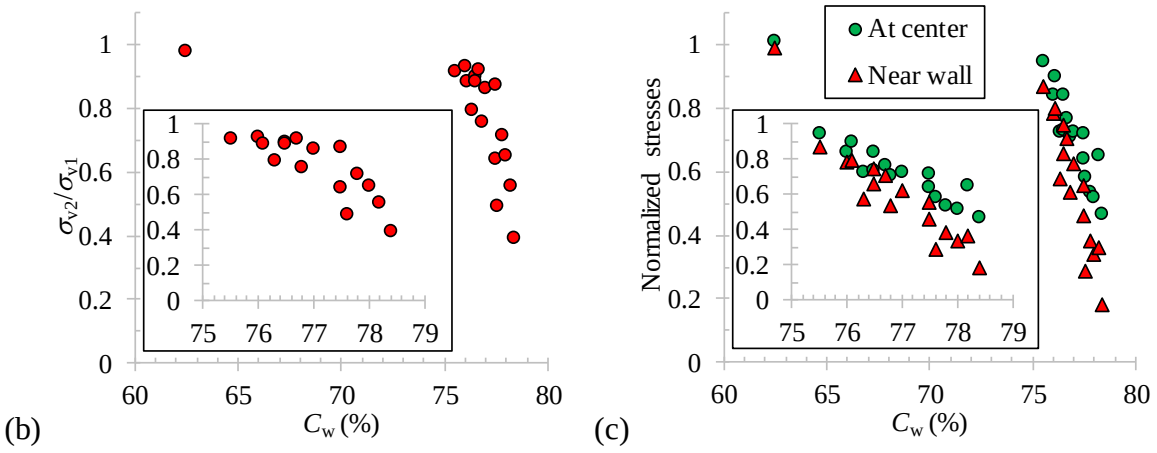

Figure 9-12: Measured vertical total stresses (a) stress ratio (b) and normalized stresses (c) at the center and close to the wall as a function of the solid content of the backfill.

To explain the variation of the vertical total stresses in paste backfill shortly after the placement in a mine stope as a function of the solid content via the slope angle α, Li and Zheng (2017) have proposed a conceptual analytical solution to estimate the ratio between the "short-term" vertical total stresses at the center (σ_{v1}) and near the wall (σ_{v2}) as follows:

$$\frac{\sigma_{v2}}{\sigma_{v1}} = \frac{3V - \pi r^3 \tan\alpha}{3V + 2\pi r^3 \tan\alpha} \qquad r_1 = r \tag{9.16}$$

$$\frac{\sigma_{v2}}{\sigma_{v1}} = 0 \qquad r_1 < r \tag{9.17}$$

where V is the total volume of the backfill placed in the column; r_1 is the radius at the bottom of the placed backfill; r is the radius of the column; α is the slope angle of the placed backfill in the column (see Eq. (9.15)).

Fig. 9-13 shows the variation of the vertical total stress ratio σ_{v2}/σ_{v1} with the normalized slump height S', obtained by stress sensors measurement and calculated by applying the proposed solution Eq. (9.16) with r = 7.75 cm and slope angle α calculated with Eq. (9.15) using the test results in Table 9-1. In the figure, the volumes of the placed backfill of 5658, 6412, 6601, and 6789 cm^3 corresponding to the backfill height H_3 of 30, 34, 35, 36 cm, respectively (see Table 9-1). It can be seen that the value of σ_{v2}/σ_{v1} increases as the backfill normalized slump height increases. The σ_{v2}/σ_{v1} ratio calculated using the proposed solution [Eq. (9.16)] correlates well with the measured results.

When the normalized slump height *S*' is as low as 0.37, the backfill can have a certain self-stand vertical height and shows a certain shear strength. The lateral flow is very limited, resulting in high slope angle and a tall cone at the top of the backfill. The value of the σ_{v2}/σ_{v1} decreases to about 0.39, indicating a low vertical total stress at the column wall. When the normalized slump height *S*' has a high value of 0.8, backfill behaves as heavy liquid and has high workability. Only a small cone is formed on top of the backfill and the value of σ_{v2}/σ_{v1} is close to one, indicating high vertical total stress at the stope wall. For backfill with a very low solid content (62.5%), the σ_{v2}/σ_{v1} is almost equal to 1 while the normalized slump height *S*' is also almost equal to 1 (see details given in Table 9-1).

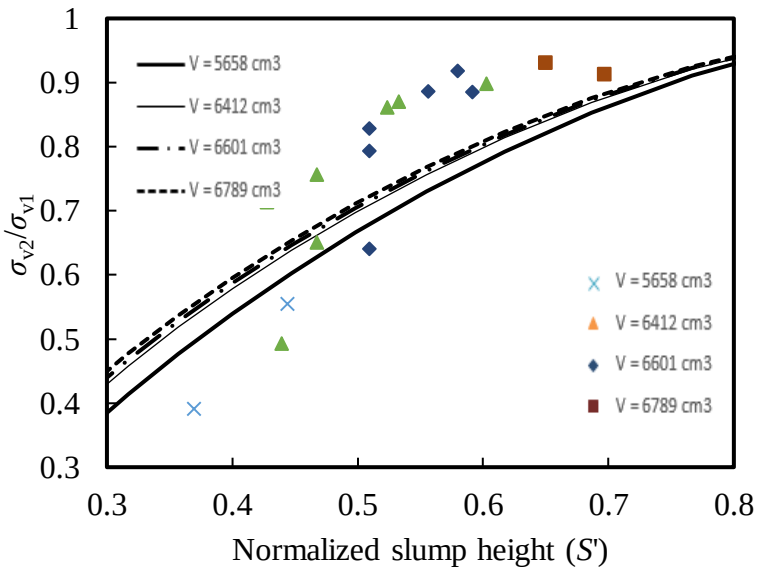

Figure 9-13: Variation of vertical total stress ratio σ_{v2}/σ_{v1} with the normalized slump height *S*', obtained by measurements and calculated by the proposed solution [Eqs. (9.15) and (9.16)] using r = 7.75)).

9.5 Discussion

A series of column tests were conducted to measure the vertical total stresses at the center and near the wall of a column by filling it with different solid contents of backfill. The measured results indicate that the vertical total stresses in a backfilled stope are related to the solid content. High solid content leads to lower vertical total stress near the wall, corresponding to the suggestions given in handbooks for barricade design. With low solid content backfill, the vertical total stresses

near the wall can be high. The construction of a strong barricade is necessary. These results indicate that the barricade design for paste backfill should take into account the backfill solid content. However, it should be noted that the laboratory tests contain some limitations.

For example, the tests only measured the vertical total stresses while the barricade design is determined by the horizontal total stresses. More work is required to measure the vertical and horizontal total stresses in paste backfilled stopes with different solid (water) contents.

The final height H_3 of the placed backfill after each column test was measured by vibrating and tamping to remove the contained air bubbles. This may change the void ratio and total volume of the placed backfill. More elaborate method to measure the volume of placed backfill is required in the future.

The proposed solution Eq. (9.16) was proposed by considering the vertical stress due to the overburden without any consideration of arching effect. The laboratory tests showed that the paste backfill can become sticky and cohesive when the solid content exceeds a certain degree, probably due to the unsaturated state and apparent cohesion. More work is required to take the arching effect into account.

9.6 Conclusions

The barricade stability is important for the successful application of backfill. For barricade designed to retain paste backfill, there is a contradictory between the handbooks suggestions and in situ measurement results. A brief review revealed that the paste backfill meeting the two criteria defined in the handbooks can be very viscous and probably unsaturated. In practice, sufficient water should be added in the backfill to facilitate the transportation and to ensure tight contact between the backfill and wide or long stope roof. The backfill can still be called paste backfill, but the criterion in terms of water bleeding defined in the handbooks is no longer satisfied. The total stresses shortly after the placement of the backfill in a stope can be as high as the iso-geostatic pressure based on the overburden. Between the two extreme cases, one can reason that the total stresses in the paste backfill should be a function of the solid content. To test this hypothesis, a series of tests were conducted to measure the vertical total stresses at the center and near the wall of a column filled with different solid contents of backfill (from liquid to viscous). The measured results show that when the solid content increases from 75.5 to 78.4%, the vertical total stresses at

the center and near the wall decrease while the vertical total stress near the wall is always lower than that at the center. The difference between the vertical total stresses at the two positions increases as the solid content increases. These results confirm that the stresses in backfilled stope depend on the solid (water) content of backfill. For the backfill with high solid content, the vertical total stress near the wall can be small. The construction of a light barricade is enough to retain the paste backfill; this corresponds to the recommendation given in the handbooks (Hassani and Archibald 1998; Potvin et al. 2005). When the solid content is low and backfill is very thin and runny, the vertical total stress near the wall can be high. An adequate design and construction of barricades is necessary.

Acknowledgements

The authors would like to acknowledge the financial aid from the Natural Sciences and Engineering Research Council of Canada (402318), Fonds de recherche du Québec—Nature et Technologies (2015-MI-191676), and the industrial partners of the Research Institute on Mines and Environment (RIME UQAT-Polytechnique; http://rime-irme.ca/). Noura EI-Harrak and Maxime Daviault are acknowledged for their kind help in the laboratory tests.

9.7 References

Ahmed, S.I., & Siddiqua, S. (2014). A review on consolidation behavior of tailings. *International Journal of Geotechnical Engineeering, 8*(1): 102-111.

Askew, J.E., McCarthy, P.L., & Fitzerald, D.J. (1978). *Backfill research for pillar extraction at ZC/NBHC*. Paper presented at the Proceedings of Mining with Backfill: 12th Canadian Rock Mechanics Symposium, CIM, Montréal, (pp. 100-110).

Aubertin, M. (1999). *Application de la mécanique des sols pour l'analyse du comportement des remblais miniers souterrains*. Short Course (unpublished notes). Paper presented at the 14th Colloque en Contrôle de Terrain, Val-d'Or, Québec.

Aubertin, M., Li, L., Arnoldi, S., Belem, T., Bussière, B., Benzaazoua, M., & Simon, R. (2003). *Interaction between backfill and rock mass in narrow stopes*. Paper presented at the Soil and Rock America 2003, Essen, Germany (pp, 1157–1164).

MineDesign queen's university. (2011). Backfill. Retrieved from http://minewiki.engineering.queensu.ca/mediawiki/index.php/Backfill

Been, K., & Sills, G.C. (1981). Self-weight consolidation of soft soils: an experimental and theoretical study. *Geotechnique*, *31*(4), 519-535.

Belem, T., Harvey, A., Simon, R., & Aubertin, M. (2004). *Measurement and prediction of internal stresses in an undergound opening during its filling with cemented fill*. Paper presented at the Symposium on Ground support in mining and underground construction. Taylor and Francis Group, London, Australia (pp. 619–630).

Bloss, M.L., & Chen, J. (1998). *Drainage research at Mount Isa Mines limited 1992-1997*. Paper presented at the 6th International Symposium on Mining with Backfill, Brisbane, Australia (pp. 111-116).

Boger, D., Scales, P., & Sofra, F. (2006). Rheological concepts. In Jewell and Fourie (Eds), *Paste and Thickened Tailings-A Guide* (2nd ed pp. 25-37).

Clayton, S., Grice, T.G., & Boger, D.V. (2003). Analysis of the slump test for on-site yield stress measurement of mineral suspensions. *International Journal of Mineral processing*, *70*(1), 3-21.

Dzuy, N.Q., & Boger, D.V. (1985). Direct yield stress measurement with the vane method. *Journal of Rheology*, *29*(3), 335-347.

Fox, P.J. (2000). *CS4: A large strain consolidation model for accreting soil layers*. Paper presented at the Geotechnics of high water content materials, ASTM International, West Conshohocken, PA.

Gade, V.K., & Dasaka, S.M. (2018). Calibration of earth pressure sensors. *Indian Geotechnical Journal*, *48*(1), 142-152.

Gawu, S.K.Y., & Fourie, A.B. (2004). Assessment of the modified slump test as a measure of the yield stress of high-density thickened tailings. *Canadian Geotechnical Journal*, *41*(1), 39-47.

Gibson, R.E. (1958). The progress of consolidation in a clay layer increasing in thickness with time. *Géotechnique*, *8*(4), 171-182.

Grice, T. (1998). *Stability of hydraulic backfill barricades*. Paper presented at the 6th International Symposium on Mining with Backfill, Victoria, Australia (pp. 117-120).

Grice, T. (2001). *Recent mine fill developments in Australia*. Paper presented at the 7th International Symposium on Mining with Backfill, Society for Mining, Littleton, Colorado (pp, 351–357).

Hassani, F., & Archibald, J. (1998). Mine backfill. (CD-ROM). Canadian Institute of Mining, Metallurgy and Petroleum, Montréal, Canada.

Helinski M, Fahey M and Fourie A. (2011) Behavior of cemented paste backfill in two mine stopes: measurements and modeling. J Geotech Geoenviron Eng, 137(2): 171–182.

Helinski, M., Fourie, A., & Fahey, M. (2006). *Mechanics of early age CPB*. Paper presented at the 9th International Seminar on Paste and Thickened Tailings, Perth, Australia (pp. 313–322).

Janssen, H.A. (1895). Versuche über Getreidedruck in Silozellen. *Zeitschrift Verein Ingenieure, 39*, 1045-1049.

Knutsson, S. (1981). *Stresses in the hydraulic backfill from analytical calculations and in-situ measurements*. Paper presented at the Application of Rock Mechanics to Cut and Fill Mining, London. (pp. 261–268).

Kuganathan, K. (2001). Mine backfilling, backfill drainage and bulkhead construction-a safety first approach. Australian Mining Monthly, (pp. 58–64).

Kuganathan, K. (2002). *A model to predict bulkhead pressures for safe design of bulkheads*. Paper presented at the Filling with Hydraulic Fills Seminar, Section 6, Australian Centre for Geomechanics, Perth, Australia.

Li, L., & Aubertin, M. (2008). An improved analytical solution to estimate the stress state in subvertical backfilled stopes. *Canadian Geotechnical Journal, 45*(10), 1487-1496.

Li, L., & Aubertin, M. (2010). An analytical solution for the nonlinear distribution of effective and total stresses in vertical backfilled stopes. *Geomechanics and Geoengineering, 5*(4), 237-245.

Li, L., & Zheng, J. (2017). *A conceptual analytical solution for estimating the short-term pressure of paste fill varying from viscous to liquid state, placed in mine stopes*. Paper presented at the 70th Canadian Geotechnical Conference, Canadian Geotechnical Society, Ottawa, Canada.

Li, L. (2013). A new concept of backfill design – application of wick drains in backfilled stopes. *International Journal of Mining Science and Technology, 23*(5), 763–70.

Li, L., Alvarez, I.C., & Aubertin, J.D. (2013). Self-weight consolidation of a slurried deposition: tests and interpretation. *International Journal of Geotechnical Engineering, 7*(2), 205–213.

Li, L., & Aubertin, M. (2009c) Horizontal pressure on barricades for backfilled stopes: Part I: Fully drained conditions. *Canadian Geotechnical Journal, 46*(1), 37–46.

Li, L., & Aubertin, M. (2009d). Horizontal pressure on barricades for backfilled stopes: Part II: Submerged conditions. *Canadian Geotechnical Journal, 46*(1), 47–56.

Li, L., & Aubertin, M. (2009a). Influence of water pressure on the stress state in stopes with cohesionless backfill. *Geotechnical and Geological Engineering, 27*(1), 1–11.

Li, L., & Aubertin, M. (2009b). A three-dimensional analysis of the total and effective stresses in submerged backfilled stopes. *Geotechnical and Geological Engineering, 27*(4), 559–569.

Li, L., Aubertin, M., & Belem, T. (2005). Formulation of a three dimensional analytical solution to evaluate stress in backfilled vertical narrow openings. *Canadian Geotechnical Journal, 42*(6), 1705–1717 (with Erratum 2006, 43(3), 338–339).

Li., L, Aubertin, M., Simon, R., Bussière, B., & Belem, T. (2003). *Modeling arching effects in narrow backfilled stopes with FLAC*. Paper presented at the 3rd International FLAC Symposium, A. A. Balkema, Rotterdam, Netherlands. (pp. 211–219).

Marston, A. (1930). The theory of external loads on closed conduits in the light of latest experiments. Iowa Engineering Experiment Station, Ames, Iowa (pp. 138-170).

Miao, X.X., Zhang, J.X., & Feng, M.M. (2008). Waste-filling in fully-mechanized coal mining and its application. *International Journal of Mining Science and Technology, 18*(4), 479–82.

Murata, J. (1984). Flow and deformation of fresh concrete. *Materiaux et Construction, 17*(2), 117-129.

Niroshan, N., Sivakugan, N., & Veenstra, R.L. (2017). Laboratory study on strength development in cemented paste backfills. *Journal of Materials in Civil Engineering, 29*(7), 04017027.

Pashias, N., Boger, D.V., Summers, J., & Glenister, D.J. (1996). A fifty cent rheometer for yield stress measurement. *Journal of Rheology, 40*(6), 1179-1189.

Pedroni, L. (2011). Étude expérimentale et numérique de la sédimentation et de la consolidation des boues de traitement des eaux acides. (Doctoral dissertation, École Polytechnique de Montréal, Montréal, Canada).

Potvin, Y., Thomas, E., & Fourie, A. (2005). *Handbook on mine fill*. Nedlands, Australia: Australian Centre of Geomechanics.

Simon, D., & Grabinsky, M. (2013). Apparent yield stress measurement in cemented paste backfill. *International Journal of Mining, Reclamation and Environment, 27*(4), 231-256.

Sivakugan, N., Rankine, K., & Rankine, R. (2006a). Permeability of hydraulic fills and barricade bricks. *Geotechnical and Geological Engineering, 24*(3), 661-673.

Sivakugan, N., Rankine, K., Lovisa, J., & Hall, W. (2013). Flow rate computations in hydraulic fill mine stopes. *Indian Geotechnical Journal, 43*(3), 195-202.

Sivakugan, N., Rankine, R.M., Rankine, K.J., & Rankine, K.S. (2006b). Geotechnical considerations in mine backfilling in Australia. *Journal of Cleaner Production, 14*(12), 1168-1175.

Soderberg, R.L., & Busch, R.A. (1985). Bulkheads and drains for high sandfill stopes. (Report of investigations 8959). United States Bureau of Mines, Spokane, Wash.

Thompson, B.D., Bawden, W.F., & Grabinsky, M.W. (2012). In situ measurements of cemented paste backfill at the Cayeli Mine. *Canadian Geotechnical Journal, 49*(7), 755-772.

Yang, P.Y., & Li, L. (2015). Investigation of the short-term stress distribution in stopes and drifts backfilled with cemented paste backfill. *International Journal of Mining Science and Technology, 25*(5), 721-728.

Yumlu, M., & Guresci, M. (2007). *Paste backfill bulkhead monitoring-A case study from Inmet's Cayeli mine*. Paper presented at the 9th International Symposium in Mining with Backfill (CD-ROM), Canadian Institute of Mining, Metallurgy and Petroleum, Montréal, Canada.

Zhang, J.X., Zhang, Q., Huang, Y., Liu, J.W., Zhou, N., & Zan, D.F. (2011). Strata movement controlling effect of waste and fly ash backfillings in fully mechanized coal mining with backfilling face. *Interntional Journal of Mining Science and Technology, 21*(5), 721–726.

Zheng, J., Li, L., Mbonimpa, M., & Pabst, T. (2018a). An analytical solution of Gibson's model for estimating the pore water pressures in accreting deposition of slurried material under one-dimensional self-weight consolidation. Part I: Pervious base. *Indian Geotechnical Journal, 48*(1), 72-83.

Zheng, J., Li, L., Mbonimpa, M., & Pabst, T. (2018b). An analytical solution of Gibson's model for estimating pore water pressures in accreting deposition of slurried material under one-dimensional self-weight consolidation. Part II: Impervious base. *Indian Geotechnical Journal, 48*(1), 188-195.

CHAPTER 10 SUMMARY AND DISCUSSION

10.1 Main results

The deposition of slurried materials in impoundments or mine stopes requires a good understanding of the excess PWP and stresses in the slurried materials during and after the deposition. This is closely related to the stability of the confining structures (dams and mine stope barricades), water and tailings volume management as well as the design of subsequent reclamation activities. In this thesis, a comprehensive study has been presented through analytical, numerical and experimental investigations on the excess PWP and stresses in slurried materials during and after the deposition.

Chapter 2 presented a literature review on the underground mining with backfill, tailings deposition. Emphasis was given on the estimation of excess PWP and stresses in accreting deposition of slurried materials in tailings impoundments or mine backfilled stopes. Chapters 3 to 9 showed the main outcomes of the thesis. They are summarized and discussed here.

Gibson (1958) proposed a model and some equations to evaluate the excess PWP in slurried materials during the slurry deposition. The equations have been taken as analytical solutions to evaluate the excess PWP in mine backfilled stopes by several researchers (Fahey et al. 2010; Shahsavari and Grabinsky 2014, 2015; Cui and Fall 2016). However, the equations of Gibson (1958) model contain an integral, which can only be estimated by numerical method. The equations of Gibson (1959) are thus not analytical solutions. To overcome this limitation, actually analytical solutions based on the Gibson (1958) model have been proposed and presented in Chapters 3 and 4 to evaluate the excess PWP during the accreting deposition, considering pervious and impervious bases. The proposed solutions have been validated against numerical results obtained by SIGMA/W. Sample calculations of the proposed solutions with EXCEL were shown. The main findings can be summarized as follows:

- When the slurry is deposited on a pervious base along which a null PWP is imposed, the excess PWP is always equal to the current total PWP. This notion has been illustrated by Gibson et al. (1989), but remains poorly known in geotechnical engineering.
- The excess PWP during the slurry deposition calculated by the proposed solution agree well with those obtained by the numerical simulations. The few experimental results obtained by

our laboratory tests showed that the excess PWP during the slurry deposition on an impervious base can be estimated by the analytical solution by using a constant c_v.

- The PWP at the end of slurry deposition is smaller than the iso-geostatic overburden pressure due to the occurrence of drainage and consolidation during the slurry deposition operation.
- The sample calculations of the proposed solutions show that the dissipation of excess PWP associated with the drainage and consolidation increases as the consolidation coefficient increases or/and the filling rate decreases.
- The excess PWP in the slurried materials can be controlled by limiting the height of the slurry deposition.

Gibson (1958) has also proposed a model to describe the evolution of the excess PWP in a slurry after the deposition on a pervious or an impervious base. An equation was proposed to evaluate the excess PWP after slurry deposition on an impervious base. The equation contain some error and cannot be used to evaluate the excess PWP. Only a governing differential equation was given to evaluate the excess PWP after slurry deposition on a pervious base. New solutions have been developed and presented in Chapters 5 and 6 to evaluate the excess PWP in slurried materials after the slurry deposition on a pervious or an impervious base. Numerical modellings were also performed with SIGMA/W to validate the proposed solutions. The main results are summarized as follows:

- The excess PWP after the slurry deposition calculated by the proposed solutions correlate well with those obtained by numerical modeling.
- The maximum PWP in the slurried materials are always smaller than the iso-geostatic overburden pressure due to the dissipation of the excess PWP associated with the drainage and consolidation during and after the slurry deposition.
- The excess PWP is very sensitive to the variation of the consolidation coefficient c_v. With a slurry having high value of c_v, the drainage can be very fast, resulting in low excess PWP.
- A high rate of deposition may result in high excess PWP in the slurried material. Long period of rest is necessary to dissipate the excess PWP after the slurry deposition.

It is important to note that design of barricades built at the base of a mine backfilled stope requires the knowledge of the total stresses during and shortly after the backfill deposition. After the slurried backfill deposition, the PWP and total stresses generally decrease with the drainage and consolidation, cementation and arching development. Chapters 7 and 8 present two pseudo analytical solutions to evaluate the PWP and stresses in backfilled stopes during the slurried backfill deposition on an impervious base and a pervious base, respectively. The arching effect and the drainage and consolidation were considered. The proposed solutions were validated by numerical modeling conducted with Plaxis2D. The findings can be summarized as follows:

- The proposed solutions can be used to evaluate the PWP, effective and total stresses in backfilled stopes.
- The stresses calculated with the proposed solutions using Rankine active earth pressure coefficient K_a agree well with those obtained by numerical modeling with Plaxis 2D.
- The total stresses are smaller than these based on the overburden solution, due to the occurrence of arching effect during the slurried backfill deposition.
- For backfill with very high consolidation coefficient (c_v > 399.96 m^2/h), the proposed solution reduces to that proposed by Li and Aubertin (2009a), who considered a submerged backfill (with a hydrostatic pressure) confined by an impervious barricade.
- The total stresses in backfilled stopes can be controlled by using a backfill of high consolidation coefficient or/and by slowing down the filling operation.

The in situ measurements conducted by Thompson et al. (2012) showed that the pressures and total stresses during the placement of cemented paste backfill can be as high as the iso-geostatic overburden pressure. These results suggest the construction of strong barricades to retain the paste backfill in the stopes. However, this does not correspond to the recommendation given in the handbooks of mining backfills (Hassani and Archibald 1998; Potvin et al. 2005), which suggest the construction of light barricades to retain cemented paste backfill in stopes. To understand this contradiction, the differences between a paste backfill strictly defined in the handbooks and those used in practice were identified. Backfilling and stress measurements were conducted with instrumented columns to study the variation of the “short-term” pressure and stresses in paste backfilled openings as a function of the solid content. The results are summarized as follows:

- The paste backfill meeting all of criteria defined in the handbooks can be very viscous and probably unsaturated. The backfill pressure and horizontal total stresses on barricade can eventually be small. However, it is difficult to apply such paste backfill in underground mine stopes. In practice, more water than the necessary (to meet the criteria defined in the handbooks) is usually added in the backfill to facilitate the transport by pipes. The pressure and total stresses in the paste backfilled stopes can be very high.
- The vertical total stresses in the backfilled openings shortly after the placement of the paste backfill decrease as the solid content of the backfill increases.
- The "short-term" vertical total stress near the wall is lower than that at the center. The difference between the vertical total stresses at the two positions increases as the solid content increases.
- With a paste backfill of high solid content, the total stresses near the stope wall can be low and the construction of a slight barricade can be enough to retain the paste backfill in the stope. With a paste backfill of low solid content, the PWP and total stresses can be large and the construction of a strong barricade is necessary.

10.2 Discussion

In the thesis, analytical or pseudo analytical solutions have been presented to evaluate the excess PWP in slurried material during and after the deposition on a pervious or impervious base. Pseudo analytical solutions have also been developed to estimate the total and effective stresses in backfilled stopes during the filling operation by jointly considering the drainage and self-weight consolidation and arching effect. The proposed solutions were validated by numerical results obtained with SIGMA/W or Plaxis 2D. The good agreements between the analytical and numerical results indicate that the proposed solutions can be used to evaluate the PWP and total stresses in the slurried materials placed in tailings impoundments or underground mine stopes. However, it should be noted that the proposed solutions presented in Chapters 3 to 8 were developed based on several explicit and implicit assumptions and limitations, which can be summarized as follows:

- In Gibson (1958) model, the assumptions of Terzaghi (1943) consolidation theory were adopted, including the small strain consolidation with constant hydraulic properties. These assumptions were inherited in the ensuing proposed solutions to evaluate the excess PWP and stresses in tailings impoundments and underground mine backfilled stopes. However, as

slurried materials usually have high water content and large void ratio, settlement can take place during the drainage and consolidation, resulting in a decrease of the permeability and an increase of the constrained modulus. The consolidation coefficient may not be a constant value. Rather, it generally increases with the drainage and consolidation (Fahey et al. 2010; Essayad 2015). More work is necessary to investigate the evolution of the consolidation coefficient c_v with the time and degree of consolidation.

- The model of Gibson (1958) considers one-dimensional drainage. Lateral drainage can take place in a tailings impoundment when waste rock inclusions are introduced to accelerate the drainage and consolidation of the tailings (Aubertin et al. 2002; Bolduc and Aubertin 2015). In underground mine backfilled mine stopes, lateral drainage can also occur through the fractures and joints of rock walls and barricades built at different levels (Sivakugan et al. 2006; Belem et al. 2016). More work is required to take into account the lateral drainage in the future.
- Upon placement of slurried materials in a confining structure, the solid particles tend to settle down under the effect of weight. The backfill can become denser and the pore water should be expelled out of the backfill. These tendencies lead to the generation of excess PWP because the backfill has a low permeability and quick drainage is impossible. The process of dissipation of excess PWP without any generation of effective stress is called sedimentation. As the drainage proceeds further, the solid particles start to contact each other. The further dissipation of the excess PWP should be accompanied with the generation of effective stress. The process of self-weight consolidation begins. In this thesis, no distinction was made between the sedimentation and self-weight consolidation of slurry deposition. More work is needed to improve the proposed solutions by making distinction between the two processes.
- In Gibson (1958) model and the ensuring solutions, the top surface of the deposition was assumed to be pervious with zero PWP. This may not always be true, especially after long period of deposition. When the slurry is placed on an impervious base, pore water flows upward and forms a decanted water pond at the top of the slurred material due to the drainage and consolidation. The hydraulic boundary condition assuming zero PWP along the top surface of the deposition could remain true (neglecting the possible evaporation), but the drainage through the top surface may not be true because the top surface of the deposition containing solids becomes the base of the decanted water pond. When the tailings are placed on a pervious base

or the backfill is retained by a pervious barricade in an underground mine stope, water can loss due to the drainage through the pervious base. The top surface of the decanted water pond can be lower than that estimated with the total volume of the deposition. If the slurry has a very high hydraulic conductivity or/and the filling rate is very small, unsaturation (with negative PWP) can even take place. More work is necessary to consider these conditions in the models.

- When a slurried backfill is placed in a mine stope, the drainage and consolidation take place first, resulting in the generation of effective stresses and arching effect. The shear stresses along the fill-rock interfaces tend to hold the backfill in place and slow down the drainage and consolidation. When the drainage and consolidation are slowed down, the increase of the effective stresses then becomes slower. The slower increase of the effective stresses in turn favors the drainage and consolidation. The treatment of the two processes needs several iterations to reach an equilibrium. A fully coupled model is needed to account for the two processes.
- Paste backfill is usually mixed with binder to fill underground mine stopes. The shrinkage or self-desiccation associated with the cementation can reduce the PWP in the backfilled stope. Neglecting this process tends to overestimate the PWP, resulting in conservative barricade design. More work is necessary to take into account the effect of the cementation, especially when the binder content is high or/and the filling rate is small.
- The proposed solutions for evaluating the excess PWP and stresses in slurried materials were mainly validated by numerical simulations. Laboratory and in situ measurements are deemed necessary to validate the proposed solutions and numerical models. A number of experimental studies have been reported to investigate the drainage and consolidation of slurried material. Most of them were conducted by following the ASTM standard (ASTM D2435-11/D2435M-11 and ASTM D4186/D4186M-12e1) or with the addition of seepage forces or external loads (Imai 1979; Sridharan and Prakash 1999; Aubertin et al. 1996; Qiu and Sego 2001; Azam 2010; Janbaz and Maher 2017). The testing conditions do not correspond to the undisturbed self-weight consolidation conditions. Only a few self-weight consolidation tests were reported. The few self-weight consolidation tests were carried out by instantaneous or very quick filling operation (Been and Sills 1981; Lin 1983; Pedroni 2011; Li et al. 2013; Saleh-Mbemba 2016). The filling rate is unknown. A few in situ measurement results are available in the literature

(Thompson et al. 2012). The results are difficult to be used to validate the proposed solutions because of the irregular stope geometry and uncertainty in the material properties (e.g. roughness of the rock wall surfaces, internal friction angle of the backfill, fractures in the surrounding rock walls). To reduce the number of uncertainties, a few self-weight consolidation tests have been realized in laboratory by filling a column with an uncemented paste backfill at a constant filling rate. The results presented in Appendix I show that the measured excess PWPs agree well with those predicted by the proposed solutions using a constant value of c_v. More work is required by considering different tests conditions (e.g. different filling rates, water contents, etc.).

In Chapter 9, the variation of the "short-term" stresses in an uncemented paste backfill as a function of the solid content has been investigated through laboratory tests. In the column tests, only the vertical total stresses were measured at the center and near the wall. However, the stability of barricades mainly depends on the horizontal total stresses. More tests are required to measure the PWP and horizontal total stresses by considering different column geometries and backfill properties. In addition, more work is necessary to investigate the uncertainty associated with the local arching effect around the stress sensors due to the contrast of stiffness between the sensors and the backfill.

CHAPTER 11 CONCLUSIONS AND RECOMMENDATIONS

11.1 Conclusion

The main objective of the thesis is to evaluate the excess PWP and stresses in the continuous deposition of slurried materials in confining structures (dams or underground mine stopes). Analytical, numerical and experimental studies were conducted to evaluate the excess PWP and stresses in the deposited slurried materials by considering the drainage and consolidation as well as the eventual arching effect in backfilled stopes. The solutions can be useful for the design of tailings impoundments or for the design of barricades in underground mine backfilled stopes. The main conclusions can be summarized as follows:

- Actual analytical solutions based on Gibson (1958) model were developed to evaluate the excess PWP during the slurry deposition on a pervious or impervious base. The proposed solutions were first validated against numerical results reported in the literature. Further validation was conducted by comparing the analytical results with the numerical results obtained with SIGMA/W and experimental results obtained by column tests with an impervious case (see Appendix I). Compared to Gibson (1958) solutions and numerical modeling, the proposed analytical solutions can be readily solved by EXCEL, which is accessible for practitioners. The proposed solutions constitute a simple and useful tool for engineers to conduct parametric sensitivity analysis in the preliminary stage of a project. According to the proposed solutions and the numerical modeling, the peak values of the PWP at the end of slurry deposition are smaller than the iso-geostatic overburden pressure. These results indicate that neglecting the drainage and consolidation, which take place during the filling operation, would overestimate the PWP and leads to overly conservative barricade design. Further analyses showed that the drainage and consolidation associated with the dissipation of excess PWP can be significantly influenced by the consolidation coefficient, filling rate and final backfilling height. The excess PWP can be controlled by using backfill of high consolidation coefficient, reducing the filling rate or/and reducing the backfill height.
- The estimation of the excess PWP in slurried materials after the slurry deposition is closely related to the stability of the confining structures as well as water and fill volume managements. The subsequent slurry deposition and reclamation activities needs evaluate the dissipation of

excess PWP and development of undrained shear strength in the deposited tailings. By solving the governing equations proposed by Gibson (1958), new pseudo analytical solutions have been proposed to evaluate the excess PWP in slurried materials after the slurry deposition on impervious and pervious bases, respectively. Numerical simulations with SIGMA/W were also conducted to validate the proposed solutions. The results show that the drainage and consolidation continuously take place after the slurry deposition. High excess PWP in the slurried material during and after the slurry deposition can be avoided by using backfill of high consolidation coefficient or/and a small filling rate. Similar results have been reported in previous studies (Fahey et al. 2009; El Mkadmi et al. 2014). However, it is for the first time that the excess PWP have been quantitatively evaluated by the application of analytical solutions. The proposed solutions constitute a simple and useful tool for evaluating the excess PWP in tailings impoundments or in underground mine backfilled stopes during the preliminary stage of a project.

- The barricade stability is closely related to the total stresses in backfilled stopes and on barricades. Pseudo analytical solutions have been presented to assess the total stresses in backfilled stopes during the filling operation by jointly considering the self-weight consolidation and arching effect. As a special case when the backfill has a very high permeability or when the filling rate is very small, the proposed solution reduces to the analytical solutions proposed by Li and Aubertin (2009a) for submerged backfill with a hydrostatic pressure. A MATLAB program was given to solve the proposed solutions and output the stresses in the backfilled stopes. The good agreements between the proposed solutions using Rankine active earth pressure coefficient K_a and the numerical results obtained by Plaxis2D indicate that the proposed solutions can be used to evaluate the effective and total stresses in backfilled stopes. Sample applications of the proposed solutions show that the stresses in backfilled stopes can be largely influenced by the consolidation coefficient, filling rate, internal friction angle of the backfill and the stope width. High consolidation coefficient or/and low filling rate is favorable for the drainage, resulting in high effective stress and low total stresses in the backfilled stopes.
- Paste backfill is gaining popularity over the years as it does not need to remove fine particles. This can help to further reduce the surface disposal of mine wastes. In addition, it can be transported by pipes without requiring a critical velocity. The in situ measurements conducted

by Thompson et al. (2012) in several mine stopes indicate that the "short-term" pressure and total stresses during the filling of paste backfill can be as high as the iso-geostatic overburden pressure due to the absence of effective stress and cementation. These results do not correspond to the suggestions given in some handbooks, which state that the pressures on barricade exerted by paste backfill can be small and the construction of light barricades is enough. To clarify this puzzling issue, column tests were conducted to measure the vertical total stresses at the center and near the wall of a column by using an uncemented paste backfill having different solid contents. The results show that the vertical total stresses at the center and near the wall decrease as the solid content of the backfill increases. The vertical total stress near the wall is always smaller than that at the center. When the backfill has high solid content, the vertical total stress near the wall can be small. The results correspond to the suggestions given in the handbooks. The construction of light barricades is enough to retain the paste backfill. When the paste backfill has low solid content, the vertical total stress near the wall can be very high. The construction of strong barricade is necessary to retain the paste backfill in place.

11.2 Recommendations

In addition to the outcomes presented in the thesis, several recommendations are given below to better understand the hydro-mechanical behaviors of the slurried materials deposited in tailings impoundments or underground mine stopes, including:

- Only a few tests have been done to validate the proposed solution for evaluating the excess PWP during the slurry deposition on an impervious base (See Appendix I). More experimental works are highly recommended to calibrate and validate the proposed solutions by considering different slurried materials, filling rates, solid contents, and column geometries.
- The proposed solutions were developed by considering small strain consolidation with constant permeability (k), constrained modulus (M') and consolidation coefficient (c_v). More experimental work is necessary to evaluate the variation of the consolidation coefficient c_v with the drainage and consolidation of the slurried materials. More work is also needed to take into account the large strain consolidation (Gibson et al. 1981; Cargill 1985; Feldkamp 1989; Morris 2002) and the evolution of the consolidation coefficient c_v.

- In the literature, several experimental results have been reported to measure the PWP and total stresses during or after the slurry deposition (e.g., Thompson et al. 2009, 2012; Grabinsky and Shahsavari 2015; Saleh-Mbemba and Aubertin 2018). These experimental data merit to be exploited by applying the proposed solutions.
- Through the calculation of the dissipation of the excess PWP, the water flow and the settlement of the slurried material during and after the deposition can be estimated. The results can be useful to manage the water and volume of materials for tailings impoundments.
- More work is necessary to analytically and experimentally study the process of sedimentation (dissipation of excess PWP without generation of effective stresses).
- For mine stope backfilled with cemented paste backfill, the cementation can take place, especially when the cement content is high and the filling rate is small. The cementation of the cemented backfill needs to consume pore water, leading to the change of the hydraulic and mechanical properties of the backfill and reduction of the PWP. For many cases, the cement content is low and the effect of the cementation can be negligible for the design of barricade. In all cases, the barricade design by neglecting the effect of cementation is conservative. Nevertheless, more elaborate models are desirable to account for the cementation in the estimation of the excess PWP and stresses in backfilled stopes.
- The proposed solutions were developed based on Gibson (1958) model, in which the moving top surface of the slurry deposition was assumed to be permeable with zero PWP. This hydraulic boundary condition does not take into account the formation of decanted water pond or unsaturation at the top part of the settled deposition. More work is necessary by considering more representative boundary conditions in the models.
- The process of drainage and consolidation and the development of arching effect can influence each other during the slurry deposition. A fully coupled model is necessary to take into account the two processes through several iterations.
- More work is necessary to extend the one-dimensional drainage and consolidation models to 2D and even 3D models by considering lateral drainage.
- More experimental work is necessary to measure the PWP, vertical and horizontal total stresses in paste backfilled columns during and shortly after the placement of the paste backfill by

considering different types of paste backfill with different solid contents, filling rates and dimensions of column.

BIBLIOGRAPHY

Abdelaal, A. (2011). *Early age mechanical behavior and stiffness development of cemented paste backfill with Sand*. Doctoral dissertation, The University of Toronto, Toronto, Canada.

Agurto-Detzel, H., Bianchi, M., Assumpção, M., Schimmel, M., Collaço, B., Ciardelli, C., … Calhau, J. (2016). The tailings dam failure of 5 November 2015 in SE Brazil and its preceding seismic sequence. *Geophysical Research Letters, 43*(10), 4929-4936.

Ahmed, S.I., & Siddiqua, S. (2014). A review on consolidation behavior of tailings. *International Journal of Geotechnical Engineeering, 8*(1), 102-111.

Alam, R., Shang, J.Q., & Islam, S. (2017). Electrophoresis and its applications in oil sand tailings management. *International Journal of Mineral Processing, 161*, 41-49.

Alberta Energy Resources Conservation Board. (2009). *Directive 074: Tailings performance criteria and requirements for oil sands mining schemes*. Calgary, AB, Canada.

Aref, K., Moss, A., & Durston, K. (1992). Design issues for low moisture content backfill. *CIM Montréal*, 270-281.

Askew, J.E., McCarthy, P.L., & Fitzerald, D.J. (1978). *Backfill research for pillar extraction at ZC/NBHC*. Paper presented at the Proceedings of Mining with Backfill: 12th Canadian Rock Mechanics Symposium, CIM, Montréal, (pp. 100-110).

Asmar NH. (2004) Partial differential equations and boundary value problems. Pearson Education, Upper Saddle River, NJ.

ASTM International. (2011). *Standard Test Methods for One-Dimensional Consolidation Properties of Soils Using Incremental Loading*. Standard ASTM D2435/D2435M-11, West Conshohocken, PA.

ASTM International. (2012). *Standard Test Method for One-Dimensional Consolidation Properties of Saturated Cohesive Soils Using Controlled-Strain Loading*. Standard ASTM D4186/D4186M-12e1, West Conshohocken, PA.

Aubertin, M., & McKenna, G. (2016). *Tailings disposal challenges and prospects for oil sands mining operation*. Paper presented at the Geo-Chicago, Chicago, USA (pp. 359-371).

Aubertin, M., Bussiere, B., & Bernier, L. (2002). *Environnement et gestion des rejets miniers. Presses* [Manual on CD-ROM]. Internationales Polytechnique, Montréal, Canada.

Aubertin, M., Bussiere, B., & Chapuis, R.P. (1996). Hydraulic conductivity of homogenized tailings from hard rock mines. *Canadian Geotechnical Journal, 33*(3), 470-482.

Aubertin, M., Bussière, B., Joanes, A.M., Monzon, M., Gagnon, D., Barbera, J.M., … Bernier, L. (1999). *Projet sur les barrières sèches construites à partir de résidus miniers, Phase II: essais en place*. (Report No. 2.22.2c). Ottawa, Ont: CANMET Secretariat.

Aubertin, M., Li, L., Arnoldi, S., Belem, T., Bussière, B., Benzaazoua, M., & Simon, R. (2003). *Interaction between backfill and rock mass in narrow stopes*. Paper presented at the Soil and Rock America 2003, Essen, Germany (pp, 1157–1164).

Aubertin, M., Mbonimpa, M., Jolette, D., Bussière, B., Chapuis, R.P., James, M., & Riffon, O. (2002). *Stabilité géotechnique des ouvrages de retenue pour les résidus miniers: problème persistants et méthodes de contrôle*. Paper presented at the Environnement et les mines: Défis et Perspectives, Rouyn-Noranda, Québec (pp, 526–552).

Aubertin, M. (1999). *Application de la mécanique des sols pour l'analyse du comportement des remblais miniers souterrains*. Short Course (unpublished notes). Paper presented at the 14th Colloque en Contrôle de Terrain, Val-d'Or, Québec.

Aubertin, M. (2013). *Waste rock disposal to improve the geotechnical and geochemical stability of piles*. Paper presented at the World Mining Congress, Montréal, Québec.

Azam, S., & Li, Q. (2010). Tailings dam failures: A review of the last one hundred years. *Geotechnical News, 28*(4), 50-54.

MineDesign queen's university. (2011). Backfill. Retrieved from http://minewiki.engineering.queensu.ca/mediawiki/index.php/Backfill.

Barbour, S.L., Wilson, G.W., & St-Arnaud, L.C. (1993). Evaluation of the saturated–unsaturated groundwater conditions of a thickened tailings deposit. *Canadian Geotechnical Journal, 30*(6), 935-946.

Beya, F.K. (2016). *Étude du transfert de chaleur dans les remblais en pâte cimentés curant sous les conditions aux frontières des chantiers miniers dans le pergélisol*. (Master's thesis. École Polytechnique de Montréal, Montréal, QC).

Been, K., & Sills, G.C. (1981). Self-weight consolidation of soft soils: an experimental and theoretical study. *Geotechnique, 31*(4), 519-535.

Behnam, F., James, M., & Aubertin, M. (2015). Effect of waste rock inclusions on the seismic stability of an upstream raised tailings impoundment: a numerical investigation. *Canadian Geotechnical Journal, 52*(12), 1930-1944.

Beier, N., Wilson, W., Dunmola, A., & Sego, D. (2013). Impact of flocculation-based dewatering on the shear strength of oil sands fine tailings. *Canadian Geotechnical Journal, 50*(9), 1001-1007.

Belem, T., & Benzaazoua, B. (2008). Design and application of underground mine paste backfill technology. *Geotechnical and Geological Engineering, 26*(2), 147-174.

Belem, T., EI Aatar, O., Bussière, B., & Benzaazoua, M. (2016). Gravity-driven 1-D consolidation of cemented paste backfill in 3-m-high columns. *Innovative Infrastructure Solutions, 1*(1), 37.

Belem, T., Benzaazoua, M., & Bussière, B. (2000). Mechanical behaviour of cemented paste backfill. Papre presented at the 53th Candadian Geotechnical Conference, Montréal, Canada.

Belem, T., Harvey, A., Simon, R., & Aubertin, M. (2004). *Measurement and prediction of internal stresses in an undergound opening during its filling with cemented fill*. Paper presented at the Symposium on Ground support in mining and underground construction. Taylor and Francis Group, London, Australia (pp. 619–630).

Benckert, A., & Eurenius, J. (2001). *Tailings dam constructions*. Paper presented at the Seminar on safe tailings dam constructions, Gällivare, Sweden.

Berilgen, S.A., Berilgen, M.M., & Ozaydin, K.I. (2006). Assessment of consolidation behavior of Golden Horn marine dredged material. *Marine Georesources Geotechnology, 24*(1), 1–16.

Berndt, C.C., Rankine, K.J., & Sivakugan, N. (2007). Materials properties of barricade bricks for mining applications. *Geotechnical and Geological Engineering, 25*(4), 449-471.

Blight, G.E. (1984). Soil mechanics principles in underground mining. *Journal of Geotechnical Engineering, 110*(5), 567-581.

Bloss, M.L., & Chen, J. (1998). *Drainage research at Mount Isa Mines limited 1992-1997*. Paper presented at the 6th International Symposium on Mining with Backfill, Brisbane, Australia (pp, 111-116).

Bloss, M.L. (1992). *Prediction of cemented rock fill stability: design procedures and modelling techniques*. (Doctoral dissertation, University of Queensland, Brisbane, Australia).

Boger, D., Scales, P., & Sofra, F. (2006). Rheological concepts. In Jewell and Fourie (Eds), *Paste and Thickened Tailings-A Guide* (2nd ed pp. 25-37).

Bolduc, F.L., & Aubertin, M. (2014). Numerical investigation of the influence of waste rock inclusions on tailings consolidation. *Canadian Geotechnical Journal, 51*(9), 1021–1032.

Bowles, J.E. (1988). Foundation analysis and design (5th ed.), Singapore: McGraw-Hill International Editions.

Brady, B.H.G., & Brown, E.T. (1993). Rock mechanics for underground mining. (2nd ed.) Chapman and Hall, London: Springer.

Brinkgreve, R.B.J., Kumarswamy, S., & Swolfs, W.M. (2014). PLAXIS (2014) [Computer software]. Delft, Netherlands.

Bussiere, B. (2007). Colloquium 2004: Hydrogeotechnical properties of hard rock tailings from metal mines and emerging geoenvironmental disposal approaches. *Canadian Geotechnical Journal, 44*(9), 1019-1052.

Caceres, C. (2005), Effect of backfill on longhole open stoping. (Master's thesis, University of British Columbia, Vancouver, Canada).

Cargill, K.W. (1984). Prediction of consolidation of very soft soil. *Journal of Geotechnical Engineering, 110*(6), 775–795.

Caughill, D.L., Morgenstern, N.R., & Scott, J.D. (1993). Geotechnics of nonsegregating oil sand tailings. *Canadian Geotechnical Journal, 30*(5), 801-811.

Canadian geotechnical Society. (2006). *Canadian foundation engineering manual* (4th ed.), Vancouver, Canada.

Chapuis, R.P., & Aubertin, M. (2003). On the use of the Kozeny-Carman equation to predict the hydraulic conductivity of soils. *Canadian Geotechnical Journal, 40*(3), 616-628.

Clayton, S., Grice, T.G., & Boger, D.V. (2003). Analysis of the slump test for on-site yield stress measurement of mineral suspensions. *International Journal of Mineral processing, 70*(1), 3-21.

Cooke, R. (2006). *Thickened and paste tailings pipeline systems: design procedure - Part 1*. Paper presented at the international seminar on Pasteand thickened tailings, ACG, Perth, Australia.

Cui, L., & Fall, M. (2008). Mathematical modelling of cemented tailings backfill: a review. International Journal of Mining, Reclamation and Environment, 1-20.

Cui, L., & Fall, M. (2016). Multiphysics model for consolidation behavior of cemented paste backfill. International Journal of Geomechnics, 17(3), 04016077.

Cui, L., & Fall, M. (2017). Modeling of pressure on retaining structures for underground fill mass. *Tunnelling and Underground Space Technology, 69*, 94-107.

Cui, L., & Fall, M. (2018). Modeling of self-desiccation in a cemented backfill structure. *International Journal for Numerical and Analytical Methods in Geomechanics, 42*(3), 558-583.

Darling, P. (2011). *SME mining engineering handbook* (3th ed.). Society for Mining, Metallurgy, and Exploration, Denver, US.

Das, B.M., & Sobhan, K. (2010). Principles of geotechnical engineering. (8th ed). Stamford: Cengage Learning.

Dobry, R., & Alvarez, L. (1967). Seismic failures of Chilean tailings dams. *Journal of Soil Mechanics and Foundations Division, 93*(6), 237-260.

Doherty, J.P., Hasan, A., Suazo, G.H., & Fourie, A. (2015). Investigation of some controllable factors that impact the stress state in cemented paste backfill. *Canadian Geotechnical Journal, 52*(12), 1901-1912.

Doherty, J.P. (2015). A numerical study into factors affecting stress and PWP in free draining mine stopes. *Computers and Geotechnics, 63*, 331-341.

Dragana, S., & Grabinsky, M. (2013). Apparent yield stress measurement in cemented paste backfill. *International Journal of Mining, Reclamation and Environment, 27*(4), 231-256.

Dzuy, N.Q., & Boger, D.V. (1985). Direct yield stress measurement with the vane method. *Journal of Rheology, 29*(3), 335-347.

El Mkadmi, N., Aubertin, M., & Li, L. (2014). Effect of drainage and sequential filling on the behavior of backfill in mine stopes. *Canadian Geotechnical Journal, 51*(1), 1–15.

Energy Resources Conservation Board. (2009). *Directive 074: Tailings performance criteria and requirements for oil sands mining schemes.* Calgary, Alberta, Canada.

Environmental Protection Agency (EPA). (1994). Design and evaluation of tailings dams. (Report No. EPA530-R-94-038). Washington.

Essayad, K. (2015). Développement de protocoles expérimentaux pour caractériser la consolidation de résidus miniers saturés et non saturés à partir d'essais de compression en colonne. (Doctoral dissertation, École Polytechnique de Montréal, Montréal, Canada).

Fahey, M., Helinski, M., & Fourie, A. (2009). Some aspects of the mechanics of arching in backfilled stopes. *Canadian Geotechnical Journal, 46*(11), 1322-1336.

Fahey, M., Helinski, M., & Fourie, A. (2010). Consolidation in accreting sediments: Gibson's solution applied to backfilling of mine stopes. *Géotechnique, 60*(11), 877-882.

Fall, M., Adrien, D., Celestin, J.C., Pokharel, M., & Toure, M. (2009). Saturated hydraulic conductivity of cemented paste backfill. *Minerrals Engineering, 22*(15), 1307-1317.

Farkish, A., & Fall, M. (2014). Consolidation and hydraulic conductivity of oil sand mature fine tailings dewatered by using super absorbent polymer. *Journal of Geotechnical and Geoenvironmental Engineering, 140*(7), 06014006.

Feldkamp, J.R. (1989). Numerical analysis of one-dimensional nonlinear large-strain consolidation by the finite element method. *Transport in Porous Media, 4*(3), 239–257.

Ferdosi, B., James, M., & Aubertin, M. (2015). Effect of waste rock inclusions on the seismic stability of an upstream raised tailings impoundment: a numerical investigation. *Canadian Geotechnical Journal, 52*(12), 1930-1944.

Fox, P.J. (2000). *CS4: A large strain consolidation model for accreting soil layers*. Paper presented at the Geotechnics of high water content materials, ASTM International, West Conshohocken, PA.

Gade, V.K., & Dasaka, S.M. (2018). Calibration of earth pressure sensors. *Indian Geotechnical Journal, 48*(1), 142-152.

Ganesalingam, D., Nagaratnam, S., & Ameratunga, J. (2012). Influence of settling behavior of soil particles on the consolidation properties of dredged clay sediment. *Journal of Waterway, Port, Coast, and Ocean Engineering, 139*(4), 295-303.

Garcia, L.C., Ribeiro, D.B., Roque, F.O., Ochoa-Quintero, J.M., & Laurance, W.F. (2016). Brazil's worst mining disaster: corporations must be compelled to pay the actual environmental costs. *Ecological Applications, 27*(1), 5-9.

Gawu, S.K.Y., & Fourie, A.B. (2004). Assessment of the modified slump test as a measure of the yield stress of high-density thickened tailings. *Canadian Geotechnical Journal, 41*(1), 39-47.

GEO-SLOPE. (2008) Stress-deformation modeling with SIGMA/ W 2007 (3th ed.). GEO-SLOPE International Ltd, Calgary, Alberta, Canada.

Gibson, R.E., Schiffman, R.L., & Cargill, K.W. (1981). The theory of one-dimensional consolidation of saturated clays. II. Finite nonlinear consolidation of thick homogeneous layers. *Canadian Geotechnical Journal, 18*(2), 280–293.

Gibson, R.E., Schiffman, R.L., & Whitman, R.V. (1989). On two definitions of excess pore water pressure. *Geotechnique, 39*(1), 169-171.

Gibson, R.E. (1958). The progress of consolidation in a clay layer increasing in thickness with time. *Géotechnique, 8*(4), 171-182.

Godbout, J., Bussière, B., & Belem, T. (2007). *Evolution of cemented paste backfill saturated hydraulic conductivity at early curing time*. Paper presented at the Canadian Geotechnical Conference, GeoMontréal, Ottwawa, Canada.

Goodwin, E.T. (1949). *The evaluation of integrals of the form* $\int_{-\infty}^{+\infty} f(x)e^{-x^2}\,dx$. Paper presented at the Mathematical Proceedings of the Cambridge Philosophical Society. Cambridge University, London, UK (pp. 241-245).

Grabinsky, M.W., Bawden, W.F., Simon, D., Thompson, B.D., & Veenstra, R.L. (2013). *In situ properties of cemented paste backfill from three mines*. Paper presented at the 66th Canadian Geotechnical Conference, Montréal, Canada.

Grabinsky, M.W., Simon, D., Thompson, B.D., Bawden, W.F., & Veenstra, R.L. (2014). *Interpretation of as-placed cemented paste backfill properties from three mines*. Paper presented at the 11th International Symposium on Mining with Backfill, Australian Centre for Geomechanics, Perth, Australia.

Grice, A.G., Wilwain, A., & Urquhart, K. (1993). *Backfilling operations at Mount Isa Mines 1998-1992*. Paper presented at the 5th International Symposium on Mining with Backfill: Minefill'93, Johannesburg, SAIMM. (pp. 369-373).

Grice, A.G. (1998a). *Stability of hydraulic backfill barricades*. Paper presented at the 6th International Symposium on Mining with Backfill, Brisbane, Australia (pp. 117-120).

Grice, A.G. (1998b). *Underground mining with backfill*. Paper presented at the 2nd Annual Summit-Mine Tailings Disposal Systems, Brisbane, Australia (pp. 234-239).

Grice, A.G. (2001). *Recent mine fill developments in Australia*. Paper presented at the 7th International Symposium on mining with Backfill, Seattle, USA (pp. 351-357).

Grice, T. (1998). *Stability of hydraulic backfill barricades*. Paper presented at the 6th International Symposium on Mining with Backfill, Victoria, Australia (pp. 117-120).

Grice, T. (2001). *Recent mine fill developments in Australia*. Paper presented at the 7th International Symposium on Mining with Backfill, Society for Mining, Littleton, Colorado (pp, 351–357).

Hambley, D.F. (2011). Backfill mining. SME Mining Engineering Handbook (3th ed.), Englewood: Society for Mining, Metallurgy, and Exploration, Inc.

Hamrin, H. (2001). Chapter 1: Underground mining methods and applications. In W.A. Hustrulid & R.L. Bullock (Eds.), *Underground Mining Methods: Engineering Fundamentals and International Case Studies*. (pp. 3-14).

Hartman, H.L., & Britton, S.G. (1992). SME mining engineering handbook (2th ed.). Denver: Society for Mining, Metallurgy, and Exploration, Inc.

Hassani, F., & Archibald, J. (1998). Mine backfill. (CD-ROM). Canadian Institute of Mining, Metallurgy and Petroleum, Montréal, Canada.

He, J., Chu, J., Tan, S.K., Vu, T.T., & Lam, K.P. (2017). Sedimentation behavior of flocculant-treated soil slurry. *Marine Georesources & Geotechnology, 35*(5), 593-602.

Helinski, M., Fahey, M., & Fourie, A. (2011). Behavior of cemented paste backfill in two mine stopes: measurements and modeling. *Journal of Geotechnical and Geoenvironment Engineering, 137*(2), 171–182.

Helinski, M., Fourie, A., & Fahey, M. (2006). *Mechanics of early age CPB*. Paper presented at the 9th International Seminar on Paste and Thickened Tailings, Perth, Australia (pp. 313–322).

Helinski, M., Fourie, A., Fahey, M., & Ismail, M. (2007). Assessment of the self-desiccation process in cemented mine backfills. *Canadian Geotechnical Journal, 44*(10), 1148-1156.

Herget, G. (1988). Stresses in rock. Rotterdam, Netherlands.

Holtz, R.D., & Kovacs, W.D. (1981). An introduction to geotechnical engineering. Englewood Cliffs: Prentice-Hall, Michigan University.

Hu, L., Wu, H., Zhang, L., Zhang, P., & Wen, Q. (2016). Geotechnical properties of mine tailings. *Journal of Materials in Civil Engineering, 29*(2), 04016220.

Hunt, W.G. (1988). The use of consolidated backfill for pillar extraction in room and pillar mining: An integrated design rationale. (Master's thesis. McGill University, Montréal, Canada).

International Commission on Large Dams. (2001). Tailings dams–risk of dangerous occurrences, lessons learnt from practical experiences (Bulletin 121). Commission Internationale des Grands Barrages, Paris.

Imai, G. (1979). Development of a new consolidation test procedure using seepage force. *Soils and Foundations, 19*(3), 45-60.

Jaditager, M., & Sivakugan, N. (2017). Influence of fly ash–based geopolymer binder on the sedimentation behavior of dredged mud. *Journal of Waterwway, Port, Coastal, and Ocean Engineering, 143*(5), 04017012.

Jahanbakhshzadeh, A., Aubertin, M., & Li, L. (2017). A new analytical solution for the stress state in inclined backfilled mine stopes. *Geotechnical and Geological Engineering, 35*(3), 1151-1167.

Jahanbakhshzadeh, A., Aubertin, M., & Li, L. (2018a). Analysis of the stress distribution in inclined backfilled stopes using closed-form solutions and numerical simulations. *Geotechnical and Geological Engineering, 36*(2), 1011-1036.

Jahanbakhshzadeh, A., Aubertin, M., & Li, L. (2018b). Three-dimensional stress state in inclined backfilled stopes obtained from numerical simulations and new closed-form solution. *Canadian Geotechnical Journal, 55*(6), 810-828.

Jakubick, A.T., McKenna, G., & Robertson, A.M. (2003). *Stabilization of tailings deposits: International experience*. Paper presented at the Mining and the Environment III, Sudbury, Ontario, Canada (pp. 1-9).

Jaky, J. (1948). *Pressure in silos*. Paper presented at the 2nd International Conference on Soil Mechanics and Foundation Engineering, Rotterdam, The Netherlands.

James, M., Aubertin, M., Wijewickreme, D., & Wilson, G.W. (2011). A laboratory investigation of the dynamic properties of tailings. *Canadian Geotechnical Journal, 48*(11), 1587-1600.

James, M. (2009). The use of waste rock inclusions to control the effects of liquefaction in tailings impoundments. (Doctoral dissertation, Ecole Polytechnique de Montréal, Montréal, Canada).

Janbaz, M., & Maher, A. (2017). Consolidation and permeability behaviour of Newark Bay's dredged sediments by seepage-induced consolidation test. *Internationa Journal of Geotechnical Engineering, 11*(2), 120-126.

Janssen, H.A. (1895). Versuche über Getreidedruck in Silozellen. *Zeitschrift Verein Ingenieure, 39*, 1045-1049.

Jaouhar, E.M., Li, L., & Aubertin, M. (2018). An analytical solution for estimating the stresses in vertical backfilled stopes based on a circular arc distribution. *Geomechanics and Engineering, 15*(3), 889-898.

Jeeravipoolvarn, S., Scott, J.D., & Chalaturnyk, R.J. (2009). 10 m standpipe tests on oil sands tailings: long-term experimental results and prediction. *Canadian Geotechnical Journal, 46*(8), 875-888.

Jeyapalan, J.K., Duncan, J.M., & Seed, H.B. (1983). Investigation of flow failures of tailings dams. *Journal of Geotechnical Engineering, 109*(2), 172-189.

Jewell, R.J., & Fourie, A.B. (2002). Paste and thickened tailings - A guide (2th ed.). ACG, Perth, Australia.

Jung, S.J., & Biswas, K. (2002). Review of current high density paste fill and its technology. *Minerral Resources Engineering, 11*(2), 165–182.

Knutsson, S. (1981). *Stresses in the hydraulic backfill from analytical calculations and in-situ measurements*. Paper presented at the Application of Rock Mechanics to Cut and Fill Mining, London. (pp. 261–268).

Komurlu, E., & Kesimal, A. (2015). Sulfide-rich mine tailings usage for short-term support purposes: An experimental study on paste backfill barricades. *Geomechanics and Engineering, 9*(2), 195-205.

Komurlu, E., Kesimal, A., & Demir, S. (2016). Experimental and numerical analyses on determination of indirect (splitting) tensile strength of cemented paste backfill materials under different loading apparatus. *Geomechanics and Engineering, 10*(6), 775-791.

Kuganathan, K. (2001). Mine backfilling, backfill drainage and bulkhead construction-a safety first approach. Australian Mining Monthly, (pp. 58–64).

Kuganathan, K. (2002). *A model to predict bulkhead pressures for safe design of bulkheads*. Paper presented at the Filling with Hydraulic Fills Seminar, Section 6, Australian Centre for Geomechanics, Perth, Australia.

Kump, D. (2001). Backfill — whatever it takes. *Mining Engineering, 53*(1), 50–52.

Lambe, T.W., & Whitman, R.V. (1969). Soil mechanics. New York: John Wiley.

Lessard, G. (2011). Essais d'infiltration sur la halde à stériles Petit-Pas de la mine Tio, Havre-St-Pierre. (Master's thesis. Polytechnique Montréal, Montréal, Canada).

Li, L., & Aubertin, M. (2008). An improved analytical solution to estimate the stress state in subvertical backfilled stopes. *Canadian Geotechnical Journal, 45*(10), 1487-1496.

Li, L., & Aubertin, M. (2009a). Influence of water pressure on the stress state in stopes with cohesionless backfill. *Geotechnical and Geological Engineering, 27*(1), 1–11.

Li, L., & Aubertin, M. (2009b). A three-dimensional analysis of the total and effective stresses in submerged backfilled stopes. *Geotechnical and Geological Engineering, 27*(4), 559–569.

Li, L., & Aubertin, M. (2009c) Horizontal pressure on barricades for backfilled stopes: Part I: Fully drained conditions. *Canadian Geotechnical Journal, 46*(1), 37–46.

Li, L., & Aubertin, M. (2009d). Horizontal pressure on barricades for backfilled stopes: Part II: Submerged conditions. *Canadian Geotechnical Journal, 46*(1), 47–56.

Li, L., & Aubertin, M. (2010). An analytical solution for the nonlinear distribution of effective and total stresses in vertical backfilled stopes. *Geomechanics and Geoengineering, 5*(4), 237-245.

Li, L., & Aubertin, M. (2011). Limit equilibrium analysis for the design of backfilled stope barricades made of waste rock. *Canadian Geotechnical Journal, 48*(11), 1713-1728.

Li, L., & Aubertin, M. (2014). An improved method to assess the required strength of cemented backfill in underground stopes with an open face. *International Journal of Mining Science and Technology, 24*(4), 549–58.

Li, L., & Yang, P.Y. (2015). A numerical evaluation of continuous backfilling in cemented paste backfilled stope through an application of wick drains. *International Journal of Mining Science and* Technology, 25(6), 897-904.

Li, L., & Zheng, J. (2017). *A conceptual analytical solution for estimating the short-term pressure of paste fill varying from viscous to liquid state, placed in mine stopes*. Paper presented at the 70th Canadian Geotechnical Conference, Canadian Geotechnical Society, Ottawa, Canada.

Li, L., Alvarez, I.C., & Aubertin, J.D. (2013). Self-weight consolidation of a slurried deposition: tests and interpretation. *International Journal of Geotechnical Engineering, 7*(2), 205–213.

Li, L., Aubertin, M., & Belem, T. (2005). Formulation of a three dimensional analytical solution to evaluate stress in backfilled vertical narrow openings. *Canadian Geotechnical Journal, 42*(6), 1705–1717 (with Erratum 2006, 43(3), 338–339).

Li., L, Aubertin, M., Simon, R., Bussière, B., & Belem, T. (2003). *Modeling arching effects in narrow backfilled stopes with FLAC*. Paper presented at the 3rd International FLAC Symposium, A. A. Balkema, Rotterdam, Netherlands. (pp. 211–219).

Li, L. (2013). A new concept of backfill design – application of wick drains in backfilled stopes. *International Journal of Mining Science and Technology, 23*(5), 763–70.

Li, L. (2013). Beneficial Experience from teaching and education to research and development. *Creative Education, 3*(7), 148–153.

Li, L. (2014). A numerical analysis of the application of wick drains for continuous backfilling in mine backfilled stopes. *Geosynthetic Mining Solutions*, (pp. 369-382).

Li, L. (2014). Analytical solution for determining the required strength of a side-exposed mine backfill containing a plug. *Canadian Geotechnical Journal, 51*(5), 508-519.

Lin, T.W. (1983). Sedimentation and self-weight consolidation of dredge spoil. (Doctoral dissertation, Iowa State University, Iowa, United States).

Mahaut, F., Mokeddem, S., Chateau, X., Roussel, N., & Ovarlez, G. (2008). Effect of coarse particle volume fraction on the yield stress and thixotropy of cementitious materials. *Cement and concrete research, 38*(11), 1276-1285.

Malekzadeh, M., & Sivakugan, N. (2017). One-dimensional electrokinetic stabilization of dredged mud. *Marine Georesources & Geotechnology, 35*(5), 603-609.

Marston, A. (1930). The theory of external loads on closed conduits in the light of latest experiments. Iowa Engineering Experiment Station, Ames, Iowa (pp. 138-170).

Matlab, M (2011). MATLAB—The language of technical computing (Version 2014). [Computer software]. Retrieved from http://www.mathworks.com/products/matlab/

Mbonimpa, M., Aubertin, M., Chapuis, R.P., & Bussière, B. (2002). Practical Pedotransfer Functions for Estimating the Saturated Hydraulic Conductivity. *Geotechnical and Geological Engineering, 20*(3), 235-259.

McLeod, H., & Bjelkevik, A. (2017). *Tailings Dam Design: Technology Update (ICOLD Bulletin)*. Paper presented at the 85th Annual Meeting of International Commission on Large Dams, Prague, Czech Republic.

Meyerhof, G.G. (1957). *Discussion on research on determining the density of sands by penetration testing*. Paper presented at the 4th International Conference on Soil Mechanics and Foundation Engineering, London, UK (pp. 110).

Miao, X.X., Zhang, J.X., & Feng, M.M. (2008). Waste-filling in fully-mechanized coal mining and its application. *International Journal of Mining Science and Technology, 18*(4), 479–82.

Mitchell, R.J., & Roettger, J.J. (1984). Bulkhead pressure measurements in model fill pours. *CIM Bulletin, 77*(868), 50–54.

Mitchell, R.J., Smith, J.D., & Libby, D.J. (1975). Bulkhead pressures due to cemented hydraulic mine backfills. *Canadian Geotechnical Journal, 12*(3), 362–371.

Molson, J.W., Fala, O., Aubertin, M., & Bussère, B. (2005). Numerical simulations of pyrite oxidation and acid mine drainage in unsaturated waste rock piles. *Journal of Contaminant Hydrology, 78*(4), 343-371.

Morris, PH. (2002). Analytical solutions of linear finite-strain one-dimensional consolidation. *Journal of Geotechnical and Geoenvironment Engineering, 128*(4), 319-326.

Murata, J. (1984). Flow and deformation of fresh concrete. *Materiaux et Construction, 17*(2), 117-129.

Naguleswaran, N., Sivakugan, N., & Veenstra, R.L. (2017). Laboratory study on strength development in cemented paste backfills. *Journal of Materials in Civil Engineering, 29*(7), 04017027.

Nehdi, M., & Rahman, M.A. (2004). Estimating rheological properties of cement pastes using various rheological models for different test geometry, gap and surface friction. *Cement and Concrete Research, 34*(11), 1993-2007.

Ning, J., Wang, J., Tan, Y., Zhang, L., & Bu, T. (2017). In situ investigations into mining-induced overburden failures in close multiple-seam longwall mining: a case study. *Geomechanics and Engineering, 12*(4), 657-673.

Niroshan, N., Sivakugan, N., & Veenstra, R.L. (2017). Laboratory study on strength development in cemented paste backfills. *Journal of Materials in Civil Engineering, 29*(7), 04017027.

Pakalnis, R.T., & Hughes, P.B. (2011). Sublevel stoping. In P. Darling (Eds.), *SME Mining Engineering Handbook* (3nd ed.).

Palarski, J. (1994). Design of backfill as support in Polish coal mines. *Journal of Southern African Institute of Mining and Metallurgy, 94*(8), 218-226.

Palarski, J. (2014). Filling of voids in coal longwall mining with caving - technical, environmental and safety aspects. In Y Potvin & AG Grice (Eds), *Mine Fill 2014*.

Pane, V., & Schiffman, R.L. (1985). A note on sedimentation and consolidation. *Géotechnique, 35*(1), 69-72.

Park, J., Chun, Y.W., Trung, H.T., & Kim, Y.U. (2014). Effect of ultrasonic energy on self-weight consolidation of clay minerals. *KSCE Journal of Civil Engineering, 18*(4), 971-974.

Pashias, N., Boger, D.V., Summers, J., & Glenister, D.J. (1996). A fifty cent rheometer for yield stress measurement. *Journal of Rheology, 40*(6), 1179-1189.

Pedroni, L., & Aubertin, M. (2008). *Evaluation of sludge consolidation from hydraulic gradient tests conducted in large size columns*. Paper presented at the 61th Canadian Geotechnical Conference and the 9th Joint CGS/IAH-CNC Groundwater Conference, Edmonton, Canada.

Pedroni, L., & Aubertin, M. (2013). *Measurement and Simulation of the Large Strain Consolidation of AMD Treatment Sludge*. Paper presented at the 66th Canadian Geotechnical

Conference, Geosciences for Sustainability, Montréal, Canada, GeoMontréal, Montréal, Canada.

Pedroni, L. (2011). Étude expérimentale et numérique de la sédimentation et de la consolidation des boues de traitement des eaux acides. (Doctoral dissertation, École Polytechnique de Montréal, Montréal, Canada).

Peele, R. (1941). Mining Engineers' Handbook. Canada: John Wiley and Sons Inc.

Peregoedova, A. (2012). Étude expérimentale des propriétés hydrogéologiques des roches stériles à une échelle intermédiaire de laboratoire. (Master's Thesis, Polytechnique Montréal, Montréal, Canada).

Pirapakaran, K., & Sivakugan, N. (2007). A laboratory model to study arching within a hydraulic fill stope. *Geotechnical Testing Journal, 30*(6), 496–503.

Pirapakaran, K., & Sivakugan, N. (2007a). Arching within hydraulic fill stopes. *Geotechnical and Geological Engineering, 25*(1), 25-35.

Potvin, Y., Thomas, E., & Fourie, A. (2005). *Handbook on mine fill*. Nedlands, Australia: Australian Centre of Geomechanics.

Priscu, C. (1999). Behavior of mine tailings dams under high tailings deposition rates. (Doctoral dissertation, McGill University, Montréal, Canada).

Qiu, Y.X., & Sego, D.C. (2001). Laboratory properties of mine tailings. *Canadian Geotechnical Journal, 38*(1), 183-190.

Queiroz, H.M., Nóbrega, G.N., Ferreira, T.O., Almeida, L.S., Romero, T.B., Santaella, S.T., … Otero, X.L. (2018). The Samarco mine tailing disaster: A possible time-bomb for heavy metals contamination? *Science of the Total Environment, 637,* 498-506.

Rankine, K.J., Sivakugan, N., & Cowling, R. (2006). Emplaced geotechnical characteristics of hydraulic fills in a number of Australian mines. *Geotechnical and Geological Engineering, 24*(1), 1-14.

Rankine, K.J. (2005). An investigation into the drainage characteristics and behaviour of hydraulically placed mine backfill and permeable minefill barricades. (Doctoral dissertation. James Cook University, Queensland, Australia).

Revell, M.B., & Sainsbury, D.P. (2007). *Paste bulkhead failures*. Paper presented at the 9th International Symposium on Mining with Backfill (Minefill'07), Montréal, Canada.

Ripley, E.A., Redmann, R.E., & Maxwell, J. (1978). *Environmental impact of mining in Canada*. Centre for Resource Studies, Queen's University, Kingston, Ontario (pp. 101-203).

Roberts, D.P., Lane, W.L., & Yanske, T.R. (1999). *Pillar extraction at the Doe Run Company 1991–1998*. Paper presented at the 6th international symposium mining with backfill. Victoria, Australia (pp. 227–233).

Roux, K.L., Bawden, W.F., & Grabinsky, M.W. (2005). Field properties of cemented paste backfill at the Golden Giant mine. *Mining Technology, 114*(2), 65-80.

Saebimoghaddam, A. (2005). Rheological yield stress measurements of mine paste fill material. (Doctoral dissertation, McGill University, Montréal, Canada).

Saleh-Mbemba, F. (2016). Assessment of drainage, consolidation and desiccation of fine-grained tailings in the presence of draining inclusions (in French). (Doctoral dissertation, École Polytechnique de Montréal, Montréal, Canada).

Saleh-Mbemba, F., & Aubertin, M. (2018). Characterization of self-weight consolidation of fine-grained mine tailings using moisture sensors. *Geotechnical Testing Journal, 41*(3), 543-554.

Seneviratne, N.H., Fahey, M., Newson, T.A., & Fujiyasu, Y. (1996). Numerical modelling of consolidation and evaporation of slurried mine tailings. *International Journal for Numerical and Analytical Methods in Geomechanics, 20*(9), 647-671.

Shahsavari, M., & Grabinsky, M. (2014). *Cemented paste backfill consolidation with deposition-dependent boundary conditions*. Paper presented at the 67th Canadian Geotechnical Conference, Canadian Geotechnical Society, Regina, Saskatchewan, Canada.

Shahsavari, M., & Grabinsky, M. (2015). *Mine backfill porewater pressure dissipation: numerical predictions and field measurements*. Paper presented at the 68th Canadian Geotechnical Conference, Canadian Geotechnical Society, Québec City, Canada (pp. 1-8).

Shahsavari, M., & Grabinsky, M. (2016). *Pore water pressure variations in cemented paste backfilled stopes*. Paper presented at the Geo-Chicago, Chicago, United States (pp. 331-342).

Simms, P., Grabinsky, M., & Zhan, G.S. (2007). Modelling evaporation of paste tailings from the Bulyanhulu mine. *Canadian Geotechnical Journal, 44*(12), 1417–1432.

Simon, D., & Grabinsky, M. (2013). Apparent yield stress measurement in cemented paste backfill. *International Journal of Mining, Reclamation and Environment, 27*(4), 231-256.

Sivakugan, N., Rankine, K., & Rankine, R. (2006a). Permeability of hydraulic fills and barricade bricks. *Geotechnical and Geological Engineering, 24*(3), 661-673.

Sivakugan, N., Rankine, K., Lovisa, J., & Hall, W. (2013). Flow rate computations in hydraulic fill mine stopes. *Indian Geotechnical Journal, 43*(3), 195-202.

Sivakugan, N., Rankine, R.M., Rankine, K.J., & Rankine, K.S. (2006b). Geotechnical considerations in mine backfilling in Australia. *Journal of Cleaner Production, 14*(12), 1168-1175.

Sivakugan, N., Rankine, K.J., & Rankine, K.S. (2006c). Study of drainage through hydraulic fill stopes using method of fragments. *Geotechnical and Geological Engineering, 24*(1), 79-89.

Skempton, A.W. (1986). Standard penetration test procedures and the effects in sands of overburden pressure, relative density, particle size, ageing and overconsolidation. *Geotechnique, 36*(3), 425–447.

Smith, J.D., & Mitchell, R.J. (1982). Design and control of large hydraulic backfill pours. *Internationa Journal of Rock Mechanics and Mining Science and Geomechanics Abstracts, 19*(6), 102–111.

Sobhi, M.A., & Li, L. (2015). *A numerical study of the stresses in backfilled stopes overlying a sill mat*. Paper presented at the 13th ISRM International Congress of Rock Mechanics, Montréal, Canada.

Sobhi, M.A., Li, L., & Aubertin, M. (2017). Numerical investigation of earth pressure coefficient along central line of backfilled stopes. *Canadian Geotechnical Journal, 54*(1), 138-145.

Soderberg, R.L., & Busch, R.A. (1985). Bulkheads and drains for high sandfill stopes. (Report of investigations 8959). United States Bureau of Mines, Spokane, Wash.

Sofra, F., & Boger, D.V. (2001). *Slope prediction for thickened tailings and pastes*. Paper presented at the Tailings and Mine Waste '01: 8th International Conference, Fort Collins, Colo., A.A. Balkema, Rotterdam, Netherlands (pp. 75-83).

Sracek, O., Choquette, M., Gélinas, P., Lefebvre, R., & Nicholson, R.V. (2004). Geochemical characterization of acid mine drainage from a waste rock pile, Mine Doyon, Québec, Canada. *Journal of Contaminant Hydrology, 69*(1-2), 45-71.

Sridharan, A., & Prakash, K. (1999). Simplified seepage consolidation test for soft sediments. *Geotechnical Testing Journal, 22*(3), 235-244.

Stephan, G. (2011). Cut-and-fill mining. In P. Darling (Ed.), *SME Mining Engineering Handbook*.

Take, W.A., & Valsangkar, A.J. (2001). Earth pressures on unyielding retaining walls of narrow backfill width. *Canadian Geotechnical Journal, 38*(6), 1220-1230.

Terzaghi, K. (1943). Theoretical Soil Mechanics. New York, USA: John Wiley and Sons.

Tesarik, D.R., Seymour, J.B., & Yanske, T.R. (2009). Long-term stability of a backfilled room-and-pillar test section at the Buick Mine, Missouri, USA. *International Journal of Rock Mechanics and Mining Sciences, 46*(7), 1182-1196.

Thompson, B.D., Bawden, W.F., & Grabinsky, M.W. (2012). In situ measurements of cemented paste backfill at the Cayeli Mine. *Canadian Geotechnical Journal, 49*(7), 755-772.

Thompson, B.D., Grabinsky, M.W., Bawden, W.F., & Counter, D.B. (2009). *In-situ measurements of cemented paste backfill in long-hole stopes*. Paper presented at the 3rd CANUS Rock Mechanics Symposium, Toronto, Canada (pp. 199).

Ting, C.H., Shukla, S.K., & Sivakugan, N. (2011). Arching in soils applied to inclined mine stopes. *International Journal of Geomechanics, 11*(1), 29–35.

Ting, C.H., Sivakugan, N., & Shukla, S.K. (2012). Laboratory simulation of the stresses within inclined stopes. *Geotechnical Testing Journal, 35*(2), 280-294.

Ting, C.H., Sivakugan, N., Read, W., & Shukla, S.K. (2014). Analytical expression for vertical stress within an inclined mine stope with non-parallel walls. *Geotechnical and Geological Engineering, 32*(2), 577-586.

Van, H. (1964). *A study of loads on underground structures*. Paper presented at the Symposium on Soil-Structure Interaction, Tucson, AZ United States (pp. 256-282).

Vick, SG. (1990) Planning, design, and analysis of tailings dams. New York: John Wiley and Sons, Inc.

Walske, M.L., & Doherty, J. (2017). Incorporating chemical shrinkage volume into Gibson's solution. *Canadian Geotechnical Journal, 55*(6), 903-908.

Williams, T.J., Bayer, D.C., Bren, M.J., Pakalnis, R.T., Marjerison, J.A., & Langston, R.B. (2007) *Underhand cut and fill mining as practiced in three deep hard rock mines in the United States*. Paper presented at the CIM conference exhibition, Montréal, Canada (pp.1-11).

Wood, D.M., Doherty, J.P., & Walske, M.L. (2016). Deposition and self-weight consolidation of a shrinking fill. *Géotechnical Letter, 6*(1), 72-76.

Xu, G.Z., Gao, Y.F., Hong, Z.S., & Ding, J.W. (2012). Sedimentation behavior of four dredged slurries in China. *Marine Georesources and Geotechnology, 30*(2), 143-156.

Yang, P.Y., & Li, L. (2015). Investigation of the short-term stress distribution in stopes and drifts backfilled with cemented paste backfill. *International Journal of Mining Science and Technology, 25*(5), 721-728.

Yang, P.Y., & Li, L. (2017). Evolution of water table and pore-water pressure in stopes with submerged hydraulic fill. *International Journal of Geomechanics, 17*(9), 04017052.

Yang, P.Y., Li, L., & Aubertin, M. (2017). Stress ratios in entire mine stopes with cohesionless backfill: A numerical study. *Minerals, 7*(10), 201.

Yang, P.Y., Li, L., & Aubertin, M. (2018). Theoretical and numerical analyses of earth pressure coefficient along the centerline of vertical openings with granular fills. *Applied Science, 8*(10), 1721.

Yang, P.Y., Li, L., Aubertin, M., & Brochu-Baekelmans, M. (2017). Stability analyses of waste rock barricades designed to retain paste backfill. *International Journal of Geomechanics, 17*(3), 04016079.

Yang, P.Y. (2016). Investigation of the geomechanical behavior of mine backfill and its interaction with rock walls and barricades. (Doctoral dissertation, École Polytechnique de Montréal, Montréal, Canada).

Yumlu, M., & Guresci, M. (2007). *Paste backfill bulkhead monitoring-A case study from Inmet's Cayeli mine*. Paper presented at the 9th International Symposium in Mining with Backfill (CD-ROM), Canadian Institute of Mining, Metallurgy and Petroleum, Montréal, Canada.

Zhang, J.X., Li, B.Y., Zhou, N., & Zhang, Q. (2016). Application of solid backfilling to reduce hard-roof caving and longwall coal face burst potential. *International Journal of Rock Mechanics and Mining Sciences, 88*, 197-205.

Zhang, J.X., Zhang, Q., Huang, Y., Liu, J.W., Zhou, N., & Zan, D.F. (2011). Strata movement controlling effect of waste and fly ash backfillings in fully mechanized coal mining with backfilling face. *Interntional Journal of Mining Science and Technology, 21*(5), 721–726.

Zhang, N., & Zhu, W. (2014). *Study of sedimentation and consolidation of soil particles in dredged slurry*. Paper presented at the Geo-Shanghai, Shanghai, China (pp.70-79).

Zhang, N., Zhu, W., He, H., & Lv, Y. (2017). Experimental study on sedimentation and consolidation of soil particles in dredged slurry. *KSCE Journal of Civil Engineering, 21*(7), 2596-2606.

Zhang, N., Zhu, W., He, H.T., Lv, Y.Y., & Wang, S.W. (2017). Experimental study on settling velocity of soil particles in dredged slurry. *Marine Georesources & Geotechnology, 35*(6), 747-757.

Zhang, Q., Zhang, J.X., Huang, Y.L., & Ju, F. (2012). Backfilling technology and strata behaviors in fully mechanized coal mining working face. *International Journal of Mining Science and Technology, 22*(2), 151-157.

Zheng, J., Li, L., Mbonimpa, M., & Pabst, T. (2018a). An analytical solution of Gibson's model for estimating the pore water pressures in accreting deposition of slurried material under one-dimensional self-weight consolidation. Part I: Pervious base. *Indian Geotechnical Journal, 48*(1), 72-83.

Zheng, J., Li, L., Mbonimpa, M., & Pabst, T. (2018b). An analytical solution of Gibson's model for estimating pore water pressures in accreting deposition of slurried material under one-dimensional self-weight consolidation. Part II: Impervious base. *Indian Geotechnical Journal, 48*(1), 188-195.

Zhu, B.T., Jardine, R.J., & Foray, P. (2009). The use of miniature soil stress measuring cells in laboratory applications involving stress reversals. *Soils and Foundations, 49*(5), 675-688.

APPENDIX A – AN EXPERIMENTAL STUDY OF THE VERTICAL AND HORIZONTAL STRESSES AND EARTH PRESSURE COEFFICIENT IN A VERTICAL BACKFILLED OPENING

A1. Introduction

In geotechnical engineering, one usually needs to evaluate the stresses in a backfill placed in a rigid confining structure, such as silos, municipal trenches, retaining walls, and underground mine stopes. When the soft backfill material is placed in the confining structure, the backfill tends to settle down under the effect of its gravity. The rigid walls tend to hold the backfill in place. The tendency of relative movement between the backfill and the confining walls leads to the generation of shear stresses along the fill-wall contacts, resulting in reduction of stresses in the backfill. This phenomenon is known as arching effect (Janssen 1895).

Marston (1930) applied the arching theory and proposed the following equations to evaluate the stresses on conduits buried in trenches:

$$\sigma_v = \frac{\gamma B}{2K\tan\delta}\left[1-\exp\left(-\frac{2K\tan\delta}{B}h\right)\right] \tag{A.1}$$

$$\sigma_h = \frac{\gamma B}{2\tan\delta}\left[1-\exp\left(-\frac{2K\tan\delta}{B}h\right)\right] \tag{A.2}$$

where σ_v (kPa) and σ_h (kPa) are the vertical and horizontal normal stresses with a backfill thickness of h (m), respectively; γ (kN/m^3) is the unit weight of the backfill; B (m) is the width of the trench; δ (°) is the friction angle along the interfaces between the backfill and surrounding walls; K (= σ_h/σ_v) is the lateral earth pressure coefficient.

The arching effect is omnipresent in several fields of geotechnical engineering. In civil engineering, it is commonly taken into account in estimating the backfill stresses behind retaining walls (Hunt 1986; Take and Valsangkar 2001; Paik and Salgado 2003; Pain et al. 2017), in silos (Richards 1966; Blight 1986; Ooi and Rotter 1990), and in trenches (Ruffing et al. 2010; Li et al. 2015). In mining engineering, arching theory has been applied to evaluate the stresses in mine backfilled stopes (Askew 1978; Aubertin et al. 2003; Li et al. 2003, 2005; Pirapakaran and Sivakugan 2007a,

2007b; Jaouhar et al. 2018). More development of the arching theory includes the consideration of pore water pressure (Li and Aubertin 2009a, 2009b), three-dimensional geometry (Winch 1999; Li et al. 2005; Pirapakaran and Sivakugan 2007*a*), non-linear stress distributions across the width of stope (Li and Aubertin 2008, 2010) and inclination of backfilled stopes (Caceres 2005; Ting et al. 2011, 2012; Deb and Jain 2018; Jahanbakhshzadeh et al. 2017, 2018a, 2018b).

Despite the numerous and extensive applications of arching theory in the stress estimation in backfilled opening, the analytical solutions have never been fully validated by experimental results. The validation of the analytical solution requires the measurement of both the vertical and horizontal stresses at a given point as well as the mechanical properties of the backfill and the opening geometry. This is however the seldom the case. For instance, some researchers (Deutsch and Schmidt 1969; Take and Valsangkar 2001) measured the horizontal stresses on the side walls of backfilled opening. The vertical stresses were not measured. Pirapakaran and Sivakugan (2007b) measured the average vertical stresses at the base without the measurement of horizontal stresses. Ting et al. (2012) measured the average vertical stresses in an inclined opening. The horizontal stresses were not measured. Li et al. (2014) measured the horizontal and vertical stresses in a backfilled silo. The filling operation was made by pouring the backfill from one top side of the silo. The backfill placed in the silo is probably nonhomogeneous. The result interpretation contained significant uncertainty. Recently, Han et al. (2018) measured the vertical stresses from the center to the wall on the bottom of a silo by adding fill layers; the horizontal stresses were not measured from the center to the wall on the bottom. Horizontal stresses on the side wall were measured by moving down the movable bottom and decreasing the fill thickness. The horizontal stresses on the side wall and the vertical stresses along the bottom were not obtained when the backfill is in the same state. Subsequently, the use and interpretation of these experimental data are difficult and may involve large uncertainty.

In addition of laboratory tests, field measurements of stresses in backfilled mine stopes were also reported. Knutsson (1981) measured the horizontal stresses on the side walls of backfilled stope without measurement of the vertical stresses. Several researchers measured the horizontal and vertical stresses in stopes with cemented backfill (Belem et al. 2004; Thompson et al. 2012; Doherty et al. 2015). The results are difficult to interpret due to the evolution of the mechanical properties with the drainage and consolidation as well as the cementation of the cemented backfill. The uncertainties associated with the stope geometries and rock walls conditions (roughness and

asperities due to blasting and hydraulic properties associated with the joints, fractures, etc.) may lead to poor estimations of the pore water pressure and effective stresses.

Another uncertainty to validate the analytical solution of arching theory is closely related to the knowledge of the lateral earth pressure coefficient *K*. This is particularly true for mine backfilled stopes.

In soil mechanics, the value of *K* is usually related to the movement of the confining structure (Coulomb 1776; Rankine 1857; Jaky 1944; Terzaghi et al. 1996). If the retaining wall does not move, the retained soil is considered in an at-rest state and the earth pressure coefficient is usually taken as the Jaky's at-rest earth pressure coefficient K_0 as follows (Jaky 1948):

$$K_0 = 1 - \sin\phi \tag{A.3}$$

where ϕ (°) is the friction angle of the retained soil.

If the retaining wall moves away, the retained soil tends to expand accompanied with a reduction in the horizontal stress σ_h. When the horizontal stress reduces to such a degree that the Mohr circle of the stress state touches the Coulomb yield envelop, the retained soil yields and reaches an active state. The earth pressure coefficient can then be expressed by the Rankine's active earth pressure coefficient K_a as follows (McCarthy 1988; CGS 2006; Das 2010):

$$K_a = \frac{1-\sin\phi}{1+\sin\phi} = \tan^2(45^\circ - \frac{\phi}{2}) \tag{A.4}$$

Because the rock walls of mine stopes remain immobile during the filling operation, some researchers suggested to use Jaky's at-rest coefficient K_0 while others (e.g., Li et al. 2003, 2005; Li and Aubertin 2009a, 2009b; Ting et al. 2012) suggested the use of Rankine's active coefficient K_a. It is however important to make difference between retaining walls and backfilled openings. For the former case, the natural soil exists first, followed by an excavation and the construction of a confining structure (retaining wall). The natural soil is initially in an at-rest state before any excavation. The immobilization of the retaining wall can thus be a necessary and sufficient condition for the natural soil to be considered in an at-rest state. For the latter case, the confining structure (rock walls) exists first, followed by the placement of a backfill. The state of the backfill placed in the opening is unknown. The immobilization of the retaining wall cannot guarantee an at-rest state of the backfill. Rather, the numerical simulations performed by Li et al. (2003) showed

that the value of K is better described by the Rankine's active earth pressure coefficient K_a at the center of the vertical backfilled opening and a value between K_a and K_0 near the walls. Good agreements were also obtained between the measured stresses and the stresses predicted using the analytical solutions by considering the Rankine's active earth pressure coefficient K_a (Li et al. 2005; Sobhi et al. 2017). Through numerical modeling, Sobhi et al. (2017) have further shown that the active state in backfilled stope is possible due to the occurrence of yielding in the backfill even though the rock walls remain immobile during or after the placement of the backfill.

Recently, Yang et al. (2017) performed numerical modeling and reported that the value of K near the opening center can be close to K_a as long as the Poisson's ratio (μ) or the backfill internal friction angle (ϕ) is smaller than their respective critical value. The mechanism for the backfill to fall into an active (yield) state has been explained by Yang et al. (2018). When the value of μ or ϕ is higher than their respective critical value, the backfill will be in an at-rest state and the value of K near the opening center is better represented by the at-rest earth pressure coefficient defined by the Poisson's ratio $(K_0)_\mu$ [= $\mu/(1-\mu)$]. Near the walls, the backfill is in yield condition, independently on the friction angle and Poisson's ratio values. The ratio between the minor and major principal stresses is close to the Rankine's active earth pressure coefficient, while the ratio of the horizontal to vertical stresses K is close to the at-rest earth pressure coefficient $(K_0)_\mu$ when interface elements were introduced between the backfill and rock wall.

The short literature review elucidates that the development of analytical solutions for estimating the stresses in backfilled openings and the investigation of the lateral earth pressure coefficient have been made, mainly based on the theoretical and numerical analyses. Their validation was made mainly against numerical results. They have never been fully validated by experimental results due to the omission of some key parameters or due to the complexity to interpret the experimental data. To partly fill this gap, laboratory tests have been performed by using a cohesionless sand and an instrumented column. The horizontal and vertical stresses were, for the first time, measured at the center and near the wall as a function of the fill thickness. The distribution of the earth pressure coefficient K was, for the first time, obtained by laboratory tests as a function of the fill thickness from the center to the wall. An analytical solution based on arching theory for estimating the stresses in a circular backfilled opening is then validated by the laboratory test results.

A2. Laboratory tests

Tested material

The tested material is a sand from a quarry at the Lac Tio in Havre-Saint-Pierre, located 52.5 km NE from Mingan, Quebec, Canada. Its particle size distribution curve is shown in Fig. A-1 with C_u = 2.6 (coefficient of uniformity) and C_c = 1.1 (coefficient of curvature). The measured specific gravity is G_s = 2.82. At the loosest state, the unit weight is γ = 16.8 kN/m^3. This value will be used in the stress estimation in the backfilled opening because the sand placed in the testing column is mostly close to the loosest state.

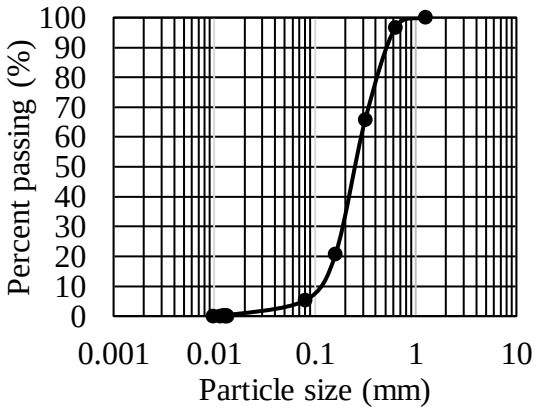

Figure A-1: Grain size distribution curve of the tested sand

Direct shear tests were conducted by following the standard ASTM D3080 to measure the internal friction angle of the sand (ϕ) and the friction angle of the interface between the sand and a piece of Plexiglas (δ). The sand material was uniformly placed in the shear box to avoid any compact. The sand placed in the shear box was thus close to the loosest state. The friction angle of the sand at the loosest state was measured as ϕ = 35°. The friction angle along the interface between the sand and Plexiglas was measured to be δ = 21°, a value close to two thirds of the friction angle of the sand (CGS 2006; Das 2010).

Instrumentation and testing procedure

The instrumentation is composed of a Plexiglas column having an inner diameter of 15.5 cm and a height of 50 cm and the four available miniature stress sensors of TML PDA-200 kPa, installed at the bottom of the column. The sensors have a diameter of 6.5 mm and a thickness of 1 mm. Figure

2 presents a schematic diagram of the testing instrumentation [Fig. A-2(a)] and a photo showing the layout of the four stress sensors in the testing column [Fig. A-2(b)].

Two stress sensors (No. 2 and 4) were fixed closely around the center, separated each other by a distance of about 1 cm due to a hole at the base center of the column. This separate distance is also desirable to minimize their mutual interference. The other two stress sensors (No. 1 and 3) were fixed near the wall at two different positions in order to take the advantage of the axis symmetry of the cylindrical column and avoid their mutual interference. Sensors 1 and 2 were glued at the bottom to ensure a tight contact between the sensors and the column bottom.

The input voltage of the sensors was 2 volts, while the output voltage from the sensors was amplified by an amplifier and measured by a multimeter. The stress sensors were calibrated before and after the backfilling and stress measurement tests. The calibration was conducted in the Plexiglas column with water at different levels.

Fig. A-3 shows the calibration results of the four stress sensors. Linear relationships were observed between the voltage difference (ΔV) and the water pressure for all of the four stress sensors. The slopes of the calibration lines were used to calculate the stresses based on the voltage differences during the backfilling and stress measurement tests.

The backfilling and stress measurement tests were started by slowly placing a first layer of sand 10 cm thick. In order to avoid or at least reduce the impact of sand placement, the used sand was first poured in a glass beak. The glass beak was then kept down to the column as close as possible to the bottom of the column (for the initial backfilling) or the top surface of the previously placed backfill. The pouring of the sand was realized by keeping an almost constant falling height to result in a uniform backfill in the column. Data readings were made when the fill height reached 10, 20, 30, 40 and 50 cm, respectively. Figure 4 shows a photo of the backfilled column at the end of the filling operation. The tests were repeated five times to see the repeatability of the experimental results.

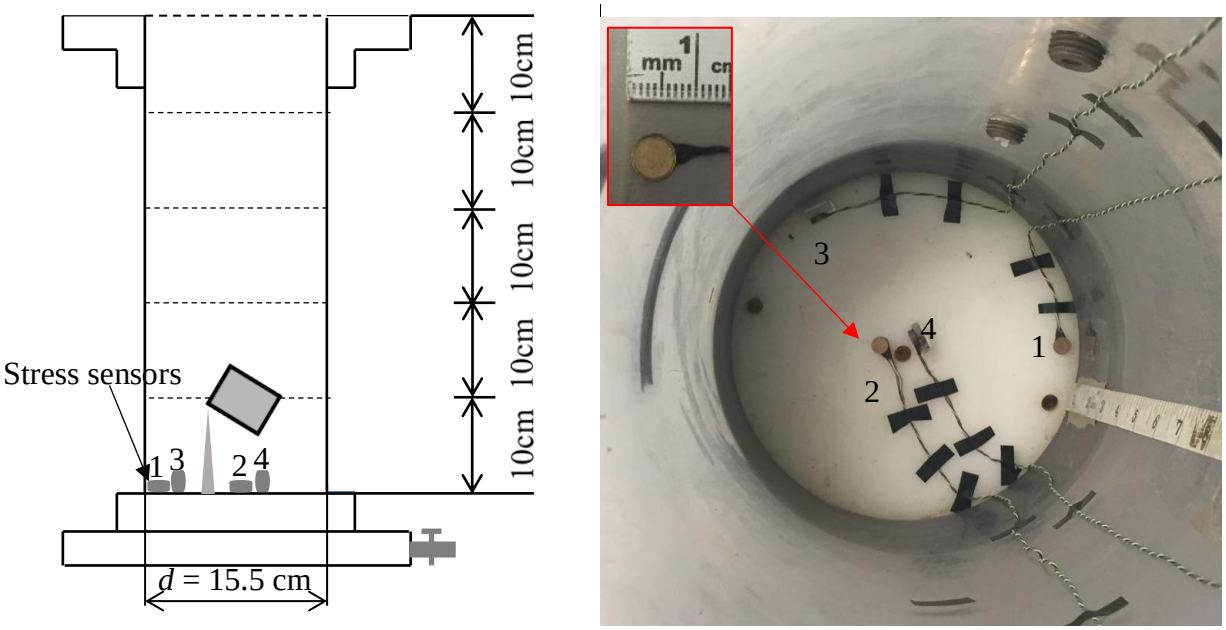

Figure A-2: Testing instrumentation: (a) schematic diagram; (b) photo showing the layout of the four stress sensors

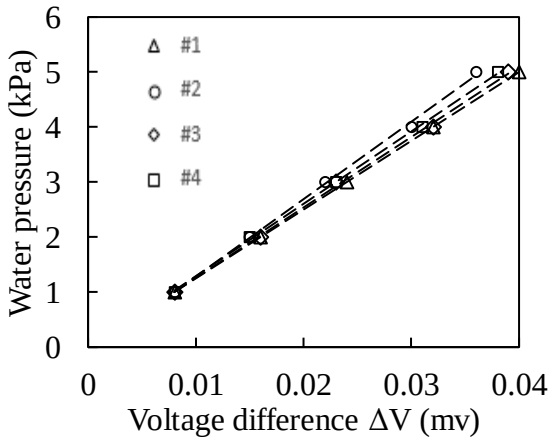

Figure A-3: Calibration results of the four miniature stress sensors

Figure A-4: Photo of the backfilled column

A3. Test results and interpretation

Fig. A-5 shows the variation of the measured vertical [Fig. A-5(a)] and horizontal [Fig. A-5(b)] stresses near the center and wall as a function of the fill thickness. The vertical ($\sigma_v = \gamma h$) and horizontal ($\sigma_h = K_0 \gamma h$) stresses based on the overburden solution have also been plotted on the figure. Despite the more or less dispersion (further addressed in the section "Discussion"), the repeatability of the test results is observed for both the vertical and horizontal stresses, indicating the validity of the tests presented in this study.

When the thickness of the fill is small (i.e. less than 10 cm), the measured vertical stresses near the center and near the wall follow almost the vertical stress based on the overburden solution. Beyond the thickness of 10 cm, the measured vertical stresses tend to become constant and much smaller than the vertical stress based on the overburden solution. Arching effect took place in the backfilled opening. From Fig. A-5(a), one sees also that the vertical stress measured near the center is higher than that measured near the wall. This trend has been illustrated by the numerical modeling performed by several researchers (Li et al. 2003; Li and Aubertin 2008, 2009c, 2010; Sivakugan and Widisinghe 2013; Jaouhar et al. 2018). The experimental results further show that the difference between the vertical stresses near the center and wall increases as the fill thickness increases, a trend corresponding to that reported in the experimental studies of Han et al. (2018).

Regarding the horizontal stress, Fig. A-5(b) shows that it increases nonlinearly with the fill thickness. It tends to become constant and always smaller than the horizontal stress based on the overburden solution. This indicates again the occurrence of arching effect in the backfilled opening. Despite the dispersion of the results, one clearly observes that the horizontal stresses measured near the center and wall are very close to each other. This tends to indicate that the horizontal stress is uniformly distributed across the width of backfilled opening as shown by the numerical modeling performed by Li and coworkers (Li et al. 2003; Li and Aubertin 2008, 2009c). It is however for the first time confirmed by the experimental results.

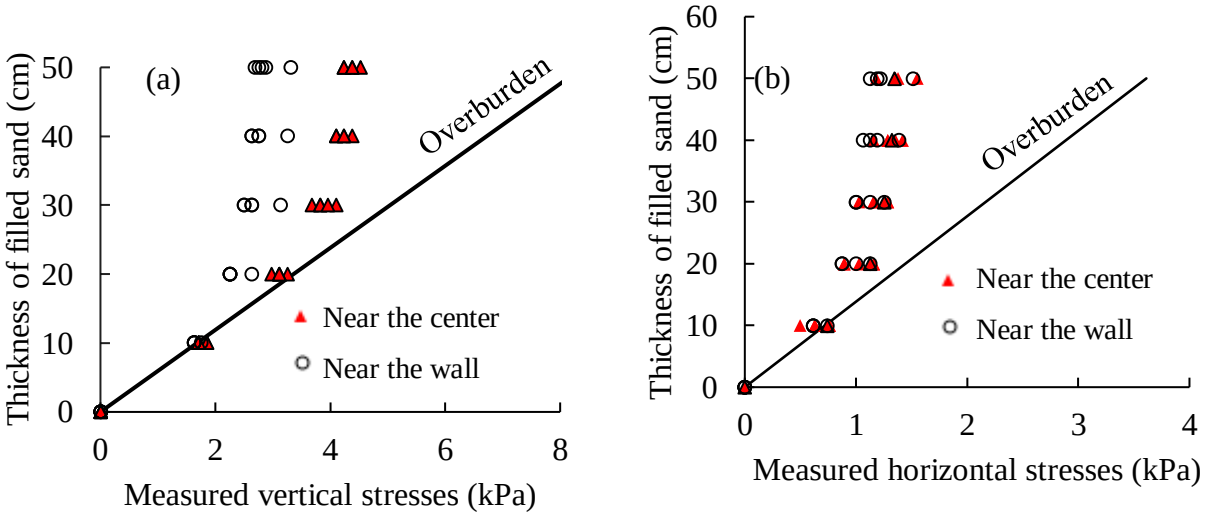

Figure A-5: Variation of the (a) vertical and (b) horizontal stresses measured near the center and wall of the column; plotting of the overburden solution with $\sigma_v = \gamma h$ and $\sigma_h = K_0 \gamma h$ [K_0 = 0. 43 based on Eq. (A.4) using ϕ = 35°].

A4. Comparisons between theoretical and experimental results

Distribution of the earth pressure coefficient *K*

From the vertical and horizontal stresses measured near the center and wall of the column, the distribution of the earth pressure coefficient K can be obtained as a function of the fill thickness as shown in Fig. A-6 shows near the center [Fig. A-6(a)] and near the wall [Fig. A-6(b)]. On the figure, Rankine's active earth pressure coefficient K_a = 0.27 [Eqs. (A.3) using ϕ = 35°] and Jaky's at-rest earth pressure coefficient K_0 = 0. 43 [Eq. (A.4) using ϕ = 35°] are also plotted. Despite the dispersion of the results, it can be clearly seen that the value of K near the center of the column is

close to the Rankine's active earth pressure coefficient K_a. These results partly confirm the numerical results of Li and coworkers (Li et al. 2003; Sobhi et al. 2017; Yang et al. 2017, 2018). An active state of the backfill along the vertical center line of the opening is possible even though the confining wall is immobile during the filling operation. Near the wall, Figure 6b clearly show that the value of K is close to Jaky's at rest coefficient K_0. These results are further discussed in the section "Discussion".

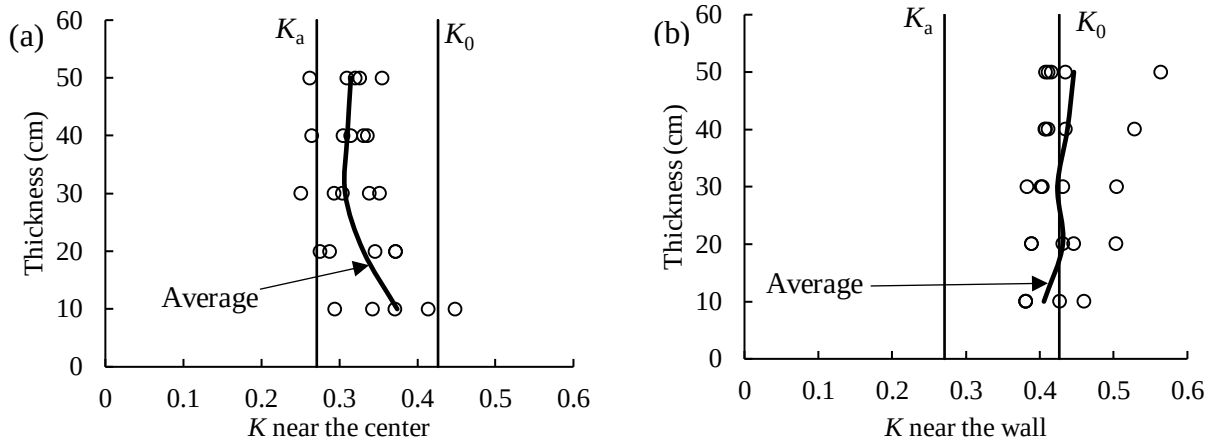

Figure A-6: Earth pressure coefficients K calculated from the mesured vertical and horizontal stresses (a) near the center and (b) near the wall, plotted with the Rankine's active (K_a) and Jaky at-rest (K_0) earth pressure coefficients.

Distribution of the vertical and horizontal stresses

The vertical and horizontal stresses measured near the center and wall as a function of the fill thickness have been presented in Fig. A-5. For circular cross section opening, an analytical solution developed based on the arching theory for estimating the vertical (σ_v) and horizontal (σ_h) stresses at the base of the backfilled opening has been given as follows (Li et al. 2014):

$$\sigma_v = \frac{\gamma d}{4K\tan\delta}\left(1-\exp\left(\frac{-4K\tan\delta}{d}h\right)\right) \tag{A.5}$$

$$\sigma_h = \frac{\gamma d}{4\tan\delta}\left(1-\exp\left(\frac{-4K\tan\delta}{d}h\right)\right) \tag{A.6}$$

where γ (kN/m^3) is the unit weight of the backfill; d (m) is the diameter of the column; δ (°) is the friction angle along the interface between the backfill and column inner wall; h (m) is the thickness of the backfill; K is the earth pressure coefficient.

Fig. A-7 shows the variation of the measured horizontal and vertical stresses near the center [Fig. A-7(a)] and wall [Fig. A-7(b)] as a function of the fill thickness, plotted with the variations of the vertical and horizontal stresses predicted by the analytical solution [Eqs. (A.5) and (A.6)] using γ = 16.8 kN/m^3, d = 0.155 m, δ = 21° and considering K as the Rankine's active ($K_a = \tan^2(45° - \phi/2)$ = 0.27) and Jaky's at-rest ($K_0 = 1 - \sin\phi$ = 0.43) earth pressure coefficients, respectively.

For the horizontal stresses σ_h near the center and wall, good agreements are obtained between the experimental results and analytical solution with both K_a and K_0. These results are straightforward by observing Eqs. (A.2) and (A.6), which show that the influence of K may become negligible at very shallow and very deep depths.

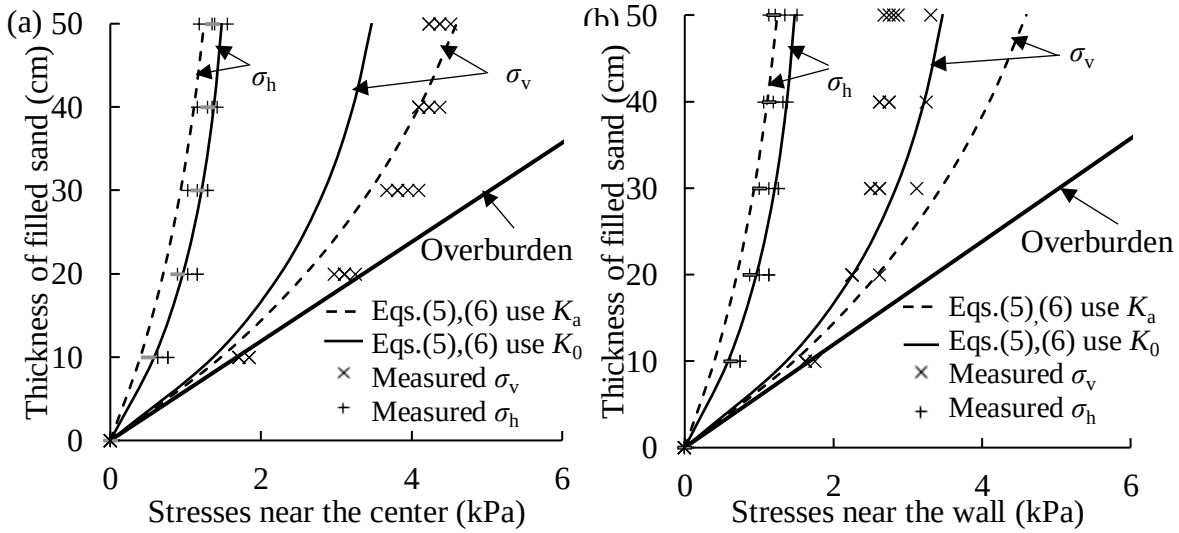

Figure A-7: Variation of the vertical and horizontal stresses as a function of the fill thickness (a) near the center and (b) near the wall of the column, measured and calculated with the arching analytical solution [Eqs. (A.5) and (A.6)] using Rankine's active (K_a) and Jaky's at-rest (K_0) earth pressure coefficients; on the figure are also plotted the vertical stresses based on the overburden solution

For the vertical stresses σ_v near the center [Fig. A-7(a)], a good agreement is obtained between the experimental results and the analytical solution [Eq. (A.5)] by considering the Rankine active earth pressure coefficient K_a. The agreement between the experimental results and the analytical solution using the Jaky at-rest earth pressure coefficient K_0 is poor. The results are consistent with the distribution of the earth pressure coefficient presented in previous section. They indicate again that the backfill can reach an active (yielding) state even though the confining wall is immobile during the placement of the backfill as shown by the numerical simulations reported by Sobhi et al. (2017) and part of the experimental results reported by Li et al. (2014).

For the vertical stresses σ_v near the wall [Fig. A-7(b)], a good agreement is obtained between the experimental results and the analytical solution [Eq. (A.5)] by considering the Jaky's at-rest earth pressure coefficient K_0. The agreement between the experimental results and the analytical solution using the Rankine's active earth pressure coefficient K_a is poor. These results are again consistent with the distribution of the earth pressure coefficient presented in previous section.

These experimental results partly confirm the analytical and numerical results reported by Li et al (2003), who conducted numerical simulation with FALC-2D and showed that the vertical stress along the vertical center line obtained by the numerical modeling agreed well with that calculated by the Marston solution using K_a while relatively good agreement was obtained between the vertical stresses near the wall obtained by the numerical modeling and calculated by the Marston solution using K_0. The horizontal stresses along the vertical center line and near the wall obtained by the numerical modeling agreed relatively well with those calculated by the Marston solution using either K_a or K_0 (somewhat better with K_0).

A5. Discussion

The vertical and horizontal stresses in a backfilled opening were simultaneously measured in the laboratory tests. The measured stresses confirmed the occurrence of arching effect during the placement of the backfill and correspond quite well to the stress analyses of Li et al (2003). Regarding the earth pressure coefficient K, the measured values at the base of the opening are close to the Rankine's active earth pressure coefficient K_a near the center. These results confirm the numerical results of Li and coworkers (Li et al. 2003; Sobhi et al. 2017; Yang et al. 2018). Near the wall, the measured K are close to the Jaky's at-rest earth pressure coefficient K_0. These results

do not confirm the numerical results obtained by Li and coworkers (Li et al. 2003; Yang et al. 2017).

Li et al. (2003) showed that the earth pressure coefficient near the wall took a value between K_a and K_0. This is probably due to the difference between the physical model (circular opening) considered in this study and the numerical model (2D plane strain without interface elements between the backfill and rock walls) considered in Li et al. (2003).

As the backfill is in an active state along the center of the backfilled opening, according to the numerical and theoretical analyses of Yang et al. (2018), the value of the unknown Poisson's ratio μ should be smaller than the critical value determined by the friction angle ϕ (i.e. $\mu \leq (1\text{-}\sin\phi)/2 = 0.213$). The numerical results similar to those of Li et al. (2003) have been obtained by Yang et al. (2017), who considered μ smaller than the critical value in the 2D plane strain numerical model without interface elements between the backfill and rock walls. When interface elements were introduced in the numerical model between the backfill and rock walls, Yang et al. (2017) showed that the value of K near the wall should be close to the at-rest earth pressure coefficient defined by the Poisson's ratio $(K_0)_\mu = \mu/(1-\mu)$. This does not correspond to the experimental results obtained in this study with a circular opening. More laboratory tests are needed to validate the theoretical and numerical analyses of Yang et al. (2017) by using a physical model close to 2D plane strain condition. Ideally, the measurement of Poisson's ratio should be part of the test program. It is however not an easy task as shown by Lambe and Whiteman (1979) and Suwal and Kuwano (2013).

It is interesting to note that the earth pressure coefficient at rest K_0 is defined as the ratio of the horizontal stress to the vertical stress under zero lateral deformation (Donath 1891; Brooker and Ireland 1965; Mesri and Hayat 1993; Lirer et al. 2011; Gao and Wang 2014). It is usually measured in oedometers with the measurement of the lateral stress on the side wall while the vertical stress was applied through a rigid plate on top of the soil sample (Brook and Ireland 1965; Mesri and Hayat 1993; Zhu and Clark 1994; Yamamuro et al. 1996; Lirer et al. 2011; Gao and Wang 2014). It is unclear if the vertical and horizontal stresses are strictly uniformly distributed in the oedometers due to the vertical loading through the top rigid plate and possible friction (arching effect) between the soil sample and side wall. Nevertheless, considering the small size of the sample, the assumption of uniform vertical and horizontal stress distributions through the sample

may not be too far from the reality. It is interesting to note that the values of K obtained by the laboratory tests performed in this study is quite close to the Jaky's at rest earth pressure coefficient K_0 both near the center and near the wall when the fill thickness is small (less than 10 cm) as shown in Figure 6. These results correspond quite well to the experimental results reported by Brooker and Ireland (1965) and Mesri and Hayat (1993) for cohesionless soils. When the fill thickness is large, the values of K deviate from Jaky's K_0 and approach Rankine's K_a. Thus, the experimental results obtained in this study do not contradict the traditional theory and experimental results in relation with the earth pressure coefficient at-rest.

Despite the interesting results and findings, several improvements are expected on the instrumentation and testing procedure to increase the accuracy and reduce the dispersion of experimental results. During the filling operation, the falling height was tried to be kept constant through manual control. However, the variation was more or less unavoidable. The backfill placed in the opening could be more or less heterogeneous along the height. In addition, the laboratory is close to a construction site, which has been lasting for more than two years. The tests have been planned in a way to avoid any major vibration by the neighbor construction. However, the minor vibration associated with the unaware neighbor construction and the possible fill heterogeneity can partly explain the dispersion of the experimental results. In the future, the test instrumentation can be improved by using a more elaborated filling system, such as air pluviation technique (e.g. Take and Valsangkar 2001). The tests should be realized without any neighbor vibration.

Another limitation is associated with the placement of the stress sensors, which were all positioned at the bottom of the column. The stress and K variations shown in this study represent only the state of the backfill at the base as a function of the backfill thickness. More work is needed and ongoing to investigate the variation of the stresses and earth pressure coefficient K at different heights for a given thickness of backfill.

In this study, the backfill is dry and the opening is vertical. More works are needed by considering the presence of water and inclined stopes. These works are ongoing and will be part of the future publications.

A6. Conclusion

In this paper, the horizontal and vertical stresses were, for the first time, measured at the center and near the wall as a function of the fill thickness. The distribution of the earth pressure coefficient was, for the first time, obtained by laboratory tests as a function of the fill thickness from the center to the wall. The main findings can be summarized as follows:

- The measured vertical and horizontal stresses follow the stresses based on the overburden solution when the fill thickness is small. The pace of increase decreases and the measured stresses tend to become constant with further increase in the fill thickness, indicating the occurrence of arching effect in the backfilled opening.
- The horizontal stress is uniformly distributed from the center to the wall of the opening. This corresponds well to the numerical results reported by Li and Aubertin (2008, 2009c, 2010). It can be estimated by the analytical solutions using either Rankine's active earth pressure coefficient K_a or Jaky's at-rest earth pressure coefficient K_0.
- The vertical stress is higher near the center than near the wall. It is not uniformly distributed from the center to the wall of the opening. This corresponds to the numerical results reported by Li and Aubertin (2008, 2009c, 2010). Good agreements were obtained between the experimental results and the analytical solution by considering the Rankine's active earth pressure coefficient K_a near the center and the Jaky's at-rest earth pressure coefficient K_0 near the wall.
- When the fill thickness is small, the ratio of the measured horizontal to vertical stresses is close to Jaky's K_0 at the center and near the wall. This result corresponds quite well to the earth pressure coefficient at-rest measured with oedometer tests for cohesionless soils.
- When the fill thickness becomes large, the values of K become close to K_a at the center and K_0 near the wall.

A7. References

Askew, J.E., McCarthy, P.L., & Fitzerald, D.J. (1978). *Backfill research for pillar extraction at ZC/NBHC*. Paper presented at the Proceedings of Mining with Backfill: 12th Canadian Rock Mechanics Symposium, CIM, Montréal, (pp. 100-110).

ASTM International. (2011). *Standard test method for direct shear test of soils under consolidated drained conditions*. Standard ASTM D3080-11, West Conshohocken, PA, USA.

Aubertin, M., Li, L., Arnoldi, S., Belem, T., Bussière, B., Benzaazoua, M., & Simon, R. (2003). *Interaction between backfill and rock mass in narrow stopes*. Paper presented at the Soil and Rock America 2003, Essen, Germany (pp, 1157–1164).

Belem, T., Harvey, A., Simon, R., & Aubertin, M. (2004). Measurement and prediction of internal stresses in an undergound opening during its filling with cemented fill. Paper presented at the Symposium on Ground support in mining and underground construction. Taylor and Francis Group, London, Australia (pp. 619–630).

Blight, G.E. (1986). Pressure exerted by materials stored in silos. Part I: Coarse materials. *Géotechnique, 36*(1), 33–46.

Brooker, E.W., & Ireland, H.O. (1965). Earth pressure at rest related to stress history. *Canadian Geotechnical Journal, 2*(1), 1–15.

Caceres, C. (2005). Effect of backfill on open stope mining methods. (Master's thesis, University of British Columbia, Vancouver, Canada).

Canadian geotechnical Society. (2006). *Canadian foundation engineering manual* (4th ed.), Vancouver, Canada.

Coulomb, C.A. (1776). Essai sur une application des règles de maximis & minimis à quelques problèmes de statique, relatifs à l'architecture. *Mémoires de mathématique & de physique présentés à l'Académie Royale des Sciences par divers savants & lus dans ses assemblées,* ***7****,* 343-382.

Das, B.M. (2010). Principles of geotechnical engineering (7th ed). Stamford: Cengage Learning.

Doherty, J.P., Hasan, A., Suazo, G.H., & Fourie, A. (2015). Investigation of some controllable factors that impact the stress state in cemented paste backfill. *Canadian Geotechnical Journal, 52*(12), 1901-1912.

Deb, D., & Jain, S. (2018). Compaction-based analytical stress model for 3D inclined backfilled stopes. *International Journal of Geomechanics, 18*(4), 04018009.

Deutsch, G.P., & Schmidt, L.C. (1969). Pressures on silo walls. *Journal of Engineering for Industry, 91*(2), 450-457.

Gao, Y., & Wang, Y.H. (2014). Experimental and DEM examinations of K_0 in sand under different loading conditions. *Journal of Geotechnical and Geoenvironmental Engineering, 140*(5), 04014012.

Han, Y., Li, D.Q., Chen, J.H., Jing, H., & Duan, J.F. (2018). Experimental study on boundary pressure and wall friction under static grain storage in silo. *Transactions of the Chinese Society of Agricultural Engineering, 34*(13), 296-302.

Hunt, R.E. (1986). *Geotechnical Engineering Analysis and Evaluation*. New York: McGraw-Hill Book Company.

Jahanbakhshzadeh, A., Aubertin, M., & Li, L. (2017a). A new analytical solution for the stress state in inclined backfilled mine stopes. *Geotechnical and Geological Engineering, 35*(3), 1151-1167.

Jahanbakhshzadeh, A., Aubertin, M., & Li, L. (2018). Three-dimensional stress state in inclined backfilled stopes obtained from numerical simulations and new closed-form solution. *Canadian Geotechnical Journal, 55*(6), 810-828.

Jahanbakhshzadeh, A., Aubertin, M., & Li, L. (2018). Analysis of the stress distribution in inclined backfilled stopes using closed-form solutions and numerical simulations. *Geotechnical and Geological Engineering, 36*(2), 1011-1036.

Janssen, H.A. (1895). Versuche uber getreidedruck in silozellen [Experiments on the grain pressure in silos]. *Deutscher Ingenieure [J. Assoc. German Eng.], 39*(35), 1045–1049.

Jaouhar, E.M., Li, L., & Aubertin, M. (2018). An analytical solution for estimating the stresses in vertical backfilled stopes based on a circular arc distribution. *Geomechanics and Engineering, 15*(3), 889-898.

Jaky, J. (1944). The coefficient of earth pressure at rest. *Journal of Society of Hungarian Architects and Engineers, 78*(22), 355–358.

Jaky, J. (1948). *Pressure in silos*. Paper presented at the 2nd International Conference on Soil Mechanics and Foundation Engineering, Rotterdam, The Netherlands (pp. 103-107).

Knutsson, S. (1981). *Stresses in the hydraulic backfill from analytical calculations and in-situ measurements*. Paper presented at the Application of Rock Mechanics to Cut and Fill Mining, London. (pp. 261–268).

Lambe, T.W., & Whitman, R.V. (*1969*). Soil mechanics. New York: John Wiley.

Li, L., & Aubertin, M. (2008). An improved analytical solution to estimate the stress state in subvertical backfilled stopes. *Canadian Geotechnical Journal, 45*(10), 1487-1496.

Li, L., & Aubertin, M. (2009a). Influence of water pressure on the stress state in stopes with cohesionless backfill. *Geotechnical and Geological Engineering, 27*(1), 1–11.

Li, L., & Aubertin, M. (2009b). A three-dimensional analysis of the total and effective stresses in submerged backfilled stopes. *Geotechnical and Geological Engineering, 27*(4), 559–569.

Li, L., & Aubertin, M. (2009c). Numerical investigation of the stress state in inclined backfilled stopes. *International Journal of Geomechanics, 9*(2), 52-62.

Li, L., & Aubertin, M. (2010). An analytical solution for the nonlinear distribution of effective and total stresses in vertical backfilled stopes. *Geomechanics and Geoengineering, 5*(4), 237-245.

Li., L, Aubertin, M., Simon, R., Bussière, B., & Belem, T. (2003). Modeling arching effects in narrow backfilled stopes with FLAC. Paper presented at the 3rd International FLAC Symposium, A. A. Balkema, Rotterdam, Netherlands. (pp. 211–219).

Li, L., Aubertin, M., & Belem, T. (2005). Formulation of a three dimensional analytical solution to evaluate stress in backfilled vertical narrow openings. *Canadian Geotechnical Journal, 42*(6), 1705–1717 (with Erratum 2006, 43(3), 338–339).

Li, L., Aubertin, J.D., & Dubé, J.S. (2014). Stress distribution in a cohesionless backfill poured in a silo. *The Open Civil Engineering, 8*(1), 1–8.

Li, Y.C., Cleall, P.J., Wen, Y.D., Chen, Y.M., & Pan, Q. (2015). Stresses in soil-bentonite slurry trench cutoff walls. *Geotechnique, 65*(10), 843-850.

Lirer, S., Flora, A., & Nicotera, M.V. (2011). Some remarks on the coefficient of earth pressure at rest in compacted sandy gravel. *Acta Geotechnica, 6*(1), 1–12.

Marston, A. (1930). The theory of external loads on closed conduits in the light of latest experiments. Iowa Engineering Experiment Station, Ames, Iowa (pp. 138-170).

McCarthy, D.F. (1988). Essentials of Soil Mechanics and Foundations: Basic Geotechnics (7th ed.). Englewood Cliffs, NJ, USA: Prentice Hall.

Mesri, G., & Hayat, T.M. (1993). The coefficient of earth pressure at rest. *Canadian Geotechnical Journal, 30*(4), 647–666.

Ooi, J.Y., & Rotter, J.M. (1990). Wall pressures in squat steel silos from simple finite element analysis. *Computers & Structures, 37*(4), 361-374.

Paik, K.H., & Salgado, R. (2003). Estimation of active earth pressure against rigid retaining walls considering arching effects. *Geotechnique, 53*(7), 643-654.

Pain, A., Chen, Q.S., Nimbalkar, S., & Zhou, Y.T. (2017). Evaluation of seismic passive earth pressure of inclined rigid retaining wall considering soil arching effect. *Soil Dynamics and Earthquake Engineering, 100*, 286-295.

Pirapakaran, K., & Sivakugan, N. (2007a). Arching within hydraulic fill stopes. *Geotechnical and Geological Engineering, 25*(1), 25-35.

Pirapakaran, K., & Sivakugan, N. (2007b). A laboratory model to study arching within a hydraulic fill stope. *Geotechnical Testing Journal, 30*(6), 496-503.

Rankine, W.J.M. (1857). On the stability of loose earth. *Philosophical Transactions of the Royal Society of London, 147*, 9-27.

Richards, J.C. (1966). *The storage and recovery of particulate solids*. Institution of Chemical Engineers, London.

Ruffing, D.G., Evans, J.C., & Malusis, M.A. (2010). Prediction of earth pressures in soil–bentonite cutoff walls. Paper presented at the GeoFlorida (Edited by Fratta, D.O., Puppala, A.J. and Muhunthan, B), geotechnical special publication, Reston, USA (pp. 2416–2425).

Sivakugan, N., & Sankha, W. (2013). Stresses within granular materials contained between vertical walls. *Inddian Geotechnical Journal, 43*(1), 30-38.

Sobhi, M.A., Li, L., & Aubertin, M. (2017). Numerical investigation of earth pressure coefficient along central line of backfilled stopes. *Canadian Geotechnical Journal, 54*(1), 138-145.

Suwal, L.P., & Kuwan, R. (2013). Statically and dynamically measured Poisson's ratio of granular soils on triaxial laboratory specimens. *Geotechnical Testing Journal, 36*(4), 493-505.

Take, W.A., & Valsangkar, A.J. (2001). Earth pressures on unyielding retaining walls of narrow backfill width. *Canadian Geotechnical Journal, 38*(6), 1220-1230.

Terzaghi, K., Peck, R.B., & Mesri, G. (1996). Soil mechanics in engineering practice. New York , USA: John Wiley & Sons.

Thompson, B.D., Bawden, W.F., & Grabinsky, M.W. (2012). In situ measurements of cemented paste backfill at the Cayeli Mine. *Canadian Geotechnical Journal, 49*(7), 755-772.

Ting, C.H., Shukla, S.K., & Sivakugan, N. (2011). Arching in soils applied to inclined mine stopes. *International Journal of Geomechanics, 11*(1), 29-35.

Ting, C.H., Sivakugan, N., & Shukla, S.K. (2012). Laboratory simulation of the stresses within inclined stopes. *Geotechnical Testing Journal*, *35*(2), 280-294.

Winch, C. (1999). Geotechnical characteristics and stability of paste backfill at BHP Cannington mine. (B.E. Hons thesis, James Cook University, Townsville, Australia).

Yamamuro, J., Bopp, P., & Lade, P. (1996). One-dimensional compression of sands at high pressures. *Journal of Geotechnical Engineering, 122*(2), 147–154.

Yang, P.Y., Li, L., & Aubertin, M. (2017). Stress ratios in entire mine stopes with cohesionless backfill: A numerical study. *Minerals, 7*(10), 201.

Yang, P.Y., Li, L., & Aubertin, M. (2018). Theoretical and numerical analyses of earth pressure coefficient along the centerline of vertical openings with granular fills. *Applied Sciences, 8*(10), 1721.

Zhu, F.Y., & Clark, J.I. (1994). The effect of dynamic loading on lateral stress in sand. *Canadian Geotechnical Journal, 31*(2), 308–311.

APPENDIX B – AN EXPERIMENTAL STUDY TO INVESTIGATE THE EFFECTIVENESS OF TYPICAL LUBRICANTS IN REDUCING THE SIDEWALL FRICTION

B1. Introduction

In soil mechanics, the sidewall friction (shear strength) along the soil-structure interfaces is one of the earliest and most important concerns for many geotechnical problems. This is particularly true for laboratory tests conducted in a slender container, including the column (self-weight) consolidation tests and earth pressure calibration tests (e.g., ASTM; Zhu et al. 2009; Pedroni and Aubertin 2013; Gade and Dasaka 2018). Due to the sidewall friction (shear force), part of the soil weight can transfer to the sidewall, resulting in reduction of the horizontal and vertical stresses in the soil. This phenomenon is well-known as arching effect (Janssen 1895; Marston 1930; Terzaghi 1943).

It is generally accepted that the side friction becomes negligible when a thin layer of lubricant is applied along the interface between the tested soil and containers inner wall. For instance, Fox and Baxter (1997) and Sridharan and Prakash (1999) applied a thin layer of grease in their column consolidation tests. The sidewall friction along the inner walls was then neglected in their result interpretation. Watabe et al. (2003) applied a combination of latex membrane and silicone grease along the triaxial cell in their K_0-consolidaiton tests. The sidewall friction (shear strength) was then considered as negligible. This same approach has been adopted by Zhu et al. (2009) in their stress sensors calibration tests and the sidewall friction along the sand-structure interfaces was neglected.

The question is if the application of these lubricant materials can completely eliminate the side friction? If not, what is the degree or effectiveness of reduction through the application of lubricant materials? To reply to these questions, a number of tests have been conducted over past years, mainly through direct shear tests. For instance, Brumund and Leonards (1973) showed that the average friction coefficients between a uniformly graded quartz sand and polished steel, Teflon coated steel, graphite coated steel, smooth mortar, Teflon coated smooth mortar, graphite coated smooth mortar and rough mortar, obtained by direct shear tests, were 0.34 (18.8^o), 0.33 (18.3^o), 0.24 (13.5^o), 0.60 (31.0^o), 0.33 (18.3^o), 0.32 (17.7^o) and 0.76 (37.2^o), respectively. The direct shear tests conducted by Tatsuoka et al. (1984) as well as Tatsuoka and Haibara (1985) showed that the

application of Dow grease with a thickness of 50 μm can reduce the friction angle smaller than 1 degree for the normal stress of 150~670 kPa and around 10 degree for the normal stress of 5 kPa (during the initial loading stage). Similar direct shear test results have been reported by Fang et al. (1994), who showed that the frictional angle between Ottawa sand and the sidewalls covered with a thin layer of silicone grease and a layer of latex rubber membrane 0.2 mm thick can be reduced to less than 1 degree for the normal stress higher than 40 kPa. Feng et al. (2017) reported that the friction coefficients between alloy steel platen and Teflon, combined Teflon and MoS_2, and MSV (a mixture of stearic acid and Vaseline), obtained by double direct-shear test in a modified true triaxial apparatus, can be reduced to as low as 0.043 (2.5^o), 0.021 (1.2^o) and 0.018 (1.0^o), respectively.

The above-mentioned studies clearly indicate that the use of lubricant material for reducing the friction is efficient at high normal stress, but less efficient at low normal stress. The latter is however for the most common testing conditions in soil mechanics laboratory tests. In addition, the testing conditions between direct shear tests and tests with cylinders are quite different. In the former case, the tested Teflon sheet or thin layer of membrane is free to move along the sliding plane without any restrictions. The weakest plane controls the strength of the system. The obtained friction (shear strength) corresponds to the smallest one among the soil-lubricant, lubricant-lubricant (in case of combined lubricant materials), and lubricant-platen interfaces. In the latter case (oedometer tests, stress sensor calibration tests, column consolidation tests, for instance), the Teflon sheet or other layer of stiff lubricant cannot freely move in the vertical direction due to the bottom restriction. The friction (shear strength) of the tested system is mainly controlled by the shear strength of the interface between the tested soil and the lubricant layer, which is in direct contact with the tested soil. In addition, the sliding planes are very different between direct shear tests and column containment tests. The former is a flat while the latter is curved. Therefore, the direct shear test results cannot be applied to the cylinder containment tests. The efficiency in reducing the friction by application of lubricant illustrated by direct shear tests is not presentative of the column containment tests.

In this paper, the effectiveness in reducing the sidewalls friction by application of several lubricants is investigated by through column containment tests. The vertical stresses at the bottom of the column due to the addition of backfill are measured. The friction angles along the side wall interface between the tested sand and selected lubricants are back-calculated. The arching degree

and the efficiency of the diverse lubricants in reducing the sidewall friction are evaluated. A series of direct shear tests were also conducted to measure the friction angle along the sand-lubricants interfaces. The back-calculated friction angles by the column tests agree well with that measured by the direct shear tests.

B2. Test materials

Air-dried Demers sand is selected as the tested soil in this study. Its particle size distribution curve is presented in Fig. B-1. Its physical and geotechnical properties were characterized as G_s = 2.74 (specific gravity) and γ = 15 kN/m^3 (at loosest state).

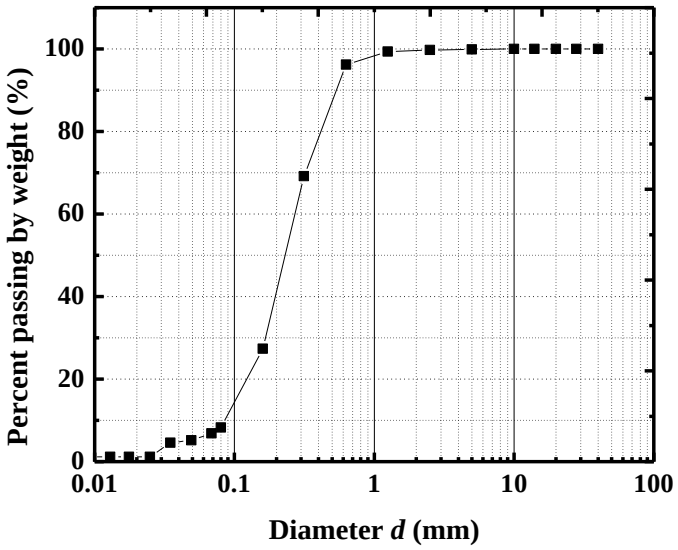

Figure B-1: Particle size distribution curve of the tested Demers sand

Fig. B-2 shows the measurement of the angle of repose for the tested sand in a loose state, with a value of α = 33.5°. The internal friction angle ϕ' of the tested sand can be considered close to the angle of repose (ϕ' = α = 33.5°) in the loose state (Ghazavi et al. 2008).

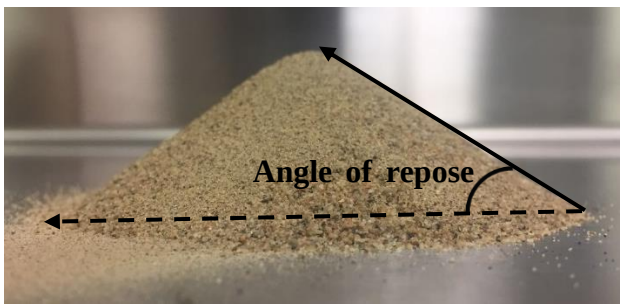

Figure B-2: The meausrement of the angle of repose for the tested sand in a loose state

In this study, two Plexiglas columns with smooth and clean inner surface wall were used. The first column has an inner diameter d_1 = 62.9 mm, a thickness t_1= 6.47 mm and a height H_1 = 180 mm, while the second one has an inner diameter d_2 = 100.8 mm, a thickness t_2 = 4.95 mm and a height H_2 = 215 mm.

Several lubricants commonly used in geotechnical laboratory tests were selected, including silicone grease, lubricant oil, JIG-A-LOO lubricant, JIG-A-LOO graphite, wax, Teflon (with a thickness of 0.15 mm), and a combined grease and Teflon.

B3. Instrumentation and testing procedures

Fig. B-3 shows the schematic diagram [Fig. B-3(a)] and a photograph [Fig. B-3(b)] of the instrumentation, inspired from the test instrumentation of Pirapakaran and Sivakugan (2007). A very thin layer of grease, oil, JIG-A-LOO lubricant, JIG-A-LOO graphite and wax were uniformly applied on the column inner wall. The combined Teflon and grease were used by applying a thin layer of grease on the column inner wall first and then covered by Teflon. When the Teflon was used, it was fixed at both ends of the column. As a comparison, the test was also conducted without using any lubricants to measure the friction angle under the unlubricated condition. The Plexiglas column was hold by a clamp with a clearance of 0.2 cm left between the column bottom and the metal tray. This gap was chosen randomly to avoid the touch between the column and metal tray. The metal tray was placed on a balance, which has a capacity of 32000 g and a precision of 0.1 g. A funnel was fixed by a clamp on a support. Its base was 25.2 cm above the metal tray.

In order to use constant sand mass in all the tests, the quantities of sand were prepared and measured before the tests, which showed that 2324 g of sand was needed to fill the large column (d_1 = 100.8 mm) to 18 cm (not including the cone), while 740 g of sand was needed to fill the small column (d_2 = 62.9 m) to 15 cm (not including the cone). The sand was placed in the columns through a funnel in two stages. At the first stage, the sand was filled to a height of h_1 (about 11 cm for the large column and 8 cm for the small column, measured from the cone toe to the column bottom). At the second stage, the rest of the prepared sand was placed in the columns with the formation of a final cone on top of the backfill. The sand height h_2 reached about 18 cm for the large column and 15 cm for the small column (measured again from the cone toe to the column bottom). The height h_3 of the cone was about 3 cm for the large column and 1.5 cm for the small column.

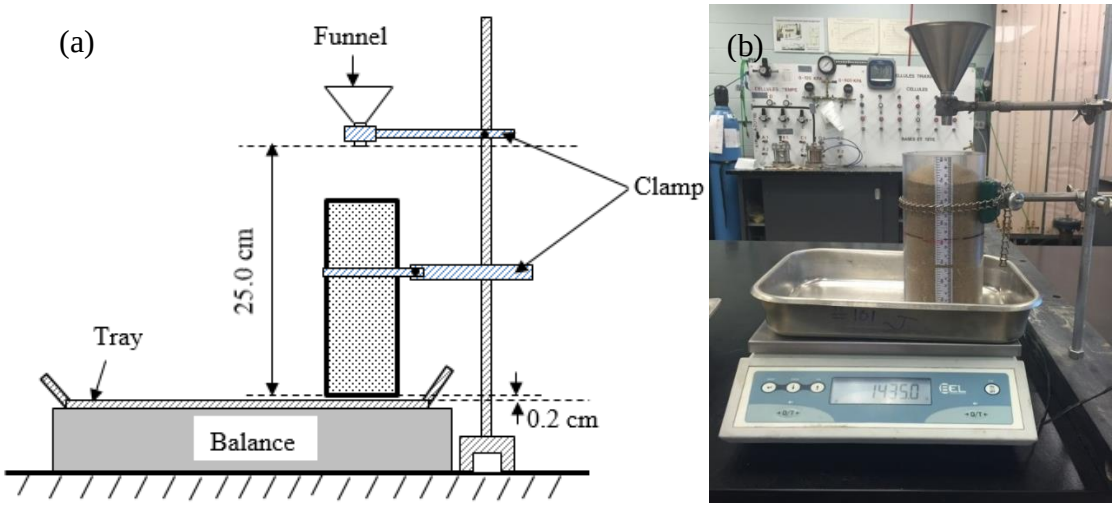

Figure B-3: Backfilled column test instrumentation: (a) a schematic diagram; (b) a photograph

B4. Test results

As the sand height reached h_1 and h_2 in the column, the balance readings were recorded as m_1 (g) and m_2 (g), respectively. The average vertical stresses σ_{vh} at the bottom of the column can be calculated as:

$$\sigma_{vh1} = \frac{m_1 g}{S} \tag{B.1}$$

$$\sigma_{vh2} = \frac{m_2 g}{S} \tag{B.2}$$

where σ_{vh1} (kPa) and σ_{vh2} (kPa) are the average vertical stresses at the bottom of the column corresponding to the sand height of h_1 (cm) and h_2 (cm), respectively; g (m^2/s) is the gravity acceleration; S (m^2) is the cross-sectional area of the column and can be computed as

$$S = \frac{\pi d^2}{4} \tag{B.3}$$

Substituting Eq. (B.3) into Eqs. (B.1) and (B.2) leads to

$$\sigma_{vh1} = \frac{4 m_1 g}{\pi d_1^{\,2}} \tag{B.4}$$

$$\sigma_{vh2} = \frac{4 m_2 g}{\pi d_2^{\,2}} \tag{B.5}$$

The test data obtained by using the large column and the average vertical stresses calculated with Eqs. (B.4) and (B.5) are shown in Table B-1 while those obtained by using the small column are presented in Table B-2.

Table B-1: Test results obtained by using the large column (100.8 mm in diameter) and different lubricant materials

Type of Lubricant	First Stage				Second Stage			
	h_1 (cm)	h_3 (cm)	m_1 (g)	σ_{vh1} (kPa)	h_2 (cm)	h_3 (cm)	m_2 (g)	σ_{vh2} (kPa)
Unlubricated	11.4	3.0	1099.2	1.35	18.0	3.0	1576.8	1.94
Grease	11.5	3.1	1017.4	1.25	18.0	3.0	1467.1	1.80
Oil	11.2	3.0	992.4	1.22	18.0	3.1	1463.6	1.80
JIG-A-LOO Lubricant	11.0	3.0	1109.8	1.36	18.0	3.0	1616.0	1.98
JIG-A-LOO Graphite	11.0	3.1	1015.0	1.25	18.0	3.0	1504.0	1.85
Wax	11.2	3.0	1017.1	1.25	18.0	3.0	1485.6	1.82
Teflon	11.0	3.0	1105.3	1.36	18.0	3.1	1625.1	1.99
Teflon + Grease	11.0	2.9	1128.3	1.38	18.0	3.0	1719.3	2.11

Table B-2: Test results obtained by using the small column (62.9 mm in diameter) and different lubricant materials

Type of Lubricant	First Stage				Second Stage			
	h_1 (cm)	h_3 (cm)	m_1 (g)	σ_{vh1} (kPa)	h_2 (cm)	h_3 (cm)	m_2 (g)	σ_{vh2} (kPa)
Unlubricated	8.0	1.5	285.5	0.90	15.0	1.5	455.1	1.44
Grease	8.2	1.5	261.0	0.82	15.3	1.6	392.3	1.24
Oil	8.0	1.6	238.3	0.75	15.0	1.5	389.9	1.23
JIG-A-LOO Lubricant	8.0	1.5	280. 7	0.89	15.0	1.5	462. 7	1.46
JIG-A-LOO Graphite	8.1	1.7	250. 7	0.79	15.0	1.5	410.3	1.29
Wax	8.0	1.5	260.0	0.82	15.0	1.7	399. 7	1.26
Teflon	8.0	1.6	291. 7	0.92	15.2	1.5	490. 7	1.55
Teflon + Grease	8.0	1.5	313. 7	0.99	15.0	1.5	506. 7	1.60

B5. Result interpretation

As shown in Fig. B-3(b), a cone was formed on top of the backfill at the intermediate and final stages of the tests. The average pressure due to the cone can be estimated as follows:

$$p = \frac{1}{3}\gamma h_3 \tag{B.6}$$

where p (kPa) is the average pressure over the top of the backfill; γ (kN/m^3) is the unit weight of the sand.

The vertical stress at the bottom of the column can be calculated by the following solution (see formulation in Appendix I):

$$\sigma_{vh} = \frac{\gamma d}{4K\tan\delta}\left(1-\exp\left(\frac{-4K\tan\delta}{d}h\right)\right)+ p\times\exp\left(\frac{-4K\tan\delta}{d}h\right) \tag{B.7}$$

where h is the height of the sand placed in the column (cone not included); δ is the friction angle along the interface between the sand and column inner wall; K is the earth pressure coefficient, which is dependent on the state of the backfill. As the confining structure walls are stiff and their deformation upon the placement of backfill is negligible, a number of researchers suggest that the backfill is in an at-rest state and the value of K can be calculated by Jaky at-rest earth pressure coefficient as follows (Jaky 1948):

$$K = K_0 = 1\text{-}\sin\phi' \tag{B.8}$$

However, Sobhi et al. (2017) and Yang et al. (2017) have shown that the backfill placed in a confining structure with immobile walls can also reach yield state and the value of the earth pressure coefficient K can be close to Rankine active earth pressure coefficient as follows:

$$K = K_a = (1\text{-}\sin\phi')/(1+\sin\phi') \tag{B.9}$$

With ϕ' = 33.5°, one can expect that the value of K can be in the range of K_a = 0.289 to K_0 = 0.448. When the column is unlubricated, as the Plexiglas wall is planar and smooth, the effective friction angle δ' along the fill-wall interface is typically taken as two thirds of the backfill effective friction angle ϕ' ($\delta' = 2/3\phi' = 22.3^o$) (Das 2004; CGS 2006; Pirapakaran and Sivakugan 2006; Pirapakaran and Sivakugan 2007). With Eq. (B.7), effective friction angle δ', and the measured results in Tables 1 and 2, the earth pressure coefficient for the two unlubricated columns can be back-calculated as K = 0.284 for the large column (d =100.8mm) and K = 0.276 for the small column (d = 62.9 mm) using Solver® of Microsoft Excel (with a sample calculation presented in Appendix II). These

values are very close to the Rankine active earth pressure coefficient K_a (= 0.289, ϕ' = 33.5°), which is consistent with the numerical results in previous studies (Sobhi et al. 2017; Yang et al. 2017).

As the earth pressure coefficient is only related to the state of sand rather than the interface properties, the values of K after applying the other lubricants can be considered to be equal to the calculated K for the case of unlubricated column. By substituting K = 0.284 and 0.276 into Eq. (B.7), the friction angle δ along the interface between the sand and different lubricants are back-calculated using Solver® of Microsoft Excel again with the experimental results shown in Tables B-1 and B-2.

Table B-3 shows the results of back-calculated δ with different lubricants. First, one notes that the back-calculated δ obtained with the large column are close to those obtained with the small column. These results are straightforward as the interface friction angle is independent of the column dimension. The close agreement between the results obtained by the two different size columns indicates a good re-productivity of the tests.

Compared to the case of unlubricated column (δ = 23.3°), slight reduction of the interface friction angle δ is noted when the column inner wall was covered with Teflon sheet, JIG-A-LOO lubricant or combined Teflon and grease. Among them, the combined Teflon and grease showed the most efficiency in reducing the side wall shear strength, resulting in an interface friction angle reduced to 18.2° to 16.8°, which are however far from being qualified as negligible.

Surprisingly, the use of grease, lubricant oil, JIG-A-LOO Graphite or wax led to increased interface friction angles. The friction angle increase effect is particularly pronounced with the application of the grease or oil, showing a friction angle between 26.7° and 29.7° (compared to a friction angle 22.3° without any lubricants). These results are counterintuitive because grease and oil are commonly used lubricants to reduce the sidewall friction in geotechnical laboratory tests.

Without any doubt, oil and grease are very low friction materials. However, they are viscous, sticky and cohesive. The effect of these (apparent) cohesion can be seen by the sand particles glued on the column inner wall during the tests. Fig. B-4 shows photographs of the column after the end of the tests when the column inner wall was not covered of any lubricants [Fig. B-4(a)] or covered of grease lubricant [Fig. B-4(b)]. With the unlubricated column, there were no evident sand particles glued on the column inner wall. When the column inner wall was covered by the grease (or oil), a layer of sand particles stuck on the inner wall of the column was clearly observed.

On the other hand, Eq. (B.7) is developed for cohesionless materials. The cohesion (adherence) along the interface is equally considered as nil ($\tau = \sigma\tan\delta$). When one applies Eq. (B.7) to back-calculate the effective friction angle δ, the apparent cohesion (c_{app}) from lubricants is translated into the shear strength of the interface (sliding plane) between the sand and lubricants. The real shear strength along the interface becomes:

$$\tau' = c_{app} + \sigma \tan\delta = \sigma \tan\delta' \tag{B.10}$$

In this study, the normal stress σ on the column wall applied by the sand is very small due to the dimension of the column, the apparent cohesion c_{app} from the lubricants can play a bigger role and significantly increase the effective friction angle of the interface. However, in the direct shear test, the normal stress can increase to megapascal which is much higher than the apparent cohesion of lubricants. The influence of the apparent cohesion of lubricants thus becomes negligible, the effective friction angle along the interface is mainly controlled by the applied normal stress in the direct shear tests. On the other hand, as stated in the section "Introduction", the lubricant, such as Teflon or combined Teflon and grease, can move freely along the sliding direction in the direct shear test, while it can hardly move in the container due to the restriction from the bottom. These two reasons may explain why previous direct shear tests always give very low effective friction angle along the interface (Tatsuoka et al. 1984; Tatsuoka and Haibara 1985; Fang et al. 1994; Feng et al. 2017).

Table B-3: Back-calculated δ using Eq. (B.7), experimental results [Tables B-1 and B-2], and Solver® of Microsoft Excel

Lubricant	d = 100.8 (mm)	d = 62.9 (mm)
	δ (°)	δ (°)
Grease	26.7	29.0
Lubricant oil	28.4	29.7
JIG-A-LOO Lubricant	21.2	22.2
JIG-A-LOO Graphite	25.1	27.4
Wax	25.9	27.9
Teflon	21.2	19.1
Teflon and Grease	18.2	16.8

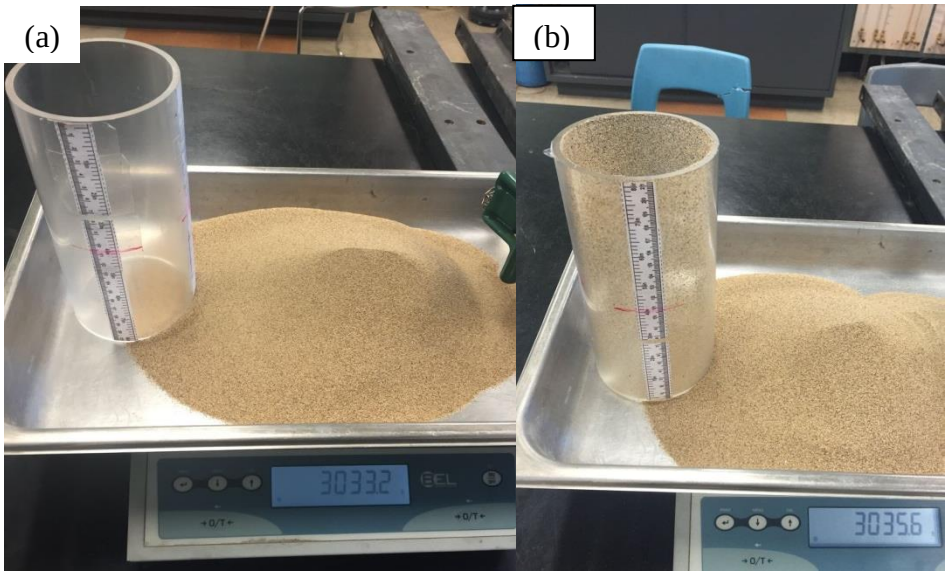

Figure B-4: The photographs of the column after the end of the tests when the inner wall was (a) not covered (i.e. unlubricated) or (b) covered of a layer of grease

To note that the apparent cohesion or adherence is not a characteristic only belonging to the grease and oil; it can manifest more or less to any material. Table B-4 shows the masses of sand attached to the column wall, measured after the end of each test. It can be seen that high amounts of attached sand masses generally correspond to the high shear strength lubricants (grease, oil and wax).

Table B-4: The mass of sand glued to the column inner wall after using different lubricants

Lubricant	Glued sand mass (g)	
	d = 100.8 mm	d = 62.9 mm
Unlubricated	0.12	0.05
Grease	10.5	4.30
Oil	7.87	3.61
JIG-A-LOO Lubricant	2.54	1.27
JIG-A-LOO Graphite	2.82	1.77
Wax	6.29	2.76
Teflon	1.08	0.54
Teflon+Grease	0.62	0.85

B6. Additional tests and validation

To validate the back-calculated δ shown in Table B-3, additional tests were conducted by fully filling the column (d = 100.8 mm) with a quasi-horizontal top surface at the end of each test, as shown in Fig. B-5.

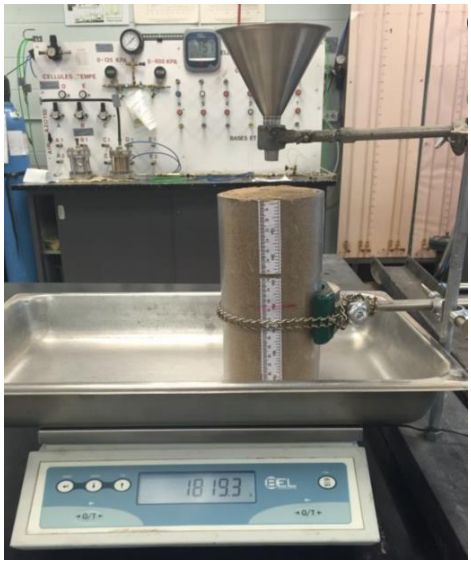

Figure B-5: Additional tests with a quasi-horizontal top surface at the end of each test

With the balance readings, the average vertical stress σ_{vH} at the bottom of the column can be calculated using Eq. (B.4). It can also be calculated using Eq. (B.7) (with p = 0 kPa) and the calculated δ shown in Table B-3. The agreement between the measured and estimated vertical stresses is shown in Fig. B-6. One sees that the agreement is generally good. But the application of the arching solution generally tends to underestimate the measured stresses for the case of Teflon and combined Teflon and grease, probably due to the overestimation of the interface friction angles shown in Table B-3.

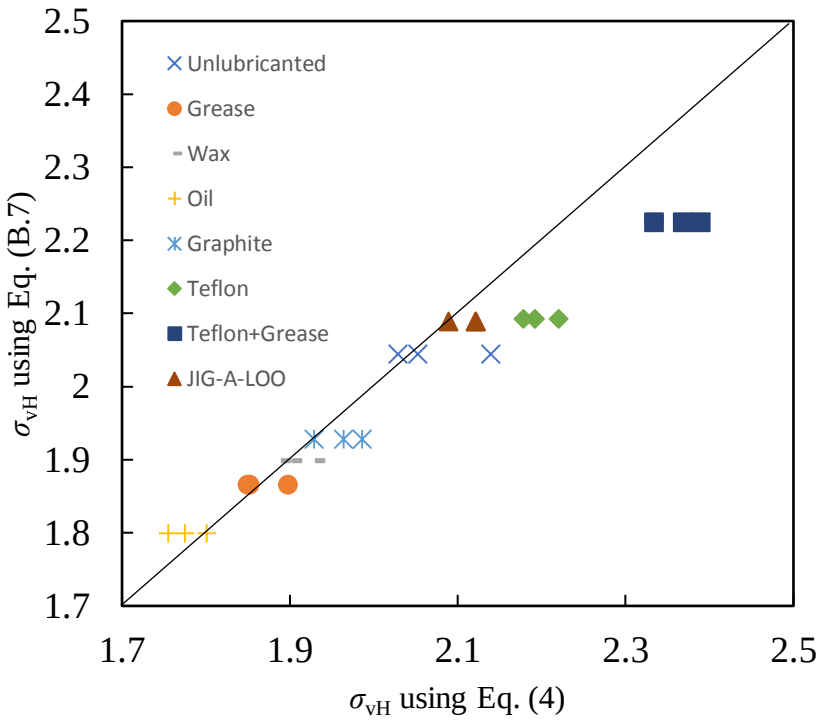

Figure B-6: Agreement between the measured average vertical stress at the bottom of the column and those estimated with Eq. (B.7) and the back-calculated K and δ shown in Table B-3

B7. Arching degree

If the column inner wall is fully smooth without any shear strength (i.e. $\delta = 0$, $c_{app} = 0$), the vertical stress can then be calculated by considering the overburden pressure p_0 at the bottom of the column:

$$p_0 = \frac{4mg}{\pi d^2} \tag{B.11}$$

When the two columns are respectively filled with sand masses of 2324 g and 740 g, the overburden pressure at the bottom of the columns should be 2.86 kPa and 2.33 kPa, respectively.

As the column inner walls are seldom totally smooth and exemption of shear strength, arching occurs more or less, resulting in lower vertical stress than the overburden pressure at the bottom of the column. In order to quantitatively evaluate the lubricants effectiveness in reducing the sidewall friction, the degree of arching U is proposed as follows:

$$U = \frac{p_0 - \sigma_{vh2}}{p_0} = 1 - \frac{\sigma_{vh2}}{p_0} \tag{B.12}$$

where σ_{vh2} is the vertical stress at the bottom of the column when the column was filled to height h_2.

When a lubricant is very efficient in reducing the sidewall shear strength, σ_{vh2} will be very close to p_0. The arching degree U will be expected to be close to 0. If the column is very small with a very rough side wall, σ_{vh2} can be expected much smaller than p_0. The arching degree U will be expected to be close to 1.

Table B-5 shows the degree of arching when the column wall is covered of different lubricant materials. It can be seen that the use of grease or oil generates very high degree of arching, which is 37% for the large column and 47.0% and 47.3% for the small column, respectively. The lowest degree of arching has been obtained by the use of combined Teflon and grease. But, the values of U equaling to 26.1% to 31.5% indicate again significant arching effect occurring in the tests.

All results shown above indicate that if lubricant materials are used to reduce the side wall friction for stress sensor calibration tests, the calibration results would definitely be inaccurate by totally neglecting the shear strength along the side walls.

Table B-5: The degree of arching for different lubricants

Type of lubricant	d = 100.8 mm		d = 62.9 mm	
	σ_{vh2} (kPa)	Arching degree (%)	σ_{vh2} (kPa)	Arching degree (%)
Unlubricated	1.94	32.2	1.44	38.5
Grease	1.80	37.0	1.24	47.0
Oil	1.80	37.0	1.23	47.3
JIG-A-LOO Lubricant	1.98	30.6	1.46	37.5
JIG-A-LOO Graphite	1.85	35.4	1.29	44.6
Wax	1.82	36.2	1.26	46.0
Teflon	1.99	30.2	1.55	33.7
Teflon+Grease	2.11	26.1	1.60	31.5

B8. Validation of the back calculated δ in Table B-3 by direct shear test results

In order to further validate the results shown in Table B-3, the authors also conducted a series of direct shear tests to measrue the internal friciton angle of the tested sand (ϕ) and the friction angle along the contact interfaces between the sand and Plexiglas (δ) with or without applying lubricants

by following the ASTM standard D3080. Fig. B-7 shows the photograph of the direct shear test apparatus. The tests were conducted in a shear box with 60 mm ×60 mm in plane, 25 mm in depth for the upper box and 20 mm in depth for the lower box. For the measurment of the internal friciton angle of the tested sand (ϕ), the air-dried sand was uniformaly poured in the shear box without any compact. The placed sand is very close to the loosest state. For the measurement of the interface friciton angle δ, a small piece of Plexiglas plate with same dimension (60 mm×60mm) as the shear box was prepared, as shown in Fig. B-8. The prepared Plexiglas and metal plate can fully fill the lower shear box half, with the top surface of the Plexiglas at the same level as the lower shear box. A thin layer of lubricant was then uniformly applied on the top surface of the Plexiglas. Air-dried sand was then uniformly placed in the upper shear box to avoid any compact. The direct shear tests were conducted at the vertical normal stress of 10.6, 20, 30, 50 kPa by consiring the low stress level in the column tests.

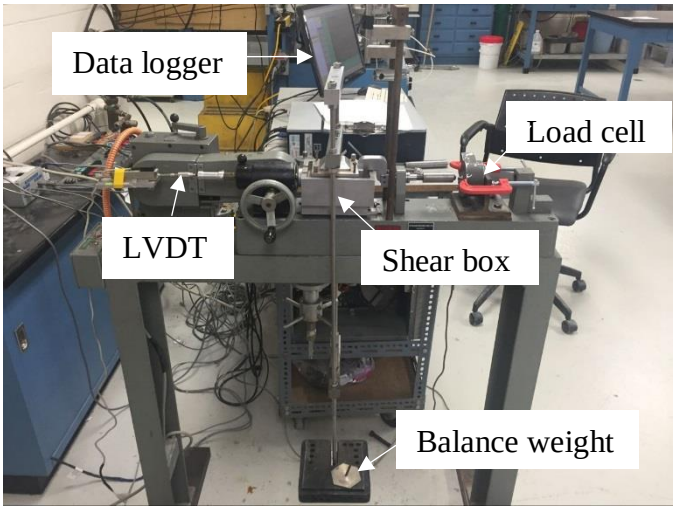

Figure B-7: Photograph of the direct shear test apparatus

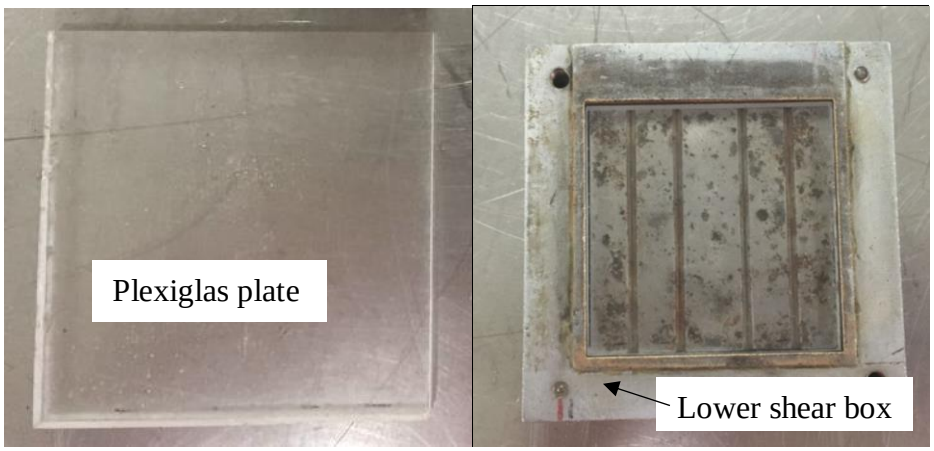

Figure B-8: The prepared Plexiglas plates

Fig. B-9 shows the shear stress- horizontal displacement curves obtained by the direct shear tests on the sand and interface between the sand and Plexiglas with or without using lubricants. One should note that the self-weight of the sand placed in the uppter shear box, the forces applied by the cap plate, the universa ball and the system of lever arm were included in the normal stresses, resulting in the normal stresses of 12, 21.4, 31.4, 51.4 kPa. The peak values of the shear stress were used to determine the friction angle.

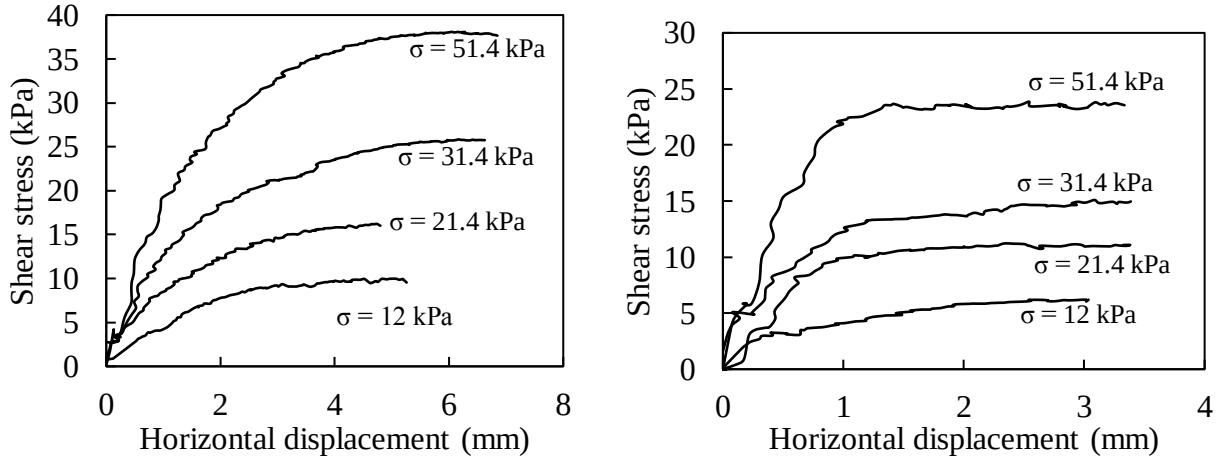

(a) Sand-Sand

(b) Sand-Plexiglas

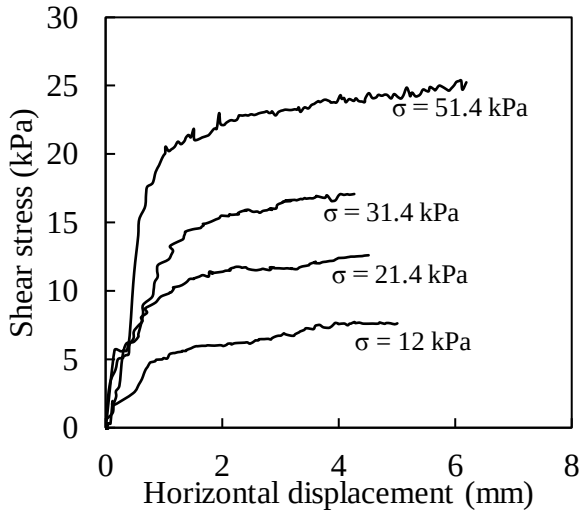

(c) Grease

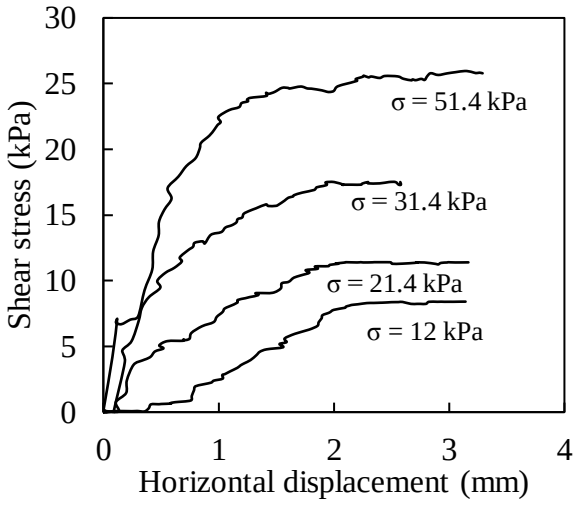

(d) Lubricant oil

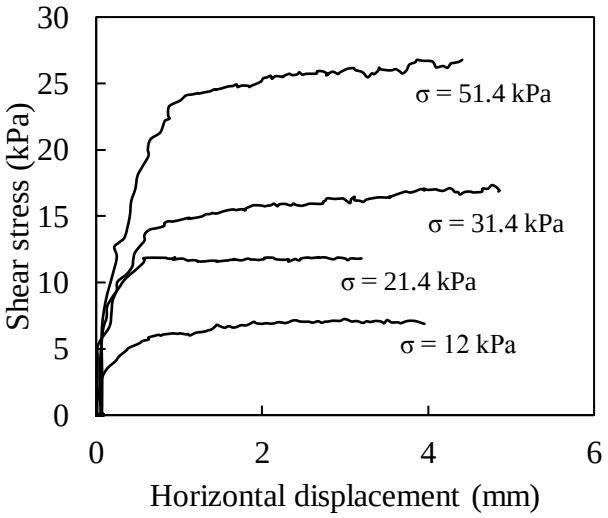

(e) JIG-A-LOO Lubricant

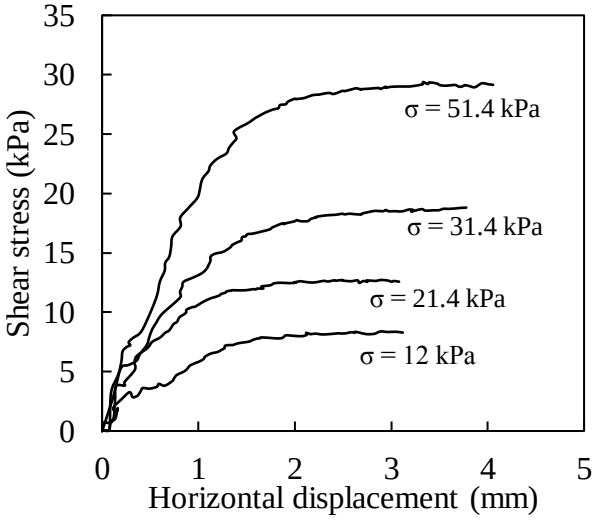

(f) JIG-A-LOO Graphite

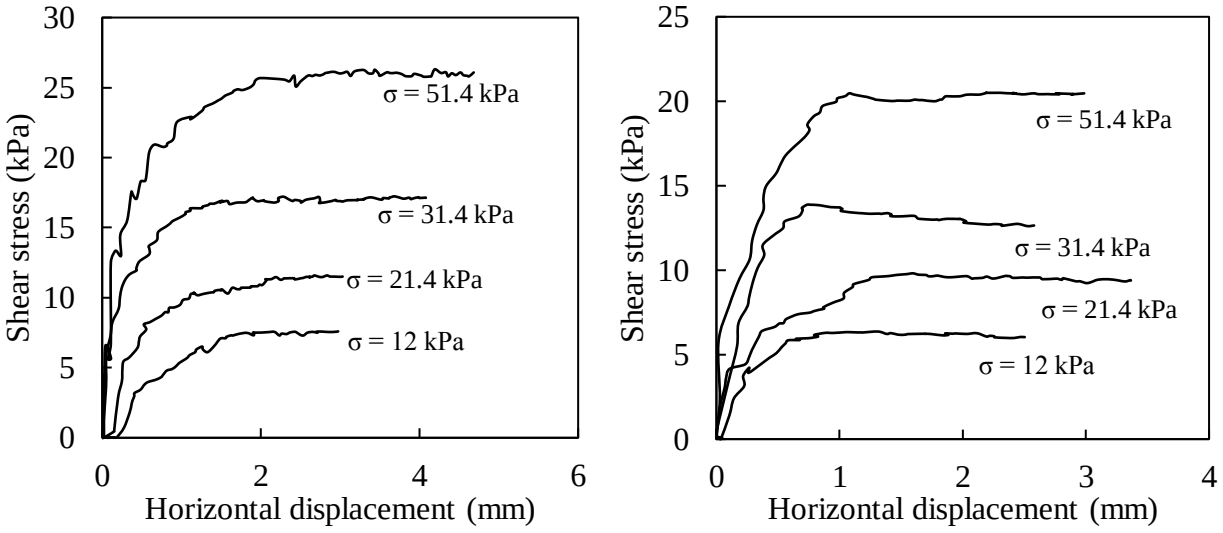

(g) Wax

(h) Teflon

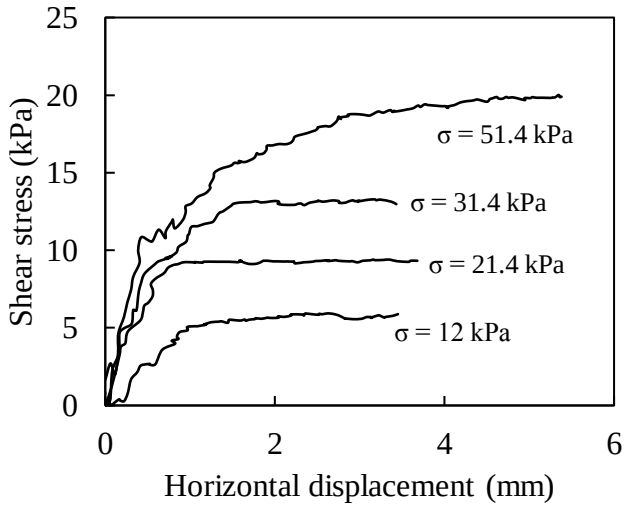

(i) Teflon and Grease

Figure B-9: Shear stress-horizontal displacement curves of the (a) Sand, (b) Sand-Plexiglas, and the interface between the sand and Plexiglas after using (c) Grease, (d) Lubriucant oil, (e) JIG-A-LOO Lubricant, (f) JIG-A-Loo Graphite, (g) wax, (h) Teflon and (i) Teflon and Grease at different normal stresses σ.

Fig. B-10 shows the Mohr-Coulomb envelop of the sand and that of the interface between the sand and Plexiglas with or without lubricants, based on the direct shear test results shown in Fig. B-9.

The friction angle can be calculated by the slope of the Mohr-Coulomb envelop. The internal friction angle of the sand at the loosest state is ϕ = 35.8°, which is close to the measured repose angle (α = 33.5°). The friction angle along the interface between the sand and Plexiglas is measured to be δ = 23.6°, a value close to two thirds of the friction angle of the sand (Das 2010; CGS 2006). Table 6 shows the friction angle along the interface between the sand and Plexiglas after applying different lubricants back calculated by the column tests and measured by the direct shear tests. It can be seen that the back calculated friction angles by the column tests agree well with that measured by the direct shear tests. The back calculated friction angles can thus be considered as valid.

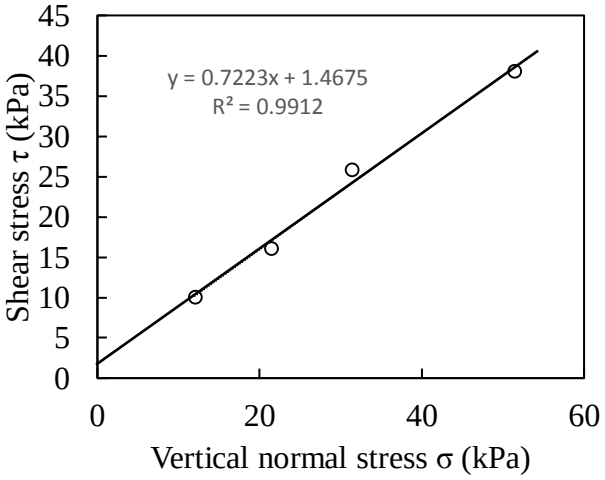

(a) Sand-Sand

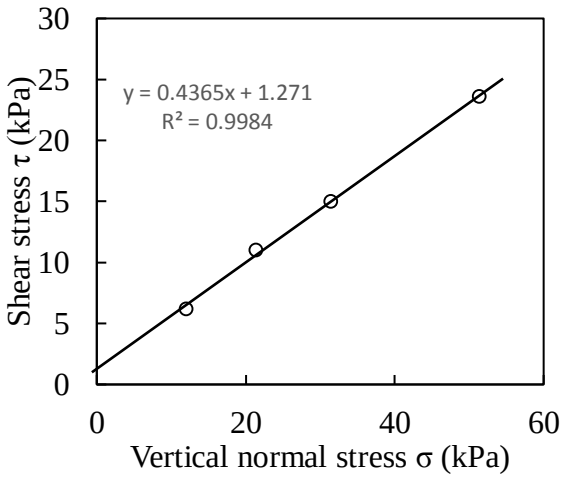

(b) Sand-Plexiglas

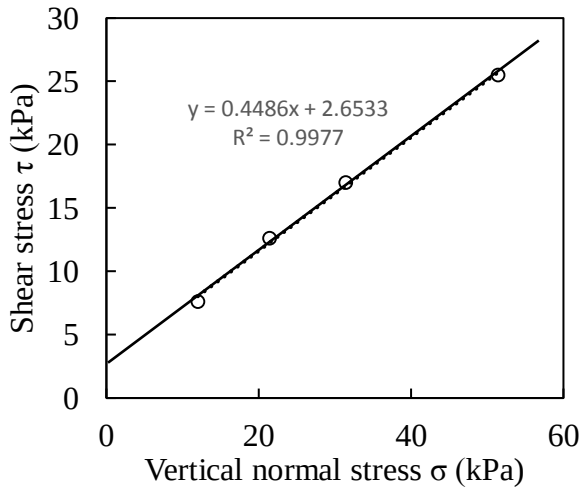

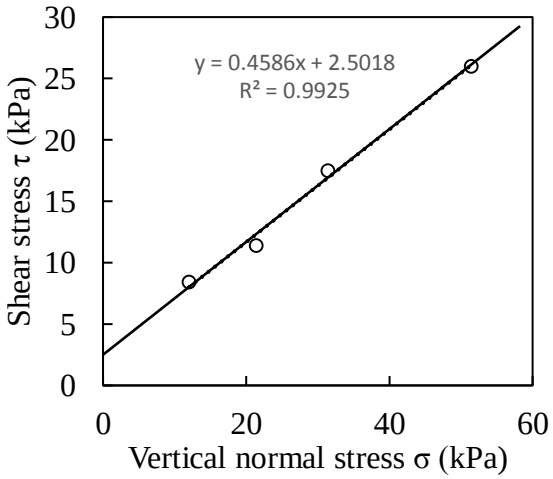

(c) Grease

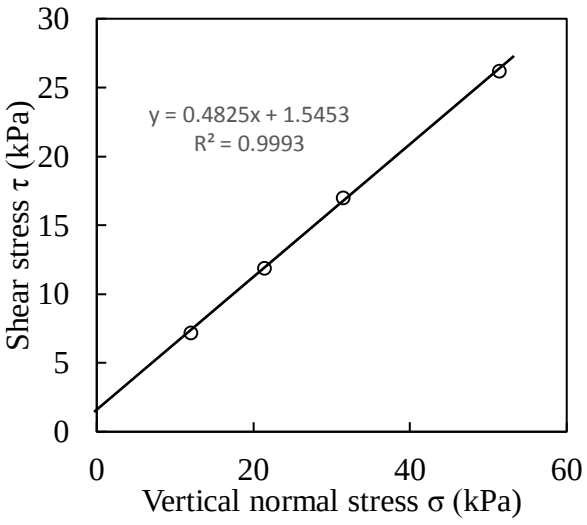

(d) Lubricant oil

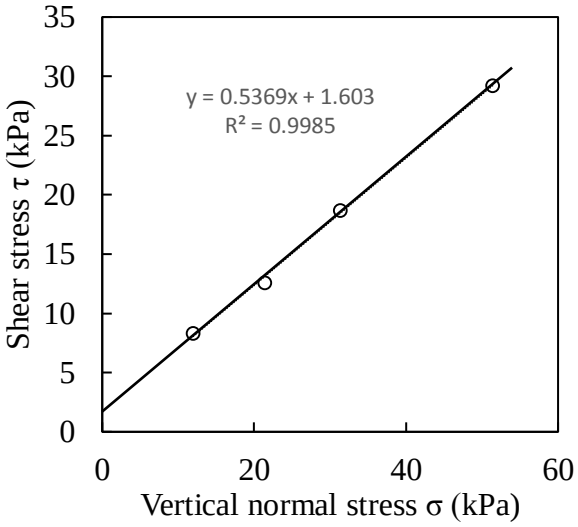

(e) JIG-A-LOO Lubricant

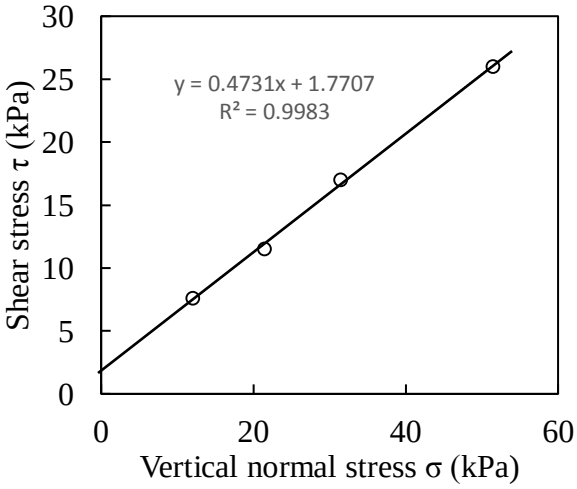

(f) JIG-A-LOO Graphite

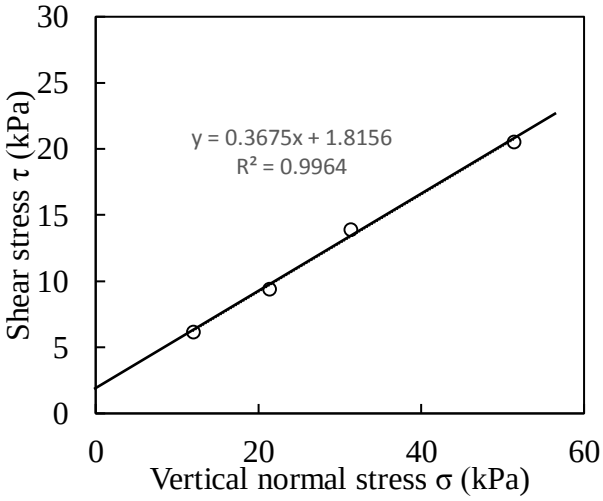

(g) Wax

(h) Teflon

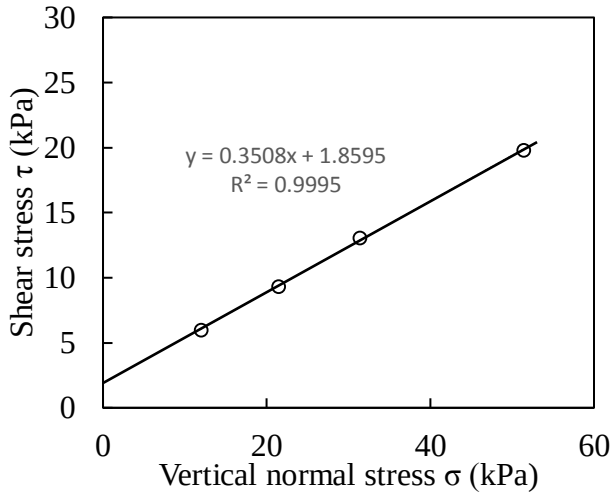

(i) Teflon and Grease

Figure B-10: Mohr-Coulomb envelops of the (a) Sand, (b) Sand-Plexiglas, and the interface between the sand and Plexiglas after using (c) Grease, (d) Lubriucant oil, (e) JIG-A-LOO Lubricant, (f) JIG-A-Loo Graphite, (g) wax, (h) Teflon and (i) Teflon and Grease

Table B-6: The friction angle along the interface (δ) back-calculated with the column test results and measured by the direct shear test

Lubricant	d = 100.8 (mm)	d = 62.9 (mm)	Direct shear test
	δ (°)	δ (°)	δ (°)
Grease	26.7	29.0	24.2
Lubricant oil	28.4	29.7	24.6
JIG-A-LOO Lubricant	21.2	22.2	25.8
JIG-A-LOO Graphite	25.1	27.4	28.2
Wax	25.9	27.9	25.3
Teflon	21.2	19.1	20.1
Teflon and Grease	18.2	16.8	19.3

B9. Discussion

In this paper, a series of sand filling tests were conducted to investigate the effectiveness of different lubricants in reducing the sidewall friction (shear strength). The friction angle δ was back calculated based on the test results and a newly proposed arching solution. The re-productivity of the back-calculated results with the large and small columns as well as the good agreement with the direct shear test results indicates that the test results and interpretation are effective and quite

reliable. Nevertheless, a few drawbacks and limitations are involved in the instrumentation and results interpretation. For instance, the earth pressure coefficient K was considered to be constant along the column height in the results interpretation with the arching solution. This may not be totally true as several studies have shown that the value of K can vary with the position (both in the horizontal and vertical directions; Sobhi et al. 2016; Janhanbakhshzadeh et al. 2017; Yang et al. 2017). More work is required to take this aspect into account.

Another limitation is related to the fixed position of the funnel during the tests. The falling height of the placed sand in the column is very high at the beginning of the filling operation. The impact associated with the mass falling was not evaluated. In addition, the sand density can change (decrease) from the column bottom to the top due to the decrease in the falling height with the filling operation. In this study, the variation of the sand density is neglected in the back calculation of K and δ.

For the interpretation of test results, the effective friction angle δ and earth pressure coefficient K were considered as unknown values and back-calculated using Solver in the authors' previous paper (Zheng et al. 2017). This is not true as detailed analysis of the test results shows that the 'Ktanδ' is actually one parameter in Eq. (B.7), resulting in infinite solution of K and δ as long as the 'Ktanδ' can generate same value.

Finally, the tested sand is dry and at the loosest state, which is expected to have no cohesion for the sand and sand-Plexiglas interface. However, Fig. B-10 shows that the Mohr-Coulomb envelops of the sand and sand-Plexiglas do not pass the origin point, indicating apparent cohesion for sand and sand-Plexiglas interface. The dead weights of the auxiliary pieces (e.g., self-weight of the placed sand, cap plate, the universa ball and the system of lever arm) were considered in the vertical normal streses. The apparent cohesions were reduced, but remain ineligible. This indicates that other influencing factors are missing. More work is needed to identify the problem of the testing system.

B10. Conclusion

The effectiveness of several lubricants in reducing the sidewall friction between the sand and column wall was investigated in this paper by conducting a series of arching tests. The friction angle along the sand-lubricants interfaces were back calculated by the column tests, which agree

well with that measured by the direct shear tests. The results showed that the selected lubricants are not efficient in reducing the sidewall friction. Compared to the tests without any application of lubricants, the use of the combined Teflon and grease is shown to be the most efficient in reducing the side friction angle. The application of JIG-A-LOO Lubricant and Teflon can only slightly reduce the sidewall friction. Surprisingly, the application of oil, grease, graphite or wax has effect to increase the side friction, mostly due to their apparent cohesive shear strength. In all cases, the results indicate that side wall frictions with the application of lubricant materials are far from being qualified as negligible. Arching takes place during the tests, which depend not only the side wall shear strength, but also the column diameter. The definition of degree of arching is proposed to quantitatively evaluate the effectiveness of the lubricants and column dimension. The results further showed that the arching degrees are 26.1% and 31.5% for the large and small column, respectively, even though the combined Teflon and grease is used, which has the lowest friction angle. Neglecting the sidewall friction (shear strength) due to the application of lubricants between the tested soil and sidewall can lead to inaccurate and even totally wrong sensor calibration results.

B11. Appendix I: Derivation process of Eq. (B.7)

Fig. B-11 shows a backfilled column with a circular cross section and various forces acting on an isolated layer element. On the figure, p is the uniform pressure acted on the column top surface, H and B are the height and diameter of the column, respectively. At a given height h, a horizontal layer is subjected to vertical forces V and V+dV, a lateral compressive force C, a shearing stress S and own weight W.

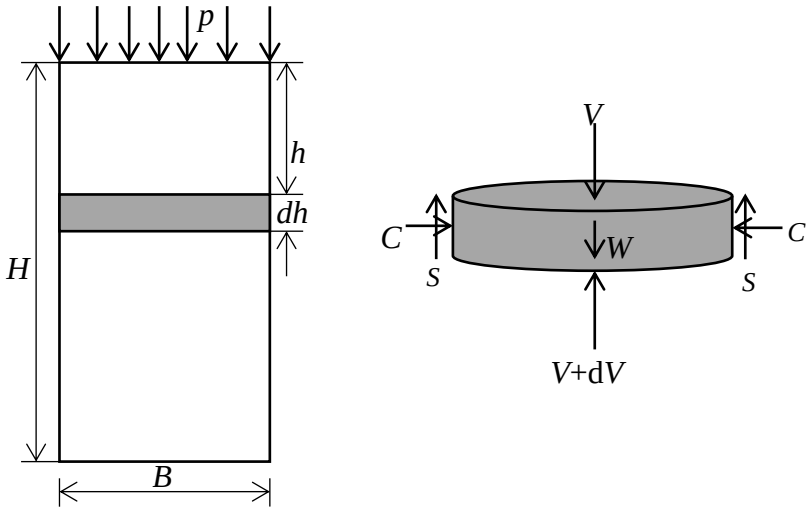

Figure B-11: A vertical backfilled column with a circular cross section and forces acting on an isolated layer element

The equilibrium of the horizontal element layer can be expressed as

$$dV + \pi BS = W \tag{B.13}$$

The weight of the backfill in this horizontal layer is given by

$$W = \gamma\pi\left(\frac{B}{2}\right)^2 dh \tag{B.14}$$

where *dh* is the thickness of the element layer.

By assuming that the vertical stress distributed uniformly along the horizontal plane, the vertical force can be expressed as

$$V = \sigma_v\pi\left(\frac{B}{2}\right)^2 \tag{B.15}$$

Using the Coulomb criterion, the shearing force acted on the element layer can be expressed as:

$$S = \sigma_h \tan\delta dh = K\sigma_v \tan\delta dh \tag{B.16}$$

Substituting Eqs. (B.14), (B.15) and (B.16) into Eq. (B.13) yields,

$$\frac{d\sigma_v}{dh} + \frac{4K\sigma_v \tan\delta}{B} = \gamma \tag{B.17}$$

Considering the boundary condition $\sigma_v = p$, at $h = 0$, the vertical stress at a given height h can be solved as:

$$\sigma_v = \frac{\gamma B}{4K\tan\delta}\left[1 - \exp(-\frac{4K\tan\delta}{B}h)\right] + p \times \exp(-\frac{4K\tan\delta}{B}h) \tag{B.18}$$

B12. Appendix II: Sample calculation of using Solver® to back calculate *K* and *δ*

Microsoft Excel® built-in optimization program, Solver®, is used to back calculate the value of *K* for the case of unlubricated column. Fig. B-12 shows an example set of calculation. Col. E

represents the measured σ_v obtained from the balance reading in Col. D using Eq. (B.4). Col. F refers to the calculated σ_v using Eq. (B.7) and the unknown K in cell D1 and δ (= 22.3°) in cell D2. Function in Col. G represents the square of the difference between the calculated σ_v in Col. F and tested σ_v in Col. E. The sum of the squared differences is shown in Cell G2 as the objective function. Solver® is used to determine the optimal K corresponding to the minimum value of summation in Cell G2. The calculated K will be used as know value to find the optimal δ (unknown) for the other lubricant materials in the Solver® by using the above-mentioned process again.

	A	B	C	D	E	F	G
1	Unlubricated		K =	0.28382342			
2			δ =	22.3	Sum of Col. G= objective Function		0.031787941
3	γ (kN/m^3)	d (m)	H (m)	Balance reading (g)	Tested σ_v (kPa)	Cal. σ_v (kPa)	(Col. F - Col. E)^2
4	15	0.1008	0.12	1130.0	1.387021067	1.467992499	0.006556373
5	15	0.1008	0.115	1098.0	1.347742594	1.426419194	0.006190007
6	15	0.1008	0.11	1098.7	1.34860181	1.383874532	0.001244165
7	15	0.1008	0.112	1070.0	1.31337393	1.401010401	0.007680151
8	15	0.1008	0.18	1608.2	1.973988743	1.898694492	0.005669224
9	15	0.1008	0.18	1567.6	1.92415418	1.898694492	0.000648196
10	15	0.1008	0.18	1595.8	1.958768334	1.898694492	0.003608867
11	15	0.1008	0.18	1535.6	1.884875708	1.898694492	0.000190959

Figure B-12. An example of back calculation of K with Solver® in Microsoft Excel

B13. References:

ASTM International. (2004). *Standard Test Methods for One-Dimensional Consolidation Properties of Soils Using Incremental Loading*. Standard ASTM D2435/D2435M, West Conshohocken, PA.

Brumund, W.F., & Leonards, G.A. (1973). Experimental study of static and dynamic friction between sand and typical construction materials. *Journal of Testing Evaluation*, *1*(2), 162-165.

Canadian geotechnical Society. (2006). *Canadian foundation engineering manual* (4th ed.), Vancouver, Canada: Bitech.

Das, B.M. (2004). *Principles of foundation engineering* (5th Ed.), New York: Thomson/Brooks/Cole.

Fang, Y.S., Chen, T.J., & Wu, B.F. (1994). Passive earth pressures with various wall movements. *Journal of Geotechnical Engineering, 120*(8), 1307-1323.

Feng, X.T., Zhang, X.W., Yang, C.X., Kong, W., Liu, X.Y., & Peng, S. (2017). Evaluation and reduction of the end friction effect in true triaxial tests on hard rocks. *International Journal of Rock Mechanics and Mining Sciences, 97*, 144-148.

Fox, P.J., & Baxter, C.D.P. (1997). Consolidation properties of soil slurries from hydraulic consolidation test. *Journal of Geotechnical and Geoenvironment Engineering*, *123*(8), 770-776.

Gade, V.K., & Dasaka, S.M. (2018). Calibration of Earth Pressure Sensors. *Indian Geotechnical Journal*, 48(1), 142-152.

Ghazavi, M., Hosseini, M., & Mollanouri, M. (2008). *A comparison between angle of repose and friction angle of sand*. Paper presented at the 12th International Conference for International Association for Computer Methods and Advances in Geomechanics (IACMAG), Goa, India (pp. 1-6).

Jahanbakhshzadeh, A., Aubertin, M., & Li, L. (2017). A new analytical solution for the stress state in inclined backfilled mine stopes. *Geotechnical and Geological Engineering*, *35*(3), 1151-1167.

Jaky, J. (1948). *Pressure in silos*. Paper presented at the 2nd International Conference on Soil Mechanics and Foundation Engineering, Rotterdam, The Netherlands (pp. 103-107).

Janssen, H.A. (1895). Versuche über getreidedruck in silozellen. *Zeitschrift Verein Ingenieure*, 39, 1045-1049.

Marston, A. (1930). The theory of external loads on closed conduits in the light of latest experiments. Iowa Engineering Experiment Station, Ames, Iowa (pp. 138-170).

Pedroni, L., & Aubertin, M. (2013). *Measurement and simulation of the large strain consolidation of AMD treatment sludge*. Paper presented at the 66th Canadian Geotechnical Conference, Montréal, Canada.

Pirapakaran, K., & Sivakugan, N. (2006). *Numerical and experimental studies of arching effects within mine fill stopes*. Paper presented at the 6th International Conference on Physical Modelling in Geotechnics, Hong Kong, China (pp. 1519-1525).

Pirapakaran, K., & Sivakugan, N. (2007). A laboratory model to study arching within a hydraulic fill stope. *Geotechnical Testing Journal, 30*(6), 496-503.

Sobhi, M.A., Li, L., & Aubertin, M. (2017). Numerical investigation of earth pressure coefficient along central line of backfilled stopes. *Canadian Geotechnical Journal, 54*(1), 138-145.

Sridharan, A., & Prakash, K. (1999). Simplified seepage consolidation test for soft sediments. *Geotechnical Testing Journal, 22*(3), 235-244.

Tatsuoka, F., Molenkamp, F., Torii, T., & Hino, T. (1984). Behavior of lubrication layers of platens in element tests. *Soils and Foundations, 24*(1), 113-128.

Tatsuoka, F., & Haibara, O. (1985). Shear resistance between sand and smooth or lubricated surfaces. *Soils and Foundations, 25*(1), 89-98.

Terzaghi K. (1943) *Theory of consolidation*. New York, USA: John Wiley.

Watabe, Y., Tanaka, M., Tanaka, H., & Tsuchida, T. (2003). K_0-consolidation in a triaxial cell and evaluation of in-situ K_0 for marine clays with various characteristics. *Soils and Foundations, 43*(1), 1-20.

Yang, P.Y., Li, L., & Aubertin, M. (2017). Stress ratios in entire mine stopes with cohesionless backfill: A numerical study. *Minerals, 7*(10), 201.

Zheng, J., Li, L., & Daviault, M. (2017). *An experimental study of the effectiveness of lubricants in reducing the sidewall friction*. Paper presented at the 19th International Conference on Civil, Environmental and Infrastructure Engineering, Kyoto, Japan.

Zhu, B.T., Jardine, R.J., & Foray, P. (2009). The use of miniature soil stress measuring cells in laboratory applications involving stress reversals. *Soils and Foundations, 49*(5), 675-688.

APPENDIX C – ADDITIONAL RESULTS RELATED TO CHAPTER 3

This section presents the sensitivity analysis of the mesh size, time step and thickness of backfill layer on the calculated excess PWP in the numerical modeling using SIGMA/W. The calculations were conducted by considering the backfill properties of E' = 864 kPa (drained Young's modulus); v = 0.2 (Poisson's ratio); k = 2.83 ×10^{-7} m/s (hydraulic conductivity); c_v = 0.1 m^2/h (consolidation coefficient); m = 1 m/h (filling rate). The same sensitivity analysis has been conducted in Chapter 4 for backfill deposited on an impervious base.

C1. Influence of mesh size

Fig. C-1 shows the distribution of the excess PWP along the full height of the backfill at the end of deposition by considering different mesh sizes of backfill. The results indicate that the mesh elements of 0.1 m quadrilateral and triangular are fine enough for the numerical modeling.

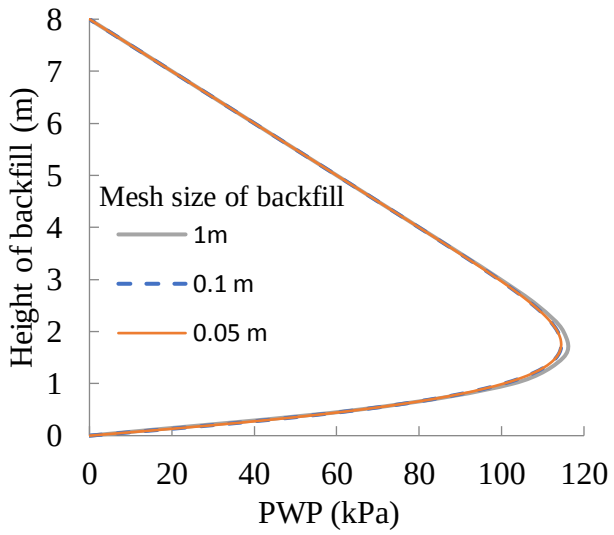

Figure C-1: Distribution of the excess PWP along the full height of the backfill at the end of deposition obtained by numerical models with different mesh sizes; calculation made with E' = 864 kPa, μ = 0.2, k = 2.83 ×10^{-7} m/s, c_v = 0.1 m^2/h and m = 1 m/h.

C2. Influence of time step

Fig. C-2 shows the distribution of the PWP along the full height of the backfill at the end of deposition by considering different time steps. The results show that excess PWP are insensitive to the variation of the time step with the considered range of the time step.

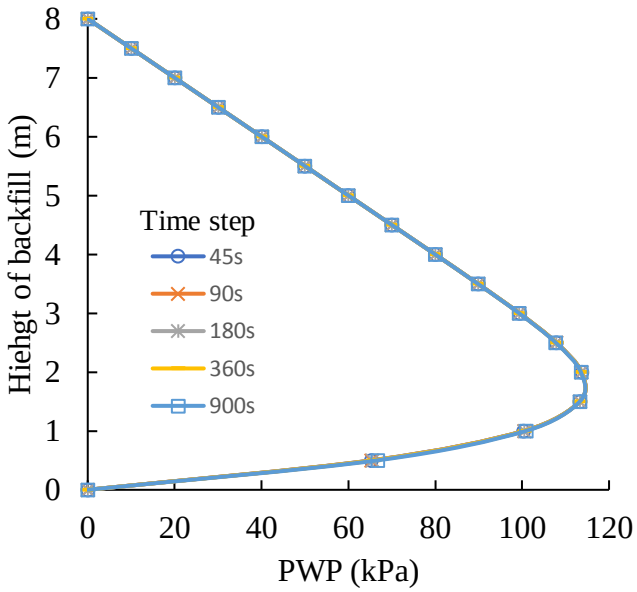

Figure C-2: Distribution of the PWP along the full height of the backfill at the end of deposition obtained by numerical models with different time steps; calculation made with E' = 864 kPa, μ = 0.2, k = 2.83 ×10^{-7} m/s, c_v = 0.1 m^2/h and m = 1 m/h.

C3. Influence of the thickness of each layer

Fig. C-3 shows the distribution of the PWP along the full height of the backfill at the end of deposition by using different thicknesses in the numerical models. The results indicate that the thickness of 0.25 m is thin enough to obtain stable numerical results.

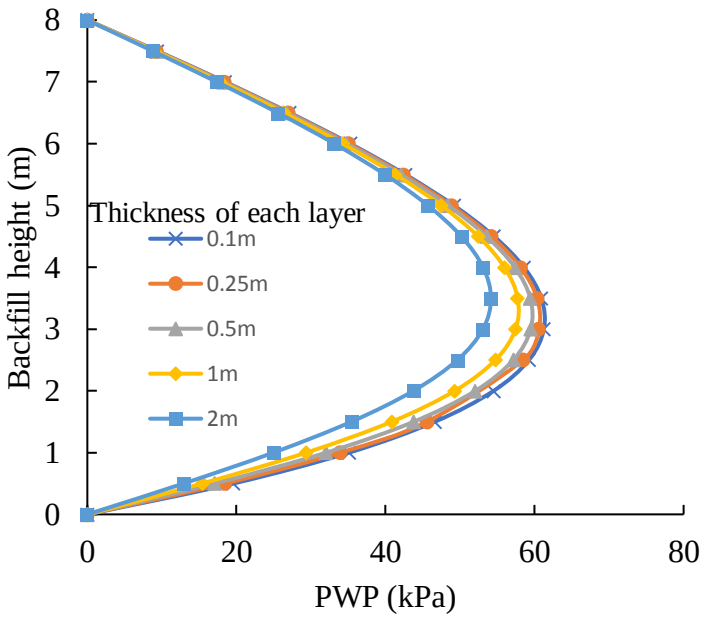

Figure C-3: Distribution of the PWP along the full height of the backfill at the end of deposition obtained by numerical models with different thicknesses of layer; calculation made with E' = 864 kPa, μ = 0.2, k = 2.83 ×10^{-7} m/s, c_v = 0.1 m^2/h and m = 1 m/h.

APPENDIX D – ADDITIONAL RESULTS RELATED TO CHAPTER 4

The sensitivity analyses to determine the optimum mesh size, time step and thickness of each layer in the numerical simulations were conducted by following the same procedure presented in Appendix C. The results are not presented here. In this section, a sample calculation of Eq. (4.12) with EXCEL is presented to evaluate the excess PWP. The sensitivity analyses of the parameters n and h_0 in the proposed analytical solution [Eq. (4.12)] are illustrated. The application of non-zero PWP along the top surface in the numerical models is presented.

D1. Sample calculation of Eq. (4.12) with EXCEL

Fig. D-1 shows the sample calculation of Eq. (4.12) using EXCEL to evaluate the excess PWP. The geometry and backfill properties are: H = 8 m (backfill height), γ' = 10.2 kN/m^3 (submerged unit weight), c_v = 0.1 m^2/h (consolidation coefficient) and m = 0.2 m/h (filling rate).

$$u = -\frac{\gamma' T c_v}{m} - \frac{2\gamma' \sqrt{T c_v h_0^2}}{\sqrt{\pi} m} \exp\left(\frac{-z^2 m^2}{4 c_v^2 T}\right) \times F(y)$$

$$F(y) = \sum_{n=-\infty}^{\infty} f(y) = \sum_{n=-\infty}^{\infty} n \times \tanh\left(n h_0 \sqrt{T}\right) \times \cosh\left(\frac{z n m h_0}{\sqrt{T} c_v}\right) \times \exp(-n^2 h_0^2)$$

	A	B	C	D	E	F	G	H	T	U	V	W	X
1		h_0=	0.5										
2		γ'=	10.2	kN/m^3									
3		c_v=	0.1	m^2/h									
4		m=	0.2	m/h									
5		H=	8	m									
6		t=	40	h									
7		T=mh/c_v=	16										
8													
9													
10			$\frac{mnh_0}{c_v\sqrt{T}}$	Z(m) =	0.001	0.005	0.01	0.1 ➡	6	6.5	7	7.5	8
11	n	$nh_0\sqrt{T}$			f(y)	f(y)	f(y)	f(y)	f(y)	f(y)	f(y)	f(y)	f(y)
12	-55	-110	-13.75		0	0	0	0	0	0	0	0	0
13	-54	-108	-13.5		0	0	0	0	1E-280	8.7E-278	7.4E-275	6.4E-272	5.4E-269
14	-53	-106	-13.25		5.5E-304	5.5E-304	5.6E-304	1.1E-303	9.3E-270	7E-267	5.3E-264	4E-261	3E-258
15	-52	-104	-13		1.4E-292	1.4E-292	1.4E-292	2.7E-292	5.1E-259	3.4E-256	2.3E-253	1.5E-250	1E-247
16	-51	-102	-12.75		2E-281	2E-281	2E-281	3.9E-281	1.7E-248	1E-245	5.9E-243	3.4E-240	2E-237
17	-50	-100	-12.5		1.8E-270	1.8E-270	1.9E-270	3.5E-270	3.4E-238	1.8E-235	9.2E-233	4.8E-230	2.5E-227

62	-5	-10	-1.25		0.009652	0.009652	0.009653	0.009728	8.72586	16.30205	30.45624	56.89974	106.3027
63	-4	-8	-1		0.073263	0.073263	0.073266	0.073629	14.7782	24.36504	40.1711	66.23091	109.1963
64	-3	-6	-0.75		0.316194	0.316196	0.316203	0.317084	14.23319	20.70781	30.12876	43.83646	63.78123
65	-2	-4	-0.5		0.735266	0.735268	0.735275	0.736185	7.402404	9.495627	12.18542	15.64079	20.0788
66	-1	-2	-0.25		0.750785	0.750786	0.750788	0.75102	1.766155	1.980321	2.225469	2.505436	2.824602
67	0	0	0		0	0	0	0	0	0	0	0	0
68	1	2	0.25		0.750785	0.750786	0.750788	0.75102	1.766155	1.980321	2.225469	2.505436	2.824602
69	2	4	0.5		0.735266	0.735268	0.735275	0.736185	7.402404	9.495627	12.18542	15.64079	20.0788
70	3	6	0.75		0.316194	0.316196	0.316203	0.317084	14.23319	20.70781	30.12876	43.83646	63.78123
71	4	8	1		0.073263	0.073263	0.073266	0.073629	14.7782	24.36504	40.1711	66.23091	109.1963
72	5	10	1.25		0.009652	0.009652	0.009653	0.009728	8.72586	16.30205	30.45624	56.89974	106.3027

117	50	100	12.5		1.8E-270	1.8E-270	1.9E-270	3.5E-270	3.4E-238	1.8E-235	9.2E-233	4.8E-230	2.5E-227
118	51	102	12.75		2E-281	2E-281	2E-281	3.9E-281	1.7E-248	1E-245	5.9E-243	3.4E-240	2E-237
119	52	104	13		1.4E-292	1.4E-292	1.4E-292	2.7E-292	5.1E-259	3.4E-256	2.3E-253	1.5E-250	1E-247
120	53	106	13.25		5.5E-304	5.5E-304	5.6E-304	1.1E-303	9.3E-270	7E-267	5.3E-264	4E-261	3E-258
121	54	108	13.5		0	0	0	0	1E-280	8.7E-278	7.4E-275	6.4E-272	5.4E-269
122	55	110	13.75		0	0	0	0	0	0	0	0	0
123				F(y)=	3.771869	3.771881	3.771918	3.776858	101.1856	161.7541	265.4125	447.2162	774.1816
124				*u* =	59.88839	59.88836	59.88824	59.87326	20.2109	15.1979	10.14545	5.069178	-0.02069

Figure D-1: Sample calculation of Eq. (4.12) using EXCEL to calculate excess PWP.

D2. Sensitivity analyses of n and h_0 in Eq. (4.12)

Eq. (4.12) contains parameters n and h_0; the value of n should be large enough while the value of h_0 should be small enough to obtain stable results of u. Fig. D-2 shows the variation of u calculated with Eq. (4.12) by using different values of n and h_0. It can be seen that stable results of u can be obtained when h_0 is taken as 0.3 and n in the range of -91 to 91.

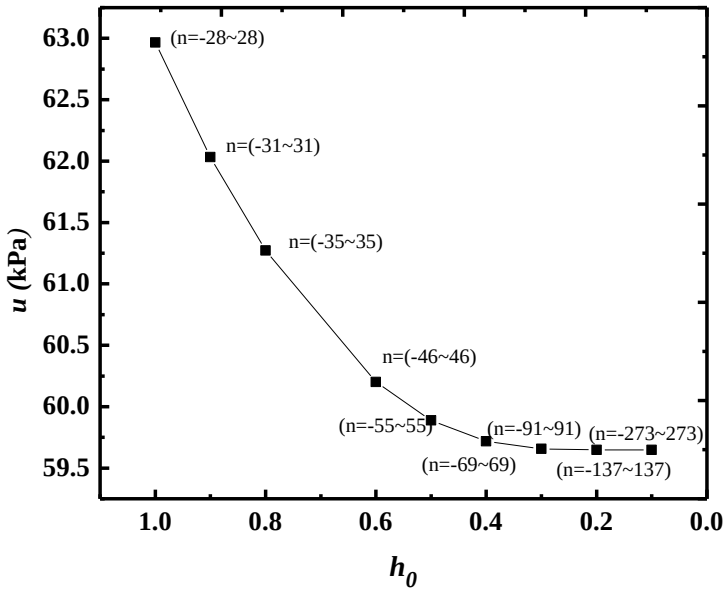

Figure D-2: Variation of excess PWP at the bottom (z = 0 m) of the backfill calculated with Eq. (4.12) using different value of n and h_0.

D3. Effect of non-zero PWP along the top surface of the slurry deposition

In the numerical simulations presented in Chapters 3 to 8, the top surface of each newly added backfill layer is assumed to be permeable with zero PWP. Fig. D-3 shows the distribution of the PWP along the height of the backfill at the end of deposition obtained with SIGMA/W by using

zero PWP and non-zero PWP boundary conditions along the top surface of each newly added backfill layer. The results show that the application of non-zero PWP boundary condition along the top surface of each newly added backfill layer can result in much higher PWP along the height of the backfill; the non-zero PWP on top surface of the backfill indicate the formation of water pond at the top surface of the backfill.

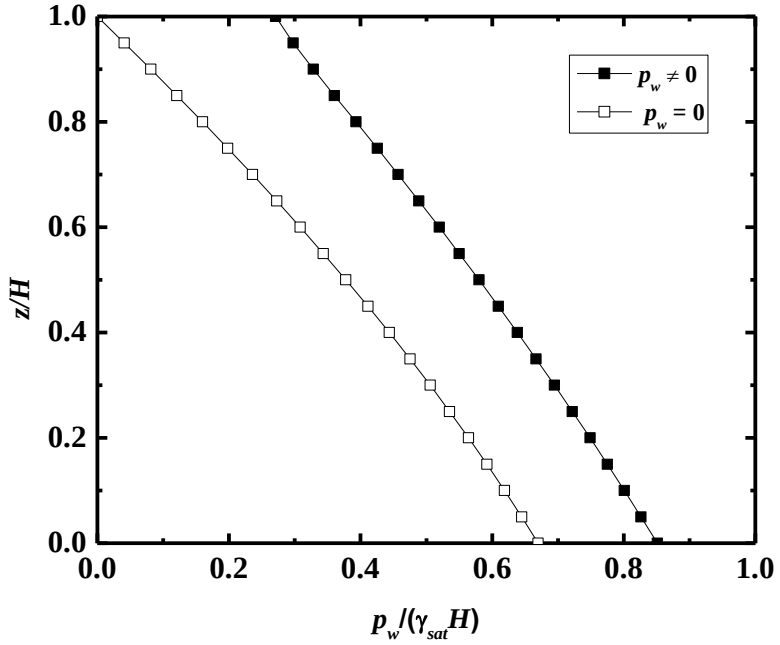

Figure D-3: Distribution of the PWP along the height of the backfill at the end of deposition obtained by SIMG/W by considering zero and non-zero PWP boundary conditions along the top surface of each new backfill layer; calculation made with c_v = 1 m^2/h, m = 0.2 m/h and H = 8 m.

APPENDIX E – ADDITIONAL RESULTS RELATED TO CHAPTER 6

This section presents the sensitivity analyses of the mesh size, time step and backfill thickness of each layer for the numerical simulations performed with SIGMA/W in Chapter 6.

E1. Influence of mesh size of the placed backfill

Fig. E-1 shows the evolution of the PWP with time at the bottom of the backfill after the end of the slurry deposition [Fig. E-1(a)] and distribution of PWP along the height of backfill 4 h after the end of deposition [Fig. E-1(b)] obtained by SIGMA/W with different mesh sizes of backfill. It can be seen that the mesh size of the backfill has almost no influence on the PWP in the backfilled stope after the end of deposition. However, as the optimum mesh size is 0.1 m quadrilateral and triangular for the case of during the accreting deposition, this mesh size is still used in the SIGMA/W for the case of after the deposition.

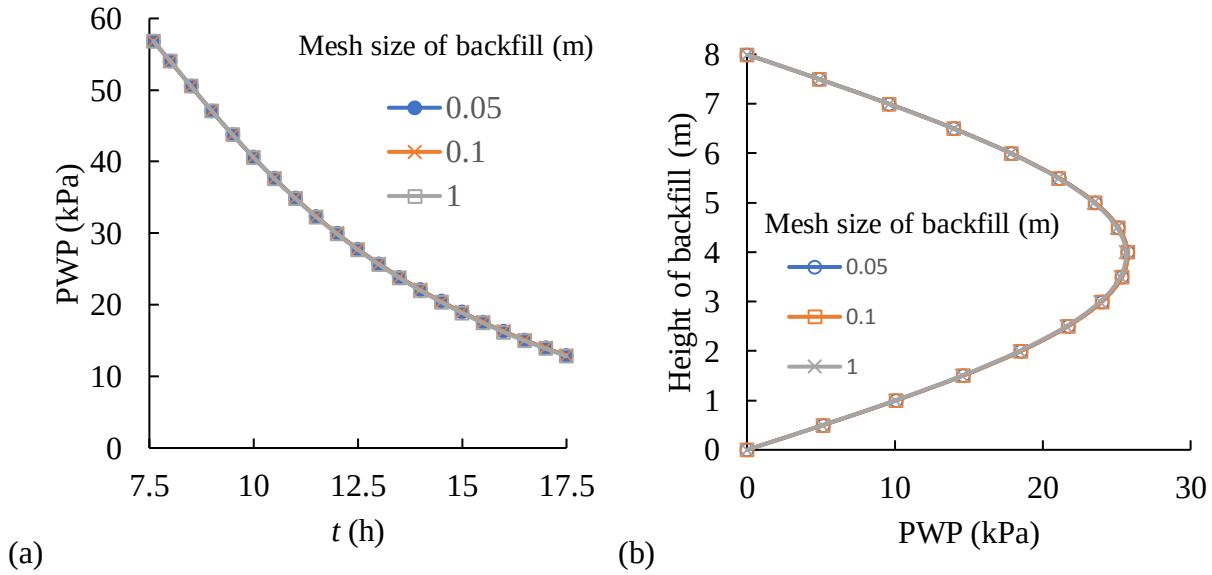

Figure E-1: (a) Evolution of the PWP with time at the bottom of the backfill after the end of deposition, obtained by numerical models with different mesh sizes; (b) distribution of the PWP along the height of backfill 4 hours after the end of the deposition, obtained by numerical models with different mesh sizes.

E2. Influence of the time step

Fig. E-2 shows the variation of the PWP in the backfill 10 h after the slurry deposition, obtained by numerical models with different time steps. The results show that a time step of 360 s is good enough to ensure the stable numerical results.

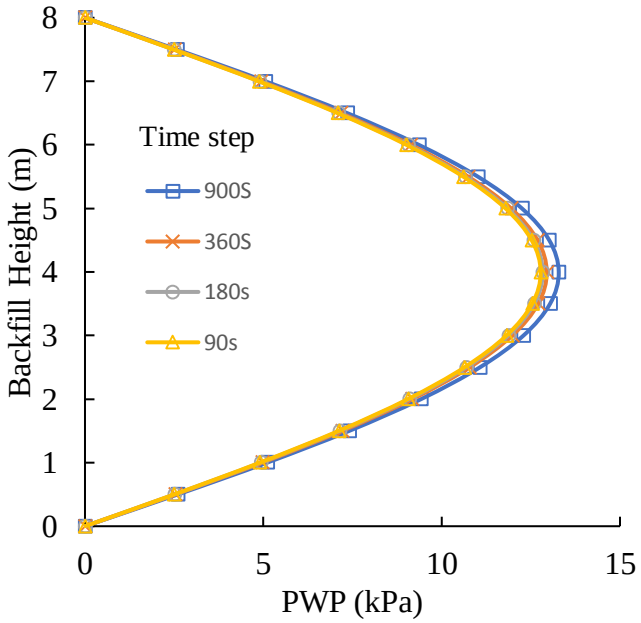

Figure E-2: Distribution of PWP along the height of the backfill 10 h after the slurry deposition, obtained by SIGMA/W with different time steps.

E3. Influence of the thickness of each layer

Fig. E-3 shows the variation of the PWP distributions along the height of the backfill 10 h after the slurry deposition, obtained by SIGMA/W with different thicknesses of each layer. One sees that a thickness of 0.25 m is thin enough to ensure stable numerical results.

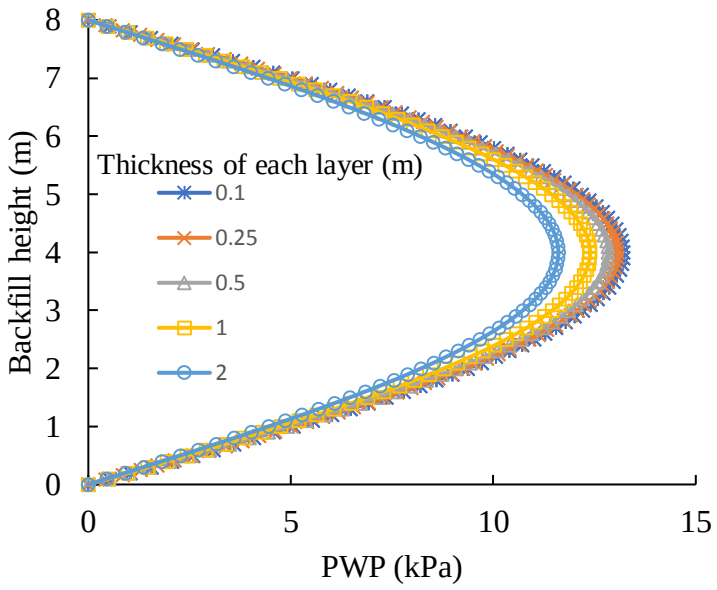

Figure E-3: Distribution of PWP along the height of the backfill 10 h after the slurry deposition, obtained by SIGMA/W with different thicknesses of each layer.

APPENDIX F – ADDITIONAL RESUTLS RELATED TO CHPTER 7

This section presents the sensitivity analyses on the mesh size and thickness of each layer in the numerical simulations conducted with Plaxis2D. Additional results for the validation of the proposed solutions [Eqs. (7.2) and (7.29)-(7.32)] are also presented.

F1. Sensitivity analysis of mesh size

In the numerical models built with Plaxis2D, the mesh size was modified through the change of coarseness factor, which indicates the local mesh refinement at a certain geometric entity. The mesh can be refined or enlarged by using a coarseness factor smaller or larger than 1, respectively. Here, the values of coarseness factor were chosen to be 0.05, 0.1, 1 and 2.

Fig. F-1 shows the distributions of PWP [Fig. F-1(a)], horizontal [Fig. F-1(b)] and vertical [Fig. F-1(c)] effective stresses, and horizontal [Fig. F-1(d)] and vertical [Fig. F-1(e)] total stresses along the full height of the backfill at the end of filling operation, obtained by Plaxis2D with different mesh sizes. It can be seen that the mesh size has almost no influence on the numerical results for the considered range of the mesh size.

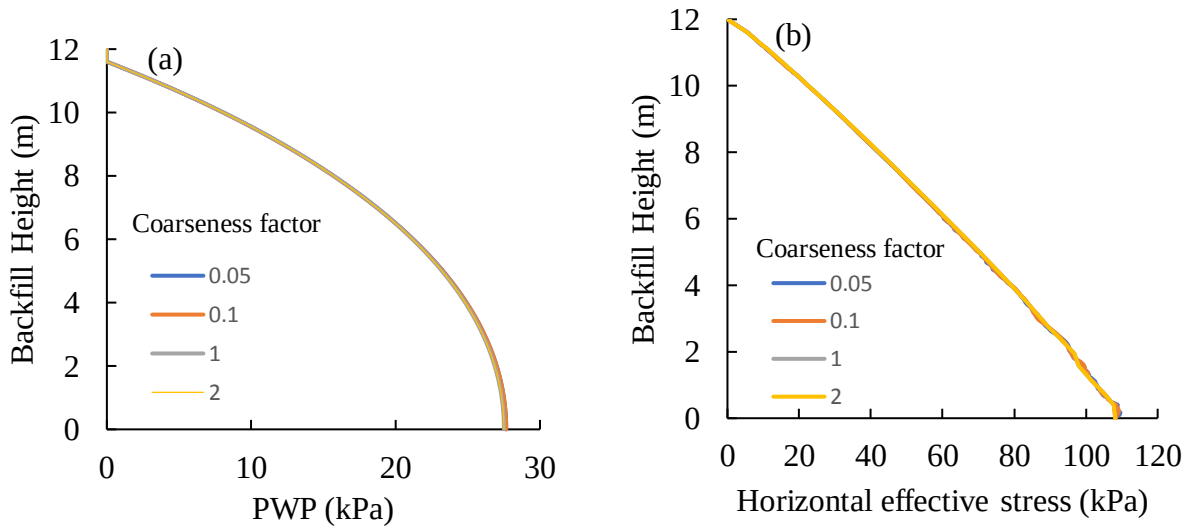

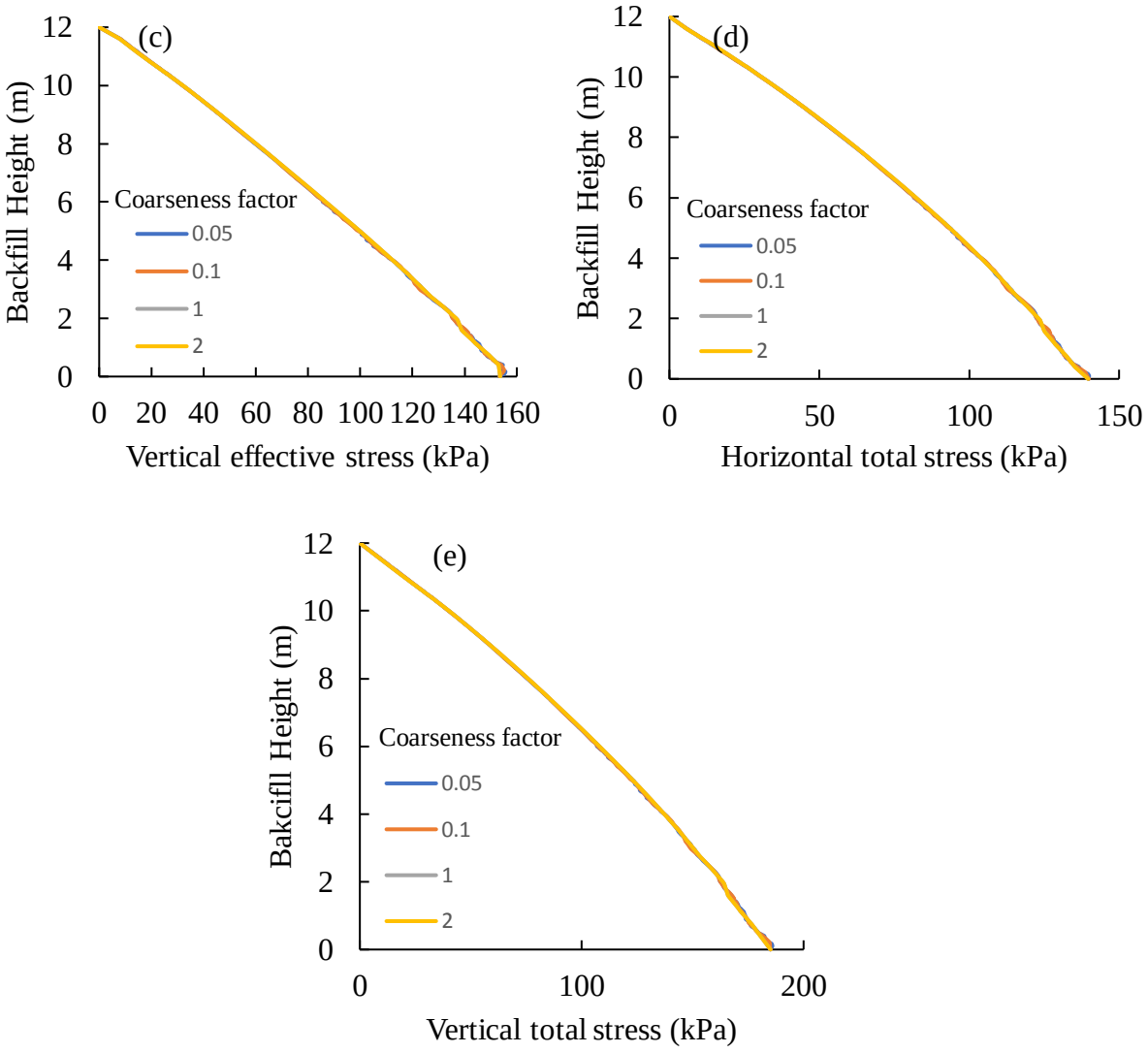

Figure F-1: Distribution of the PWP (a), horizontal (b) and vertical (c) effective stresses, and horizontal (d) and vertical (e) total stresses along the full height of the backfill at the end of filling operation, obtained by Plaxis2D with different coarseness factors.

F2. Sensitivity analysis of thickness of each layer

Fig. F-2 shows the distributions of the PWP [Fig. F-2(a)], horizontal [Fig. F-2(b)] and vertical [Fig. F-2(c)] effective stresses, and horizontal [Fig. F-2(d)] and vertical [Fig. F-2(e)] total stresses along the full height of the backfill at the end of filling operation, obtained by numerical modeling with Plaxis by considering different thicknesses to simulate a continuous backfilling. The results show that a thickness of 0.4 m is thin enough to ensure stable numerical results.

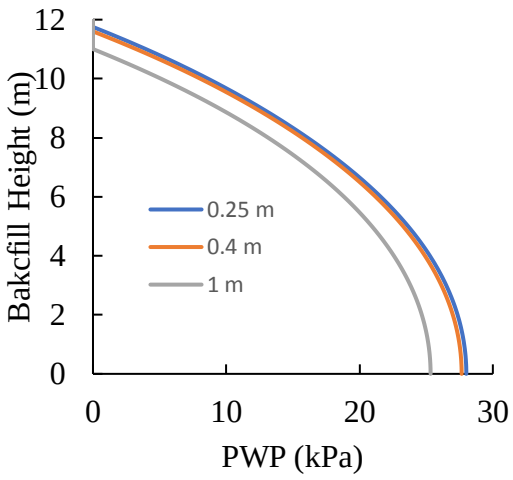
Bakcfill Height (m)
PWP (kPa)
0.25 m
0.4 m
1 m

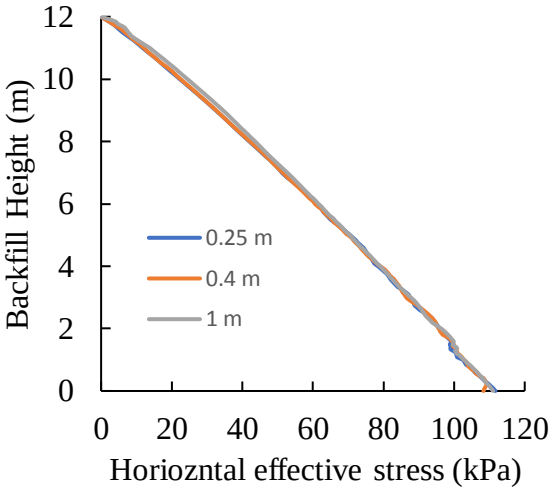
Backfill Height (m)
Horiozntal effective stress (kPa)
0.25 m
0.4 m
1 m

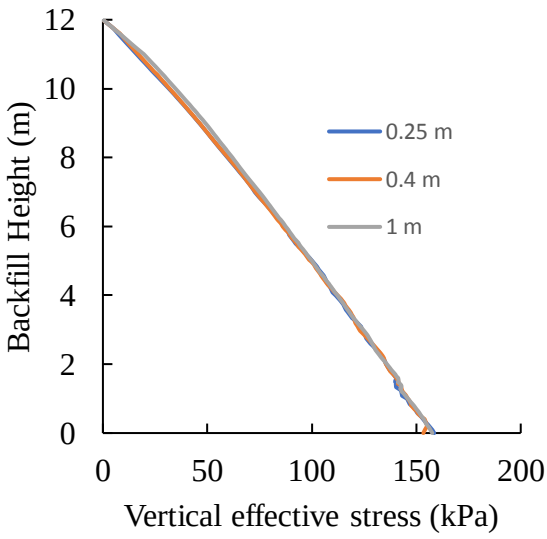
Backfill Height (m)
Vertical effective stress (kPa)
0.25 m
0.4 m
1 m

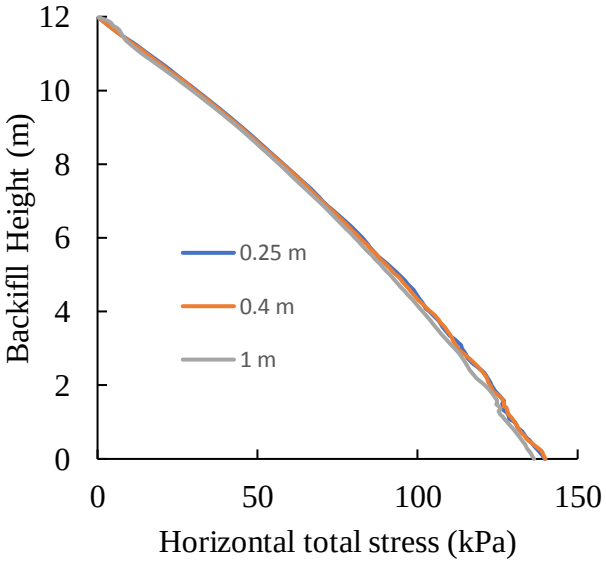
Backifll Height (m)
Horizontal total stress (kPa)
0.25 m
0.4 m
1 m

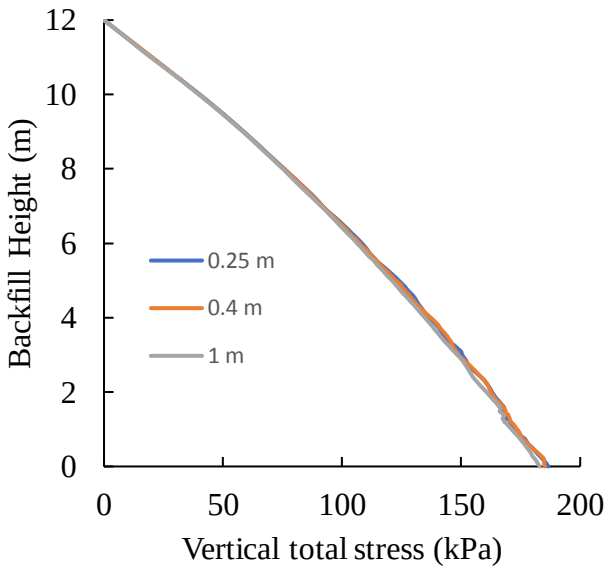

Figure F-2: Distribution of the PWP (a), horizontal (b) and vertical (c) effective stresses, and horizontal (d) and vertical (e) total stresses along the full height of the backfill at the end of filling operation, obtained by numerical modeling with Plaxis by considering different thicknesses for each layer.

F3. Additional results of validation of the proposed solutions

Fig. F-3 shows an additional validation of the proposed solutions [Eqs. (7.2), (7.29)-(7.32)] presented in Chapter 7. The analytical results are compared with the distributions of the excess PWP [Fig. F-3(a)], effective [Fig. F-3(b)] and total [Fig. F-3(c)] stresses along the full height of the backfill, obtained by numerical modeling with Plaxis. The good agreements between the analytical and numerical results indicate that the proposed solutions can be used to evaluate the excess PWP and stresses in backfilled stopes.

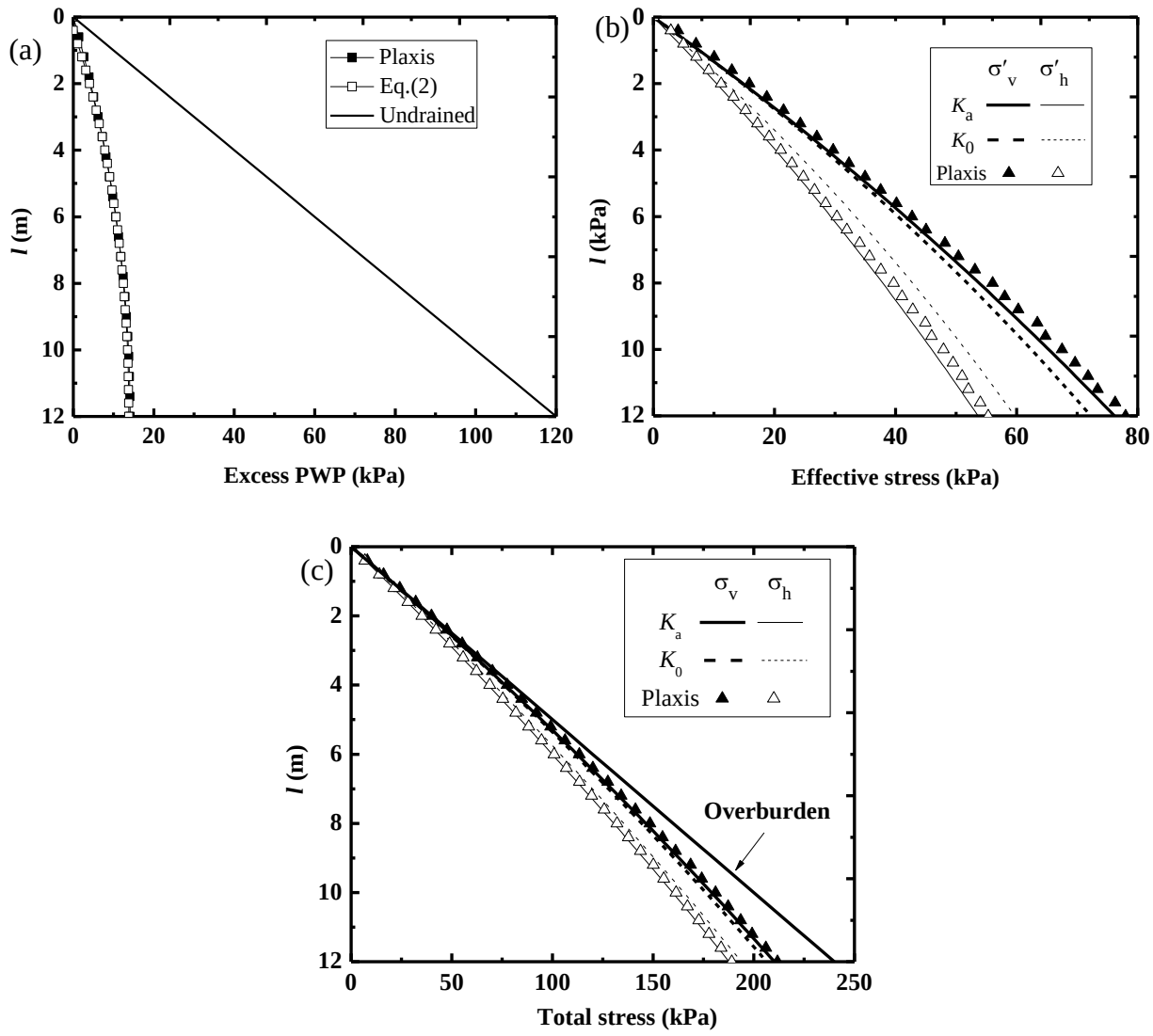

Figure F-3: Distribution of the excess PWP (a), effective (b) and total (c) stresses along the VCL of the stope at the end of filling operation (at t = 24 h and $h = H$ = 12 m), obtained by numerical modeling with Plaxis2D and calculated with the proposed solutions [Eqs. (7.2), (7.29)-(7.32)] using K_a, K_0, $k = 5.80\times10^{-5}$ m/s, $c_v = 20$ m^2/h, $m = 0.5$ m/h, and $\phi' = 10°$.

APPENDIX G – ADDITIONAL RESULTS RELATED TO CHAPTER 8

The sensitivity analyses of the mesh size and thickness for each layer in the numerical simulations were conducted by following the same procedure presented in Appendix F (not shown). This section presents an additional validation of the proposed solutions [Eqs. (8.2), (8.28)-(8.30)] in Chapter 8. The calculations are made with k = 5.80×10^{-5} m/s, c_v = 20 m^2/h, m = 0.5 m/h, and ϕ' =10° for the backfill. The other material parameters for the backfill and surrounding rock mass were taken as the same as those used in the model of validation presented in Section 8.3.

Fig. G-1 shows the distribution of the excess PWP [Fig. G-1(a)], effective [Fig. G-1(b)] and total [Fig. G-1(c)] stresses along the full height of the backfill, obtained by the numerical simulations and calculated by the proposed solution [Eqs. (8.2), (8.28)-(8.30)]. Good agreements are obtained between the analytical and numerical results.

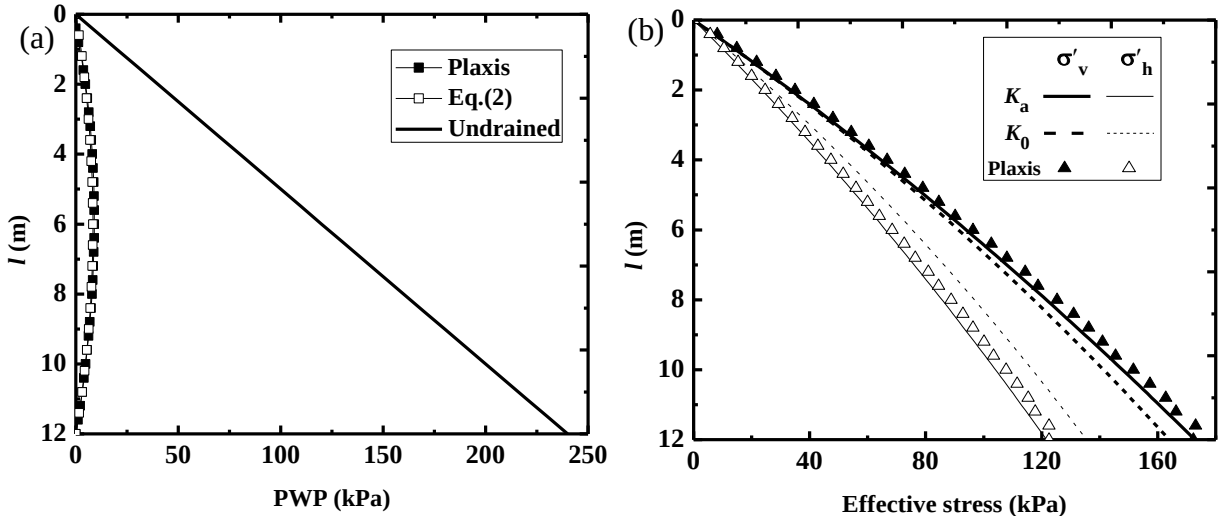

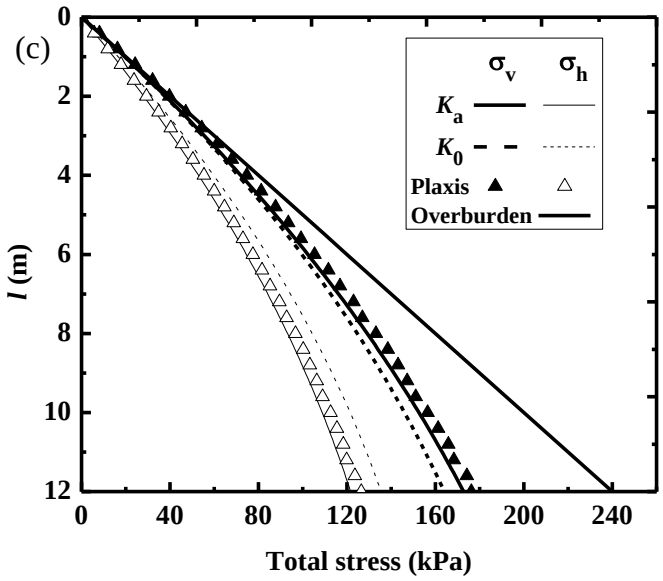

Figure G-1. Distribution of the (excess) PWP (a), effective (b) and total (c) stresses along the vertical center line of the backfilled stope at the end of filling operation (at t = 24 h and $h = H$ = 12 m), obtained by numerical modeling with Plaxis2D and calculated using the proposed solution [Eqs. (8.2), (8.26), (8.19) and (8.20)] by considering K_a, K_0, $k = 5.80\times10^{-5}$ m/s, $c_v = 20$ m^2/h, m = 0.5 m/h, and $\phi' = 10°$.

APPENDIX H – ARTICLE 8: A CONCEPTUAL ANALYTICAL SOLUTION FOR ESTIMATING THE SHORT-TERM PRESSURE OF PASTE FILL VARYING FROM VISCOUS TO LIQUID STATE, PLACED IN MINE STOPES

Li Li; Jian Zheng

Article published in GeoOttawa 2017

Abstract: In mine stope backfilling, a key issue is to estimate the fill pressures on barricades constructed to retain the cemented paste backfill in place. Recent experimental results obtained by field measurements indicate that the pressures of cemented paste backfill shortly after the placement are close to the iso-geostatic pressure (commonly called hydrostatic pressure) based on the overburden of the backfill, due to the absence of arching effect. These results do not correspond to the barricade design recommendations given in textbooks, which suggest slight construction of barricade to retain paste backfill. In this paper, a conceptual analytical solution is proposed to estimate the ratio of the vertical total stress at the stope center to that at the stope wall after taking into account the yield stress of the backfill. When the backfill is very viscous with a very high yield stress, the vertical total stress ratio can become very small, indicating very small pressure on the stope wall and barricade. A slight construction of barricade is indeed sufficient. When the backfill contains a lot of water and has a very low yield stress, the vertical total stress ratio may be close or equal to one, indicating high stresses on the wall or barricade. The barricade should be designed and constructed adequately.

H1. Introduction

Paste backfill is widely used in underground mines in Canada, Australia and elsewhere. It is made of all-coming tailings and has several advantages compared to hydraulic backfill. For example, it has few problem of segregation during the transportation by pipelines. It does not require elimination of a portion of the fine particles and thus has less mine wastes to be disposed of on surface. As the application of other types of backfill, the application of paste backfill underground improves ground stability, reduces ore dilution and increases ore recovery (Miao et al. 2008; Zhang et al. 2011; Li 2013; Li and Aubertin 2014).

Despite the diverse advantages, a successful application of the mining backfill requires a good estimation of the stresses in the backfilled stopes and on barricade, a confining structure constructed at the base of the stopes to retain the backfill in place. For barricade design, knowledge of the backfill pressure shortly after the placement is particularly important. Several cases of barricade failure reported in the literature indicate that serious consequences can result from a barricade failure (Yumlu and Guresci 2007; Sivakugan et al. 2013).

Over the years, extensive studies have been reported on the investigation of stresses in backfilled stopes, mainly from two aspects. First, when a backfill is placed in a stope, the backfill tends to settle down under the effect of its own weight. As the stope rock walls are usually much stronger and stiffer than the backfill, shear stresses develop along the fill-wall interfaces, resulting in a stress transfer from the backfill to the rock walls and smaller stresses in the backfill than those based on the overburden pressure. This phenomenon is well-known as “arching effect” (Janssen 1895; Marston 1930; Aubertin et al. 2003).

Secondly, when a slurry backfill is placed in a stope, the solid particles of the backfill tend to settle down and become denser. The volume diminution in the backfill then tends to expulse water toward the outside of the backfill. If the backfill has a low permeability, fast outflow (i.e. drainage) is not possible, resulting in generation of excess pore water pressure and absence of arching effect. The generation and dissipation of the excess pore water pressure due to the self-weight of the backfill is a phenomenon well-known as sedimentation and self-weight consolidation (Gibson 1958; Been and Sills 1981; Fox 2000; Pedroni 2011; Zheng et al. 2018a, 2018b). The absence of arching effect and high backfill pressure shortly after the placement of backfill in mine stopes have been observed in laboratory tests (Li et al. 2013) and field measurements (Thompson et al. 2012). These results

do not correspond to what has been observed by some researchers and practitioners, who are convinced that the backfill pressure is very small and the construction of a weak of barricade is enough to retain paste backfill in mine stope (Hassani and Archibald 1998; Potvin et al. 2005).

This paper aims to investigate the contradictory observations and proposes a conceptual analytical solution that can be used to evaluate the stresses in paste backfill shortly after its placement in mine stopes. “Short-term” in this paper is used to refer to the time shortly after the placement of the backfill in the mine stope. It does not have the same meaning in soil mechanics where short-term means the undrained and unconsolidated condition.

H2. Paste backfill and pressure in backfilled stopes

The definition of paste backfill is not yet unanimously accepted. Potvin et al. (2005) have defined a paste backfill as a material made of at least 15% of fine particles smaller than 20 μm. In addition, the backfill should not bleed water even after a prolonged period after deposition. A paste backfill meeting these criteria is typically in a very viscous state, probably becomes unsaturated once out of the transportation pipes. The pressures exerted by such backfill on a barricade can be very small and even nil if the barricade is positioned far enough from the stope. The barricade construction to retain such backfill in stopes can indeed be slight. This type of paste backfill can be interesting for surface tailings disposal, especially where water shortage is a serious problem. For underground mines, this type of paste backfill is not appropriate due to the low flowability (workability), which may require heavy pumps to transport the backfill from surface backfill plant to underground stopes. In addition, the low flowability of the backfill may render the full filling and tight contact between the backfill and stope roof very difficult, if not impossible. This is particularly true for the case of wide and/or long stopes.

In underground mines, the paste backfill must contain enough water to reach the required flowability. Subsequently, the paste backfill typically looks like a fluid. The almost horizontal surface of the backfill typically observed through the long stopes indicates that the backfill has low shear strength. It is thus oversaturated and close to a state of liquid. Shortly after the placement in the stope, arching effect is absent in such backfill. This was confirmed by several in situ measurements conducted in different underground mines (Belem et al. 2004; Helinski et al. 2011; Thompson et al. 2012). The measured vertical (σ_v) and horizontal (σ_h) total stresses and pore water pressure (u_w) increased linearly at the same pace with the height of the backfill. They were equal

to each other over the initial period of filling, indicating the absence of effective stresses (i.e., $\sigma'_h = \sigma'_v = 0$; where σ'_h and σ'_v are the horizontal and vertical effective stresses, respectively) and arching effect.

As the backfill does not have any effective stress and behaves like a liquid, the horizontal and vertical total stresses and the pore water pressure are all equal to the iso-static pressure (usually called hydrostatic pressure) based on the overburden of the backfill (i.e., $\sigma_h = \sigma_v = u_w = \gamma h$; where γ is the unit weight of saturated backfill, h is the depth of the calculation). Therefore, the pressures on the barricade at the base of the stope can be very high. A slight construction of barricade suggested by handbooks (Hassani and Archibald 1998; Potvin et al. 2005) is probably not enough and particular attention is needed on the barricade design.

H3. A conceptual analytical solution for estimating the stresses in backfilled stope by considering the viscosity of paste backfill

In the previous section, it was shown that the pressure in paste backfilled stopes can be very small or very high, depending on the rheological, hydraulic and mechanical properties of the backfill, which are mainly controlled by the water content (usually expressed by solid content). Subsequently, the requirement on the barricade design can vary from very strong to very slight as two extreme cases.

In this paper, a conceptual analytical solution is proposed to evaluate the vertical total stresses in paste backfilled stopes. The solid content or water content is taken into account through the consideration of the yield stress.

Fig. H-1 schematically shows a slump test using a cylindrical mold. In the figure, d_1 is the inner diameter and H is the height. In the slump test, the cylinder is filled with the material and then the mold is removed vertically. The reduction in height of the backfill sample s is defined as the slump height of the backfill. The intact (unyielded) region is quantified by the height h_0 (or normalized height $h'_0 = h_0/H$), while the deformed (yielded) region is characterized by the height h_1 (or normalized height $h'_1 = h_1/H$).

The slump height is usually taken as an indicator of the viscosity characterized by the yield stress τ_y. The yield stress is defined as the minimum shear stress required to fully mobilize a Bingham fluid. For cemented paste backfill, its value generally ranges from 100 to 800 Pa (Potvin et al. 2005;

Boger et al. 2006; Niroshan et al. 2017). But a value as high as 1100 Pa has also been reported by Simon and Grabinsky (2013).

Pashias et al. (1996) proposed an equation to relate the normalized slump value s' (= s/H) and normalized yield stress τ'_y [= $\tau_y/(\gamma H)$; where γ is the unit weight of the backfill] as follow:

$$s' = 1 - 2\tau'_y[1 - \mathrm{Ln}(2\tau'_y)] \tag{H.1}$$

The normalized heights h'_0 and h'_1 were further related to the normalized yield stress τ'_y as follows (Pashias et al. 1996):

$$h'_0 = 2\tau'_y \tag{H.2}$$

$$h'_1 = -2\tau'_y \mathrm{Ln}(h'_0) \tag{H.3}$$

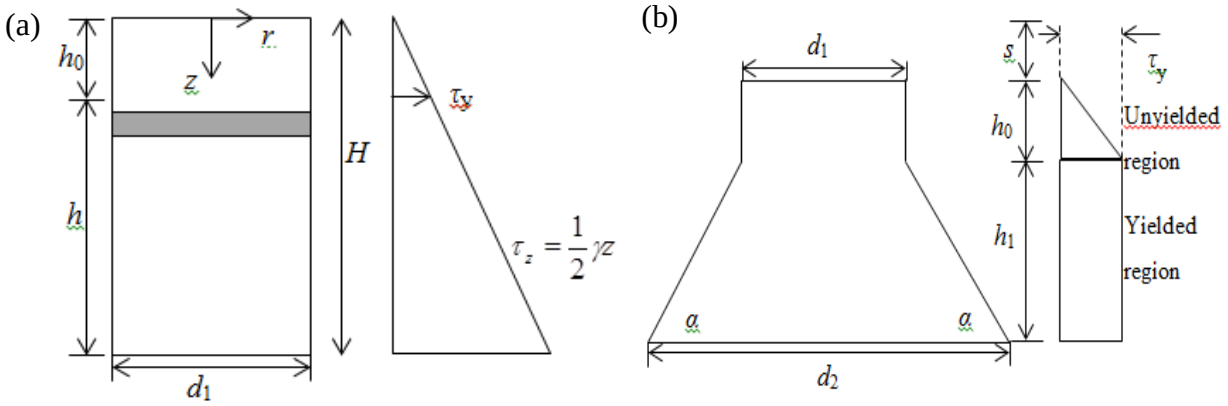

Figure H-1: Schematic diagram of the geometry and initial (a) (τ_z is the maximum shear stress at depth z) and final (b) stress state distribution for a cylindrical slump test (adapted from Pashias et al.1996)

Using the diverse normalized dimensions, a dimensionless volume of the material in the cylindrical mold before collapse [Fig. H-1(a)] is calculated as:

$$V'_1 = \frac{\pi}{4}(d'_1)^2 \times (h'_0 + h') \tag{H.4}$$

where

$$d'_1 = \frac{d_1}{H} \tag{H.5}$$

$$h' = \frac{h}{H} \tag{H.6}$$

After collapse [Fig. H-1(b)], the total volume of the sample can be expressed as

$$V_2' = \frac{\pi}{4} \times (d_1')^2 h_0' + \frac{1}{12}\pi (d_2')^2 \times \frac{d_2'}{2} \tan\alpha$$
$$-\frac{1}{12}\pi (d_1')^2 \times \frac{d_2'}{2} \tan\alpha + \frac{1}{12}\pi (d_1')^2 h_1' \tag{H.7}$$

where α is the slope angle of the deformed region; the dimensionless bottom radius d'_2 of the collapsed portion is given as follows:

$$d_2' = d_1' + 2h_1' \cot\alpha \tag{H.8}$$

Considering the volume constant before and after collapse (i.e., $V'_1 = V'_2$) leads to

$$4(h_1')^3 (\cot\alpha)^2 + 6(h_1')^2 d_1' \cot\alpha + 3(d_1')^2 \times (h_1' - h') = 0 \tag{H.9}$$

Solving the equation results in:

$$\tan\alpha = \frac{4(h_1')^2}{-3h_1'd_1' + d_1' \times \sqrt{3h_1'(4 - 4h_0' - h_1')}} \tag{H.10}$$

As shown in Fig. H-2, the stress distribution in paste backfilled stope can significantly be affected by this slope angle. With a slurry backfill of high water content, a horizontal surface is formed on the top of the backfill [Fig. H-2(a)]. The vertical total stress at a given height is probably uniform across the width of the stope. With a solid-like backfill of high yield stress, a cone-shaped surface may form at the top of the backfill [Fig. H-2(b)]. The vertical total stress at a given height then becomes non-uniform across the width of the stope. It is expected to be higher at the stope center than near the wall due to the difference in the height of the overburden.

At the bottom of the stope, the vertical stress is noted as σ_{v1} at the stope center and σ_{v2} near the wall. Assuming the vertical total stresses be approximated by the overburden, one can then express the vertical total stresses ratio as follows:

$$\frac{\sigma_{v2}}{\sigma_{v1}} = \frac{h_3}{h_2} = 1 - \frac{h_4}{h_2} \tag{H.11}$$

where h_2 and h_3 are the backfill height at the stope center and close to stope wall, respectively; h_4 is the height of the cone [Fig. H-2(b)].

h_2 and h_4 are dependent on the total volume and yield stress of the placed backfill. From Fig. H-2(b), one sees that h_4 can be calculated as:

$$h_4 = r\tan\alpha \qquad r_1 = r \tag{H.12}$$

$$h_4 = r_1\tan\alpha \qquad r_1 < r \tag{H.13}$$

where r_1 is the base radius of the placed backfill; r is the half width of the mine stope; α is the repose angle of the deposited backfill, which can be taken as that obtained from the cylindrical mold slump test using Eq. (H.10).

For a stope having a square section, the total volume V of the placed backfill is expressed as follows:

$$V = (2r)^2 \times (h_2 - h_4) + \frac{1}{3} \times \pi r^2 h_4 \qquad r_1 = r \tag{H.14}$$

$$V = \frac{1}{3}\pi r_1^2 h_4 \qquad r_1 < r \tag{H.15}$$

Eqs. (H.14) and (H.15) can further be changed as follows:

$$h_2 = \frac{3V - r^2 h_4(\pi - 12)}{12r^2} \qquad r_1 = r \tag{H.16}$$

$$h_2 = h_4 \qquad r_1 < r \tag{H.17}$$

Substituting Eqs. (H.14) and (H.16) or Eqs. (H.15) and (H.17) into Eq. (H.11) leads to

$$\frac{\sigma_{v2}}{\sigma_{v1}} = \frac{3V - \pi r^3\tan\alpha}{3V + r^3\tan\alpha(12 - \pi)} \qquad r_1 = r \tag{H.18}$$

$$\frac{\sigma_{v2}}{\sigma_{v1}} = 0 \qquad r_1 < r \tag{H.19}$$

For a stope having a circular section, the total volume of the placed backfill can be calculated as:

$$V = \pi r^2 \times (h_2 - h_4) + \frac{1}{3}\pi r^2 h_4 \qquad r_1 = r \tag{H.20}$$

$$V = \frac{1}{3}\pi r_1^2 \times h_4 \qquad r_1 < r \qquad \text{(H.21)}$$

Eqs. (H.20) and (H.21) can further be changed as follows:

$$h_2 = \frac{V}{\pi r^2} + \frac{2}{3}h_4 \qquad r_1 = r \qquad \text{(H.22)}$$

$$h_2 = h_4 \qquad r_1 < r \qquad \text{(H.23)}$$

Substituting Eqs. (H.20) and (H.22) or Eqs. (H.21) and (H.23) into Eq. (H.11) leads to

$$\frac{\sigma_{v2}}{\sigma_{v1}} = \frac{3V - \pi r^3 \tan\alpha}{3V + 2\pi r^3 \tan\alpha} \qquad r_1 = r \qquad \text{(H.24)}$$

$$\frac{\sigma_{v2}}{\sigma_{v1}} = 0 \qquad r_1 < r \qquad \text{(H.25)}$$

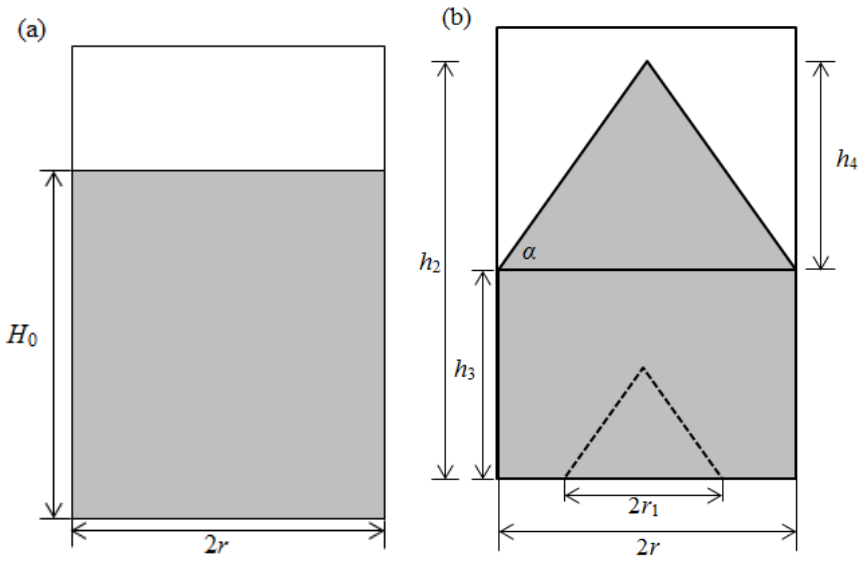

Figure H-2: Idealized shapes of a paste backfill placed in stope: (a) with a liquid-like paste backfill; (b) with a solid-like paste backfill

Eqs. (H.18) to (H.19) constitute the conceptual analytical solution for estimating the vertical total stresses ratio along the base of the stope.

To illustrate the application of the proposed analytical solution for estimating the pressure of paste backfilled stopes, one considers a stope having a horizontal section of 10×10 m (r = 5 m), filled with a paste backfill having a unit weight of γ = 20 kN/m^3. The inner diameter d_1 and height H of

the cylindrical mold are taken as 20 cm and 40 cm, respectively. The normalized $d_1^{'}$ then equals to 0.5.

Fig. H-3 shows the variation of the repose angle of the fresh deposited backfill with the dimensionless yield stress, calculated using Eq. (H.10). The repose angle α increases as the dimensionless yield stress $\tau_y^{'}$ increases. When $\tau_y^{'}$ is close to zero, the backfill behaves like a liquid. The flow and deformation of the backfill can be similar to water, resulting in an almost zero repose angle. For backfill with extremely high yield stress, the repose angle can reach 90°, corresponding to the case when the material is very hard and strong and there is no collapse in the slump tests.

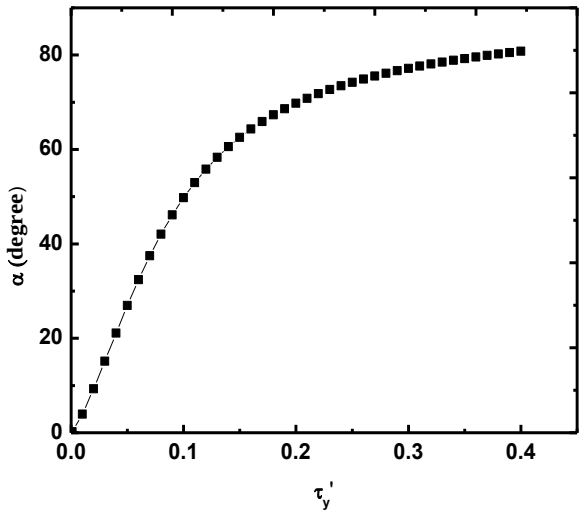

Figure H-3: Variation of the repose angle α as a function of the normalized yield stress τ_y'

Fig. H-4 shows the variation of vertical total stress ratio as a function of the normalized yield stress τ'_y. It is seen that the vertical total stress ratio decreases as the yield stress increases, indicating that the stress on the wall decreases with increased yield stress of the backfill.

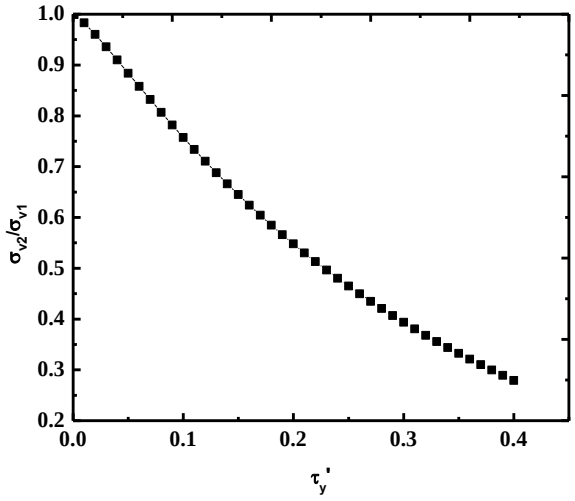

Figure H-4: Variation of vertical total stress ratio as a function of the normalized yield stress; calculation made with r = 5 m and V = 2000 m^3.

H4. Discussion

In this paper, a conceptual analytical solution is proposed to estimate the short-term vertical total stress ratio in paste backfill stopes by considering the yield stress of the backfill. The results show that the proposed solution can generally capture the main features of paste backfill placed in stope. However, the model contains several limitations.

One limitation of the model is related to the utilization of the repose angle α calculated from the slump tests as that of the paste backfill placed in mine stopes. Obviously, the conditions are very different between the slump test and stope backfilling. In a slump test, the backfill confined in a cylindrical mold is initially in a static equilibrium state. The yield or collapse occurs due to the self-weight of the backfill once the cylindrical mold is removed. The observed slope angle can be considered as the static repose angle of the collapsed backfill. For the case of mine stopes, impact is unavoidable when the paste backfill is poured into the stope, resulting in smaller repose angle. The utilization of the repose angle calculated from the slump tests tends to overestimate the vertical total stress ratio and underestimate the vertical (and horizontal) total stress on the wall. More work is required to improve the analytical solution.

When the backfill is placed in mine stopes, self-weight consolidation occurs, resulting in the development of effective stress and arching effect (Li et al. 2005; Li and Aubertin 2009a, 2009b;

Yang and Li 2015). The influence of the arching effect on the stress estimation needs to be investigated.

Another limitation is related to the top shape of the placed backfill, which was assumed to be a cone in this paper. In practice, the shape is probably to be a dome. The influence of the actual shape of the backfill needs to be studied further in the future.

Finally, the proposed solution can only be used to estimate the vertical total stress ratio. More work is required to estimate the vertical and horizontal stresses in paste backfilled stopes.

H5. Conclusion

In this paper, a conceptual analytical solution has been proposed to estimate the ratio between the vertical total stress at the stope center and that at the stope wall as a function of the yield stress of the backfill. Sample calculations using the proposed analytical solution show that the backfill yield stress, total deposited volume and stope geometry (not shown) can significantly influence the vertical total stress ratio. When the backfill is very viscous and has a very high yield stress, the vertical total stress ratio can become very small, indicating very small stress on the stope wall. For a given yield stress, the vertical total stress ratio and the stresses on the stope wall can also become very small if the stope has a very large horizontal section. These results can explain well why some researchers and practitioners suggest that slight construction of barricades is enough to retain paste backfill. The proposed solution also shows that the vertical total stress ratio can become close to unity when the yield stress of the backfill is very small. In this case, the stress on the stope wall may be very large. Therefore, a slight construction of barricade is probably not adequate.

Acknowledgement

The authors would like to acknowledge the financial support from the Natural Sciences and Engineering Research Council of Canada (NSERC 402318), Institut de recherche Robert-Sauvé en santé et en sécurité du travail (IRSST 2013-0029), Fonds de recherche du Québec – Nature et Technologies (FRQNT 2015-MI-191676), and industrial partners of the Research Institute on Mines and the Environment (RIME UQAT-Polytechnique; http://rime-irme.ca/). The authors also thank the anonymous reviewers for the positive and constructive comments.

H6. References

Aubertin, M., Li, L., Arnoldi, S., Belem, T., Bussière, B., Benzaazoua, M., & Simon, R. (2003). *Interaction between backfill and rock mass in narrow stopes*. Paper presented at the Soil and Rock America 2003, Essen, Germany (pp, 1157–1164).

Been, K., & Sills, G.C. (1981). Self-weight consolidation of soft soils: an experimental and theoretical study. *Geotechnique, 31*(4), 519-535.

Belem, T., Harvey, A., Simon, R., & Aubertin, M. (2004). *Measurement and prediction of internal stresses in an undergound opening during its filling with cemented fill*. Paper presented at the Symposium on Ground support in mining and underground construction. Taylor and Francis Group, London, Australia (pp. 619–630).

Boger, D., Scales, P., & Sofra, F. (2006). Rheological concepts. In Jewell and Fourie (Eds), *Paste and Thickened Tailings-A Guide* (2nd ed pp. 25-37).

Fox, P.J. (2000). *CS4: A large strain consolidation model for accreting soil layers*. Paper presented at the Geotechnics of high water content materials, ASTM International, West Conshohocken, PA.

Gibson, R.E. (1958). The progress of consolidation in a clay layer increasing in thickness with time. *Geotechnique, 8*(4), 171–182.

Hassani, F., & Archibald, J. (1998). Mine backfill. (CD-ROM). Canadian Institute of Mining, Metallurgy and Petroleum, Montréal, Canada.

Helinski, M., Fahey, M., & Fourie, A. (2011). Behavior of cemented paste backfill in two mine stopes: measurements and modeling. *Journal of Geotechnical and Geoenvironment Engineering, 137*(2), 171–182.

Janssen, H.A. (1895). Versuche über Getreidedruck in Silozellen. *Zeitschrift Verein Ingenieure, 39*, 1045-1049.

Li, L. (2013). A new concept of backfill design – application of wick drains in backfilled stopes. *International Journal of Mining Science and Technology*, *23*(5), 763–70.

Li L and Aubertin M. (2014) An improved method to assess the required strength of cemented backfill in underground stopes with an open face. *International Journal of Mining Science and Technology, 24*(4), 549–58.

Li, L., Alvarez, I.C., & Aubertin, J.D. (2013). Self-weight consolidation of a slurried deposition: tests and interpretation. *International Journal of Geotechnical Engineering, 7*(2), 205–213.

Li, L., Aubertin, M., & Belem, T. (2005). Formulation of a three dimensional analytical solution to evaluate stress in backfilled vertical narrow openings. *Canadian Geotechnical Journal, 42*(6), 1705–1717 (with Erratum 2006, 43(3), 338–339).

Li, L., & Aubertin, M. (2009a). Influence of water pressure on the stress state in stopes with cohesionless backfill. *Geotechnical and Geological Engineering, 27*(1), 1–11.

Li, L., & Aubertin, M. (2009b). A three-dimensional analysis of the total and effective stresses in submerged backfilled stopes. *Geotechnical and Geological Engineering, 27*(4), 559–569.

Marston, A. (1930). The theory of external loads on closed conduits in the light of latest experiments. Iowa Engineering Experiment Station, Ames, Iowa (pp. 138-170).

Miao, X.X., Zhang, J.X., & Feng, M.M. (2008). Waste-filling in fully-mechanized coal mining and its application. *International Journal of Mining Science and Technology, 18*(4), 479–82.

Niroshan, N., Sivakugan, N., & Veenstra, R.L. (2017). Laboratory study on strength development in cemented paste backfills. *Journal of Materials in Civil Engineering, 29*(7), 04017027.

Pashias, N., Boger, D.V., Summers, J., & Glenister, D.J. (1996). A fifty cent rheometer for yield stress measurement. *Journal of Rheology, 40*(6), 1179–1189.

Pedroni, L. (2011). Étude expérimentale et numérique de la sédimentation et de la consolidation des boues de traitement des eaux acides. (Doctoral dissertation, École Polytechnique de Montréal, Montréal, Canada).

Potvin, Y., Thomas, E., & Fourie, A. (2005). *Handbook on mine fill*. Nedlands, Australia: Australian Centre for Geomechanics.

Sivakugan, N., Rankine, K., Lovisa, J., & Hall, W. (2013). Flow rate computations in hydraulic fill mine stopes. *Indian Geotechnical Journal, 43*(3), 195-202.

Simon, D., & Grabinsky, M. (2013). Apparent yield stress measurement in cemented paste backfill. *International Journal of Mining, Reclamation and Environment, 27*(4), 231-256.

Thompson, B.D., Bawden, W.F., & Grabinsky, M.W. (2012). In situ measurements of cemented paste backfill at the Cayeli Mine. *Canadian Geotechnical Journal, 49*(7), 755-772.

Yang, P.Y., & Li, L. (2015). Investigation of the short-term stress distribution in stopes and drifts backfilled with cemented paste backfill. *International Journal of Mining Science and Technology, 25*(5), 721-728.

APPENDIX I – ARTICLE 9: ANALYTICAL AND EXPERIMENTAL STUDIES OF THE EVOLUTION OF THE EXCESS PORE WATER PRESSURE DURING THE DEPOSITION OF A SLURRIED MATERIAL

Li Li; Jian Zheng

Article published in GeoOttawa 2017

Abstract: The fast-growing of mining industry is accompanied by the generation of large volume of tailings, which are usually pumped to tailings pond, made of tailings dams. Tailings can also be used as backfill material to return and fill underground mine stopes. Similar practice in civil engineering is the disposal of dredged sludge excavated from river or sea beds in a containment structure. Among these practices, a common point is the disposal of a slurried material in a confining structure. To ensure the stability of this structure, it is important to have a good estimation of the pore water pressure (PWP) during the placement of the slurried material in the confining structure. Recently a truly analytical solution has been developed by the authors based on a model proposed by Gibson. However, the analytical solution has never been validated by experimental results. In this paper, the truly analytical solution is first recalled. A simple laboratory test instrumentation is presented. The measured pressures are compared with the analytical solution. The good agreement between the experimental and analytical results indicates that the analytical solution is validated even though it contains some simplifying assumptions.

I1. Introduction

The rapid growth of mine industry is accompanied by the production of large quantity of mine wastes. These mine wastes are in terms of tailings and waste rock, which needs to be properly managed. Tailings usually contain a lot of water. They are sent by pipe to a tailings pond and confined by tailings dams. Tailings are also used to fill the underground mine stopes to improve ground stability, decrease ore dilution and reduce the surface disposal of mine wastes (Hassani and Archibald 1998; Kump 2001; Aubertin et al. 2002; Jung and Biswas 2002; Bussiere 2007; Cui and Fall 2018). In civil engineering, the large amount of dredged sludge accompanied by the cleaning operation of river or sea beds needs to be transported by pipes and disposed in a containment structure. As these slurried materials usually have high water content and low permeability, their deposition is typically accompanied with the generation of excess pore water pressure. A good understanding of the self-weight consolidation and evolution of the excess pore water pressure (PWP) is necessary to access the stability of the confining structures and manage the subsequent filling or deposition operations (Priscu 1999; Azam and Li 2010; Fahey et al. 2010; Farkish and Fall 2014; Zheng et al. 2018a, 2018b).

The self-weight consolidation of slurried material during the deposition or filling operation is a complex issue. With the continuous deposition or filling, the excess PWP can be instantaneously generated and slowly dissipated. This is different from the traditional consolidation theory of Terzaghi (1943), in which the consolidation takes place under an external applied load.

A solution has been proposed by Gibson (1958) by considering a continuous increasing of the slurry thickness. The Gibson (1958) solution contains an integral part, which can only be evaluated through numerical calculation. A truly analytical solution based on the Gibson (1958) model has been developed by Zheng et al. (2018b). The analytical solution constitutes a very useful tool to estimate the evolution of the excess PWP during the slurry deposition. However, the Gibson (1958) model and ensuing analytical solution have never been validated by experimental results.

In the past decades, numerous experimental studies have been conducted to investigate the compressibility and consolidation of slurried materials. Most of them were performed by following the standard consolidation process suggested by ASTM (ASTM D2435-11/D2435M-11 and ASTM D4186/D4186M-12e1). The tests were thus conducted with the application of an external load (Aubertin et al. 1996; Qiu and Sego 2001; Azam 2010). As slurried material usually has high

water content and low (no) shear strength, a few researchers have made use of seepage force to investigate the compressibility and permeability behavior of slurried material (Imai 1979; Sridharan and Prakash 1999; Lee and Fox 2005; Janbaz and Maher 2017).

The aforementioned testing methods tend to disturb the drainage condition. The testing conditions are not representative of the field condition of slurry deposition. Self-weight consolidation tests without applying any load were also conducted to study the consolidation characteristics of slurried material (Been and sills 1981; Lin 1983; Pedroni 2011; Li et al. 2013; Saleh-Mbemba 2016). The testing conditions are closer to the field condition than previously mentioned tests, which were however conducted by instantaneously or quickly pouring the slurried material in a column, without noting the filling rate.

To better investigate the consolidation characteristics of the slurried material during the accreting deposition, laboratory tests were conducted by placing slurried tailings in a column with a constant filling rate. Four PWP sensors were installed along the height of the column to measure the PWP variation during the deposition. The measured excess PWP were compared with those predicted by the analytical solution proposed by Zheng et al. (2018b).

I2. Analytical solution of the Gibson (1958) model

Fig. I-1 shows the Gibson (1958) model with an accreting deposition of slurried material on an impervious base. The thickness of the slurried material increases at a constant filling rate m. At a given time t, the thickness of the slurry reaches h (= mt). At the end of the deposition operation the final thickness of the slurried material reaches H. x is the calculation point from the base of the slurry ($0 \leqslant x \leqslant h$)

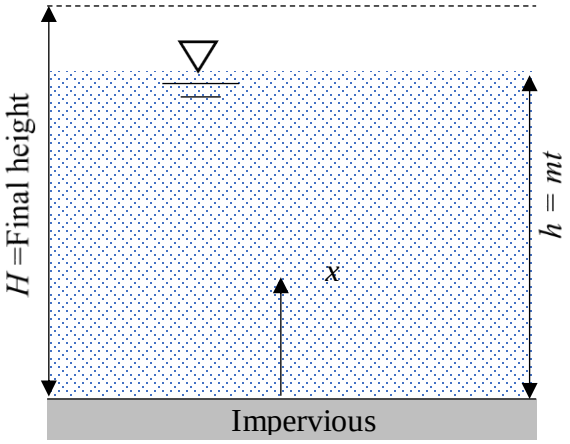

Figure I-1: Accreting deposition of slurried material on an impervious base (Gibson 1958).

By applying the same assumptions as the consolidation theory of Terzaghi (1943), Gibson (1958) proposed the following equation to evaluate the excess PWP during the accreting deposition:

$$c_v \frac{\partial^2 u}{\partial x^2} = \frac{\partial u}{\partial t} - \gamma' \frac{dh}{dt} \tag{I.1}$$

where u (kPa) is the excess PWP; c_v (m^2/h) is the consolidation coefficient; t (h) is the filling time; γ' (kN/m3) is the submerged unit weight of the slurried material.

Solving Equation (I.1) leads to the following equation (Gibson 1958):

$$u = \gamma' mt - \frac{\gamma'}{\sqrt{\pi c_v t}} \exp\left(-\frac{x^2}{4c_v t}\right) \times \int_0^\infty \xi \tanh\left(\frac{m\xi}{2c_v}\right) \times \cosh\left(\frac{x\xi}{2c_v t}\right) \times \exp\left(-\frac{\xi^2}{4c_v t}\right) d\xi \tag{I.2}$$

where ξ is an integration variable ($0 \le \xi \le \infty$).

Equation (I.2) contains an integral that can only be evaluated numerically. A truly analytical form has been proposed by Zheng et al. (2018b) through the transformation of Goodwin (1943) as follow:

$$u(x,t) = \gamma' mt - \frac{\gamma'}{\sqrt{\pi c_v t}} \times \exp\left(-\frac{x^2}{4c_v t}\right) \times \frac{h_0}{2} \sum_{n=-\infty}^{\infty} \left\{ 4c_v t n h_0 \times \tanh\left(mnh_0 \sqrt{\frac{t}{c_v}}\right) \times \cosh\left(\frac{xnh_0}{\sqrt{c_v t}}\right) \times \exp(-n^2 h_0^2) \right\} \tag{I.3}$$

where n is a series number ($-\infty < n < +\infty$), h_0 is the step length of x. To obtain stable results, sensitivity analysis should be made on the series number n for a given value of h_0 between 0 and 1. For most cases, Zheng et al. (2018b) have shown that stable results of u can be obtained when n is taken between -91 and 91 and h_0 is taken as 0.3.

I3. Test material and procedure

Tailings

The tailings used in this study are from Canadian Malartic Mine. The tailings have a specific gravity of 2.71. They are characterized by a uniformity coefficient of C_u = 5.88 and curvature coefficient of C_c = 0.62. Slurry specimens were obtained by thoroughly mixing dry tailings and water to the desired water content of w = 50% (kg/kg). The obtained tailing slurry has a saturated unit weight 18 kN/m^3.

Instrumentation

Fig. I-2 shows a photograph of the test apparatus used to measure the variation of the PWP with the placement of tailings slurry. The column has an inner diameter of 30 cm and a height of 108.5 cm. In order to obtain a homogeneous specimen and minimize any possible segregation, the prepared tailings slurry was stored in a bucket and continuously mixed with a portable mixer during the tests. The filling or deposition operation was performed through pumping. The filling rate is about m = 0.156 m/h. Four PWP sensors were installed along the height of the column at 4.5, 35.5, 65.5 and 95.5 cm from the bottom of the column, respectively to measure the PWP variation during the deposition. The PWP sensors were kept saturated and protected by saturated cigarettes filter to prevent any conglomeration by the fine particles. A layer of sand of 4.5 cm was placed at the bottom of the column. A thin layer of geotextile was placed on the sand layer which is saturated with water before the deposition. The top surface of the geotextile is in the same level as the bottom PWP sensor. The four PWP sensors were calibrated with water before and after each filling test. The linear variation between the voltage and water head indicated that the four PWP sensors are reliable.

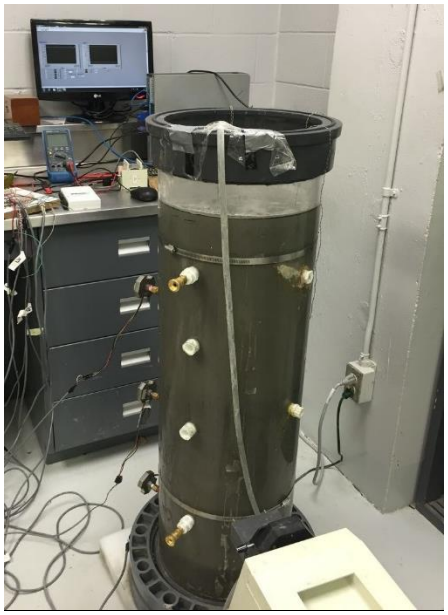

Figure I-2: Photograph of the test apparatus used to measure the variation of the PWP with the placement of tailings slurry

I4. Test results and comparison with analytical solution

Fig. I-3 shows the distribution and evolution of the measured excess PWP along the height of the column. The results calculated with the analytical solution [Eq. (I.3)] using c_v = 0.025 m^2/h and m =0.156 m/h are also plotted on the figure. The used value of c_v = 0.025 m^2/h is in the range of measured results reported in the previous studies. For example, Essayad (2015) found that the value of c_v should be in the range of 0.0936 to 0.368 m^2/h while Saleh-Mbemba and Aubertin (2017) obtained a range of 0.036 to 0.072 m^2/h for c_v.

It is interesting to note that good agreements are obtained between the experimental results and the analytical results by using a constant c_v. These results indicate that the Gibson (1958) model and ensuing analytical solution can be used to estimate the variation of evolution of the excess PWP during the slurry deposition. Nevertheless, it should be noted that only one group of tests were conducted. More tests are needed to verify if this conclusion is valid under different testing conditions.

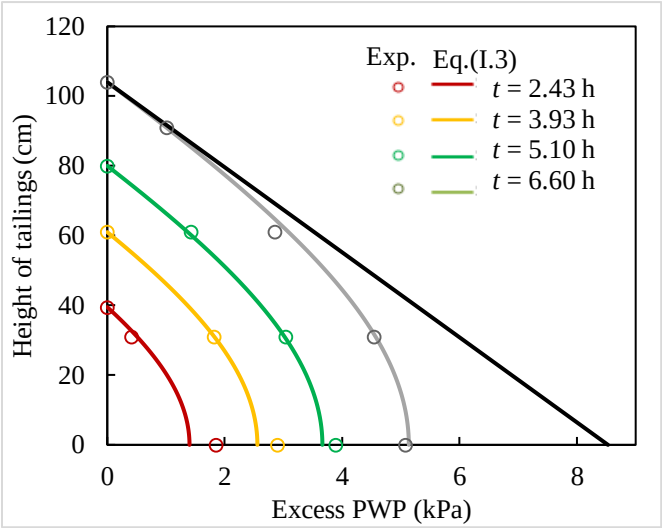

Figure I-3: Distribution and evolution of the excess PWP along the height of the tailings, measured from the laboratory tests and calculated with the analytical solution (Zheng et al. 2018b) using c_v = 0.025 m^2/h and m = 0.156 m/h

I5. Conclusions

In this paper, an analytical solution based on the Gibson (1958) model was recalled. The solution was proposed to evaluate the excess PWP in accreting deposition of slurried materials. A column test was conducted to study the consolidation and excess PWP dissipation in the accreting deposition of tailings with a constant filling rate. The measured excess PWP distributions were compared with those calculated by the analytical solution using a constant value of c_v. The good agreements between the experimental and analytical results indicate that analytical solution can be used to evaluate the variation and evolution of the excess PWP during the accreting deposition, using a constant consolidation coefficient c_v. More tests are needed to verify if this conclusion is valid under other testing conditions.

Acknowledgement

The authors would like to acknowledge the financial support from the Natural Sciences and Engineering Research Council of Canada (NSERC 402318), Fonds de recherche du Québec—Nature et Technologies (FRQNT 2015-MI- 191676), and industrial partners of the Research Institute on Mines and the Environment (RIME UQAT-Polytechnique; http://rime-irme.ca/).

I6. References

ASTM International. (2011). *Standard test methods for one-dimensional consolidation properties of soils using incremental loading*. Standard ASTM D2435/D2435M-11, West Conshohocken, PA.

ASTM International. (2012). *Standard test method for one-dimensional consolidation properties of saturated cohesive soils using controlled-strain loading*. Standard ASTM D4186/D4186M-12e1, West Conshohocken, PA.

Aubertin, M., Bussiere, B., & Bernier, L. (2002). *Environnement et gestion des rejets miniers. Presses* [Manual on CD-ROM]. Internationales Polytechnique, Montréal, Canada.

Aubertin, M., Bussiere, B., & Chapuis, R.P. (1996). Hydraulic conductivity of homogenized tailings from hard rock mines. *Canadian Geotechnical Journal, 33*(3), 470-482.

Azam, S., & Li, Q. (2010). Tailings dam failures: A review of the last one hundred years. *Geotechnical News, 28*(4): 50-54.

Azam, S. (2010). Large strain settling behavior of polymer-amended laterite slurries. *International Journal of Geomechanics, 11*(2), 105-112.

Been, K., & Sills, G.C. (1981). Self-weight consolidation of soft soils: an experimental and theoretical study. *Geotechnique, 31*(4), 519-535.

Bussiere, B. (2007). Colloquium 2004: Hydrogeotechnical properties of hard rock tailings from metal mines and emerging geoenvironmental disposal approaches. *Canadian Geotechnical Journal, 44*(9), 1019–1052.

Cui, L., & Fall, M. (2018). Modeling of self-desiccation in a cemented backfill structure. *International Journal for Numerical and Analytical Methods in Geomechanics, 42*(3), 558-583.

Essayad, K. (2015). Development of experimental protocols for the characterization of saturated and unsaturated tailings consolidation from compression tests in columns (in French). (Master's thesis, École Polytechnique de Montréal, Montréal, Canada).

Fahey, M., Helinski, M., & Fourie, A. (2010). Consolidation in accreting sediments: Gibson's solution applied to backfilling of mine stopes. *Géotechnique, 60*, 877–882.

Farkish, A., & Fall, M. (2014). Consolidation and hydraulic conductivity of oil sand mature fine tailings dewatered by using super absorbent polymer. *Journal of Geotechnical and Geoenvironmental Engineering, 140*(7), 06014006.

Gibson, R.E. (1958). The progress of consolidation in a clay layer increasing in thickness with time. *Géotechnique, 8*(4), 171-182.

Goodwin, E.T. (1949). *The evaluation of integrals of the form* $\int_{-\infty}^{+\infty} f(x)e^{-x^2}dx$. Paper presented at the Mathematical Proceedings of the Cambridge Philosophical Society. Cambridge University, London, UK (pp. 241-245).

Hassani, F., & Archibald, J. (1998). Mine backfill. (CD-ROM). Canadian Institute of Mining, Metallurgy and Petroleum, Montréal, Canada.

Imai, G. (1979). Development of a new consolidation test procedure using seepage force. *Soils and Foundations, 19*(3), 45-60.

Janbaz, M., & Maher, A. (2017). Consolidation and permeability behaviour of Newark Bay's dredged sediments by seepage-induced consolidation test. *Internationa Journal of Geotechnical Engineering, 11*(2), 120-126.

Jung, S.J., & Biswas, K. (2002). Review of current high density paste fill and its technology. *Minerral Resources Engineering, 11*(2), 165–182.

Kump, D. (2001). Backfill — whatever it takes. *Mining Engineering, 53*(1), 50–52.

Lee, J., & Fox, P.J. (2005). Efficiency of seepage consolidation for preparation of clay substrate for centrifuge testing. *Geotechnical Testing Journal, 28*(6), 577-585.

Lin, T.W. (1983). Sedimentation and self-weight consolidation of dredge spoil. (Doctoral dissertation, Iowa State University, Iowa, United States).

Li, L., Alvarez, I.C., & Aubertin, J.D. (2013). Self-weight consolidation of a slurried deposition: tests and interpretation. *International Journal of Geotechnical Engineering, 7*(2), 205–213.

Pedroni, L. (2011). Étude expérimentale et numérique de la sédimentation et de la consolidation des boues de traitement des eaux acides. (Doctoral dissertation, École Polytechnique de Montréal, Montréal, Canada).

Priscu, C. (1999). Behavior of mine tailings dams under high tailings deposition rates. (Doctoral dissertation, McGill University, Montréal, Canada).

Qiu, Y.X., & Sego, D.C. (2001). Laboratory properties of mine tailings. *Canadian Geotechnical Journal, 38*(1), 183-190.

Saleh-Mbemba, F. (2016). Assessment of drainage, consolidation and desiccation of fine-grained tailings in the presence of draining inclusions (in French). (Doctoral dissertation, École Polytechnique de Montréal, Montréal, Canada).

Sridharan, A., & Prakash, K. (1999). Simplified seepage consolidation test for soft sediments. *Geotechnical Testing Journal, 22*(3), 235-244.

Terzaghi, K. (1943). Theoretical Soil Mechanics. New York, USA: John Wiley and Sons.

Zheng, J., Li, L., Mbonimpa, M., & Pabst, T. (2018a). An analytical solution of Gibson's model for estimating the pore water pressures in accreting deposition of slurried material under one-dimensional self-weight consolidation. Part I: Pervious base. *Indian Geotechnical Journal, 48*(1), 72-83.

Zheng, J., Li, L., Mbonimpa, M., & Pabst, T. (2018b). An analytical solution of Gibson's model for estimating pore water pressures in accreting deposition of slurried material under one-dimensional self-weight consolidation. Part II: Impervious base. *Indian Geotechnical Journal, 48*(1), 188-195.